

SECOND

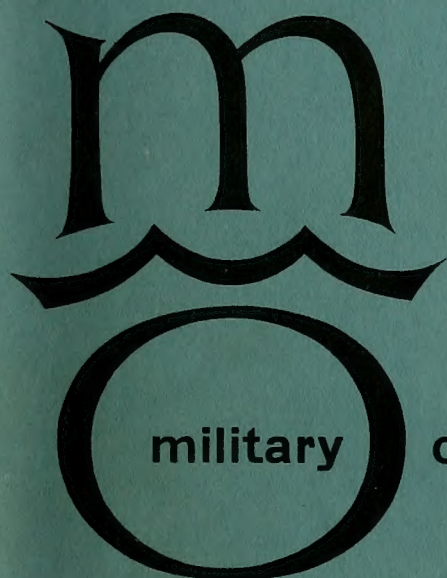
UNITED

STATES

NAVY

SYMPOSIUM

ON



military

oceanography

5-7 MAY 1965

THE PROCEEDINGS  
OF THE SYMPOSIUM

VOLUME I

UNITED STATES NAVAL ORDNANCE LABORATORY WHITE OAK  
SILVER SPRING, MARYLAND

V  
396.3  
.45  
2nd



US Navy Symposium  
 May, 5-7 May 65,  
 Silver Spring, Md.

RETURNED	
8 Nov 65	
10 Jan 66	
24 July 68	
11 a/m 69	
19 Dec 1971	
5 July 73	

806  
 10/10/69  
 10/10/69

Papers have been printed in this publication  
 substantially as submitted by the authors.

are available  
 at the Library of the Navy,

published in a  
 copies of the  
 addressed to

See also volume II  
classified 246-C-65

SECOND

UNITED

STATES

NAVY

SYMPOSIUM

ON



**oceanography**

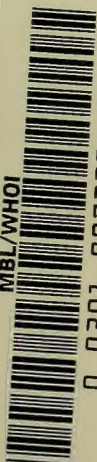
5-7 MAY 1965

THE PROCEEDINGS

OF THE SYMPOSIUM

VOLUME I

MBL/WHOI



0 0301 0072228 6



## WELCOME

From the Commander  
United States Naval Ordnance Laboratory White Oak  
Silver Spring, Maryland

The Naval Ordnance Laboratory is honored to host this second annual U. S. Navy Symposium on Military Oceanography.

Your direct interest and active participation are the key ingredients that will combine to make this second symposium as highly successful as the first. The quality of the papers that have been submitted and selected for presentation are advance indicators of your deep interest in this challenging frontier.

It is a great pleasure having you as our guests. The arrangements that have been made are directed towards making these sessions a success. We hope that you will find them so.

R. E. ODENING

Captain, USN  
Commander



from the Oceanographer of the Navy  
MESSAGE

MESSAGE

from the Oceanographer of the Navy

Our first U. S. Navy Symposium on Military Oceanography in June 1964 was, like all firsts, an experiment.

The high calibre of the representatives from private industry, scientific and educational institutions and government agencies who attended, the quality of papers presented, the free flow of ideas that were generated in the open forum discussions, plus the generally enthusiastic reaction, made it inevitable that the symposium should become an annual affair.

The problems that confront the Navy as a member of the U. S. defense team are as pressing as ever and it is not too much to say that our survival as a nation may, in the end, depend upon our continued leadership in the field of oceanographic research and development. The success of all anti-submarine operations will be enhanced immeasurably as our increased knowledge of ocean environment becomes an integral part of Fleet operations. Should your deliberations result in ideas leading to a better solution to any one of these problems the effort involved in this symposium will have been well worthwhile both for military operations as well as our broad national welfare.

As sponsor of these symposiums, I want to express my appreciation to the U. S. Naval Ordnance Laboratory for acting as your host on this occasion. I know that the arrangements they have made will contribute to the success of your deliberations. I am confident that all of you will find in these sessions an opportunity to gain new and imaginative insights into your own many and varied interests in the oceanographic factors that affect military problems and specifically Fleet operational capabilities.

As I said to those who attended the first symposium, ideas are our weapons, good luck and good hunting.

DENYS W. KNOLL

Rear Admiral, USN  
Oceanographer of the Navy

U. S. NAVY SYMPOSIUM  
ON  
MILITARY OCEANOGRAPHY

SPONSORS

---

Office of Chief of Naval Operations  
Office of Naval Research  
Chief of Naval Material  
Bureau of Naval Weapons  
Bureau of Ships  
Bureau of Yards and Docks  
U. S. Naval Air Development Center  
U. S. Naval Civil Engineering Laboratory  
U. S. Naval Oceanographic Office  
U. S. Naval Ordnance Laboratory  
U. S. Naval Ordnance Test Station  
U. S. Naval Research Laboratory  
U. S. Naval Underwater Ordnance Station  
U. S. Naval Underwater Sound Laboratory  
U. S. Naval Weather Service  
U. S. Navy Electronics Laboratory  
U. S. Navy Mine Defense Laboratory

STEERING COMMITTEE

---

Commander J. C. Fry, USN, CNO (Op-09B5)  
Lieutenant Commander R. G. Reed, USN, CNO (Op-716)  
A. T. Jaques, NOL  
B. King Couper, BUSHIPS  
Murray H. Schefer, BUWEPS  
Bruce Bingham, ONR  
Frederick Knoop, BUDOCKS

PROGRAM COMMITTEE

---

A. T. Jaques, Chairman  
R. E. Arthaud  
Julius Castigliola  
Ermine A. Christian  
Commander D. W. Smith



# TABLE OF CONTENTS

	Page
THE ROLE OF THE NAVY IN OCEANOGRAPHY, by Honorable Robert W. Morse . . . . .	1
TRENDS IN THE NAVY OCEANOGRAPHIC PROGRAM, by Commander John C. Fry, USN. . . . .	9
NAVY-MAN-IN-THE-OCEAN, by Commander Willard F. Searle, Jr., USN . . . . .	25
OCEANOGRAPHY EDUCATION AT THE UNITED STATES NAVAL PORTGRADUATE SCHOOL, by Glenn H. Jung . . . . .	35
ANALYTICAL PREDICTION OF OCEANOGRAPHIC INFLUENCES ON BOTTOM-REFLECTED SOUND, by Rodney O. Davidson. . .	43
DEEP RECTILINEAR TOWING WITH PARALLEL TUBES, by Norman W. Lord. . . . .	55
THE ACCURACY AND POTENTIAL USES OF COMPUTER BASED WAVE FORECASTS AND HINDCASTS FOR THE NORTH ATLANTIC, by Willard J. Pierson, Jr., and Leo J. Tick . . . . .	69
THE RESPONSES OF THE OCEAN TO THE ACTION OF ATMOSPHERIC FORCES AND ACCOUNTING OF THESE RESPONSES IN U. S. FLEET NUMERICAL WEATHER FACILITY'S OCEAN- OGRAPHIC ANALYSIS AND FORECASTING PROGRAMS, by Commander W. E. Hubert, USN, Commander R. C. Slusser, USN, and T. Laevastu. . . . .	83 ✓
PREDICTION OF SUMMER THERMOCLINE DEPTH OFF MISSION BEACH, by James L. Cairns and E. C. LaFond. . . . .	111 ✓
THE NUMERICAL PREDICTION OF MEANDERS IN THE GULF STREAM, by James G. Welsh . . . . .	133
A MOORED OCEANOGRAPHIC DATA ACQUISITION SYSTEM, by William C. Green and Leon DeVilleneuve. . . . .	145
DEEP OCEAN BIOLOGY IN RELATION TO CONSTRUCTIONAL MATERIALS, by James S. Muraoka. . . . .	163
A PRELIMINARY STUDY OF THE DIRECTIONAL SPECTRUM OF SHORT-PERIOD INTERNAL WAVES, by H. Charnock . . . . .	175
PRECISION FATHOMETER RECORDER, by Richard G. Popovici and Thomas K. DeWitt. . . . .	179

# TABLE OF CONTENTS

	Page
DEEPLY-TOWED ECHO-SOUNDER RECONNAISSANCE OF A FLEET TACTICAL RANGE SITE, by Michael S. Loughridge .	207
PHYSICAL CHEMISTRY OF THE DEEP OCEAN ENVIRONMENT, by R. A. Horne. . . . .	221
DEEP SEA FREE INSTRUMENT PACKAGE, by Philip P. Bedard. . . . .	235
A DESCRIPTION OF INSTRUMENTATION AND THE MEASUREMENT TECHNIQUES USED FOR THE DETECTION OF EXTREMELY LOW FREQUENCY ELECTROMAGNETIC ENERGY IN THE SEA, by James F. Orr. . . . .	243
GLASS AND CERAMIC HULLS FOR OCEANOGRAPHIC APPLICATIONS, by J. D. Stachiw. . . . .	255
SYNTACTIC FOAM BUOYANCY MATERIALS FOR SUBMERGED RESEARCH VEHICLE, by Israel Resnick . . . . .	317
THERMAL AND SOUND VELOCITY MICROSTRUCTURE DATA TAKEN WITH AN UNMANNED RESEARCH VEHICLE, by S. R. Murphy and G. E. Lord . . . . .	343
ECONOMIC CONSTRAINTS ON THE DESIGN OF AN EXPENDABLE INSTRUMENT SYSTEM, by W. V. A. Clark, Jr. . . . .	361
A SHIPBOARD NAVIGATIONAL AND GEOPHYSICAL PROCESSING SYSTEM, by Carl O. Bowin. . . . .	367
INVESTIGATIONS OF SEDIMENT PROPERTIES IN SONAR BOTTOM REFLECTIVITY STUDIES, by James J. Gallagher and Vito A. Nacci . . . . .	375
TEMPERATURE STRUCTURE IN THE TRANSITION REGION OF THE NORTH PACIFIC, by Margaret K. Robinson and John Northrop . . . . .	403
SOUND VELOCITY STRUCTURE OF THE OCEAN BETWEEN BERMUDA AND THE ANTILLES, by R. E. Payne and J. C. Beckerle. . . . .	433



THE ROLE OF THE NAVY IN OCEANOGRAPHY

by

Honorable Robert W. Morse

Assistant Secretary of the Navy for  
Research and Development





## THE ROLE OF THE NAVY IN OCEANOGRAPHY

by

Honorable Robert W. Morse

Assistant Secretary of the Navy for Research and Development

Admiral Knoll, distinguished guests, ladies and gentlemen. It is a privilege for me to be here this morning to address the Second Annual Symposium on Military Oceanography, held under the auspices of the Oceanographer of the Navy and sponsored this year by the Naval Ordnance Laboratory. I appreciate being asked to speak because I strongly endorse the objectives of this Symposium: to stimulate discussion among scientists and engineers from industry, from our universities, and from the Navy, in an annual forum devoted to the Navy's oceanographic program. Certainly one can view the proceedings of this meeting as comprising an annual status report on the Navy program.

I would like to share with you today some thoughts as to the role presently played by the Navy in ocean science and to suggest future changes in that role which might be necessary to enhance the Navy's effectiveness in oceanography and to support this Nation's peaceful goals in using the ocean.

In the past several years, the entire Nation has become much more aware of the oceans. At all levels, there is a growing recognition that we must understand, explore, and exploit fully this large part of the world we inhabit.

These concerns have led to a strengthening of the oceanographic programs of several other federal agencies which have roles and missions concerned with the ocean. The Navy has gained because virtually all that is learned about the ocean is of potential naval value. Growth of the Navy's own oceanography program also has been substantial in the past several years but continues to be based on the necessity of exploiting the sea for national defense.

To avoid duplication between the Navy and other federal agencies as well as to encourage a purposeful national program, the Interagency Committee on Oceanography (ICO) of the Federal Council for Science and Technology was established in 1960. The ICO reviews and endorses or recommends modification to the agencies' programs within the context of the overall national effort but also acknowledges the priorities of the separate missions of the member agencies. Within this natural restriction, I believe the Committee has been effective. The primary forces of the ICO are communication, debate, coordination, and a unified sense of purpose which has enabled planning in the individual agencies to be carried out in full knowledge of the purposes and actions of the other agencies.

In spite of the fact that oceanography recently has assumed a new importance both within the Federal Government and in the public mind, there are expressions of concern that progress is too slow, particularly in the area of exploiting the ocean's resources. In Congress this concern takes form in a number of bills before the current session.

American industry has been restive, too. The publicity accorded oceanography in recent years has led some to expect massive federal projects with an impact upon industry comparable to that of the space program, and a spin-off of new technological competence that would put established firms in a new and lucrative business. This has not developed - and - may not!

I, personally, am not convinced that organizational changes is the prime requirement. Required most of all are well-planned, imaginative programs.

In my mind, there has been much too much talking in vague generalities about: "exploiting the sea," "exploiting the continental shelf," etc., and too little specific examination of real goals that might be attainable.

The concerns expressed by both Congress and industry about progress in ocean technology are well founded. However, before organizational questions can be focussed, before accelerated spending is justifiable or before new industries are launched, it will be necessary to develop specific programs, establish priorities, and clarify the roles to be played by the Federal and State Governments, industry, and other private institutions. But clearly the existing federal agencies and, in particular, the Navy, utilizing fully the Interagency Committee on Oceanography, should take a strong lead in developing such programs.

Within the Navy there are many similarities to the national program since oceanography cuts across virtually all parts of the Navy structure. There is hardly an admiral who does not have in his command some group that concerns itself directly with ocean science and technology. You will get a feeling for the magnitude of this problem within the Navy by an examination of the President's National Oceanographic Program document for Fiscal Year 1966. This document shows the Navy's share as approximately 50 per cent of the national program. However, a full accounting of total oceanographic efforts of the Navy completely eclipses the activities of all other agencies. There is no vertical structure in the Navy that embraces all of this and exerts line control over all of oceanography. This would be neither feasible nor desirable. However, it is clearly essential that the Navy have well developed and coherent objectives for its total oceanographic effort.

The aims are clear. The Navy is determined that it shall continue to be the federal agency most knowledgeable about the ocean. We intend to have, for the foreseeable future, a program in ocean science, technology, operations, and services, second to none in the world. The Navy intends to take an increasingly aggressive leadership in the National Oceanographic Program because nothing that goes on in the ocean can be without impact upon the Navy's mission.



If we make this abundantly clear, and, at the same time, emphasize that the Navy is actively interested in the growth of effective ocean programs in other agencies, I feel that concern over a national program can be eventually eliminated.

What should we do within the Navy? One easy suggestion might be to collect all the Navy's oceanographic activities under one command. This unfortunately would make as little sense as collecting all the Nation's marine activities under one agency. As ocean science is vital to the mission of various federal agencies in a variety of ways, so it is vital in a variety of ways to the mission of the many branches of the Navy.

Basic research in the science of the sea has a long range bearing upon every part of the Navy and is rightly separated organizationally from branches with operational missions and is overseen by the Chief of Naval Research.

The Navy's bureau must pursue applied research as it bears upon their missions of providing the hulls, facilities, and weapons systems required by the Fleet.

The Navy laboratories, each with its own mission in applied research to back up development projects, must do this research within the real ocean and thus with a direct understanding of it.

Finally, the Fleet must be provided with, and have a competence to use, the best possible environmental information in order to maximize its effectiveness.

The Navy is well organized for all these functions and its oceanographic activities are in the hands of officers and civilian scientists of clear capabilities. Nevertheless, I can identify three possible shortcomings to which we must continue to give attention.

We do not have sufficient in-house competence for advanced environmental research. We do, however, sponsor the work of many of the world's best scientists in the universities and nonprofit laboratories.

In spite of much effort we are not doing as much as we should to familiarize our future admirals with ocean science and technology. Barely sufficient for today's Navy perhaps, but not for the vastly more complex Navy of the future. We do have the beginnings of an excellent program at the Navy Postgraduate School that is addressing itself to this problem and we must do much more.

There are shortcomings in communication between our own establishments and with the outside. Basic research is not always well communicated to the applied laboratories or applied research to the bureau developments or to operating forces. A bright point is the success of the Oceanographer in providing environmental information to the Fleet.

Although we tend to give much of our attention to our shortcomings, we are definitely proud of the Navy's posture in ocean science and technology. During the last two decades, we have taken a leading role in the development of the Nation's competence. Notably, we have provided continuing support to university departments and nonprofit laboratories and the industrial laboratories. Our bureaus have faced up to new technological problems in areas such as deep water structures. The private institutions were full partners in many of the early ventures where the store of pertinent information was minimal. A similar role is now being taken by industrial organizations which have learned with us and, in many cases, have become the major sources of competence.

The changes have been rapid. Jobs at sea, which ten years ago were legitimate concerns of those doing the most basic research, are now considered in the sphere of routine surveying. Historically, we learn slowly and with great difficulty how to do things at sea and then almost overnight it becomes standard practice.

There has been considerable public interest in our developing a capability for operations in the deep ocean. Perhaps we have been too deliberate but we have been pushing forward nevertheless. We have done this by exploiting and improving specialized vehicles, including ALVIN and the NOTS vehicles, and by encouraging company developments and leasing their vehicles. Now, we have a well-conceived program to develop search and rescue vehicles and, as recently announced, a program to develop a small nuclear powered, long range research submarine. These developments must build upon firm foundations of technological knowledge, and we have to learn how to use these new tools.

One of our great hopes is that we will be able to observe ocean parameters synoptically and be able to predict short-term changes. Many facets of the Navy's program are converging upon this goal: The ASWEPS program at NAVOCEANO has been striving to build an operational system on existing scientific and technological frameworks. At the Fleet Numerical Weather Center a somewhat different approach using historical information and available synoptic data is being tried. Part of the ONR program at private institutions is aimed at improving the scientific basis for prediction. Both Navy laboratories and institutions are gaining valuable experience with observing arrays and an industrial development of a well-engineered unmanned ocean data station is nearing completion.

In addition to strengthening the Navy's oceanographic efforts internally, we shall undertake to expand our assistance to the other federal agencies involved with the sea. Not only will our facilities be made increasingly available to these agencies, but our entire oceanographic research and development programs will be programmed to insure maximum benefit to other agencies as well as the Navy. I must emphasize that this is not a one way street - the Navy will also gain from the fruits of their research, development, and operations.

I would like to give you two examples of areas in which the Navy is prepared to expand our work with other agencies. First, through our Deep Submergence Program we are developing a capability for placing man deeper and deeper into the sea. Part of this is directed towards man living for extended periods under water - capable of doing useful work. Another part concerns the design and construction of vehicles for taking man to greater depths and performing useful tasks. Although this is a program directed to clearly defined military purpose, I am confident that the technology resulting from the Deep Submergence Program will greatly accelerate the information of a broad technical base for future exploration of the ocean.

Second, the Navy has the broad problem of predicting weather and sonar conditions at sea. In order to do this, we must have elaborate devices for measuring, transmitting, and analyzing data collected at sea. This will involve networks of buoys, communication systems, and computation centers. These developments and the outputs of such systems are also relevant to agencies such as the Weather Bureau or the Bureau of Commercial Fisheries. We shall make every attempt to provide useful support to such agencies in our programs in this area.

The oceans represent a great potential to our country, and it is an obligation of the Navy, under its mission to insure freedom and beneficial use of the seas, to know as much as possible about this environment. The Navy must have an outstanding oceanographic program, must provide leadership in this field for the Nation, and must be willing to cooperate and work closely with any other group, inside or outside of the Federal Government, having similar interests.





TRENDS IN THE NAVY OCEANOGRAPHIC PROGRAM

by

Commander John C. Fry, USN

Office of the Chief of Naval Operations  
Washington, D.C.





## TRENDS IN THE NAVY OCEANOGRAPHIC PROGRAM

by

Commander John C. Fry, USN

Office of the Chief of Naval Operations, Washington, D. C. 20390

Mr. Chairman, ladies and gentlemen, it is a privilege for me to have the opportunity this morning to present "Trends in the Navy Oceanographic Program" which, broadly speaking, should set the stage for a discussion of scientific and technical achievements to follow throughout this meeting.

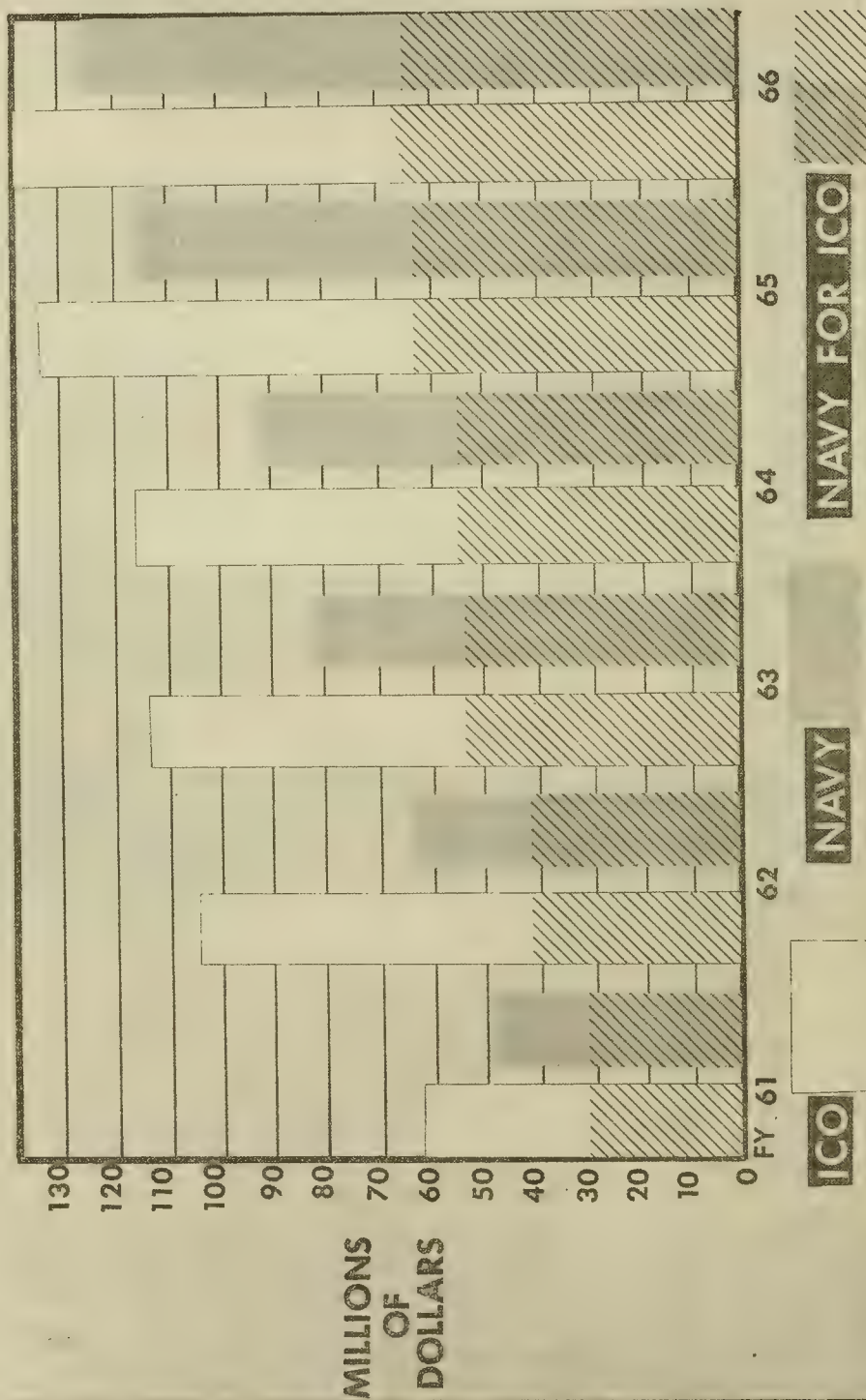
Figure 1 shows the budget for the total Navy oceanographic program compared year by year with the total national oceanographic program, which is coordinated by the Interagency Committee on Oceanography. The Navy includes only its unclassified programs in the national oceanographic program, and this is shown as the shaded area of these bars. During this period the Navy portion of the ICO program has decreased from roughly 60 percent of the total Navy program to about 50 percent this year, which reflects a relative increase in classified operations. If classified Navy programs were to be included, the national oceanographic budget would be increased by more than 40 percent, and, as it stands now, the doubling time of the Navy program is roughly 4 years, a rate somewhat greater than 10 percent per year.

Figure 2 shows how FY 1966 funds, if appropriated by the Congress, will be balanced among participants in the Navy's oceanographic program and applied to new ship construction: 23 percent of the total to the Office of Naval Research, 48 percent to the U. S. Naval Oceanographic Office, 8 percent to the Bureau of Ships, about 1 percent to the Bureau of Naval Weapons, less than 1 percent to the Bureau of Yards and Docks, and 19 percent for ship construction. The ship construction funds are intended for two AGORs for the Office of Naval Research and one large hydrographic surveying ship for the Naval Oceanographic Office.

I would also like to show by Figure 3 how FY 1966 funds will be balanced among the appropriation categories: 38 percent for research, development, test and engineering; 32 percent for operations and maintenance; 19 percent for ship construction; 4 percent for other procurement; and 6 percent for military personnel.

A complementary document to the Navy's long range plan for oceanography, TENOC, is the Navy Oceanographic Program Summary, pictured in Figure 4, which has been prepared by the Office of the Oceanographer of the Navy to aid in program analysis and planning. This summary gives a brief resume of all tasks included within the Navy oceanographic program, defining their objective, approach, progress, plans, and keywords to aid





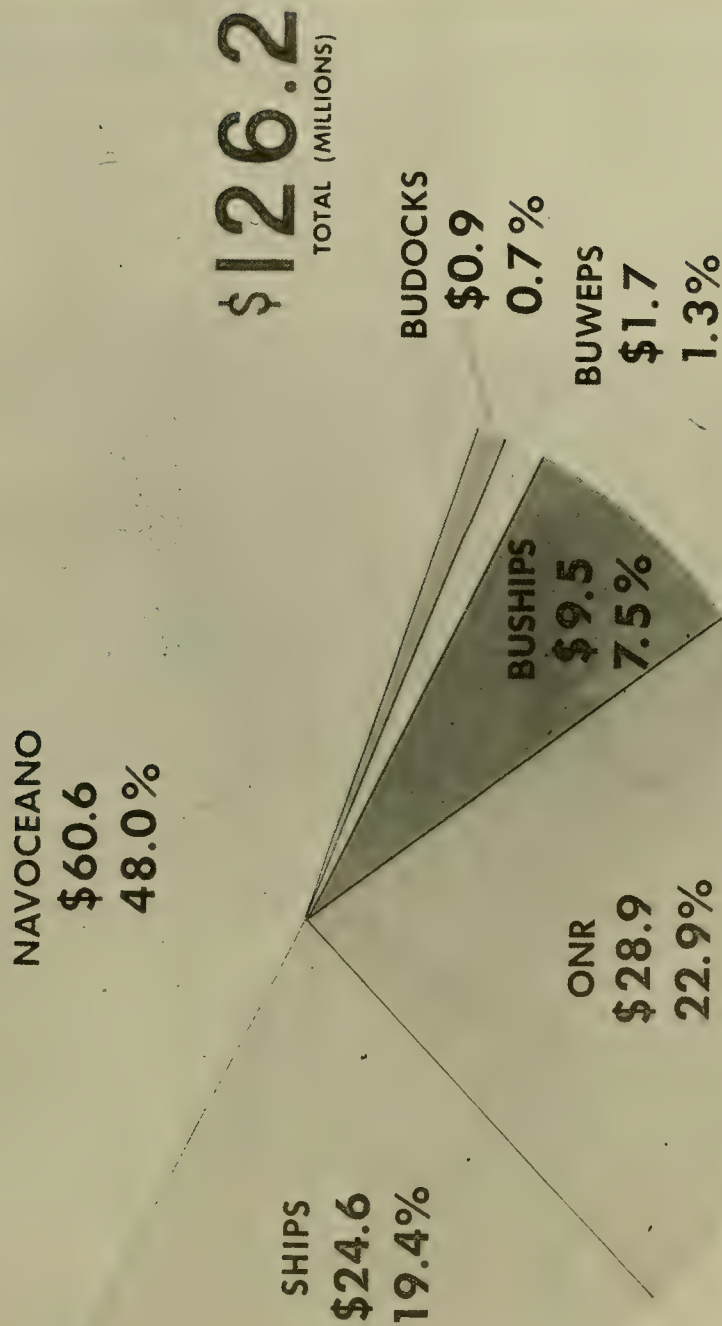


FIGURE 2 FY 1966 BUDGET IN OCEANOGRAPHY BY NAVY ACTIVITIES



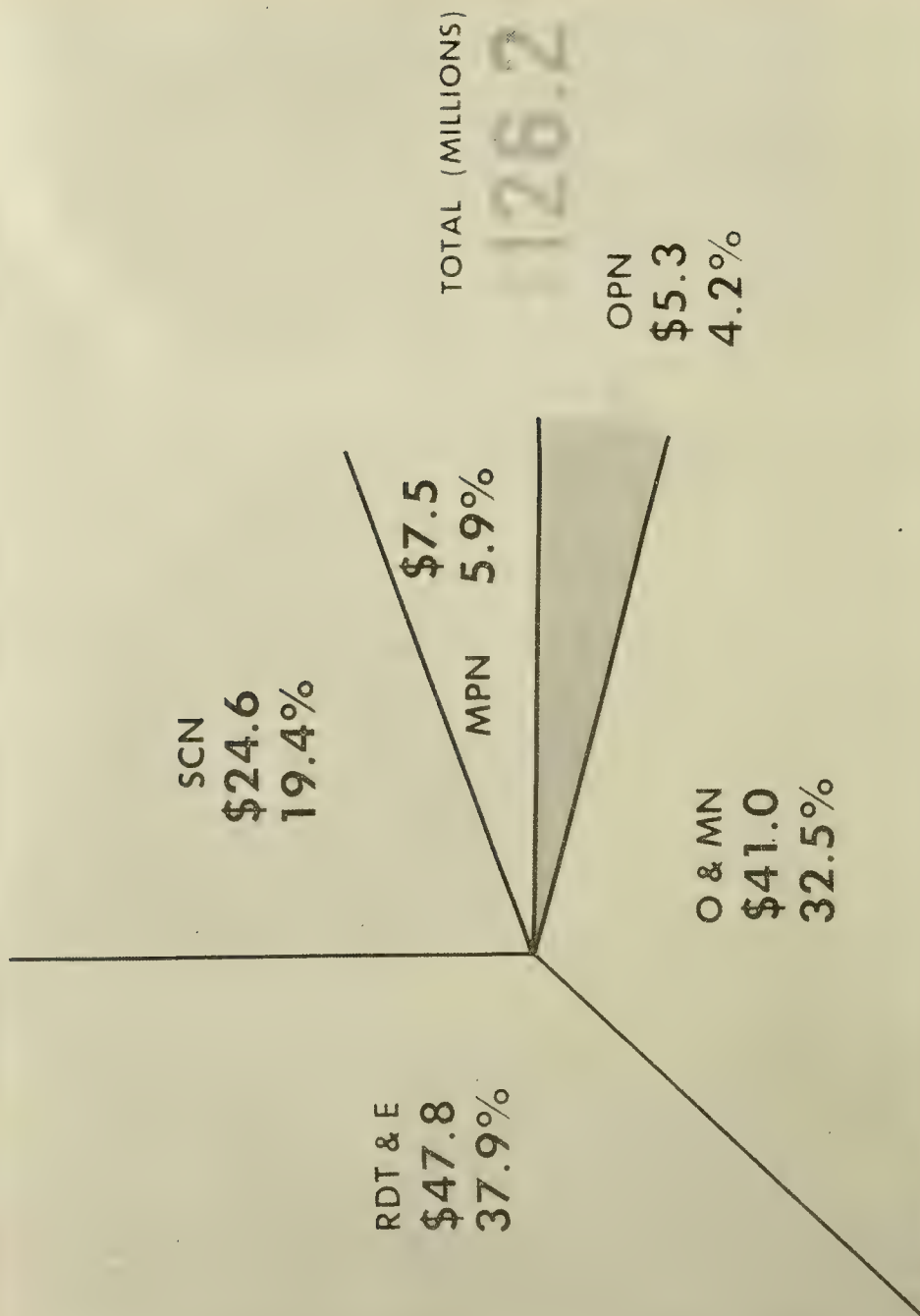


FIGURE 3 FY 1966 BUDGET IN OCEANOGRAPHY BY FUNDING CATEGORY

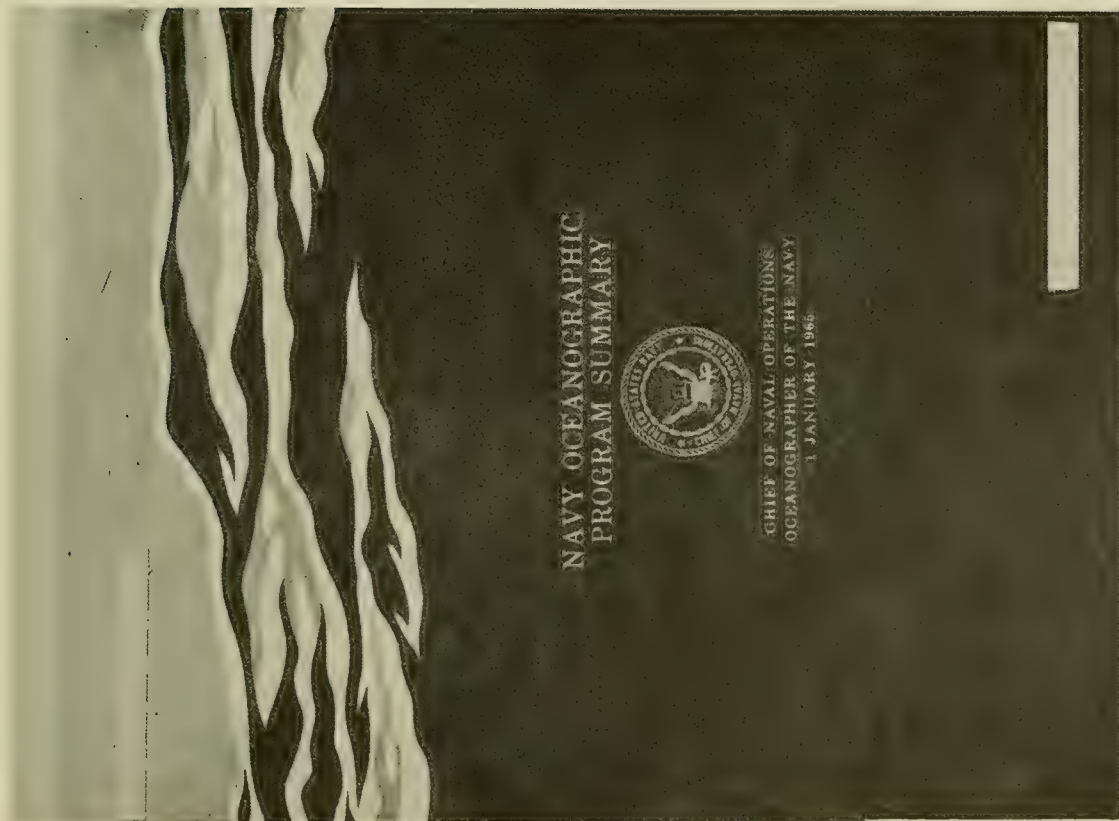


FIGURE 4 PICTURE OF PROGRAM SUMMARY COVER

in task identification. The program summary will be used to assess progress in TENOC and, at the same time, to determine whether the program has appropriate balance and scope. Whereas TENOC is the Navy long range plan in oceanography, the program summary contains both the current annual plan and mid-range objectives in consonance with the five-year force structure and financial plan.

Although oceanographic buoys and aircraft are being developed, the Navy will have to depend largely on ships to support the bulk of its oceanographic program for many years.

Figure 5 shows the TENOC plan for oceanographic survey and research ships that will enter service through 1973, a plan for new construction well-supported by Navy requirements.

In the FY 1966 program a new design has been proposed for the oceanographic research ships. Now that we have had some operational experience with the first of these ships and have had an opportunity to assess their performance and capabilities, some design modifications have been proposed for the two ships to be used by Scripps and Woods Hole Oceanographic Institutions. If the changes are approved, these ships will be slightly larger with a wider beam, they will accommodate a larger scientific party, and several major options in design will be possible, for example, one option is the capability to handle and support deep research vehicles; another is a large center well and drilling equipment for sea floor studies.

Figure 6 compares the funding of the Navy RDT&E program in oceanography with research in the national oceanographic program. The Office of Naval Research, through several of its branches, broadly supports research and development in oceanography at universities and oceanographic institutions in this country and at several universities abroad, and to an extent in private industry. This program supports research and development by some of the country's leading oceanographers, the operation of research ships assigned to the various institutions and universities, the development of improved oceanographic instrumentation and vehicles, ship conversion and outfitting with equipment and scientific instruments, and the expansion of university facilities for marine research.

I should like to mention several significant accomplishments of this program this past year, which comprises 60 percent of the RDT&E effort. A new **technique** was developed which permits a single ship to rapidly determine the changing path of the Gulf Stream. By measuring horizontal temperature gradients with a new temperature-sensing instrument towed at a depth of 200 meters, Woods Hole scientists were able to trace the course of the Gulf Stream over a distance of 1,600 miles. This technique has already found commercial application, being used by tankers enroute from the Gulf coast to east coast ports, to remain near the axis of the Gulf Stream and thus shorten their voyage. In another project a number of new knolls were discovered on the bottom of the eastern portion of the Gulf



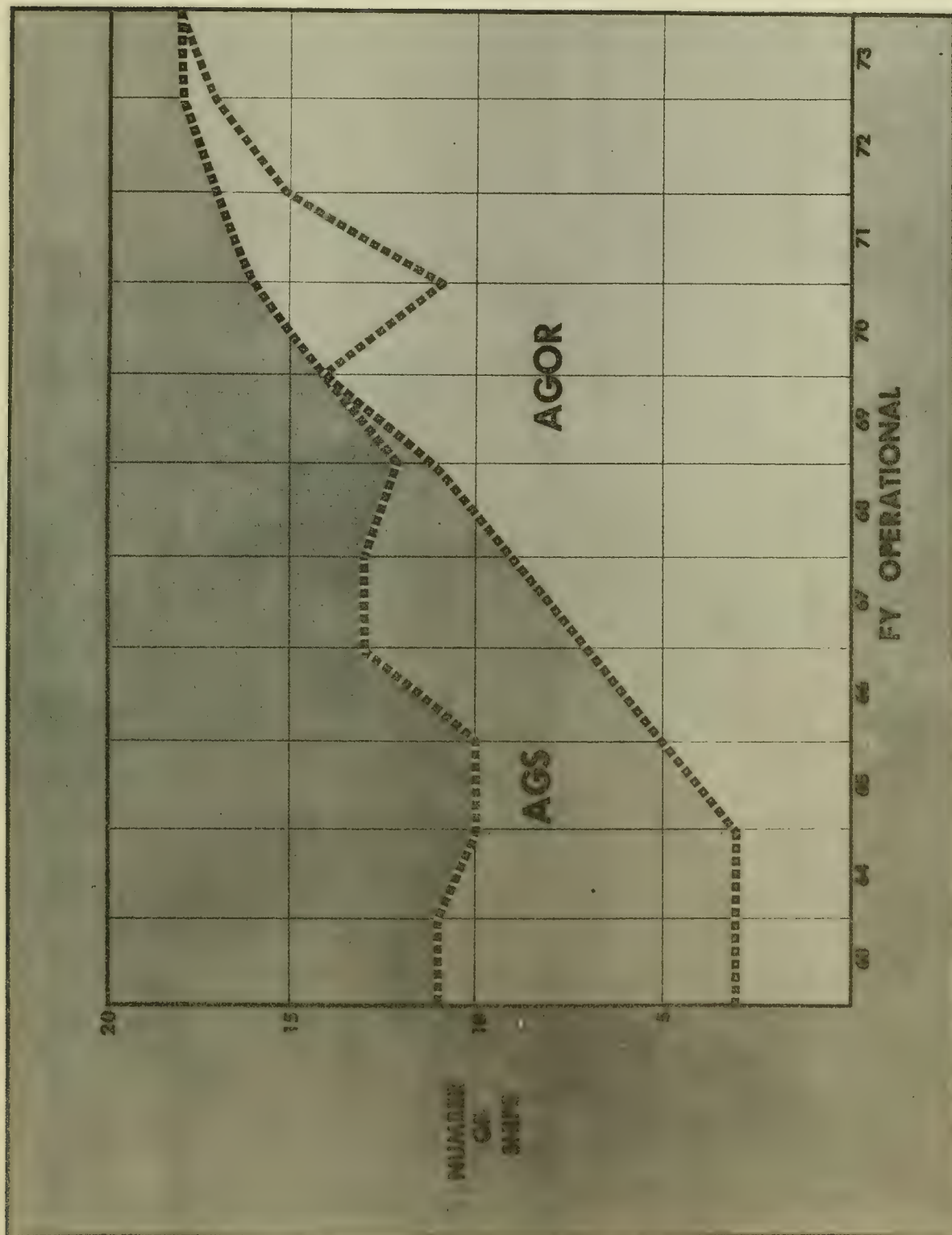


FIGURE 5 NUMBER OF SHIPS

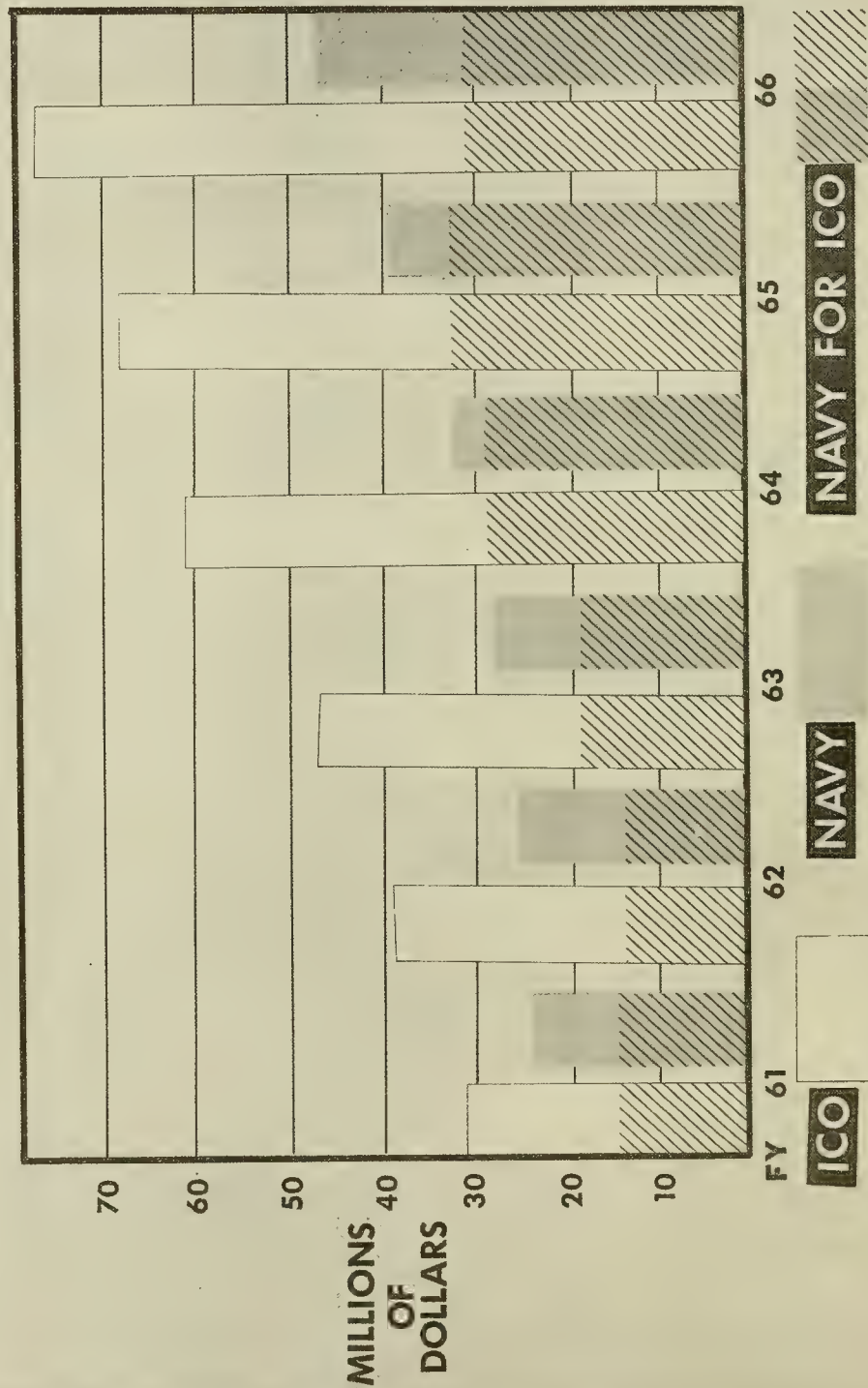


FIGURE 6 RESEARCH FUNDS

of Mexico at depths of about 12,000 feet. The geophysical evidence indicates that these could be salt domes, which may be commercially important, because salt domes commonly are found in the vicinity of petroleum deposits.

The Naval Material Support Establishment has established research and development programs in oceanography within the Bureau of Ships, the Bureau of Naval Weapons, and the Bureau of Yards and Docks, accounting for another 25 percent of the oceanographic RDT&E effort. These are programs centered at the Bureau's laboratories, that are generally mission-oriented to support approved system development and engineering programs.

One of the major oceanographic programs in this category is supported by the Bureau of Ships and conducted at the Naval Electronics Laboratory in San Diego, where they have a balanced program of sea floor studies; physical oceanography; marine biology, concentrating on investigations of the deep scattering layer; and sea ice and Arctic studies.

The Bureau of Naval Weapons has a research and development program in oceanography, which is still small, but is being strengthened at the Naval Ordnance Laboratory and other in-house and contract laboratories. The purpose of this program is to develop oceanographic models and obtain oceanographic data, with which to improve the design and effectiveness of future naval weapon systems.

In addition, the Special Projects Office of the Bureau of Naval Weapons supports oceanographic and underwater acoustical research and development to provide a strengthened foundation in marine science and technology for FBM submarine operations and advanced sea based deterrent systems; now, however, an additional program of research and development in oceanography is required to adequately support the development and world wide employment of deep submergence systems.

The third major program in the Naval Material Support Establishment is that sponsored by the Bureau of Yards and Docks. This is an expanding program being conducted at the Naval Civil Engineering Laboratory at Port Hueneme, California, to investigate the physical properties of marine sediments influencing the design of undersea foundations and to develop and select optimum procedures and material for deep sea construction and engineering.

Thus far we have accounted for roughly 85 percent of the Navy's RDT&E program in oceanography. The remaining 15 percent of RDT&E and the total O&MN program in oceanography is concentrated at the Naval Oceanographic Office, which, in the main, produces oceanographic and hydrographic products for naval operating forces, although to an increasing extent, oceanographic surveys and studies are performed for other Offices and Bureaus of the Navy Department as well. In general, the RDT&E program at the Naval Oceanographic Office is devoted to the development, test, and calibration of oceanographic instruments, the development of oceanographic and



hydrographic survey techniques, the improvement of procedures and equipment for the efficient printing and distribution of nautical charts and publications, and development of the Antisubmarine Warfare Environmental Prediction System.

Figure 7 presents a comparison of the Navy and national survey programs. Broadly speaking, the surveys performed by the Naval Oceanographic Office fall into four categories. First, Inshore Surveys are conducted in overseas areas to support amphibious and mine warfare training and operational planning.

Second, Strategic Coastal Surveys are performed to meet requirements of the Defense Intelligence Agency for improved nautical charts.

Third, Project Surveys, required to obtain data for the development, installation, and operation of underseas systems. Several examples of these are the oceanographic surveys required for Project CAESAR; for COLOSSUS I; for AUTEC; for the Pacific Missile Range; and for nuclear submarine operations.

As the Navy's program in oceanography expands, a greater number of naval officers subspecializing in this field will be needed. To obtain these officers a new course in oceanography has been established at the Naval Postgraduate School in Monterey and the annual input of naval officer students is being increased from 12 in FY 1965 to 24 this year, and may be further increased to 40 by 1968 as shown in Figure 8. At the same time the graduate students will be distributed differently: half of them will attend major graduate schools in oceanography and the remaining half will attend the course at Monterey. For example in the fall of 1965, 12 naval officers will enter the program at Monterey, and 12 will enter graduate schools in oceanography at the Scripps Institution of Oceanography, Texas A&M, the University of Washington, and the Institute of Marine Sciences of the University of Miami. In addition, an introductory course in oceanography has been established for all midshipmen at the U. S. Naval Academy in their first year, and they can now concentrate in the field of environmental sciences their last two years.

When we take a broad view of the Navy's oceanographic program, as we must at least annually, it is most essential to re-evaluate its objectives, its balance and emphasis, and most importantly the opportunities it offers to contribute substantially to naval progress and the tangible national goals established for marine science and technology. We have done this, and are convinced the program is essentially sound. It is a program that has increased in funding by a factor of 6 in the past ten years; it has more than doubled in the last five years. Its growth rate is nearly twice that of the federal research and development program. It has provided 5 new construction oceanographic ships in the past 4 years, and 9 more have been authorized and funded. It has greatly accelerated research and development within the Navy and its laboratories, within industry, and within

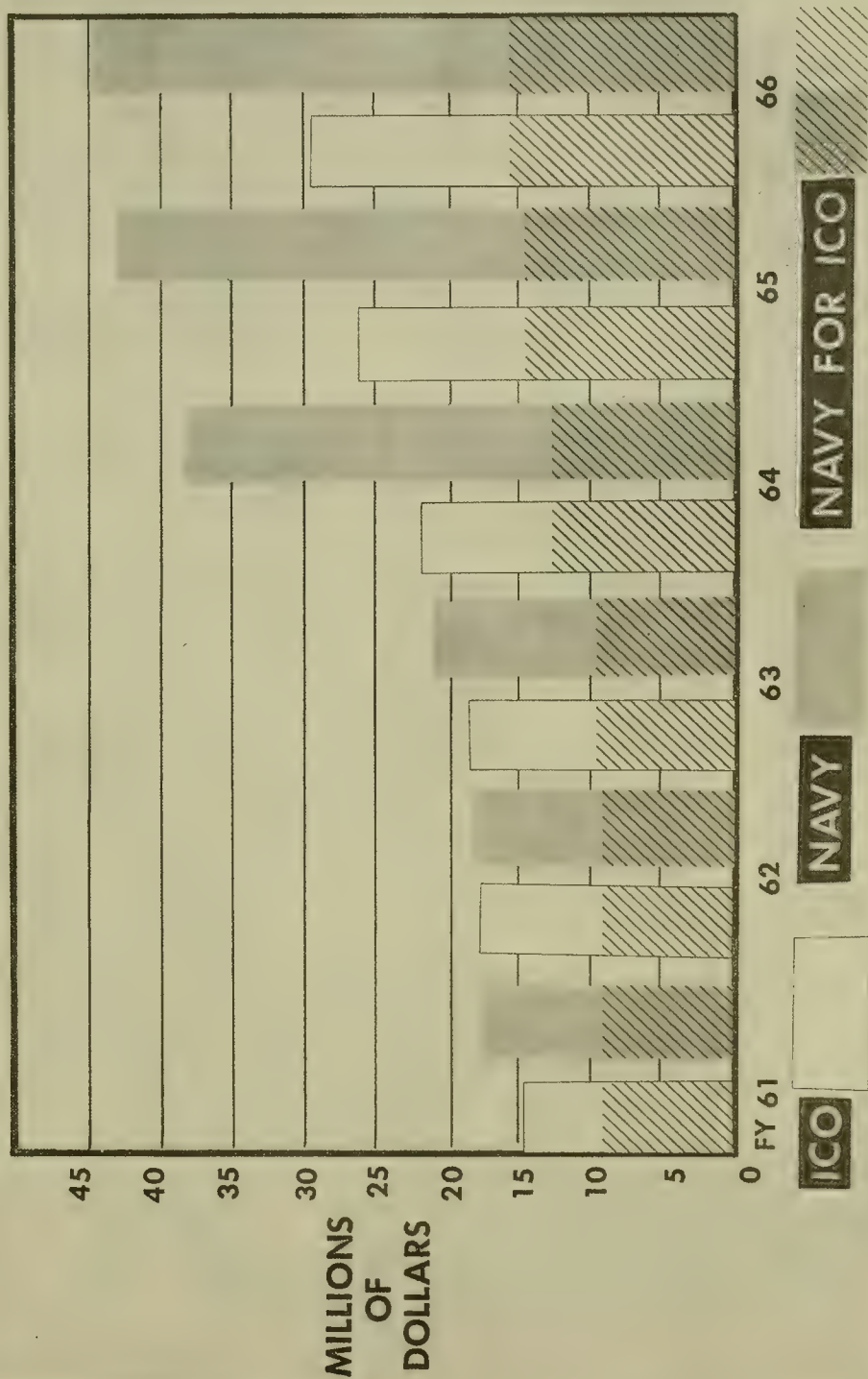


FIGURE 7 SURVEYS

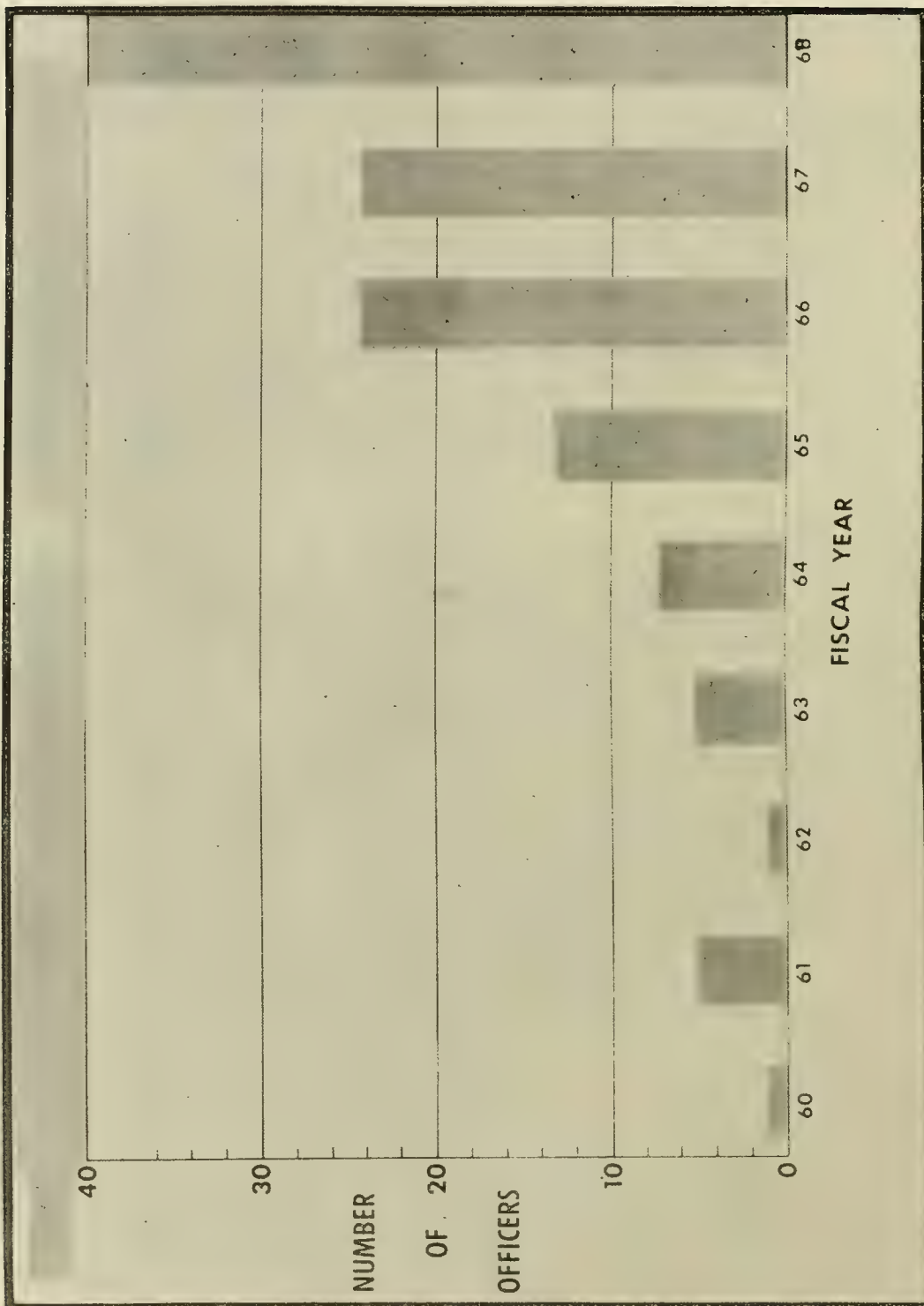


FIGURE 8 NAVY POSTGRADUATE PROGRAM IN OCEANOGRAPHY



private institutions and universities, thus providing firm Navy guidance and leadership in the national oceanographic program. And, most importantly, it has increased an awareness within the Navy of the relevance of oceanography to current missions and of opportunities to reshape these missions to exploit marine science and technology in the national interest.

Nonetheless, in the face of changing requirements within the Navy and the federal government, I believe there may well be areas of the Navy program we might wish to examine more closely to search for improvement.

First, perhaps, we should re-examine the emphasis in the program, wherein the first and foremost requirement is to provide oceanographic information in useable form to optimize decisions concerned with the design and employment of advanced naval systems. In view of the complex influence of the environment on underseas system performance, we can ill-afford to delay required oceanographic programs until such systems are being procured in production quantities, and the need becomes urgent. Rather, oceanographic program must be identified and harmonized with system development to obtain accurate oceanographic models for system analysis prior to the selection among alternative designs, and to obtain required oceanographic data prior to fleet employment. With greater emphasis in the Department of Defense being placed on technically and financially sound systems management, we have no recourse but to stress system oriented oceanographic programs to a much greater degree than we have in the past.

This is not to say, however, that we would at the same time unbalance the research effort in oceanography, for such a policy would lead in the long run to diminishing returns and ultimate stagnation. The mainstream of effort in research, development, and surveys must, of course, continue, but all programs would be subject to critical analysis in terms of their potential contribution to Navy objectives.

Secondly, I believe we should intensify our programs for exploring dynamical processes in the sea that would lead to more efficient models for oceanographic prediction and forecasting. ASWEPS, being developed by the Naval Oceanographic Office, is a logical start in this direction; however, this is confined to a single area of the northwestern Atlantic. In other areas the data are more sparse, the circulation and turbulence models are less well-defined, and there can be no doubt that we will have to utilize oceanographic-meteorological buoys in substantial numbers to augment the meager oceanographic data available from transiting ships, weather stations ships, fixed stations and aircraft. I visualize that a network of ocean buoys, collecting and transmitting oceanographic and meteorological data to satellites, will be required in the future to obtain reliable models of dynamical processes in the sea and air-sea interaction relationships for practical application.

Oceanographic and meteorological information from a network of ocean buoys would have important military and economic applications; it would

substantially improve oceanographic forecasting techniques, it would augment available environmental data for fleet operating forces, to achieve greater effectiveness in ASW, amphibious, and mine warfare operations; and it would improve efficiency in ship routing and long range weather forecasting.

Concerning these benefits, I might mention the recent publication of the National Academy of Sciences' Committee on Oceanography entitled, "Economic Benefits from Oceanographic Research". In this excellent document the Committee concludes that fuel consumption and time at sea can be reduced 10 percent and weather losses can be reduced 20 percent through improved ship routing, with a benefit/cost ratio of 2.8 to 1. Similarly, the Committee concludes that long range weather forecasts can be improved through increased understanding of air-sea interactions with a benefit/cost ratio of 6.5 to 1. Certainly, all aspects of oceanographic prediction and forecasting programs should be re-evaluated in appraising the balance of the Navy's total oceanographic program.

In conclusion, let me quote a remark by Rear Admiral John D. Hayes, USN (retired), on the occasion of his acceptance of the U.S. Naval Institute's annual prize essay award. In discussing the rationale for his excellent article, Admiral Hayes urges "the U. S. Naval profession to lift its sights beyond warships and weapons, to include the whole, wide, maritime horizon." And, as he points out in his essay, this includes oceanography.

NAVY-MAN-IN-THE-OCEAN

by

Commander Willard F. Searle, Jr., USN  
Supervisor of Salvage, U. S. Navy





## NAVY-MAN-IN-THE-OCEAN

by

Commander Willard F. Searle, Jr., U. S. N.  
Supervisor of Salvage, U. S. Navy

The primary purpose of this paper will be to define for you the breadth of the Navy's present capability for placing man in the ocean for the execution of one task or another, and, having defined this rather extensive capability, to suggest to you that this part of the Navy and the men who do the work in the ocean, and generally under its surface, constitutes a separate and distinct corps of the service. Call this corps of the service "Navy-Man-in-the-Ocean". It might also be called "Navy Man Underwater"; or perhaps someone will come up with a better generic term, paralleling "Naval Aviation".

This paper deliberately avoids use of the term "Man-in-the-Sea" because this term has come to represent a specific program. The program's purpose is to extend the capability of the existing Man-in-the-Ocean corps of the Navy. In fact, the Man-in-the-Sea Program only covers one of the several basic missions of the Navy Man-in-the-Ocean corps. It covers only submarine rescue and salvage and the R and D areas -- those tasks which will be described later on as falling under a Logistic and Service mission. The Man-in-the-Sea Program does not cover either the offensive or defensive underwater missions. This essay addresses, therefore, not the program but, rather, the overall arm of the service -- Navy-Man-in-the-Ocean -- which is manned by swimmers and divers of one type or another.

By way of history it may be pointed out that underwater men have been an important part of the Navy for well over a hundred years. The advent of underwater machinery -- shafting, propellers and sea suction -- and underwater ordnance in the form of mines and torpedoes, provided the stimulus for early specialized training in underwater work. For example, in an article which he wrote in 1879, Admiral Stephen B. Luce stated that:

"...a corps of divers for the Navy has come to be a necessity of the times, and these divers, besides being trained as seamen, should be trained also for submarine warfare."

Luce envisaged a corps of divers. Did he also envisage a corps of fliers? Whether or not he did, today we can use the term "Navy-Man-in-the-Ocean" to describe this underwater corps much as one uses the term "Naval Aviation" to describe our air corps. The generic term "Naval Aviation" conjures up a picture of the very large, very vital, very well known, well

organized (and advertised) air arm of the Navy. Naval Aviation includes all sorts of capabilities: from defensive fighter craft, to strike bombers; from logistic service craft to research vehicles. Naval Aviation also encompasses very distinct organizational units, such as ASW, Strike, Recon, Transport and so on, and very distinct types of people -- Navy-Man-in-the-Air, if you wish -- to man or pilot them.

Here the term Navy-Man-in-the-Ocean is used in the very same sense. This corps of the Navy also is separate and unique. It includes both defensive and offensive, or strike, capabilities. It also includes logistic and research services. It includes several very distinct types of people -- underwater pilots, if you will -- who are to be found in many different organizational units.

At this point it will be well to tie down whether or not the submarine service is a part of the definition of Navy-Man-in-the-Ocean. Submarine boats, as we know them today, wherein the personnel who man them are living and working in a more or less normal ambient atmospheric environment, are not a part of Navy-Man-in-the-Ocean. The crews are certainly not in the ocean; except in the escape situation, they are neither directly nor potentially affected by the ambient conditions around them as are Navy-Men-in-the-Ocean and naval aviators. Perhaps the day will come when ambient pressure inside a submarine hull will be increased, thereby increasing the boat's maximum operating depth. When that day comes, the submarine's crewmen will certainly be at least cousins to the fraternity of divers. At this point in time, however, so far as Navy-Men-in-the-Ocean are concerned, men in submarines, like crews of destroyers, are a part of the "sea goin'" Navy. They are sailors -- submarine sailors. So we very quickly put this subject into perspective -- there are sailors; there are aviators; and there are Men-in-the-Ocean or, for lack of a better word, divers.

So much for introduction and definition. Where do you find the Navy-Man-in-the-Ocean capability -- organizationally speaking?

The best way to audit this overall capability is to consider Navy-Man-in-the-Ocean as serving three separate and distinct missions, as follows:

- Logistics and Service
- Offensive
- Defensive

Expanding on these three categories, and recognizing that there are overlaps between them, we can show essentially all the different diver and related tasks in the Navy, as follows:

- Logistics and Service

- Repair, maintenance and construction.



Salvage.  
Aviation and submarine rescue and escape assist.  
R and D services.  
Training.

#### Offensive

Amphibious assault recon and preparation.  
Mine clearance.  
Underwater strike warfare.  
Clandestine operations.

#### Defensive

Explosive ordnance disposal and rendering safe.  
Harbor surveillance and inspection of ships hulls.

From an organizational standpoint, the operating personnel who perform these several tasks will be found scattered throughout the Navy. The logistic tasks are distributed as follows:

#### Repair, Maintenance and Construction

##### Service Force

Repair Ships and Drydocks (AR; ARD)  
Salvage Ships and Tugs (ARS; ARSD; ATF; AGB)  
Construction Battalions (SEABEES)

##### Other Type Commanders

Tenders (AS; AD; ARG)

##### Shore Establishment

Shipyards and Repair Facilities  
Public Works activities

#### Salvage, Aviation Rescue and Submarine Escape Assist

##### Service Force

Salvage Ships and Tugs (ARS; ARSD; ATF)  
Harbor Clearance Units (ARST; HCU)

##### Submarine Force

Rescue Ships (ASR)

## SS Escape Training Facilities

### Aviation Activities

Crash Boat Crews (AVR)  
Helicopter Rescue Crews

### R and D Services

#### Ships

Oceanographic Survey Ships (AGS; AGB; AGOR)  
Ocean Engineering Ships (ARC; ARS; ARSD; AN; ATF)

Navy Laboratories, Test and Field Stations

Navy and Civilian Divers

### Training

Diving and Damage Control Schools  
SCUBA Schools at Laboratories  
Escape Training and EDU

The offensive tasks are distributed as follows:

#### Amphibious Assault Recon and Preparation

Navy Underwater Demolition Teams (UDT)  
Marine Recon Battalions

#### Mine Clearance

Explosive Ordnance Disposal Units (EODU)  
Mine Hunting/Clearance Ships (MHC; MSC)  
Underwater Demolition Teams (UDT)

#### Underwater Strike Warfare

UDT Elements) From Naval Operational  
                  )  
SEAL Teams ) Support Groups

#### Clandestine Operations

SEAL Teams  
Special Intelligence and Counter Insurgency Ops

The defensive tasks are distributed as follows:

#### Explosive Ordnance Disposal and Rendering Safe

##### Shipboard and Deployed Units

- Ammunition Ships (AE; AOE; AD; AS)
- Carriers and Missile Ships (CVA; CVAN; CLG)
- Minecraft (MHC; MSC)
- Explosive Ordnance Disposal Units (EODU)
- Mobile Harbor Defense Units (MHDU)
- Underwater Demolition Units (UDT)

##### Shore Activities

- Naval Ammunition Depots
- Naval Air Stations

#### Harbor Surveillance and Inspection of Ships Hulls

##### Navy

- Harbor Defense Units (HDU; MHDU)

##### Coast Guard

##### Harbor Security Units

With such a wide spectrum of tasks under the three basic missions, one would expect to find a variety of specialists in Man-in-the-Ocean corps of the Navy. Such is indeed the case. Just as Naval Aviation has pilots who specialize in ASW work; others who are "tail-hook" or carrier pilots; still others who are helicopter pilots; multi-engine logistic pilots, so too in the underwater business. Reviewing the Naval Officer Classifications (NOC) and Naval Enlisted Classifications (NEC) one finds 16 NOC's and 12 NEC's that are related to Navy-Man-in-the-Ocean and which require some degree of diver qualification.

These NOC and NEC are as follows:

##### Officers

NOC	TITLE
0090	Submarine Medical Officer
7215	Diving and Salvage Equipment Engineer
8855	Underwater Photographer
9230; 9231; J-931	Explosive Ordnance Disposal



9293	UDT/SEAL
9294; J-935	UDT
9312	Diving Officer - General
9313; J-927	Diving Officer - Deep Sea HeO <sub>2</sub>
9314; J-928	Diving Officer - Salvage
9375	Ship Salvage Operations Officer
J-903	SCUBA Diver
-----	Marine Recon

#### Enlisted

NEC	TITLE
5321	UDT Swimmer
5322	UDT Swimmer/EOD Technician
5332	EOD Technician
5341	Master Diver
5342	Diver First Class
5343	Diver Second Class
5344	Diver- Salvage (Mobilization only)
5345	SCUBA Diver
8136	Underwater Photographer
8285	Helicopter Rescue Crewman
8492	Hospital Corpsman - UDT/SEAL
8493	Hospital Corpsman - Diving Technician
----	Damage Control Diver - Shallow
----	Marine Recon

In addition to these officer and enlisted Man-in-the-Ocean classifications, there are also at least two civilian diver categories in the Navy -- the diver, general, and the SCUBA diver. Most of the diver scientists and engineers are strictly SCUBA divers, leaving the general diving to non-professional personnel (per-diem employees) such as shipyard "hard hat" divers.

Space does not permit a description of the depth or equipment capabilities of all the NOC/NEC. Note merely that, with the exception of the Damage Control Diver, all are SCUBA qualified. That is to say, open circuit SCUBA qualified. This implies the use of the famous "Aqua-Lung". We should be reminded that this is a specific brand name -- "Aqua-Lung" being to open-circuit SCUBA what "Frigidaire" was to refrigerators. Aside from having other brand names of approved open-circuit SCUBA, we even have a miniature open-circuit apparatus called LUBA -- "Limited Underwater Breathing Apparatus" -- which is used by the Helicopter Rescue Crewmen.

The classification titles which include the word "diver" are all qualified in surface supplied equipment of one type or another and, of course, their diver's depth limitation is a function of the equipment he

is qualified to use. We generally refer to these chaps as "Hard-Hat Divers".

The UDT and EOD divers have all sorts of special diving equipment, which in general can be considered as sophisticated or exotic SCUBA gear. Again, the equipment legislates the depth of operation. Closed circuit SCUBA is a pure oxygen apparatus, used only by UDT and SEAL and has a 33 foot depth limitation. It is silent and bubble-free for clandestine use.

Semi-closed circuit SCUBA is mixed gas apparatus, employed by UDT, SEAL and EOD and can be used to considerable depths. The Mark V and Mark VI units are operational and, in fact, the latter is now coming into use by R and D divers -- specifically in the SEALAB Program. This gear is non-magnetic and can be adjusted to operate relatively noise and bubble-free for short periods of time. These features are especially important to the EOD Technician when on a mine disposal job.

The description of the three basic missions and the variety of tasks performed by Navy-Man-in-the-Ocean will have given an idea of the magnitude of our current underwater capability. There are in the Navy today nearly four-thousand billets calling for the NOC's and NEC's listed above. These billets are not all filled, chiefly because we cannot keep up with the recruiting and training.

It is not generally recognized that this Man-in-the-Ocean corps of the Navy is as extensive as it is. This probably is because the individual Man-in-the-Ocean units are spread so far and wide and because there is no coordinated administration of this arm of the Navy. These 4,000 billets are actual man-underwater billets. Unlike Naval Aviation which counts non-flying ground personnel at Air Stations and onboard carriers as a part of that corps of the Navy, the underwater types have not yet gotten around to being able to include surface support people as a part of Navy-Man-in-the-Ocean.

As an example of the billet strength of Navy-Man-in-the-Ocean, following is a condensed tabulation of allowances in the Pacific area alone, as of a year ago:

	Officers	Enlisted	Note
NAVAIRPAC	16	140	
CRUDESAPAC	12	44	
SUBPAC	33	211	J-903 not included
PHIBPAC	35	288	Includes PHIBTRAPAC
MINPAC	18	46	
SERVPAC	70	264	
FMFPAC	15	94	
Area Commands	8	36	Japan/Phil/Marianas
Districts	<u>24</u>	<u>156</u>	COM 11 thru 17
TOTAL	231	1,279	
GRAND TOTAL		1,510	

While this Man-in-the-Ocean corps of the Navy does place requirements on the Military Oceanographic community, and is, therefore, a customer of that community, these underwater men must also be considered to be partners in the business of Military Oceanography. This partnership is particularly evident in the logistic and service mission. On the other hand, in the defensive and offensive missions, the Men-in-the-Ocean are chiefly customers to the techniques and accumulated data of Military Oceanography.

One further analogy must be drawn between the Navy underwater corps and Naval Aviation. That is to point out that our Man-in-the-Sea Program is to us what the Space Program -- "Man-on-the-Moon" Program -- was at its outset to the aviation people. Now whether or not the Man-in-the-Sea Program evolves into a NASA-like Ocean Sciences Office remains to be seen. Whether it does or not the comment of the eminent British biologist and entomologist, Sir Julian Huxley, is pertinent. He was the principal speaker at the 100th Anniversary celebration of Harvard's Agassiz Museum of Natural Science. It was in 1959, shortly after SPUTNIK. It was the period of awakening and intense and excited interest in space. After giving due attention to space and to the possible interest of biologists, entomologists, and the like in what might be found on the moon, Sir Julian very tersely got back to earth by saying -- British accent, portly professor, pince-nez glasses and all --

"...and frankly, I should much rather see the sea's bottom than the moon's behind."



OCEANOGRAPHY EDUCATION AT THE  
UNITED STATES NAVAL POSTGRADUATE SCHOOL

by

Glenn H. Jung

U. S. Naval Postgraduate School  
Monterey, California



OCEANOGRAPHY EDUCATION AT THE  
UNITED STATES NAVAL POSTGRADUATE SCHOOL

by

Glenn H. Jung  
U. S. Naval Postgraduate School, Monterey, Calif.

Oceanography was introduced at the United States Naval Postgraduate School beginning in 1946 by Professor George Haltiner who introduced courses in ocean waves and shallow water oceanography. The first professional oceanographer to join the faculty was Professor J. B. Wickham in 1951. A limited number of oceanography courses were introduced at this time as a minor field of interest for meteorology students being educated to man the Naval Weather Service billets for the Fleet. The number of courses offered in oceanography expanded somewhat with the arrival of Professor Warren C. Thompson in 1953. Professor Glenn H. Jung joined the faculty in 1958 to complete the faculty in oceanography during phase I of the development reported here, which occupies the period from 1946-1961. Each of these faculty members had practical experience as service weather forecasters during World War II.

In this interval of time, courses had been developed to include: Introduction to Oceanography; Physical Oceanography; Shallow Water Oceanography; Waves Forecasting (including laboratory); Oceanographic Factors Affecting Underwater Sound; Sea Ice Forecasting (including laboratory); and Oceanographic Factors Affecting Underwater Sound II, which included thermal structure forecasting and a laboratory. The three courses for which laboratory portions are indicated were developed in response to particular sponsor requirements. By 1956, the Secretary of the Navy had instructed the Naval Weather Service to be prepared to furnish forecasts in those three indicated areas which are not normally covered in meteorological education. As a result of these directives, the courses developed in the fields of wave forecasting, sea ice forecasting, and thermal structure forecasting appear to be unique in their laboratory applications to particular Navy interests. I will return to these courses again in a later section of this paper.

The length of the educational programs for the Naval Weather Officer in the then Department of Aerological Engineering varied from one to two years. Certificates of Completion, Bachelor of Science and Master of Science Degrees were awarded during this period to student officers varying in number from 28 in 1951 to 43 in 1961. Each officer had some education in oceanography with students after 1958 having seven oceanography courses as a part of their curricular program.



In 1961 the curricular programs which most concerned Meteorology and Oceanography Department faculty included one which terminated in a Bachelor's Degree in Meteorology and a second one which terminated in a Master's Degree in Meteorology; both curricular programs extended over a two-year period. Officer students entering each program need to have a minimum of two years of college, ordinarily, which includes physics and mathematics. Almost all entering students have Bachelor's Degrees now. Graduates of either program are able to fill Naval Weather Service billets.

In 1962, the next phase in development of oceanography education was initiated with the introduction of a new curriculum in the school, entitled Air-Ocean Environment. This was done at the request of the Naval Oceanographic Office in order to provide officers especially trained for staffing billets within the developing ASWEPS program during its operational test and afterward. The curriculum was visualized as essentially half oceanography and half meteorology courses, initially. The Naval Weather Service imposed a later requirement that these officers, too, must possess the capability of manning a meteorology billet within the Naval Weather Service with a resulting decrease in the ratio of oceanography courses to meteorology courses. This curriculum leads to a Master of Science Degree in Environmental Science.

Concurrently, the Bachelor's level meteorology curriculum was modified to include additional oceanography courses and it was redesignated as a Bachelor's level Air-Ocean Environment curriculum.

The first student officer graduates from these two Air-Ocean Environment curricula numbered 25 in 1964; the graduates in 1965 will number 39 officers and 22 additional officers should be graduated in 1966. Present plans call for the 1966 graduates to include the final output from the Master's Degree curriculum in Air-Ocean Environment. These numbers do not include graduates from the Meteorology Master's Degree curriculum which has continued its oceanography minor program throughout this period.

Certain more or less external administrative factors were instrumental in determining the final design for the Air-Ocean Environment curricula established in 1962. These administrative factors included: (a) a substantial student input to the Master's Degree curriculum was visualized for only a short period, i.e., two years; (b) a very short time interval elapsed between proposal of the curriculum and its implementation; students were selected for the curriculum only a few weeks (about six) after initial requests were received for its establishment; students were on board for the program less than one year after initial correspondence was received at the U. S. Naval Postgraduate School; (c) there was a curious inability at this particular time for the U. S. Naval Postgraduate School to acquire additional oceanography faculty members to shoulder the substantial increase in oceanography teaching load imposed by the new curriculum.

The new curriculum was designed to provide a minimum of readjustment from then existing schedules, accordingly. Meteorology courses were followed in much the same pattern as for the two Meteorology curricula, with most oceanography courses scheduled primarily for the second year of the new program; this was not ideal in arrangement, but provided essential transition time for the limited faculty to produce the new courses entailed in the curriculum.

A military oceanography billet was established for our department during this period, capably filled by CDR Richard M. Haupt from 1962 to the present time.

Also during this period, there were increased requirements to provide oceanography courses for non-Environmental Sciences curricula at the Naval Postgraduate School. As a result, nine sections of the introductory course in oceanography were taught during 1963-64, which included 276 officer students. Of these, only 56 officers were Environmental Sciences curricular students in three sections. These sections ranged in size from eight to 41 officers.

The third phase in the development of oceanography in our Department began in 1964 and continues through the present. At this time a curriculum leading to a Master's Degree in Physical Oceanography was established. The initial student input of ten officers has been depleted by one, since he has been selected for the Navy Ph.D. Program to study oceanography at Massachusetts Institute of Technology beginning this autumn.

In August, 1964, two professors were added to our Oceanography faculty, Professors Warren W. Denner and Victor T. Neal.

Courses added especially for the Oceanography curriculum include introductory courses in geological, biological, and chemical oceanography; additional courses in dynamical oceanography, in waves theory, tides, descriptive oceanography, and in geophysics; there are courses in oceanographic observations and instrumentation, and in field experience which were added in 1962 as well, in addition to the oceanography courses taught to all curricula in Environmental Sciences. The field courses are materially aided by acquisition of a 65-foot boat, especially equipped for oceanographic work, during the second phase of our development.

The Oceanography faculty staffing situation has improved further. Two professors have been recruited to join our faculty during the coming year. However, Professor Thompson is going on leave during this period, and CDR Haupt is being transferred. The military oceanography billet he vacates remains unfilled for the coming year as of this date. His duties will be assumed in part by a meteorology instructor who has partially completed a program for a Master's Degree in Oceanography. The Navy appears to have

more urgent needs elsewhere for their few officers educated through the small oceanography program of the immediate past.

The three courses mentioned earlier pertaining to ocean waves forecasting, sea ice forecasting, and oceanographic forecasting demonstrate two aspects of the capabilities of the U. S. Naval Postgraduate School as reflected by our Department of Meteorology and Oceanography: 1) to respond quickly to particular Navy requirements and 2) to undertake the development of courses in new and essentially untried fields; the latter aspect depends heavily on current research, often contributed by various Navy agencies and often aided by our own research efforts.

The Ocean Waves Forecasting course differs from conventional courses offered in several of the civilian oceanography departments of the United States in that laboratory exercises have been developed to give the student officer experience in application of the various principles described in the lectures; the final and major problem of the term involves working with actual weather charts over a period of several days in the North Pacific Ocean to prepare wave forecasts for nearby Point Sur, California. Wave records measured in the nearshore region at Point Sur have been obtained for the same period and have been analyzed with great care for use in verification.

The Sea Ice Forecasting course, after reviewing the latest Russian and United States developments, again goes to laboratory exercises to give practical experience in preparing sea ice forecasts. Two recent Master's theses have dealt with improvement and computerizing the ice forecasting models now in use.

The Oceanographic Forecasting course reviews current research on ocean thermal structure as related to other oceanographic and weather parameters, and attempts to evaluate the various forecasting methods through laboratory exercises. The current state of this art is explained and areas of needed research are pointed out. The course includes examples of using oceanographic charts in preparing sonar range charts for tactical use and reviews these various applications. Several Master's theses have dealt with empirical forecasting equations and with model studies to evaluate the relative importance of various air-sea interaction processes in determining upper ocean thermal structure.

#### SUMMARY

The Department of Meteorology and Oceanography at the United States Naval Postgraduate School includes a capable and experienced group teaching oceanography with a view toward particular Navy needs. The present capability is in physical oceanography, but new faculty members possess capabilities in the biological and engineering aspects of oceanography and it is expected that a widening scope of oceanography aspects will be included



in Departmental course offerings in the future. At present, there are programs which include educational minor support for the Meteorology majors who will staff the Naval Weather Service; there are also a major program in Physical Oceanography, a special program in Air-Ocean Environment, and introductory courses for general education purposes for Naval officers with a wide spectrum of particular interests. Certain of the courses offered appear to be unique in the educational world such as the sea ice forecasting laboratory, waves forecasting laboratory, and oceanographic forecasting laboratory. Research in areas of improvement of these techniques is encouraged for students and faculty in the Department.



ANALYTICAL PREDICTION OF OCEANOGRAPHIC INFLUENCES  
ON BOTTOM-REFLECTED SOUND

by

Rodney O. Davidson

Vitro Laboratories

Division of Vitro Corporation of America  
West Orange, New Jersey





ANALYTICAL PREDICTION OF OCEANOGRAPHIC INFLUENCES  
ON BOTTOM-REFLECTED SOUND \*

by

Rodney O. Davidson  
Vitro Laboratories  
Division of Vitro Corporation of America  
200 Pleasant Valley Way, West Orange, New Jersey

INTRODUCTION

This paper presents a technique for predicting selected acoustic parameters of a bottom-reflected sound field as a function of sonar range. The technique is applicable under a wide spectrum of environmental and tactical situations. It has the advantage that it obviates the need for case-by-case sound ray computations and thus provides a means for tactical decision-making without the use of elaborate computational schemes. The acoustic parameters to be considered are: (1) slant range; (2) travel time; (3) source or depression angle; (4) receiver angle; (5) bottom grazing angle; (6) geometrical spreading loss; (7) absorption loss.

Assumptions

In order for the technique to be applicable in a given situation the following assumptions are made:

- (1) The ocean bottom and surface are horizontal planes;
- (2) The maximum sound velocity in the medium occurs at the ocean bottom;
- (3) The distribution of sound velocity is cylindrically symmetric about an axis perpendicular to the surface through the source;
- (4) The sound source and receiver depths are fixed;
- (5) Ray theory is an adequate description of sound transmission in the ocean;
- (6) The values of sonar range must correspond to source angles between zero and  $42^\circ$ ; sonar ranges not covered by this interval can be adequately treated by assuming that no refraction of the sound rays takes place.

---

\* Research sponsored by the US Navy Underwater Sound Laboratory under Contract N140(70024)76683B whose Technical Director has been Mr. Thaddeus G. Bell. Mr. Carl T. Moore, US Naval Oceanographic Office, assisted this research by supplying valuable environmental data.

A few comments about the scope of the technique and the assumptions are in order. First, the set of acoustic parameters can be enlarged. That is, the technique is sufficiently basic to be used as a tool in the investigation of more extensive and more difficult problems. Secondly, the set of assumptions can be reduced. In particular, source and receiver depth can be varied. This has not been done in the present paper because it does not contribute to an understanding of the basic techniques. Thirdly, bottom-limited profiles (that is, profiles with a maximum velocity in the surface layers) can also be included if a small portion of the sound field is eliminated from the prediction system. This is a special case which will not be treated in this paper.

#### PROBLEM DEFINITION

The establishment of a prediction system that will perform the tasks just described must deal with the following three general problem areas:

- (1) Characterization and description of the state of the environment-both spatially and temporally
- (2) Performance of the computations to obtain the set of acoustic parameters which describe the sound fields
- (3) Display, presentation, and indexing of the output of the prediction system.

The technique presented below addresses itself to each of these problem areas.

The first task is to answer the following question: Given (1) The value of sonar range, say  $H_k$ , and (2) A variation in the sound velocity profile, say from  $P_1$  to  $P_2$  in Figure 1, which describes the total variation in the sound velocity structure through which the rays must pass, then what are the extreme values of the acoustic parameters that can occur at the range  $H_k$ ?

#### DESCRIPTION OF TECHNIQUE

In Figure 1 the shaded region between the two profiles depicts the region through which  $P_1$  must pass to assume the position of  $P_2$ . Corresponding to this variation in the profile is the variation of the sound rays, shown on the right in Figure 1 as a shaded region in a vertical cross-section of the ocean. Assuming, for the moment, that we know these extreme values, it is observed that if the difference between the extreme values of the acoustic parameters is sufficiently small, then the average of these extreme values is a prediction with which is associated a known possible error. This error is the difference between the average value and either of the two extreme values. This error is also dependent on the size of the ocean area in which the prediction is to be valid. Therefore, the ability to specify the region in which the prediction is valid will provide some control over the magnitude of these errors.



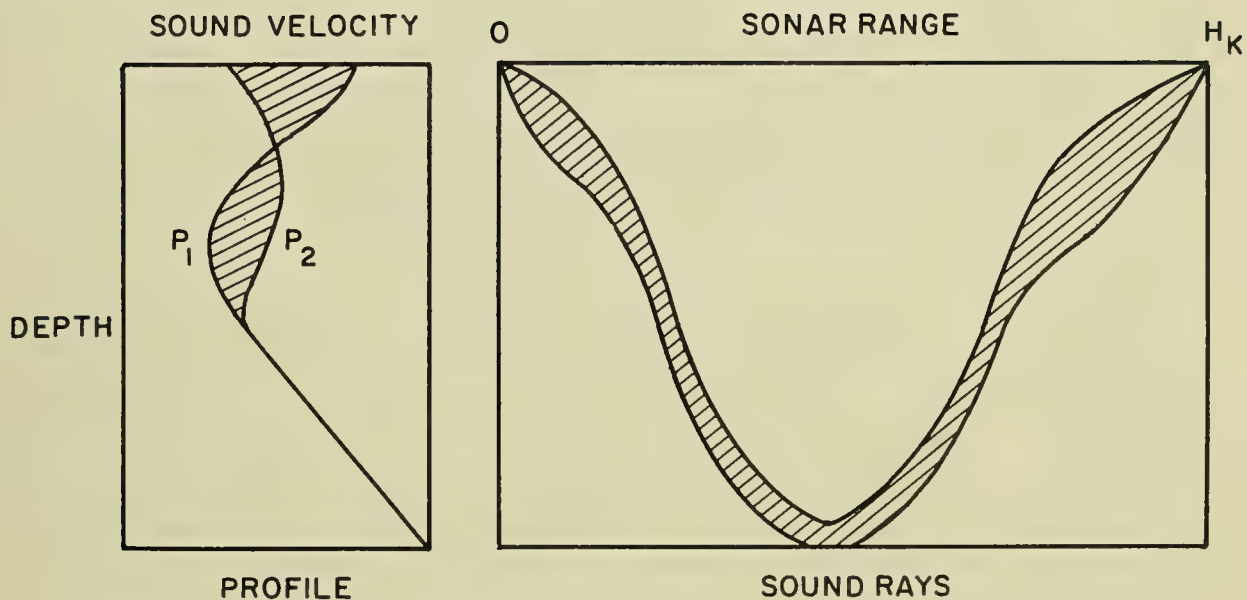


FIGURE 1 VARIATION OF ENVIRONMENT AND ASSOCIATED SOUND RAYS TO  $H_k$

It is also observed that the variation in the profile in Figure 1 need not take place at a single location, but may take place anywhere in the vertical cross-section of the ocean between the source and the range value  $H_k$ . We are, therefore, including in this hypothesis the influence of horizontal gradients. The horizontal gradients being introduced are the radial gradients about the axis which passes through the source and is perpendicular to the surface. The distribution of sound velocity is then cylindrically symmetric about this axis.

### Variation of Profiles

The variation in the profile from  $P_1$  to  $P_2$  in Figure 1 generates an infinite set of sound velocity profiles all contained in the shaded region. To each of these profiles corresponds a ray in the shaded region on the right of Figure 1, which extends to the range  $H_k$ . Each of these rays has associated with it a value of Snell's Constant. It is observed then, that by holding the range fixed, we have established a correspondence between the sound velocity profiles and the value of Snell's Constant. Although little can be said about the general aspects of this correspondence, enough specific information can be obtained to determine the extreme values of the acoustic parameters.

The difficulty in attempting to describe a sound velocity profile arises because the profile is, in a sense, infinitely dimensional. That is, an infinite set of values of sound velocity can occur at an infinite number of depth points. However, this paper is concerned with a description of the environment so as to attain the extreme values of the acoustic parameters. That is, our description of the environment does not have to be specific for the intermediate values of the acoustic parameters. This simplifies the first of the above three problem areas with which the evolution of a prediction system must cope.

### Environmental Inputs

The next task is to determine the state of the environment which gives rise to the extreme values of the acoustic parameters. This state turns out to be the extreme sound-velocity profiles that can exist in a given region. In addition to the two extreme profiles we must also know the depths of the source, receiver, and ocean bottom, and, in addition, the velocity of sound at the source.

This description of the environment has several operational implications. The extreme profiles can be accurately established from historical data. In that case, the extreme profiles are valid over a large oceanographic area, and, in most cases, are valid for the entire year. It is therefore unnecessary to measure the sound velocity profile during Fleet operations. A determination of the source and bottom depths can be easily made. The same is true of the sound velocity at the source. It is emphasized that the entire scope of this paper is restricted to bottom-reflected sound in water, sufficiently deep, to eliminate bottom-limited profiles.

The extreme values of the sound velocity profile can be obtained by constructing the envelope of the profiles existing in a given area. A determination of these envelopes has been commenced by the US Naval Oceanographic Office. The results are contained in NavOceanO Technical Report No. TR-171, "An Interim Report on the Sound Velocity Distribution in the North Atlantic Ocean", March 1965.

Using this report we have constructed the six regions, or oceanographic provinces, shown in Figure 2. (The original report contained a finer subdivision of the provinces for each of four seasons.) The shaded areas represent transition zones that change from season to season. Each of the six regions in Figure 2 has associated with it an envelope of the sound-velocity profiles existing in that region. This partitioning of the North Atlantic Ocean is of course an interim result. Additional data is needed in many areas. This additional data would very likely alter the presentation in Figure 2. The modification, however, could only be expected to delineate the zones more accurately. The size of the zones, and their general location are, it is felt, well established by the above-mentioned NavOceanO report.

In Figure 3 there are two sound velocity profiles labeled  $P_1$  and  $P_2'$  which are indicated by heavy black lines. These two profiles were constructed by taking the envelope of all profiles measured in Zone 2 (Fig 2), i.e. the North American Basin. These two sound velocity profiles represent in essence the extreme conditions which the environment can assume in Zone 2.

It will later be shown that the errors associated with the predictions increase as the envelope increases. An improvement in the prediction of the sound velocity envelope at any given moment can be made through a better knowledge of the behavior of water masses. Thus, for instance, it is known that large positive gradients tend to be unstable. This instability is also a function of depth. Studies performed by Vitro Laboratories in conjunction with the ASWEPS program indicated that an upper bound to the positive gradients existing in the first 100 feet of Zone 2 is 0.04 ft/sec/ft. An upper bound to positive gradients existing below 100 feet in this area was found to be 0.0175 ft/sec/ft. This information, in conjunction with the known value of surface velocity, permits a sound velocity profile to be constructed that intersects the value of sound velocity at the surface and the profile  $P_2'$  (Fig 3). The profile  $P_2$  which borders the shaded region on the right and the profile  $P_1$  can now be used as the environmental inputs to the computations.

#### Variation of Acoustic Parameters

A schematic depiction of the variation in the acoustic parameters at a fixed value of sonar range are shown in Figure 4(b) through 4(f). Figure 4(a) shows a graph of normalized range  $\mu_k$  versus a normalized Snell's index,  $\nu$ . The values of slant range,  $s$ , and travel time,  $t$ , are also normalized.



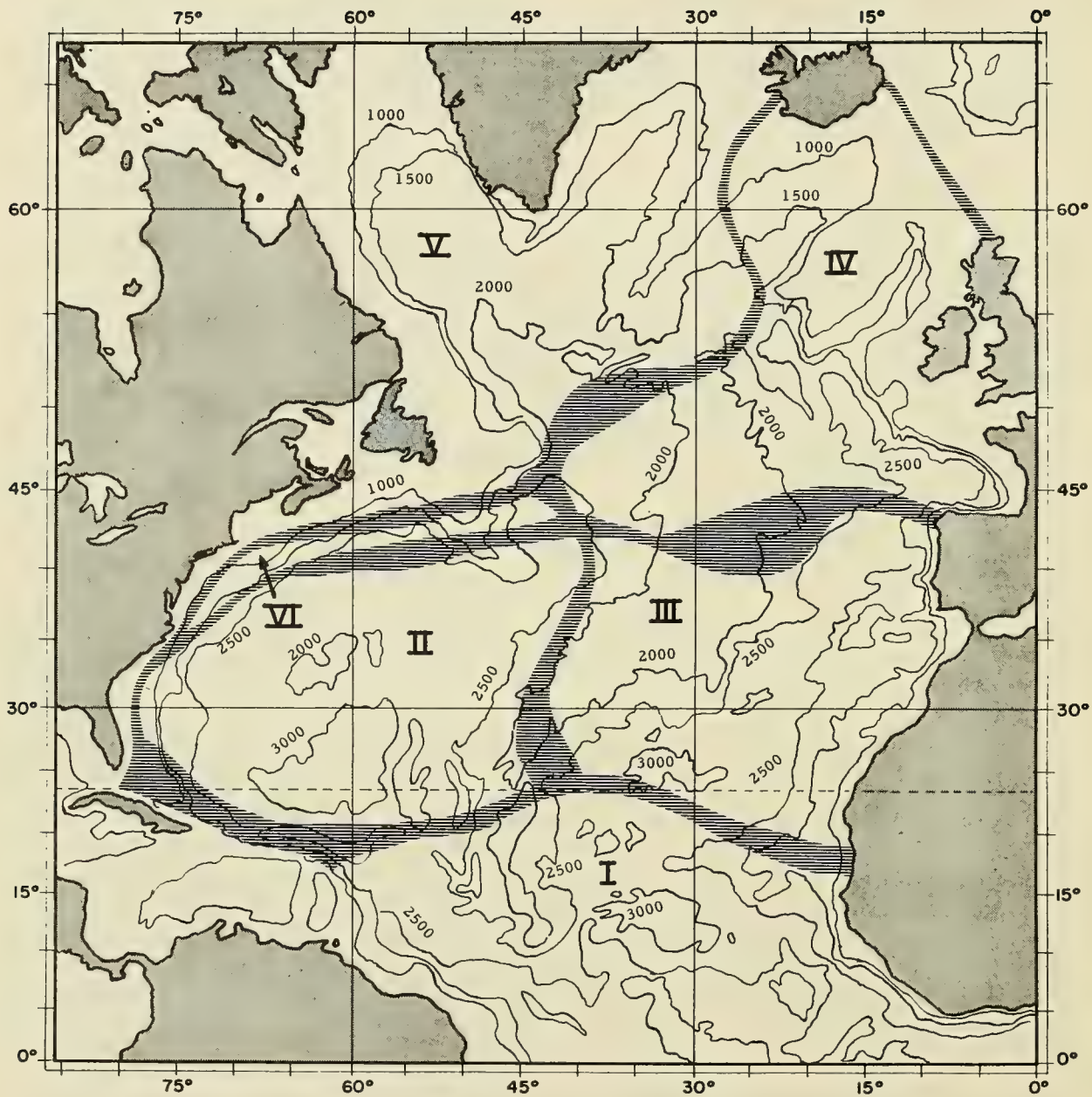


FIGURE 2 PARTITIONING OF NORTH ATLANTIC OCEAN



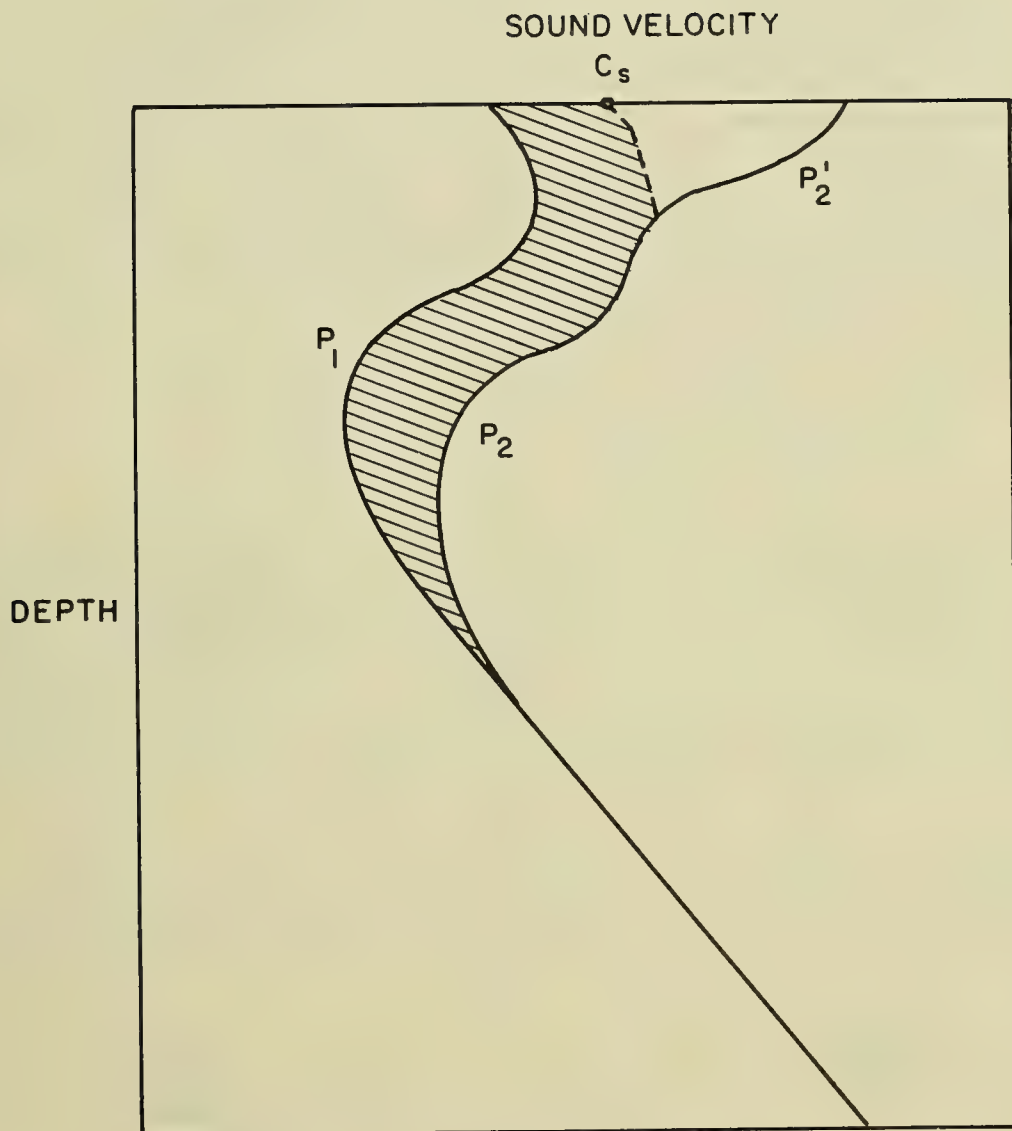


FIGURE 3 MINIMUM AND MAXIMUM PROFILES IN  
NORTH AMERICAN BASIN (ZONE 2)

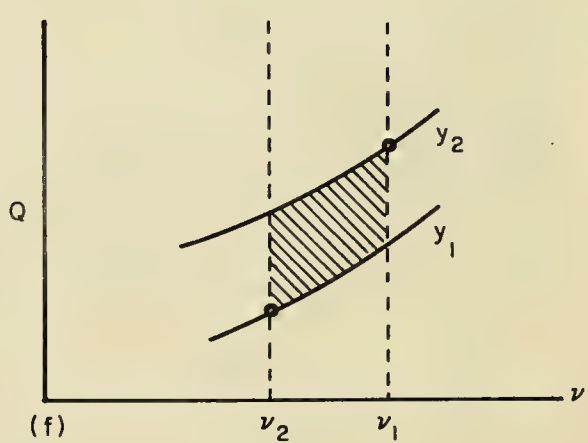
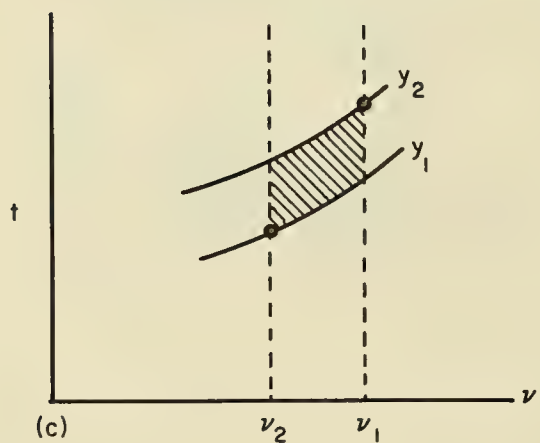
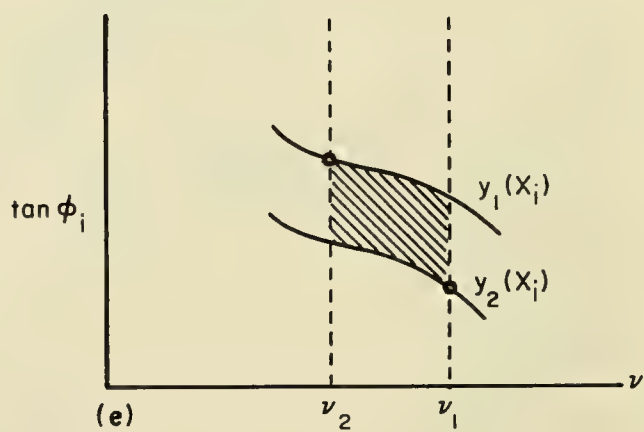
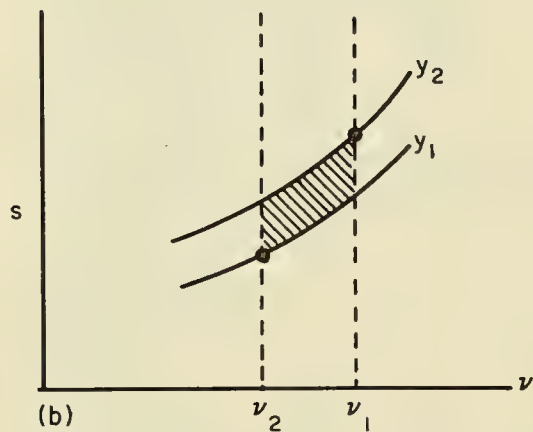
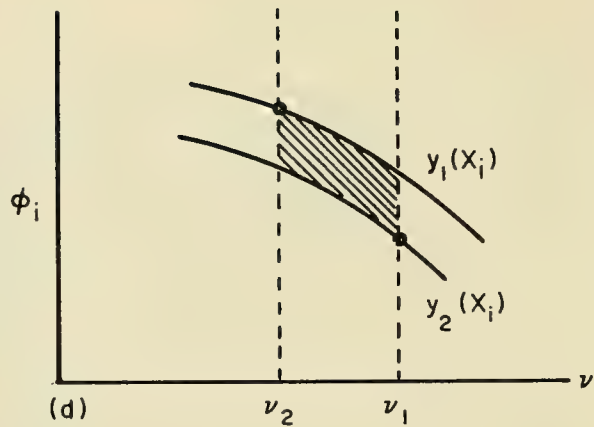
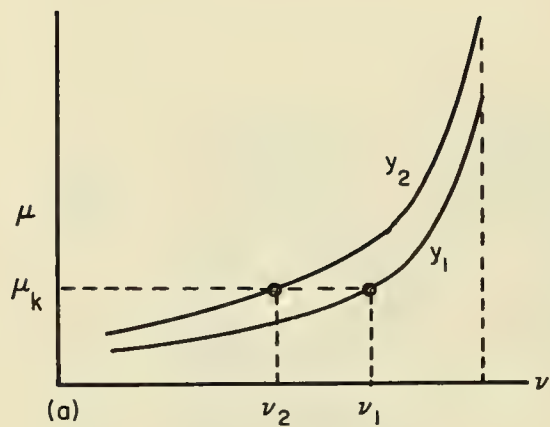


FIGURE 4 VARIATION OF ACOUSTIC PARAMETERS AT  $\mu_k$

The symbols  $y_1$  and  $y_2$  represent the normalized minimum and maximum sound-velocity profiles, respectively. In Figure 4(f), the factor  $Q$ , which is also normalized is a complex term that represents, in part, the derivative of sonar range with respect to source angle. The  $\phi_i$  and  $\tan\phi_i$  parameters in Figure 4(d) and 4(e) are valid for any  $i$ th point in the sound velocity profile. The geometrical spreading loss is computed as the product of terms involving  $\tan\phi_i$ ,  $Q$ , a simple ratio of sound velocities, and a constant. In each graph of Figure 4 the curves denoted by  $y_1$  and  $y_2$  can be computed with standard ray theory techniques.

Three observations concerning Figure 4 can be rigorously proven:

- (1) Any profile between  $P_1$  and  $P_2$  in Figure 3 will generate a  $\mu$  versus  $\nu$  curve between  $y_1$  and  $y_2$  in Figure 4(a);
- (2) Every curve in Figure 4 is either monotonically increasing or decreasing.
- (3) The values of the acoustic parameters in Figure 4(b) through 4(f) must lie between the  $y_1$  and  $y_2$  curves.

These three observations will now be used to compute the extreme values of each acoustic-parameter. In Figure 4(a) the sonar range (normalized) is held fixed at  $\mu_k$ . Corresponding to  $\mu_k$  is an interval of  $\nu$  values (Snell's index) between  $\nu_2$  and  $\nu_1$ . This interval of  $\nu$  values contains every  $\nu$  that can possibly produce the sonar range  $\mu_k$ , when the profile varies from  $P_1$  to  $P_2$ , as in Figure 3. This interval of  $\nu$  values can now be used in conjunction with the curves in the remaining graphs to delineate the shaded regions in Figure 4(b) through 4(f).

The extreme values of each parameter can now be computed by combining the profile and the  $\nu$  value that corresponds to the upper and lower corners of the shaded regions. The extreme values of the acoustic parameters not explicitly depicted in Figure 4 can be easily obtained from the above computations.

#### FEATURES OF THE NEW TECHNIQUE

The technique just described for predicting the bottom-reflected sound field has the following essential features.

- (1) No computations need be performed by the user of the prediction system.
- (2) All quantities can be indexed by area, bottom depth, and sound velocity at the source. Historical data corresponding to the oceanographic province, and the remaining two indices can easily be determined during operations. It is estimated that one volume can be used to graphically depict the acoustic parameters associated with regions as large, or larger, than the North American Basin.

- (3) The accuracy of the prediction system should be adequate for operational purposes. Supporting computations will be made in the near future as part of the continuing research. It has been ascertained, however, that all depression angles in the North American Basin where the technique is applicable, can be predicted with a maximum error of approximately one half degree. This small error suggests that the remaining parameters can also be adequately predicted.

A final comment about the theoretical significance of this effort is in order. A method often used in approaching the problems discussed here, is to analyze statistically, the distribution of the sound-velocity profiles, and then the corresponding distribution of the computed acoustic parameters. It is currently felt that the errors associated with the techniques just outlined, will, in many cases, eliminate the need and the uncertainties of the statistical approach.



DEEP RECTILINEAR TOWING WITH PARALLEL TUBES

by

Norman W. Lord

Hudson Laboratories of Columbia University  
Dobbs Ferry, New York



# DEEP RECTILINEAR TOWING WITH PARALLEL TUBES\*†

by

Norman W. Lord  
Hudson Laboratories of Columbia University  
Dobbs Ferry, New York

## ORIGINS

Our need for a device which would tow an object in a straight line while suspended at great depths arose out of sound velocimeter studies we started about four years ago.

In deep water we had encountered unexpected variations in sound velocity recorded on a meter that was merely suspended from an anchored ship as shown in Figure 1. The so-called patch represents a small region the water-space, where the sound velocity is either greater or smaller than in the surrounding region. This is not a general representation for we can also have spatial distributions of sound velocity whose topology would not admit such a region. This would be the case of internal waves as opposed to the picture here which would commonly arise from turbulent mixing. However, considering the time-scale of recorded variations on the meter, it is highly unlikely that they arise by anything other than some kind of spatial distribution sweeping past it rather than by an internally generated time variation. Swinging on such a suspended cable the meter easily acquires undetermined velocities of a meter per second and this is superposed upon unknown deep water currents that are generally below half a meter per second. Obviously we have little hope of finding the basic spatial variation from the record of the meter which would normally be taken with respect to time. On these experiments we could make a decent guess as to the statistics of the variation but the uncertainty almost equals the magnitude of the parameter, not a rare state of affairs in marine experiments.

\* Hudson Laboratories of Columbia University Contribution No. 224.

† This work was supported by the Office of Naval Research under Contract Nonr-266(84).

In most underwater acoustic and oceanographic measurements we are faced with just such an uncomfortable area of ignorance concerning the stability and precise location of deeply suspended instruments. To impose the ideal laboratory frame of reference with fixed and known positions upon a remote deep-sea environment is almost always impossible. However, when we recognize that the deep sea is perpetually in motion with respect to the earth, we see that in most experiments other than seismological it would be rare to require a fixed placement or even the knowledge of absolute placement for deeply suspended instruments. In fact we would know more about the physical situation if we imposed a known movement that was much larger than unknown and varying sea motion. If we can achieve truly rectilinear movement and measure it using sensitive radio navigation such as Loran C, then in the observational variations recorded by the deep instruments we can account for it and know precisely what the influences of the sea itself have been.

#### TOWING DYNAMICS AND PRINCIPLES OF THE PARALLEL TUBE DEVICE

Consider the problem of towing in a straight line in terms of the perturbations in tow path introduced by the rocking motion of the ship. This situation is depicted in Figure 2. A key element that simplifies the complexities of this problem is due to John Ess of our laboratory who made the following observation while towing a few tons at the end of a cable about 7000 ft long. Tracking closely an extremely sensitive depth gage, he was able to observe a strong correlation between small movements imparted by rotating the winch and small depth changes in the load at the end of the cable. Within seconds, hauling in 3 or 4 ft of cable would be reflected in a 3 or 4 ft decrease in depth. It was clearly as if the shape of the catenary in the cable were essentially invariant over the order of at least 10 seconds. This is not so unreasonable when we consider the spaces involved and the enormity of the drag forces on the long cable which could easily act like a giant sheave.

Starting from this point we can relate a change in height  $\Delta$ , imparted by the ship at the suspension point, to a change in depth  $Y$  of the suspended object. The angle  $\phi$  will be constant for all  $Y$  greater than a thousand feet since it is determined almost entirely by the ratio of horizontal drag force on the object to its weight. As long as the deep currents are small, this drag force will be determined solely by the towing speed. The ship motion is then resolved into components perpendicular to and along the suspension cable. In what follows we have to compare the merits of towing between using a dead weight and using parallel tubes. To be fair, the advantage gained with small  $\theta$  is cancelled out, using the rather crude approximation  $y/1$  for  $\sin \theta$ .

The idea of a possible advantage in using, instead of dead weight, some system that traps a large water mass is shown in Figure 3. To damp a motion imparted at the surface on a cable which retains its shape requires that the tension suspending the weight below vary so as to allow the elas-



ticity of the cable to accommodate a difference between ship-imparted motion as shown in Figure 2 and depth variation of the weight. For a dead weight the steady tension always equals the instantaneous tension except for a resonating periodicity in the ship motion. If we now add a pair of light-weight tubes which temporarily entrap a water mass of say double the dead weight attached, we have the possibility of instantaneous tensions as great as 3 times the steady tension and probably as low as  $1/3$  the steady tension upon release of the upward pull. Naturally the same possible resonating periodicity exists, and I would imagine that these cases should be treated separately. However, for nonresonant conditions we clearly have the possibility of damped vertical motion for the parallel tubes. For the sake of easy recollection we can calculate casually that the ship-imparted motion may be cancelled by as much as the cable strain difference due to an excess as deficiency of tension equal to  $W \sec \theta$ .

## DESCRIPTION OF DEVICE AND ITS TEST IN A MODEL BASIN

A device which follows the foregoing principles and, as a natural concomitant, rigidly constrains the orientation of any arrangement of sensors mounted upon it is shown in Figure 4.

To fix the plane of the tubes horizontally, most of the dead weight was mounted on a rigid extension about 3 ft below the suspension point providing a restorative couple that keeps the tubes horizontal. The vertical vane well behind the centroid constrains the tubes to align with the towing direction. A small nearly horizontal vane can be adjusted so that even over a speed range of several knots the unit does not tilt downward or upward but keeps the tube axes in the horizontal plane.

During tests run in a model basin and in subsequent deep water sound velocity surveys, two sound velocimeters are mounted at the front end of the device. Since the meter designated Lockheed uses an unfolded path, it could be oriented in such a way that, in addition to the sound velocity as a function of path position, readings of the two meters give the rate at which water sweeps by the meters. To calibrate this effect and also adjust the horizontal vane for speed range up to 3 knots, the complete unit was tested in January 1964 at the David Taylor Model Basin. Figure 5 shows the general features of the tank used in the test. The whole tank is about 2600 ft long and the positions are marked every 30 ft running from west to east. Carriage 5 operates on the eastern half of the southern side of the tank which is divided at the 1100-ft mark by a wave-making machine.

For active towing we used the length between 1500 ft and 2400 ft. The overhead cranes can service the carriage only at the eastern end past the 2600-ft marker; therefore all runs had to start and end there. Our towed vehicle is 10 ft long and was suspended at an interior part of the carriage from one of its overhead tubular joists. Because of the turnaround required at the unserved end of the tank one probably cannot test a towing device that is longer than 20 ft.

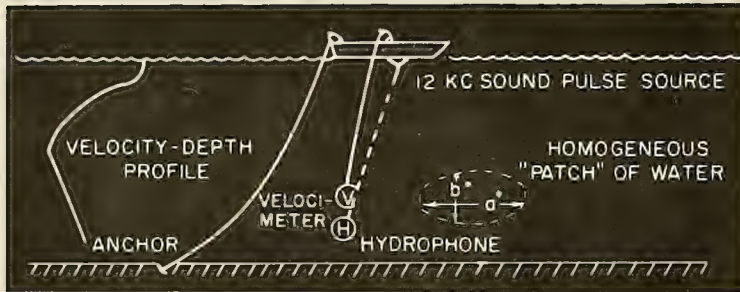


FIG 1 SOUND VELOCITY MEASUREMENT WITH A SUSPENDED METER

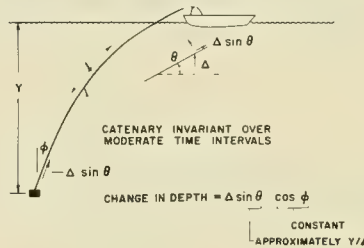


FIG 2 DYNAMICS OF DEPTH CHARGES IN A WEIGHT ON A LONG CABLE

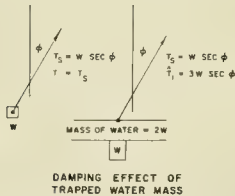


FIG 3 DAMPING EFFECT OF WATER MASS

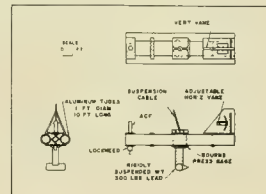


FIG 4 PARALLEL TUBE TOWING DEVICE

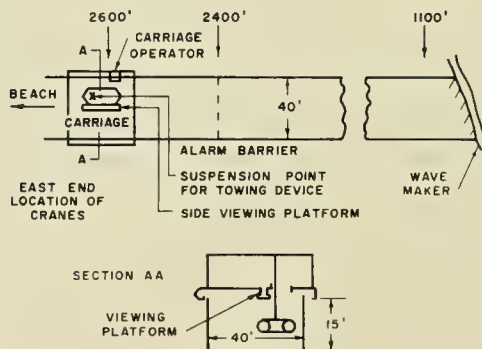


FIG 5 TEST IN MODEL BASIN

Initial runs were made solely to adjust the vane. Lying down on the carriage I was able to see the towing condition and slope of the tubes at all of the speeds. From the front end of the carriage I could watch how the azimuthal orientation was controlled by the vertical vane. Even the lowest speed of 0.50 knot was enough to turn the tubes in the proper direction. Once aligned there was no discernible change or oscillation in the azimuthal angle. The vertical declination of the tubes was observed visually from a low platform that was only an inch above the water. I sat on it and kept my line of sight to the tow point on the tubes perpendicular to the path. The tubes hanging from a cable 15 ft long were about 8 ft below the surface, and I was sitting about 5 ft to the side of the tow path. Because the line of sight is then at a glancing angle into water, the tubes appear curved upward at their ends. Adjusting the view as I did makes the upward end curves symmetrical when the tubes are horizontal. The best procedure is to observe the change that occurs with speed. At 0.50 knot or less, because of the careful balance of the tubes, they always appear horizontal. With the adjustment vane perfectly horizontal the tubes turned downward at 2 knots, and this declination was much more marked at 3 knots. The angle needed for the vane proved to be extremely sensitive in its influence on tube elevation in the speed range 2 to 3 knots. A final adjustment had the tubes moving down a few degrees between 2 and 3 knots with level flight at 2. For the presently contemplated use this is probably safest since any upward angle tends to be accentuated. The drag on the stabilizing weight and strut is reduced and a lift seems to work on the tubes themselves.

Such extremely well-mannered behavior for a towing device made it possible to calibrate the velocimeter assembly in terms of speeds that could in the final analysis be set and measured to 0.02 knot or about 1 centimeter/sec (Lord [1964]).

## TESTS AT SEA FOR TOWED VELOCIMETER SURVEYS

The device was used at sea for the first time in March 1964 and it is possible to compare depth fluctuation data on these runs with those obtained on an earlier test which used only a dead weight to hold down a single velocimeter. This was done in July 1962 at a series of four latitudes ranging north of the island of Bonaire in the Caribbean. The parallel tube work was done at 3 locations, west of the Windward Island chain, east of the same chain, and finally southwest of Bermuda. Naturally the choice of these locations was relevant to our study of sound velocity variation, not to towing characteristics. However, weather plays such a large role in these matters that we can use the depth records accumulated as if all possible variations in towing characteristics were covered with equal comprehension in the two sets of runs.

Towing depth fluctuations were assessed by calculating them as deviations from a moving average. In all runs the towing speed was around 2 knots or 1 meter/sec and a moving average embracing around 210 meters or  $3\frac{1}{2}$  minutes of towing was calculated for most of the run. The instantaneous depth readings then depart from this as shown in the three typical



examples of Figure 6. Each of the tow paths shown is 1000 meters long with a similarly exaggerated vertical scale. Dead weight towing is shown in Figure 6a as it was experienced with the ship steaming eastward against steady winds and currents, with 1006 meters of suspended cable. Parallel tube towing as experienced in the Grenada Trough on a westward drift is shown in the next figures. Over 1200 meters of cable are suspended in the case of Figure 6b and over 1500 meters of cable in that of Figure 6c. As you can see the scope, or ratio between depth and cable length, is lower in the parallel tube case. This has so far proved to be generally what happens and it is quite disappointing. What seems to happen is this: At great depths very frequently our device encounters steady currents directed laterally to its tow course. Being steady, they exert, upon the big areas such as the vertical vane, a force which slowly rotates the plane containing the tow course and the cable about the suspension point on the ship. In every case where the effect is accentuated, that is, reduced scope, we have observed the strong fairing of the cable to one side. Whenever the cable streamed directly aft of the ship our scope was good, generally between 0.8 and 0.9.

Only two weeks ago, towing a weightier version of the device, we have been able to counter the sideways shift by dragging a large sea anchor behind it. This might be one solution to the problem but it limits our scope by the extra drag and we will have to find a more subtle approach.

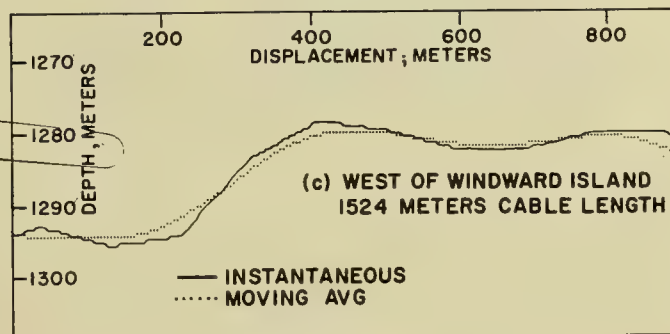
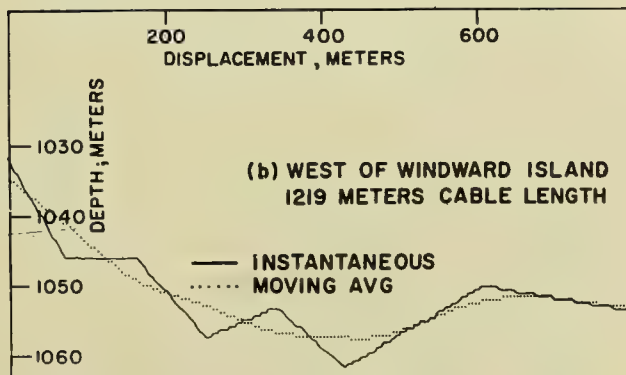
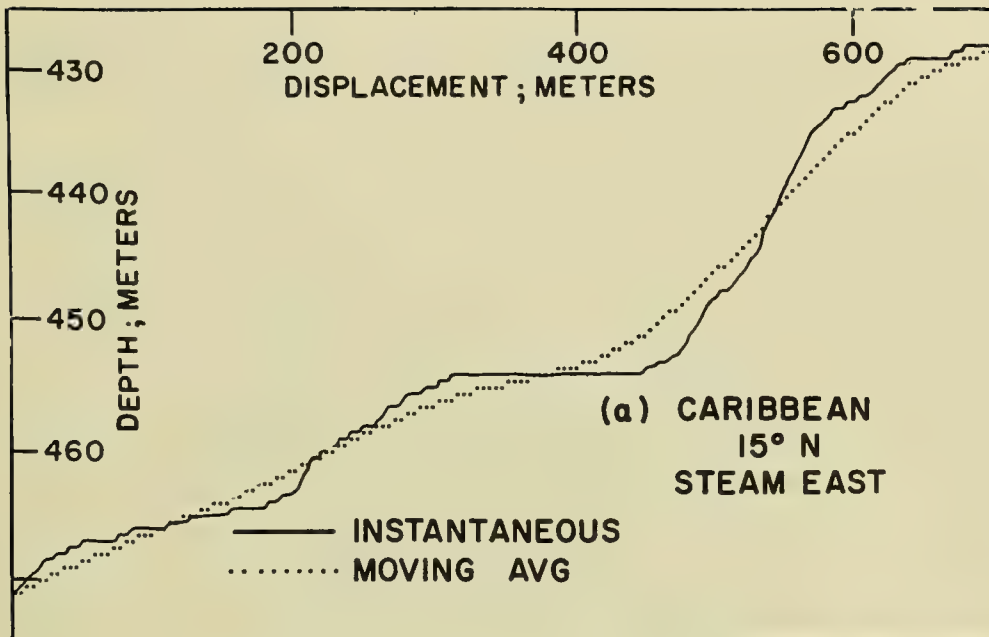
In all, we have nine detailed records of dead-weight tow paths and the most relevant parameters of the depth variation statistics are shown in Table 1. The entries in the last column,  $(h)$ , do not have an absolute significance but serve mainly to make a fair comparison with the counterpart statistics for parallel tube towing. As I have pointed out we can expect the depth fluctuations to be proportional to the scope. Therefore, in comparing two towing systems we cancel its effect in the auxiliary parameter,  $h$ . For the variety of towing conditions experienced in this series we can remember the rms  $(h)$  of 1.98 meters as that expected depth fluctuation in dead weight towing when the scope is unity.

This parameter rms  $(h)$  is reduced in parallel tube towing as we can see from Table 2, which ranges over the three locations. All the runs here are for drifting at about 2 knots except for those labeled R during which the ship steamed at 2 knots against the drift. Here we see that the rms  $(h)$  is 1.37 meters for location  $\alpha$ , 1.05 meters for location  $\beta$ , and 1.46 for location  $\gamma$ . I think that the weather near Bermuda was particularly bad for towing. Winds were between 20 and 25 knots and of course the seas were rough. This probably is behind the large value of rms  $(h)$ .

## CONCLUDING EVALUATION

As a final, perhaps more complete, form of comparison we have a set of histograms which display the frequency distribution of the  $h$  - values. Figure 9 shows that for dead weight towing. Each subtended area is proportional to the number of  $h$  - values that fell within its range. Figure 10





FIGURES 6a, b and c TOWING DEPTH RECORDS

Caribbean Sea North of Bonaire Island, July 1962  
Length of Cable, 1 , always 1525 meters. Columns c, d, e, f, in meters.

(a) Latitude	(b) Direction	(c) rms ( $\Delta y$ )	(d) y max	(e) y min	(f) $\bar{y}$	(g) $\bar{y}/h$	(h) col.(c)/col.(g)				
13N	West	0.914	695	550	623	0.620	1.50				
13N	East	1.373	931	649	790	0.786	1.75				
14N	West	0.900	862	778	820	0.815	1.02				
14N	East	2.347	916	681	799	0.795	2.95				
15N	West	0.923	950	920	935	0.930	0.98				
15N	East	1.568	479	428	459	0.456	3.44				
15N	West	0.647	870	839	855	0.850	1.02				
16N	East	1.475	884	563	723	0.720	2.05				
16N	West	0.913	646	603	625	0.622	1.47				
						rms(h)	1.98				

FIGURE 7 TABLE I: SIMPLE DEAD WEIGHT TOWING, MARCH 1964

Locations:  $\alpha$  = West of Windward Islands,  $\beta$  = East of Windward Islands,  $\gamma$  = Southwest of Bermuda  
 Lengths and depths in meters. R = reversed course.

(a) Location	(b) Cable length, l	(c) $\frac{l}{\text{rms}(dy)}$	(d) $y_{\text{max}}$	(e) $y_{\text{min}}$	(f) $\bar{y}$	(g) $\frac{y}{\bar{y}}$	(h) $\frac{\text{col. c}}{\text{col. g}}$
$\alpha$	305	0.717	280	267	274	0.899	0.798
$\alpha$	610	0.647	594	539	547	0.897	0.710
$\alpha$	915	0.621	791	763	777	0.860	0.731
$\alpha$	1219	2.005	1095	1021	1038	0.851	2.380
$\alpha$	1524	1.151	1296	1270	1287	0.845	1.353
$\alpha$	1524R	0.768	999	601	800	0.524	1.465
						rms (h)	1.37
$\beta$	610	0.453	358	351	355	0.582	0.778
$\beta$	915	0.254	442	439	441	0.483	0.522
$\beta$	1219	0.723	576	521	549	0.450	1.607
$\beta$	1219R	0.593	802	664	733	0.601	0.987
						rms (h)	1.05
$\gamma$	305	0.580	299	277	283	0.529	0.624
$\gamma$	610	0.311	428	410	419	0.687	0.484
$\gamma$	915	1.700	577	327	852	0.604	2.815
$\gamma$	1219	0.562	702	674	688	0.564	0.318
						rms (h)	1.46

FIGURE 8 TABLE II: PARALLEL TUBE TOWING, MARCH 1964

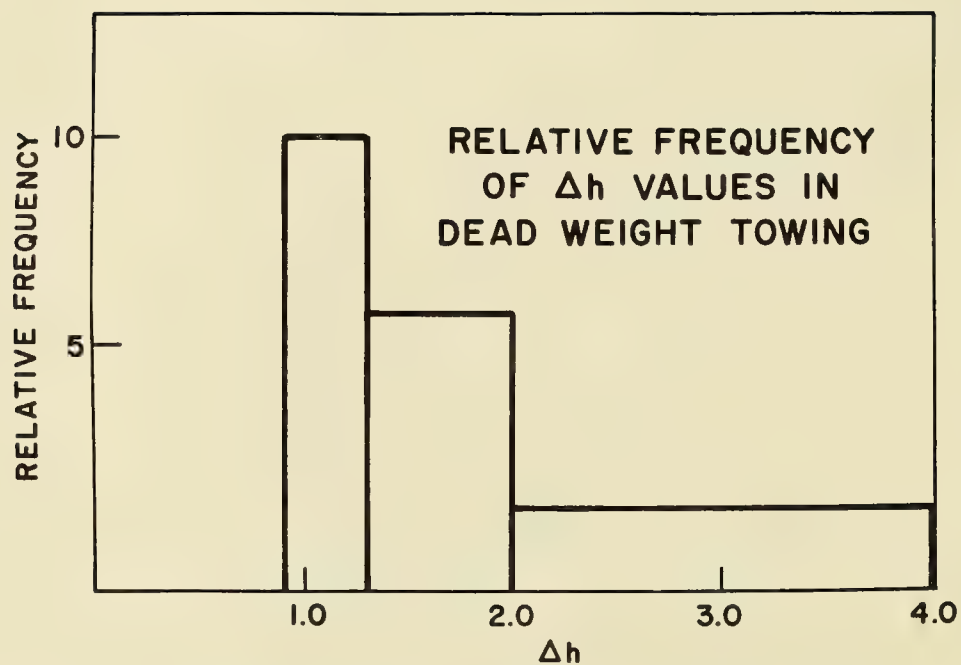


FIGURE 9 DISTRIBUTION OF  $\Delta h$  VALUES IN DEAD WEIGHT TOWING

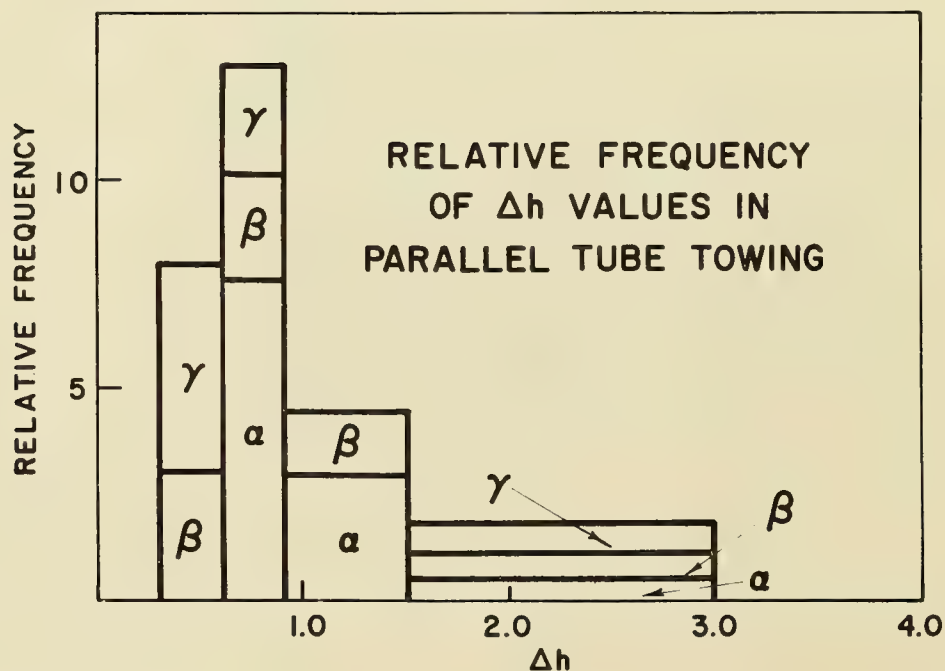


FIGURE 10 DISTRIBUTION OF  $\Delta h$  VALUES IN PARALLEL TUBE TOWING



shows a similar graph for parallel tube towing over all three locations. The total areas of the two histograms are equal to each other. The shape is similar and it is quite clear that the parallel tube device moves the distribution considerably toward smaller  $h$  - values.

For both sets of data the same ship and the same cable were used. The decline in  $h$  is around 0.8 meters as nearly as we can estimate it on such a crude test that is really composed of by-product data from sound velocity studies. The excess and deficiency in tension would be around 500 pounds and it would act on average on about 3000 ft. This particular cable would yield a strain in this case of 31.5 in. or 0.80 meters which with fortuitous accuracy predicts our improvement in  $h$ .

Besides the minimizing of the depth fluctuation, the parallel tube device offers the probably more important advantage of orientation stability. The two tubes form a perfect platform for mounting, besides velocimeters, arrays of hydrophones or self-operated sources which can thereby be towed and yet have their complete orientation fixed and known.

In effect a fairly large set of tubes would provide an experimental facility similar to that of a deeply submerged submarine. Characteristics usually sought in a submarine such as steady slow motion, constant orientation, sonic and electrical silence are all quite natural with towed tubes.

## REFERENCE

Lord, N. W., 1964, The principles and first test of a new device for deep rectilinear towing, Hudson Laboratories of Columbia University Technical Memorandum No. 72.



THE ACCURACY AND POTENTIAL USES OF COMPUTER BASED  
WAVE FORECASTS AND HINDCASTS FOR THE NORTH ATLANTIC

by

Willard J. Pierson, Jr., and Leo J. Tick

New York University, Bronx, New York





# THE ACCURACY AND POTENTIAL USES OF COMPUTER BASED WAVE FORECASTS AND HINDCASTS FOR THE NORTH ATLANTIC

by

Willard J. Pierson, Jr. and Leo J. Tick  
New York University, Bronx, New York 10453

## ABSTRACT

The work to be described was a part of a much larger project. The aim of the project was to predict the changes in airframe design that would be needed to optimize performance of the automatic landing control system (AN/SPN-10) to be used on aircraft carriers. To do this, carrier motions have to be described, and to describe the carrier motions the wave conditions have to be determined.

Computer based hindcasts for fifteen months of historical data have been made that describe the directional spectra of the wind generated waves and swell on the North Atlantic. The months were December 1955, November 1956, and December 1958 through December 1959. The computed frequency spectra agree well with the spectra obtained by an analysis of wave records obtained by British weather ships. Verification statistics show that the bias is negligible. About 40% of the hindcasts are within three feet of the observed significant wave height. About 60% are within six feet.

The wind field proved to be the most difficult part of the problem of hindcasting the waves. Errors in the wind field due in part to inadequate data coverage were responsible for the largest errors in the hindcasts. Ways to improve the determination of the wind field by a finer grid and by further calibration of ship reports are available.

The climatological wave data so obtained have many potential uses in military oceanography besides their original purpose. The usefulness of any naval vessel, or of any floating structure in the deep sea can be studied by means of the same input wave data. Instead of specifying that a certain military device should function in some particular sea state, a more meaningful statement would be that the device should have assigned characteristics whenever the wave spectrum, no matter what its features, as hindcasted every twelve hours for a particular year of data yields a significant wave height less than 20 feet and whenever the wind is under 33 knots as an example.

Wave forecasts will soon be prepared using the computer programs developed for wave hindcasting. The observed winds and sea level pressures prior to and at a given surface weather map time will be used to generate a description of the present state of the sea. These results will be saved for climatological purposes. Forecasts of the winds for the next thirty hours at six hour intervals will then be used to prepare the wave forecast valid thirty hours from the last available surface map. It is not expected that the forecasts will be as accurate as the hindcasts, because errors in predicting the wind fields will cause errors in the wave forecasts. However, the verification statistics just cited were for areas where the sea state varies rapidly due to sequences of rapidly developing and moving cyclones, and for a large area of the Atlantic the swell emanating from cyclones that have already developed and died down will be properly forecasted.

At each of 519 points on the Atlantic, 180 numbers will describe the directional spectrum of the waves. From this data on significant wave height, wave direction, swell height, and swell direction can be extracted.

Were it possible to provide a particular ship with 180 numbers describing the directional spectra, a prediction of the motions and capabilities of that ship could be made. Other applications are ship routing and eventually mine warfare problems.

## THE CARRIER LANDING PROBLEM

The design of an engineering system for maximal effectiveness at minimum cost requires knowledge of the class and relative frequency of tasks to be performed by the system as determined in part by the environment in which the system is to be used. This is especially true for weapon systems. A crucial aspect in the design of aircraft to be operated from carriers concerns the loads which will be incurred on landing.

Over the years the Navy has made continuing studies on the contact conditions between the landing gear and the deck so as to evolve proper design criteria for the aircraft structure. In the expected conversion of the landing procedure to an automatic one involving the landing control central AN/SPN-10, the possibility is large that this conversion of operating procedures will create a substantial change in the distribution of the loads environment of the entire airframe. Therefore, it appears to be the case that a new series of studies will have to be made over a considerable period of time in order to determine this new loads distribution with any sort of accuracy. If the changes in the distribution due to this new doctrine are large, the landing system will either be inadequate to its task or be over-designed thus reducing performance. The question then arises as to whether it is possible by some means to obtain this landing loads distribution other than by the lengthy empirical approach.

An alternate attack to this problem would be to make an analytic model of the entire carrier landing operation. It is then only necessary to verify

that the model is correct in order to obtain the distribution of contact conditions. This would require a much smaller volume of observations. To this end the Air Frame Design Division of the Bureau of Naval Weapons undertook a study to evolve such a model and to perform computer simulations and analyses on this model. This problem breaks down into the following phases:

1. Determination of the distribution of wave conditions.
2. Determination of the transfer function characteristics of a class of aircraft carriers.
3. Deriving a mathematical model of the landing control system, i. e. the AN/SPN-10.

Under ordinary circumstances the first item would be carried out by analyzing the wave climatology of the relevant operating areas. However, such data are not available especially so since a rather detailed description of the surface in terms of its spectral characteristics is required. The only environmental data on an ocean-wide scale which were available were the atmospheric pressure patterns. In order to obtain any wave data, it would be necessary to be able to compute rather than observe. To this goal, a contract was let to New York University School of Engineering and Science by way of the U. S. Naval Oceanographic Office to derive a computer-based procedure for calculating the spectral distributions of the waves on the surface of the North Atlantic from surface pressure and wind data, and to calculate, using this procedure, a wave climate of the North Atlantic for the year 1959. From these data, distributions of carrier motions would be determined by the David Taylor Model Basin and finally the distribution of landing conditions for certain set of conditions would be computed by the Bell Aerosystems Company. This paper reports the results of the New York University effort. It should also be stated here that the California Division of the Lockheed Aircraft Corporation also participated.

## THE WAVE HINDCASTING PROBLEM

The basic problem was to develop a computer oriented numerical procedure for computing the directional wave spectra using the wind velocity field as the driving mechanism. Originally it was thought that the atmospheric pressure field could be used to determine the wind field.

Preliminary descriptions of the procedures used have been given by Pierson and Tick (1964). Reports on the details of the computer based numerical procedure are in the first draft stage of preparation, and should appear first as Technical Reports at New York University and later as papers in the Journal of Geophysical Research. †

---

† (See Trans. Amer. Geophys. Un., vol. 46, no. 1, March 1956, p. 109 papers 059 and 060.)



The general geometry consists of a grid of 519 space points equally spaced on a Lambert Conformal map. The directional spectra at each of these points consists of the values for 12 directions and 15 frequencies. The development and verification phases of this study required certain basic wave and atmospheric data.

#### Wave, Pressure, and Wind Data.

The basic data on waves are described in reports by Moskowitz, Pierson and Mehr (1962, 1963), Bretschneider, Crutcher et al (1952) and Pickett (1962). These reports reproduce the spectra obtained by an analysis of wave records obtained by weather ships of the United Kingdom and by the U. S. Naval Oceanographic Office at Argus Island.

These spectra as computed have provided a basic source of data for many problems concerning waves. The supply of the reports by Moskowitz, Pierson and Mehr (1962, 1963) is currently exhausted, but it is planned to reissue it. These data are also available on magnetic tape.

In order to compile wave climatology for the year 1959 (which was the one chosen) it was necessary to have surface wind fields. Such data were not available. The atmospheric data which were available were pressure fields every 12 hours over the JNWP grid. A subsidiary problem, but one which turned out to require the most effort, was to generate correct wind fields. This was not possible only in terms of the available pressure observations. In addition to these pressure observations some 300,000 ship reports had to be obtained.

It was a difficult task to use these data to obtain wind fields at six hour intervals for the desired elevation above sea level. Wave hindcasts (and forecasts) are extremely sensitive to the wind field, and it is our belief that a major part of the error of our present procedure is due to errors in describing the wind field.

The computer program for determining the wind field over the North Atlantic is quite interesting. A regression analysis of the pressure field and ship reports as described by Thomasell and Welsh (1963) yields a first estimate. The key ships are the weather ships and the U. S. Navy ships. For these, anemometer heights are known, and the reported speeds are corrected by the logarithmic wind profile to a constant reference level of 19.5 meters above the sea surface. These corrected winds were used to refine the first estimate of the wind field computed from the pressure field. The anemometer heights on these ships vary over a wide range and bias the wind field in an uncontrollable way unless this correction is made.

The pressure fields were available on magnetic tape only every 12 hours at 00Z and 12Z. To get the winds at 06Z and 18Z, it was necessary to devise an interpolation scheme that may have degraded the hindcasts to some extent. The low centers on the 00Z and 12Z charts were located



according to the nearest point on the JNWP grid, and the wind fields at these times were translated to the point half way between and averaged inside a circle of appropriate radius. After all lows were treated in this way, points not translated were simply averaged. The procedure treated the moving low pressure systems in such a way as not to distort the wind field around the lows. The sub-tropical highs could be averaged, or interpolated, without translations.

### The Wave Hindcasting Procedure

Once adequate representations of the wind fields were available every six hours, it was possible to generate the wave hindcasts according to the application and extension of the results of Baer (1962), Moskowitz (1964), Pierson and Moskowitz (1964) and Pierson (1964). The hindcasting procedure accounts for the effects of spectral growth (both due to duration and fetch), propagation, and the dissipation by turbulence due to a local wind sea of those spectral components that are traveling against the wind.

## RESULTS

In this paper, only a very small portion of the results can be given. For each point in the field a set of 180 numbers was obtained to describe the wave spectrum every six hours. The numbers represent the contribution to the total variance within given ranges of frequencies and directions in the following representation.

$$\int_{f_1}^{f_2} \left[ \int_{\theta_1}^{\theta_2} S(f, \theta) d\theta \right] df$$

Fifteen frequency ranges and twelve direction ranges for a total of 180 values were obtained.

A sample of one such spectrum for 17 December 1959 at 06Z at grid point 72 is given in Table 1. The units are (ft)<sup>2</sup>. The direction and frequency ranges are shown. Also tabulated is the sum over all directions for a given frequency range.

One of the developmental samples was from about 15 December 1959 to 28 December 1959. A graph of the significant wave height as observed and as hindcasted at four surrounding grid points is shown in Figure 1. The waves range in significant height from 12 feet to nearly 40 feet and the hindcasting procedure tracks the hourly variation in wave height quite well.

Figure 2 shows a scatter diagram of observed versus predicted heights. The observed heights are instrumentally observed and have been computed in terms of the area under a frequency spectrum (corrected for instrument response) estimated from a 15 minute long wave record. The sampling variability is about 10% of the value of the observed height and

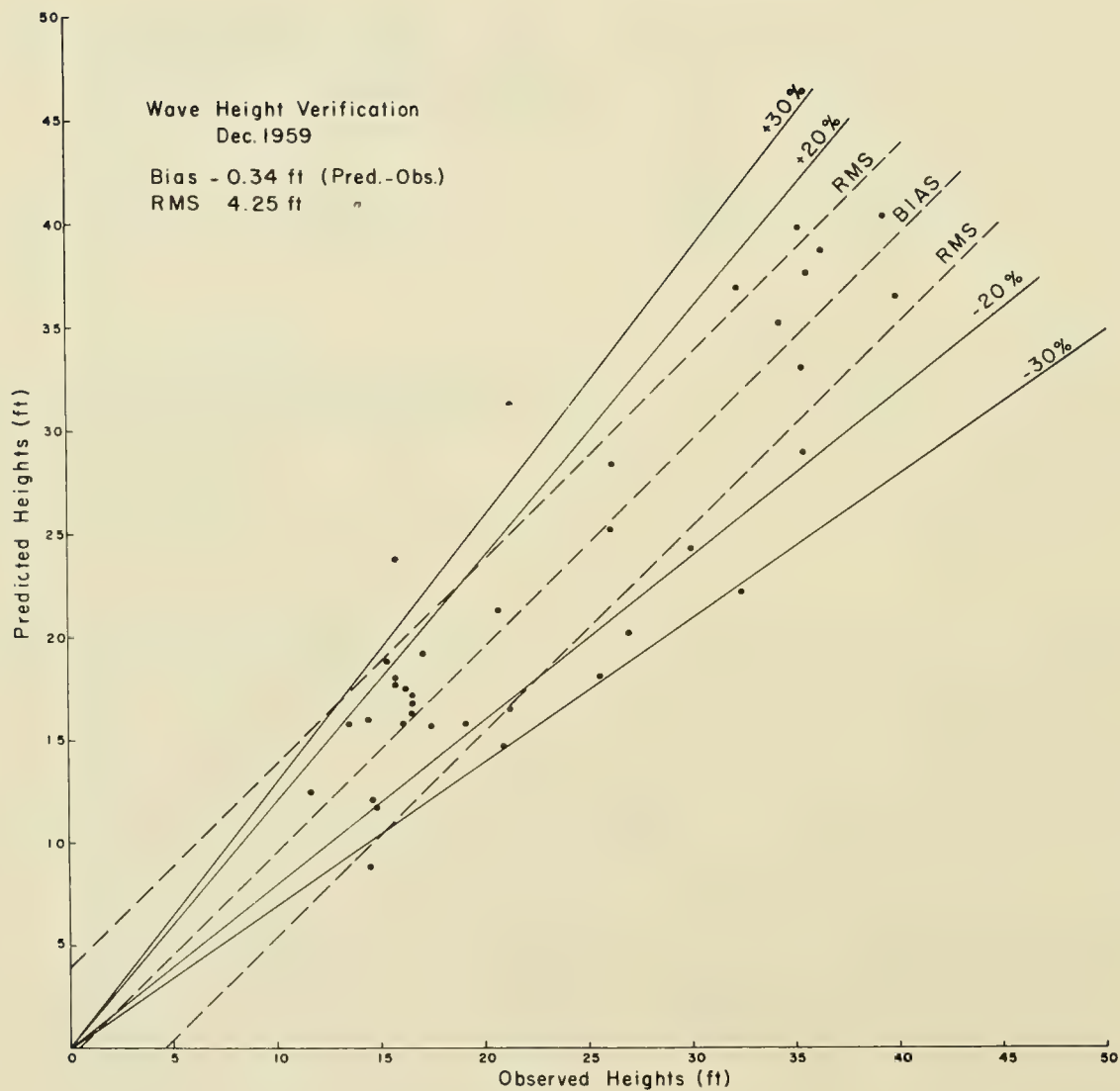


FIGURE 1 GRAPH OF SIGNIFICANT WAVE HEIGHT AT FOUR GRID POINTS AS  
HINDCASTED AND AS OBSERVED AT POSITION J IN THE NORTH  
ATLANTIC FOR DECEMBER 1959

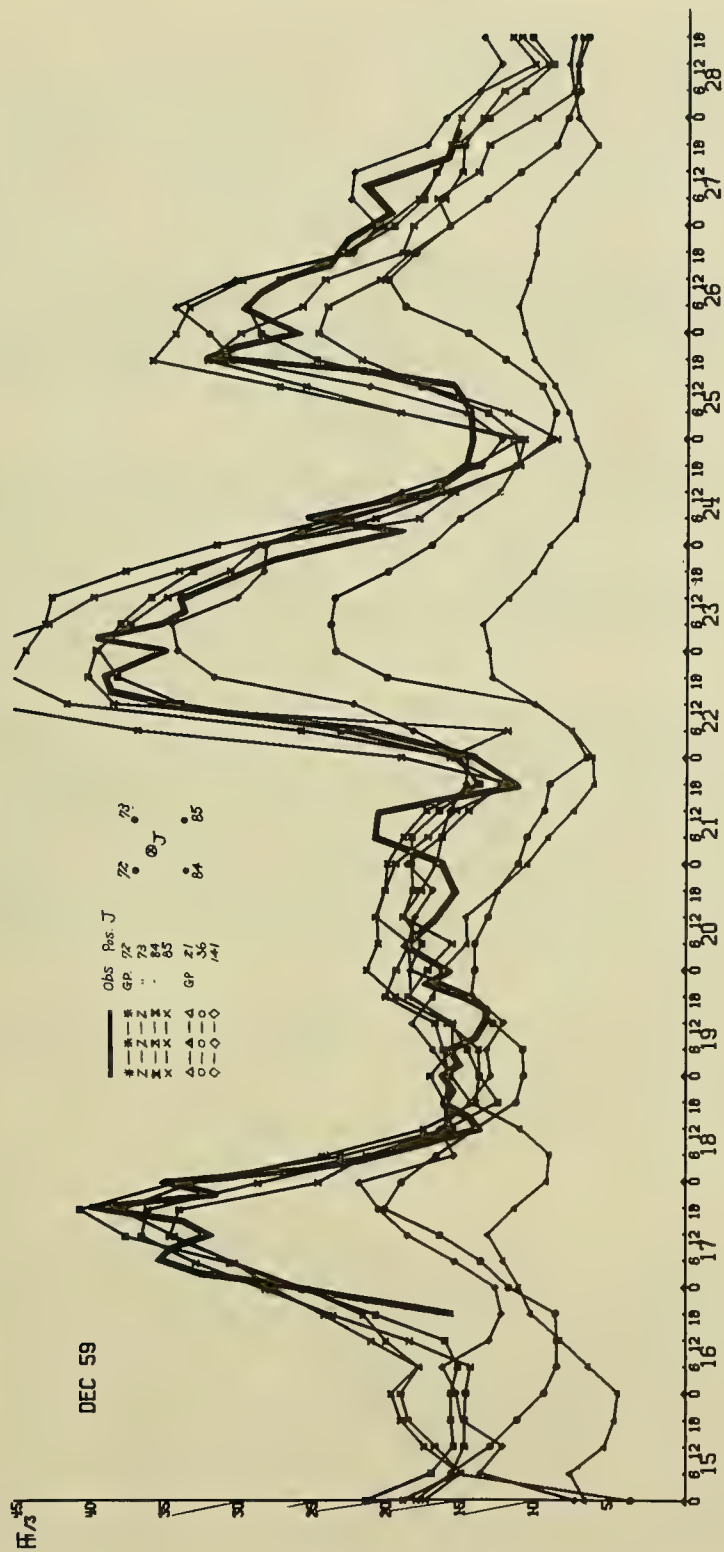


FIGURE 2 PREDICTED VERSUS OBSERVED WAVE HEIGHTS FOR DECEMBER 1959

thus waves with a significant height of 40 feet could, if many more wave records had been taken near the ship in the same general area (say, within an area 10 miles on a side) actually be more precisely represented by a significant height that nine times out of ten would be somewhere between 44 feet and 36 feet.

The bias in the hindcasting procedure is negligibly small, and the rms error of 4.25 feet is nearly the same as the sampling variability of the higher waves. Of the 38 hindcasts, about 75% fall within  $\pm 4.25$  feet of the observed value. A forecast, if it could be made, that the significant height of the waves at a certain point on the ocean at a certain time would be between 31 and 39 feet would be a very useful forecast.

A correct hindcast of the significant height implies a correct hindcast of the total volume under the directional wave spectrum; that is, it implies that the sum of the numbers in Table 1 is correct. However, the errors in height produce larger percentage errors in variance. A five percent error in significant height implies a ten percent error in variance, and a twenty percent error in height (too high) implies a forty-four percent error in variance.

It was not possible to verify the results of Table 1. However, the sum column of Table 1 could be verified. Figure 3 shows a portion of such verifications for 20, 21, and 22 December 1959. The agreement between the hindcasted and observed frequency spectra is quite good for the first day and for the last two observations on 22 December. The waves grew in the hindcast for 06Z 22 December too rapidly to provide a good verification although a few hours earlier the hindcast spectrum probably would agree quite well with the spectrum that was observed.

The final output of this project was 60 reels of magnetic tape containing approximately one million spectra of the form of Table 1. They represent the essential information on the state of the sea for a 15 months period every six hours at 519 points on the North Atlantic Ocean.

#### Use of Results.

The primary purpose of this work was described in the introduction. Toward this goal the data will be used to compute the motions of aircraft carriers in the waves, and since the wind is also given, the landing conditions can be found. Its usefulness extends far beyond its original purpose to many problems in the design of vehicles and platforms to be used on the open sea. It is immediately obvious that the procedure has operational significance. Interest has already been indicated by those connected with the design of merchant ships. It would also be possible to improve on various ship routing procedures by testing various models on these data. Numerous studies based on these results can be made. The accuracy at low frequencies in the spectral hindcasts is currently not too good. For mine warfare problems, our present results would need improvement before the waves could be refracted to shallow water and used to predict



Frequency band	DIRECTION												SUM
	345°-15°	15°-45°	45°-75°	75°-105°	105°-135°	135°-165°	165°-195°	195°-225°	225°-255°	255°-285°	285°-315°	315°-345°	
29.5/180 to ∞	0	0	0	0	0	0	0	.250	.281	.281	.281	.188	1.281
25.5/180 to 29.5/180	0	0	0	0	0	0	0	.313	.344	.313	.313	.219	1.500
22.5/180 to 25.5/180	0	0	0	0	0	0	.031	.438	.469	.500	.500	.313	2.250
19.5/180 to 22.5/180	0	0	0	0	0	0	.094	.156	.906	.969	.938	.406	3.469
17.5/180 to 19.5/180	.219	0	0	0	0	0	.031	.813	1.094	1.156	1.125	.656	5.094
15.5/180 to 17.5/180	.500	0	0	0	0	0	.469	.625	1.688	1.906	1.844	.656	7.688
14.5/180 to 15.5/180	.406	0	0	0	0	.031	.406	.688	1.125	1.344	1.313	.438	5.750
13.5 /180 to 14.5/180	.531	0	0	0	0	.031	.531	.406	1.375	1.656	1.625	.531	6.688
12.5/180 to 13.5/180	.281	0	0	0	0	0	.656	.344	1.625	1.969	2.031	.625	7.531
11.5/180 to 12.5/180	.281	0	0	0	0	0	.781	.719	1.813	2.188	2.344	.656	8.781
10.5/180 to 11.5/180	.688	0	0	0	0	0	0	0	1.844	2.281	2.188	.594	7.594
9.5/180 to 10.5/180	.531	0	0	0	0	0	.625	0	1.656	1.938	1.781	.438	6.969
8.5/180 to 9.5/180	0	0	0	0	0	0	.313	0	1.063	.906	.969	.188	3.438
7.5/180 to 8.5/180	.031	0	0	0	0	0	.063	0	.031	.219	.250	.125	.719
6.5/180 to 7.5/180	0	0	0	0	0	0	0	0	0	.031	0	9	.031

TABLE 1 SAMPLE WAVE SPECTRUM DEC 17, 1959 06Z AT GRID POINT 72. WIND SPEED 42 KNOTS  
WIND DIRECTION 268 DEGREES. SIGNIFICANT WAVE HEIGHT AS HINDCASTED 33 FEET.  
DIRECTION FROM WHICH SPECTRAL COMPONENT IS COMING IS GIVEN.

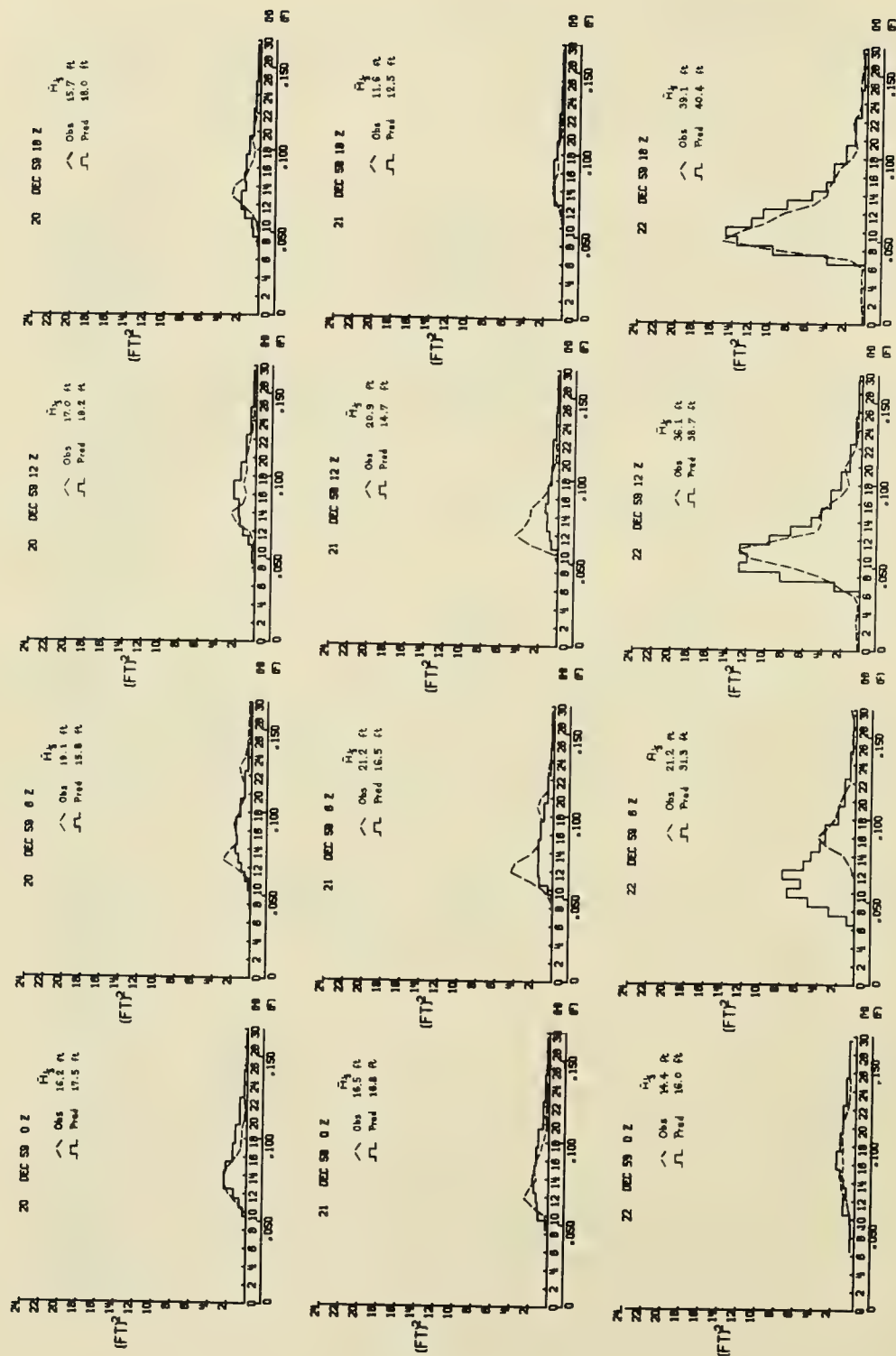


FIGURE 3 SELECTED SPECTRAL VERIFICATIONS FOR 20, 21, AND 22 DECEMBER 1959

mine response.

## WAVE FORECASTS

A data link is being established between the U. S. Naval Oceanographic Office and New York University. Within a few months, charts representing the state of the sea as of the last available synoptic chart and as a 30 hour wave forecast will be prepared on a daily basis for transmittal to the Oceanographic Office. There are many ways in which such forecasts can be improved by modifications in the current procedure, but even as presently given they represent an important advance in providing maritime interests with results of great day to day usefulness.

Current plans call for providing only significant height and dominant wave directions and periods. When ways to use the full spectral information operationally are developed, more detailed information can be provided.

One more level of computation should make it possible to provide an ASW group with a detailed prediction of its operational potential for the next day. If the responses of the various naval vessels at sea could be entered in a master file along the lines of the results already available at the David Taylor Model Basin for carriers, it would be possible to guide refueling operations, search and rescue operations, and predict the movement of vessels across the seas.

It is hoped that these methods will be extended to the North Pacific. Some work on great circle propagation and on ways to handle this much greater oceanic area is under way. The importance of a capability of this nature for the North Pacific and its marginal seas in the present world situation can hardly be underestimated.

## CONCLUSIONS

To our knowledge, this work represents the first time a wave forecasting procedure was developed by first getting the best available data on waves and by employing computer techniques to develop the wind field and the wave spectrum based on a consistent concept of the way wave spectra change over the ocean. The computer program for the waves can run for the equivalent in real time of a year and by far the best initial conditions for each successive time step are the previously hindcasted spectral values. A synoptic wave recording and wave reporting system would improve the forecasts as would better coverage by ships of the wind field.

## ACKNOWLEDGMENTS

This program was administered by the U. S. Naval Oceanographic Office under contract N-62306-1042 as part of a BuWeps Airframe Design Division Project (Code RAAD-22). Preparation of this paper was sponsored by the Office of Naval Research under contract Nonr 285(57).

## REFERENCES

- Baer, L. 1962 An experiment in numerical forecasting of deep water ocean waves. Lockheed Missiles and Space Division LMSC 801296.
- Bretschneider, C. L., H. C. Crutcher, et al 1962 Data for high wave conditions observed by the OWS Weather Reporter in December 1959. Deutsche Hydrographische Zeitschrift, Band 15, Heft 6, pp. 243-255.
- Moskowitz, L. 1964 Estimates of the power spectrums for fully developed seas for winds of 20 to 40 knots. Journal of Geophysical Research, v. 69, no. 24, pp. 5161-5179.
- Moskowitz, L., W. J. Pierson, and E. Mehr (1962, 1963 Wave spectra estimated from wave records obtained by the OWS Weather Explorer and the OWS Weather Reporter. GSL Reports No. 63-5, New York University, School of Engineering and Science.
- Pickett, R. L. 1962 A series of wave power spectra. Informal manuscript report No. 0-65-62, Marine Sciences Department, U.S. Naval Oceanographic Office (unpublished manuscript).
- Pierson, W. J. 1964 The interpretation of wave spectrums in terms of the wind profile instead of the wind measured at a constant height. Journal of Geophysical Research, v. 69, no. 24, pp. 5191-5203.
- Pierson, W. J., and L. Moskowitz 1964 A proposed spectral form for fully developed wind seas based on the similarity theory of S. A. Kitaigorodskii. Journal of Geophysical Research, v. 69, no. 24, pp. 5181-5190.
- Pierson, W. J., and L. J. Tick 1964 Wave spectra hindcasts and forecasts and their potential uses in military oceanography. First Symposium on Military Oceanography 17-18-19 June 1964. U.S. Naval Oceanographic Office, Washington, D. C.
- Thomasell, A. and J. G. Welsh 1964 Studies of the specification of surface winds over the ocean. Final Report, The Travelers Research Center, Inc.



THE RESPONSES OF THE OCEAN TO THE ACTION OF ATMOSPHERIC  
FORCES AND ACCOUNTING OF THESE RESPONSES IN U. S. FLEET  
NUMERICAL WEATHER FACILITY'S OCEANOGRAPHIC ANALYSIS AND  
FORECASTING PROGRAMS

by

Commander W. E. Hubert, USN, Commander R. C. Slusser USN  
and T. Laevastu

U. S. Navy Fleet Numerical Weather Facility, Monterey, California



THE RESPONSES OF THE OCEAN TO THE ACTION OF ATMOSPHERIC  
FORCES AND ACCOUNTING OF THESE RESPONSES IN U. S. FLEET  
NUMERICAL WEATHER FACILITY'S OCEANOGRAPHIC ANALYSIS AND  
FORECASTING PROGRAMS

by

Commander W.E. Hubert, USN, Commander R.C. Slusser, USN  
and T. Laevastu  
U.S. Navy Fleet Numerical Weather Facility, Monterey, Calif.

ABSTRACT

Traditional studies have considered the ocean in general to be quite conservative in contrast to the atmosphere. Assuming that the ocean is sluggish and slow to react to atmospheric driving forces, oceanographic analysis and prediction should be closely associated with climatological data and should utilize large-scale interaction models. However, since a number of studies indicate rapid and pronounced changes in the ocean that are linked to action in the atmosphere, oceanographic analysis and forecasting should be based on synoptic meteorological analysis and forecasting and on quantitative knowledge of the interactions between the ocean and atmosphere.

Operational oceanographic programs at FNWF are in consonance with energy exchange theory and utilize inputs from atmospheric analyses and forecasts. This permits reconstruction of oceanographic parameters that show excellent agreement with observed values even where large changes are taking place.

In order to present a cohesive picture of the forces involved, a general description is presented of the FNWF scheme of oceanographic analyses and predictions. Examples are given of the following analyses and/or forecasts: sea surface temperature and its large- and small-scale pattern separation (anomalies), sea and swell, surface currents, mixed layer depth and subsurface thermal structure. A summary is given of the principles on which these analyses and forecasts are based. The small-scale extraction and analysis/forecast is briefly demonstrated, with an example.

It is concluded that the relatively large changes that occur over short periods in the surface layers are closely related to atmospheric forces. As a result, the oceanographic analysis and forecasting periods must be relatively short (comparable to meteorological practice), and oceanographic analyses and forecasts should be carried out in an integrated meteorological/oceanographic scheme as used at FNWF.

## INTRODUCTION

One of the assigned missions of the U.S. Fleet Numerical Weather Facility (FNWF) at Monterey, California, is to prepare meteorological and oceanographic analyses and forecasts in support of fleet and other operations throughout the Navy. As the activity's title implies, these products are prepared numerically using the fastest appropriate high-speed electronic computers. The approach used at FNWF has been to apply a combination of dynamic theory and empirical experience to problem solving by computer. In general, only problems which have direct Navy application and which show promise of operational usefulness within one year's time are undertaken at FNWF. In this sense, the developmental efforts at the facility should be called engineering application rather than 'basic research.'

While early efforts at Monterey were concentrated on atmospheric analysis and forecasting, emphasis has been shifting more and more in the last two years to oceanographic problems and, in particular, to sea-air interactions. The atmosphere and the oceans are considered to be one environment as far as naval operations are concerned. Each of the media affects conditions in the other and their behavior should not, and cannot, be treated independently.

In this paper we present examples of FNWF oceanographic analyses and predictions and indicate the basic principles used in their derivation. Detailed descriptions of the programs and the theoretical and empirical basis are found in other FNWF publications. It is also demonstrated in this paper that relatively large changes take place in the surface layers of the ocean over short periods of time and that these changes are mainly caused by atmospheric forces. Hence it is shown that oceanographic analysis should be carried out in relatively short time intervals, compatible to synoptic meteorological analysis frequencies and that successful oceanographic analyses and forecasts should be done in connection with meteorological ones. It can be easily demonstrated that the 5-day composite oceanographic analyses, done by some institutions, present neither the initial nor the final nor average conditions and that 14-day and longer analyses of past data of some elements approach the mean past conditions.

## THE FNWF SCHEME FOR OCEANOGRAPHIC ANALYSIS AND PREDICTION

Figure 1 outlines the scheme developed at Monterey for numerical analysis and prediction of oceanographic elements and processes (see FNWF Tech. Memo No. 5). The figure clearly demonstrates the complexity of the numerical program being undertaken by FNWF in the general field of oceanographic analyses and forecasts. This scheme has been developed almost entirely independently of the ASWEPS program and may, in fact, be considered to be competitive.

Looking first at the column headed Basic Data, one can see that a large part of the input data to this program is derived from meteorological



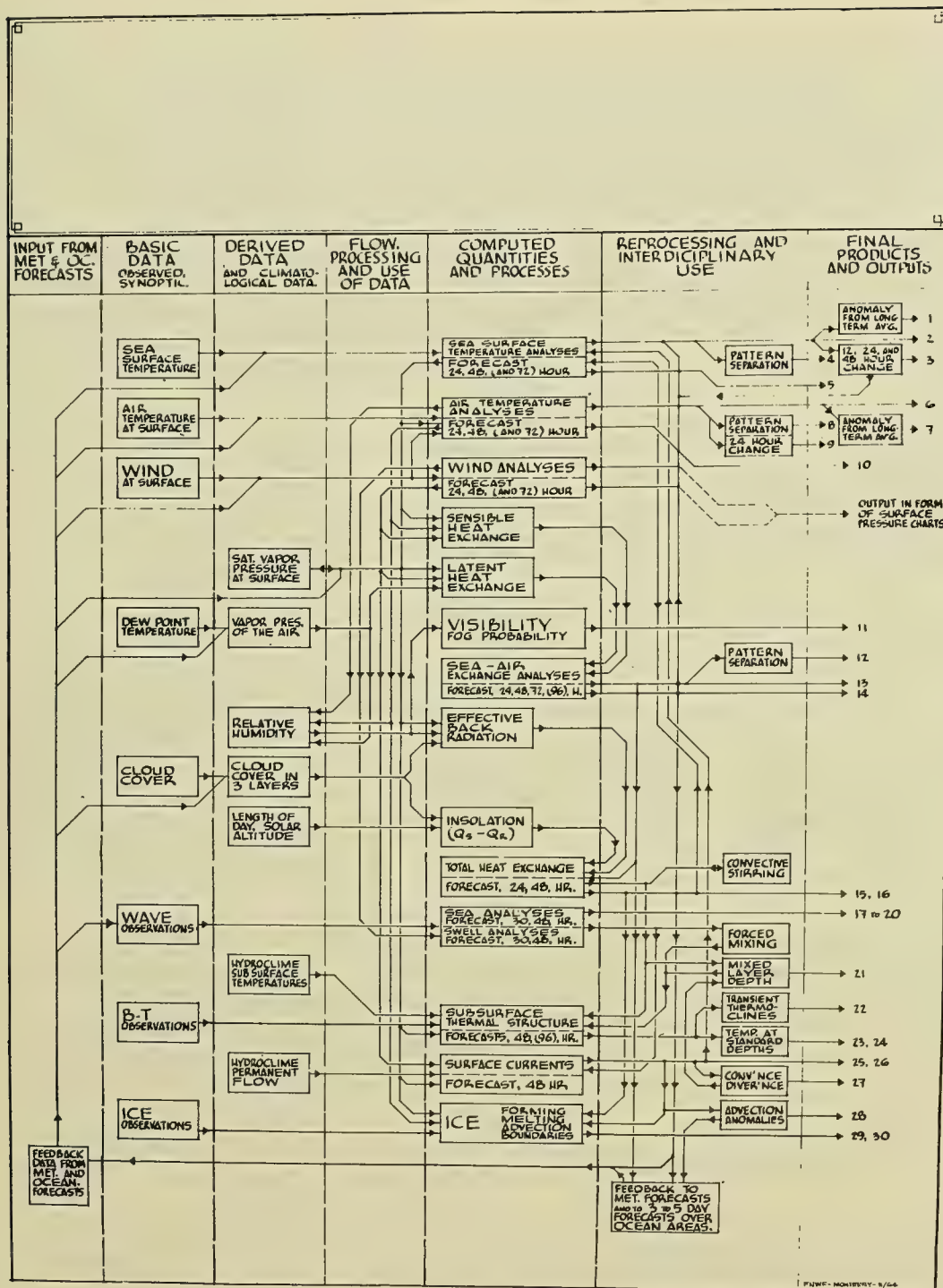


FIGURE 1 FLEET NUMERICAL WEATHER FACILITY, MONTEREY, MASTER SCHEME OF NUMERICAL ANALYSIS AND PREDICTION OF OCEANOGRAPHIC ELEMENTS AND PROCESSES

observations. Since the number of BT observations is insufficient for truly synoptic oceanographic analysis (except perhaps in limited areas), we are forced to derive the maximum information from meteorological reports at the ocean surface. The basic approach at FNWF has been to obtain the first estimate of oceanic thermal structure from purely exchange considerations and then to modify this 'guess' with BT data where available.

The various computations involved in this method of oceanographic analysis and prediction are summarized in the middle of Figure 1 under the column headed Computed Quantities and Processes. The flow diagram leading to and resulting from these computations serves to emphasize the entire concept of sea/air exchange utilized in the FNWF oceanographic scheme.

Table 1 summarizes the principal environmental inputs to Submarine Warfare programs; there are others, such as bottom effects, but those listed here are the problem areas under attack at Monterey. Besides these inputs there are other oceanographic programs produced and under development at FNWF for support of surface and amphibious operations.

## EXAMPLES OF FNWF OCEANOGRAPHIC ANALYSES AND FORECASTS

Figure 2 shows an example of hemispheric sea surface temperature analysis, and Figures 3 and 4 present the large- and small-scale pattern separations respectively. These pattern separations indicate the anomalies (in meteorological sense) and in addition the small-scale pattern can be used to determine the positions of oceanic fronts (see Fig 15B). The methods and procedures of these analyses have been described in other FNWF publications (Wolff, 1964; Wolff, Carstensen and Laevastu, 1965; Wolff, Laevastu and Hubert, 1964; and Holl, 1963).

An example of an FNWF wind wave analysis is given in Figure 5. The following wave parameters are analyzed and/or forecast: wind wave significant height, swell height, combined sea height and significant periods. These forecasts are based on surface wind forecasts from which are computed wind duration, fetch length, stability, decay distance and time.

The detailed description of the method is given by Hubert (1964 and 1965). The forecasts have been verified by direct wave observations and reports.

Figure 6 is an example of an ocean current chart (in nautical miles per day) obtained at FNWF on a synoptic basis. As can be seen from this figure, well-known features such as the Gulf Stream, Kuroshio, Equatorial Counter Current, etc., are quite well defined by this procedure. Since the computations are carried out in component ( $u, v$ ) form, directional fields are also available.

In order to obtain a single continuous field displaying both direction

PROGRAM AREA

SEA STATE	- DERIVED FROM GEOSTROPHIC SURFACE WINDS CORRECTED FOR LOW-LEVEL STABILITY. INFLUENCE SUBMARINE WARFARE PROGRAMS THROUGH NOISE AND MECHANICAL MIXING OF SURFACE LAYER.
SURFACE CURRENTS	- DERIVED FROM SURFACE WINDS AND OCEAN THERMAL STRUCTURE. INFLUENCE SUBMARINE WARFARE PROGRAMS THROUGH ADVECTION OF SST AND BY CONVERGENCE/DIVERGENCE.
SEA SURFACE TEMP. (SST)	- ANALYZED FROM SHIP REPORTS. FORECAST FROM ADVECTION AND HEAT FLUX CONSIDERATIONS. USED AS ANCHOR POINT FOR THERMAL STRUCTURE WORK.
HEAT TRANSFER	- COMPUTED FROM HEAT EXCHANGE FORMULAE INVOLVING PRIMARILY METEOROLOGICAL PARAMETERS. INFLUENCES SUBMARINE WARFARE PROGRAMS THROUGH TRANSIENTS AND CONVECTIVE MIXING.
LAYER DEPTH & THERMOCLINE INTENSITY	- DERIVED FROM MECHANICAL AND CONVECTIVE MIXING PLUS CONVERGENCE/DIVERGENCE. IMPORTANT TO SOUND PROPAGATION.

TABLE 1 FNWF ENVIRONMENTAL INPUTS TO SUBMARINE WARFARE PROGRAMS





FIGURE 2 OPERATIONAL SEA SURFACE TEMPERATURE (SST) ANALYSIS  
FOR 00 GMT 1 FEBRUARY 1965. DEGREES C



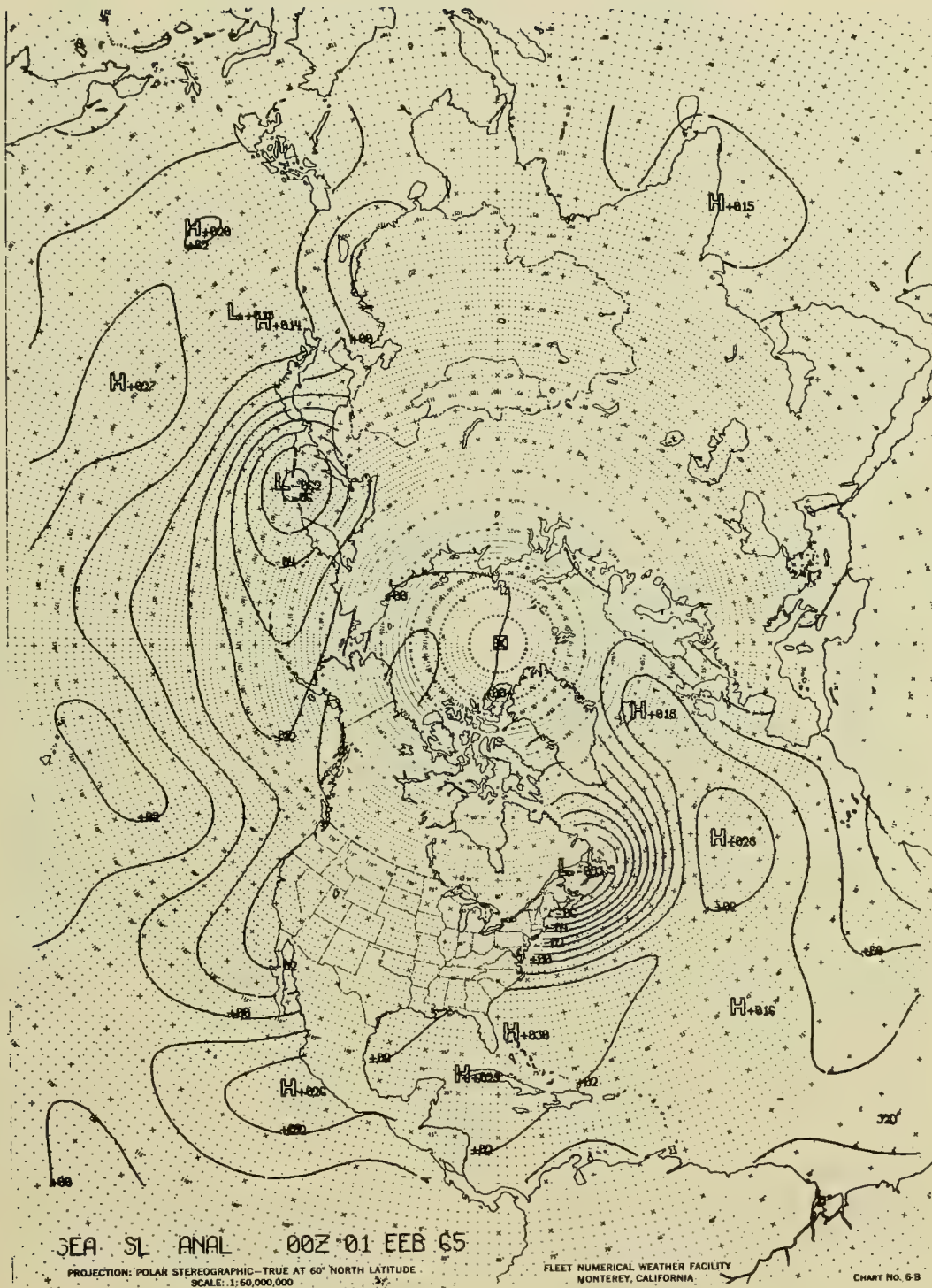


FIGURE 3 LARGE-SCALE PART OF SST ANALYSIS FOR 00 GMT 1 FEBRUARY 1965. RESULT OF SCALE AND PATTERN SEPARATION





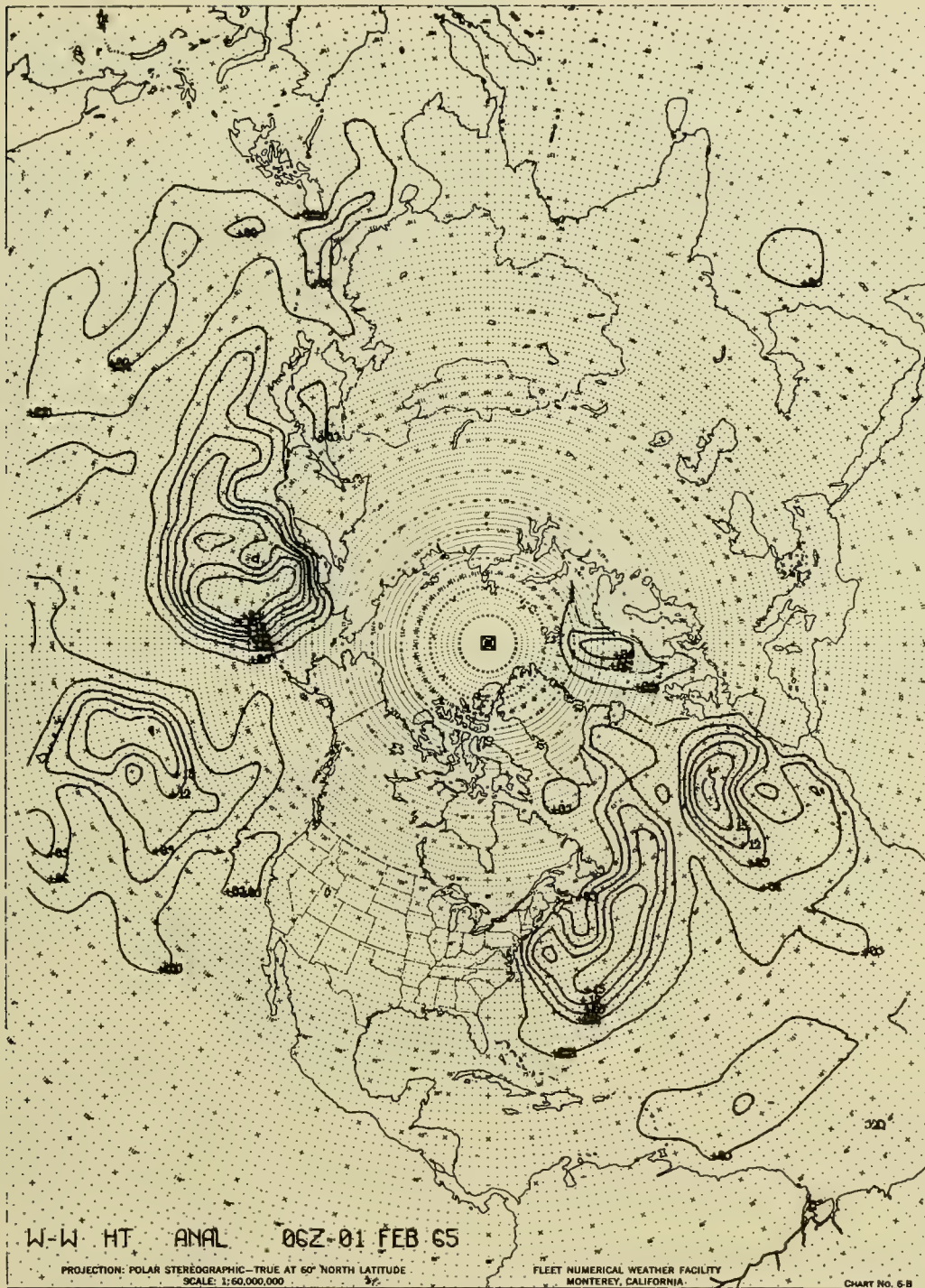


FIGURE 5 WIND WAVE ANALYSIS FOR 06 GMT 1 FEBRUARY 1965.  
SIGNIFICANT HEIGHTS IN FEET



FIGURE 6 OCEAN CURRENT COMPUTATION AT 06 GMT 1 FEBRUARY 1965.  
TRANSPORT IN NAUTICAL MILES/DAY. TRANSPORT OVER  
12 NM/DAY STIPPLED.



and speed of the computed currents, a stream function ( $\psi$ ) analysis is made using methods similar to those employed by Bedient and Vederman (1964) to represent atmospheric flow in the tropics.

The stream function field which corresponds to the ocean current chart in Figure 6 (06 GMT 1 February 1965) is shown in Figure 7. Current vectors have been plotted at selected grid points to show the degree of fit. The fact that the derived stream function is nondivergent while there is divergence in the initial velocity field explains some of the cross contour flow. In general, however, this appears to be small in most places, and the stream field provides a good representation of the current pattern.

The surface current forecasts are verified with sea surface temperature analyses and heat exchange and advection computations. Detailed procedures are described by Hubert (1964 and 1965). Besides the direct use of this product in various naval operations, it is used for computation of divergence/convergence for thermocline depth and subsurface thermal structure forecasts and for forecasting the advective portion of sea surface temperature change.

Figure 8 is a further breakdown of the scheme discussed earlier. As can be seen, all of the computational programs described in the preceding section enter into the determination of thermal structure with depth. The analyses will be built downward from the surface (where the most reports are available).

The previous day's analysis will first be modified by mechanical and convective mixing, where applicable, and large-scale convergence and divergence in the surface layers. Climatological (hydroclimate) restraints will be used to keep computed changes within reasonable limits. Finally, BT observations will be introduced by means of a median seeking technique such as used in the SST analysis program.

Most of the components needed to assemble the complete subsurface analysis and prediction package have been programmed for numerical solution. The first major portion completed is a hemispheric analysis and prediction of mixed layer depth, which is shown in Figure 9. A partly subjective, partly computerized thermal structure and sound speed profile forecasting is now being done daily for twelve points in the Pacific. Examples of these forecasts at three points, together with verifying observation and climatology, are shown in Figure 10.

It should be noted that hemispheric oceanographic analyses and predictions have certain limitations. They do, e.g., not give enough details of complex conditions within about 100 miles of major current boundaries, nor near coasts and islands. These charts also do not present the truly short-term fluctuations (12 hours or less) caused, e.g., by tides. Special explanatory notes on these short-term and small-scale processes have been issued by FNWF to the users of the analyses and

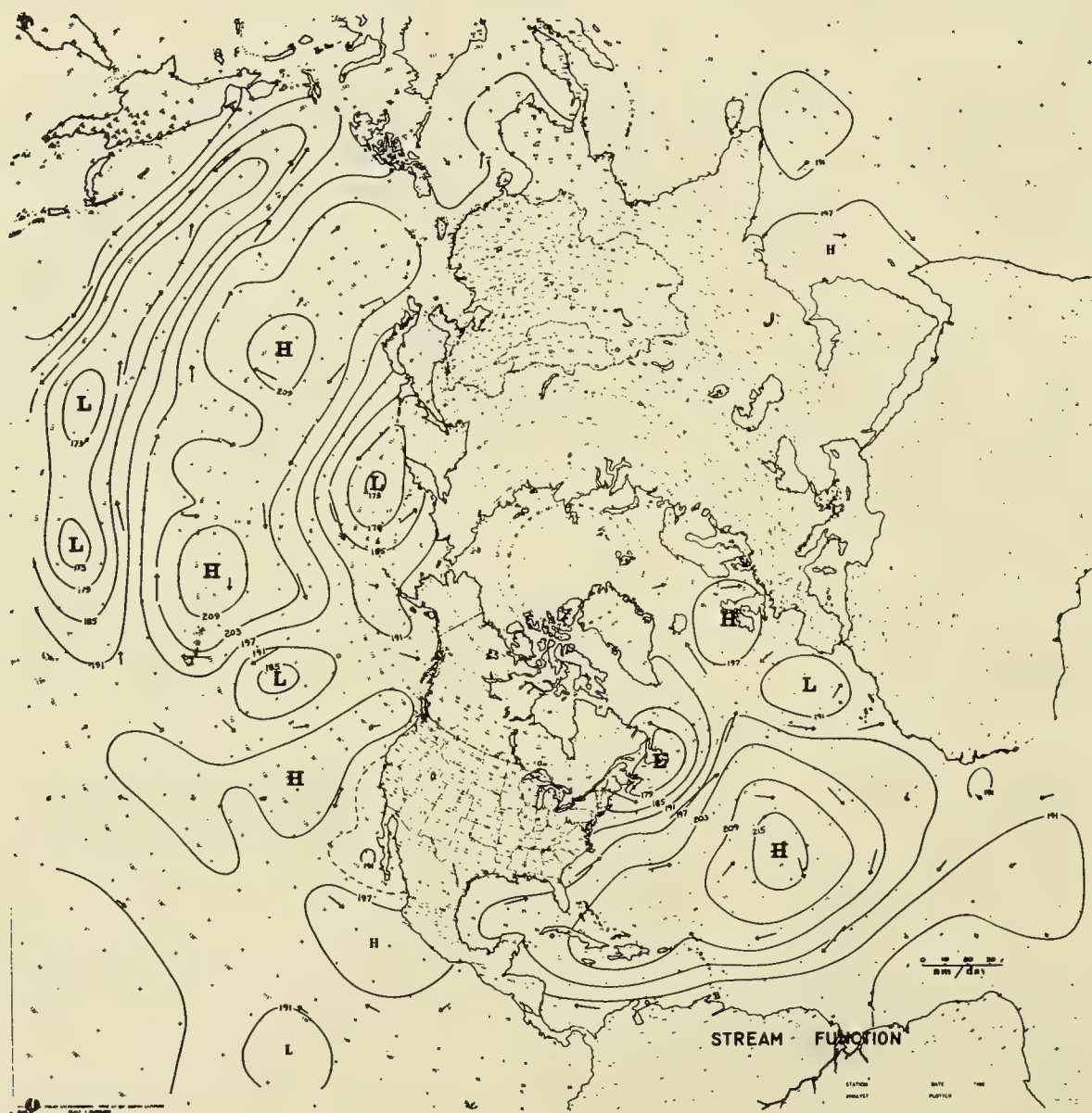


FIGURE 7 CURRENT STREAM FUNCTION ANALYSIS FOR 06 GMT 1 FEBRUARY 1965. UNITS  $10^7 \text{ SEC}^{-1}$  CURRENT ARROWS TO SCALE PLOTTED AT SELECTED GRID POINTS

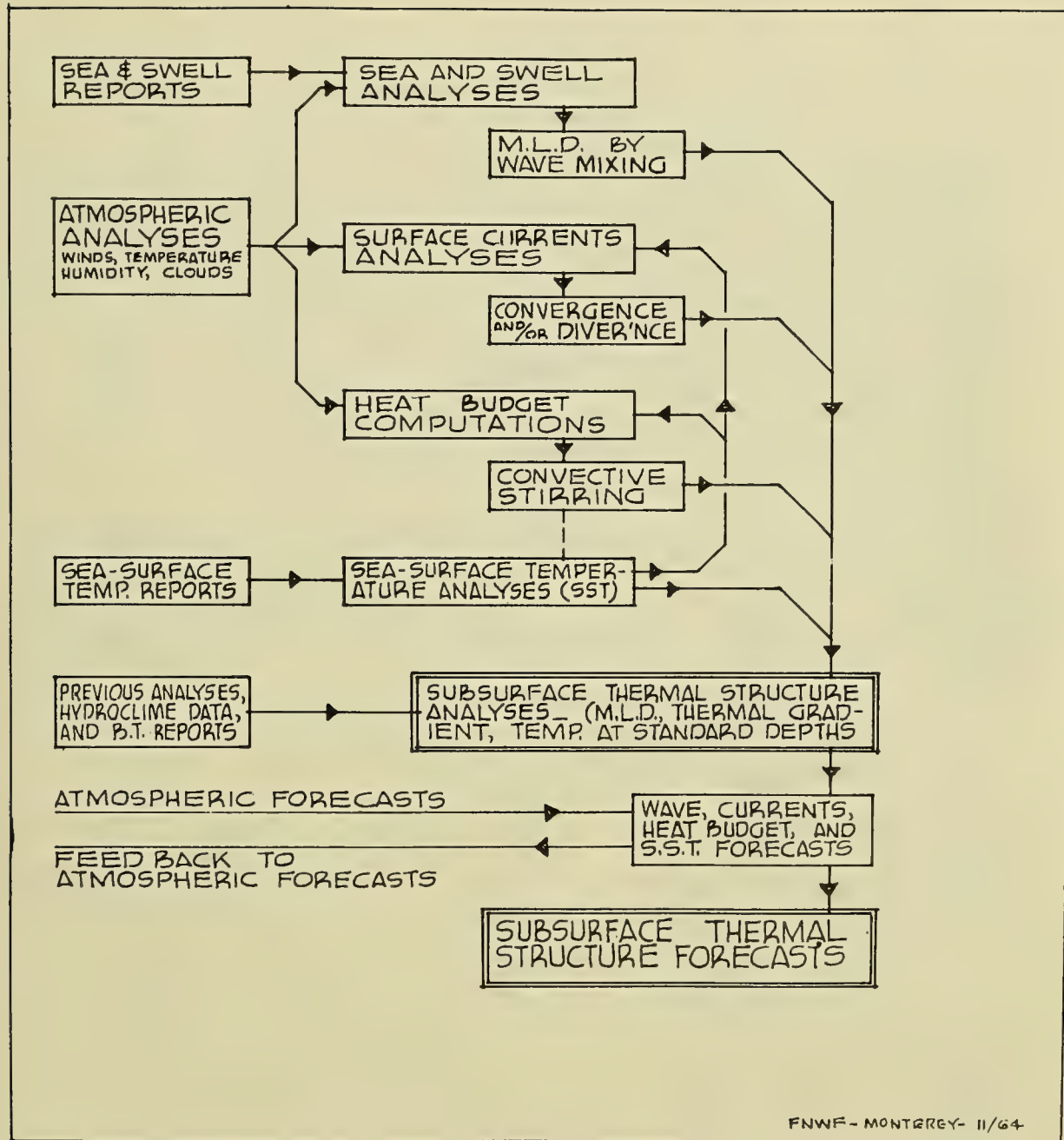


FIGURE 8 FLEET NUMERICAL WEATHER FACILITY, MONTEREY,  
SCHEME FOR SUBSURFACE THERMAL STRUCTURE  
ANALYSES AND FORECASTING

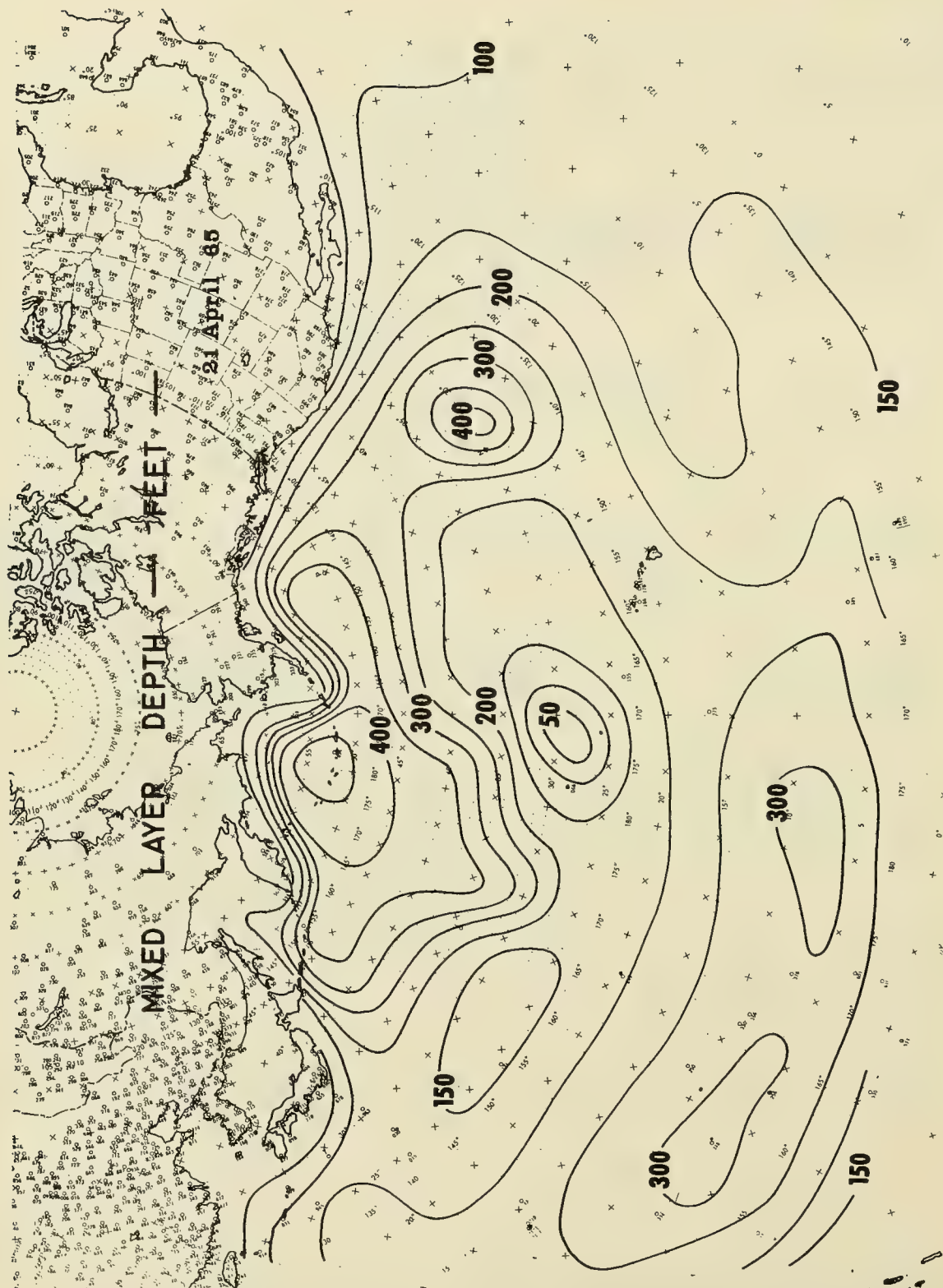


FIGURE 9 HEMISPHERIC THERMOCLINE DEPTH ANALYSIS FOR 1200 GMT 21 APRIL 1965



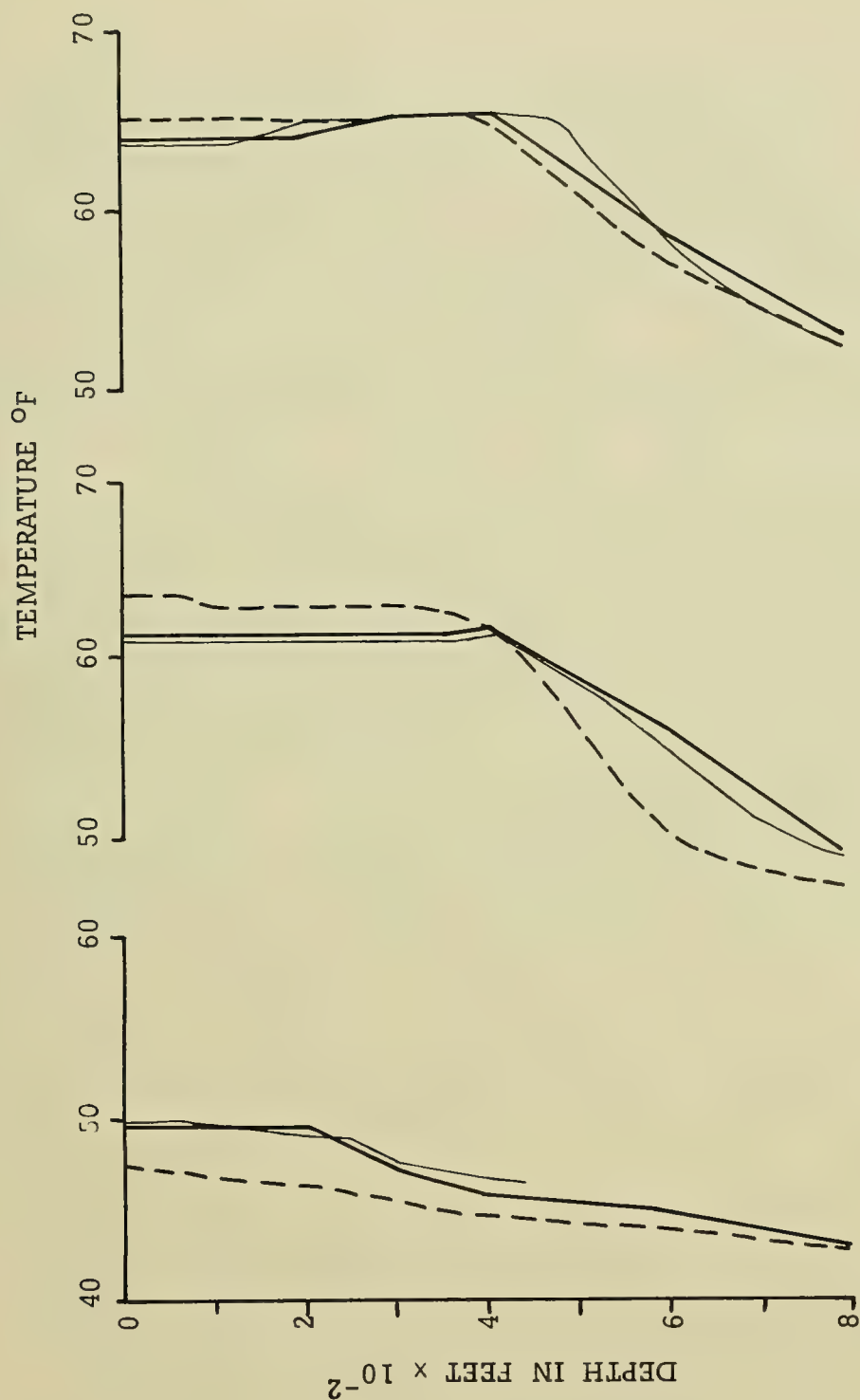


FIGURE 10 24-HOUR TEMP PROFILE FORECASTS AT 3 SPECIFIC LOCATIONS, NORTH PACIFIC (6 APRIL 1965). INTERPOLATED CLIMATOLOGY DOTTED LINES. VERIFYING OBSERVATION (AVERAGE OF 2 BT CASTS) THIN LINES

forecasts.

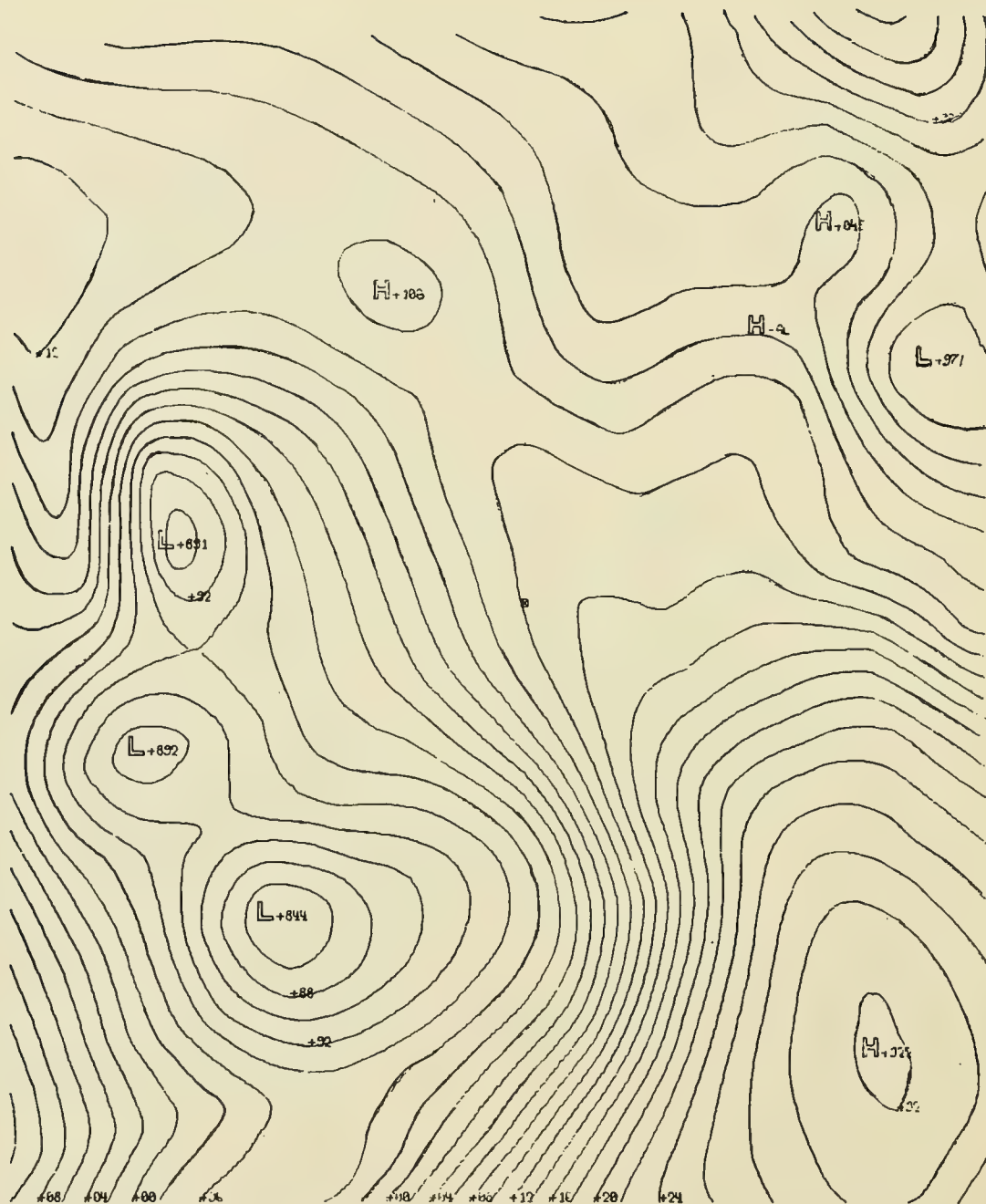
Detailed small-scale analyses are prepared for specific operation areas, and can be prepared in any area if and when requested by operating forces. This is done by specifying four positions (corners) of the area, extracting information from the standard large-scale analyses/forecasts made at FNWF and expanding it to new 63x63 grid, to which additional details can be added by reanalysis. This is illustrated in Figures 11 and 12. The minimum (and optimum) grid size of such small-scale analysis is greatly determined by data density, rate of change of properties and complexity of local modifying factors.

#### THE SPEED AND MAGNITUDE OF RESPONSE OF THE OCEAN TO THE ACTION OF ATMOSPHERIC FORCES, AND THEIR EFFECTS ON OCEANOGRAPHIC ANALYSIS AND FORECASTING PROGRAMS

A number of recent synoptic studies and surveys indicate relatively fast and pronounced response of surface layers of the ocean to the atmospheric driving forces. The relatively rapid response of the surface layers to the synoptic surface weather conditions was demonstrated with synoptic sea surface temperature and surface weather analysis and time series BT messages by Wolff, Laevastu and Russell (1965). They also demonstrated that the sea surface temperature fluctuations have shorter periods in higher latitudes in the areas of migrating cyclones and longer periods in lower latitudes in the areas of highs. The magnitude of short-term sea surface temperature fluctuation depended on its gradient and could reach 4°C in 48 hours but was, on the average, about  $\pm 0.3^\circ\text{C}$  in the same period. The sea-surface temperature fluctuation patterns were large in scale and corresponded to past wind fields, thus demonstrating the importance of advective contribution to these changes. Numerous examples of rapid response of the surface layers of the sea to the atmospheric driving forces can be obtained daily. A few of these are given below. Figure 13 shows a plot of sea surface temperature from 15 March to 6 April 1965 at OSV November. The relatively sudden SST changes between 23 - 24 March and 29 - 30 March (2 to 3°C in 24 hours) are obviously mainly advective as the surface pressure charts on the same figure indicate. During the period of small SST fluctuations, OSV November is in a high pressure area with relatively weak winds.

Another more complex type of rapid response of the sea to atmospheric forces is illustrated in Figures 14 and 15. The relatively large fluctuations of sea surface temperature (Fig 14A) close to a major current boundary and in an area of sharp horizontal temperature gradients are caused by migrating cyclones, which push the cold, less saline water from the St. Lawrence Gulf over warmer more saline water (Fig 15B), as already shown by Wolff, Laevastu and Russell (1965). The passing cyclones cause extensive, relatively large-scale, meandering of the surface layers, as shown in Figures 14B, C and 15A. The details of this process are somewhat more complex than is possible to describe here. Figure 14B also shows the climatological 200 m temperature boundary,



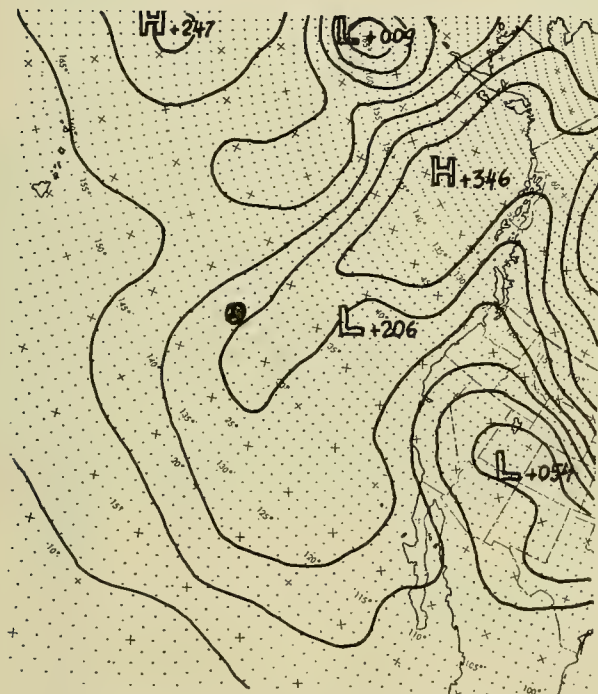
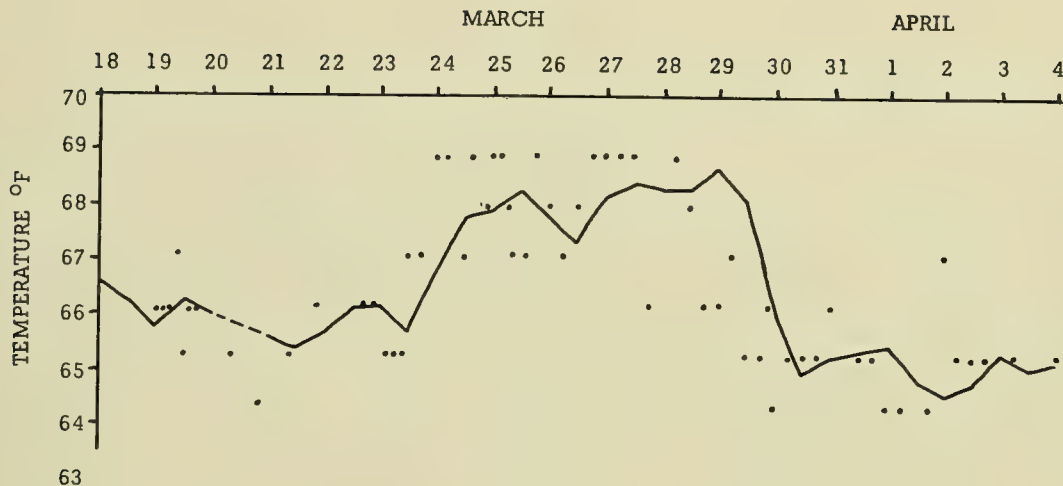


SFC PRES ANAL 12Z 01 OCT 64

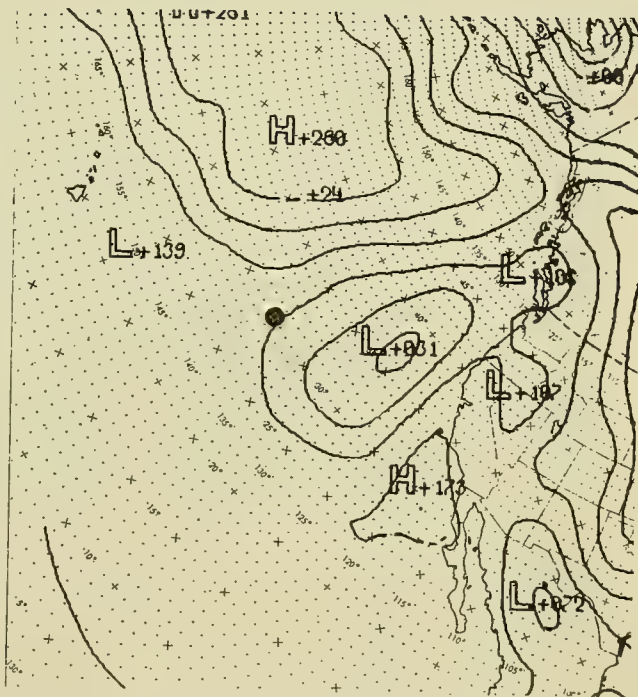
01

FIGURE 12 EXTRACTED, EXPANDED AREA (SHOWN ON FIG 11),  
CONTOURED TO 2-mb INTERVAL





SFC PRES ANAL 06Z 23 MAR 1965



SFC PRES ANAL 00Z 30 MAR 1965

FIGURE 13 SEA SURFACE TEMP ANALYSIS AT OSV NOVEMBER ( $30^{\circ}\text{N}$ ,  $140^{\circ}\text{W}$ ) FROM 18 MARCH TO 4 APRIL 1965; SURFACE PRESSURE ANALYSIS ON 06Z 23 MARCH AND 00Z 30 MARCH 1965



FIGURE 14A SEA SURFACE TEMPERATURE ANALYSIS AT 41.3°N, 61.7°W  
FROM 18 MARCH TO 4 APRIL 1965



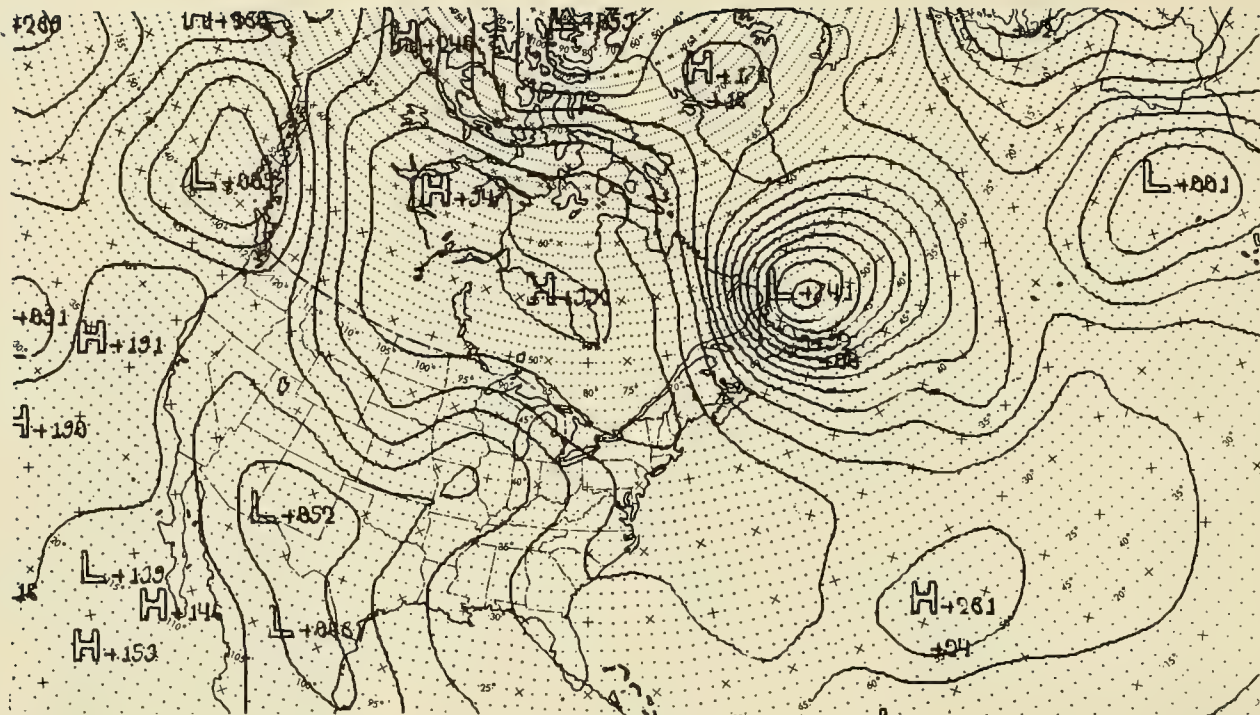


FIGURE 15A SURFACE PRESSURE ANALYSIS ON 00Z 29 MARCH 1965 AND

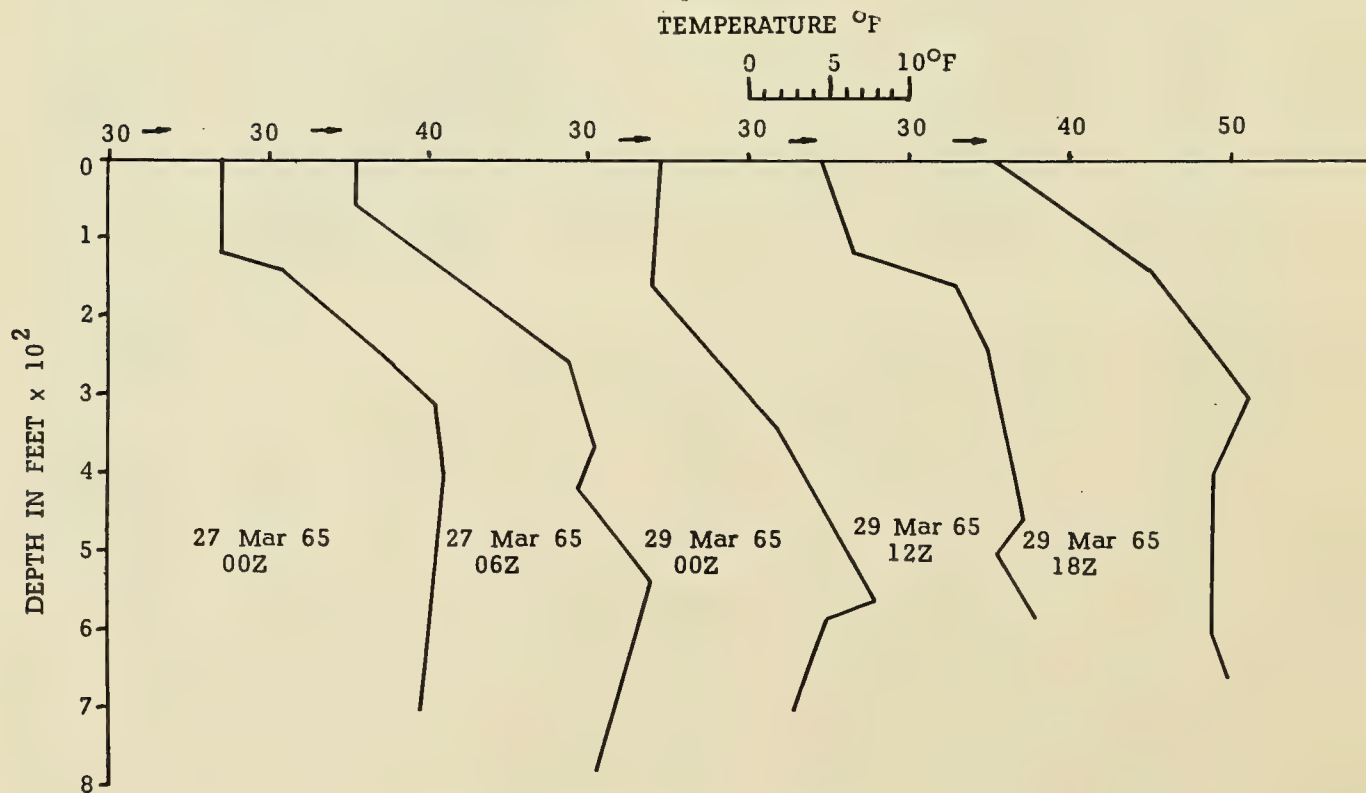


FIGURE 15B SOME BT REPORTS FROM 41.3°N, 61.7°W FROM 23 TO 31 MARCH 1965



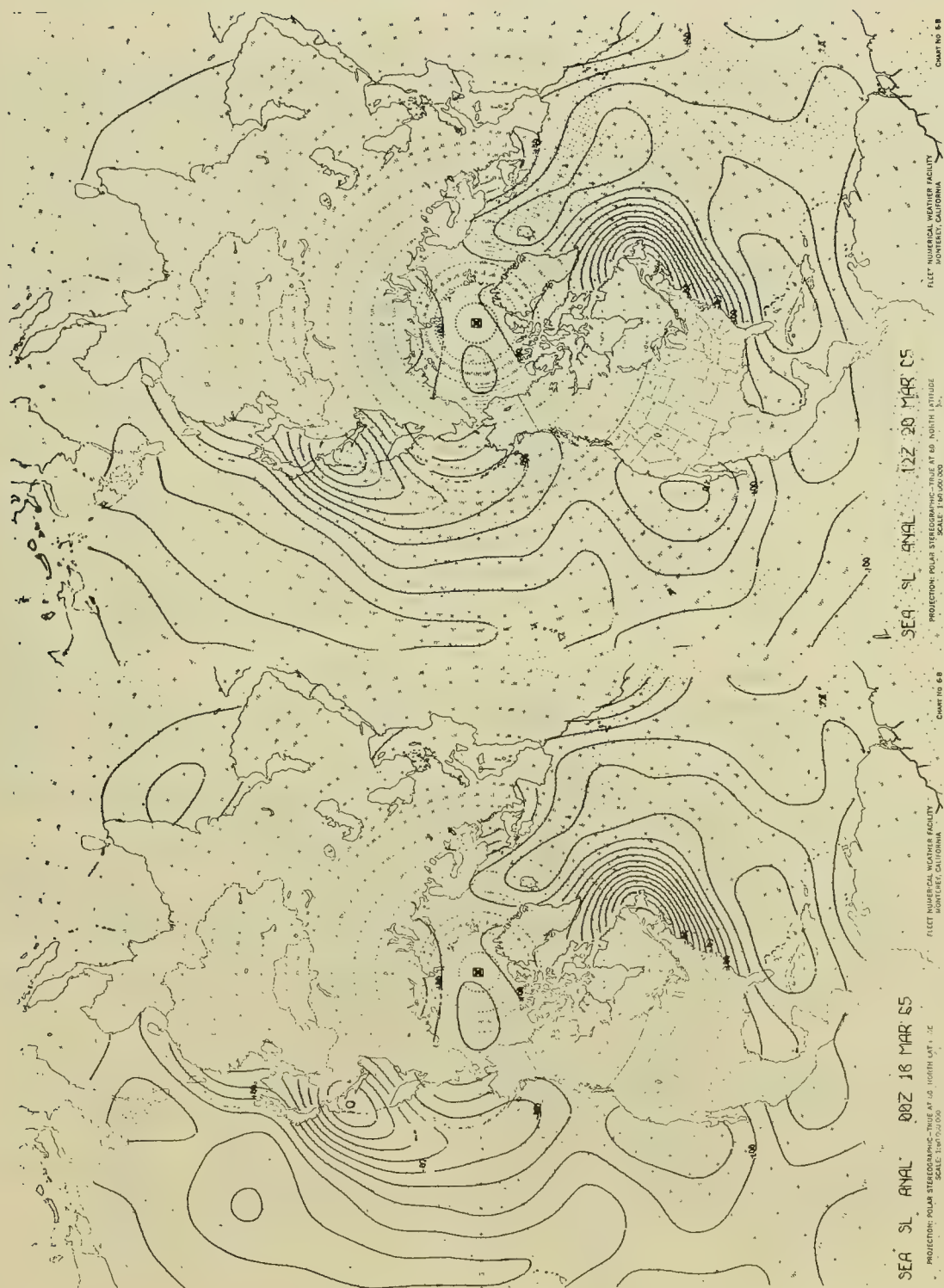


FIGURE 16 SEA SURFACE TEMPERATURE SL PATTERN ON 00Z 18 MARCH 1965  
 AND 12Z 20 MARCH 1965

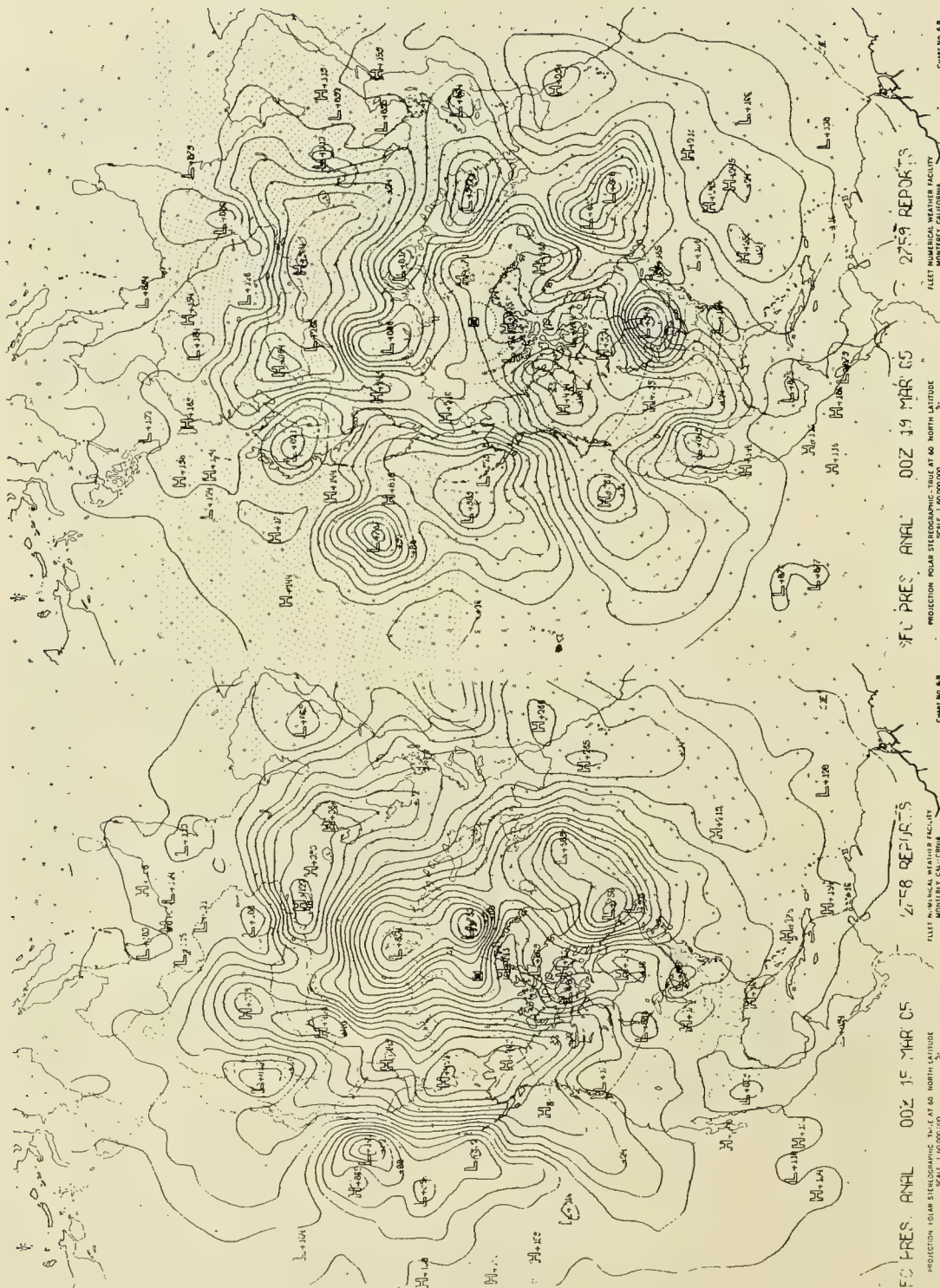


FIGURE 17 SURFACE PRESSURE ANALYSIS ON 00Z 15 MARCH 1965  
AND 00Z 19 MARCH 1965

which seems to fluctuate but very little, as earlier studies by Schroeder (1963) and Dietrich (1964) also indicate. A detailed dynamical model of the fluctuations in this complex but important area is under consideration at FNWF.

The atmospheric driving forces (winds) can also cause rapid changes in large-scale sea surface temperature patterns over short periods (few days). This is indicated with the changes off California in Figure 16, the causes of which are obvious from Figure 17. More detailed descriptions of these anomaly charts are given by Wolff, Laevastu and Hubert (1964).

It can be concluded from these and numerous other examples that the oceanographic analyses and forecasts should be done with short period meteorological analyses/forecasts as a basis (e.g., hourly to 6 hourly), and the displays of analyses and forecasts should be made in 12 to 24 hour periods in order to indicate significant changes in the ocean. This condition requires that oceanographic analyses and forecasts be made in connection with weather analyses and forecasts and by the same facilities.

## REFERENCES

- Bedient, H.A. and J. Vederman 1964 Computer analysis and forecasting in the tropics. Monthly Weather Review, Vol. 92, No. 12, pp 565-577.
- Dietrich, G. 1964 New hydrographical aspects of the Northwest Atlantic. Paper presented at ICNAF Environmental Symposium, Rome, January 1964.
- Fleet Numerical Weather Facility 1965 Outline of synoptic numerical oceanographic analysis and forecasting programs at U.S. Fleet Numerical Weather Facility. FNWF Tech. Memo No. 5.
- Holl, M.M. 1963 Scale-and-pattern spectra and decompositions, Tech. Memo No. 3, Meteorology International, Monterey, Calif.
- Hubert, W.E. 1964 Operational forecasts of sea and swell. 1st U.S. Navy Symp. on Military Oceanogr. Proc. 113-124.
- Hubert, W.E. 1964 Computer produced synoptic analyses of surface currents and their application for navigation. Presented 1964 National Marine Navigation Meeting, San Francisco, Dec 1964.
- Hubert, W.E. 1965 U.S. Fleet Numerical Weather Facility activities relating to sea-air interactions on synoptic scale. FNWF Tech. Note No. 5.



- Schroeder, E.H. 1963 North Atlantic temperatures at a depth of 200 meters. Serial Atlas of the Marine Environment. Folio 2 Am. Geogr. Soc.
- Wolff, P.M. 1964 Operational analyses and forecasting of ocean temperature structure. 1st U.S. Navy Symp. on Military Oceanogr. Proc. 171-195.
- Wolff, P.M., T. Laevastu and W.E. Hubert 1964 Numerical scale and pattern separation of sea surface temperature for the Northern Hemisphere. FNWF Tech. Note No. 3.
- Wolff, P.M., T. Laevastu and J. Russell 1965 Short-term fluctuations of sea surface temperature, their magnitudes, causes and effects. FNWF Tech. Note No. 6.
- Wolff, P.M., L.P. Carstensen and T. Laevastu 1965 Analyses and forecasting of sea surface temperature. FNWF Tech. Note No. 8.



PREDICTION OF SUMMER THERMOCLINE DEPTH OFF MISSION BEACH

by

James L. Cairns and E. C. LaFond

U. S. Navy Electronics Laboratory, San Diego, California

.



## PREDICTION OF SUMMER THERMOCLINE DEPTH OFF MISSION BEACH

by

James L. Cairns and E. C. LaFond  
U. S. Navy Electronics Laboratory, San Diego, California 92152

### INTRODUCTION

A strong thermocline occurs, during the summer, in the ocean off Southern California. Vertical oscillations of the thermocline, as high as 50 feet, have been measured. It is important to the Navy to acquire more knowledge of this phenomenon in view of its importance to naval operations. This is due to the facts that the depth, strength, and general nature of the thermocline influence the propagation and transmission of underwater sound; the refraction properties of the gradient layer differ from those of the surrounding ocean; and the water, above and below the thermocline, may move in opposite directions or at varying speeds.

Within this thermocline is normally a high plankton content, which hampers visual or optical observation. Therefore a prediction of the thermocline depth in this region is valuable to the Navy. This study presents a new insight into the vertical motion of the water layers associated with the Southern California offshore summer thermocline, and provides a procedure for predicting its depth within usable limits.

### DATA COLLECTION

The thermal structure data for this study were obtained from the USNEL Oceanographic Research Tower located about a mile off Mission Beach, California (Fig 1). Daily bathythermograph records have indicated that a thermocline becomes established along the Southern California coast by the end of March, reaches a well-developed state by mid-May, and remains strong until late September. During the May-August period, the vertical thermal gradient within the layer is on the order of  $0.5^{\circ}\text{F}$  per foot.

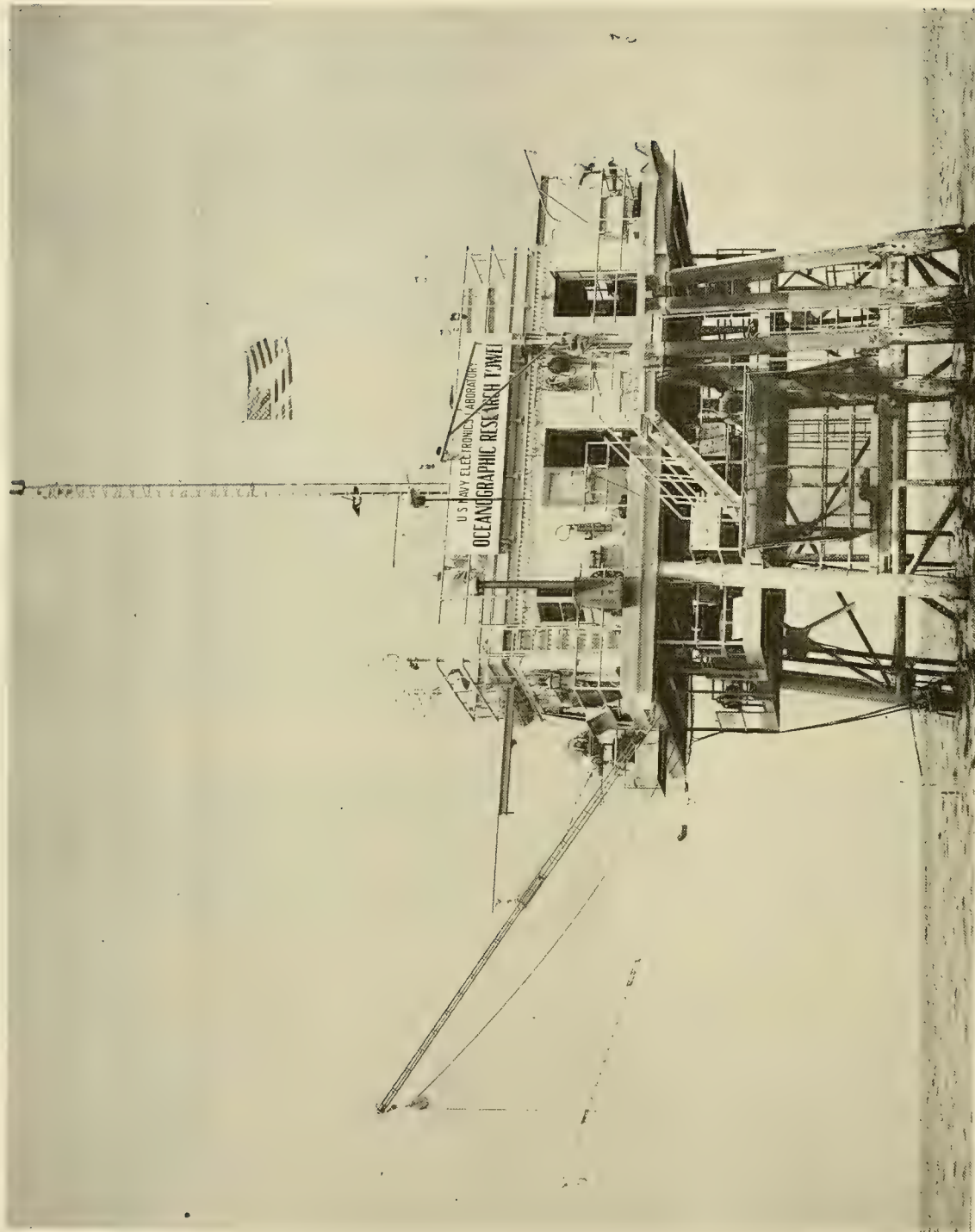


FIGURE 1 U. S. NAVY OCEANOGRAPHIC RESEARCH TOWER, SHOWING  
DEPLOYMENT OF ISOTHERM FOLLOWERS



For this study four months of nearly continuous thermocline depth data were collected using isotherm followers (LaFond 1961), instruments which follow and record the depth of an isotherm as it moves with the thermocline. Three such devices, suspended from booms on the tower, were operated throughout the May-August period (1961), when the gradient was the strongest. Supplemental wind\* and tide\*\* data taken nearby during the same period were used to determine the influence of these forces on the thermal structure.

#### Data

The nearly continuous recording of the depth of an isotherm in the middle of the thermocline showed that the thermocline undergoes high-amplitude vertical oscillations. In addition to the short-period internal waves, these are predominantly of diurnal and semidiurnal periods. Figure 2 shows a typical example of 3 days of recorded isotherm depth together with the corresponding period of wind and tide data. These thermocline oscillations are about 30 feet high, but during other periods they may measure as much as 50 feet in height at the Mission Beach Site.

The normal summer wind off Mission Beach is an onshore sea breeze that develops in the morning, becomes strongest in the afternoon, and recedes in the evening. There is usually a weak, offshore breeze in the early morning. Thus the dominant wind cycle is diurnal.

The tide has a semidiurnal cycle with a mean range of 3.6 feet.

#### DATA ANALYSIS

According to the wind transport theory formulated in 1902 by V. W. Ekman (1905), the total mass transport by the wind, in the open

\*The wind was recorded at the U. S. Weather Bureau Station at Lindbergh Field, 4 1/2 miles from the tower.

\*\*The tide was measured at the Scripps Institution of Oceanography pier near La Jolla, 6 miles from the tower.

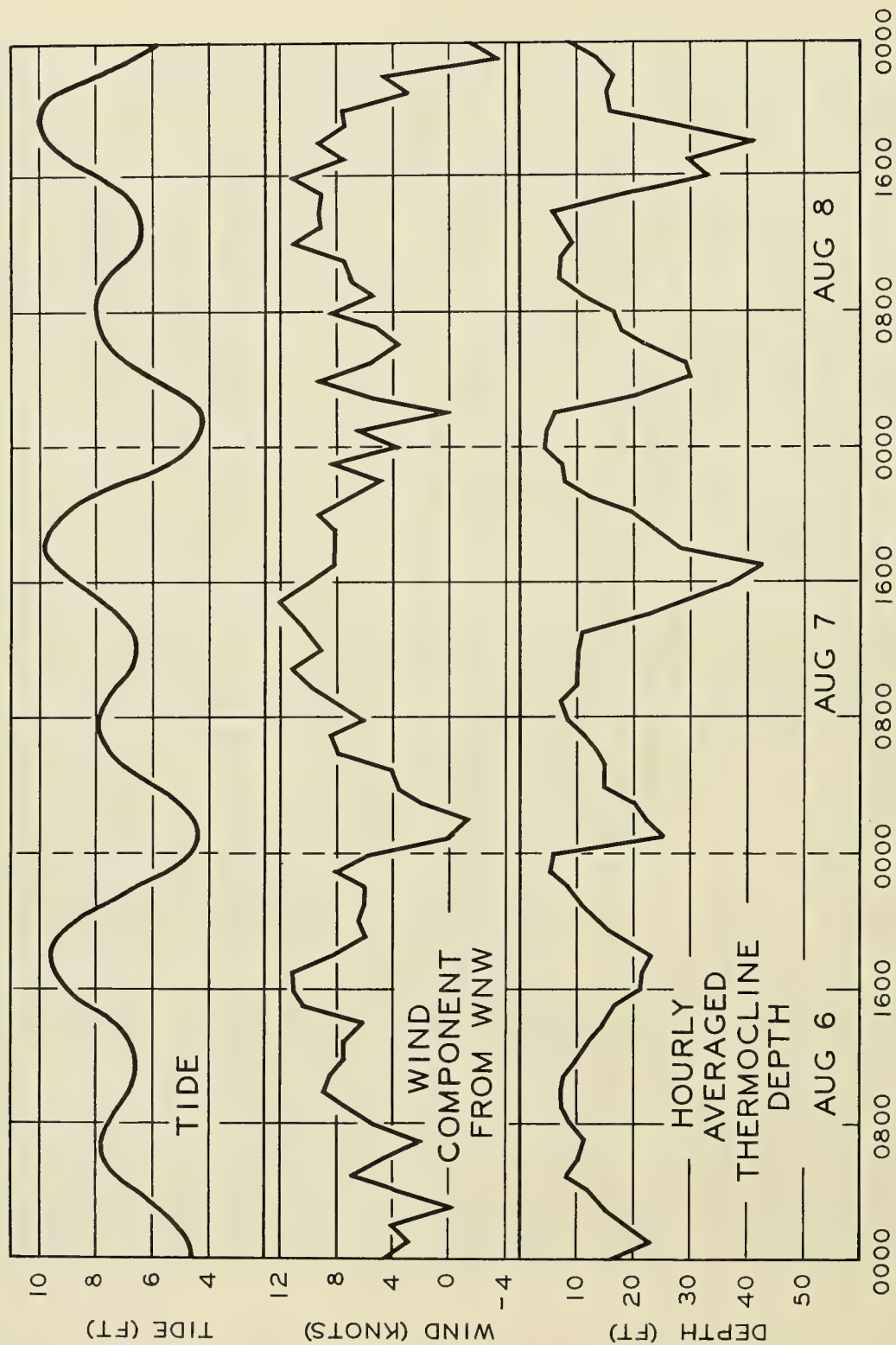


FIGURE 2 COMPARISON OF THREE TYPICAL DAYS OF THERMOCLINE DEPTH, WIND, AND TIDE

sea, is directly proportional to the square of the wind velocity and is at right angles to the wind regardless of (1) the depth to which the wind current reaches and (2) the variations of eddy viscosity with depth (Sverdrup, et al, 1942). In the northern hemisphere this transport is directed 90° to the right of the wind. Thus a wind blowing to the north in the nearshore region of a western coast creates a net transport toward the coast in the upper layers. The boundary presented by the coast, however, prohibits an eastward flow of the water. It should be expected then that an accumulation of surface water would occur in the coastal region, accompanied by a downward bending of the isothermal and isohaline surfaces along the coastline (Fig 3A). A wind blowing toward the equator along the same coastline should create an offshore transport in the upper layers and a corresponding upward bending of the isothermal and isohaline surfaces along the coast (Fig 3B).

To examine the data from the Mission Beach site for Ekman transport effects, daily averages of the continuous thermocline depth measured by the isotherm followers were made. The 24-hour averages are desirable, in that they minimize any influences of the diurnal and semidiurnal tidal oscillations. Corresponding daily averages of the wind velocity components parallel to the coast (along the WNW-ESE axis) were computed from the hourly measured wind data and compared to the daily averaged thermocline depths. Figure 4 reveals that the isothermal surfaces in this coastal location respond to the wind in the manner predicted by the Ekman theory. The mathematical relationship between the two curves may be expressed as

$$D = 36 - 2.6 W_{wnw}$$

where D is the depth in feet to the center of the thermocline and  $W_{wnw}$  is the wind velocity component in knots parallel to the coast, but from the previous day. It is easily shown that the dependence of the gradient depth on the first power of the wind velocity corresponds with the dependence of the volume transported on the square of the wind velocity, as predicted by theory.

#### Wind Lag

Figure 4 shows that there is a long-term, upward trend of the thermocline which is accounted for, at least in part, by the wind.

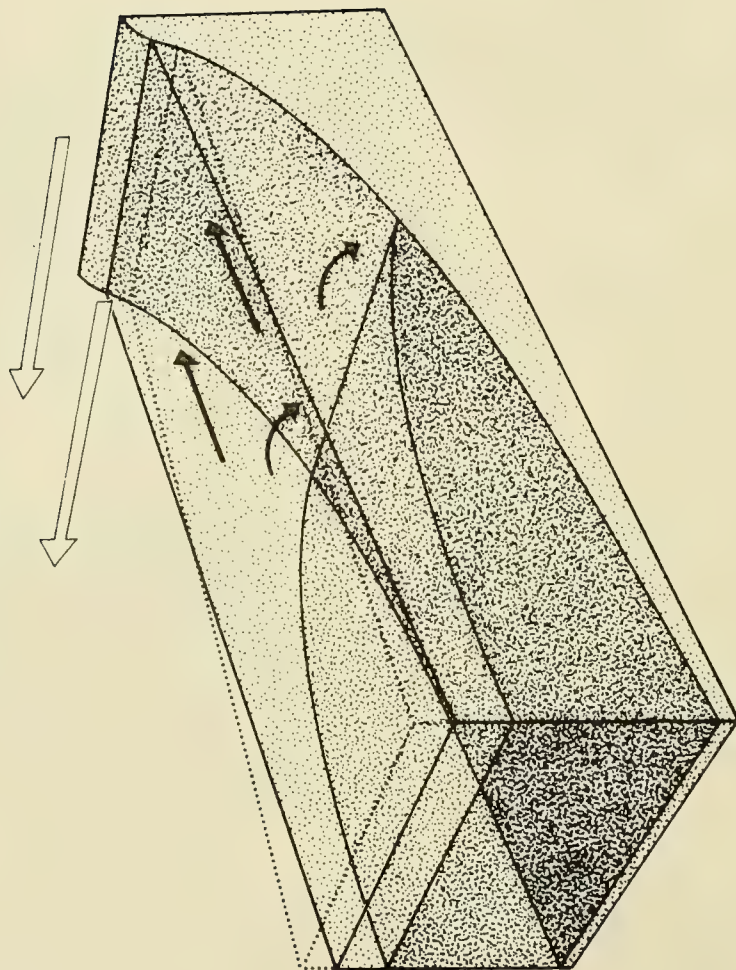


FIGURE 3a SCHEMATIC REPRESENTATION OF THERMOCLINE  
ORIENTATION VERSUS WIND DIRECTION



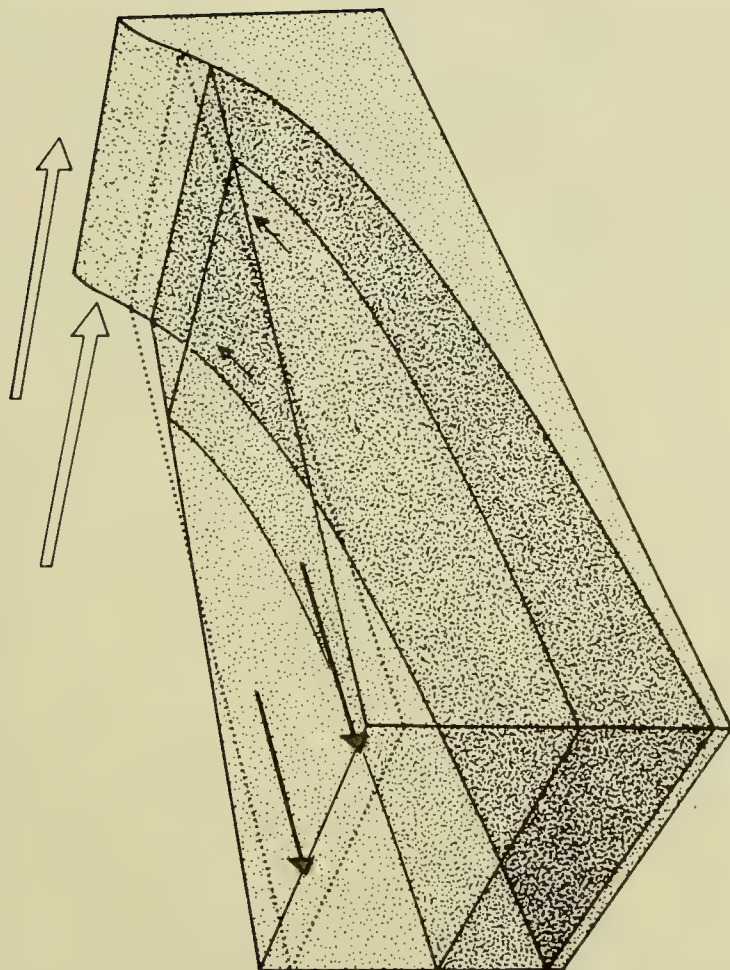


FIGURE 3b SCHEMATIC REPRESENTATION OF THERMOCLINE  
ORIENTATION VERSUS WIND DIRECTION

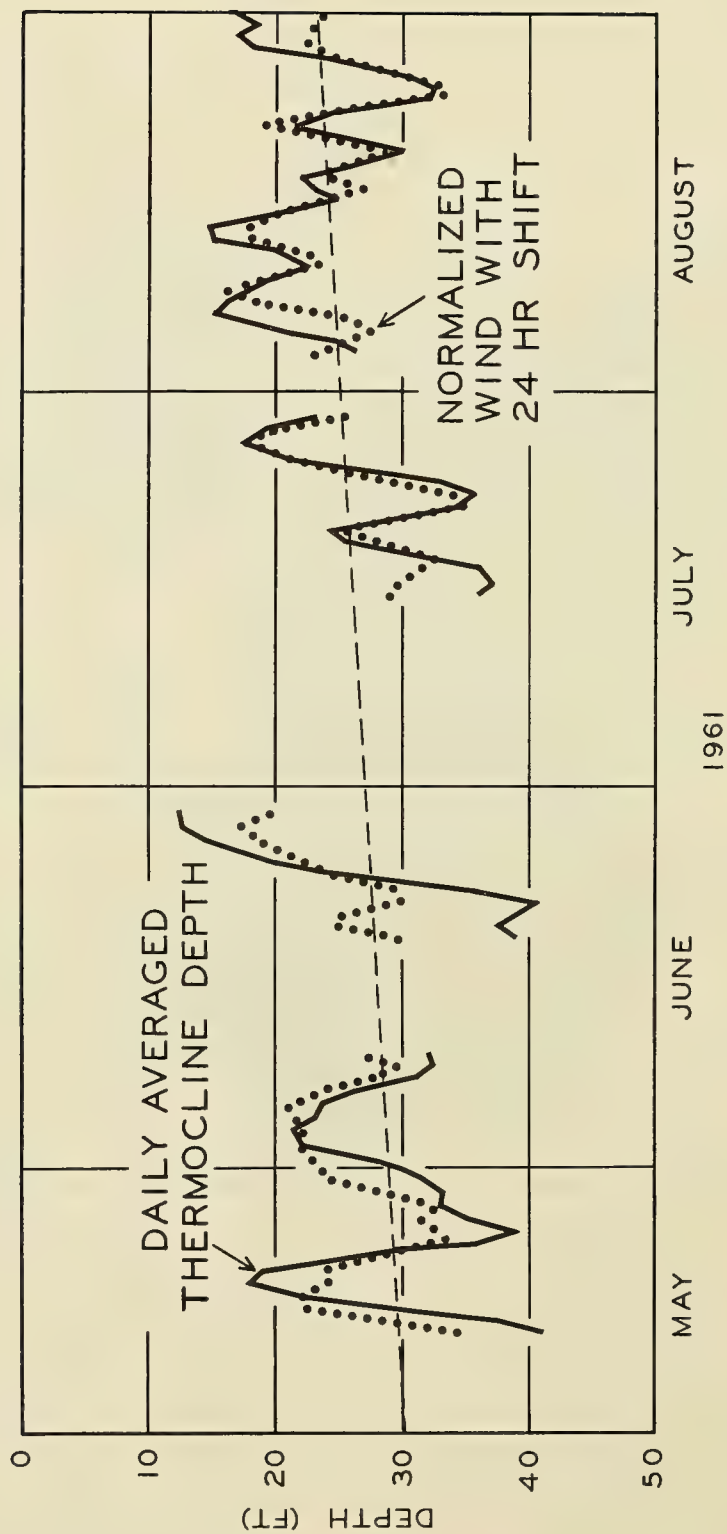


FIGURE 4 MEASURED THERMOCLINE DEPTH AND WIND VELOCITY

There are also 4- to 5 day oscillations of the thermocline, which have counterparts in the wind and are a result of Ekman transport.

The Ekman transport theory is formulated assuming that the wind and current systems have attained steady-state conditions. To examine the application of the wind transport theory to relatively short-term phenomena, a phase comparison was made between the average diurnal thermocline depth cycle and the average diurnal wind cycle for the month of August. It was found that the depth changes lagged behind the wind changes by 14 to 16 hours. Using this value as an approximation of the response time of depth to wind changes, we can rewrite the linear dependence equation as: ✓

$$D_{w,t} = 36 + 2.6 \bar{W}_{t-15} \quad \text{Equation (1)}$$

where

$D_{w,t}$  is the wind-predicted depth in feet to the center of the thermocline at time  $t$ , and

$$\bar{W}_{t-15} = 1/4 (2W_{t-15} + W_{t-14} + W_{t-16})$$

where

$W_{t-x}$  is the hourly average wind component from the WNW at  $x$  hours prior to time  $t$ .

#### Wind Direction

To confirm that the raising and lowering of the thermocline (Fig 4) are governed by the wind component parallel to the coastline, and do not correlate better with the wind normalized along some slightly different axis, a directional search was made in which the depths predicted by equation 1 were compared with the corresponding measured thermocline depths at hourly points throughout a 33-day period. The results, presented as the standard deviation between the measured and predicted points as a function of normalization direction, are shown in Figure 5.

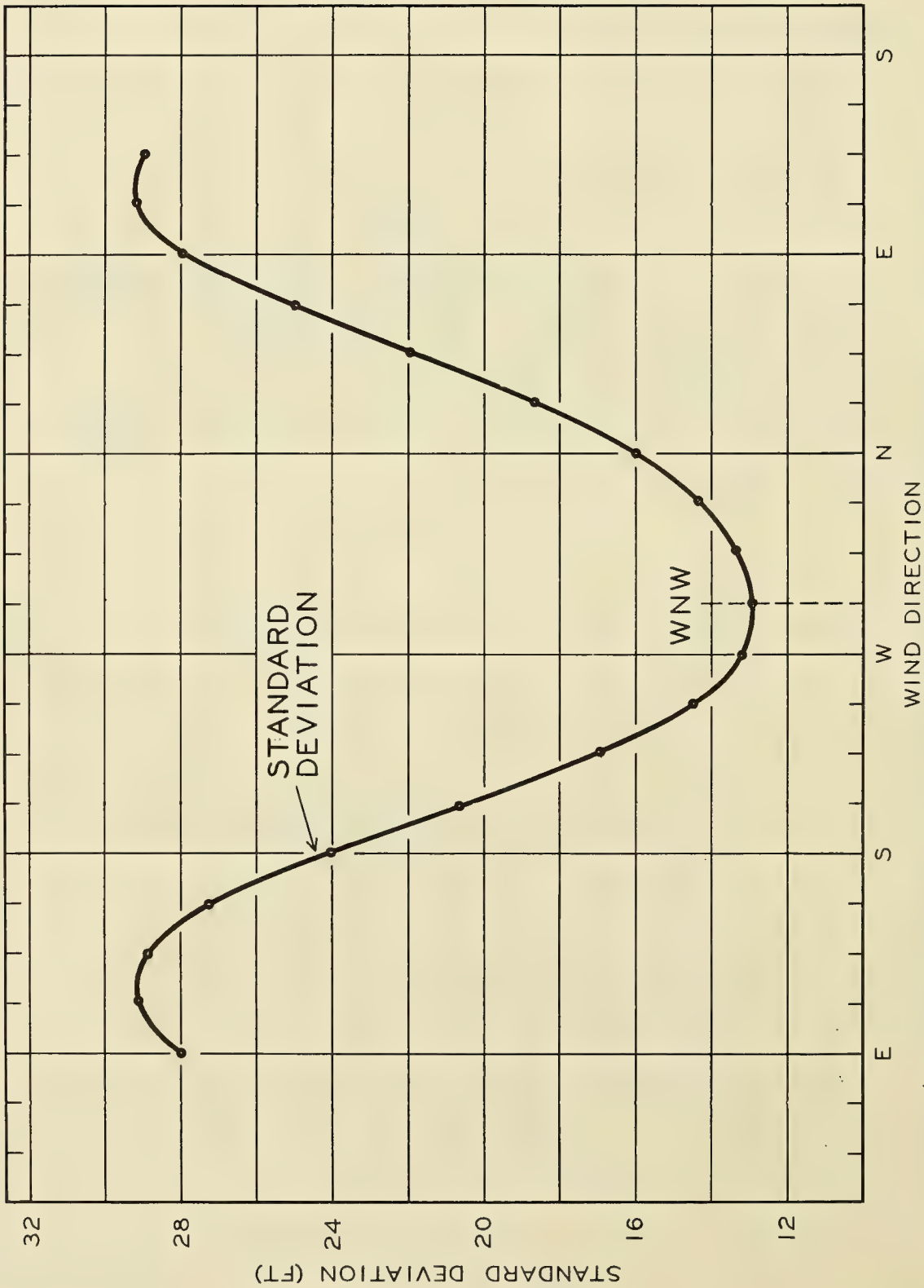


FIGURE 5 STANDARD DEVIATION BETWEEN OBSERVED THERMOCLINE DEPTHS AND THOSE CALCULATED FROM VARIOUS DIRECTIONAL COMPONENTS OF THE WIND



The best agreement between the two variables is obtained when the wind component from the WNW is used.

The standard deviation is  $\pm 13$  feet when the axis parallel to the coast is used for normalization.

It should be mentioned that although equation (1) was used in the direction search, the computed direction of best fit is independent of the constants in the equation. That is, the parameters of the equation have no effect on the choice of optimum direction since the equation could simply be written as:

$$D_{w,t} = -\bar{W}_t - 15$$

without any change of the locations of the maxima and minima of the curve as a function of direction.

#### Tidal Relation to Isotherm Depth

To further examine the data for short-term wind transport effects, it was necessary to determine the extent of tidal influences on the thermocline motion. To do this, equation (1) was applied to the August diurnal wind cycle to generate a diurnal depth cycle predicted as a function of wind only. The resulting curve was then compared with the measured diurnal thermocline depth cycle averaged over the same period (Fig 6). The pointwise difference between these two curves was then computed and compared with that of the August diurnal tidal cycle. Except for a small additive constant (which has been removed), the pointwise differences between the measured and wind-predicted depth cycles match the tidal cycle almost exactly (Fig 7).

According to this fit, the internal tide is five times\* as great in amplitude as the surface tide and lags behind it by 3 hours. Using this

\*The factor of 4 appearing in equation (2) seems to disagree with this. However, equation (2) predicts the depth from the surface, which is itself oscillating with tidal amplitude.

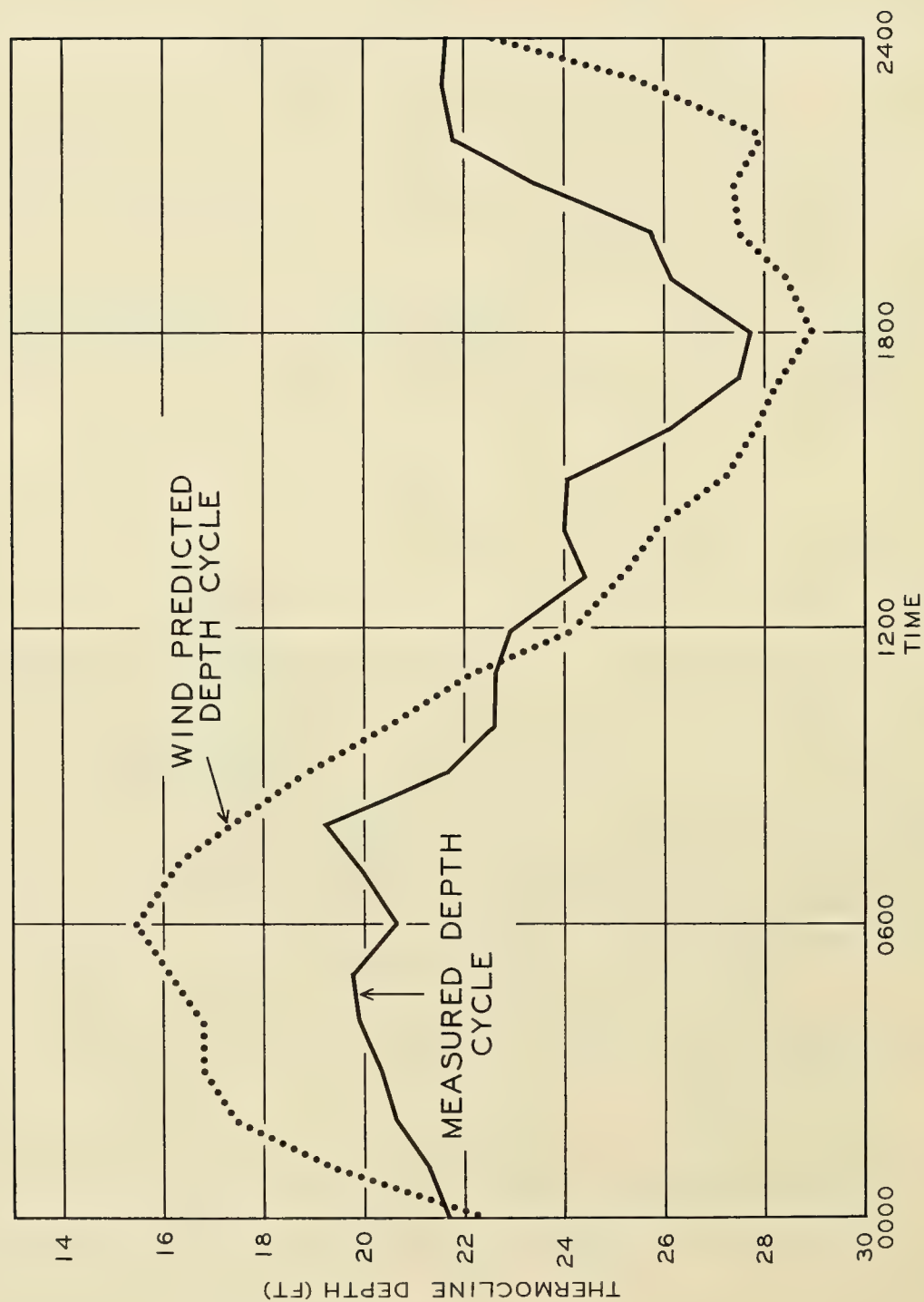


FIGURE 6 COMPARISON OF DIURNAL CYCLE OF THERMOCLINE DEPTH AND  
PREDICTED DEPTH BASED ON WIND FROM A WNW DIRECTION

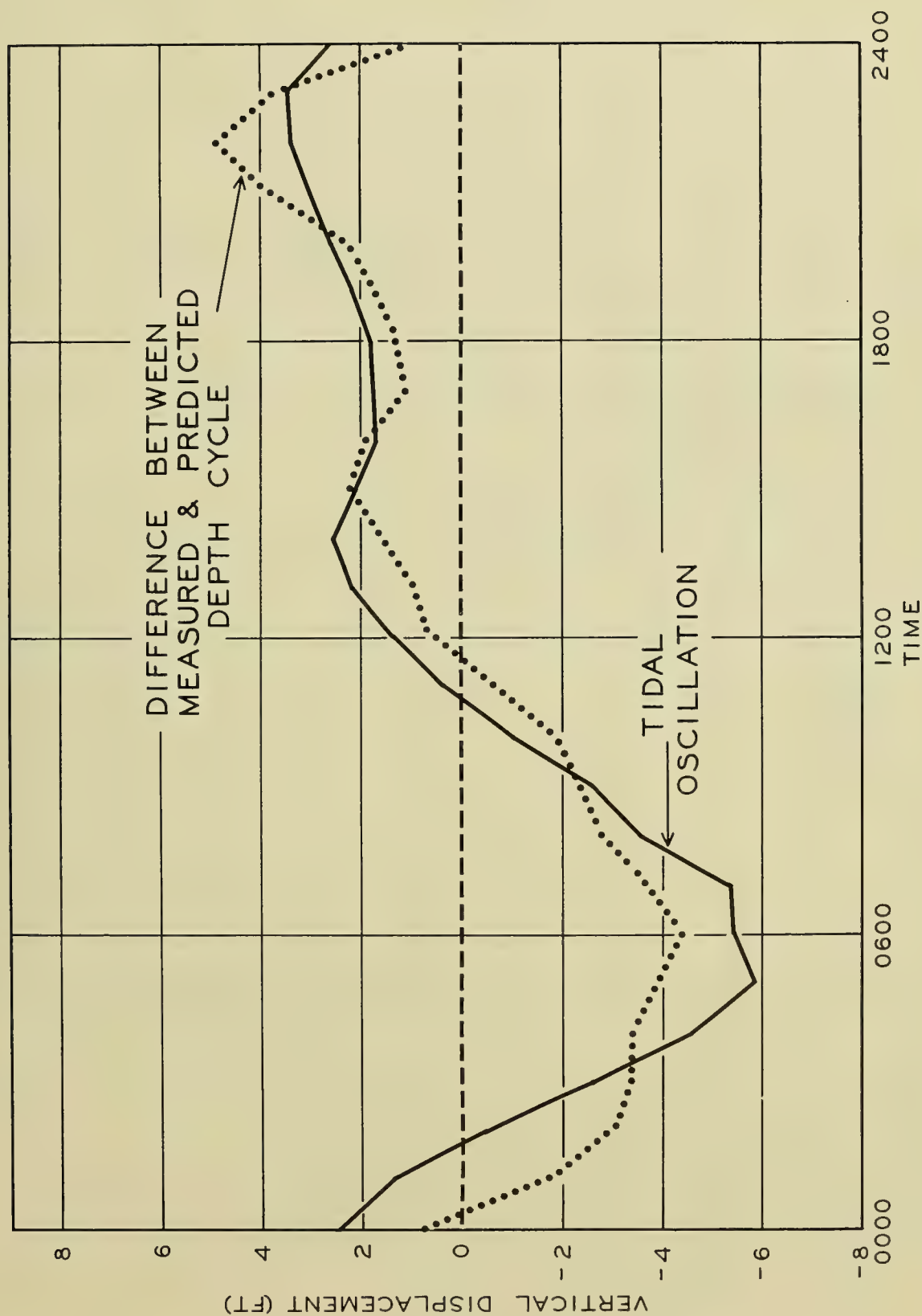


FIGURE 7 COMPARISON OF THE DIURNAL CYCLE OF TIDE HEIGHT AND THAT OF THE DIFFERENCE OF PREDICTED THERMOCLINE DEPTH AND MEASURED THERMOCLINE DEPTH

information, we can rewrite the depth prediction equation to contain a tidal correction term in addition to the wind effect term

$$D_{W,T,t} = 37.5 - 2.6 \bar{W}_{t-15} + 4 (\bar{T} - T_{t-3}) \quad \text{Equation (2)}$$

where 37.5 is the zero wind depth (in feet) adjusted to account for the constant discrepancy present in equation (1) and  $(\bar{T} - T_{t-3})$  is the tidal oscillation about the mean 3 hours prior to time  $t$ .

A comparison of the diurnal depth cycle, as predicted by equation (2), with the measured diurnal depth cycle shows very close agreement (Fig 8). The tidal effect on the predicted diurnal depth tends to decrease the high amplitude diurnal cycle that would be expected if only wind effects were considered.

In addition to the results obtainable from the essentially quantitative survey, one fact of thermocline motion has been brought out by direct inspection of the 4-month record of thermocline depth, i.e., tidal oscillations about the mean thermocline depth decrease in amplitude as the general level of the thermocline approaches either the upper or lower water boundaries. This has also been observed to occur for shorter period internal waves (LaFond, 1961).

## DISCUSSION OF ANALYSIS

To determine more clearly influences of wind and tide on thermocline motion, and to establish whether or not significant features of the motion occur that are not directly related to either wind or tide, a power spectra analysis was carried out on 33 days of unbroken hourly data. The spectra that were calculated are listed below and presented in Figures 9 and 10:

Hourly measured thermocline depth data,  $(D_{m,t})$   
 Hourly predicted depths using equation (1)  $(D_{w,t})$   
 Hourly values of  $D_{m,t} - D_{w,t} = \Delta_t$   
 Hourly measured surface tide,  $T_t$ .

A study of the spectra reveals a long-term trend of the thermocline motion that is partially, but not entirely, a wind effect. This is



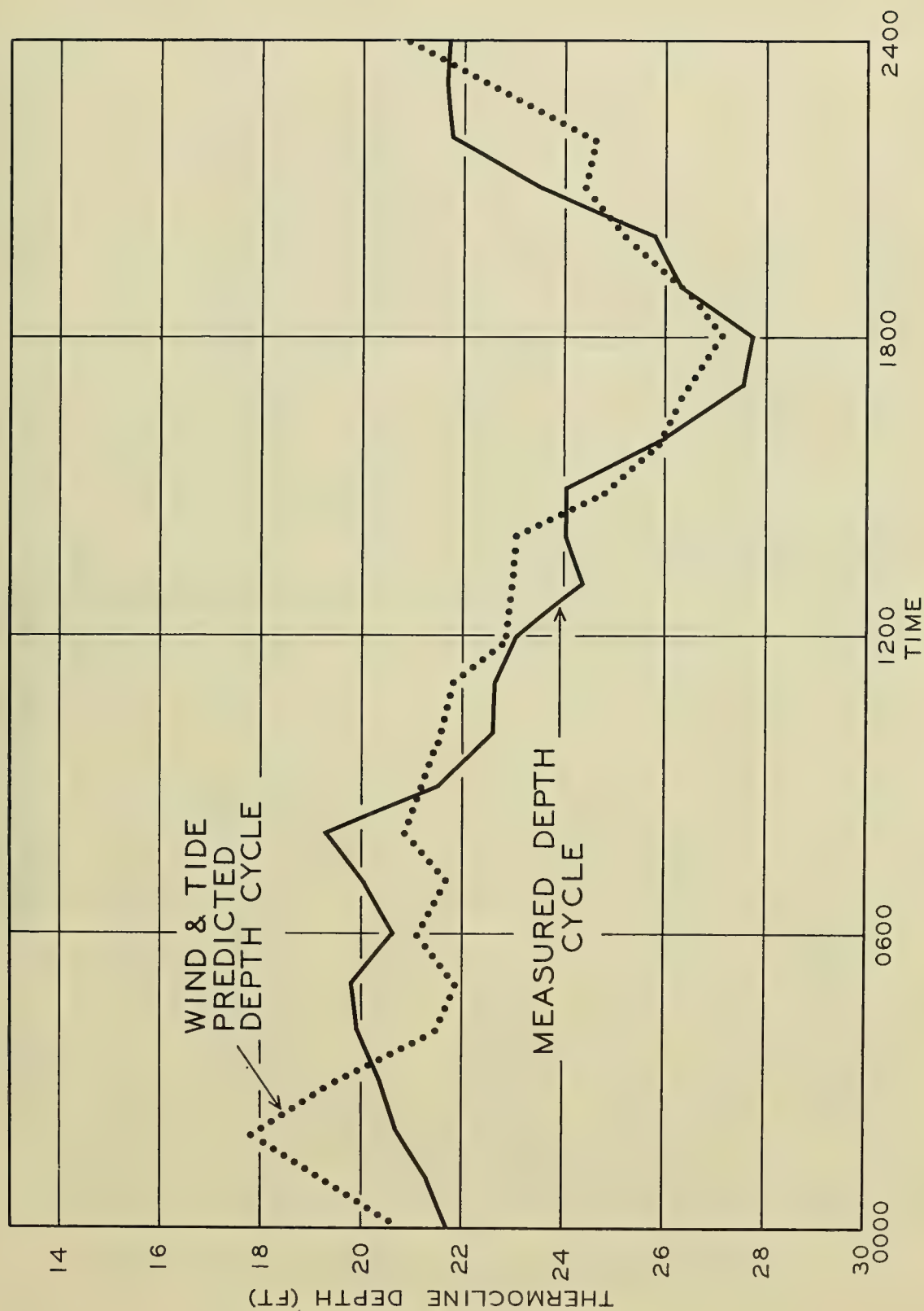


FIGURE 8 COMPARISON OF DIURNAL CYCLE OF MEASURED THERMOCLINE DEPTH AND PREDICTED DEPTH BASED ON WIND AND TIDE

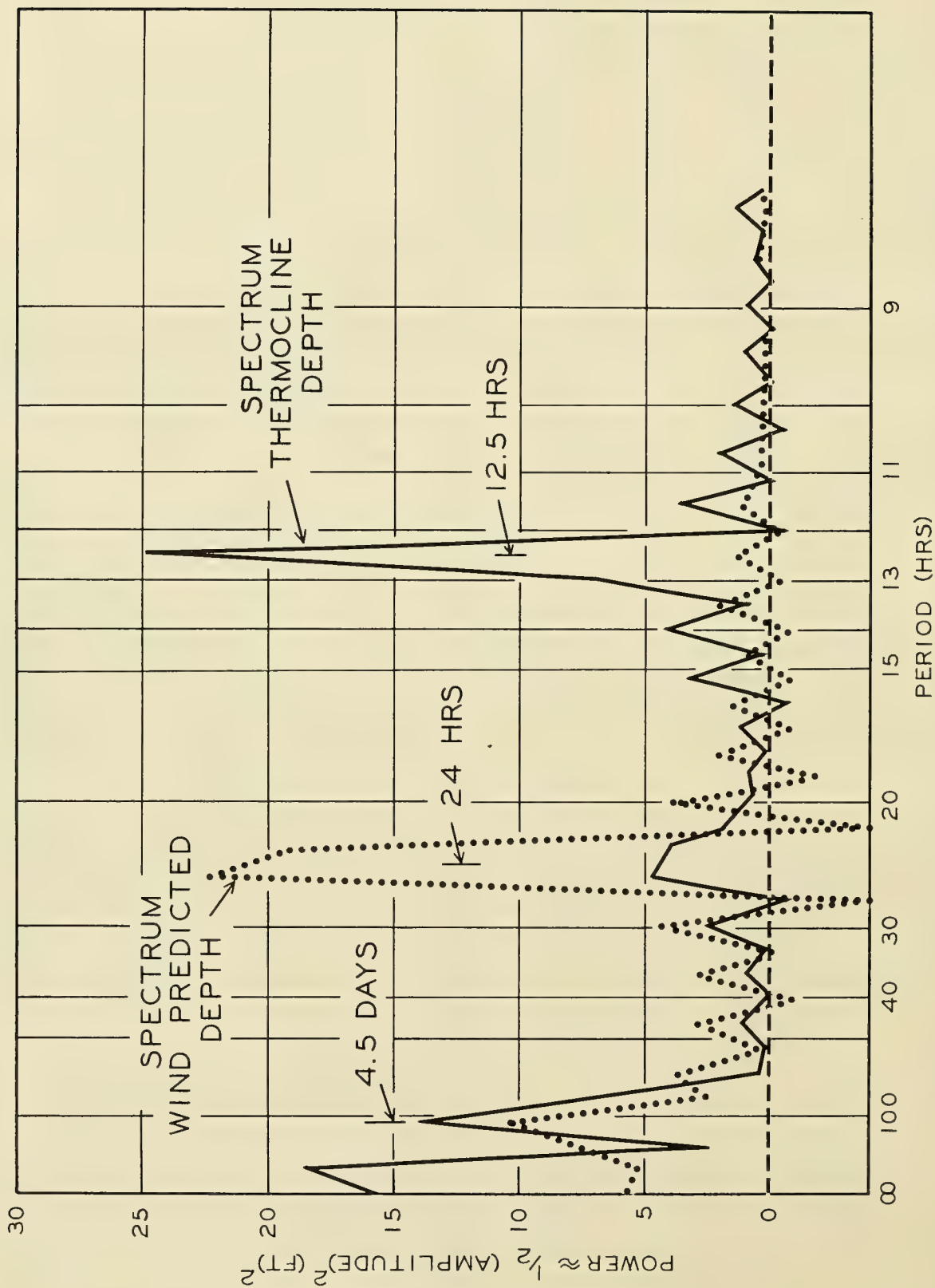


FIGURE 9 COMPARISON OF POWER SPECTRUM OF MEASURED THERMOCLINE DEPTH AND PREDICTED DEPTH

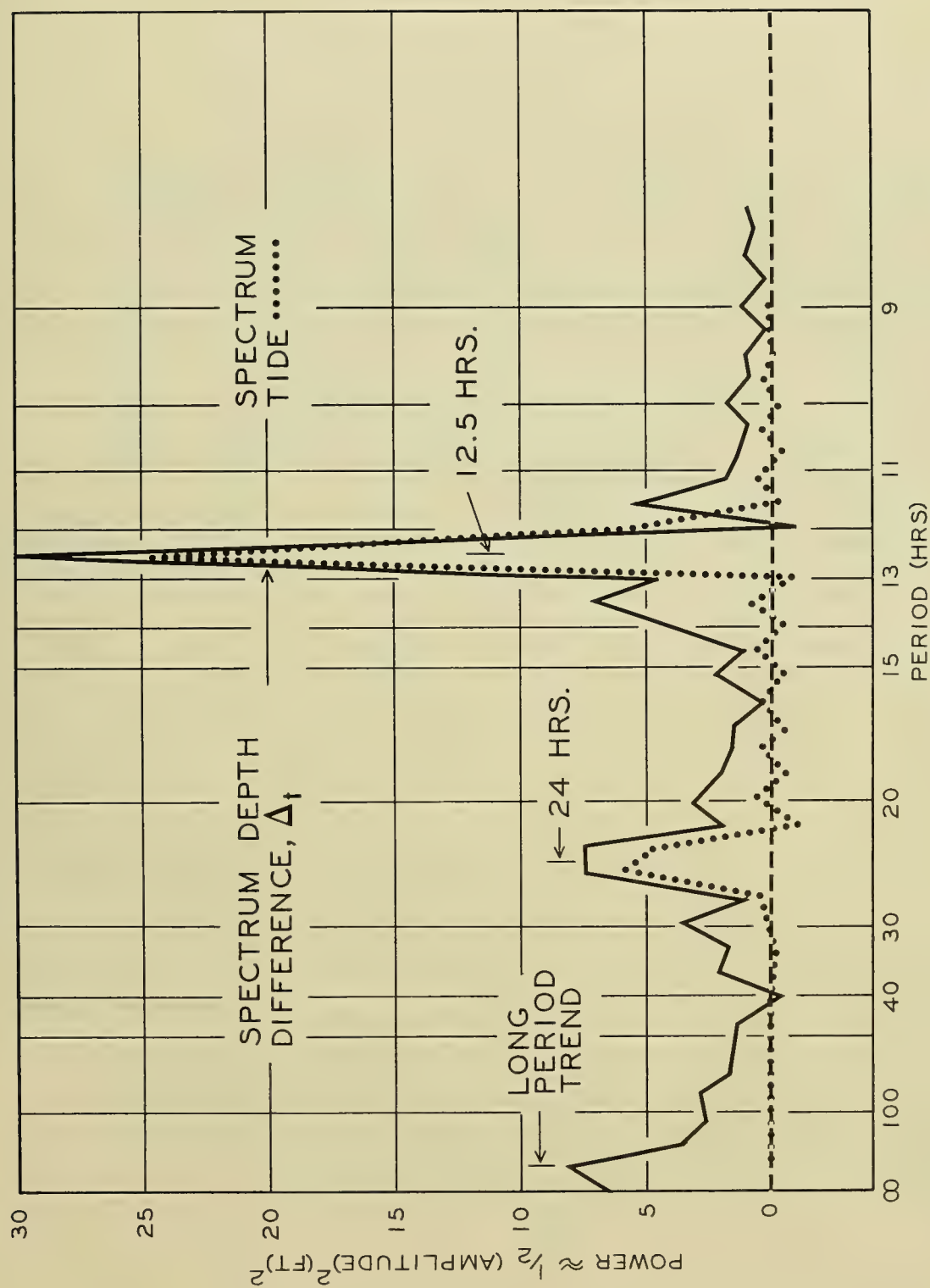


FIGURE 10 COMPARISON OF POWER SPECTRUM OF THE DIFFERENCE BETWEEN PREDICTED DEPTH OF THE THERMOCLINE BASED ON WIND AND MEASURED DEPTH, AND TIDE HEIGHT

reasonable, because there is likely to be a long-term trend in the motion related to the annual heating cycle. In addition, the spectra show that the dominant periods of thermocline oscillation are  $4\frac{1}{2}$  days, 24 hours, and  $12\frac{1}{2}$  hours. It can be seen that no peaks exist, in either the wind or tide spectra, that do not also appear in the measured depth spectrum. The  $4\frac{1}{2}$  day oscillation appears to be accounted for entirely by the wind and is no doubt a direct result of wind transport. The 24-hour oscillation, however, is over-predicted on the basis of wind alone. That is, the diurnal depth cycle as predicted by wind transport is of higher amplitude than that actually observed. This over-prediction appears as the 24-hour peak in the  $\Delta_t$  spectrum in Figure 10. This is compensated for by the 24-hour peak in the tidal spectrum. This result is in complete agreement with the conclusion reached earlier, that the diurnal thermocline oscillation is diminished by the tide. The  $12\frac{1}{2}$  hour oscillation of the thermocline is seen to be entirely an effect of the semidiurnal component of the tide. It was concluded earlier that the internal tide is four to five times as great as the surface tide. This result is also inferred from the power spectra study. If it is assumed that the oscillations under study are sinusoidal in nature, then the spectral ordinates of the various peaks may be set equal to one-half of the squares of the amplitudes. The tidal spectrum in Figure 10 has been multiplied by  $4^2$ , which is the factor necessary to normalize it to the  $\Delta_t$  spectrum. Thus, the spectra also indicate that the internal tide is four or five times as great in amplitude as the surface tide.

To confirm the 3-hour phase lag between the surface and internal tides, a cross-correlation of the tide data and the  $\Delta_t$  difference data was computed. This correlation supported the original estimate of a 3-hour phase shift between the tides.

## APPLICATION

The information thus far gained as to the nature and magnitude of the thermocline vertical oscillations finds immediate application in predicting the thermocline depth. It has been shown (Fig 4) that the daily average depth is adequately described by a linear relationship involving only the wind. The standard deviation between the two curves of Figure 4 is  $\pm 5$  feet. For more detailed predictions, equation (1)



was used for hourly points over a 33-day period, with a standard deviation of  $\pm 13$  feet (Fig 5). To check the validity of the prediction scheme, equation (1) was applied to the hourly wind data points and the results compared to the hourly measured thermocline depth averages throughout the entire May-August period. The results were equally good for the entire period; the  $\pm 13$  feet deviation calculated for the month of August is probably typical of the accuracy that can be expected of wind-based predictions.

A similar check on the thermocline depths predicted as a function of wind and tide did not support the validity of equation (2). Instead, it was found that while the surface and internal tides are closely coupled in frequency and phase, they are only loosely coupled in amplitude. Both schemes previously used to determine the ratio of surface to internal tidal amplitudes have used long-term averages, and thus have failed to account for variations in the ratio. Results indicate, however, that the variations become quite large; these are as yet unpredictable, but it is believed that the variations are at least partially a function of the density gradient across the thermocline. The determination of this effect is one purpose of a planned experimental program; however, the depth prediction capabilities of equation (1) are sufficient for most practical purposes.

## SUMMARY AND CONCLUSIONS

This study has shown that the gross vertical migrations of the thermocline along the coast are driven by the winds. Various modes of layer motion were found to be:

1. a long-term, upward trend throughout the summer, which occurs in response to a similar trend in the wind, and may be related to the annual heating cycle,
2. an oscillation of  $4\frac{1}{2}$  day period, not previously known to be present in the thermocline motion, which is a direct result of a  $4\frac{1}{2}$  day cycle in the wind,
3. a diurnal oscillation that is also a wind effect, although somewhat decreased by the diurnal tidal cycle, and
4. a semidiurnal oscillation of tidal origin.

It has been demonstrated at the Mission Beach Site, and on the basis of wind alone, that it is possible to forecast the daily average thermocline depth with a standard deviation of  $\pm 5$  feet, and to forecast the average hourly depth with a standard deviation of  $\pm 13$  feet.

It has been established that, although the overall motion of the thermocline is in response to the wind, internal tidal oscillations are superimposed on this motion. These are shown to be frequency-coupled to the surface tide and are, on the average, about five times as great in amplitude.

The results of this program are in excellent agreement with the Ekman transport theory. It is therefore believed that the linear form of equation (1), with appropriate parameters, will be applicable to any extended coastline.

#### REFERENCES

- LaFond, E. C., 1961, "The Isotherm Follower," J. Mar. Res., 19, 1 : 33-39.
- Ekman, V. W., 1905, "On the Influence of the Earths Rotation on Ocean-Currents," Akr. Mat. Astr. Fys., 2, 11 : 52 pp.
- Sverdrup, H. U., M. W. Johnson, R. H. Fleming, 1942, The Oceans, 12 : 494-500.
- LaFond, E. C., 1961, Boundary Effects on the Shape of Internal Temperature Waves," Indian J. Met. Geophys., 12, 2 : 335-338.

THE NUMERICAL PREDICTION OF MEANDERS IN THE GULF STREAM

by

James G. Welsh

The Travelers Research Center, Inc.  
Hartford, Connecticut





# THE NUMERICAL PREDICTION OF MEANDERS IN THE GULF STREAM

by

James G. Welsh  
The Travelers Research Center, Inc.  
250 Constitution Plaza  
Hartford, Connecticut 06103

## INTRODUCTION

The equivalent barotropic model has enjoyed considerable predictive success in meteorology. That this same model can be adapted to oceanographic prediction is suggested by work of Warren (1963), in which he demonstrates that the observed meander patterns in the Gulf Stream agree remarkably well with constant potential-vorticity trajectories along the Continental Rise.

The work described here is being carried out by The Travelers Research Center, Inc., under contract to the U.S. Naval Oceanographic Office. The purpose of this work is to investigate the possibility for useful dynamical prediction of the Gulf Stream with an equivalent barotropic model especially adapted for the ocean.

## DERIVATION OF THE EQUIVALENT BAROTROPIC MODEL FOR THE OCEAN

When formulating hydrodynamic models, one must always impose certain conditions and assumptions on the theoretical fluid in order to facilitate the derivation of a practical set of mathematical equations. The equivalent barotropic model, as formulated for the ocean, is based upon these assumptions:

The fluid is incompressible.

The fluid is homogeneous.

The fluid is inviscid.

The fluid is in hydrostatic equilibrium.

The direction of the flow is independent of depth except for the possibility of reversal, but the speed may have an arbitrary variation.

The last assumption contributes "equivalent" to the model's name, since both speed and direction of a barotropic flow are independent of depth. It is further assumed that:

The fluid is bounded on top by a rigid, horizontal surface.

The fluid is bounded below by a rigid bottom with variable slope.

The flow is essentially horizontal and non-divergent and may therefore be defined by a stream function.

As a point of departure for deriving the prediction equation appropriate to the model, we start with the vorticity equation:

$$\frac{\partial \zeta}{\partial t} + \mathbf{V} \cdot \nabla (\zeta + f) + (\zeta + f) \nabla \cdot \mathbf{V} = 0, \quad (1)$$

where  $\bar{\zeta}$  is the vertical component of the relative vorticity of the current  $\mathbf{V}$ , and  $f$  is the coriolis parameter. This form of the vorticity equation does not consider the twisting effect of differential vertical advection of vorticity or the baroclinic (solenoidal) generation of relative vorticity, but does include the generation of relative vorticity by horizontal divergence in the current. Flow over a sloping bottom will cause both horizontal divergence and vertical motion that enter into equation (1); so long as this divergence and vertical motion are small, it is safe to assume that the current is essentially horizontal and non-divergent.

Since the fluid is assumed incompressible, the continuity equation can be written

$$\frac{\partial w}{\partial z} + \nabla \cdot \mathbf{V} = 0, \quad (2)$$

where  $w$  is the vertical component of the flow. The assumption that the flow is vertically constant in direction is expressed by

$$\mathbf{V}(x, y, z, t) = A(z) \bar{\mathbf{V}}(x, y, t), \quad (3)$$

where the bar operator, when applied to the flow, is defined by

$$\bar{\mathbf{V}} \equiv \frac{1}{h} \int_0^h \mathbf{V} dz. \quad (4)$$

The depth field  $h(x, y)$  is measured positive; thus the directional sense of the  $z$ -axis is reversed from the normal right-handed Cartesian coordinate system. The vertical profile parameter  $A$  is in reality also a function of  $x$ ,  $y$ , and even  $t$ , but it is permissible to limit  $A$  to variation only in the  $z$  direction. The vorticity of equation (3) is given by

$$\bar{\zeta} \equiv \mathbf{k} \cdot \nabla \times \mathbf{V} = \mathbf{k} \cdot \nabla \times (A \bar{\mathbf{V}}) = A (\mathbf{k} \cdot \nabla \times \bar{\mathbf{V}}) = A \bar{\zeta}. \quad (5)$$

Equations (3) and (5) are now substituted in the vorticity equation (1), and the result is integrated vertically with the bar operator, equation (4):

$$\frac{1}{h} \int_0^h \frac{\partial}{\partial t} (A \bar{\zeta}) dz + \frac{1}{h} \int_0^h (A \bar{\mathbf{V}}) \cdot \nabla (A \bar{\zeta} + f) dz + \frac{1}{h} \int_0^h (A \bar{\zeta} + f) \nabla \cdot (A \bar{\mathbf{V}}) dz = 0,$$

or

$$\frac{\partial \bar{\zeta}}{\partial t} \frac{1}{h} \int_0^h A dz + \bar{\mathbf{V}} \cdot \nabla \left[ \bar{\zeta} \frac{1}{h} \int_0^h A^2 dz + f \frac{1}{h} \int_0^h A dz \right] + \left[ \bar{\zeta} \frac{1}{h} \int_0^h A^2 dz + f \right] \nabla \cdot \bar{\mathbf{V}} = 0,$$

and finally,

$$\frac{\partial \bar{\zeta}}{\partial t} + \bar{\mathbf{V}} \cdot \nabla (\bar{A}^2 \bar{\zeta} + f) + (\bar{A}^2 \bar{\zeta} + f) \nabla \cdot \bar{\mathbf{V}} = 0, \quad (6)$$

as

$$\frac{1}{h} \int_0^h A dz = 1, \quad \frac{1}{h} \int_0^h A^2 dz = \bar{A}^2. \quad (7)$$

Equation (6) is the vorticity equation of the vertically-averaged velocity  $\bar{\mathbf{V}}$ . By being prescribed in a special manner, the vertical variability of the current has been integrated out of the vorticity equation leaving only the parameter  $\bar{A}^2$ . An expression for the divergence  $\nabla \cdot \bar{\mathbf{V}}$  of the mean flow must be derived to accomodate the effect of bottom topography.

By expanding the expression for  $\nabla \cdot \bar{\mathbf{V}}$ , we have:

$$\nabla \cdot \bar{\mathbf{V}} = \nabla \cdot \left[ \frac{1}{h} \int_0^h \mathbf{V} dz \right] = -\frac{\nabla h}{h} \cdot \left[ \frac{1}{h} \int_0^h \mathbf{V} dz \right] + \frac{1}{h} \nabla h \cdot \mathbf{V}_h + \frac{1}{h} \int_0^h \nabla \cdot \mathbf{V} dz,$$

or

$$\nabla \cdot \bar{\mathbf{V}} = -\frac{1}{h} \bar{\mathbf{V}} \cdot \nabla h + \frac{1}{h} \mathbf{V}_h \cdot \nabla h + \frac{1}{h} \int_0^h \nabla \cdot \mathbf{V} dz. \quad (8)$$

The last term on the right side of equation (8) can be evaluated by applying the bar operator, equation (4), to the continuity equation (2):

$$\frac{1}{h} \int_0^h \nabla \cdot \mathbf{V} dz = \frac{1}{h} \int_0^h \left( -\frac{\partial w}{\partial z} \right) dz = \frac{1}{h} (w_0 - w_h). \quad (9)$$

The vertical velocities  $w_0$ , at the top of the fluid, and  $w_h$ , at the bottom of the fluid, must satisfy the kinematic boundary condition that there be no cross-boundary flow; therefore:

$$w_0 = 0, \quad w_h = \mathbf{V}_h \cdot \nabla h. \quad (10)$$

When equations (8), (9), and (10) are combined, we have the following:

$$\nabla \cdot \bar{\mathbf{V}} = -\frac{1}{h} \bar{\mathbf{V}} \cdot \nabla h = -\bar{\mathbf{V}} \cdot \nabla \log h. \quad (11)$$

Substitution of equation (11) into the integrated vorticity equation (6) yields the equation

$$\frac{\partial \bar{\zeta}}{\partial t} + \bar{\mathbf{V}} \cdot \nabla (\bar{A}^2 \bar{\zeta} + f) - (\bar{A}^2 \bar{\zeta} + f) \bar{\mathbf{V}} \cdot \nabla \log h = 0,$$

or

$$\frac{\partial \bar{\zeta}}{\partial t} + \bar{\mathbf{V}} \cdot \nabla (\bar{A}^2 \bar{\zeta} + f - f_0 \log h) = 0, \quad (12)$$

where  $f_0$  is an average value of the coriolis parameter for the fluid. Equation (12) is the mathematical relationship which describes the equivalent barotropic model for the ocean. This equation differs from that for a simple barotropic model in the terms  $\bar{A}^2$ , which is a measure of the vertical variability of the current, and  $-f_0 \log h$ , which results from the sloping bottom topography. In the application of equation (12), a stream function  $\bar{\psi}(x, y, t)$  is introduced, from which the vertically-averaged current and vorticity can be derived. The resulting model equation is then

$$\nabla^2 \frac{\partial \bar{\psi}}{\partial t} + \mathcal{J}(\bar{\psi}, \bar{A}^2 \nabla^2 \bar{\psi} + f - f_0 \log h) = 0, \quad (13)$$

where  $\nabla^2$  is the Laplacian operator  $\nabla \cdot \nabla$  and  $J$  is the Jacobian with respect to  $x$  and  $y$ .

## PERTURBATION ANALYSIS

To subject the model to perturbation analysis, the  $x$ -axis and a constant basic current  $U$  are aligned parallel to isopleths of  $g = f - f_0 \log h$ . A velocity perturbation along the gradient of  $g$  is introduced in the form:

$$v = F e^{ik(x-ct)}, \quad (14)$$

where  $i = \sqrt{-1}$ ,  $k$  is the wave number of the perturbation, and  $c$  is the phase velocity of the perturbation. The total velocity is then:

$$\bar{V} = U i + v j, \quad (15)$$

and the relative vorticity is given by:

$$\bar{\zeta} = \frac{\partial v}{\partial x} - \frac{\partial U}{\partial y} = \frac{\partial v}{\partial x} = ik F e^{ik(x-ct)} = ik v. \quad (16)$$

Also note that

$$\frac{\partial \bar{\zeta}}{\partial t} = ck^2 v, \quad \frac{\partial \bar{\zeta}}{\partial x} = -k^2 v. \quad (17)$$

Substituting these perturbation relationships into the model, equation (12) yields:

$$\frac{\partial \bar{\zeta}}{\partial t} + U \frac{\partial}{\partial x} (\bar{A}^2 \bar{\zeta}) + v \frac{\partial \bar{\zeta}}{\partial y} = 0,$$

or

$$ck^2 v - k^2 \bar{A}^2 U v + v \gamma = 0,$$

which finally gives:

$$k^2 (c - \bar{A}^2 U) + \gamma = 0, \quad (18)$$

where  $\gamma = \partial g / \partial y$ . Equation (18) is similar to Rossby's long-wave speed formula, except for  $\bar{A}^2$  and  $\gamma$ ;  $\gamma$  includes the effect of the sloping bottom as well as the earth's rotation. Note here that the effect of bottom topography is to enhance (or diminish) the usual  $\beta$  effect, and  $\bar{A}^2$  effectively increases the strength of the basic flow  $U$ .

For the special case of stationary perturbation, the phase velocity  $c$  is zero. Solving equation (18) for the stationary wavelength  $\lambda_s = 2\pi/k_s$  yields:

$$\lambda_s = 2\pi \sqrt{\frac{\bar{A}^2 U}{\gamma}}. \quad (19)$$



Table 1 lists values of  $\lambda_s$  for several typical values of  $\bar{A}^2 U$  and  $\gamma$ . Since the basic current is essentially westerly, features with wavelengths longer than  $\lambda_s$  for a given  $\bar{A}^2 U$  and  $\gamma$  will have easterly phase velocities (i.e., they retrogress) and features with wavelengths shorter than  $\lambda_s$  will have westerly phase velocities less than  $\bar{A}^2 U$ .

## THE VERTICAL PROFILE OF THE CURRENT

The parameter  $\bar{A}^2$  in the model equations (12) or (13) is a measure of the vertical variability of the current. It should be evaluated from observations of the current profile extending all the way from the surface to the bottom. Unfortunately, adequate observations do not exist. Many current profiles in the Gulf Stream extend only a few hundred meters below the surface; also they assume a level of no motion near 200 meters. Direct measurements of the current are almost entirely restricted to the surface of the ocean. At depth, direct observations are simply too sparse to allow a realistic evaluation of  $\bar{A}^2$ .

If  $\bar{A}^2$  cannot be evaluated, its behavior can be studied from hypothetical current profiles. Table 2 summarizes such a calculation. The surface current speed is given as  $V_0$ , and the current at the bottom, 5000 meters, is assumed to be  $1/10 V_0$ . The current is constant from the bottom to some intermediate depth  $d$ , and varies linearly from  $d$  to the surface. From Table 2 and similar profiles, it is observed that a reasonable range for  $\bar{A}^2$  is 1.0 to 2.5.

## APPLICATION OF THE MODEL

To apply the model, an array of grid points is laid over a portion of the Gulf Stream and the change of stream function  $\psi$  at the grid points from some initial condition is computed by equation (12).

The prediction area (Fig. 1) that has been used is in the form of a channel containing the Gulf Stream from Cape Hatteras to the Grand Bank. The inflow to the channel extends across the Gulf Stream for about 800 km in a southeasterly direction from Cape Hatteras. The outflow from the channel lies approximately along  $50^\circ W$ . One side of the channel lies along an arbitrary isobath of the Continental Shelf. The deep side of the channel follows a broad arc passing west and north of Bermuda and about 700 km from the edge of the Continental Shelf.

The grid points laid over the Gulf Stream are rectilinear on a polar stereographic map projection and are 50 km apart. A computer program (IBM 7090) has been written to accept as initial conditions a bottom topography at all grid points and a stream-function profile along the inflow. The program generates an innocuous field of stream function at all grid points from the specified inflow. The outflow stream-function profile is linear and no flow is allowed across the sides of the channel. From this initial condition, the model is numerically integrated in time steps of about one hour. It is hoped

Table 1

Stationary Wavelengths for Various Basic Flows and Bottom Slopes

Basic Current $\bar{A}$ U(knots)	Stationary Wavelengths (naut. mi.)		
	Steep Rise $\gamma = .5 \times 10^{-9} \text{ m}^{-1} \text{ sec}^{-1}$	Moderate Rise $\gamma = .2 \times 10^{-9} \text{ m}^{-1} \text{ sec}^{-1}$	Horizontal Bottom $\gamma = \beta = .2 \times 10^{-10} \text{ m}^{-1} \text{ sec}^{-1}$
1.0	109.	172.	544.
0.3	60.	94.	299.
0.1	34.	54.	172.
0.03	19.	30.	94.
0.01	11.	17.	54.

Table 2

Current Profile Parameter  $\bar{A}^2$  for Several Hypothetical Profiles

d(meters)	$\bar{V}$	$\bar{A}^2$
250.	$0.12 V_o$	1.7
500.	$0.15 V_o$	2.1
750.	$0.17 V_o$	2.2
1000.	$0.19 V_o$	2.2
1500.	$0.24 V_o$	2.1
2500.	$0.33 V_o$	1.8
3500.	$0.42 V_o$	1.5
5000.	$0.55 V_o$	1.2

Surface current =  $V_o$  , bottom current =  $1/10 V_o$  , bottom depth = 5000 meters. Current is constant from the bottom to depth  $d$  , linear from  $d$  to the surface.

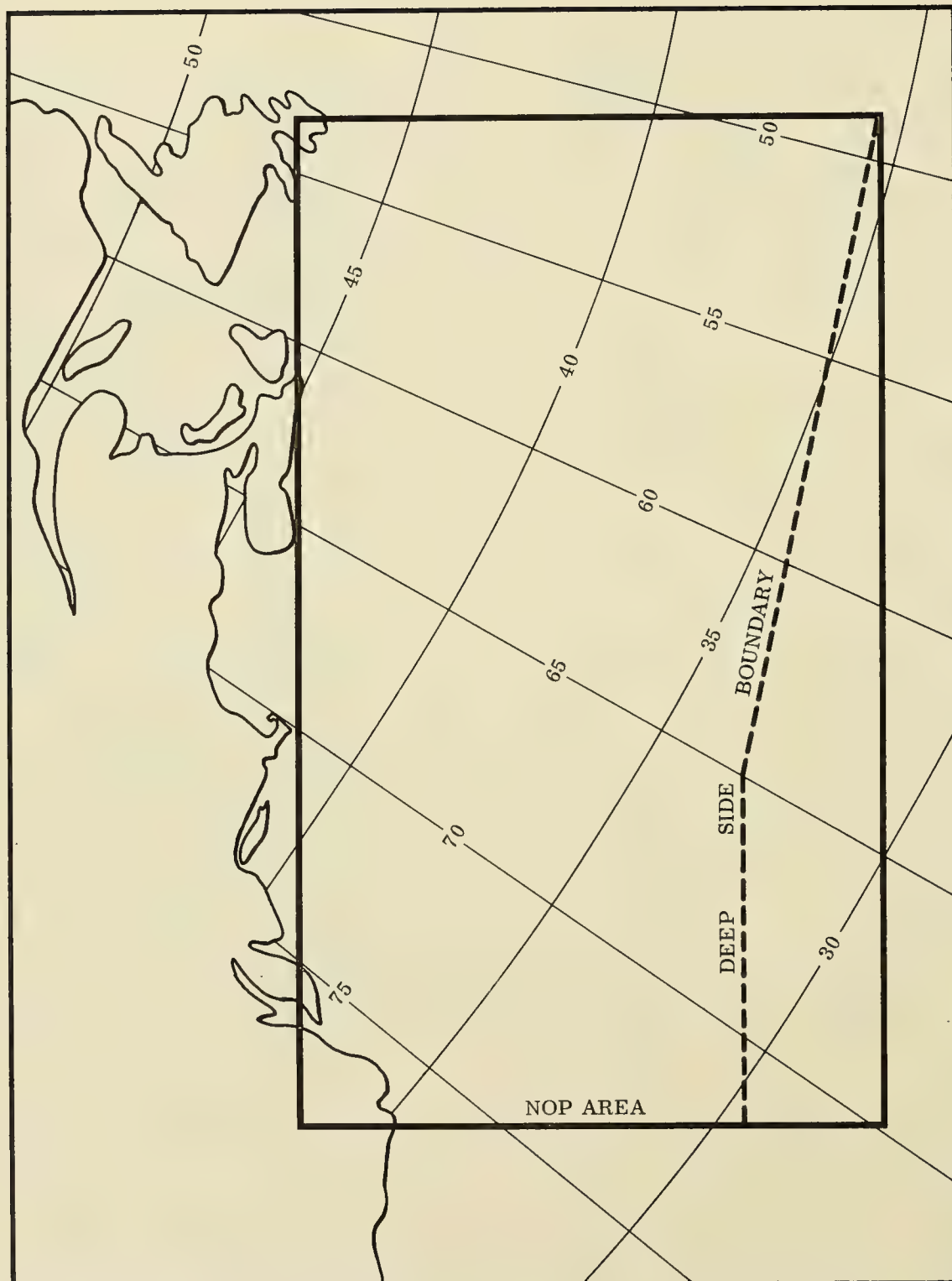


FIGURE 1 THE NUMERICAL OCEAN PREDICTION AREA



that from the innocuous initial condition, interesting and realistic features will form in the channel.

## RESULTS

In practice, the model has developed features with wavelengths typically on the order of 400 km. Although some interesting features form, especially near the sea mounts extending southeastward from New England, the usefulness of the predictions is marred by an instability near the inflow. Tests to study the effect of inflow profile and  $\bar{A}^2$  were conducted, but the occurrence of the instability near the inflow may well obscure the true result of such tests.

The instability is in the form of a single amplifying wave extending in from the inflow, with a wavelength of about 350 km. The amplification is such that after typically 10 to 15 days, the prediction is completely unrealistic near the inflow. The present effort is directed toward a theoretical understanding of the instability and toward devising the optimum means to control it, since it does not seem to be an observed phenomenon of the Gulf Stream. Two preliminary results of this investigation are discussed in the last two sections of the paper.

## INFLOW-OUTFLOW BALANCE

The first modification to the model concerns the net transport of vorticity through the channel. It will be shown that a net accumulation or depletion of relative vorticity will occur in the channel unless the inflow and outflow are selected to avoid it. Returning to equation (12), we may rewrite it as:

$$\frac{\partial \bar{\zeta}}{\partial t} + \bar{\mathbf{v}} \cdot \nabla p = \frac{\partial \bar{\zeta}}{\partial t} + \nabla \cdot (p \bar{\mathbf{v}}), \quad (20)$$

where  $p = \bar{A}^2 \bar{\zeta} + f - f_0 \log h$ , and the divergence of  $\bar{\mathbf{v}}$  is neglected. Now, by integrating equation (20) over the area  $R$  of the channel,

$$\iint_R \frac{\partial \bar{\zeta}}{\partial t} dA + \iint_R \nabla \cdot (p \bar{\mathbf{v}}) dA = 0. \quad (21)$$

The left-hand integral in equation (21) represents the total accumulation or depletion of relative vorticity in the channel. This should be zero for any long-term prediction. The right-hand integral in equation (21) can be transformed by Greene's theorem into a line integral,

$$\iint_R \nabla \cdot (p \bar{\mathbf{v}}) dA = \oint_S p \bar{\mathbf{v}} \cdot \mathbf{n} ds = 0, \quad (22)$$

for balanced inflow-outflow;  $\mathbf{n}$  is the outward-directed normal on the boundary  $S$  of  $R$ . For the prediction channel, there is no cross-boundary flow along the sides. At the inflow  $\bar{\mathbf{v}} \cdot \mathbf{n} = -v$ , and at the outflow  $\bar{\mathbf{v}} \cdot \mathbf{n} = v$ .

This yields, finally, the inflow-outflow balance for no vorticity accumulation

$$\int_{\text{outflow}} p v dx - \int_{\text{inflow}} p v dx = 0. \quad (23)$$

The model is applied by specifying an inflow which resembled the Gulf Stream on a section extending southeastward from Cape Hatteras. Equation (23) states that the outflow from the channel should not be selected arbitrarily. In the tests of the model that have been conducted, the outflow stream-function profile has been constructed to be linear. This, unfortunately, has not generally satisfied the inflow-outflow balance. In tests which differ essentially in the sign of the inflow-outflow imbalance, the phase of the instability near the inflow is reversed. Although no reduction of instability was indicated, the striking difference in phase, apparently due to differing inflow-outflow imbalance, points to some sort of interaction between the imbalance and instability.

#### FREE-SURFACE MODEL

The second modification which may help control instability in the model is to relax the rigidity of the top of the fluid. The fluid then possesses not only a rigid, sloping bottom, but also a free top surface. To outline the derivation of the model equation for this case, we return to the kinematic boundary conditions, equation (10), which will now be:

$$w_s = \frac{ds}{dt}, \quad w_h = \mathbf{V}_h \cdot \nabla h, \quad (24)$$

where  $s(x, y, t)$  is the free-surface top of the fluid. When the geostrophic assumption is introduced to relate the free surface to the stream function, the model equation similar to equation (13) becomes:

$$\nabla^2 \frac{\partial \bar{\Psi}}{\partial t} + \bar{\mathbf{V}} \cdot \nabla (\bar{A}^2 \nabla^2 \bar{\Psi} + f - f_0 \log h) - \frac{f_0^2}{g h_0} \frac{\partial \bar{\Psi}}{\partial t} = 0. \quad (25)$$

The difference between equations (13) and (25) is the term  $-\frac{f_0^2}{g h_0} \frac{\partial \bar{\Psi}}{\partial t}$  (the Helmholtz term). A perturbation analysis of this model demonstrates that the Helmholtz term serves to reduce the speed of long waves.

Testing of the free-surface model awaits the completion of the investigation (now under way) into the instability which has been encountered. Inclusion of the Helmholtz term in the model would seem to be beneficial since it can be expected to counteract, to some extent, the unstable amplification which has been encountered near the inflow.

#### REFERENCE

- Warren, Bruce A. 1963 Topographic influences on the path of the Gulf Stream. *Tellus*, v. 15, no. 2, pp. 167-183.

A MOORED OCEANOGRAPHIC DATA ACQUISITION SYSTEM

by

William C. Green and Leon DeVilleneuve

Institute of Marine Science, University of Miami  
Miami, Florida





# A MOORED OCEANOGRAPHIC DATA ACQUISITION SYSTEM<sup>1</sup>

by

William C. Green and Leon deVilleneuve  
Institute of Marine Science, University of Miami  
#1 Rickenbacker Causeway, Miami, Florida 33149

## INTRODUCTION

In order to correlate ambient noise in the sea with surface disturbances, a permanently moored oceanographic environmental sensing system to measure certain environmental factors has been installed one mile west of North Bimini, Bahamas (Fig 1). It was designed for this location where the water is 100 feet deep with a sandy bottom. The water currents are of variable direction with velocities of 0 to 3 knots. These waters, which are generally navigated by small craft, lie in the hurricane belt (Fig 2).

## SYSTEM

The environmental factors being measured are wind speed and direction, wave height, current speed and direction, water temperature and ambient noise. The sensors measuring these parameters are sequentially sampled by a submerged commutator selector, converted to a frequency analog and transferred by cable to tape recorders on shore. The data are then processed by computers for analysis (Fig 3).

Because the requirements for mounting the different sensors vary so widely, two platforms were installed to support them. The anemometer and wave height sensors were mounted on a spar buoy and the current speed, current direction meter and temperature sensors were mounted on a submerged buoy.

## SPAR BUOY

The spar buoy (Fig 4), fifty-five feet long and one foot in diameter, floats with fifteen feet of its length exposed above the water. It is fabricated of three sections of polyvinyl chloride pipe filled with high density expanded polyurethane. The pipe joints are reenforced with steel collars and the buoy is externally guyed with stainless steel wire to minimize flexing. A disc-shaped counterweight, to dampen vertical motion due to surface waves, is suspended 27 feet below the spar. The buoy is secured at its center of pressure by horizontal tether wires fastened to the mooring lines of two large floats (Fig 5). The horizontal wires have no vertical force components due to currents and therefore, tilting and vertical excursion of the buoy due to currents is minimized. The two floats, 30 feet away from, and on opposite sides of the buoy, are in line with maximum expected currents.

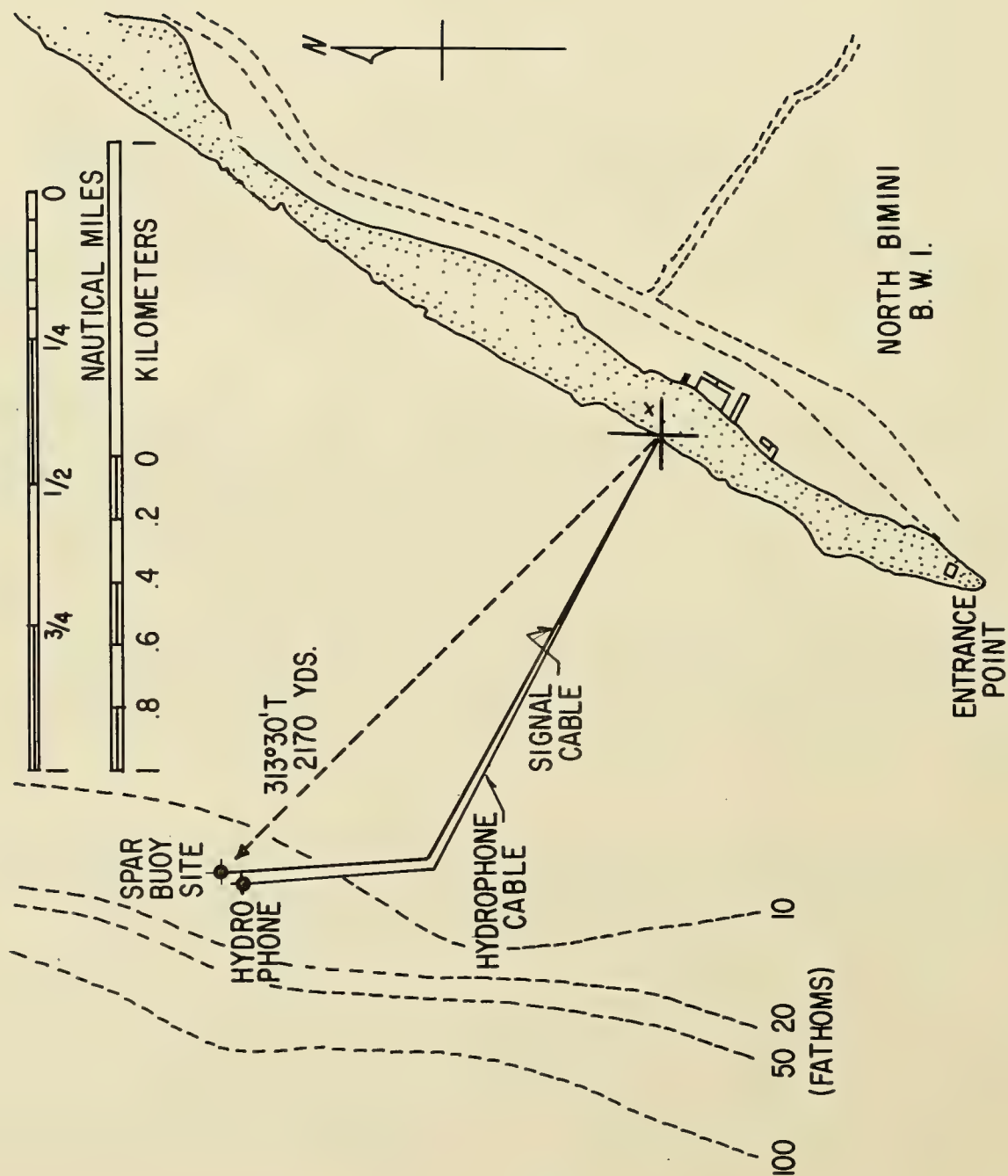


FIGURE 1 SENSOR SYSTEM LOCATION, BIMINI

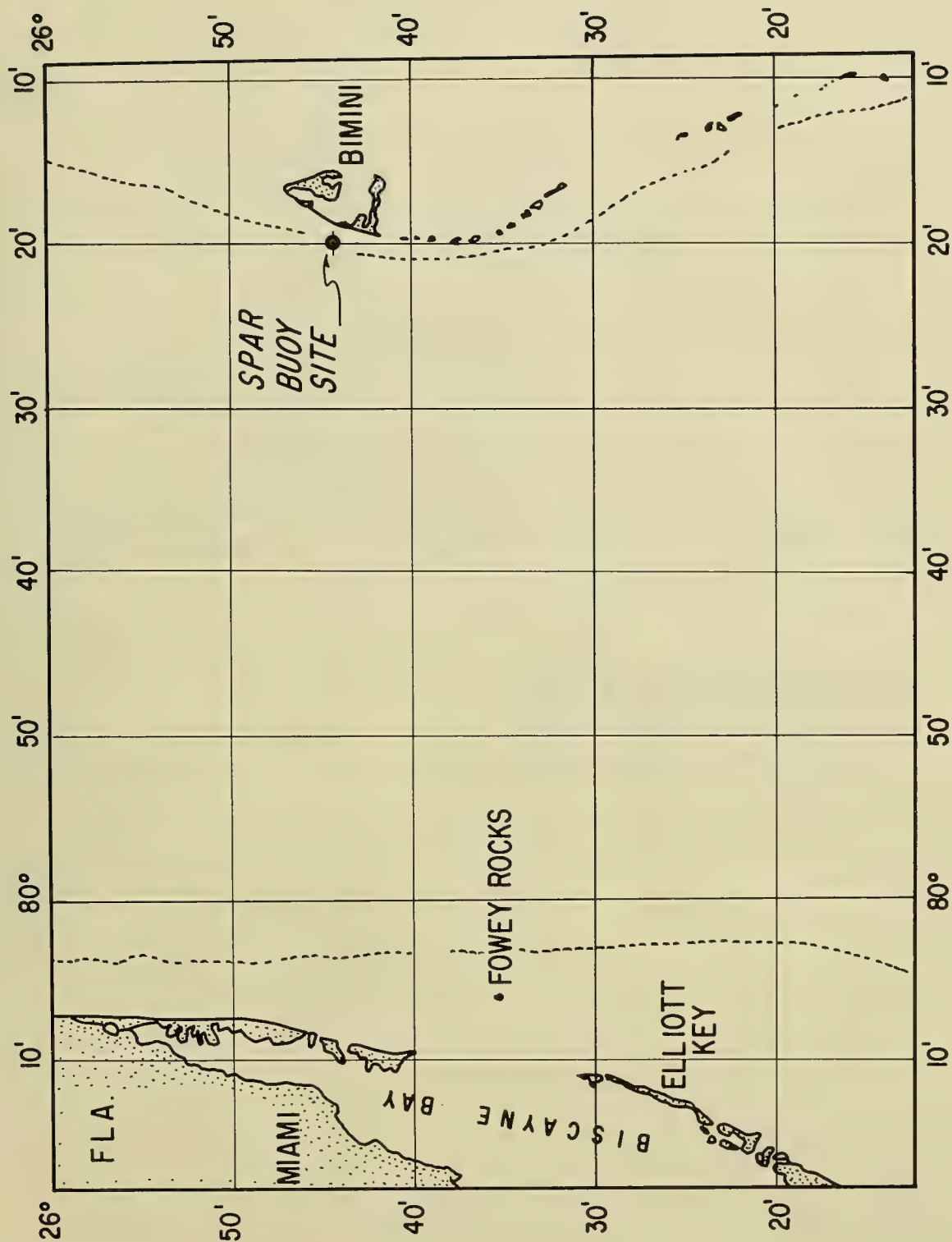


FIGURE 2 STRAITS OF FLORIDA

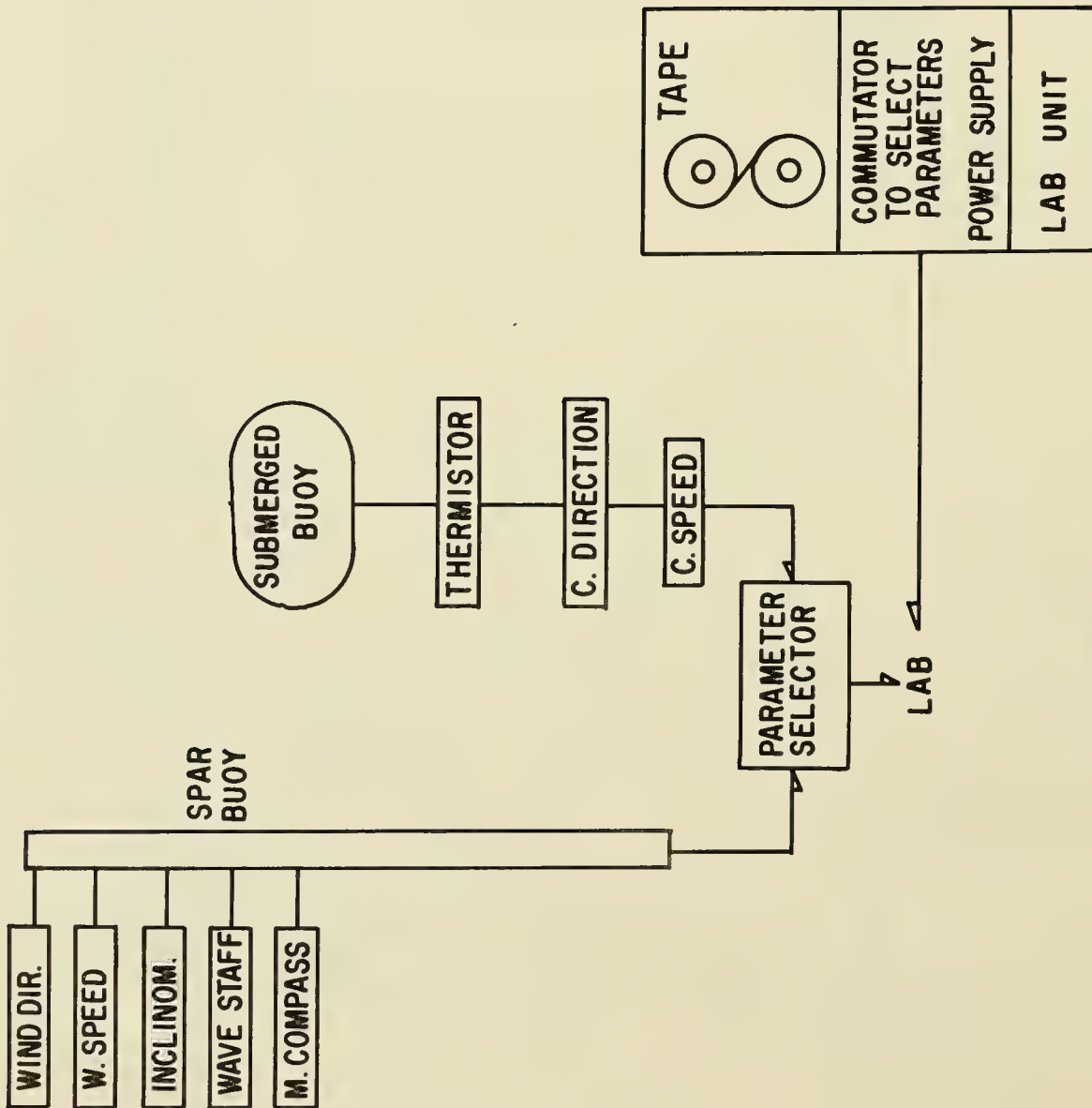


FIGURE 3 DATA ACQUISITION SYSTEM



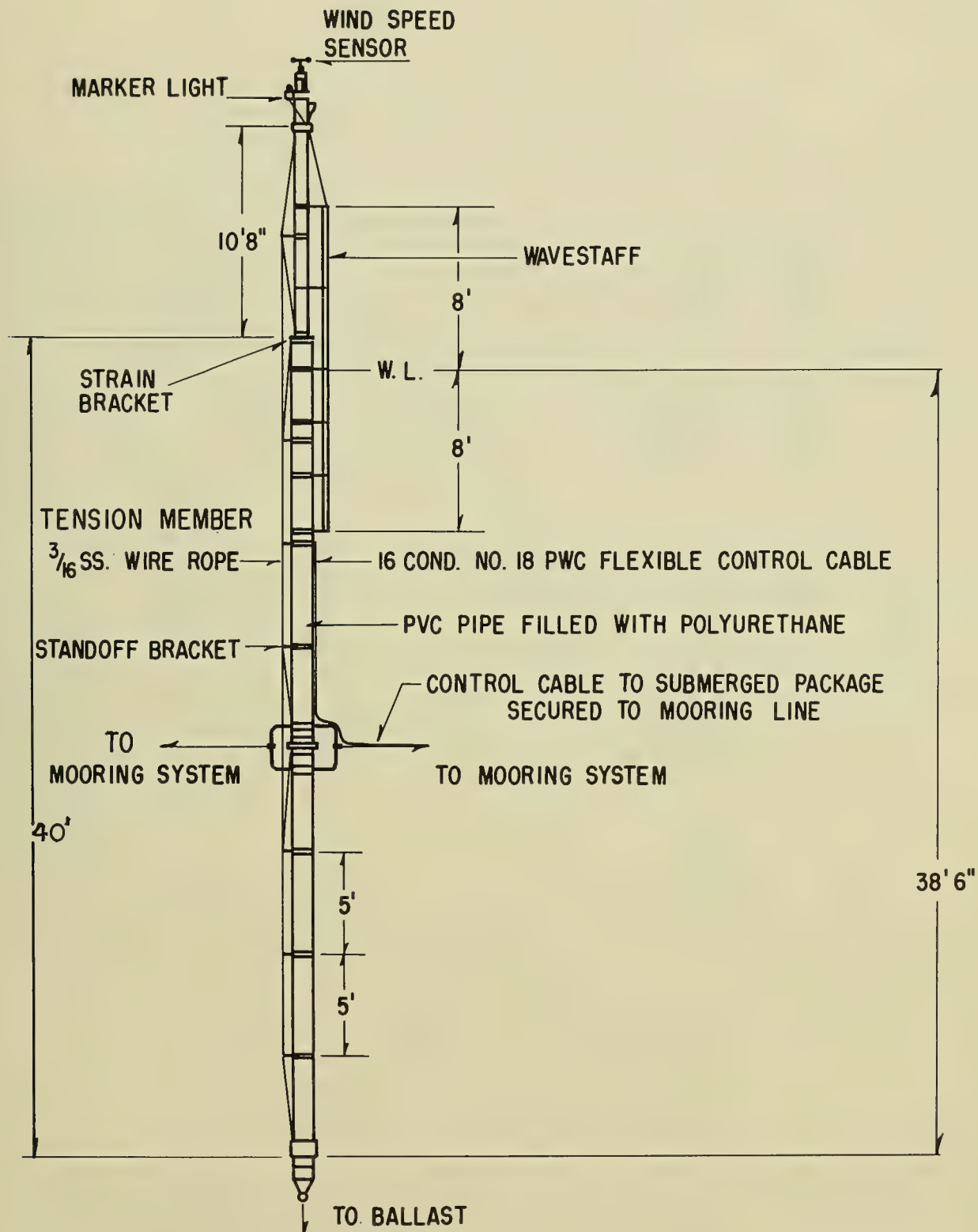


FIGURE 4 SPAR BUOY ASSEMBLY

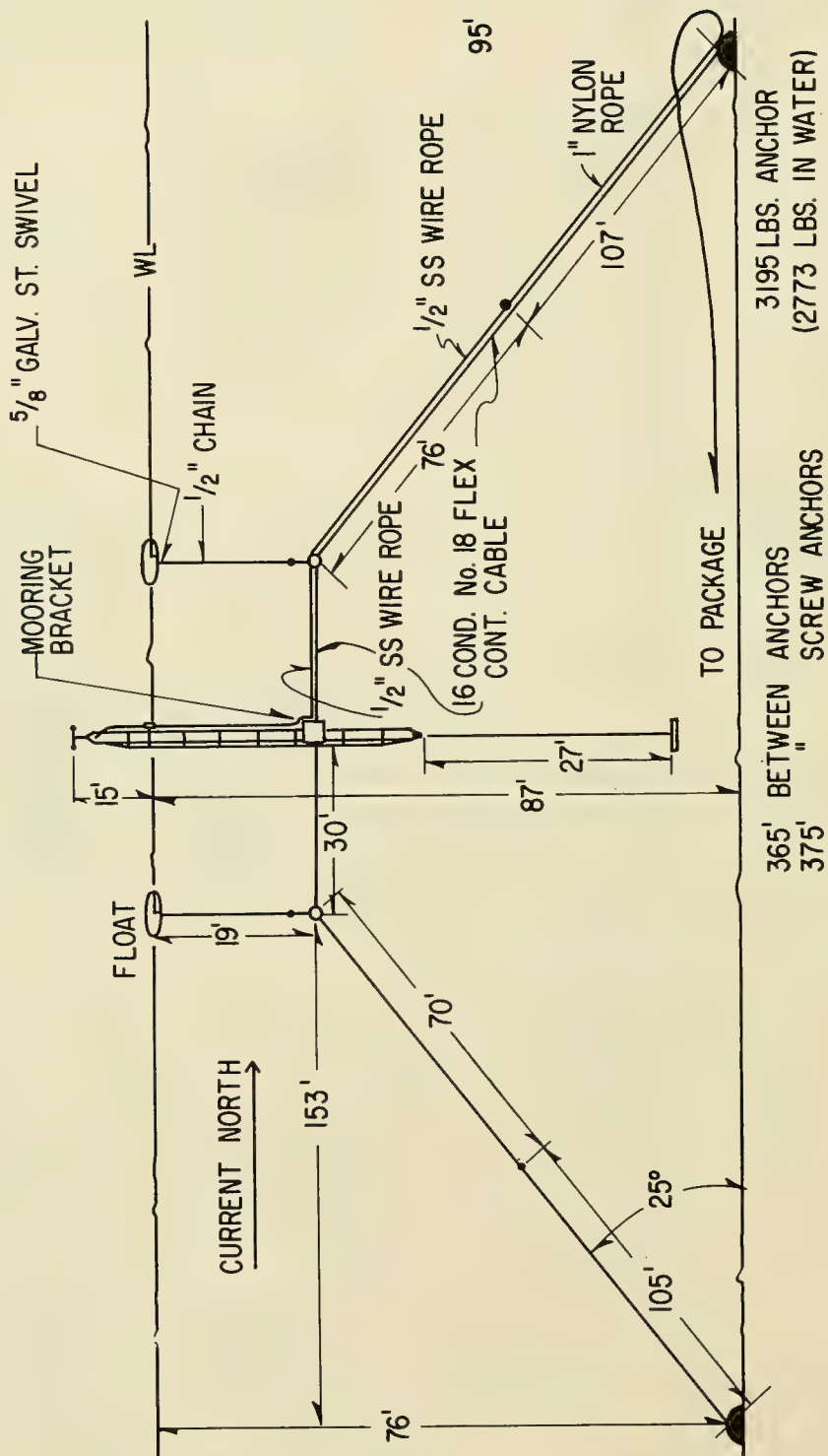


FIGURE 5 MOORING SYSTEM

## A MOORED OCEANOGRAPHIC DATA ACQUISITION SYSTEM

Originally, the spar buoy was installed with only one large float, but variable tidal currents and wind caused the spar to rotate around its mooring anchor and foul its mooring line. This dual float system eliminates the rotation of the spar due to currents and wind. Plastic pipes were installed over the tether wires to prevent loops and possible fouling with the spar. The lower half of the floats' mooring lines are nylon and are secured to smooth, low profile dead weight anchors. Auxiliary floats were installed on the nylon line to keep it off the bottom and prevent chafing. The electrical signal cable is secured to the tether wire and mooring line with nylon straps. The anemometer is mounted on top of the spar and the wave height sensor is secured to the side of the spar.

### SUBMERGED BUOY

The submerged buoy<sup>2</sup> (Fig 6), is fabricated of fiberglass and is partially filled with expanded high density polyurethane to provide a positive buoyancy of 2000 pounds. Thrust bearings have been installed on the buoy's mooring axle to allow the buoy to head into the currents, thereby permitting the instruments below it to remain fixed. Current speed and direction meters are mounted below the buoy. This system is moored 25 feet below the surface with a multiconductor double armored cable, the armor being the strength member. Three temperature sensors are fastened to the mooring cable at 25 foot intervals.

### SENSORS

The wind speed sensor (Fig 7) is of a standard four cup design whose shaft is magnetically coupled to sealed reed switches. The first wind speed meters installed became inoperative after a few weeks of service due to corrosion and salt accumulation between the shaft and bearings. Installing nylon bearings, chrome plating the shaft and leaving .005 inch clearance between shaft and bearings to allow rain water to flush out salt deposits has substantially reduced these problems. After several months of operation, the new wind speed meter showed virtually no signs of wear or corrosion. Its calibration curves show it to be substantially linear to 100 miles per hour.<sup>3</sup>

The wind direction sensor is mounted directly below the wind speed meter. A low torque resistive potentiometric wind direction sensor was originally used, but failed after a few months of service due to excessive wear over a limited section of the resistive element. Prevailing Southeast winds and jitter in the vane caused the excessive wear. To overcome this problem, a non-ambiguous, incremental type sensor was developed which utilizes twenty magnetically actuated reed switches, thereby, giving a resolution of 18°. <sup>4</sup> It is oriented to a magnetic compass mounted directly below it.

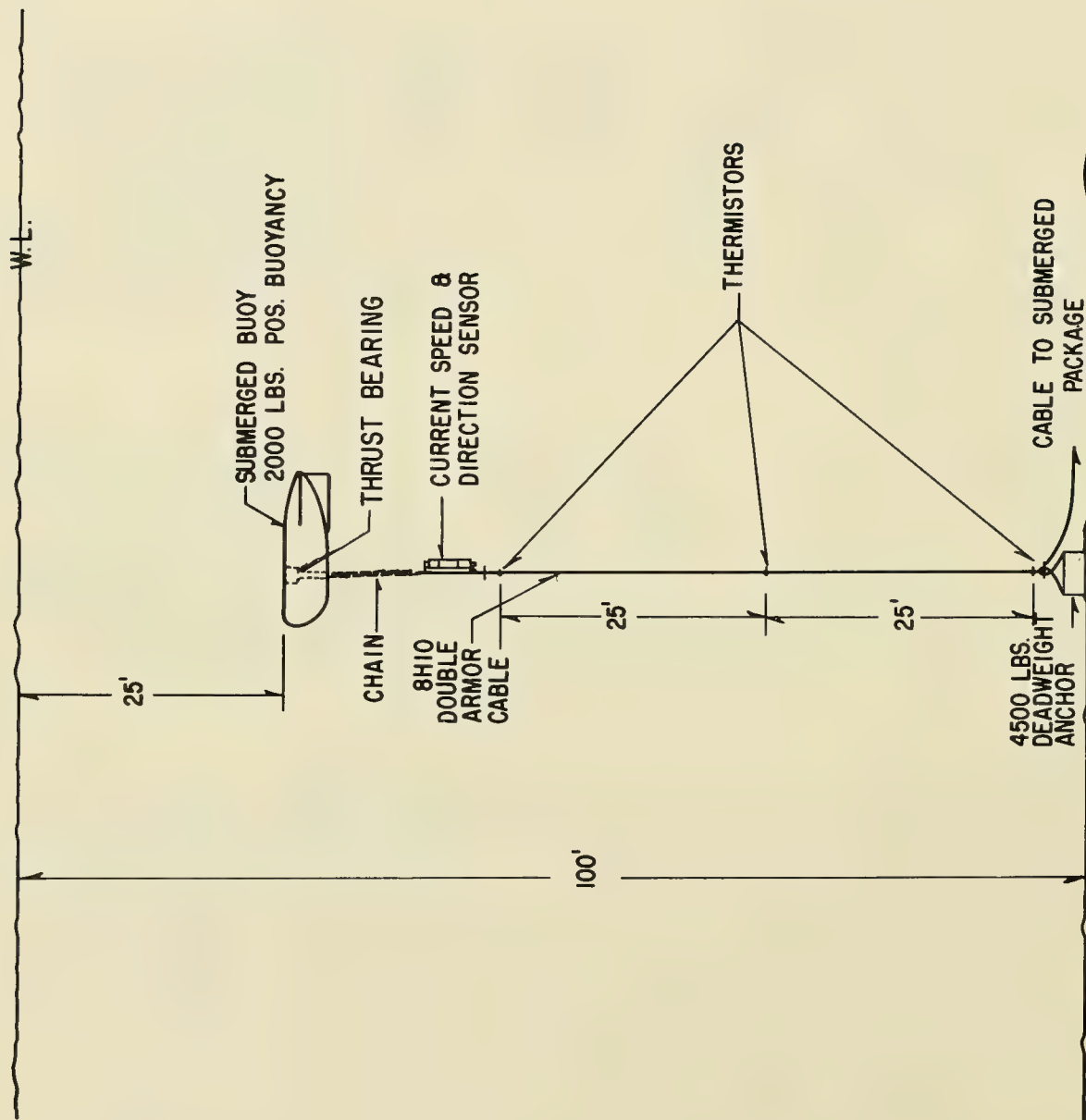


FIGURE 6 SUBMERGED BUOY ASSEMBLY



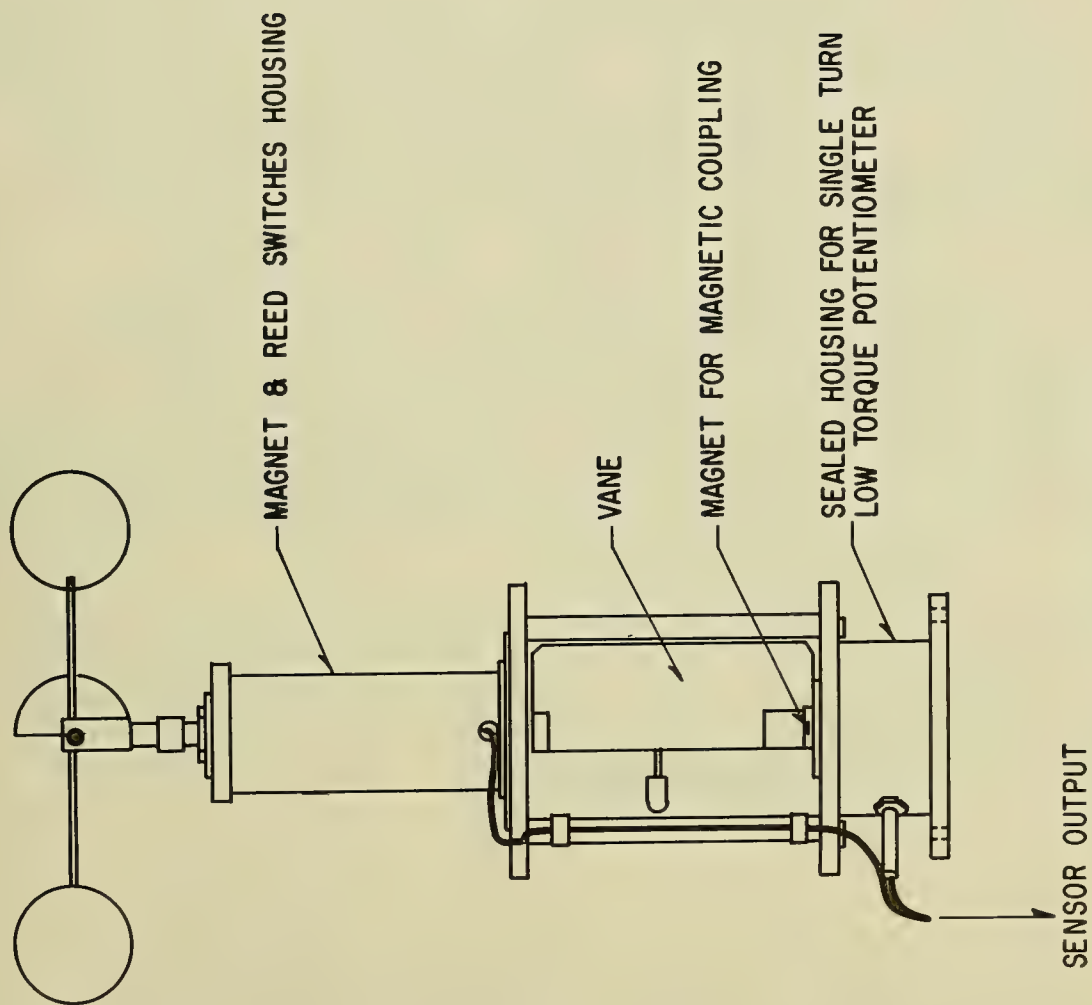


FIGURE 7 SENSOR ASSEMBLY

## A MOORED OCEANOGRAPHIC DATA ACQUISITION SYSTEM

The wave height sensor is a sixteen foot staff utilizing a floating magnet in a slotted aluminum tube that actuates series connected sealed reed switches (Fig 8).<sup>4</sup> The reed switches are housed in a sealed oil-filled polyvinyl chloride pipe that is attached to the aluminum tube. This design eliminates the objectional features of residual resistance in exposed resistance type staffs and the aluminum tube prevents jamming of the float. The staff is secured to the side of the buoy with 8 feet of its length exposed above water. The reed switches are mounted on 3 inch centers so that waves from six inches to sixteen feet can be monitored. The entire wave staff is painted with an organic tin base antifouling paint.

The current speed meter (Fig 9), suspended six feet below the submerged buoy, is a Savonius rotor type of molded plastic supported in an aluminum housing which is magnetically coupled to sealed reed switches. It has been calibrated to five knots. The current direction meter, mounted above the rotor, is magnetically coupled to a 360° resistive potentiometer whose shaft is magnetically linked to a magnetic compass. Tungsten bearings and antifouling paint were used to give maximum life to the instruments. Resolution of the current speed and direction meters are .1 knot and 20° respectively.<sup>1</sup>

To measure ambient noise, two preamplifier-hydrophone assemblies are mounted on the bottom. Because of the high signal levels coming from the commutator package to the laboratory, separate cables connect the hydrophones to shore in order to avoid cross talk. They are placed two hundred feet from the buoys to keep buoy generated noise from masking the ambient noise. Frequency response of the hydrophone-preamplifier-cable system is 20 cps to 2000 cps  $\pm$  1 dB. The sensitivity of the hydrophone is -92 dBV<sub>µb</sub> and the preamplifiers have a gain of 40 dB.

### SPLICES AND SEALS

The commutator package is a bottom mounted aluminum cylinder weighted down with concrete ballast (Fig 10). To afford a more flexible system and prevent total failure if one or more of the connecting cables floods, a separate bulkhead connector and plug is used for each sensor's output. Commercially available waterproof plugs and bulkhead connectors are used at all cable entrances, both above and below water.<sup>5</sup> All splices were hand taped with self amalgamating polyethylene or neoprene tape and antihosing stops were installed in each splice.

### INSTALLATION

To install this system, a careful survey was made by SCUBA divers to check water depth and topography. Anchor, commutator package and cable positions were carefully marked and buoyed. A converted 90 ton "T" boat was

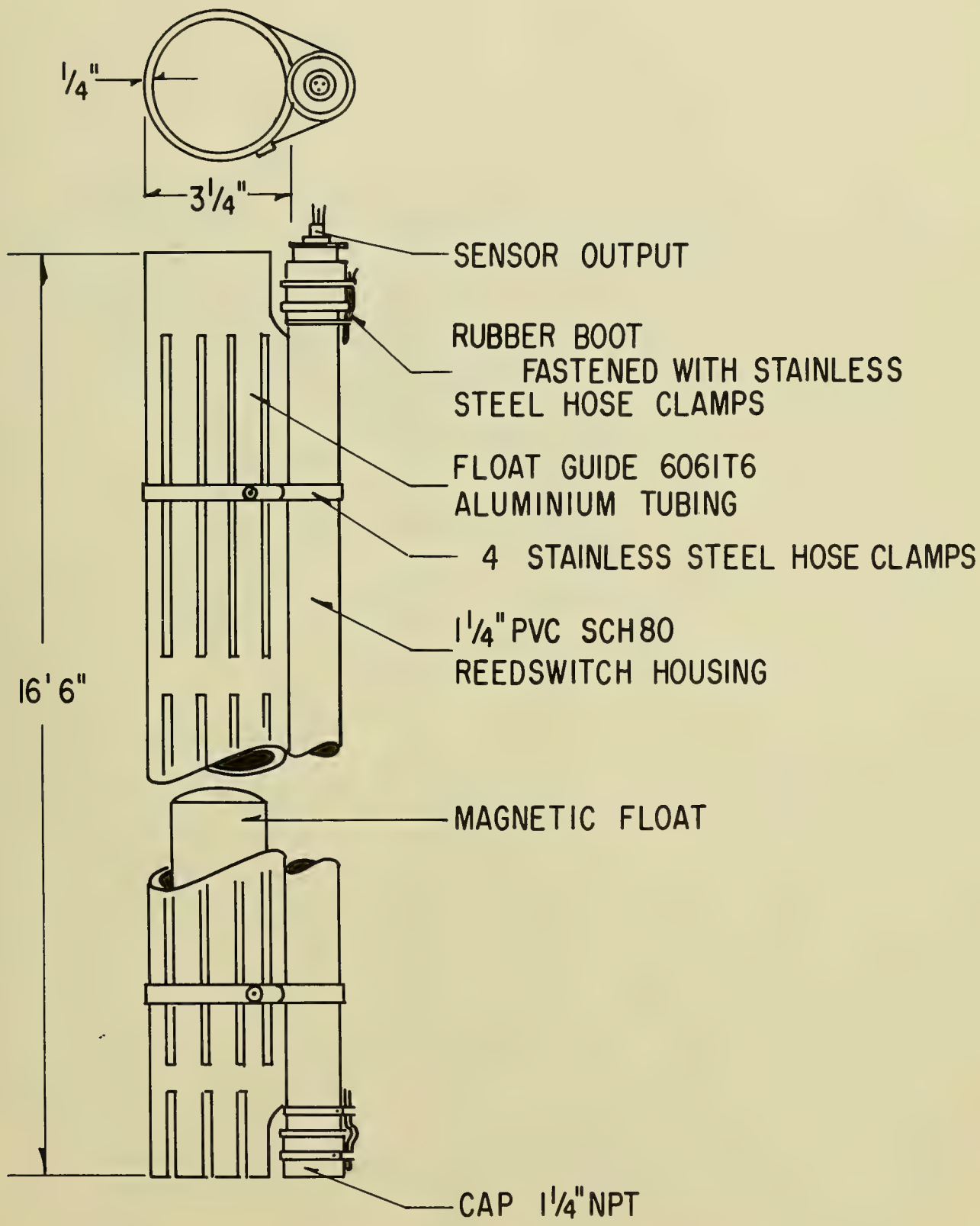


FIGURE 8 WAVE STAFF ASSEMBLY

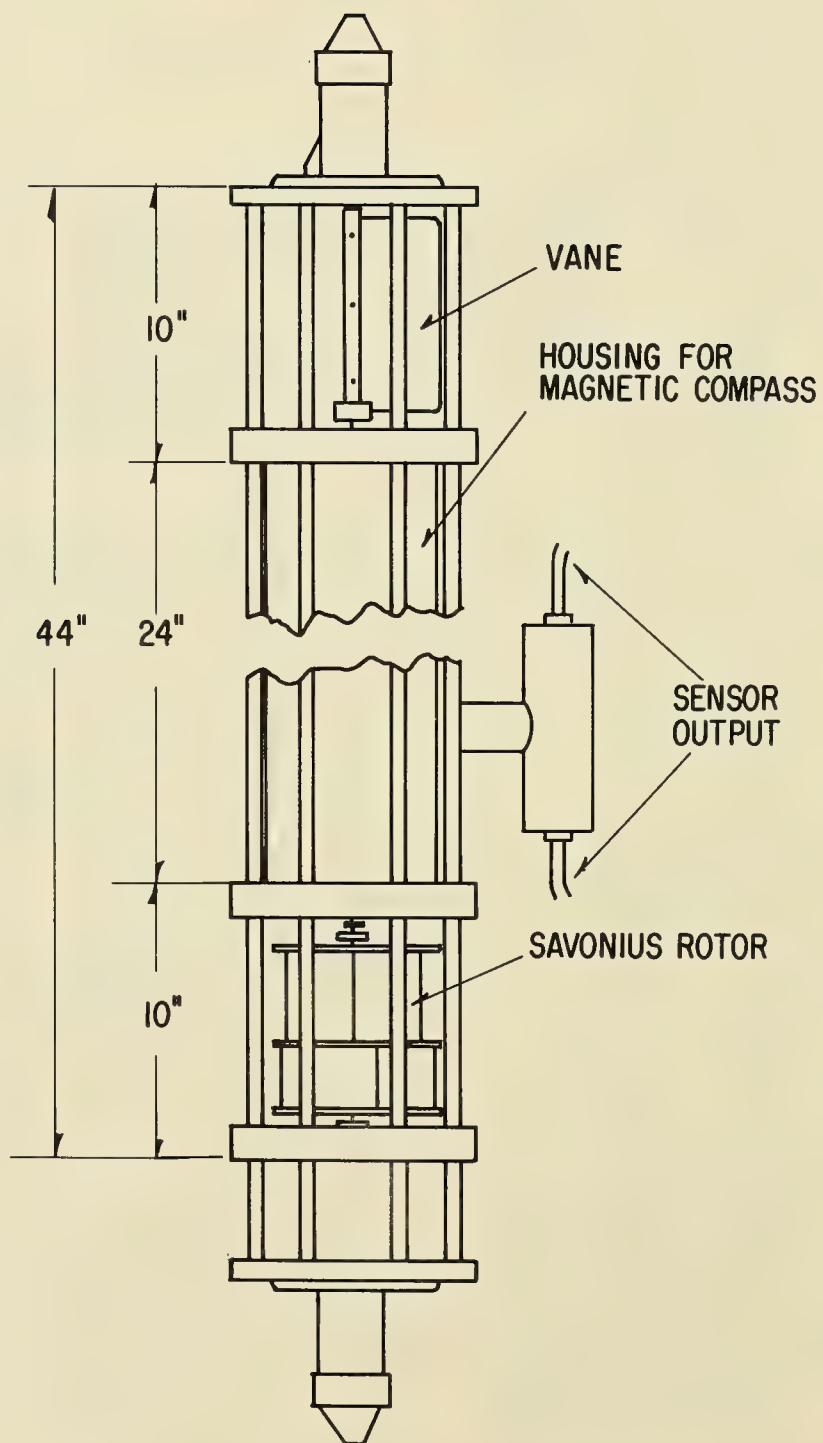


FIGURE 9 CURRENT SPEED AND DIRECTION METER ASSEMBLY



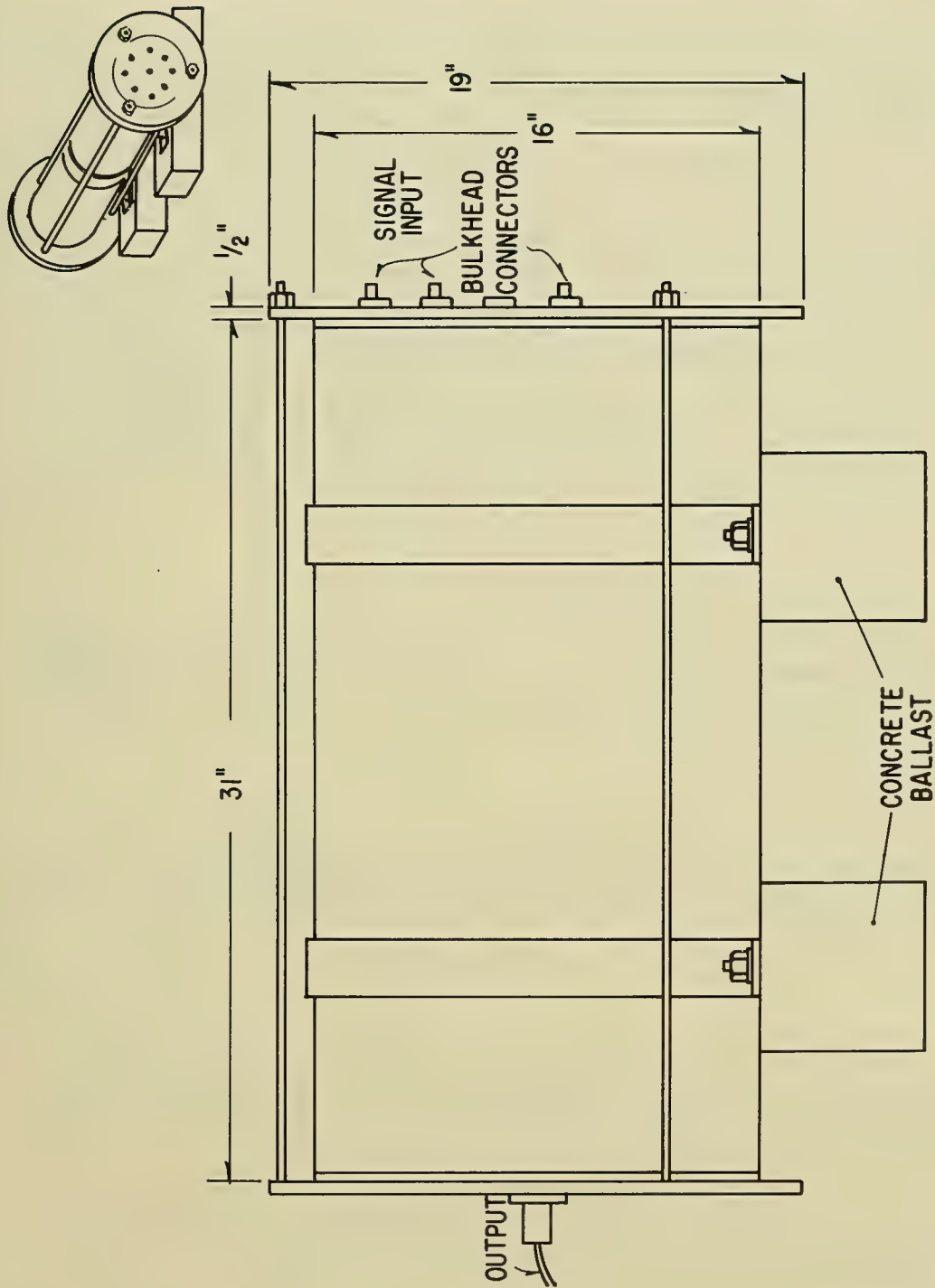


FIGURE 10 SUBMERGED COMMUTATOR SELECTOR PACKAGE

## A MOORED OCEANOGRAPHIC DATA ACQUISITION SYSTEM

used to install the anchor and submerged buoy. A thirty foot utility boat was used to tow the buoy into position and connect it to its mooring lines. Constant underwater to surface telephone communication between divers and boats was maintained to insure that the equipment was accurately placed.

### MAINTENANCE

This system was designed with a life expectancy of two years. It should require relatively low maintenance because the buoys were built of synthetic materials that have high corrosive resistance to the environment. All metals were chosen on the basis of their compatibility with each other and the environment. Military specification grade zinc anodes were used on all metal parts for cathodic protection. All components subject to fouling were coated with antifouling paint. Few available design criteria can be relied upon when choosing materials or dimensions because of unpredictable amounts of corrosion, loading, wear and fatigue. Therefore, frequent regular inspections are made of the entire system.

### CONCLUSION

It is difficult to maintain fixed buoy installations of this nature for long periods in the ocean. Several failures have proven that no compromise can be taken in the most insignificant details of design, material or workmanship. Information gained from solving problems will certainly result in improving future systems.

### ACKNOWLEDGEMENTS

The authors are indebted to Drs. John C. Steinberg and William Richardson and Messrs. Morton Kronengold, Jack M. Loewenstein and Raul Murciano of the Institute of Marine Science, University of Miami for their assistance and encouragement in this work.

### REFERENCES

- <sup>1</sup>Contribution No.602 from the Institute of Marine Science, University of Miami, Florida. This work was supported in part by research contract Nobs 90190.
- <sup>2</sup>Braincon Manufacturing Company, Marion, Massachusetts.
- <sup>3</sup>Georgia Institute of Technology, Daniel Guggenheim School of Aeronautics, Atlanta, Georgia

## A MOORED OCEANOGRAPHIC DATA ACQUISITION SYSTEM

<sup>4</sup>Morton Kronengold, Jack M. Loewenstein and Gerald A Berman, "Sensors For The Observation Of Wave Height And Wind Direction".

<sup>5</sup>Marsh and Marine Manufacturing Company, Houston, Texas  
Electro-Oceanics, Encinitas, California.





DEEP OCEAN BIOLOGY IN RELATION TO CONSTRUCTIONAL MATERIALS

by

James S. Muraoka

U. S. Naval Civil Engineering Laboratory

Port Hueneme, California



# DEEP OCEAN BIOLOGY IN RELATION TO CONSTRUCTIONAL MATERIALS

by

James S. Muraoka

U. S. Naval Civil Engineering Laboratory, Port Hueneme, California 93041

## INTRODUCTION

The U. S. Naval Civil Engineering Laboratory at Port Hueneme, California, is conducting a long-term research program to determine the effects of deep-sea environment on materials. In connection with this study, submersible test units (STUs) were designed and fabricated on which many test specimens can be mounted. The STUs can be lowered to the ocean bottom and left for long periods of exposure. To date the Laboratory has placed five STUs on the ocean floor and three of these have been recovered.

Thus far, two test sites have been selected. Test Site 1 (nominal depth of 6,000 feet) is approximately 81 nautical miles southwest of Port Hueneme. Test Site 2 (nominal depth of 2,500 feet) is 75 nautical miles west of Port Hueneme. Additional test sites at a depth of 12,000 and 18,000 feet will be chosen.

This paper presents the materials and methods employed for attracting, collecting, and evaluating deep-sea fouling and boring organisms and the results of field and laboratory investigation of the recovered STU materials. The materials studied were exposed for a period of 6 months at a depth of 2,340 feet (Test Site 2) and similar materials exposed for a period of 3 years at a depth of 5,300 feet (Test Site 1).

A literature survey has already been published on fouling and boring organisms and their effects upon various materials submerged in the deep ocean (Muraoka, 1962).

## OCEANOGRAPHIC INFORMATION

Concurrently with the STU program, numerous oceanographic and biological data-collecting cruises to STU sites have been conducted. These have produced information about the environmental parameters, such as salinity, temperature, oxygen content, and biological activity. Such information is essential in evaluating changes in the materials, especially corrosion of metals, exposed on the ocean floor. Table 1 summarizes the environment at Test Sites 1 (Gray, 1965) and 2 (Reinhart, 1965).

Table 1. Summary of Environment at the Test Sites

	Surface Water	Test Site 1	Test Site 2
Depth		5300 ft	2300 ft
Water Temperature	13.0 C	2.53 C	7.2 C
Dissolved O <sub>2</sub> Conc.	5.6 ml/l	1.26 ml/l	0.42 ml/l
Salinity	33.6 ppt	34.66 ppt	34.37 ppt
pH	7.9	7.44	7.46
Hydrostatic Pressure		2500 psi	1030 psi
Current		0.5 knots	0.3 knot max.
Sediment		green mud containing glauconite, Foraminifera tests, quartz, etc.	green mud containing glauconite, Foraminifera tests, quartz, etc.



## BIOLOGICAL ACTIVITY

Deep-sea photographs show that the surface of the ocean floor at Test Site 1 is very irregular with numerous mounds built by benthic mud-dwelling animals. This indicates that considerable biological activity is occurring at this site. Also, a 5- to 6-foot-long shark-like fish was photographed at the test site drifting near the ocean floor.

### Rock Samples

Rock specimens were desired from these areas to study any fouling organisms attached to the rocks since these fouling organisms could be expected to attach themselves to other materials placed there. A 10-inch-diameter by 36-inch-long steel pipe with retaining rods welded across the lower end of the pipe was employed for collecting rocks from the ocean floor. The pipe dredge was lowered to the ocean floor from an oceanographic vessel, USNS DAVIS, and the area dredged for rock specimens. Several passes were made over Test Site 2 but no rock specimens could be obtained. However, numerous large and small rock samples were obtained near Test Site 1 at a depth of 6,000 feet. Various species of bryozoa, tube worms, Foraminifera, and a species of chiton were found on these rocks. Some rocks had holes made by Pholads, a rock boring mollusk.

### Sediment Samples

Sediment samples for bacteriological and biological analysis were obtained with:

1. A gravity core sampler, which takes cores up to 4 feet long.
2. NCEL's scoop-type bottom sampler which collects about 225 cubic inches of sediment from a soft bottom.
3. A modified ZoBell bacteriological sampler was used to collect a mixture of sea water and sediment. The sampler consists of a 100-ml rubber bulb (deflated) connected with a rubber tube to a glass tube (sealed at one end). The sterilized unit is attached to the side of an NCEL bottom sampler with the glass tube protruding below the scoop sampler. When the heavy sampler touches bottom, the glass tube shatters and the rubber bulb expands, drawing in the surface layer of the bottom sediment and sea water.

Marine bacteria are one of the major biological agents in the deterioration and fouling of various materials and equipment submerged in the sea. To determine the type and activity of bacteria in the deep ocean, sediment samples were obtained with the above samplers and analyzed in the laboratory using standard microbiological methods.

Approximately 1,500,000 aerobic and 5,000 anaerobic bacteria were found in a gram of sediment (wet weight) collected at the sediment-sea water interface. Sulfate-reducing bacteria were also present in the sediment samples.

The sulfate reducers are anaerobic bacteria which obtain their energy by the reduction of sulfate and sulfites in water in the absence of free oxygen. The end product of their metabolic process is hydrogen sulfide ( $H_2S$ ). These microbes are considered to be responsible for the anaerobic corrosion of metals.

The sediment samples obtained with a scoop sampler were washed through a screen to collect mud-dwelling organisms. The animals were bottled and preserved in a 5-percent glycerol-alcohol solution for laboratory analysis.

A variety of animals was found in these sediment samples. Amphipods and annelids were the marine organisms collected most abundantly in the vicinity of both STU test sites.

## TEST MATERIALS

For evaluating nonmetallic test specimens to deep sea biological effects, two aluminum biological test specimen racks (bio-racks) were built which could be attached to a STU. Each rack could hold several plastic rods and tubes each 3 feet long, and a 30- by 12- by 1/8-inch phenolic laminated plastic sheet. Numerous smaller test specimens were attached to the plastic sheet; one sheet was secured to the upper section of a bio-rack, and an identical sheet was secured to the bottom. In order to expose the test materials to biodeterioration in mud as well as water, the two racks were attached to the STU so that the lower portions would be buried in the bottom sediment and the upper portions exposed to sea water about 3 feet above the mud line.

The bio-rack specimens were carefully prepared for deep-sea exposure. The 2- by 6- by 1/2-inch wood panels were cut from a sound lumber. These wood panels were employed to collect any deep sea fungi and marine borers which might be present on the ocean floor. The sections of 3-foot-long plastic rods, tubes, pipe, and rubber tubes were treated in different ways. One section of each rod was roughened, a second section was wrapped in burlap, a third section was taped with plastic and rubber electrical tape, and the fourth section was left smooth. Each such section was about 6 inches long. The various wrappings were to provide a favorable foothold for growth of deep sea fouling and boring organisms. A length of 2- by 4-inch untreated pine wood was fitted around each of the 3-foot plastic specimens to act as bait to attract and lead borers into direct contact with each of the plastic specimens (Fig 1).

Four different kinds of rope, such as synthetic plastic fiber rope (nylon and polypropylene) and natural fiber rope (cotton and Manila), were placed on the bio-racks. Electrical cables covered with rubber or plastic insulation of various thicknesses were also placed on the bio-racks. A small pine wood piece was fitted around each electrical cable specimen to act as bait to attract and lead any marine boring animals into direct contact with the cable specimens.

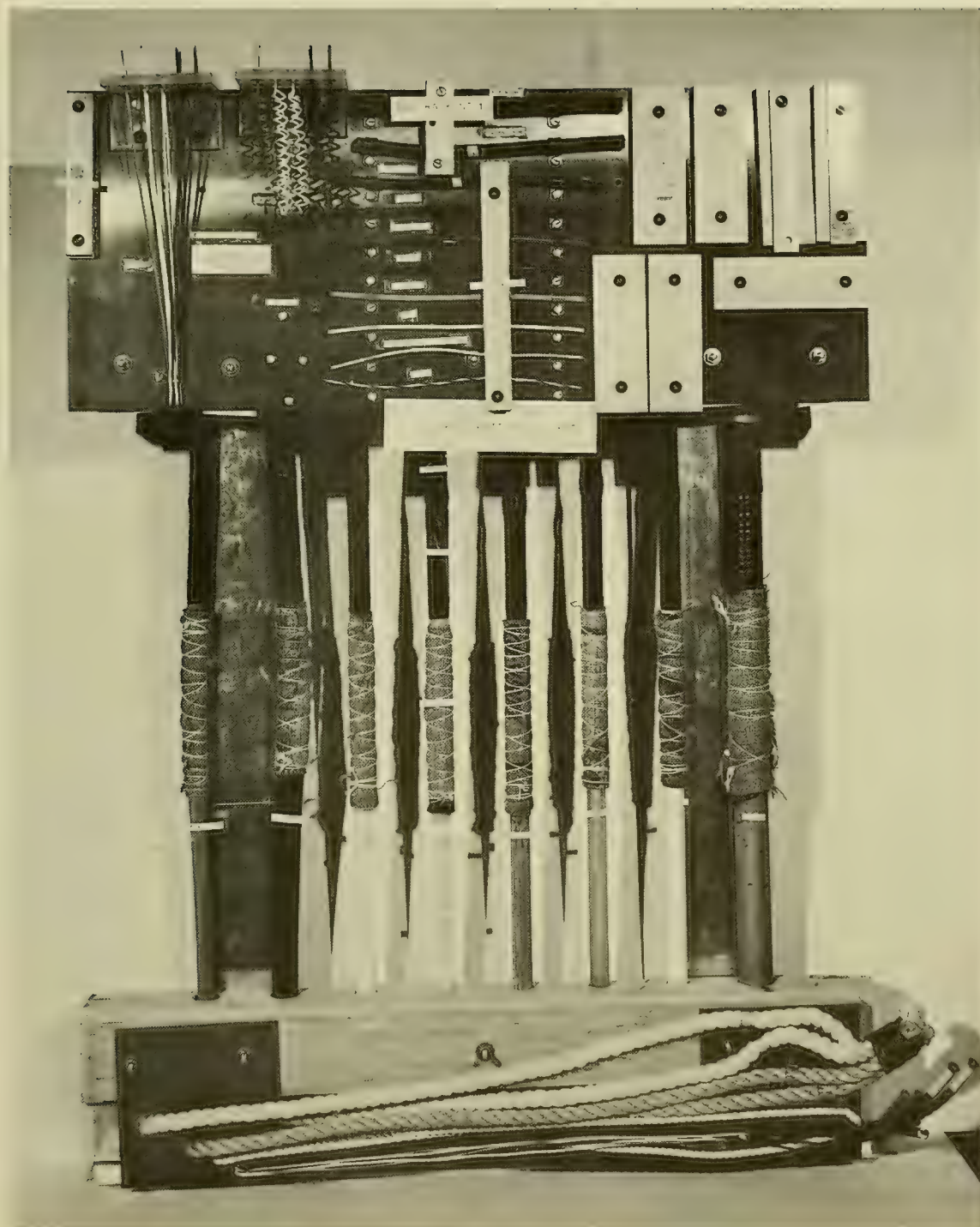


FIGURE 1 ARRANGEMENT OF VARIOUS KINDS OF MATERIALS ON A BIOLOGICAL TEST SPECIMEN RACK BEFORE EXPOSURE IN THE DEEP-SEA ENVIRONMENT



Materials containing antifouling paints or other toxic substances were excluded from exposure aboard the STU. The current velocity at a depth of 2,340 feet and 5,300 feet was not great enough (less than 0.5 knot) to carry away any toxic substance which might alter the natural biological fauna found in the immediate vicinity of the STU.

## RESULTS

### STU II-1 Materials

Test specimens on STU II-1 (Test Site 2) recovered after 6 months exposure on the ocean floor in 2,340 feet of water were examined for signs of biodeterioration, fouling and boring organisms. Teredo-like molluscan borers, Xylophaga washingtona, were found boring into wood panels such as pine, fir, ash, oak, maple and even redwood which is considered highly resistant to insect and to decay damage. Some of the borers were about 1/8 inch in diameter and had penetrated over 5/16 inch into the wood. These borers were also found boring into plastic specimens such as acrylic, polystyrene, cellulose acetate rods, vinyl tubes, and plastic electrical tape.

Most of the borers were found boring into the solid plastic along the edge of the plastic tape wrapping. Approximately 150 borer holes were present around a 1-inch diameter acrylic rod along the edge of the plastic tape wrapping. The depth of penetration was about 1/64 inch and the diameter of these borers was about 1/32 inch.

The borers were also found over the entire length of two 5-foot Manila rope specimens severing the fibers as they bored into the rope. There were several hundred borers per lineal inch of the rope and it was estimated that 75% of the tensile strength of the rope was destroyed. The fibers of cotton rope and jute (burlap) wrapping were decayed by microbiological activity. About 50% of the tensile strength of 1/2-inch diameter cotton rope specimens was destroyed. The nylon and polypropylene rope specimens were in good condition. Silicone rubber insulation over electrical conductors exposed on the sea floor were deteriorated by the nibbling and biting action, possibly by the crabs and amphipods which were found on the bio-racks. In some area of the insulation, the bare wire was exposed to the sea water.

### STU I-1 Materials

Teredo-like molluscan borers had also damaged plastic and wood specimens exposed for 35 months at a depth of 5,300 feet in water at Test Site 1.

The damage to the above materials by the borers was very extensive as compared to damage of materials recovered from a depth of 2,340 feet after 6 months exposure.



The 2- by 4- by 30-inch pine wood bait pieces which were fitted around the plastic rod and tube specimens were not recovered because these wood pieces were totally destroyed by the marine borers. However, two 3/4- by 3- by 24-inch pine wood pieces which were sandwiched in between two metal plates were recovered and the wood pieces were found riddled by borers. The size of some of the borer tunnels measured about 3/4 inch in diameter (Fig 2).

A piece of Greenheart, a hard tropical wood specimen, which is considered resistant to marine borers was also riddled by the borers.

The borers had made numerous shallow to deep grooves on the surface of plastic rods and tubes in an area under the wooden bait piece. The plastics damaged by the borers include vinyl plastic, delrin, nylon, polycarbonate, teflon, PVC, cellulose acetate, polyethylene, acrylic and polystyrene. There were over 100 shallow to deep grooves around a 1 inch diameter cellulose acetate rod (Fig 3). Some of the grooves measured over 1/4 inch in diameter and about 1/16 inch deep.

The cotton and Manila rope specimens were completely destroyed by microorganisms and marine borers, and only a few pieces of the deteriorated rope materials were recovered.

Two species of marine borers were found boring into wood and rope specimens recovered from a depth of 5,300 feet. These have been identified as Xylophaga washingtona Bartsch and Xylophaga duplicata Knudsen (Turner, R. D.). However, only Xylophaga duplicata were found in Greenheart wood.

The discovery of these Teredo-like borers on wooden test panels exposed at a depth to 5,640 feet of water in the Pacific was very surprising (Muraoka, 1964 and 1965), although there have been reports of finding Xylophaga sp. in the Atlantic (Turner, 1961) and in the Tongue of the Ocean, Bahamas (DePalma, 1962).

#### FUTURE PLANS

Investigation of the effects of deep-ocean environment upon materials is continuing. Plans are being readied to recover two STUs during 1965. One STU has been exposed on the ocean floor in 5,600 feet for a period of 18 months. A second STU exposed at a depth of 6,800 feet will be recovered during the latter part of 1965 after 2 years in the sea. It is anticipated that interesting and unusual information about corrosion and growth of marine life upon materials will be obtained when these are recovered and examined. The results of these findings will be reported.

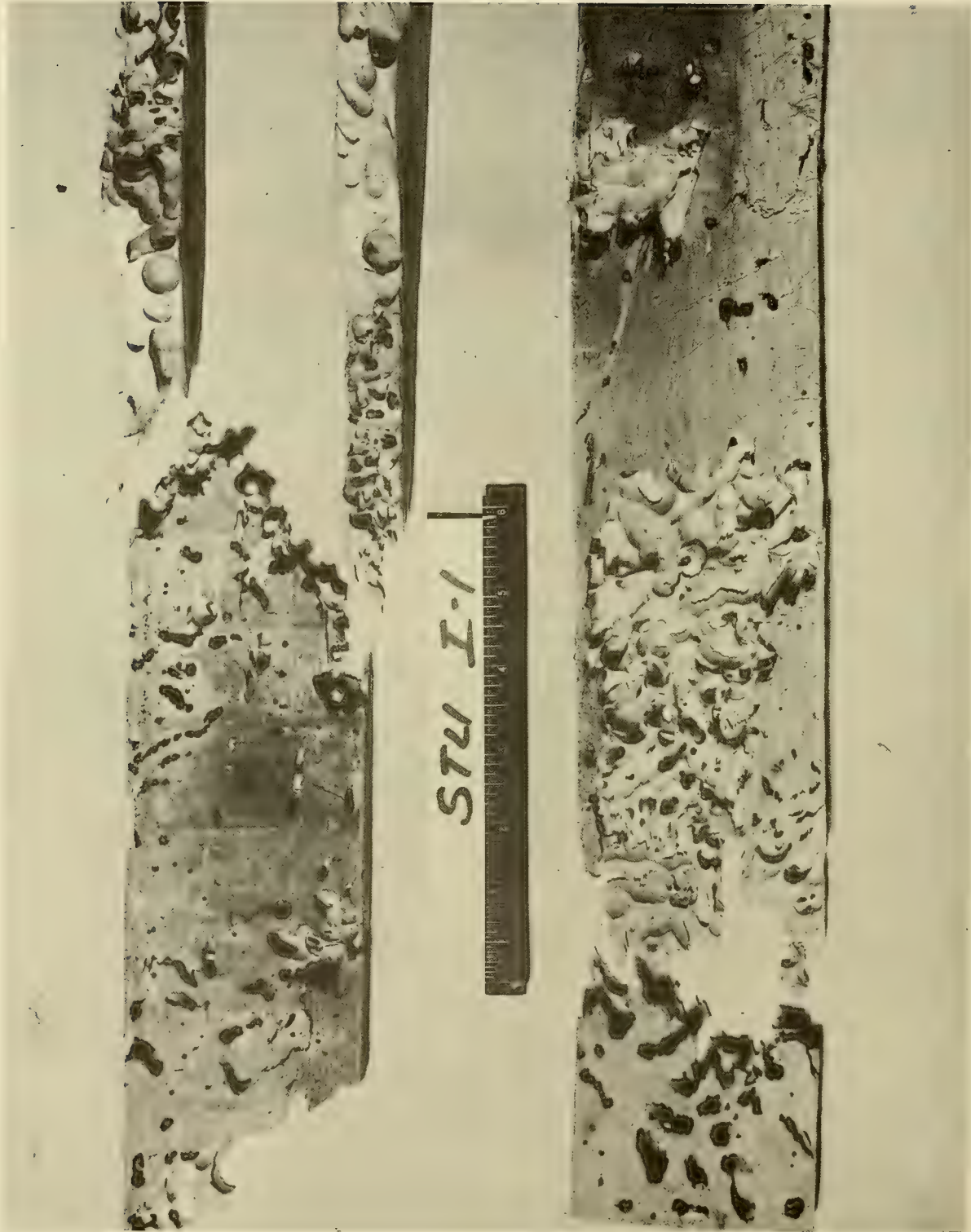


FIGURE 2 PINE WOOD TEST PANEL ATTACKED BY MARINE BORERS, XYLOPHAGA  
WASHINGTONA AND XYLOPHAGA DUPLICATA. WOOD PANEL EXPOSED  
ON THE OCEAN FLOOR IN 5,300 FEET OF WATER

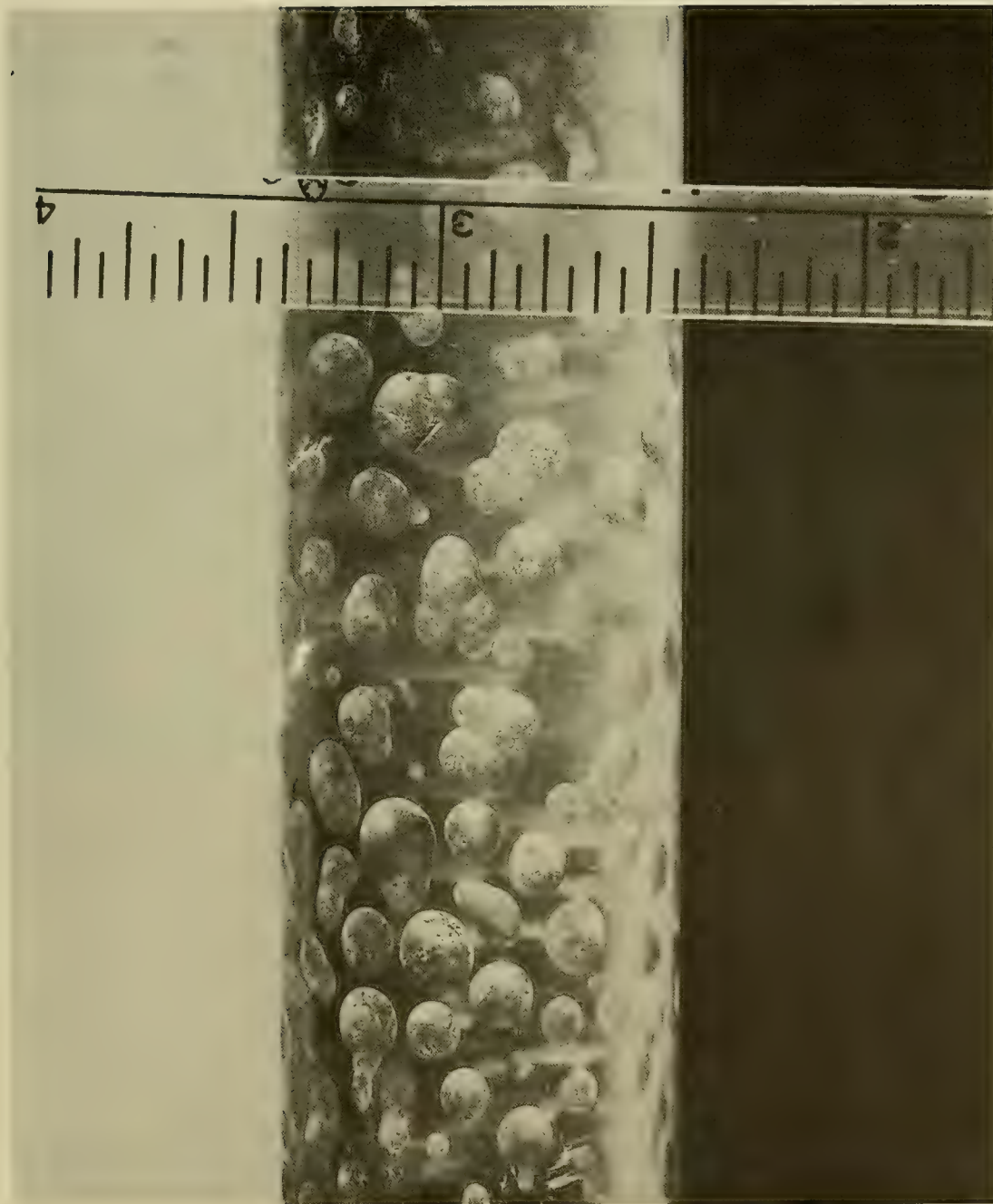


FIGURE 3 OVER 100 SHALLOW-TO-DEEP GROOVES (SOME  $\frac{1}{4}$ " DIA AND  $\frac{1}{16}$ " DEEP) BY MARINE BORERS AROUND A CELLULOSE ACETATE PLASTIC ROD BELOW THE WOODEN BAIT PIECE. (EXPOSED AT 5300 FT DEPTH FOR 3 YEARS)



## REFERENCES

- Muraoka, James S. 1962 The effects of marine organisms on engineering materials for deep-ocean use. Technical Report 182. U. S. Naval Civil Engineering Laboratory, Port Hueneme, Calif.
- Gray, Kenneth O. 1965 Environment of deep ocean test sites (nominal depth, 6000') latitude 33°46'N, longitude 120°37'W. Technical Note 657. U. S. Naval Civil Engineering Laboratory, Port Hueneme, Calif.
- Reinhart, Fred M. 1965 Examples of corrosion of materials exposed on STU II-1 in the deep ocean (2340 feet of depth for 197 days). Technical Note 695. U. S. Naval Civil Engineering Laboratory, Port Hueneme, Calif.
- Turner, Dr. Ruth D. Identified marine borers. Museum of Comparative Zoology, Harvard University, Cambridge, Mass.
- Muraoka, James S. 1964 Deep-ocean biodeterioration of materials — part I. four months at 5,640 feet. Technical Report 329. U. S. Naval Civil Engineering Laboratory.
- Muraoka, James S. 1965 Deep-ocean boring mollusk. BioScience, v. 15, no. 3, p. 191. March 1965.
- Turner, Harry J. 1961 Deep teredo. Oceanics, v. 8, no. 2, p. 11. December 1961.
- DePalma, John R. 1963 Marine fouling and boring organisms in the Tongue of the Ocean. Report No. 0-64-62. Unpublished manuscript. U. S. Naval Oceanographic Office, Washington, D. C.



A PRELIMINARY STUDY OF THE DIRECTIONAL SPECTRUM  
OF SHORT-PERIOD INTERNAL WAVES

by

H. Charnock

UK National Institute of Oceanography  
Wormley, Surrey



# A PRELIMINARY STUDY OF THE DIRECTIONAL SPECTRUM OF SHORT-PERIOD INTERNAL WAVES

by

H. Charnock

UK National Institute of Oceanography, Wormley, Surrey

## INTRODUCTION

The material on which this work is based was collected on Cruise 21 of R.V. 'Chain' (Woods Hole Oceanographic Institution) in September 1961. The Chief Scientist was Professor J. B. Hersey and the observations were made under the supervision of Mr. R. Frassetto.

The object was to study the short-period internal waves on the seasonal thermocline in deep water between Madeira and Gibraltar and the main tool was the Woods Hole thermistor chain which was used to record temperature fluctuations at intervals down to a depth of about 100 m.

To gain some information about the directional properties of the internal waves, the ship followed a track in the form of a regular octogram. Each leg was about 40 km long and took about 2 hours.

## ANALYSIS AND RESULTS

The thermistor chain provides an analogue record of the depth of selected isotherms as a function of time. These were first read off and prepared in digital form for analysis on a digital computer.

The mean temperature distribution had an almost isothermal layer about 50 m thick, overlying a thermocline in which the temperature fell by about 5°C in 30 m. This basic temperature structure stayed fairly constant over the 16 hours of recording but the individual isotherms fluctuated in depth. The typical range was 5 to 10 m with extremes beyond 20 m.

Further analysis has so far been limited to the study of fluctuations in the depth of the 20°C isotherm, which is thought to be typical of the motion about the mid-depth of the thermocline. The mean square fluctuation in the depth of this isotherm varied, but its variation was not systematic with either course or time. Most of the variation was associated with the longer-period components of the spectrum which were poorly sampled.

A spectral analysis was made of the eight records of the 20°-isotherm depth, one for each of the eight courses. The records were, of course, in time but they have been interpreted in terms of distance on the reasonable assumption that the ship's speed was constant. The wave-number range was from zero to 6 cycles/km.

The general form of the spectrum is such that the (amplitude)<sup>2</sup> per unit wave-number decreased with increasing wave-number, approximately as (wave-number)<sup>2</sup>. There is some indication that at the lowest wave-numbers, below about 1 cycle/km, the falloff was less rapid.

This spectral form can perhaps be interpreted in terms of a recent proposal by O. M. Phillips, based on the hypothesis that the amplitude of internal waves is limited by shearing instability at their troughs and crests.

No clear directional property of the spectra was found - those from all eight courses are virtually indistinguishable. This is consistent with their monotonic form and provides an interesting negative result.

If internal waves are generated by the nonlinear interaction of surface waves then their directional spectra must be broad. No quantitative estimate of the directional spread seems to be possible. Equally, since we have no clear idea of the damping and decay of internal waves, they may be interpreted as a residue or continuum of internal waves generated at other places and at other times.

It must always be borne in mind that the analysis of records such as these in terms of internal waves may not provide the most useful interpretation. It may be more useful to consider them as turbulent fluctuation in an hydrostatically stable layer.

Further analysis planned will attempt to assess the vertical structure of the temperature fluctuations so as to provide information on the best interpretation. This will be used to design further observations using a British thermistor chain and to make a quantitative estimate of the effect of the thermal inhomogeneity on sound transmission in the ocean.

A further account of the investigation is being prepared for publication elsewhere.



# PRECISION FATHOMETER RECORDER

by

Richard G. Popovici and Thomas K. DeWitt

Electrographic Systems Department, Raytheon Company  
Submarine Signal Division, Portsmouth, Rhode Island



# PRECISION FATHOMETER RECORDER

by

Richard G. Popovici and Thomas K. DeWitt  
Electrographic Systems Department, Raytheon Company  
Submarine Signal Division, Portsmouth Rhode Island

## INTRODUCTION

With approximately 98 per cent of the ocean still unsurveyed, the problem of compiling contour charts is ever so growing. Moreover, the demand is increasing for surveys of numerous strategic areas which must be executed with speed, accuracy, and reliability.

Contour charting of the ocean floor is achieved by compilation of profiles obtained along the ship's track with a sonic transceiver and a precision paper recorder. The precision recorder is a vital instrument in this operation since it provides a continuous integrated and precise display of the bottom and sub-bottom topography on a permanent record.

Many of times we have heard statements from the Navy Oceanographic Office expressing their deep concern over the reliability and maintainability of oceanographic instrumentation. It was said recently at a marine symposium that over 75% of the instrumentation was inoperative or not functioning properly at the time of delivery.

This fact, coupled with the ever-increasing demand for precision recorders in survey work, has prompted Raytheon to develop an instrument that will do justice in this or related assignments. The development of the Precision Fathometer Recorder, PFR-193, was a challenge for experienced engineers to break the barrier of technological dissatisfaction.

This paper covers in detail the design concepts and novel features of the PFR-193.

## FUNCTIONAL DESCRIPTION

### General

The PFR-193 is a small, self-contained precision electromechanical recorder, which generates precise solid state keying pulses for the companion sonar transceiver, and prints the return echoes with a timing stability of 2 ppm over the operating temperature range. The recording medium used is dry electrosensitive paper, which provides high resolution and excellent white-to-black contrast on a good dimensionally-stable base.

The recorder consists of a mechanical assembly unit and an electrical assembly unit, (Fig 1), both housed in a rugged cabinet. The mechanical unit sweeps the styli across the paper at a uniform linear rate while advancing the paper under the styli from a paper feed to a take-up system. The mechanism also generates, through the timing pulse generator, highly accurate and stable timing pulses to initiate actions of keying, gating, and calibration marking.

The electrical assembly, responsible for control and power generation functions, features a highly stable power source of 2 ppm which supplies power to the synchronous motor in the mechanical unit. In addition, it processes the timing signals from the mechanical unit and translates these into key-pulse, gate, and calibration marking signals. The print amplifier processes the sonar receiver output information, which, in the end product, provides the operator with recordings of excellent quality and highest resolution.

### Sweeping

The components of the sweeping function (Fig 2) are responsible for the transformation of a precision frequency into a smooth jitter-free linear motion of the styli across the paper. A 60-cps oscillator, with a frequency stability of +2 ppm over the recorder operating temperature range, and a stability of  $\pm 1$  ppm over any  $10^{\circ}$  C range, provides a square wave output to the DC-to-AC inverter. The inverter is a high efficiency source of 110-V AC power to the synchronous motor that in turn generates the stylus motion. In addition, 5 watts of precision AC is available at a rear-mounted receptacle, so that a wall clock or other timing device may be driven by the recorder. Through an auxiliary connection, the recorder can be driven by an external 60-cps source, to check its accuracy with WWV, or to play back tapes of soundings. The DC-to-AC inverter is fed from a regulated DC voltage supply, thus assuring voltage regulation at the synchronous motor. This 4-pole 1800-rpm motor has been designed to run precisely at synchronous speed, while maintaining high damping and extremely little jitter. The motor shaft is connected to a precision gear train, containing three electromagnetic clutches. Energizing the proper clutch selects the gear ratio corresponding to the scale in use. The sync pulley is attached to the output



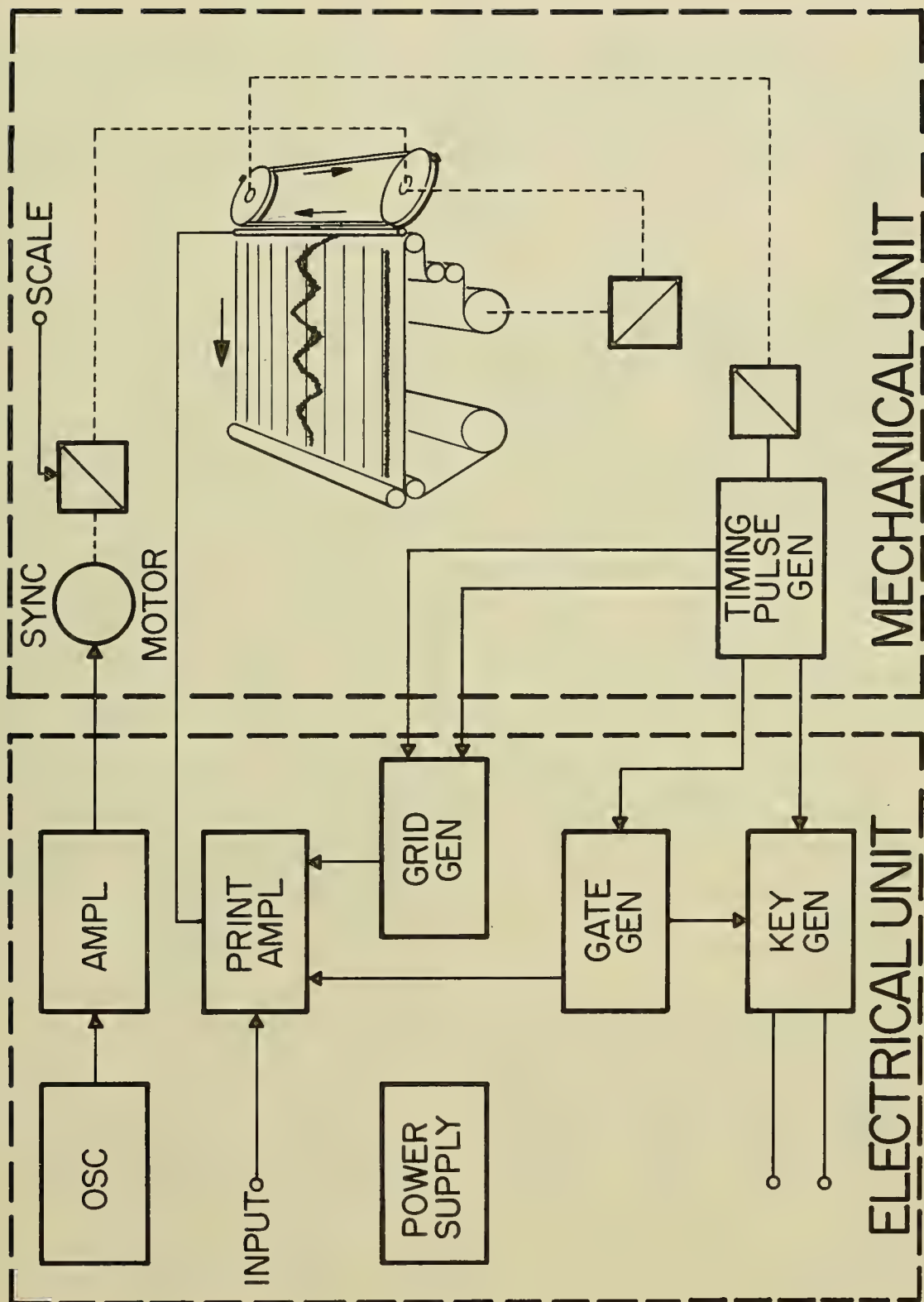


FIGURE 1 GENERAL BLOCK DIAGRAM

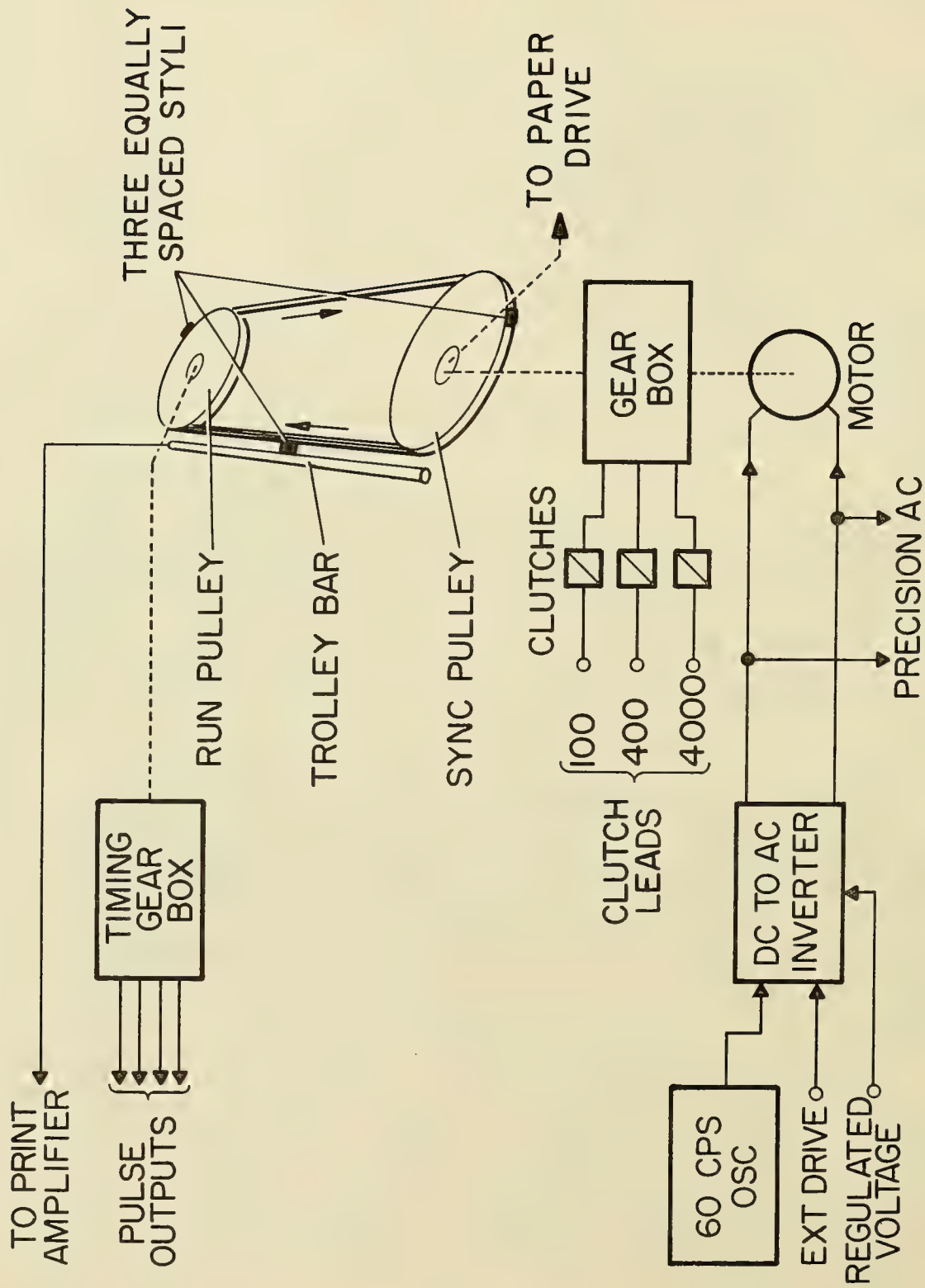


FIGURE 2 SWEEP FUNCTION DIAGRAM

of the gear train, and drives the rubber timing belt which serves to transport the styli, precisely guided by a trolley bar, across the paper. The trolley also serves as the electrical connection between the print amplifier and the active styli. The run pulley drives the timing gear box which generates key, gate, and calibration grid timing pulses. A saturated photo-optical device digitally generates extremely accurate pulses.

### Paper Feed

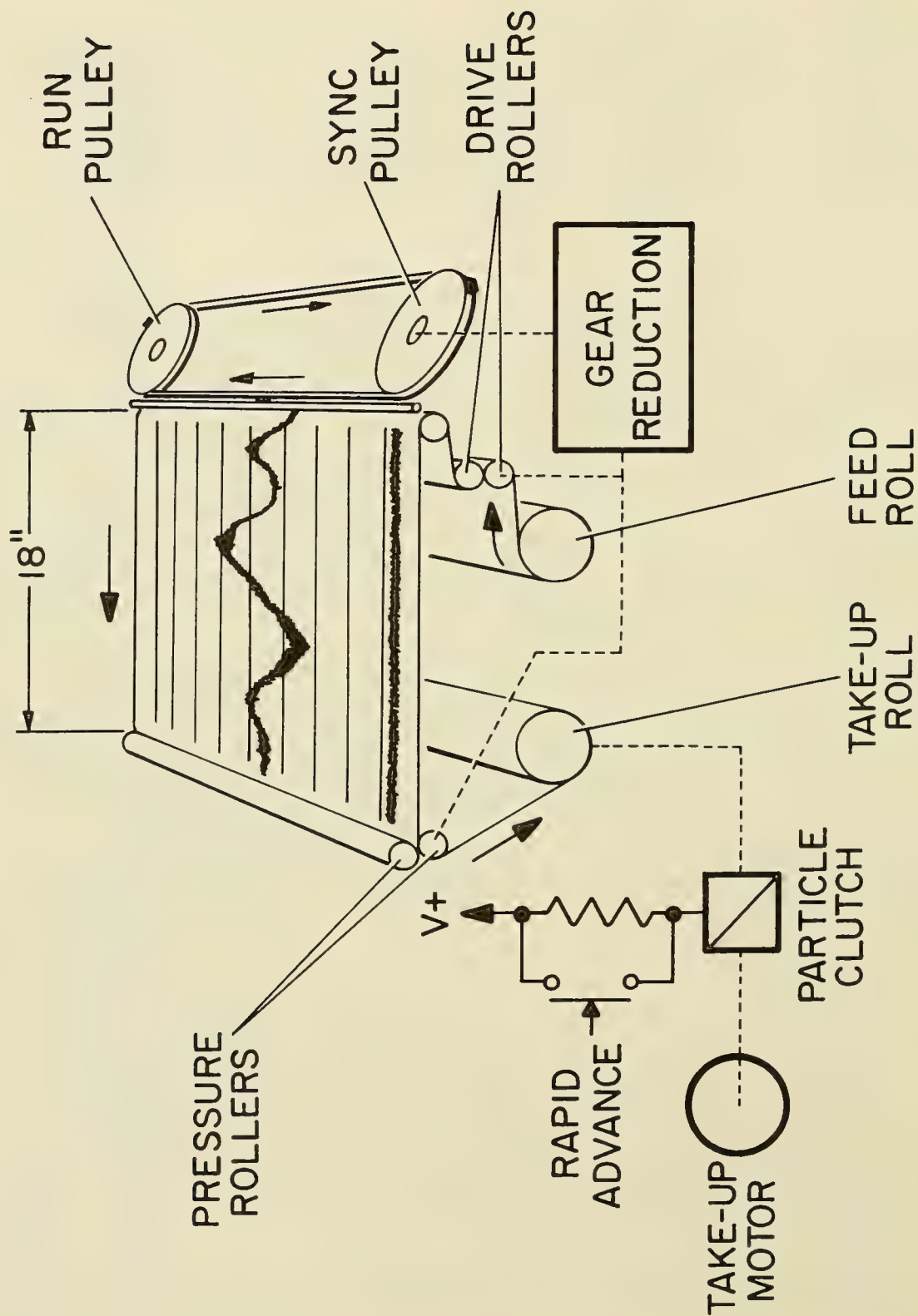
It is essential to advance the paper with the same precision as the stylus sweep to achieve constant and accurate amplification of the bottom profile at fixed ship speeds. The paper feed system (Fig 3) originates at the feed roll from where the paper is fed through the drive rollers, driven through a gear train coupled to the sync-drive pulley, at a constant rate of 150 lines per inch. From the drive rollers, the paper is fed past the styli and across an 18-inch long platen which is the area viewed by the operator. The platen allows the operator to make annotations easily on the chart. The paper then passes through the pressure rollers, which keep tension on the paper and assure a smooth flow, the rollers being geared directly to the drive rollers. The paper is then fed to the take-up roll, where the take-up motor and clutch provide even tension.

The purpose of the pressure rollers and the take-up mechanism is twofold. First, if it is desired to review past charts, the chart may be unwound from the take-up roll without disturbing normal paper feed, due to the isolating effect of the pressure rollers. Then, after review, if the rapid chart advance button is pressed, the slipping action of the clutch is cancelled, and the paper is rewound at a fast rate. Second, since the take-up motor has the ability to override the paper feed mechanism when directly coupled, it also acts as an automatic rapid paper advance. Manual advance, using the knobs on the end of the rollers, can also be accomplished.

### Print Amplifier

The print amplifier (Fig 4), a key module in the PFR-193, provides the operator with much more closely controlled recording characteristics and flexibility than has been available previously. In addition, residue generated by the writing process with electrosensitive recording papers has been suppressed to a new low by closely controlling the energy to the stylus, resulting in an optimum power transfer. The small amount of residue occurring is removed almost completely by a highly efficient blower and carbon filter system.

The input to the print amplifier is the output from the transceiver, sending and receiving sonar pulses. The print amplifier processes and





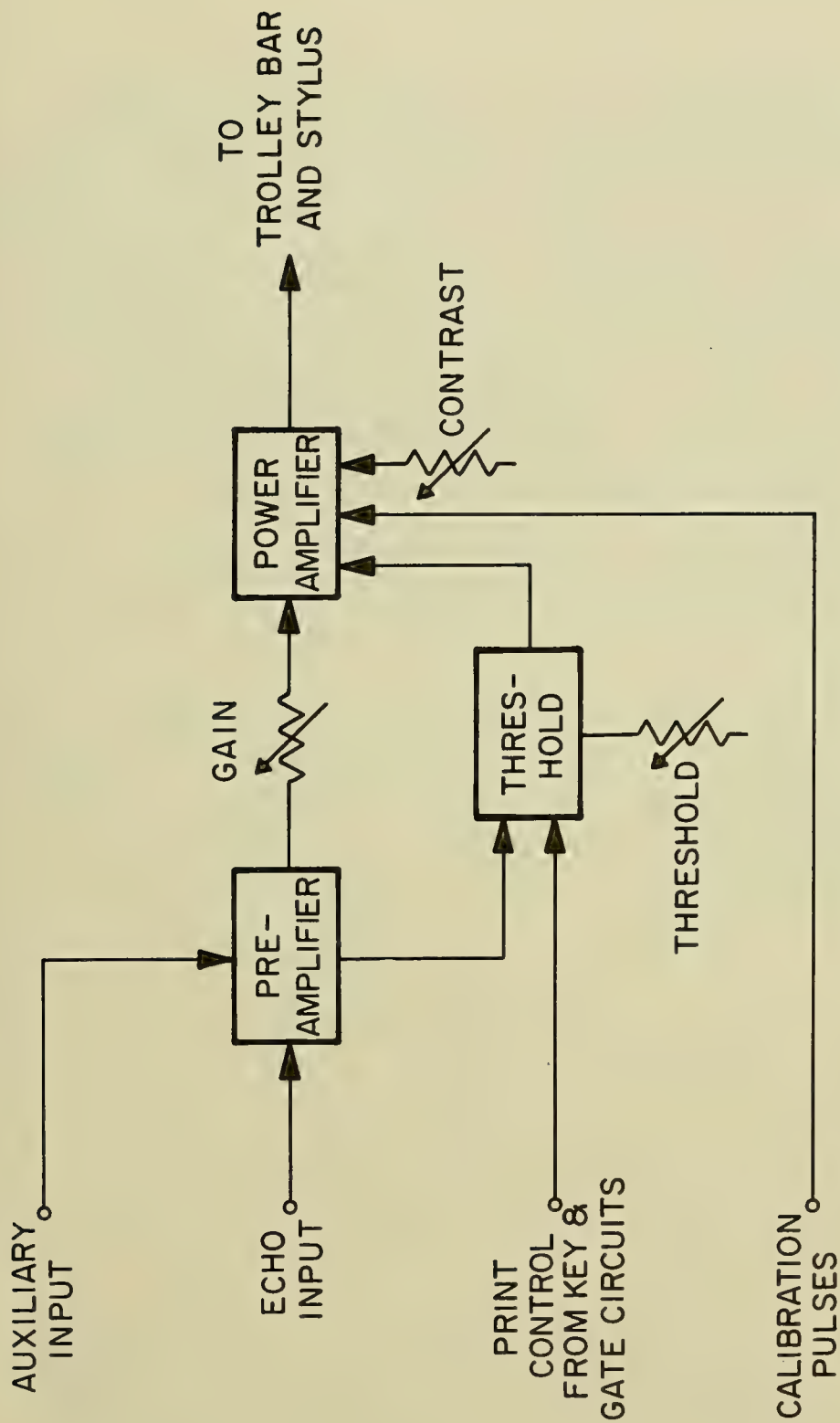


FIGURE 4 PRINT AMPLIFIER BLOCK DIAGRAM

reproduces these signals on the chart, resulting in a high contrast recording of the bottom profile. This is accomplished by variable amplification with the gain control, threshold to eliminate background noise, and contrast, which allows the amplifier dynamic range to be changed to suit variations in input signal-to-noise ratio.

The threshold circuit allows the setting of the minimum signal that the recorder will print. If the input is below a predetermined signal level, there will be no output from the print amplifier. If the input goes above this level, the recorder will print a shade determined by the setting of the gain control. It may be noted that the gain control follows the threshold voltage pick-off point, allowing threshold to be set independently of gain. Full limiting is included to eliminate the possibility of allowing too much energy to reach the stylus, which would result in excessive black printing during the outgoing pulse.

The contrast control allows the dynamic range of the recording to be varied. This differs from the gain control in that the latter simply varies the absolute input range that will cause the recording to go from white to black. (See Fig 15 and Fig 16 for sample recordings.)

The operation of the three controls, in a typical condition (Fig 5), would be as follows: If the input echo, which is usually the main signal of interest, has a dynamic range of 14 db, the gain control would normally be set so that the echo signal peak would print black. Any input signal above this level will not print heavier due to the limiting feature. The threshold control would be set at a point approximately -13 db from the peak input echo; the signal to the power amplifier would then consist of a 13 db input signal variation. The contrast control is next set to give the best quality record which, in this case, would probably be such that the dynamic range of the print amplifier would cause a recording to go from white to black in a range of 13 db. If additional detail of the lower amplitude second echoes is desired, the contrast range would be greater, e.g., 25 db. AGC has not been included in the present design until adequate sea tests can be completed to insure that this function is merited in this application.

The print amplifier also prints grid marks on the chart, which are generated by the grid marking generator. Interruption of printing for various functions is achieved through the print control lead, which acts as an on-off switch.

The input impedance of the PFR-193 print amplifier is 5000 ohms, with a constant frequency response from 1 to 20 kc of the processed input. The auxiliary input will accept signals from 10 cps to 100 kc to permit printing of auxiliary inputs enabling the recorder to check external functions. A typical application might be to record the ticks of a watch, checking its accuracy. Available as an option is a facsimile converter which converts the PFR-193 to standard 120-rpm facsimile recorder, when used in a standard facsimile communication network.

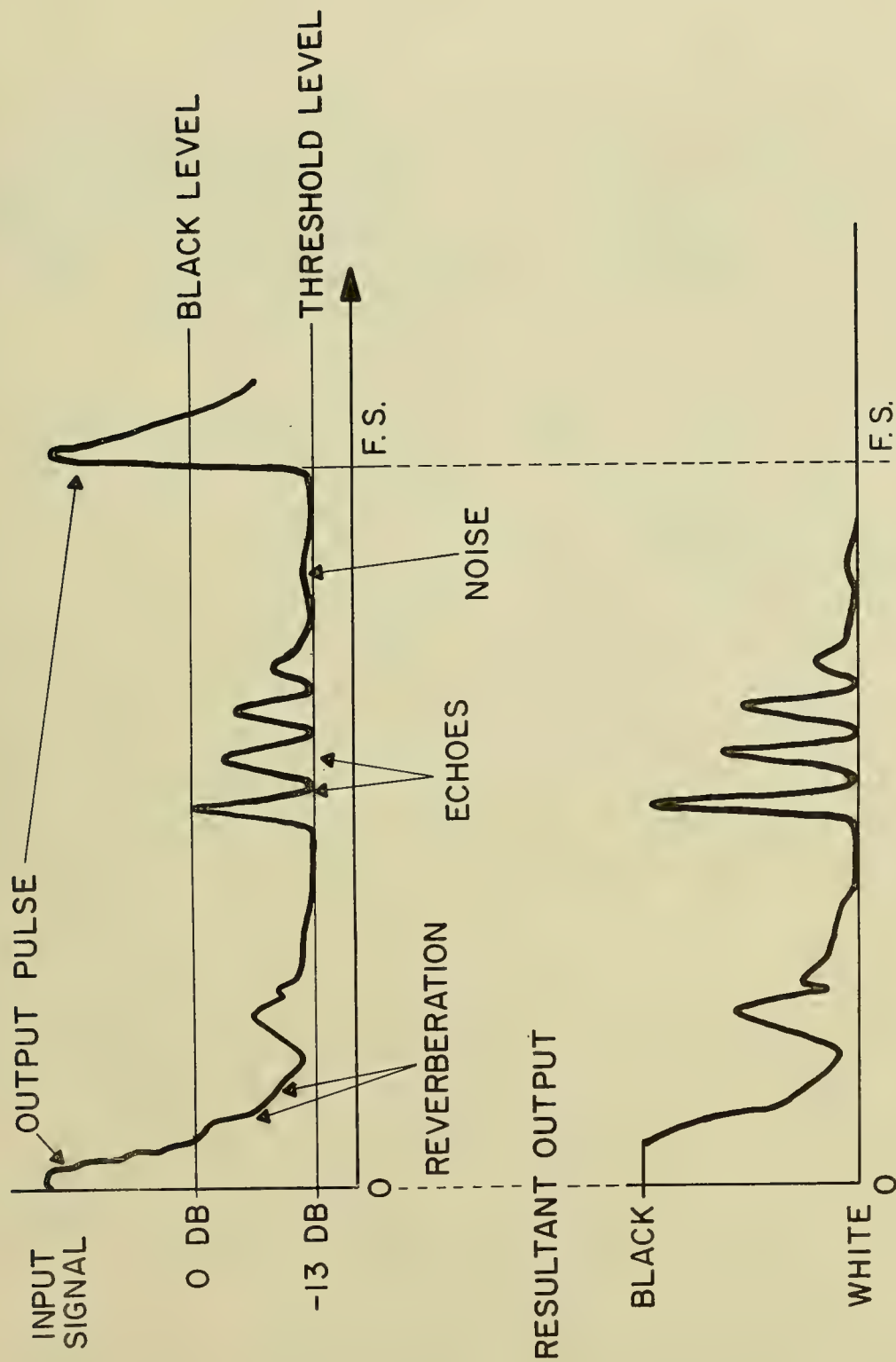


FIGURE 5 PRINT AMPLIFIER TYPICAL ADJUSTMENT

## Gating

The gating circuit (Fig 6) is entirely digital for precise repeatability and stability. The gating ranges are in fixed incremental steps, identified by an accurate calibration dial. The circuitry operates on a constant time basis; for example, it will allow keying for 5 seconds and recording for 5 seconds. As a result, when the recorder is switched from the 400 to the 100-fathom scale, the times for gating and keying remain the same. This allows expanded scale operation on the 100-fathom scale at depths where gating is needed, without adjustments when scales are switched.

The gating cycle is controlled by a timing pulse which is generated in the timing pulse generator gearbox. This pulse normally occurs once per scan when the stylus is precisely at the middle of the chart. When the gate circuit causes the recorder to change from key to record or vice versa, the change-over point occurs at the center of the chart. The timing pulse is divided by a string of binary, integrated circuit flip-flops. On the 400-fathom scale, the once-per-second pulse is fed to FF3, and FF3 through FF6 divide the pulse by an integer ratio. The Gate Range switch selects how often that the Gate FF is triggered. The Gate FF provides a binary control signal for the key or record interval.

When the recorder is on the 100-fathom scale, FF1 and FF2 divide the timing pulse (now at 4 per second) by a factor of 4, such that the input to FF3 is again at one pulse per second. The gate operation now is the same as on 400 fathoms, with the exception that 4 keys per second are now made. This assures the same sampling density, in time, regardless of scale. Gating is disabled by grounding the Gate FF output, thus allowing simultaneous keying and recording for identification of scattering layer structures.

## Key Circuit

The key circuit (Fig 7) provides an accurate, fixed-length contact closure simulation to an external sonar transceiver. The time of occurrence of the pulse is also controlled by the timing pulse generator, which generates a highly stable and accurate pulse to trigger the keying circuitry. The jitter of this pulse is in the order of  $\pm 1$  sec. Since the key timing pulse occurs at the zero edge of the chart, the gate and key timing pulses can be interchanged to provide center of chart keying. Both pulses can be adjusted with relation to the paper with a micrometer-type screwdriver adjustment, allowing the leading edge of the key pulse to be adjusted easily with respect to the chart.

The pulse from the timing generator is fed to the "key" multivibrator which generates the length of the keying interval. This length is varied in two ranges by a front panel control from 0.2 to 20 ms. The output of the multivibrator is fed to the Key Gate which has as a second input the



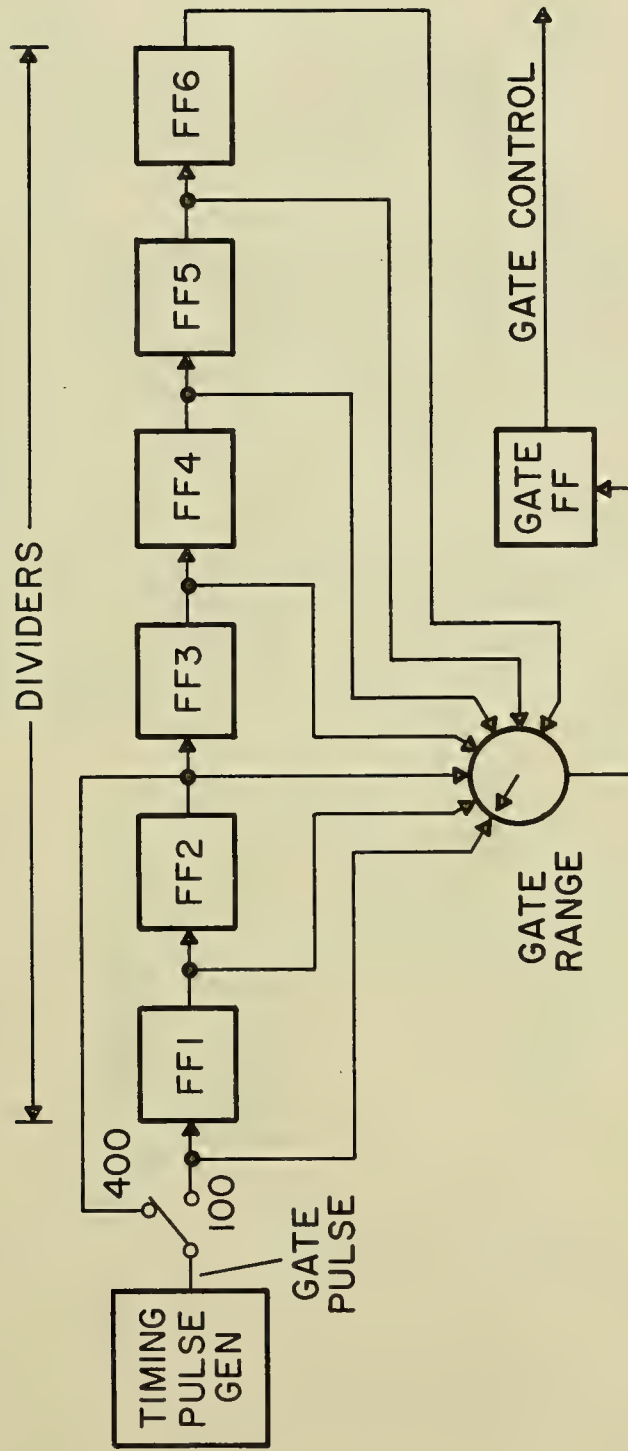


FIGURE 6 GATE CIRCUIT BLOCK DIAGRAM

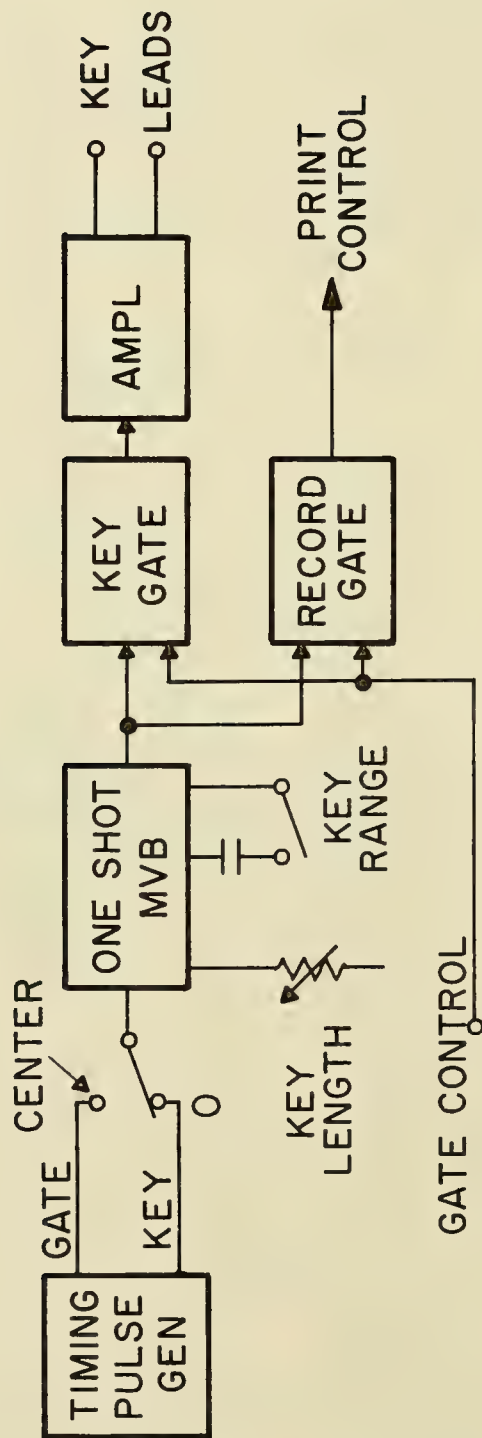


FIGURE 7 KEY CIRCUIT BLOCK DIAGRAM

Gate FF. When the Gate FF is in the key state, or when the gate function is disabled, the key pulse is fed to the amplifier circuit which generates the simulated contact closure with sharp rise and fall times. The key amplifier output leads are isolated from ground. The maximum voltage which can be applied to the key leads is 200 volts of either polarity, and the maximum current is 0.2 amp.

The Record Gate generates the print control signal, fed to the Print Amplifier. This gate is normally controlled by the Gate FF, and disables the print circuitry during the keying cycle, except during the key pulse interval. Thus, the recorder will not print during the keying cycle, except when a sonar pulse is generated, allowing the leading edge of the key pulse from the sonar transceiver to be always printed.

### Calibration Pulse Generator

The PFR-193 generates its own calibration marks which are printed on the chart. Twenty grid marks are printed on the 100 and 400-fathom scales, and 10 on the 4000-fathom scale. The calibration marks are interrupted every five minutes by a precision switch. The possible ambiguity that might result by using the same number of grid marks on the 100 and 400-fathom scales has been resolved by making the length of the five minute interruptions four times longer when the 100-fathom scale is used.

Two grid mark timing pulses are generated by the timing pulse generator (Fig 8). On the 4000-fathom scale, ten evenly spaced pulses per scan are used, starting at zero. When the recorder is switched to 100 or 400 fathoms, the 4000-fathom scale pulses are summed in a gate with another timing pulse, which fills in the in-between pulses. The gate output triggers a one-shot multivibrator, which provides a standard pulse for printing. In addition, the gate is controlled by a signal from a precision switch, which serves as the grid interruption control, for a period of 10 seconds every five minutes.

### Control Functions

The recorder contains two precision motors and gear trains. One is located in the mechanical assembly and is used to generate the sweep time base. The other, the program timer (Fig 9), generates the grid interrupt and deep scale time base functions. The purpose of the deep scale switchover is to allow the PFR-193 to be used in applications where an operator is not continually present. The recorder will automatically check the base line of the 400-fathom scale by switching to 4000 fathoms for 30 seconds. Deep scale operation will occur 1, 2, or 4 times per hour. The frequency of occurrence of this event is determined by the scale switch, which controls the scale clutches and scale relays. The grid interruption switch and the deep scale switches are mechanically

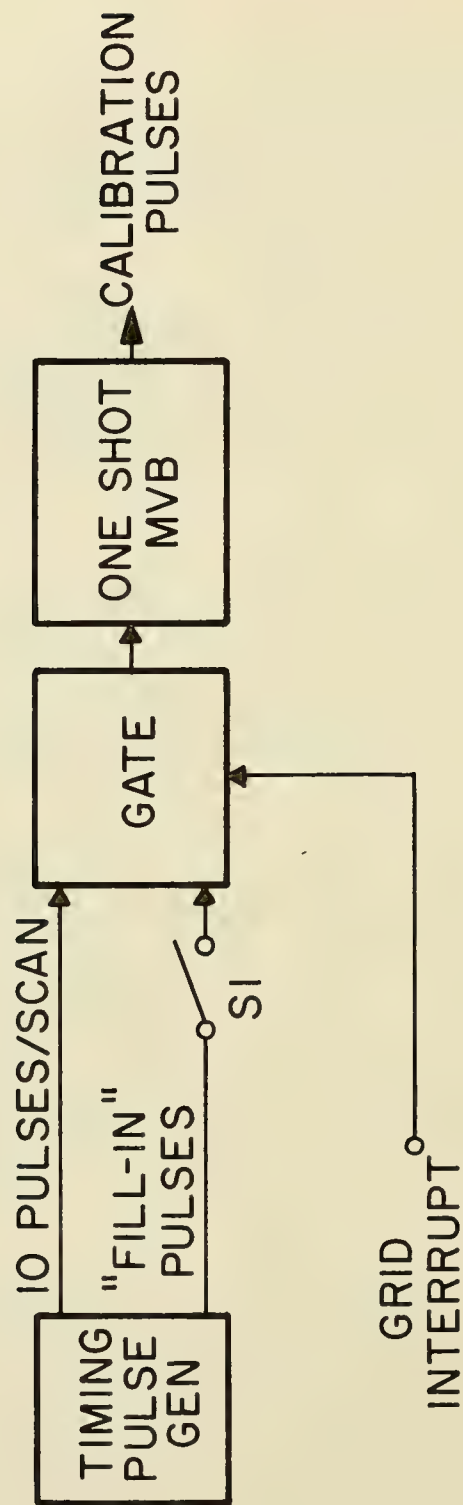


FIGURE 8 CALIBRATION PULSE GENERATOR BLOCK DIAGRAM



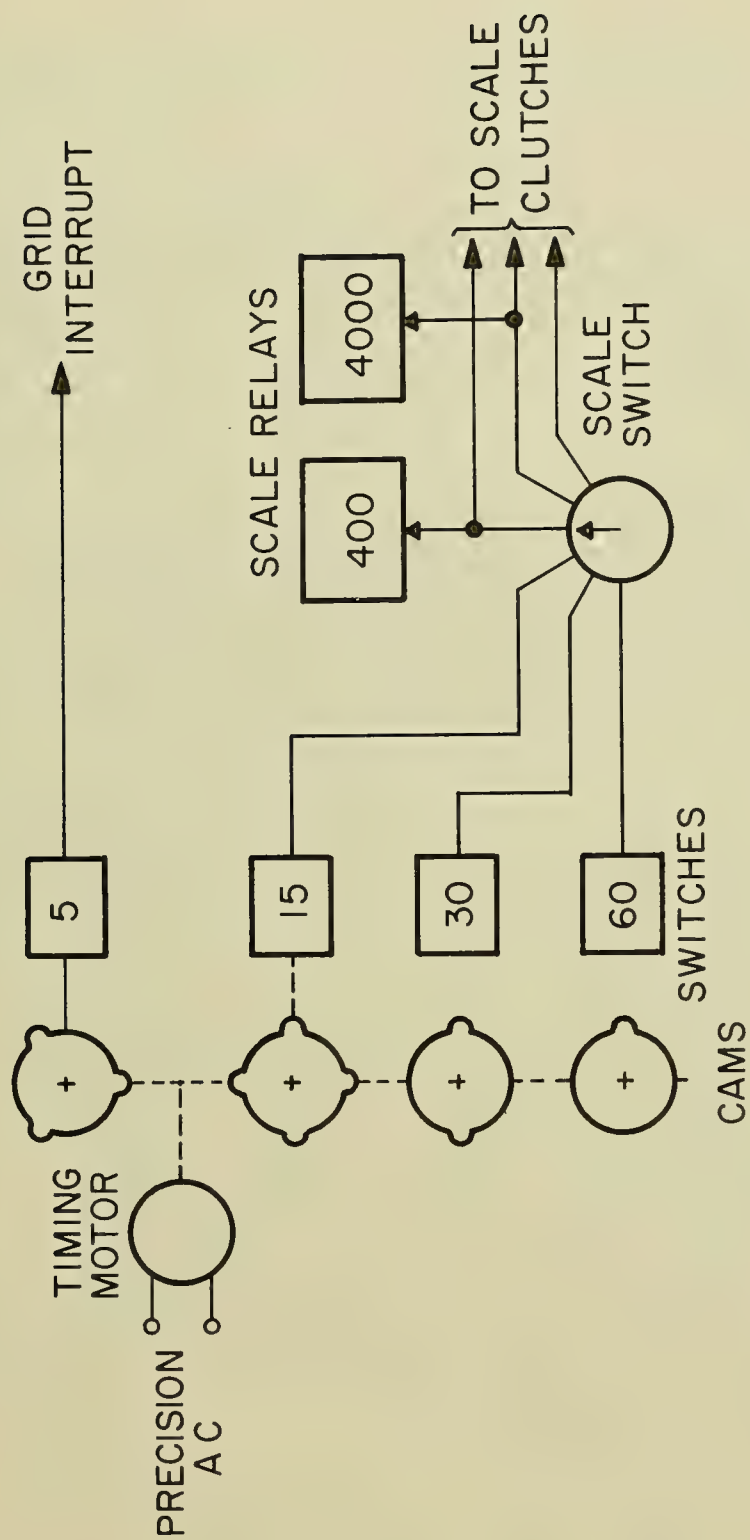


FIGURE 9 CONTROL BLOCK DIAGRAM

interlocked, allowing them to be phased as one unit. Deep scale operation will normally occur during the 55th to 60th minutes of the hour, when properly phased.

## CONSTRUCTION

The face of the recorder cabinet is 34.5 inches wide and 25 inches deep with a height of 11 inches, and is constructed of a high strength, non-combustible polyester glass (Fig 10). Clean modern appearance and functional rigidity have been combined in one. The cabinet can be made completely RFI-proof should the need require. A glass panel over the chart area is easily removable to allow operator annotation of the chart. A rigid bar in the front of the machine provides handhold for the operator as well as a means of handling.

The recorder, designed with consideration of shipboard mounting space, is extremely versatile in the number of ways that it can be mounted, either bulkhead or table. If it is necessary to review past records, the recorder would be mounted with the paper feeding toward the front, allowing the operator to review the past record with ease. If adequate side space is available, or it is not necessary to review the past record, the recorder can be turned 90 degrees, allowing the operator to see a true-oriented picture of the bottom profile.

The construction of the mechanical unit reflects utmost rigidity throughout with the use of castings wherever possible (Figs 11 and 12). The castings are of 356-T6 aluminum as specified in MIL-E-16400, insuring good dimensional stability within the extreme environmental conditions at sea. The modular approach is used for a few significant items, such as the gearbox and the timing pulse generator. These plug-in units are easily replaceable for minimum downtime. All other materials conform to MIL-E-16400 or higher requirements to further insure long life and dependable operation. The PFR-193 has been proven to meet the requirements of MIL-S-901 (Shock) and MIL-STD-167 (Vibration).

Access to the electronics is obtained by swinging back the control panel (Fig 13). The electrical components are packaged in plug-in modules and printed circuit boards which are mounted on a removable flat plate. Numerous test points are used which, when combined with the test meter at the front and the master test point data and function schematic plate, allow easy fault location. Solder-type, fixed-pin connectors have been used throughout the equipment to allow easy field servicing at remote locations should the need occur.

## RELIABILITY

As stated earlier, reliability was one of the most important considerations in the PFR-193 design. Every circuit and mechanical detail was analyzed through an exhaustive process to minimize failure rates.

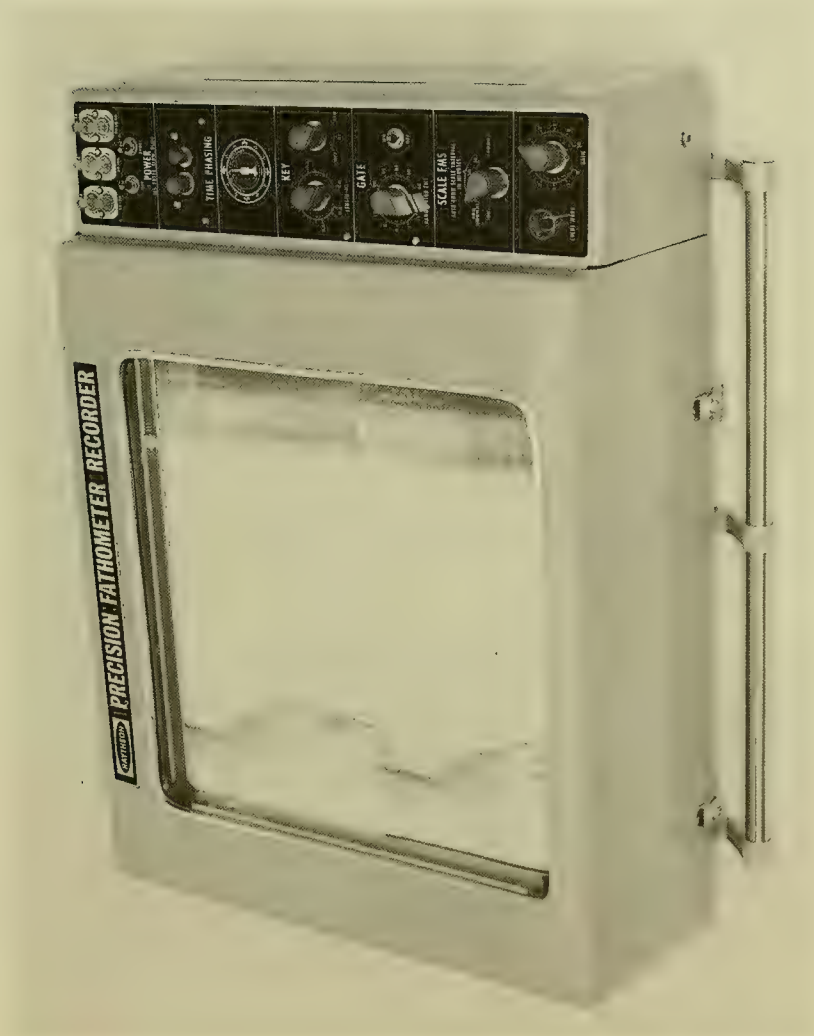


FIGURE 10 FACE VIEW OF PRECISION FATHOMETER RECORDER

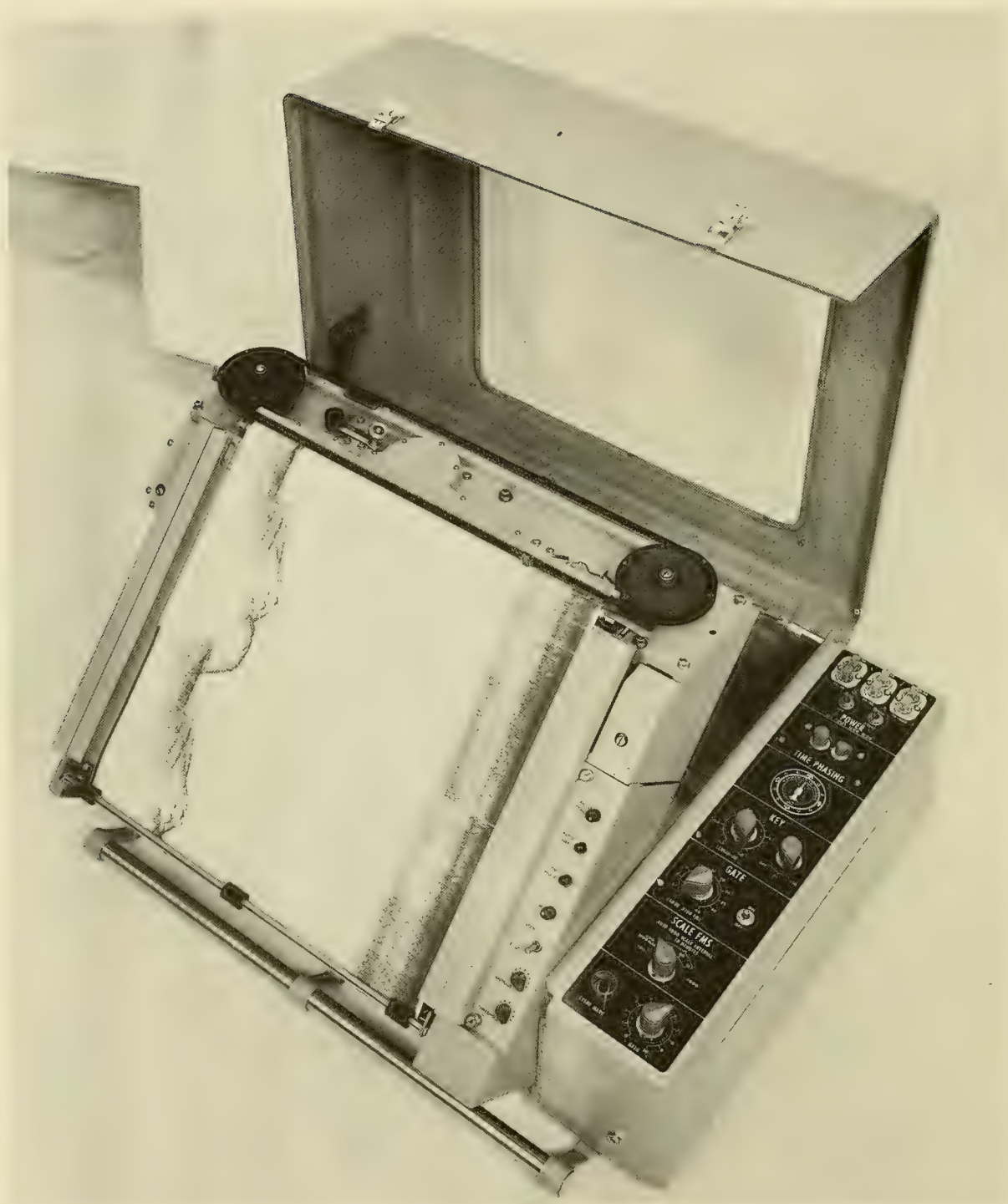


FIGURE 11 VIEW WITH COVER OPENED



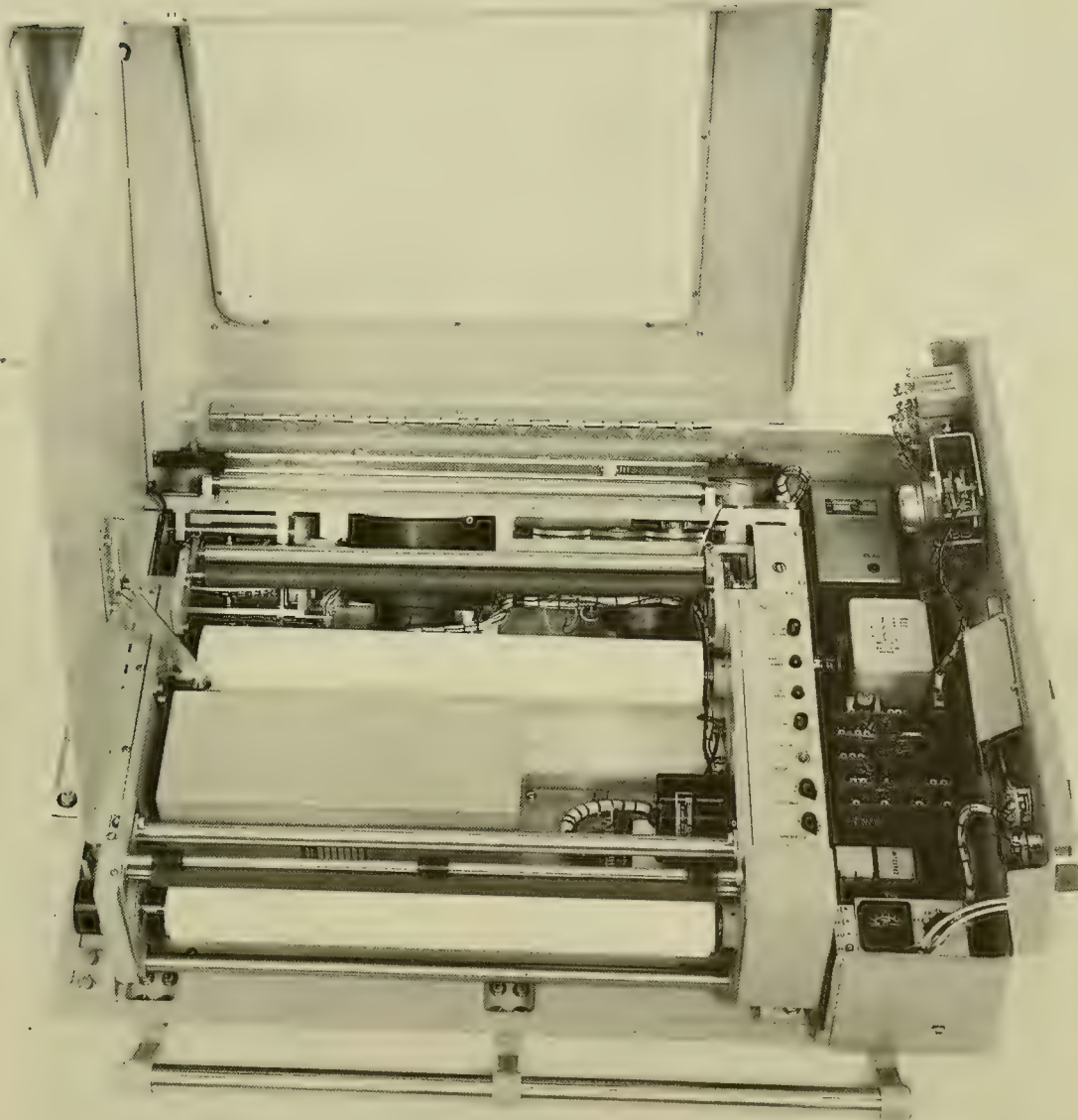


FIGURE 12 VIEW SHOWING PAPER FEED AND OTHER UNITS



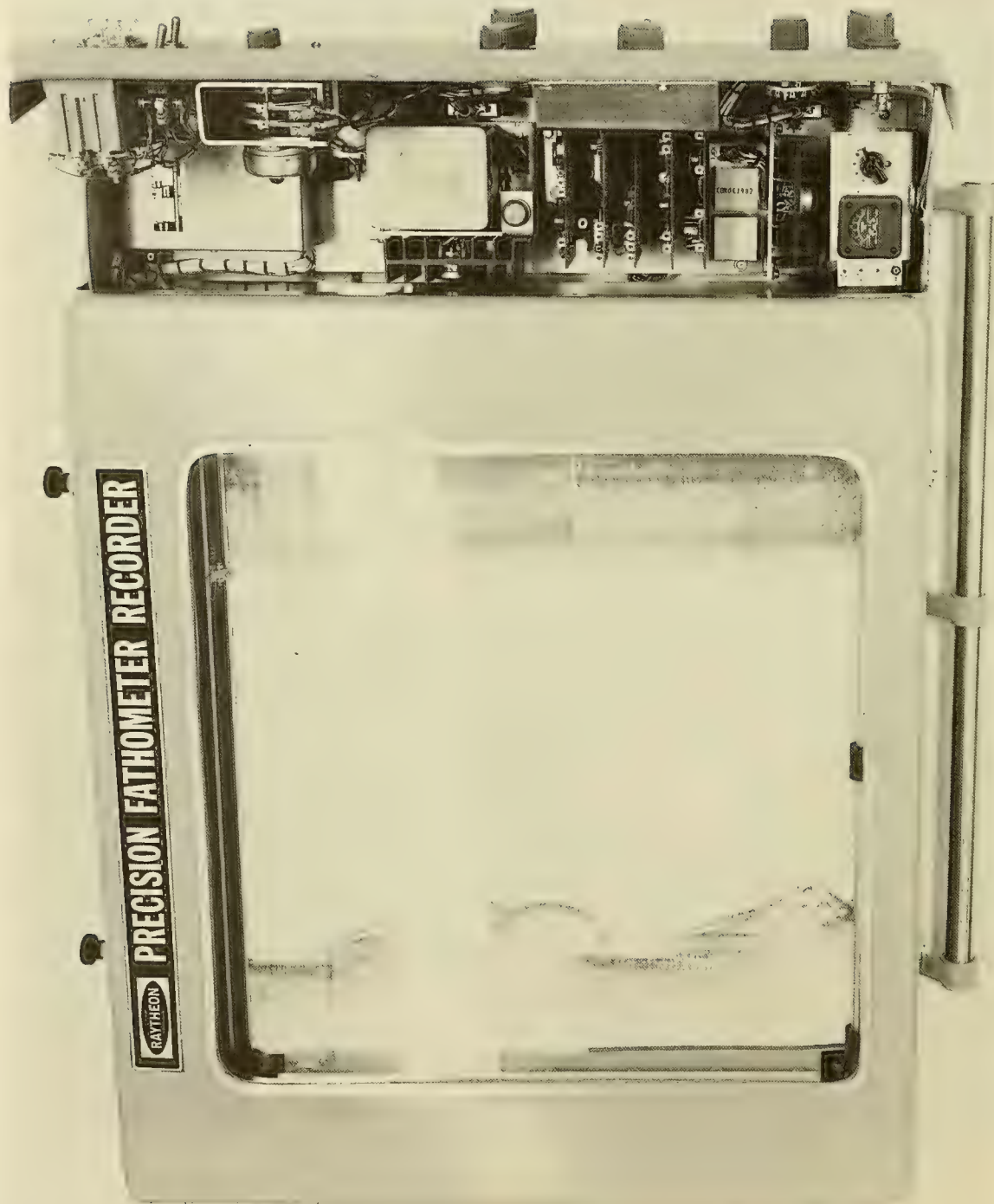


FIGURE 13 VIEW SHOWING ELECTRONICS COMPONENTS

The measure of PFR-193 reliability is expressed in the commonly known MTBF (Mean Time Between Failures). The prediction analysis using component failure rates from NAVSHIPS 93820 shows that this instrument has a theoretical MTBF of 3400 hours. This number was obtained by identifying all the parts with their respective failure rates, which then were summed for the equation:

$$\theta_R = (K_A \sum_{\mu=1}^{\mu=n} \lambda_{\mu})^{-1}$$

where

$\theta_R$  = MTBF in hours

$K_A$  = adjustment factor

$\lambda_{\mu}$  = reliability of any unit

Figure 14 shows the breakdown of units within the recorder and their calculated failure rates.

#### OTHER APPLICATIONS

The PFR-193 can easily be modified for application in such areas as:

ASW Systems -

- Tracking
- Detection
- Classification

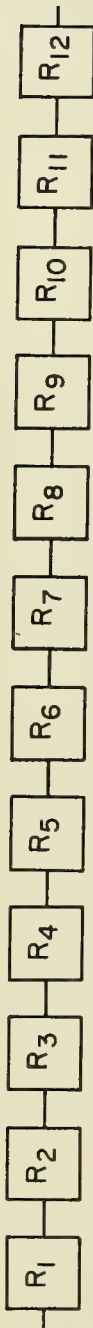
Facsimile -

- Weather Maps
- Messages
- Pictures

Oceanographic Data Recording -

- Temperature
- Velocity
- Current

In fact, this recorder can be adapted to meet many other requirements where utmost precision is necessary.

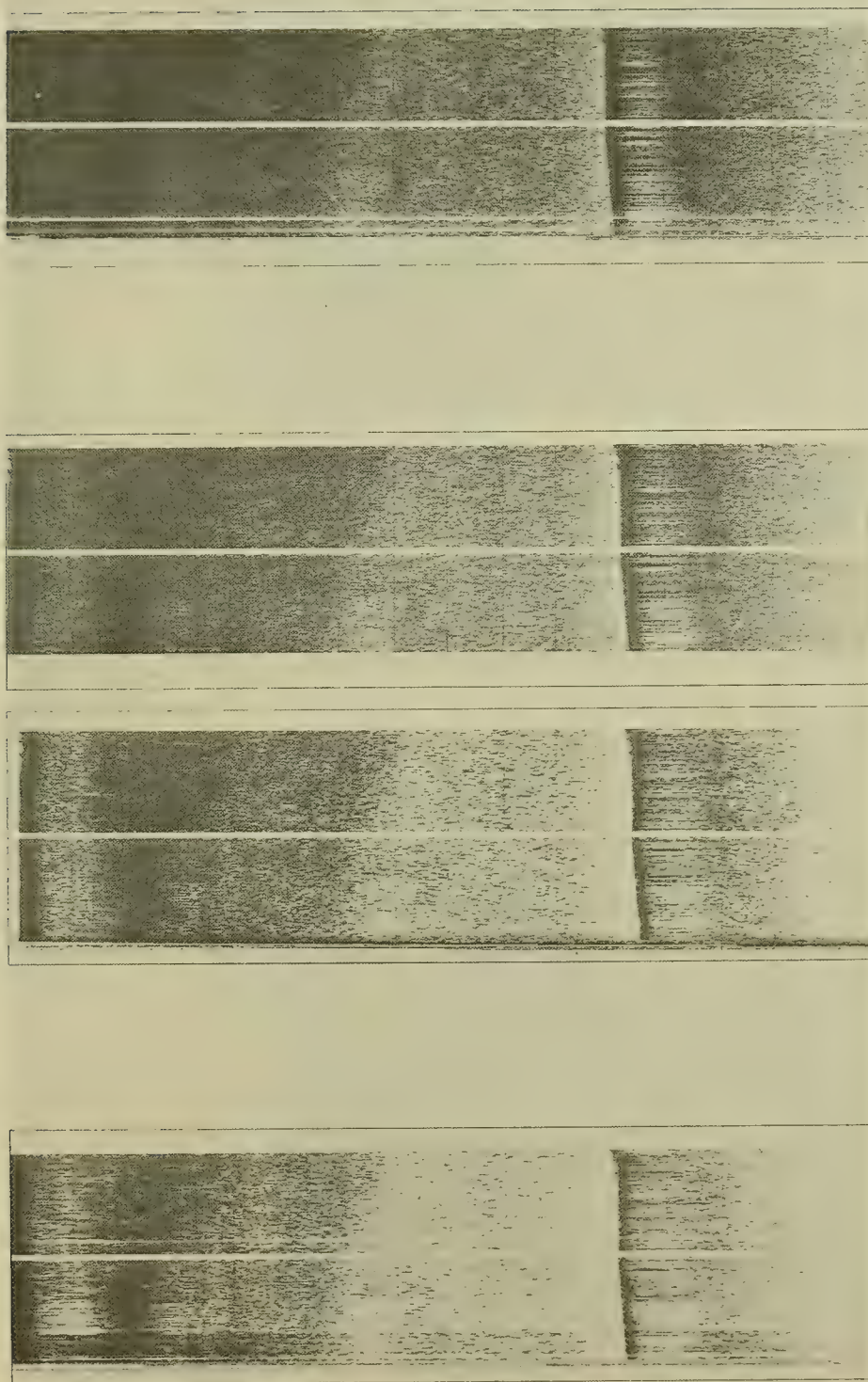


UNIT NUMBER	UNIT NAME	UNIT FAILURE RATE (X 10 <sup>6</sup> HOURS)
R <sub>1</sub>	PRINT AMPLIFIER 1	13.8
R <sub>2</sub>	PRINT AMPLIFIER 2	13.2
R <sub>3</sub>	KEY	13.4
R <sub>4</sub>	GATE	17.7
R <sub>5</sub>	SYNC. MOTOR AMPLIFIER	12.3
R <sub>6</sub>	MECH. UNIT ELECTRICAL PARTS	23.8
R <sub>7</sub>	ELECTRONIC CHASSIS	72.8
R <sub>8</sub>	SYNC. AMPLIFIER OUTPUT MODULE	7.2
R <sub>9</sub>	CONTROL PANEL ASSEMBLY	7.8
R <sub>10</sub>	PRINT AMPLIFIER OUTPUT MODULE	12.3
R <sub>11</sub>	MISC. MECH. PARTS	12.7
R <sub>12</sub>	POWER SUPPLY	58.8
TOTAL		265.8

$$\text{SYSTEM MTBF IN HOURS } (\theta_R) = (K_A \sum_{\mu=1}^{\mu=n} \lambda_{\mu})^{-1} = [(1.1)(265.8)]^{-1} =$$

3400 HOURS

FIGURE 14 PFR SYSTEM MTBF



D. MINIMUM THRESHOLD  
LOW CONTRAST

C. MAXIMUM THRESHOLD  
LOW CONTRAST

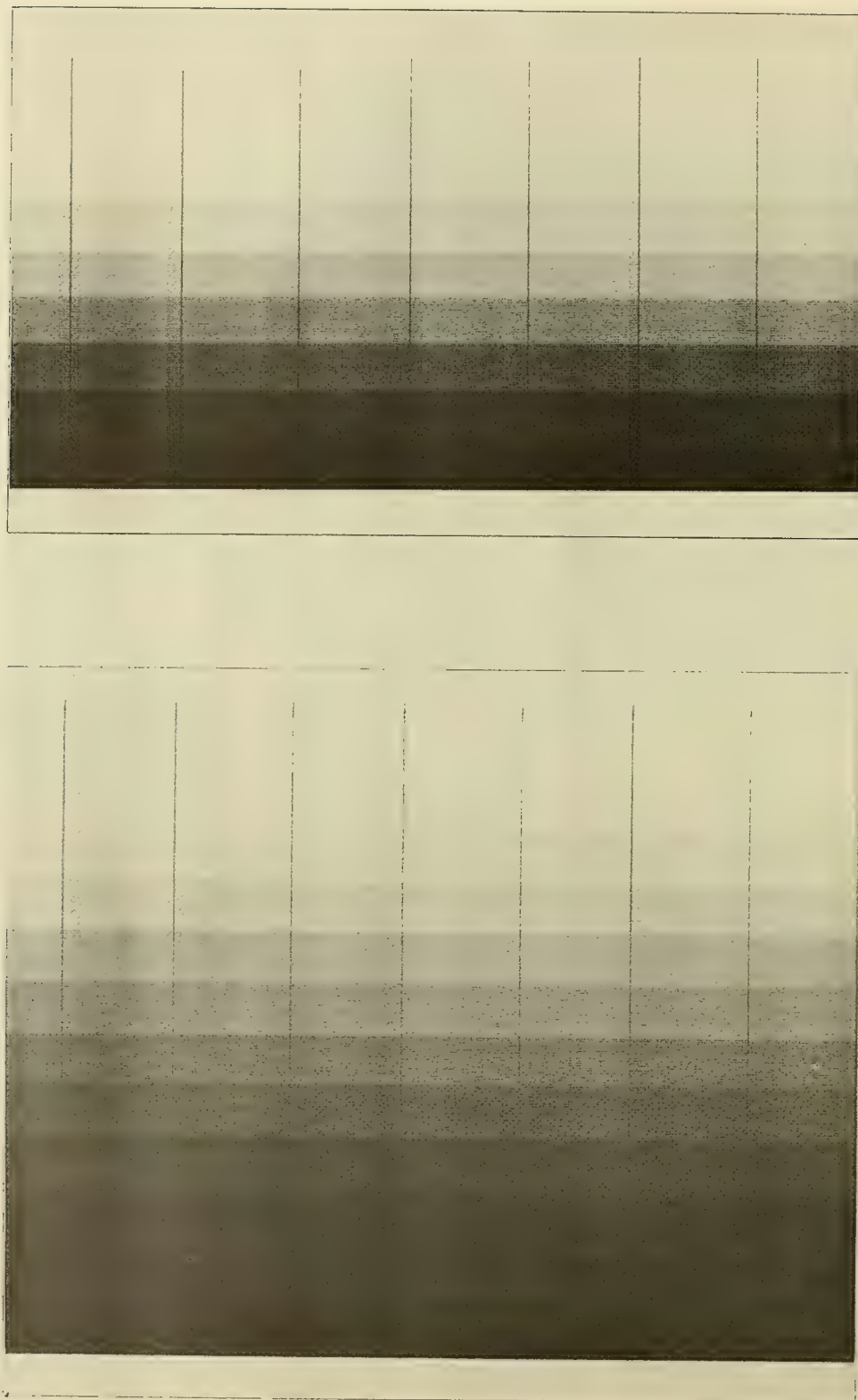
B. MINIMUM THRESHOLD  
HIGH CONTRAST

A. MAXIMUM THRESHOLD  
HIGH CONTRAST

Showing Effect of Threshold  
and Contrast Settings  
• 400 fm scale, depth 2500 fm,  
taken aboard R.V. CHAIN,  
courtesy of Woods Hole  
Oceanographic Institution

FIGURE 15 PFR-193 RECORDINGS FROM SEA TAPE





A. CONTRAST LOW  
OVERALL DYNAMIC RANGE 26 dB

B. CONTRAST HIGH  
OVERALL DYNAMIC RANGE 16 dB

Block Threshold = 0.5 v rms  
Signal Input = 5 kc  
Signal Steps = 2 dB

FIGURE 16 PFR-193 GREY SCALE RECORDING

## CONCLUSION

The design features of the PFR-193 are summarized as follows:

- Rugged construction (proved to meet MIL-S-901 high impact shock and MIL-STD-167 Vibration.)
- High reliability for long uninterrupted operation.
- Simplified maintenance through modular electromechanical construction.
- Versatility in mounting.
- Signal Data Processing with:
  - High Contrast
  - High Resolution
  - Minimum energy transfer
  - Low carbon residue
  - Low RFI
- Accurate gating in distinct increments.
- Automatic base line check.
- Review of past record while in operation.

---

## ACKNOWLEDGMENT

The authors wish to acknowledge the substantial contributions of Jonas Vakarietis to the overall design of the PFR-193.



DEEPLY-TOWED ECHO-SOUNDER RECONNAISSANCE  
OF A FLEET TACTICAL RANGE SITE

by

Michael S. Loughridge and F. N. Spiess  
University of California, San Diego  
Marine Physical Laboratory of the  
Scripps Institution of Oceanography  
San Diego, California





# DEEPLY-TOWED ECHO-SOUNDER RECONNAISSANCE OF A FLEET TACTICAL RANGE SITE

by

Michael S. Loughridge and F. N. Spiess

University of California, San Diego  
Marine Physical Laboratory of the  
Scripps Institution of Oceanography  
San Diego, California 92152

## INTRODUCTION

At the request of the Applied Physics Laboratory, University of Washington, Seattle, personnel and a ship, the R/V OCONOSTOTA, from the Marine Physical Laboratory, University of California, San Diego, participated in precision bathymetric studies west of the island of Kauai in late October and early November 1964. This work was part of the oceanographic site studies for a proposed Fleet Tactical Range west of the island of Kauai and was intended to supplement precision narrow-beam bathymetric work done from ships of the U. S. Naval Oceanographic Office. Figure 1 is an index chart of the area studied which shows the location of the probable range area and the Pacific Missile Range FPS-16 Radar Facility.

The Marine Physical Laboratory effort consisted of two parts. The first part made use of MPL's deeply-towed echo-sounder system and it is this data with which we are concerned in this paper. The second part of our effort was a conventional echo-sounder survey with Raydist navigation in a shallow water area to the northwest of Nohili Point. The data from this work were given directly to the Applied Physics Laboratory for their use in planning cable runs.

It has been demonstrated in previous MPL work that the MPL deeply-towed system has a capability for delineating small features on the ocean floor that are rarely detected by conventional surface echo sounders and could provide valuable topographic information necessary for the successful installation of underwater devices and in planning cable runs to these underwater installations.

To achieve the desired end, six deeply-towed echo-sounder profiles were made in the area of interest. The locations of these profiles are shown in Figure 2.

The data obtained are readily adaptable to an analysis of bottom slopes and it was quickly recognized that such an analysis could be of importance in estimating fire control performance of bottom bounce sonars. This point is a particularly important one in that our newer bottom bounce sonars will probably be used extensively in the new Fleet Tactical Range.

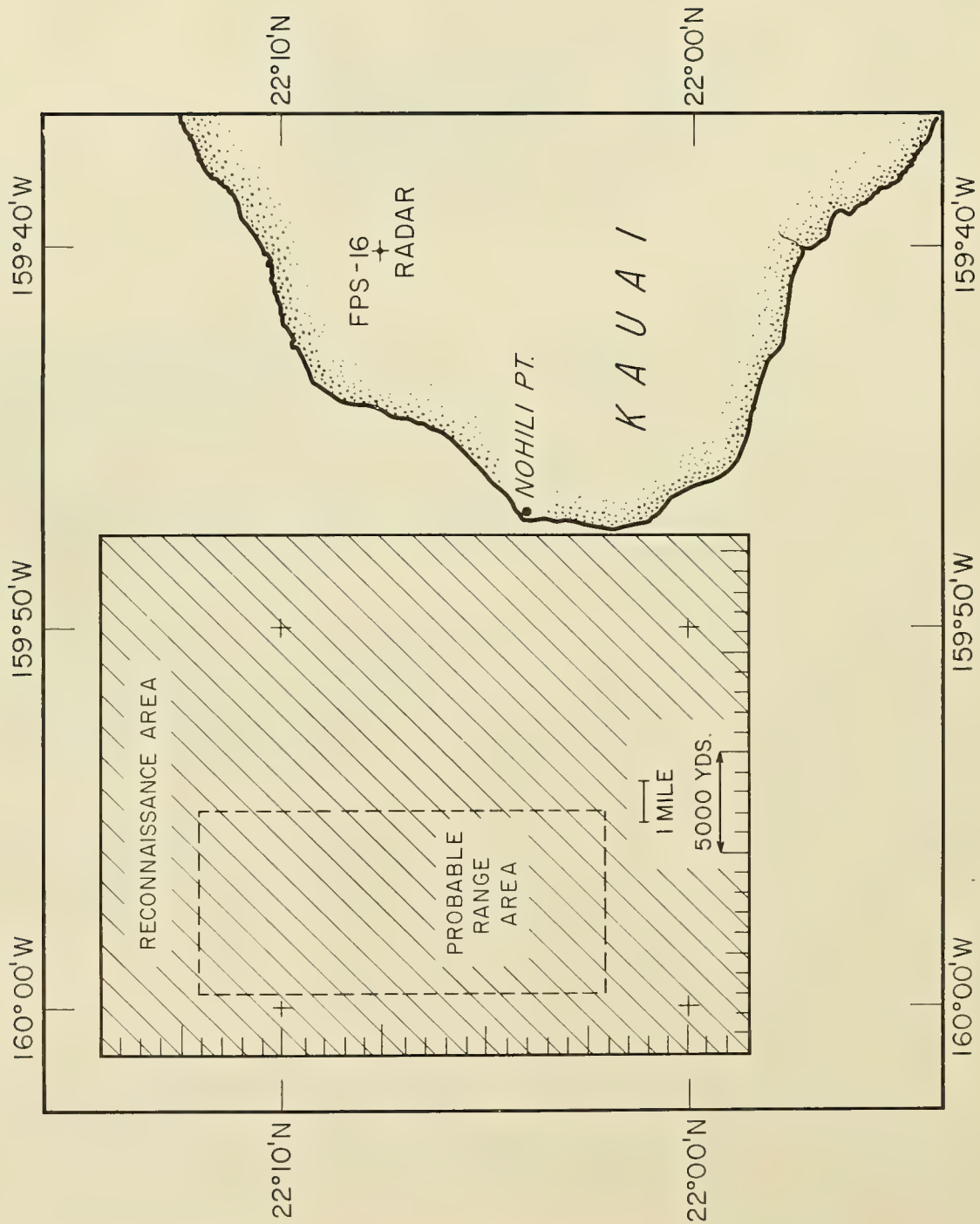


FIGURE 1 INDEX CHART OF RECONNAISSANCE AREA WEST OF KAUAI

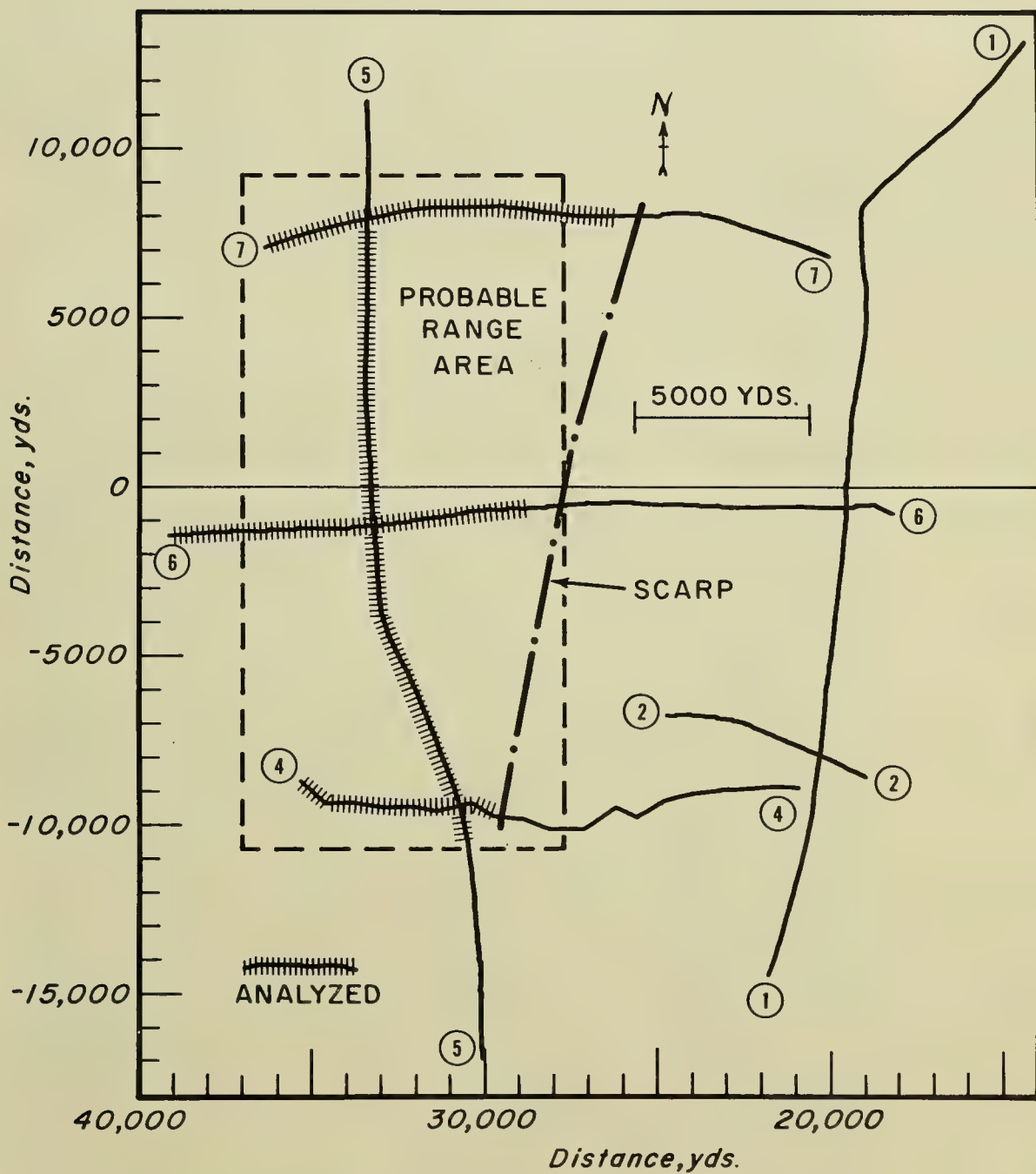


FIGURE 2 PROFILE LOCATIONS WITHIN RECONNAISSANCE AREA

The reconnaissance area is divided into two topographic entities by a northeast-southwest trending steep break in slope. This scarp separates the shallow water of the eastern half of the area from the deeper water to the west where the probable range area is located.

Note that in Figure 2 certain portions of several tracks are marked as having been analyzed. These portions of the individual runs were subjected to a simple statistical analysis of bottom slope. The portions of the runs selected for analysis all fall to the west of the scarp and approximately within the probable range area. This area was selected partially on the basis of the existence of the scarp and it is for this reason that we have confined our slope analysis to the portions of the runs which fall in the area of operational significance.

## EQUIPMENT AND METHOD OF OPERATION

The MPL deeply-towed echo sounder consists of an instrumented vehicle which is towed in proximity to the ocean bottom by means of a well-logging type cable. The actual echo sounding is done from this vehicle, and travel times are measured both to the bottom and to the surface. The downward-looking echo sounder is a narrow-beam system with a beam width of about 2 degrees by 5 degrees. The upward-looking system has considerably less directivity and is used to monitor the depth of the "fish" at all times. In rugged topography such as that west of Kauai proximity of the fish to the bottom can only be maintained by paying out or reeling in wire as needed. It is for this reason that the upward-looking system is so important, for it provides the means by which the changing fish depths are continuously monitored.

All control of the echo-sounding equipment remains at the ship. Power and commands for the electronics in the fish are sent down the coaxial conductor of the well-logging cable and echo-sounding information is returned via the same wire. All sounding information is recorded in conventional fashion on the ship on an Alden Precision Graphic Recorder.

A typical record is shown in Figure 3. The upper half of the record shows the trace of the upward-looking system and the trace of the conventional surface ship echo sounder. Since the ship is always ahead of the fish, the topography can be monitored at all times to prevent disastrous surprises. The lower half of the record shows the trace of the narrow-beam downward-looking system. At any given instant the sum of the travel times from the upward-looking system and the downward-looking system is the time equivalent of the surface-to-bottom distance.

It is from data of this sort that our study was made and upon which our conclusions are based.

It is interesting to note that most of this work was done in rough weather with sea state 4 prevailing most of the time. This made the handling of equipment from a small ship such as the R/V OCONOSTOTA rather hazardous especially during launching and retrieval of the fish.



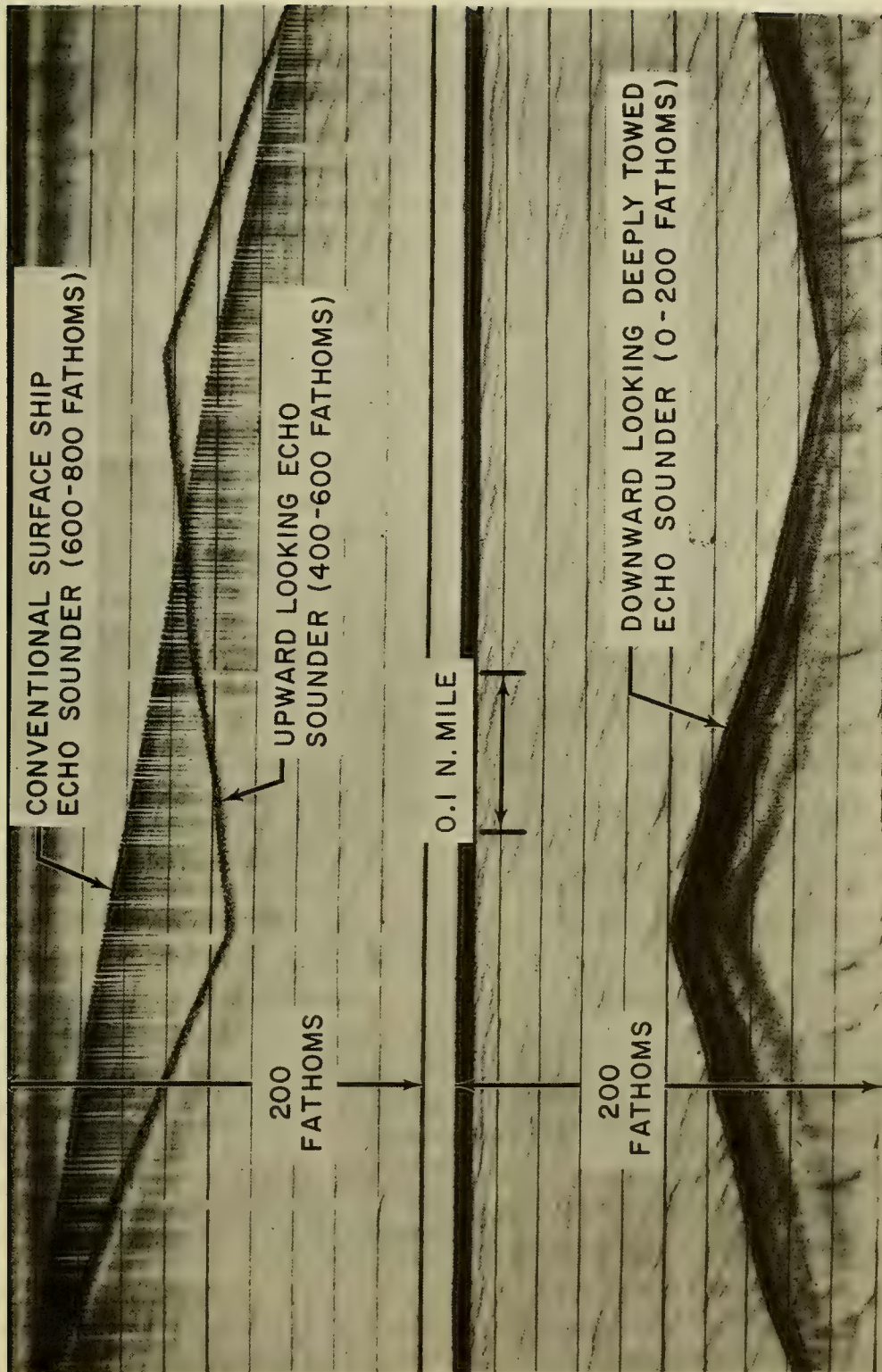


FIGURE 3 TYPICAL DEEPLY-TOWED ECHO-SOUNDING RECORD

## NAVIGATION

Precision navigation for the deep-tow work was furnished by the FPS-16 Radar Facility of the Pacific Missile Range on the island of Kauai. This facility was unable to furnish assistance during run number four due to other commitments, therefore navigation for run number four was by means of ship's radar.

The FPS-16 Radar navigation fixed the position of the ship three times each minute during profile runs. These fixes were tabulated by the FPS-16 computer facility as ranges, bearings, and depression angles to the ship.

This precision navigation information was not available on the ship during the runs so it was necessary to monitor progress along the run by means of ship's radar. As an additional check on progress along the runs and to make sure the FPS-16 Radar was tracking the correct target, a rough plot was maintained at the Radar Facility.

The precision of the navigation for the ship provided by the FPS-16 Radar Facility probably exceeds our need for knowing ship's position; however, it is necessary to have a horizontal component of bottom slope for the analysis. In these profiles, the speed of the fish is essentially that of the ship so the precision navigation is assumed to apply to the fish as far as speed over the ground is concerned. In the analysis of the data the horizontal component of the bottom slope is that determined by the precision radar navigation for all runs except number four. The horizontal component for run number four is determined from the ship's radar navigational information.

## GENERAL TOPOGRAPHIC RESULTS

The most important topographic feature of the reconnaissance area is a scarp which trends from southwest to northeast through the eastern portion of the area. It essentially forms the eastern margin of the range area.

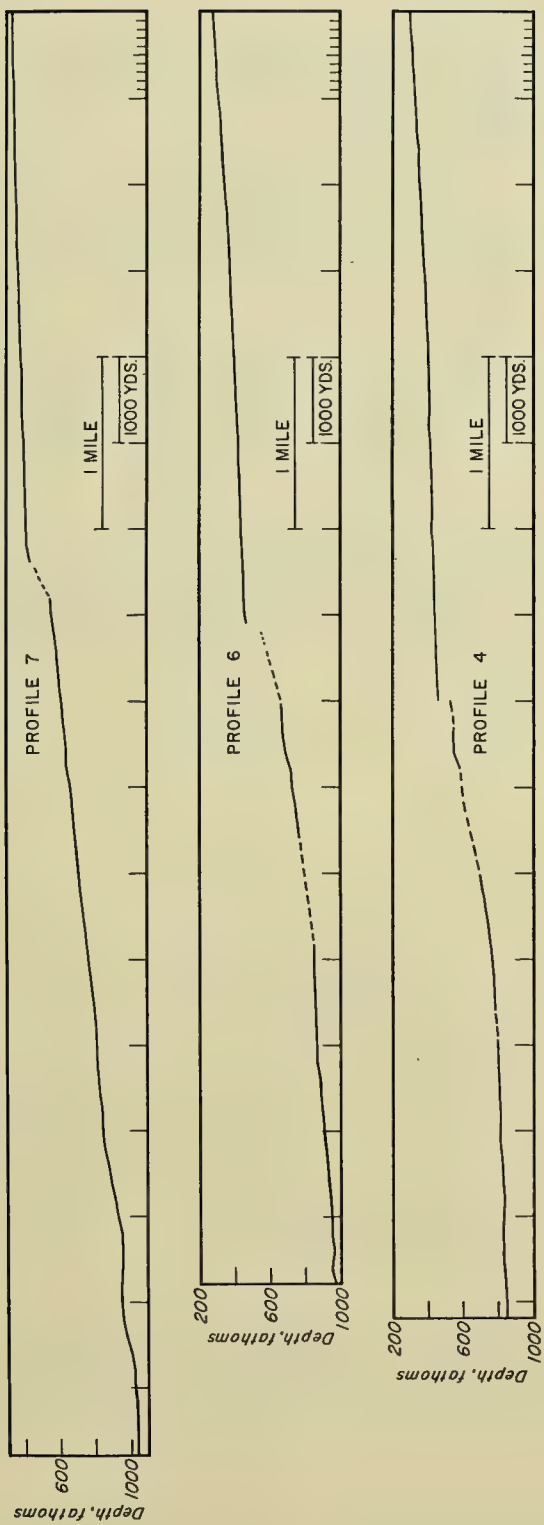
This scarp is typified by depth changes of the order of 600 to 1000 feet and slopes in excess of 35 degrees and possibly as much as 60 degrees.

Figure 4 shows the three east-west profiles which cross the scarp. The topography east of and above the scarp is relatively featureless and smooth with bottom slopes of 2 to 4 degrees. Below the scarp in these profiles the depth increases in a gently undulatory fashion from about 550 fathoms at the base of the scarp to approximately 1000 fathoms toward the western end of the profiles.

Note that the bottom slopes are moderately steep in the western portions of the profiles. It is this steepness which first suggested the value of a slope analysis and its application to the bottom bounce sonar bearing error problem.

## SLOPE ANALYSES

The data for the slope analyses came from profiles 4, 5, 6 and 7. Profiles 4, 6 and 7 are east-west trending and profile 5 is north-south trending. The records for each of these runs were read at 200-yard intervals of horizontal distance and the tan-



LOUQUERRE  
MAR. 24 9341(U)/R&DP 12/15/84

FIGURE 4 EAST-WEST TOPOGRAPHIC PROFILE



gent of the bottom slope angle was computed.

A simple statistical analysis was then performed on the individual east-west profiles and the north-south profile. The mean, median and standard deviation for these profiles were obtained and are shown in Figure 5.

For purposes of estimating sonar fire control performance the data of the three east-west profiles were lumped together to obtain an east-west composite distribution. The statistical parameters for this composite and the north-south profile number 5 are also shown in Figure 5.

Figure 6 shows the data of the east-west composite plotted on arithmetic probability paper. Note that the data points fall almost on a straight line between the 10th and 90th percentile lines indicating a close approximation to a normal distribution about a mean of +8.3 percent bottom slope, where the + sign indicates a downslope to the west.

Figure 7 shows the data of the north-south profile plotted on arithmetic probability paper. Note that the data points fall almost on a straight line between the 12th and 88th percentile lines indicating a close approximation to a normal distribution about a mean of 2.5 percent bottom slope where the + sign in this case indicates a downslope to the north.

The linear transverse error at the target when bottom bounce sonar paths are used is given approximately by

$$e = 2 d \tan \alpha$$

where  $d$  is the bottom depth at the reflection point and  $\alpha$  is the bottom slope.

Assuming a general water depth of 1000 fathoms (2000 yards), the mean error to be expected for bottom bounce paths with north-south azimuths is approximately 330 yards. This error represents a fire control bias which could be corrected for if it were not for the unfortunate fact that the standard deviation for the east-west profiles is equivalent to bottom slope deviations of 7.6 percent which is almost as great as the mean slope. It is important to remember also that essentially 30 percent of the errors will be greater than 330 yards even if allowance is made for the mean slope.

A typical steeper slope (12 percent) occurring with modest frequency in the east-west direction, will cause a transverse error of 480 yards.

In the case of the north-south profile the mean slope of 2.5 percent (error of 100 yards) is less than for the east-west profiles but the standard deviation of 6.6 percent (slope) is almost as great. This implies that even though the correction that could be made is less, it would not help the situation any more than for the east-west profiles.

Given sufficient coverage of the area of interest one could construct an error map which would give expected errors along particular azimuths for selected bottom reflection points. With the data on hand one can pass an "average" plane through the

PROFILE	EXPRESSED IN % SLOPE		
	MEAN	MEDIAN	STANDARD DEVIATION
7	9.5	9	
6	7.9	8	
4	6.4	6	
E-W Composite	8.3	8	7.6
5 (N-S)	2.5	2.3	6.6

FIGURE 5 STATISTICAL RESULTS OF SLOPE ANALYSIS



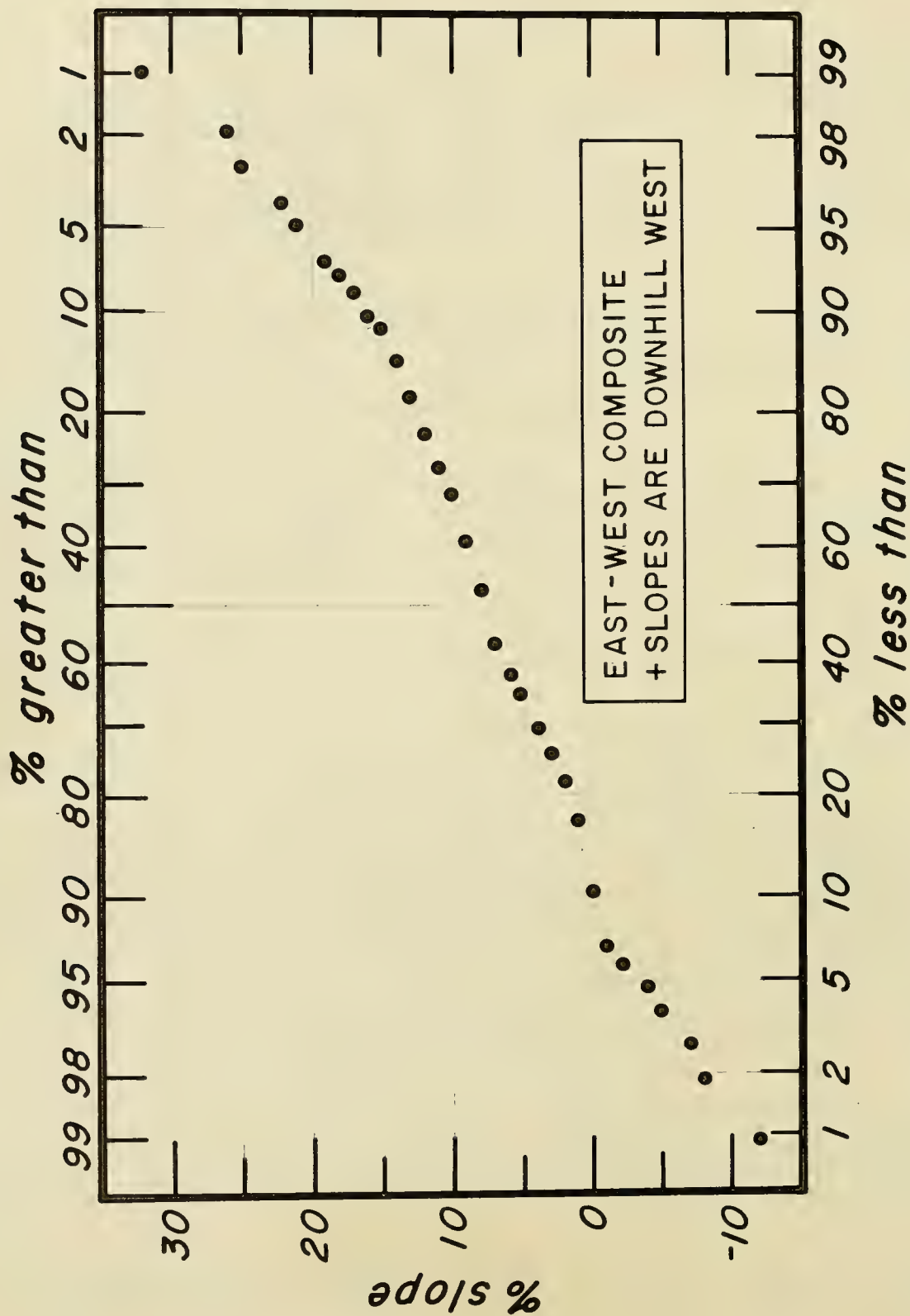


FIGURE 6 ARITHMETIC PROBABILITY PLOT OF EAST-WEST DATA

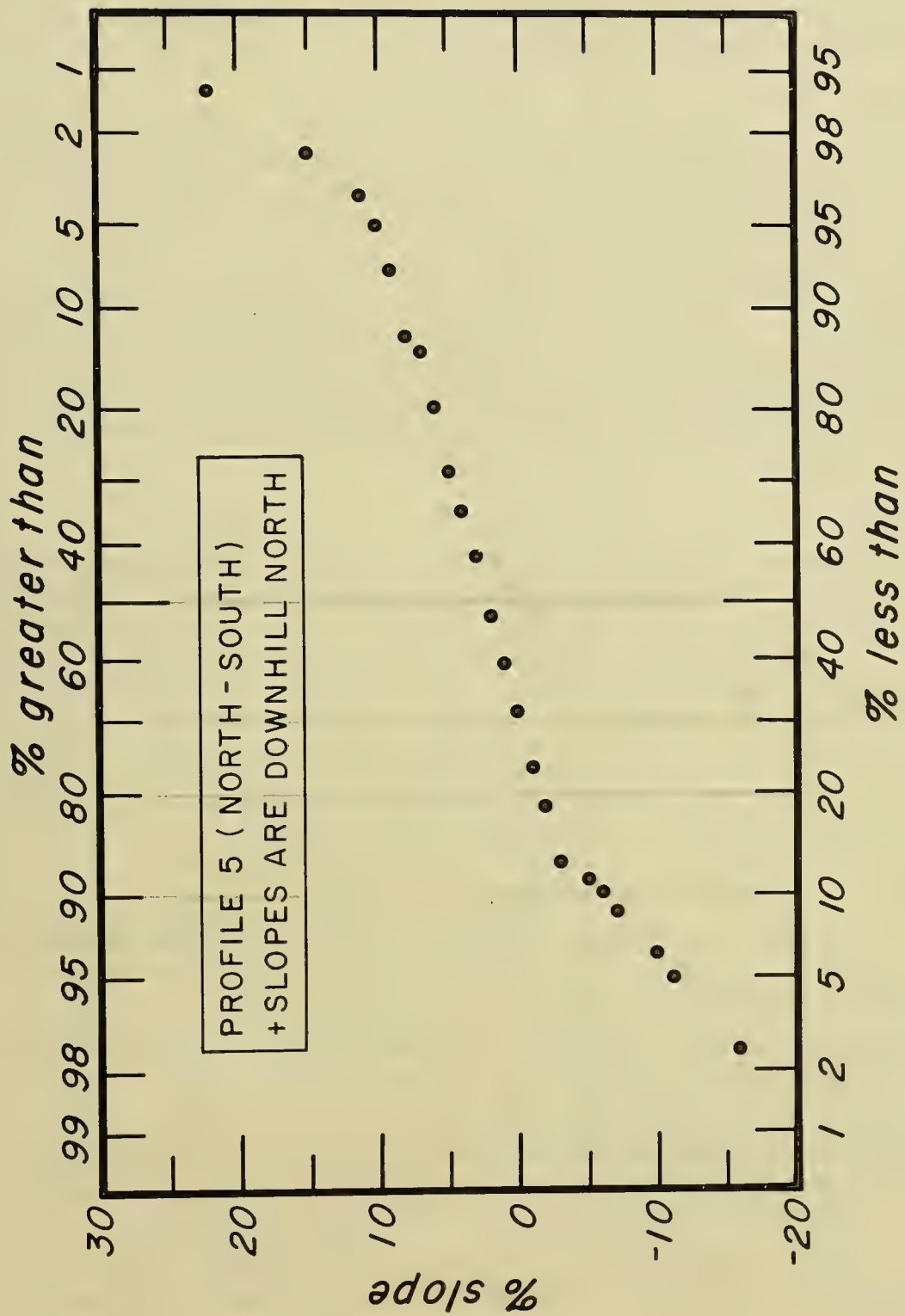


FIGURE 7 ARITHMETIC PROBABILITY PLOT OF NORTH-SOUTH DATA

area of interest which has a mean slope of 8.7 percent and whose direction of maximum slope is along true bearing 287°. The mean expected error for sonar azimuths at right angles would then be approximately 348 yards.

## CONCLUSIONS

One of the purposes of a tactical range is the evaluation of weapons systems according to their performance. An attempt must be made to sort out the shortcomings of the system from those related to the medium and its boundaries.

We have demonstrated in this paper that the environmental effects may be significant in this area. Suppose, for example, fire control effectiveness evaluations involving bottom bounce sonars are conducted in the tactical range west of Kauai. If these tests produce observed fire control errors of 300-500 yards, the expected errors due to bottom slope which we have mentioned become extremely important. The observed fire control errors may not be the fault of the system at all, but may be almost entirely due to the effects of the medium.

## ACKNOWLEDGMENTS

MPL participants in the Kauai work in addition to the authors were M. S. McGehee, senior engineer; D. E. Boegeman, senior electronics technician, and H. J. McQuern, laboratory mechanic. Liaison with APL, University of Washington, was provided by Dr. G. R. Garrison of APL. His help in the survey work and in acquiring the navigational assistance of the FPS-16 Radar Facility were sincerely appreciated. Dr. C. D. Lowenstein of MPL provided considerable assistance in the data analysis and his comments on the manuscript were both pertinent and helpful.

In addition the continued assistance of the officers and crew of the R/V OCONOSTOTA under Captain Terry Hansen is gratefully acknowledged.

## REFERENCES

- Garrison, G. R. 1965 Oceanographic evaluation of a Fleet Range Site off the west coast of Kauai, Hawaii. APL-UW 6513, Applied Physics Laboratory, University of Washington, Seattle, p. 35. 7 January 1965.
- McGehee, Maurice S. 1964 A high resolution differential pressure gage for deep sea use. Marine Physical Laboratory, University of California, San Diego Technical Memorandum 145. 27 February 1964.
- Loughridge, Michael S. 1964 A deeply-towed narrow-beam echo sounder. Proceedings of First U. S. Navy Symposium on Military Oceanography, Washington, D. C. 17-19 June 1964.
- Spiess, F. N., H. W. Menard and D. C. Krause. 1959 Some sources of sonar bearing errors. U. S. Navy Journal of Underwater Acoustics, v. 9, no. 2, pp 259-268. April 1959.

PHYSICAL CHEMISTRY OF THE DEEP OCEAN ENVIRONMENT

by  
R. A. Horne

Arthur D. Little, Inc., Cambridge, Massachusetts





# PHYSICAL CHEMISTRY OF THE DEEP OCEAN ENVIRONMENT

by

R. A. Horne

Arthur D. Little, Inc., Cambridge, Massachusetts 02140

## INTRODUCTION

Naval operations occur above, on, and in a medium which is easily one of the most complex and ill-understood substances known to man - sea water. The concurrence of relatively low temperatures ( $-1$  to  $+4^{\circ}\text{C}$ ) and high hydrostatic pressures (up to about  $15,000 \text{ lbs/in}^2$ ) in the ocean depths further complicates the situation and makes the deep ocean perhaps the most extraordinary environment in our universe. This paper reviews the results of some simple experiments which we have performed in our laboratory over recent years in a simulated deep ocean environment (Fig 1).

## THE STRUCTURE OF SEA WATER\*

There are several theories of the structure of water. There is also a minority opinion which insists that water has no structure at all. But at the present time in the United States the most popular model for the state of affairs in pure water appears to be that of Frank and Wen (1957), who proposed that water consists of transient "clusters" of more-or-less ordered, H-bonded water (sometimes, perhaps unfortunately, referred to as "ice-like") swimming in and in equilibrium with "free", monomeric water (Fig 2). Nemethy and Scheraga (1962) have calculated the size and concentration of these clusters as a function of temperature. The application of pressure or the addition of an electrolyte also affect the extent of water structure.

Roughly speaking sea water is an  $0.5\text{M NaCl}$  solution with a trace of  $\text{MgSO}_4$ . The addition of electrolytes further complicates the structure of the system. If an ion, such as  $\text{Na}^+$ , is placed in water the coulombic attraction between the ion's charge and the partial charges of opposite sign of the water dipoles results in a crowding or "electrostriction" of the water molecules about the ion and an overall volume decrease (Fig 3). If the spacial distribution of water molecules in the first solvation sheath of an ion is symmetrical, such as  $\text{Na}(\text{H}_2\text{O})_4^+$ , the ion will be a structure-maker and will tend to make the surrounding water more ordered as reflected in an increase in

---

\* For a more detailed discussion of the physical chemistry and structure of sea water see R. A. Horne, J. Water Resources Res., in press, 1965.

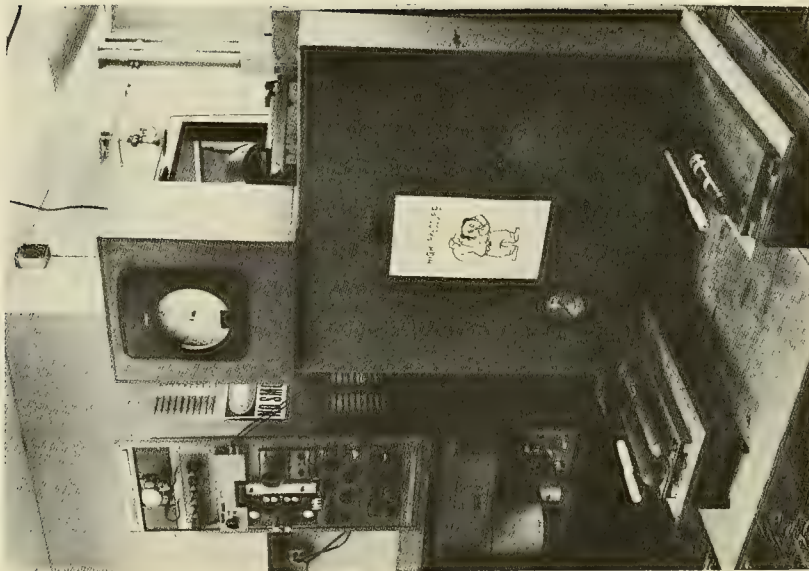


FIGURE 1A HIGH PRESSURE EQUIPMENT  
FRONT VIEW

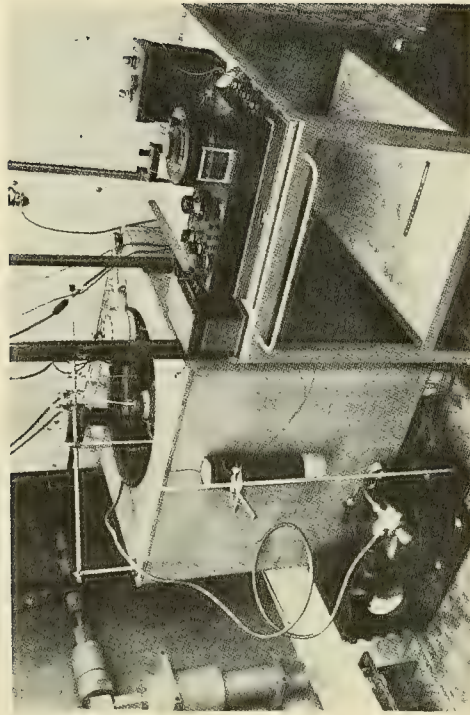


FIGURE 1B HIGH PRESSURE EQUIPMENT  
REAR VIEW

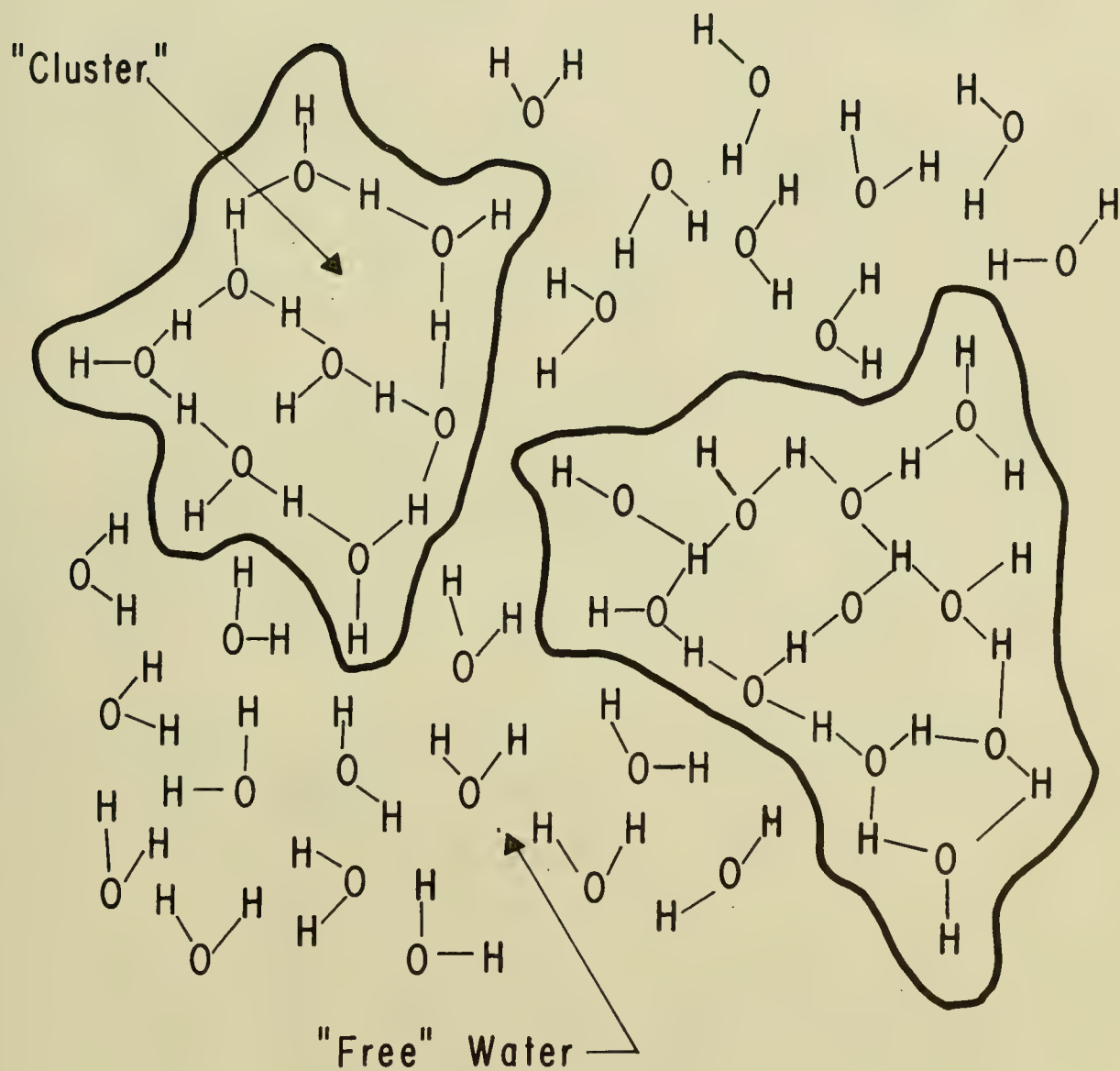


FIGURE 2 SCHEMATIC DIAGRAM OF THE FRANK-WEN WATER MODEL

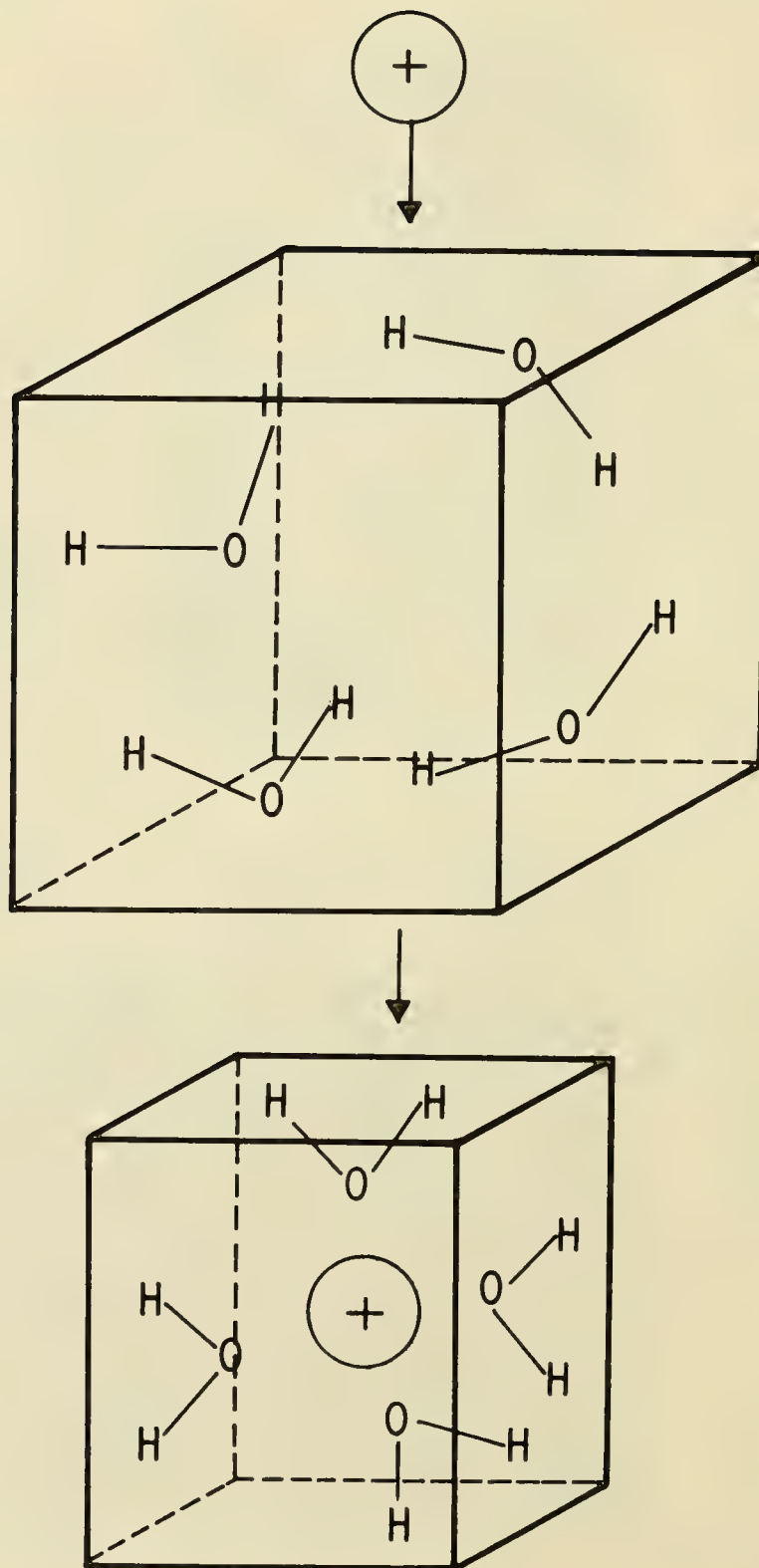


FIGURE 3 DECREASE IN WATER VOLUME PRODUCED BY ELECTROSTRICTION



relative viscosity (Fig 4) whereas if the first hydration sheath is asymmetrical, such as  $K(H_2O)^+$  or  $Cl(H_2O)^-$ , the ion will be a structure-breaker and will tend to make the surrounding water less ordered as reflected in a decrease in relative viscosity (Fig 4) (Horne, 1964).  $Mg(H_2O)_6^{++} SO_4(H_2O)_{12}^{=}$ , it is interesting to note, like many other 2:2 electrolytes is a very powerful structure-maker (Fig 4).

#### THE ELECTRICAL CONDUCTIVITY OF SEA WATER

Electrical conductivity,  $\Lambda$ , can be treated as a rate process and its activation energy,  $E_a$ , calculated from the integrated form the the Arrhenius equation

$$(1) \quad E_a = (\log \Lambda_2 - \log \Lambda_1) 4.576 T_2 T_1 / \Delta T$$

where the T's are absolute temperatures.  $E_{a, \text{cond.}}$  for sea water exhibits a maximum (Fig 5) and for chlorinities less than about 10 ‰ the maximum occurs at the temperature of maximum density (Horne, 1964). The rate-determining step of the "normal" electrical conductivity of aqueous solutions of strong 1:1 electrolytes is "hole" or vacancy formation in the solvent. The process occurs both in the free and clustered water, and the decrease in  $E_{a, \text{cond.}}$  with decreasing temperatures at temperatures below the maximum reflects the fact that "hole" formation is facilitated by the increasing amount of less dense, more open, clustered water (Horne, 1964 and Horne and Courant, 1964).

We have measured the effect of pressure on the electrical conductivity of sea water (Horne and Frysinger, 1963). In the range of oceanographic interest, pressure, like temperature, decreases  $E_{a, \text{cond.}}$  indicating that its application tends to disorder liquid water (Horne, Myers and Frysinger, 1963). We found that Walden's rule

$$(2) \quad \Lambda^\circ \eta^\circ = \text{Constant}$$

where  $\eta$  is the viscosity is a good approximation for sea water under the condition of varying temperature but not varying pressure (Horne and Courant, 1964). However, we found that we were able to curve fit the observed pressure-dependence of the electrical conductivity of sea water by simple corrections for (1) the increased dissociation of  $MgSO_4$  (Fisher, 1962), (2) the compressibility, and (3) the square of the viscosity (Horne and Courant, 1964). The apparent dependence on  $\eta^2$  is an artifact arising from the reduction of the radii of hydrated ions by pressure (Horne, 1963) - a phenomenon first noted by Zisman (1932). The structural effects of pressure differ in one very important respect from those of temperature: temperature breaks up the structure of the bulk water but does not greatly affect the local water structure near ions, pressure, on the other hand, destroys both the bulk structure and the hydration atmospheres of ions.



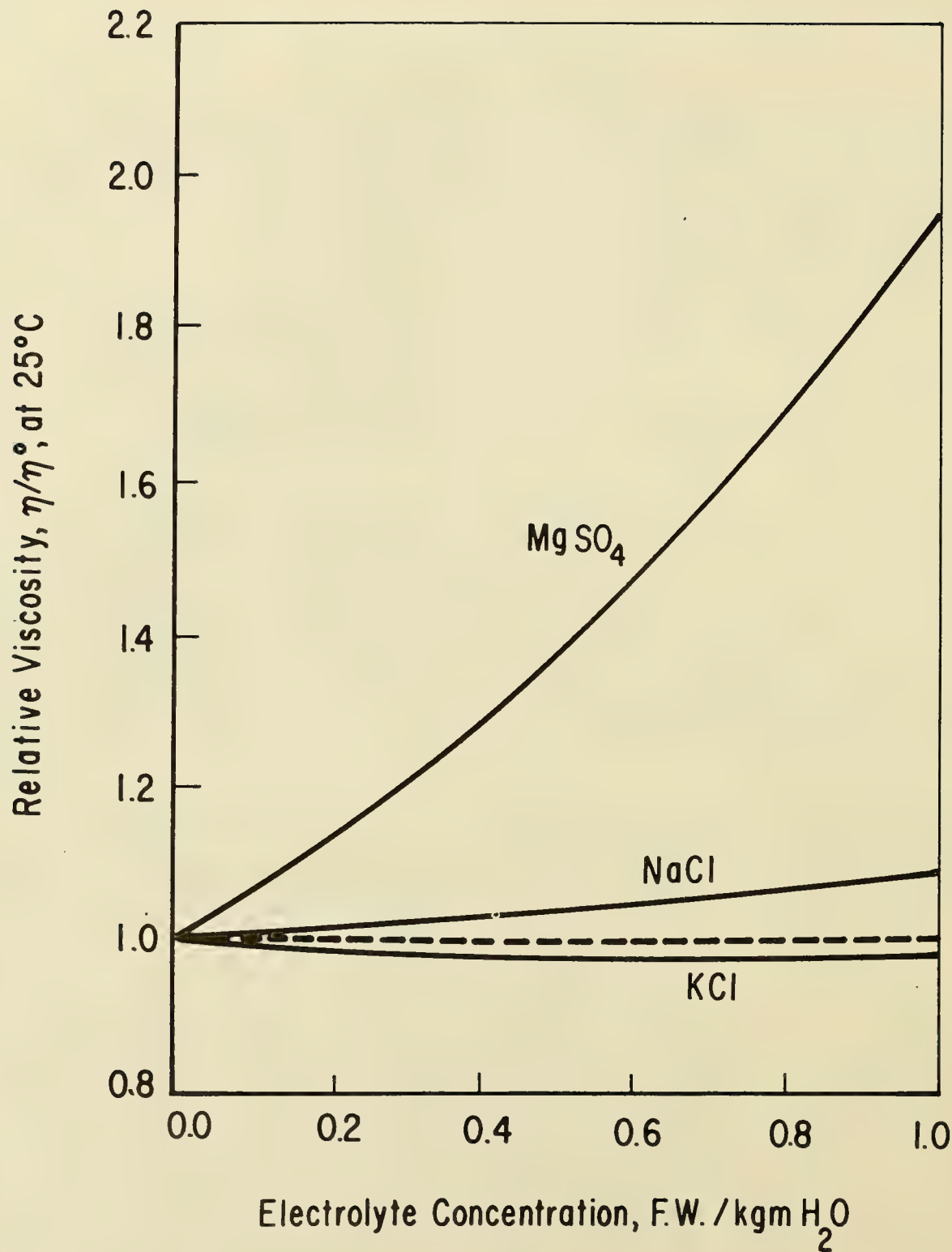


FIGURE 4 THE EFFECT OF ELECTROLYTE ADDITION ON THE RELATIVE VISCOSITY OF WATER

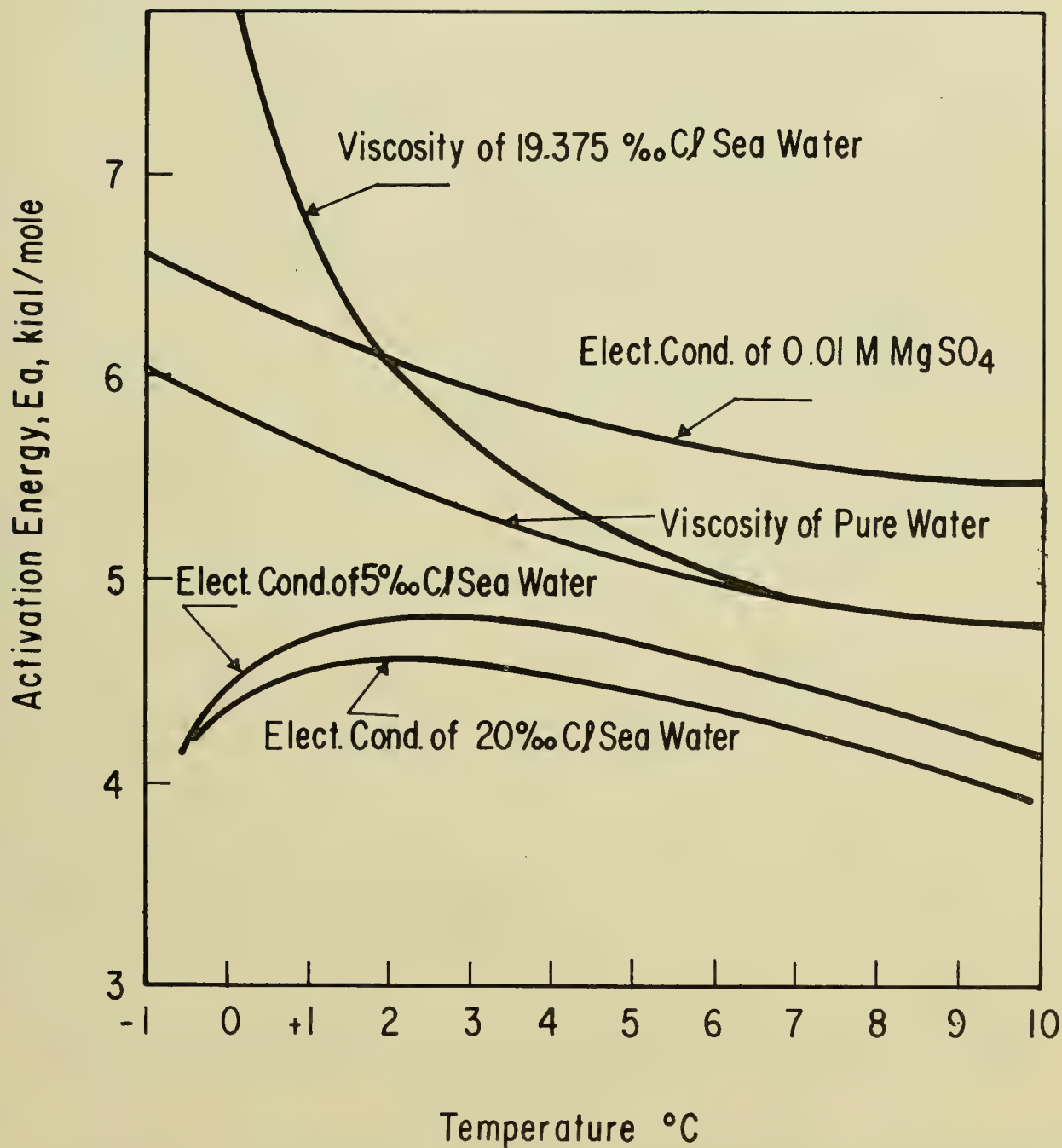


FIGURE 5 THE TEMPERATURE-DEPENDENCE OF THE ACTIVATION ENERGY OF VARIOUS TRANSPORT PROCESSES IN WATER

## THE VISCOSITY OF SEA WATER

On the basis of what now appears to have been a superficial similarity of their activation energies electrical conductivity, viscous flow, self-diffusion, and dielectric relaxation in water were believed to all involve the same rate-determining step (Glasstone, Laidler and Eyring, 1941, and Wang, Robinson and Edelman, 1953). However, more detailed examination, especially in the 0 to +10°C region reveals important differences. Miller (1963) reports no discontinuities in  $E_{a,vis.}$  at 4°C in the viscosity of water and our recent measurements (Horne, Courant, Johnson, and Margosian, 1964) on both pure water and sea water yield the same result.  $E_{a,vis.}$ , unlike  $E_{a,cond.}$  shows no maximum (Fig 5) hence the mechanism of viscous flow is different from that of normal conduction, possibly involving some kind of rotational tumbling of the clusters through the free water.

At the present time we are just completing an experimental study of the effect of pressure on the viscosity of pure water and sea water. The data have not been analyzed yet in detail, but qualitatively they show the same phenomena revealed by the much earlier work of Cohen (1892) on aqueous NaCl solutions, namely an initial decrease in viscosity with increasing pressure due to the destruction of the structure in liquid water and then, after the order has been destroyed, an increase in viscosity with increasing pressure as observed for "normal" non-associated liquids.

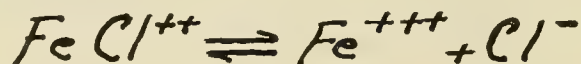
## THE ELECTRICAL CONDUCTIVITY OF AQUEOUS MAGNESIUM SULFATE SOLUTIONS

Earlier we mentioned that  $MgSO_4$  is a very powerful structure maker.  $E_{a,cond.}$  of aqueous  $MgSO_4$  solutions (Horne and Johnson, 1965) has a temperature dependence similar to that of viscous flow rather than normal ionic conduction (Fig 5). Evidently  $MgSO_4$  is so highly hydrated that its species are too large to fit into the "holes" and as a consequence the mechanism of their transport in aqueous solution resembles that of the water clusters.

## MISCELLANEOUS STUDIES

In addition to fundamental research on the physical-chemistry of sea water we have also turned our attention to problems of more immediate practical consequence. Our interest in marine corrosion at great depths prompted us to examine the effect of pressure on the dissociation constant of the chloride complex of a constructional metal.

(3)



Due to electrostriction (see above) the application of pressure tends to force this reaction to the right increasing the dissociation constant by about 20 fold in going from 1 to 2,000 atmospheres (Horne, Myers and Fry-singer, 1964). The performance of unshielded electro-chemical devices such as batteries on the ocean floor has been of concern to us (Horne, 1963) and

we have examined the effect of hydrostatic pressure on the electrical conductivity of some typical battery electrolytes (see Table 1) (Horne, Bannon, Sullivan and Frysinger, 1963). Notice the relatively large effect in the case of sulfuric acid due, in part, to the increased dissociation of bisulfate ion by electrostriction (Horne, Courant and Frysinger, 1964).

(4)

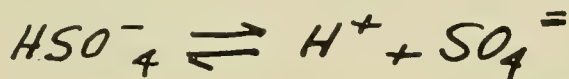


Table 1

Effect of Pressure on the Conductivity of Battery Electrolytes

<u>Battery Electrolyte</u>	<u>% Increase in Elect. Cond. at 1,000 atm. at 25°C</u>
Potassium Hydroxide	1.5
Sulfuric Acid	5
NaCl enriched with $MgCl_2$	2

Measurements of voltage versus current for button-type Ni-Cd and Leclanche cells under simulated deep ocean conditions yielded results that still leave us baffled. We expected the structure-breaking properties of pressure to decrease the structure at the electrolyte-electrode interface thereby facilitating the transport of ions and decreasing polarization, however, contrary to expectation, polarization appears to worsen with increasing pressure (Fig.6). We hope to look into this matter further (for studies of the performance of lead-acid batteries under pressure, see Schumaker, 1961).

Certain marine sedimentary materials such as montmorillonite have exchangeable cations. The effect of pressure on ion exchange equilibria had never been previously examined. Needless to say, we could not resist the temptation of applying our equipment to this purpose. We found little effect of pressure on the  $K^+/H^+$  exchange on a synthetic, strong, sulfonic acid type, cation exchange resin, however, in the case of the  $Sr^{++}/H^+$  exchange as pressure increases the resin's preference for  $Sr^{++}$  increases (Horne, Courant, Myers and George, 1964). Evidently the pressure-produced dehydration of the more heaving hydrated  $Sr^{++}$  ion is more marked than for the proton, hence the charge density (and thus the coulombic attraction for the resin sites) increases more steeply with increasing pressure for  $Sr^{++}$  than for  $H^+$ .

CONCLUSION

Today one frequently hears of the application of the specialized knowledge of the various disciplines to marine science. This certainly need not be a one-way exchange of advantage. I hope that the experiments I have discussed

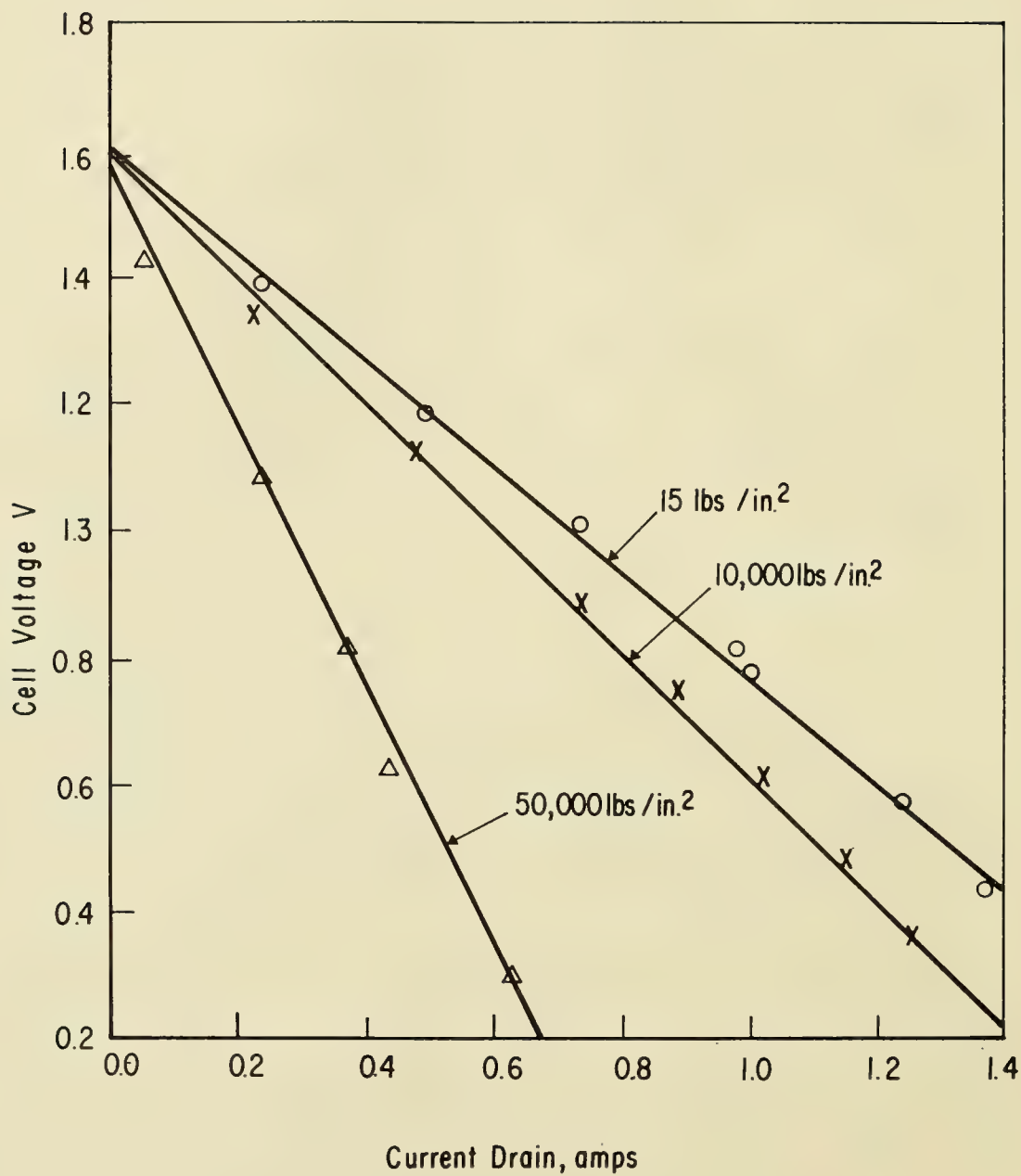


FIGURE 6 DISCHARGE CHARACTERISTICS OF AN EVEREADY SIZE AA DRY CELL AT 25°C UNDER PRESSURE



will provide an illustration of how what began as an interest in the simulation of the deep ocean environment in due course lead to fundamental research in solution physical chemistry. Oceanography has reopened, not a new, but a neglected field of physical chemistry, a field which I am convinced will prove to be a most fascinating and fruitful one - the effect of pressure on aqueous electrolytic solutions.

#### ACKNOWLEDGEMENT

This work was supported in part by the Office of Naval Research.

#### REFERENCES

- Frank, H. S. and Wen, W. Y. 1957 Discussions of the Faraday Society, v. 24, p. 133. 1957.
- Nemethy, G. and Scheraga, H. A. 1962 Journal of Chemical Physics, v. 36, p. 3382. 1962.
- Horne, R. A. 1964 Structure makers and breakers in water. Arthur D. Little, Inc., Technical Report number 3, ONR Contract Nonr-4424(00). 30 September 1964.
- Horne, R. A., and Courant, R. A. 1964 Journal of Geophysical Research, v. 69, p. 1152. 1964.
- Horne, R. A., and Courant, R. A. 1964 Journal of Physical Chemistry, v. 68, p. 1258. 1964.
- Horne, R. A., and Frysinger, G. R. 1963 Journal of Geophysical Research, v. 68, p. 1967. 1963.
- Horne, R. A., Myers, B. R., and Frysinger, G. R. 1963 Journal of Chemical Physics, v. 39, p. 2666. 1963.
- Horne, R. A., and Courant, R. A. 1964 Journal of Geophysical Research, v. 69, p. 1971. 1964.
- Fisher, F. H. 1962 Journal of Physical Chemistry, v. 66, p. 1607. 1962.
- Horne, R. A. 1963 Nature, v. 200, p. 418. 1963.
- Zisman, W. A. 1932 Physics Review, v. 39, p. 151. 1932.
- Glasstone, S., Laidler, K. J., and Eyring, H. 1941 The theory of rate processes. McGraw-Hill Book Company, Inc., New York, New York. 1941
- Wang, J. H., Robinson, C. V., and Edelman, I. S. 1953 Journal of the American Chemical Society, v. 75, p. 466. 1953.

- Miller, A. A. 1963 Journal of Chemical Physics, v. 38, p. 1568. 1963.
- Horne, R. A., Courant, R. A., Johnson, D. S., and Margosian, F. F. 1964 The activation energy of viscous flow of pure water and sea water in the temperature region of maximum density. Arthur D. Little, Inc., Technical Report number 4, ONR Contract Nonr-4424(00). 31 October 1964.
- Cohen, R 1892 Ann. Physik, v. 45, p. 666. 1892.
- Horne, R. A., and Johnson, D. S. 1965 The electrical conductivity and structure of aqueous magnesium sulfate solutions in the -2 to +12°C range. Arthur D. Little, Inc., Technical Report number 7, ONR Contract Nonr-4424(00). 31 January 1965.
- Horne, R. A., Myers, B. R., and Frysinger, G. R. 1964 Inorganic Chemistry, v. 3, p. 452. 1964.
- Horne, R. A. 1963 Undersea Technology, v. 4, no. 7, 16. 1963. Naval Engineering Journal, v. 7, p. 807. 1963.
- Horne, R. A., Bannon, W. J., Sullivan, E., and Frysinger, G. R. 1963 Journal of the Electrochemical Society, v. 110, p. 1282. 1963.
- Horne, R. A., Courant, R. A., and Frysinger, G. R. 1964 Journal of the Chemical Society, London, p. 1515. 1964.
- Shumaker, L. A. 1961 Evaluation of external battery power supply for bathyscaph TRIESTE - for studies of the performance of lead-acid batteries under pressure. Navy Electronics Laboratory, Report number 1063. 18 August 1961.
- Horne, R. A., Courant, R. A., Myers, B. R., and George, J. H. B., Journal of Physical Chemistry, v. 68, p. 2578. 1964.

DEEP SEA FREE INSTRUMENT PACKAGE

by

Philip P. Bedard

Narragansett Marine Laboratory  
University of Rhode Island  
Kingston, Rhode Island



## DEEP SEA FREE INSTRUMENT PACKAGE

by

Philip P. Bedard

Narragansett Marine Laboratory, University of Rhode Island, Kingston, R.I.

### INTRODUCTION

The buoy that will be described in this presentation was conceived as a solution to the problem of obtaining oceanographic data from very near the ocean bottom. The specific aim of the project is to obtain current readings from the bottom of the Gulf Stream. As of this date, four current meter installations, totaling 75.8 hours, have been made on the ocean floor, one of these installations being in the Gulf Stream.

### THE SYSTEM

#### Available Methods

There are a number of alternatives that can be considered when one desires to make measurements very near the ocean floor. One method would be by the means of instruments attached to an anchor line that extends upward to a surface buoy (Richardson, et al, 1963). In an area such as the Gulf Stream, the maintaining of such a mooring can be a difficult proposition. Another method is the use of a current meter suspended from a drifting ship (Pratt, 1963). Current meters have been mounted on manned deep submersibles (LaFond, 1962). Information regarding bottom currents has also been inferred from photographs of bottom ripple marks (Hurley and Fink, 1963).

#### Free Falling Buoy

Our instrument package uses a method described by Isaacs and Schick (1960), where a free falling vehicle falls to the bottom and spends a desired amount of time there collecting and storing data. At the end of this time the ballast holding the instrument package on the ocean floor is released, and the package rises to the surface under the force of its self-contained flotation material.

#### Instruments Used

The oceanographic sensor selected for such an instrument package must be capable of self-contained operation for the length of time over which it is desired to make observations. Due to the limited amount of flotation available in our particular configuration, equipment weight in



water must be kept low. The current meter selected for this project was a Richardson type instrument, Model A-100, manufactured by the Geodyne Corporation of Waltham, Massachusetts. The meter as used was capable of making continuous current observations for  $3\frac{1}{2}$  days. In the intermittent mode, readings could have been made one minute out of twenty for a period of 10 weeks.

The device used to release the anchor was also manufactured by the Geodyne Corporation. This mechanism can be set to release after a desired number of twenty minute intervals (up to a total of 140 days). When the desired time interval has elapsed, an explosive squib is fired and the ballast is released, allowing the package to rise to the surface.

#### Flotation Package

The key to the success of the buoy is the flotation material that maintains the current meter in a vertical position while the data is being gathered, and then provides the buoyant force necessary to return the instruments to the surface for recovery.

The depth for which the package was designed was 6,000 meters (9,000 psi). Initially, it was desired to use containers filled with gasoline to provide the necessary flotation. This was discarded for the following reasons: the impossibility of carrying gasoline aboard our research vessel TRIDENT; handling difficulties caused by the mass required; and the horizontal drag forces that would be placed on the buoy while the equipment was on the bottom. Other materials considered were: filled epoxy materials; aluminum spheres; and glass spheres. The cost of a pound of flotation varies considerably from one material to the next. The filled epoxy was \$16.50 per pound; the aluminum spheres \$7.60 per pound; and the glass spheres \$2.70 per pound. These costs are for the flotation material alone and do not take into consideration the problems of attaching the sensor and of providing a platform on which location aides can be mounted.

Glass spheres were selected to provide the flotation. These units, manufactured by Corning Glass Works, are 10 inches in diameter, with a  $\frac{1}{4}$  inch wall, and are designed for service up to 10,000 psi. The spheres were specified as providing 11  $\frac{3}{4}$  pounds of buoyancy each, but subsequent investigation revealed the buoyancy to be 12.5 to 13.0 pounds per unit.

The spheres were sandwiched between two aluminum discs, the resulting float having the shape of a flat disc with a thickness to diameter ratio of 0.2. The discs were cut out in a honeycomb pattern to reduce drag and weight. Support of the equipment required 109 pounds of buoyancy; thirteen spheres were used, leaving an assumed net buoyant force of 44 pounds. This was later revised to 57 pounds when the difference in the buoyancy of the spheres was discovered.

A pressure case containing a small radio transmitter and a flashing xenon light was placed in the center of the float assembly, resulting in a

stable, although low, platform for these location aids. Approximately one meter of line was used between units, with the current meter being located 3.5 meters off the bottom.

#### Instrument Descent Speed and Overshoot

To estimate the speed of descent of the instrument package, the following formula for form drag was employed (Rouse, p. 244).

$$F_d = \frac{1}{2} C_d \rho A v^2 \quad \text{eqn 1}$$

where  $F_d$  = drag force

$C_d$  = dimensionless, shape-dependent drag coefficient

$\rho$  = density of fluid through which float travels

$A$  = cross sectional area normal to direction of motion

$v$  = velocity of moving body

The drag coefficient was estimated as 1.0 (Rouse, Table III, p. 249). The cross sectional area of the float was 1.68 square meters. On descent the drag force was made equivalent to the difference between the net buoyant force and the ballast weights; on ascent the drag force was taken as equal to the net buoyant force. The drag forces were designed to be equal at approximately 178 newtons (40 pounds) apiece, yielding a speed of 45 cm/sec.

Instrument overshoot on hitting the bottom did not prove to be a problem. The following linearized equation was taken as an approximate description of the motion of the instrument package immediately after the ballast weights hit bottom:

$$m \frac{d^2 x}{dt^2} + k \frac{dx}{dt} = F \quad \text{eqn 2}$$

where  $x$  = vertical displacement of instrument

$m$  = total mass of instrument package

$k$  =  $\frac{1}{2} C_d \rho A v_0$

$v_0$  = descent velocity (terminal velocity)

$F$  = restoring force (equal to force exerted by ballast)

Using the values of  $v_0$  and  $C_d$  as obtained from our instrument records, the overshoot was considered negligible; and no attempt was made to solve for the overshoot based on the proper expression for drag force involving the square of the velocity.

The records derived from our current meters gave an excellent check on the velocities of ascent and descent, the transit time being very clearly defined. It is not known to what extent the deviation from a vertical path caused the transit time to be increased. From our records, the average descent velocity was 46.2 cm/sec and the average ascent velocity was 46.2 cm/sec. The discrepancy in velocity is largely accounted for by the increased buoyancy actually provided by our glass spheres.

From these velocities and the known value of the ballast weights released, the drag coefficient for the entire instrument package is calculated as  $0.78 \pm 0.06$ .

### Summary of Results

A total of four installations and recoveries of this system were made during the summer of 1964. Table 1 is a summary of the locations and length of records obtained.

Table 1

#### Current Meter Installations - Locations and Depths

Installation Number	Location	Depth Meters	Record Length Meters
1	32°11'N, 68°13'W	5192	15.7
2	32°05'N, 68°12'W	5182	7.4
3	32°24'N, 69°47'W	5337	35.8
4	36°04'N, 73°13'W	3584	17.0

The first two observations occurred sixty-four hours apart. Records from both these installations indicate a current of 10 to 20 cm/sec at a heading of 125° to 130°. In the third observation the indicated velocities were of the order of zero to 2 cm/sec. These readings must be interpreted with caution, since they lie in a range of speeds for which the Savonius rotor may be non-linear (Gaul, 1962; Sexton, 1964). In the Gulf Stream observations, a current of 10 cm/sec at 033° is indicated (Knauss, in press).

### SUMMARY

Adoption of this technique of a free falling package makes possible the acquisition of oceanographic data from near the ocean bottom. The present configuration, while limited in payload to fairly small instruments, is easily handled over the side of a ship without the need for special handling techniques and equipment.

### ACKNOWLEDGEMENTS

This work was done under the direction of John A. Knauss. Ferris Webster lent assistance in the reduction of the data. The work was supported in part by Contract Nonr-396(08) of the Office of Naval Research.

## REFERENCES

- Gaul, R.D. 1962 The Savonius rotor current meter. Dept. of Oceanography and Meteorology A & M College of Texas Technical Report 62-2T 36 pp.
- Hurley, R.J., and L.K. Fink 1963 Ripplemarks show that countercurrent exists in Florida Straits. Science v. 139 no. 3555: pp 603-605.
- Isaacs, J.A. and G.B. Schick 1960 Deep sea free instrument vehicle Deep Sea Research, v. 7: pp 61-67.
- Knauss, J.A. A technique for measuring ocean currents close to the bottom and some preliminary results. Journal of Marine Research, in press.
- LaFond, E.C. 1962 Deep current measurements with the Bathyscaphe Trieste. Deep Sea Research v. 9: pp 115-116.
- Pratt, R.M. 1963 Bottom currents on the Blake Plateau. Deep Sea Research, v. 10: pp 245-249.
- Richardson, W.D., P. B. Stimson, and C.H. Wilkins 1963 Current measurements from moored buoys. Deep Sea Research, v. 10: pp 369-388.
- Rouse, Hunter 1946 Elementary Mechanics of Fluids. John Wiley & Sons, New York 1946 376 pp.
- Sexton, R. 1964 Some tow tank calibrations of the Savonius rotor. Lamont Geological Observation, Columbia University. Ref. cu-11-64 38 pp (unpublished).



## ERRATA

### Page 3 Last Paragraph

Using the values of  $v_p$  and  $C_d$  as obtained from our instrument records, the overshoot was calculated to be 4.4 cm. This was considered negligible, and no attempt was made to solve for the overshoot based on the proper expression for drag force involving the square of the velocity.

### Page 4 Sentence 3

From our records, the average descent velocity was 46.2 cm/sec and the average ascent velocity was 56.2 cm/sec.

### Page 4 Caption, Table 1

Record Length  
Hours



A DESCRIPTION OF INSTRUMENTATION AND THE  
MEASUREMENT TECHNIQUES USED FOR THE DETECTION OF  
EXTREMELY LOW FREQUENCY ELECTROMAGNETIC  
ENERGY IN THE SEA

by

James F. Orr

U. S. Navy Underwater Sound Laboratory  
New London, Connecticut



# A DESCRIPTION OF INSTRUMENTATION AND THE MEASUREMENT TECHNIQUES USED FOR THE DETECTION OF EXTREMELY LOW FREQUENCY ELECTROMAGNETIC ENERGY IN THE SEA

by

James F. Orr

U. S. Navy Underwater Sound Laboratory, New London, Conn. 06321

## INTRODUCTION

In the past decade there has been a renewed interest in the Extremely Low Frequency (ELF) region. Reflecting this interest, the U. S. Navy Underwater Sound Laboratory has extended its oceanographic program to include a determination of the electromagnetic characteristics of the sea. Previously very little ELF atmospheric noise data was available, and virtually none had been taken in the sea. No background of information existed, except in the power and acoustical region. The extremely low electromagnetic levels to be measured demanded careful design consideration, especially in the preamplifiers and antennas.

The ultimate purpose of this project will be to obtain absolute ELF measurements of atmospheric and sea-generated noise and to relate them to some of the physical parameters of the sea, such as sea state and electrical conductivity. With these goals in mind, a series of trips on the Navy's General Oceanographic Survey Vessels (AGOR's) was planned.

## DESCRIPTION OF INSTRUMENTATION

The instrumentation system installed on the USNS GILLISS (AGOR-4) for the measurement of atmospheric and ambient electromagnetic noise in the sea consisted of preamplifiers, 60-cycle reject filters, level adjusting attenuators, amplifiers, FM modulators, and a tape recorder (Fig. 1). In addition, general-purpose test equipment was included for on-the-spot analysis, observation of wave forms, measurement of antenna impedance, and other experiments. This equipment was installed in three standard 6-foot instrumentation racks.

The frequency range of interest is approximately from 5 to 1000 cycles (Fig. 2). This frequency range includes the  $1/f$  noise region of common amplifying devices.

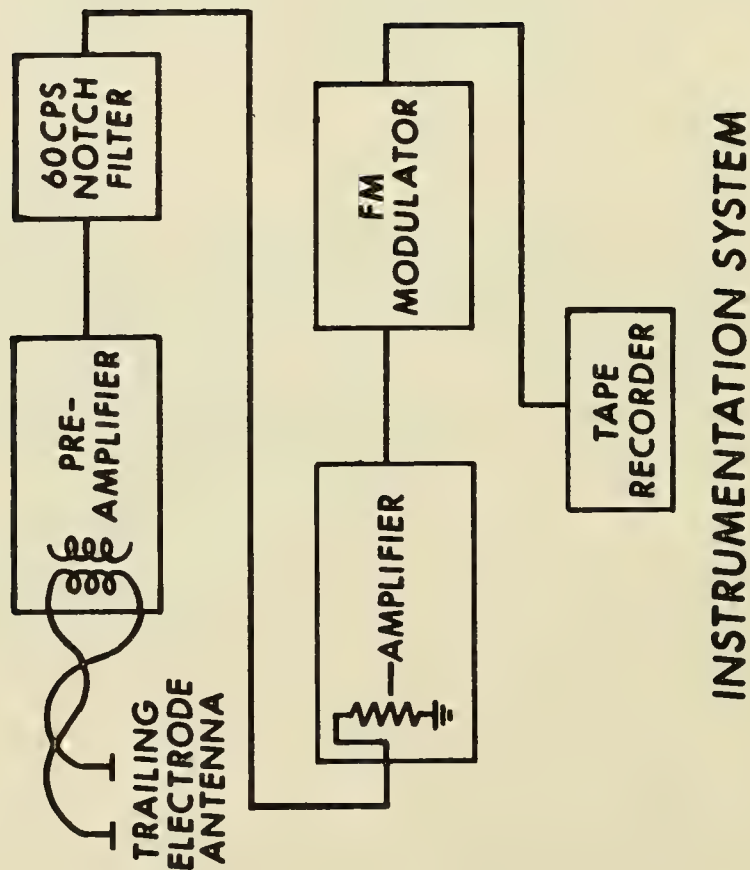


FIGURE 1 INSTRUMENTATION BLOCK DIAGRAM

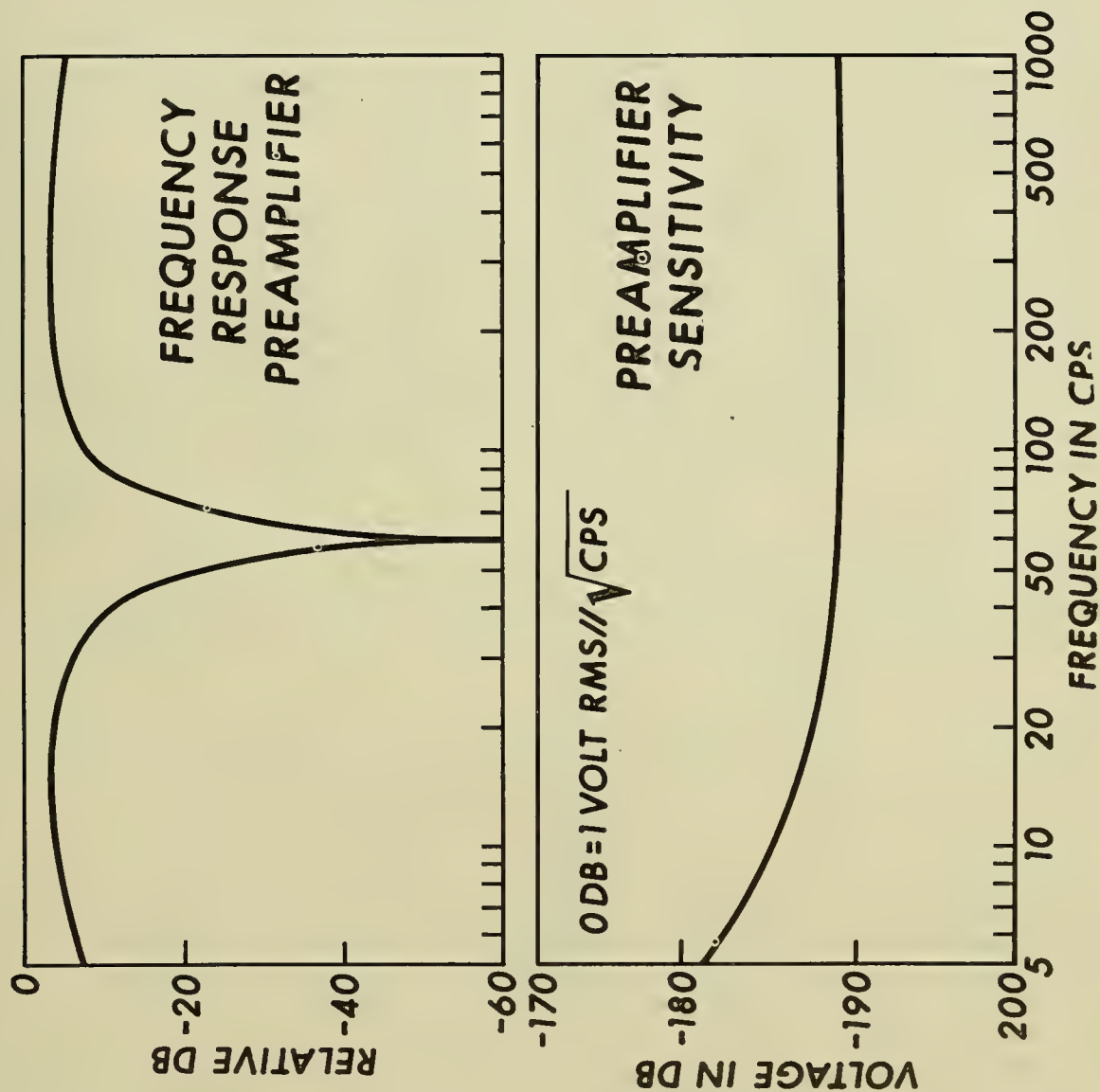


FIGURE 2 PREAMPLIFIER FREQUENCY RESPONSE AND SENSITIVITY CURVES



To keep the noise of the amplifying device below or equal to the thermal noise of the antenna, a geophysical-type transformer working into an RCA Nuvistor was used in the input circuit of the preamplifier.

There are two basic sensors that can be used for detecting electromagnetic energy in the sea. They are a loop antenna, which responds to the magnetic field component, and a pair of electrodes, which respond to the electric component. When measurements are being made at sea or in the sea from a moving platform, the sensor is subjected to motion with respect to the earth's magnetic field. Since such motion induces large currents in loop antennas, an electrode antenna was chosen as the sensor. The sensor is towed astern of the ship. At low speeds this trailing electrode antenna is essentially insensitive to vibration.

The overall length of the trailing electrode antenna line installed on the GILLISS was 360 meters (Fig. 3). Two stainless-steel electrodes were located at the trailed end of the line and were spaced 75 meters apart. A miniature, bellows-type pressure transducer was installed near the end of the line to monitor the depth of the antenna. A dummy antenna was located in the line near the electrode closest to the ship to monitor the transmission line for cable contamination. The line was depressed to approximately 30 meters by a 12-inch by 12-inch depressor designed by Taylor Model Basin.

The voltage that is induced in a pair of electrodes in a medium of uniform conductivity is directly proportional to electrode spacing. Thus, the electrodes were spaced 75 meters apart to increase the system sensitivity. Sources of noise, such as velocity-induced noise, thermal noise, and polarization noise are independent of spacing.

The major fixed noise source affecting sensitivity is the phenomenon of polarization. This is the gradual build-up of corrosion by-products at the electrode-sea water interface. This coating, in the case of most stainless steels, builds up a lossy capacitive film that further inhibits corrosion. However, the coating is not stable; it is constantly breaking down, changing the corrosion process, and consequently changing the electrical equilibrium. This changing corrosion process produces the electrode self-noise. Continuing experiments with various materials have found carbon to be unaffected by polarization, and a new trailing electrode antenna that utilizes carbon as the electrode material is being designed.

The trailing cable was manufactured by Samson Cordage Works, Shirley, Mass., from a design developed by the Underwater Sound Laboratory and Samson. The physical characteristics of the trailing electrode antenna line are interesting. Several special features had to be incorporated into the manufacture of this line. The first feature was that the supporting line be non-metallic. Because of the nature of the electric dipoles, it is essential that no metal be in the vicinity of the

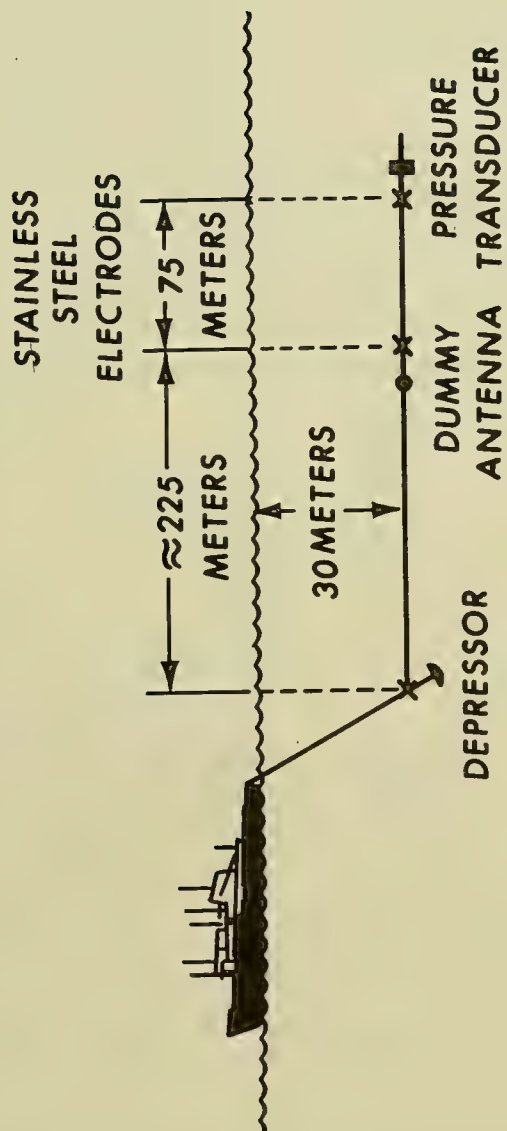


FIGURE 3 TOWING SCHEME FOR THE TRAILING ELECTRODE ANTENNA

electrodes. Any material whose conductivity is greater than that of the sea water will distort the electric field pattern and consequently alter the sensitivity of the antenna. Exposed metal could also react with the electrodes and result in unwanted corrosion currents. These DC corrosion currents could be modulated by mechanical motion of the line and cause unwanted noise.

The second feature concerned specific gravity. The specific gravity of the line must be close to the specific gravity of sea water in order to maintain a known distance between electrodes and hence measure the horizontal component accurately. The only material that would fulfill the above requirements was polypropylene. It is non-metallic, and its specific gravity is 0.9.

In addition to having a neutral buoyancy and being non-metallic, the cable had to have sufficient strength to withstand the tension developed from towing. The cable elongation, while towing, had to be kept to a minimum to prevent the electrical connecting wires from being permanently deformed and weakened. As fabricated, the trailing cable, in addition to the electrical leads, contained an inner core, an intermediate braid, and a cover braid (Fig. 4). Most of the strength was in the core and intermediate braid, while the cover braid protected the line from abrasion. With this construction the line would only elongate 5 percent at the top speed of an AGOR.

The line was manufactured on the cordage company's normal production machines with the three twisted pairs of electrical leads constrained in the center by the two outer layers of multi-filament polypropylene braid. The nominal diameter of the line was 1.25 inches and was essentially neutrally buoyant throughout its entire length. The stainless-steel electrodes, 60 inches long by 2 inches wide, were spiraled on top of the intermediate braid and covered with the outer braid.

Two of the major electrical problems in the trailing electrode antenna were the lead resistance and susceptibility to electromagnetic interference. The wire size had to be large enough not to add unduly to the thermal noise of the overall antenna impedance. The No. 14 wire used in connecting the electrode pair to the instrumentation adds 6.5 ohms to the nominal 1.5 ohms of the electrode pair. The wire was covered with extruded teflon and was tested in manufacture with a high voltage to insure that there were no ruptures in the jacket. A tightly twisted pair was selected over a coaxial type cable because it is easier to manufacture, tolerates physical elongation, and provides lower susceptibility to surrounding magnetic fields.

For example, in a one-gauss field the voltage induced in a single twist of the twisted pair of 100 cycles is  $1 \times 10^{-7}$  volt. The coefficient of coupling between two of the twisted pairs was  $5 \times 10^{-3}$ . With this low susceptibility and coefficient of coupling, the transmission line would be unaffected by ambient electromagnetic noise fields on or near the ship.

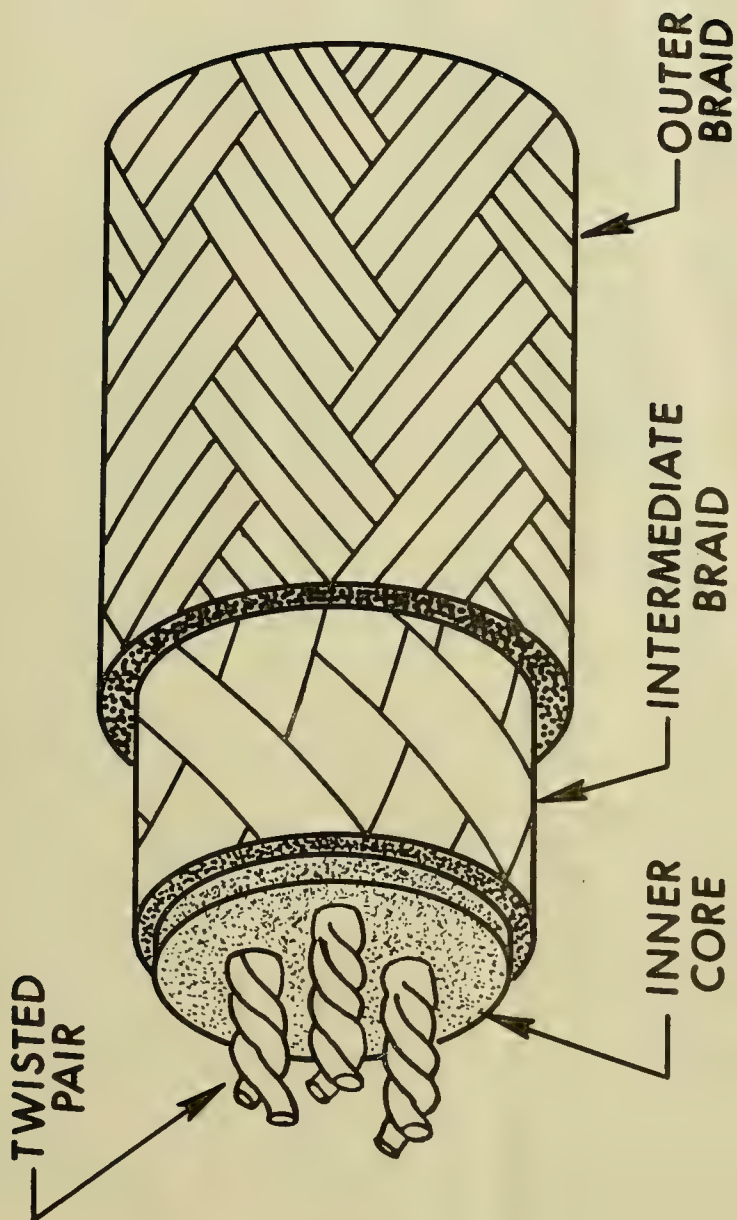


FIGURE 4 CONSTRUCTION DETAILS OF TRAILING ELECTRODE ANTENNA LINE



## MEASUREMENT TECHNIQUES

The calibrations made on the GILLISS are based on the hypothesis that the voltage induced in an isolated electrode pair is numerically equal to the product of the field strength and the antenna length. Because the impedance of the electrode antenna is very low as compared with the input impedance of the preamplifier, a field-induced voltage at the antenna may be simulated by means of a calibration voltage injected in series with the electrode pair.

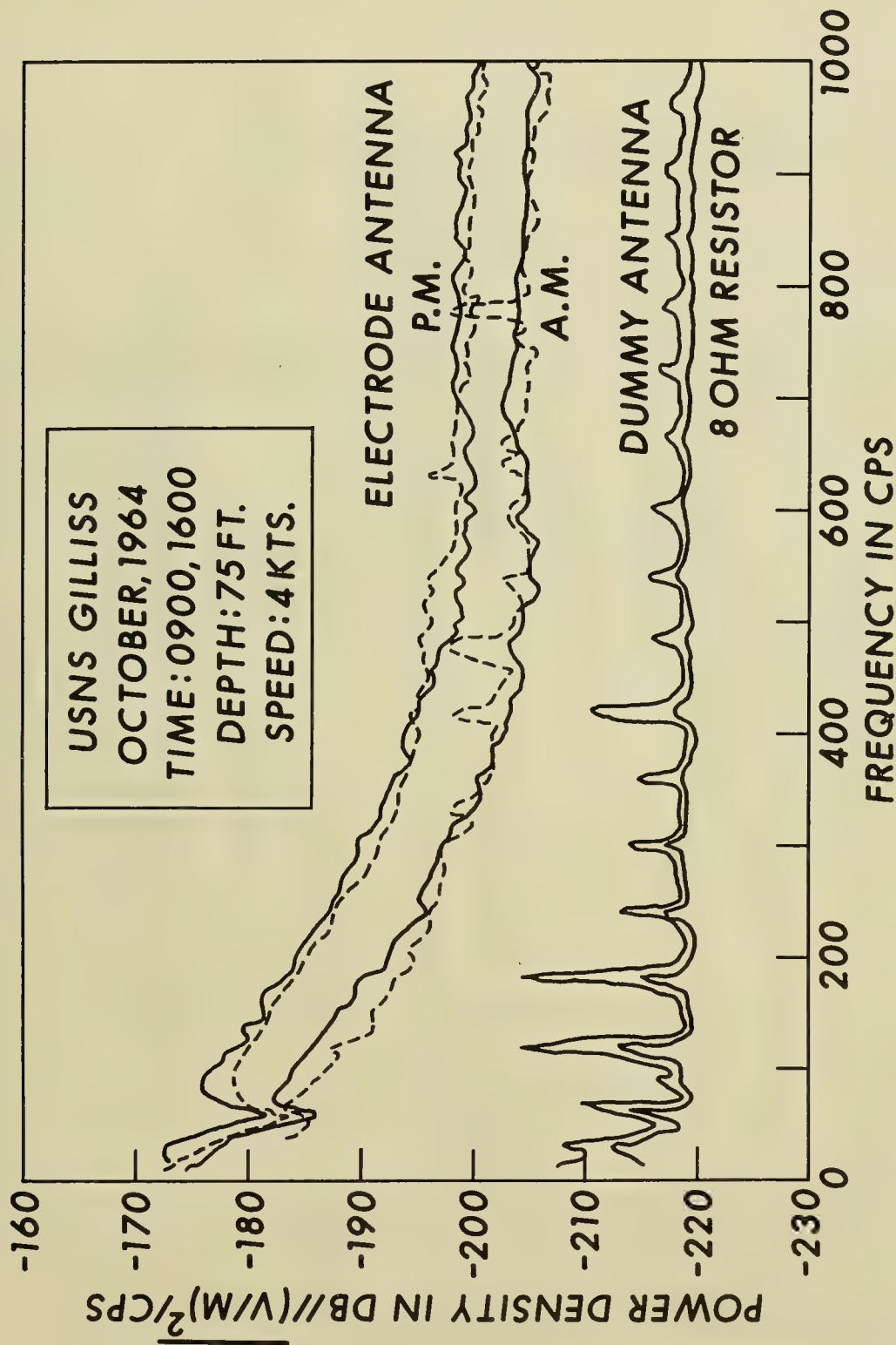
To insure that any changes in system sensitivity would be detected, three calibration measurements were made. In one case the preamplifiers were terminated with a dummy resistor at the input terminals, and the calibration measurements were compared with laboratory data taken before sailing. In the second calibration measurement, the dummy resistor was located at the trailed end of the electrode antenna. This second measurement checked the antenna cable and lead-in wires. The third calibration measurement was made on the antenna. The system was calibrated throughout its full frequency range at the beginning and end of the trip, and a spot calibration was recorded during each measuring period.

Measurements were made on the GILLISS at sunrise, mid-day, sunset, and post-sunset with the electrodes depressed approximately 30 meters below the surface. The ship trailed the antenna at about 3 knots; this slow speed kept the electrode velocity-induced noise to a minimum.

A power spectrum analysis has been performed on some data from the October 1964 trip on the GILLISS. The analysis was performed on 152-second data samples using a 12.5 cps bandwidth in the spectrum analyzer. One hundred different frequencies were analyzed in the range between 10 and 1000 cps. These results are shown in Figs. 5 and 6. In addition to the power spectra of the electrode antenna, the power spectra of both the dummy antenna and an 8-ohm resistor at the input to the preamplifier terminals are shown. As shown by these two spectra, there was a small amount of hum in the system. Figure 5 compares two samples taken within a half hour of each other. Note the spread of approximately 3 db. Figure 6 compares data of different days—two morning samples and two afternoon samples. Note the possible morning and afternoon differences.

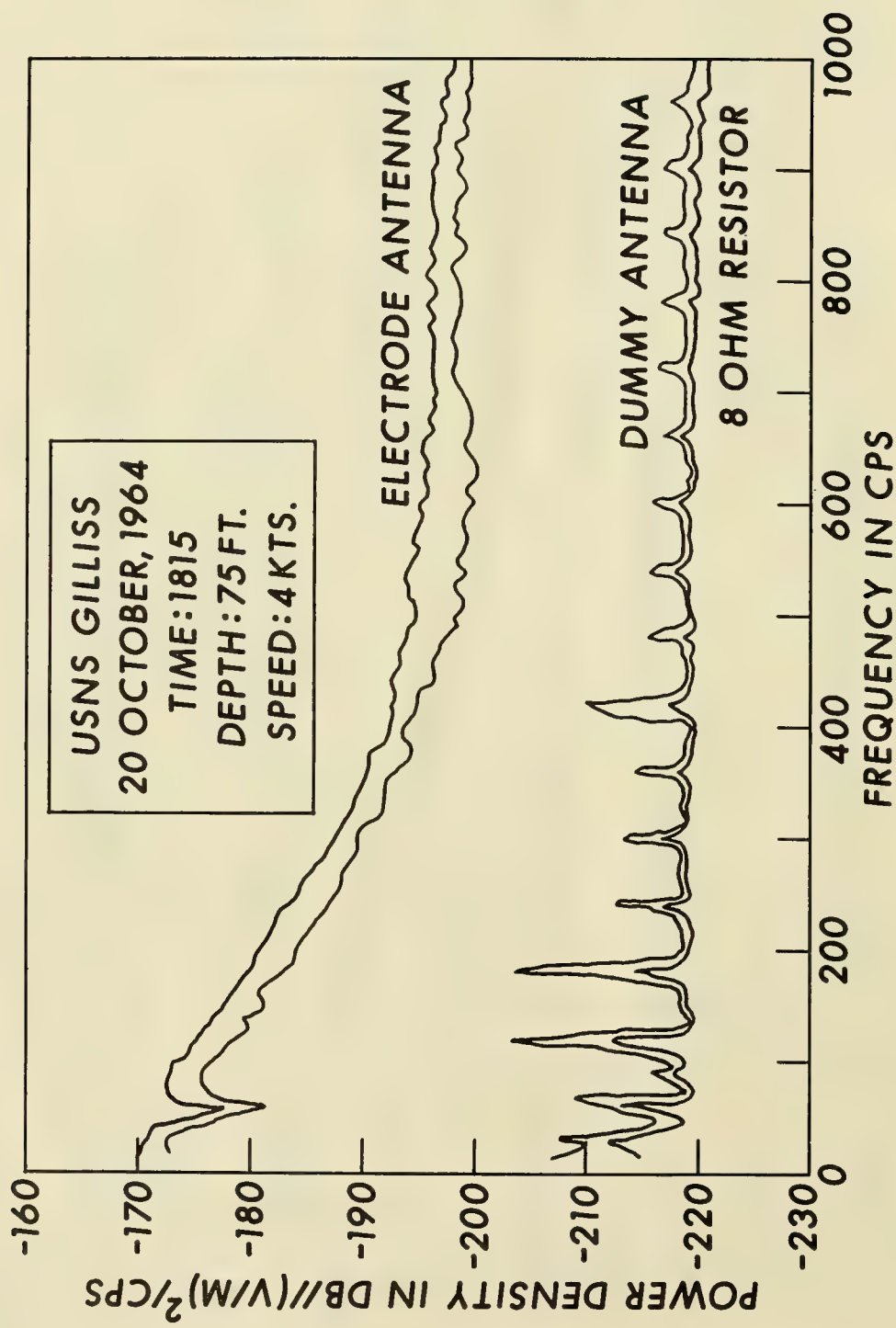
Ultimately the analysis of these data will result in quantitative ELF electromagnetic noise levels as a function of frequency, time of day, season, geographic location, and meteorological and oceanographic conditions.





## NOISE POWER DENSITY

FIGURE 5 COMPARISON OF CONSECUTIVE RECORDINGS



## POWER DENSITY COMPARISON OF CONSECUTIVE RECORDINGS

FIGURE 6 COMPARISON OF MORNING AND AFTERNOON DATA

GLASS AND CERAMIC HULLS FOR OCEANOGRAPHIC APPLICATIONS

by

J. D. Stachiw

U. S. Naval Civil Engineering Laboratory  
Port Hueneme, California



# GLASS AND CERAMIC HULLS FOR OCEANOGRAPHIC APPLICATIONS

by

J. D. Stachiw  
U. S. Naval Civil Engineering Laboratory  
Port Hueneme, California

## INTRODUCTION

More than five years have passed since glass and ceramics appeared on the horizon of the deep submergence materials application field. Since that time, a sufficient number of papers,<sup>1</sup> articles<sup>2,3,4</sup> and reports<sup>5,6,7,8</sup> has been published to convince even the most conservative scientist and engineer that glass and ceramics do indeed possess the highest compressive strength and compressive strength to weight ratio of all the known commercially available structural materials. The superiority of these materials' ability to withstand compressive stresses has been described and proven to such a point that it can be considered axiomatic, and no need exists to belaborate this point further.

Since the point has been proven that these materials are superior in compression and, therefore, worthy of consideration for the construction of deep submergence structures, the question arises as to what uses these materials have already been put in that field and in which applications they promise to succeed in the near future. It is hoped that this brief paper will summarize the progress made in applying glass and ceramics to the deep submergence structures field and will, possibly, crystallize the thinking for future research plans in this field.

## STATEMENT OF PROBLEMS

After the discovery that glass and ceramics possess outstanding compressive strength properties and thus would seem to be ideal choices for application in deep submergence structures, unlimited vistas arose as to their use in that field. They could be used for the hulls of deep-diving submarines, torpedoes, mines, buoys, instrumentation capsules, permanent ocean-bottom installations, and as components of other deep submergence equipment where their high compressive strength and/or optical transparency make them desirable. No matter which application was considered, the problems of designing with unfamiliar materials, of fabricating complex and large structures, of joining glass and ceramics to each other



and to dissimilar materials, of protecting against point and shock loading, and of establishing adequate quality control had to be tackled and at least partially solved. From the very beginning, three distinct streams of research in the use of glass and ceramics for deep submergence applications became discernible (Figure 1). First, there was the research directed to the use of glass and ceramics for hulls of deep submergence buoys; second, the research applying itself to the utilization of these materials for deep submergence ASW torpedoes and instrumentation capsules; and third, the research dedicated to the solution of the engineering problems blocking the path to the use of glass in submarine hulls. Each one of these areas of research has produced tangible results which testify to the progress made in these rather distinct research areas. In addition, glass and ceramics could also be applied to hulls of permanent sea floor installations where their resistance to corrosion, creep, and leakage is found advantageous. However, due to lack of interest and funding, no work has yet been done in this very promising area of research.

Since the author's work has been centered, primarily, in the research area of deep submergence oceanographic instrumentation capsules and ASW weapon hulls, the discussion of this research area will form the main body of the paper, while the work in the other research areas will be discussed only peripherally.

## BUOYS

Glass and ceramics saw their first application in the deep submergence engineering field as buoys. Buoys, generally made in spherical shapes, are very simple structures, as their main application is to provide buoyancy for diverse oceanographic systems. Since their main application is simply providing buoyancy to other oceanographic systems, the structures consist only of a hull, which is either a monolithic sphere or is made up of two hemispheres held together mechanically or with the help of adhesives. Up to this time, the spherical deep submergence buoys have been made available on a commercial basis only in Coor's Porcelain AD-99C alumina and Corning Glass Works' Pyrex glass with approximate weight to displacement ratios of .27 and .37, respectively. The buoys are available in 1- to 12-inch diameters in alumina and in 2- to 23-inch diameters in Pyrex. Both the alumina and Pyrex buoys have an operational depth of 20,000 feet, while their implosion depths vary from 25,000 to 40,000 feet depending on the buoy's size, type of joint, gasket material in the joint, and deviation from nominal diameter, wall thickness and sphericity.

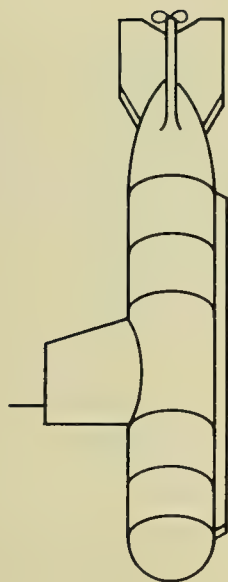
Instrumentation

&

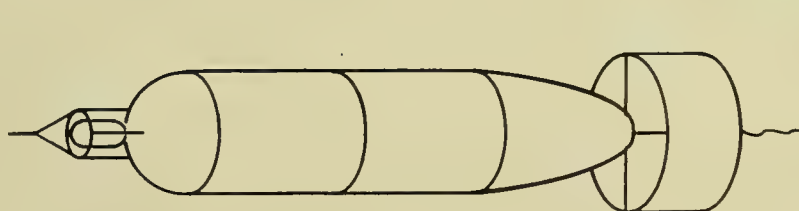
ASW

Weapons

Buoys



Submarine Hulls



Ocean Floor Installations

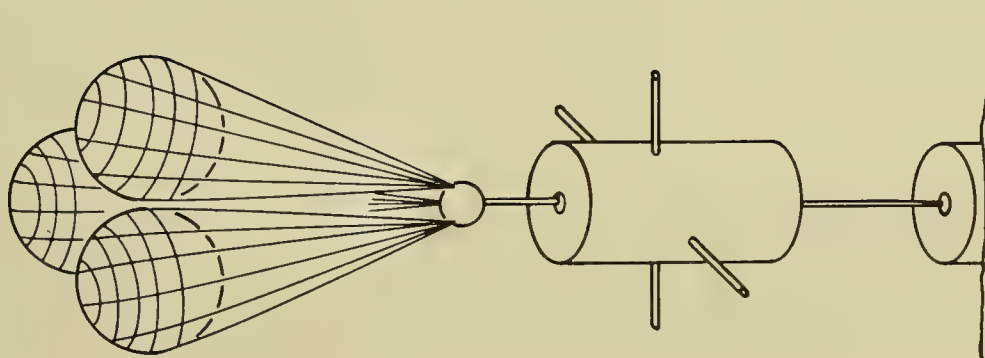
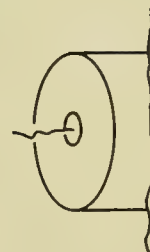


FIGURE 1 FIELDS OF APPLICATION FOR GLASS AND CERAMIC  
DEEP SUBMERGENCE HULLS

Experimental data shows that in order to maximize the implosion strengths of the spherical buoys, the hemispheres should be fused if the construction material is glass, or should rely on a fabrication method that produces monolithic hulls if the material is alumina ceramic. Using such assembly methods, Pyrex spheres can be expected to withstand at least 120,000 psi and AD-99C alumina ceramic spheres at least 300,000 psi compressive stress in the hull prior to implosion. The use of joints with or without gaskets with either one of the materials invariably lowers the implosion pressure of the buoys. Although different gasket materials have been experimented with, the buoys with beveled hand-lapped joints without gaskets have shown to have the highest resistance, in some cases approaching the strength of fused or monolithic buoys. Gasketless joints with beveled and hand-lapped surfaces in 99-percent alumina ceramic buoys withstood between three to four times higher compressive stresses than Pyrex buoys.

In addition to commercially available items, there are various custom-made items which have proven interesting in experiments. Chemically strengthened glass spheres, fabricated from Pittsburgh Plate Glass' Herculite II strengthened glass and Corning Glass Works' Chemcor strengthened glass, have been found capable of withstanding somewhat higher compressive bearing stresses than semi-tempered or annealed Pyrex spheres. Also, custom-made spheres of Corning Glass Works' Pyroceram #9606 have been found to withstand approximately the same compressive bearing stresses in a lapped ceramic to ceramic joint as the alumina ceramic.

At the present time, the commercially available glass and ceramic buoys are of small diameter, but development is being carried on at glass and ceramic industry research facilities which will result in the immediate future in buoys of up to 4 feet in diameter with 20,000-foot depth capability. Such larger buoys will probably also permit lowering of the price per pound of buoyancy. The current price for Pyrex buoys purchased in small lots is \$5 per pound of buoyancy, and for such buoys bought in large lots, the price is \$2.50 per pound of buoyancy. The lowered price should reach approximately \$2 per pound of buoyancy in 1000-pound buoyancy Pyrex spheres. In comparison, alumina ceramic buoys are currently selling for approximately twice that of Pyrex spheres, but improving mass production techniques promise to bring these buoys in line with prices for Pyrex spheres.

With the increased availability, larger diameter, and lowered price, glass and ceramic buoys (which already surpass metallic, glass-fiber epoxy, and syntactic foam buoys on a buoyancy basis) will also become competitive on cost per pound of buoyancy basis. It appears that the future of glass and ceramic in the deep submergence buoy field is assured as economical structure materials without peer in compressive strength.



It would be an omission not to mention here also small low-quality buoys made for the fishing trade. Although not designed or fabricated for deep submergence application but for use as fishing net surface buoys, some of these buoys can withstand safely depths of 20,000 feet. Available from Blenco Manufacturing Company in the United States, and as imports from Japan and in sizes from 2 to 10 inches in diameter, their cost is less than \$1 per pound of buoyancy when purchased in small lots and less than 50 cents per pound of buoyancy in large lot quantities. Their price is very attractive, and because of it they have found some use in deep submergence applications;<sup>10</sup> but unless each buoy is proof tested to its operational depth prior to use in the ocean, they cannot be relied upon. It may be that improved mass production techniques will improve the reliability of these inexpensive glass spheres to such an extent that they can be used, without testing, to some specified operational depths.

## SUBMARINES

The most glamorous application for which glass and ceramics are being groomed<sup>11</sup> is that of a hull for deep submergence submarines. At last a hull will be in the possession of man which will permit him to descend to the very bottom of the oceans without recourse to flotation buoys or liquid-filled dirigibles, like Trieste, for support of the hull containing the crew. Glass or ceramic spherical and cylindrical hulls are certainly capable of providing a weight to displacement ratio of .4 which is thought sufficient for providing buoyancy to men and associated equipment in a submarine with an operational depth of 35,000 feet. Glass, in particular, is desirable for such an application because it would not only provide the necessary strength for the hull, but would also provide almost unlimited visibility for the crew, a dream long cherished by submarine crews who today feel that they are actually strangers and intruders in the sea.

Work initiated in 1962<sup>1</sup> in this area has brought forth many fruits. It has been confirmed in both theoretical studies and in actual experiments that the resistance of unprotected glass hulls of different shapes to underwater shock increases with depth to more than 20,000 feet of depths. It was also discovered that a plastic or rubber overlay on the glass hull increased its resistance to shock waves still further. Models of surface-compressed glass spherical hull with a simple circumferential joint, glass entry hatch, and metallic feed throughs were tested to more than 20,000 feet depth without failure while the compressive stress in the hull was approximately 65,000 psi. Silver foil was used as the gasket material for the joints between the hemispheres and between the hatch and its seat. The use of tensioned metallic cages on surface-compressed glass hulls was shown to prevent shattering of the hull when it was locally cut or fractured.

In general, the progress shown in applying glass to submarine hull construction has been encouraging and has been steadily progressing from the feasibility study stage to the model study stage. Still, a considerable amount of design, engineering and production experience will have to be accumulated before glass and ceramic submarine hulls can be considered predictably reliable and safe structures. This experience can be accumulated readily if the designer of glass submarines draws heavily upon extensive work being done in the glass and ceramic oceanographic instrumentation capsule and ASW weapon hull fields.

## OCEANOGRAPHIC INSTRUMENTATION CAPSULES AND ASW WEAPON HULLS

### The Morphology of Design

The area of research concerning itself with free-diving oceanographic instrumentation capsules and ASW weapon hulls is an interesting one because it is located midway between the buoys, on the one hand, and submarine research, on the other hand, as far as the scope of its endeavors is concerned. The design and fabrication of a free-diving oceanographic instrumentation capsule and of ASW weapon hulls require more engineering and fabrication knowledge of glass and ceramics than is necessary for the design and fabrication of buoys, but less than is required for submarines. Furthermore, design and engineering advances in the free-diving capsule field are directly applicable to the submarine design if parameters of size and weight are properly taken into consideration.

The fact that free-diving instrumentation capsules and ASW weapon hulls are generally smaller, less costly, and unmanned are further reasons why experimentation with these structures has been so prolific. The small size of the various free-diving capsules places them definitely in the present state of the fabrication art so that many relatively inexpensive units can be built and experimented with for the same cost that would be involved in building even one manned submarine hull, while the fact that they are unmanned imposes less requirements on the reliability of the experimental design or fabrication method. Because of this, free-diving instrumentation capsules can be designed and fabricated on a much more limited basis of knowledge and experience. However, once such a capsule design has been built and found safe for a given set of operational parameters, it immediately becomes a scale model of a large manned free-diving buoy or submarine with similar operational parameters. In addition, with few dimensional changes the hull of a free-diving instrumentation capsule becomes the hull of a deep submergence propelled or unpropelled ASW weapon. If one looks at the free-diving glass and ceramic oceanographic instrumentation capsule field from the above-mentioned vantage



points, then the number of different free-diving instrumentation capsules built so far, although numerically substantial, is indeed meager. As a matter of fact, it may not be farfetched to postulate that the future of glass and ceramic deep submergence manned submarines would be more assured and would arrive sooner if more efforts were directed at the present time to design, fabrication, and evaluation of glass and ceramic deep submergence free-diving oceanographic capsules and ASW weapon hulls, rather than to feasibility studies of manned glass and ceramic submarines. The more deep submergence free-diving capsules and ASW weapon hulls are designed and built from these materials, the more engineering problems pertaining to the use of these materials in deep submergence structures will be brought to light and, after some experimentation with design parameters, solved.

So far, the design and fabrication of free-diving oceanographic capsules and of submarines has pivoted around two dissimilar approaches to the problem of providing more buoyancy for the carrying of larger payloads. One approach relies on the design and fabrication of progressively larger hemispheres, which, when joined, provide more and more payload-carrying buoyancy. The other approach, to which the author personally subscribes, is to provide increasing amounts of buoyancy, not just by building larger and larger monolithic hemispheres whose size is severely limited by the fabrication capability of the glass and ceramic industry, but by joining many cylindrical shell sections into longer cylindrical hulls.

The reason for using spherical hulls is obvious; it is an extremely simple design, requires no stiffeners, and an ordinary glass to glass joint will satisfy the joint requirements, particularly when a metal band is used on the outside of the joint to hold the two hemispheres together. The disadvantages of this approach to providing larger and larger buoyancy for carrying of internal payload are many, the principal ones being the poor hydrodynamic shape and severe fabrication size limitation, unless polyolithic designs and assembly methods are resorted to, at which time the joint problem becomes much more complex and difficult than the joint for cylindrical hull sections.

The approach to the fulfillment of requirements for larger and larger payload-carrying capabilities of free-diving capsules utilizing the concept of joining several cylindrical shell sections together is firmly rooted in past ASW weapon engineering practice and in the evaluation of the glass and ceramic industry in fabrication capability. The custom of using cylindrical shapes in ASW weapon hulls and free-diving instrumentation capsules is grounded in the well-known property of cylindrical hulls to possess less hydrodynamic drag than spherical hulls of equal displacement. Not only that, their capability of carrying payloads can be varied according

to payload requirements by varying the total number of cylindrical shell sections in the hull. As far as fabrication is concerned, it is much easier to fabricate cylindrical shell sections than spherical shell sections of equal diameter; and since a sphere must be of much larger diameter than a long cylinder in order to carry the same payload, the comparison between the cost and difficulty of fabricating spherical and cylindrical hulls for the same payload becomes more and more favorable for the cylindrical hulls.

There are, however, some problems connected with the use of cylindrical shell sections, too. The two major problems are, first, the need to incorporate ribs into the cylindrical shells to make them elastically stable, and, second, the need to provide the many shell sections in the hull with mechanically reliable and strong metallic joints. The incorporation of ribs into the shell structure makes their design more complicated and fabrication more difficult, but without the ribs the walls of the cylinder would have to be excessively thick in order to prevent failure of the glass or ceramic shell by elastic instability. The need to join the many shell sections by metallic joints requires the design of a joint that is not only compatible with the glass or ceramics that it joins, but that is also capable of withstanding the large column loads and hydrostatic pressure loading at operational depths not to mention the high bending moments imposed on the hull during launchings or retrieval operations.

#### Experimental Deep Submergence Ceramic Shell Series

To provide the cylindrical hulls for glass and ceramic deep submergence free-diving instrumentation capsules, it was necessary then to investigate the design of ribs for glass and ceramic shells and their fabrication. For this purpose a series of ceramic rib-stiffened shells was designed<sup>8</sup> in 1962. Two materials were used, Corning's Pyroceram #9606 and Coor's 99-percent alumina. These two materials were chosen because of their high moduli of elasticity, high compressive strength, and above average flexural strength. Since transparency of the deep submergence hull for ASW weapons or instrumentation capsules is not necessary for ultimate utilization, no drawbacks were considered to be associated with the selection of opaque ceramics for the experimental series of cylindrical hulls. Although the behavior of rib-stiffened ceramic shells under hydrostatic pressure was the main objective of the investigation, sufficient additional shells were ordered to permit investigation also of several additional points of interest. As the depth capability of 20,000 feet is considered to be sufficient to operate in 90 percent of the hydro-space, all of the shells in the exploratory series were designed for that operational depth. In order to cover the field adequately, one shell design had only end stiffeners (Figure 2), one design had an additional

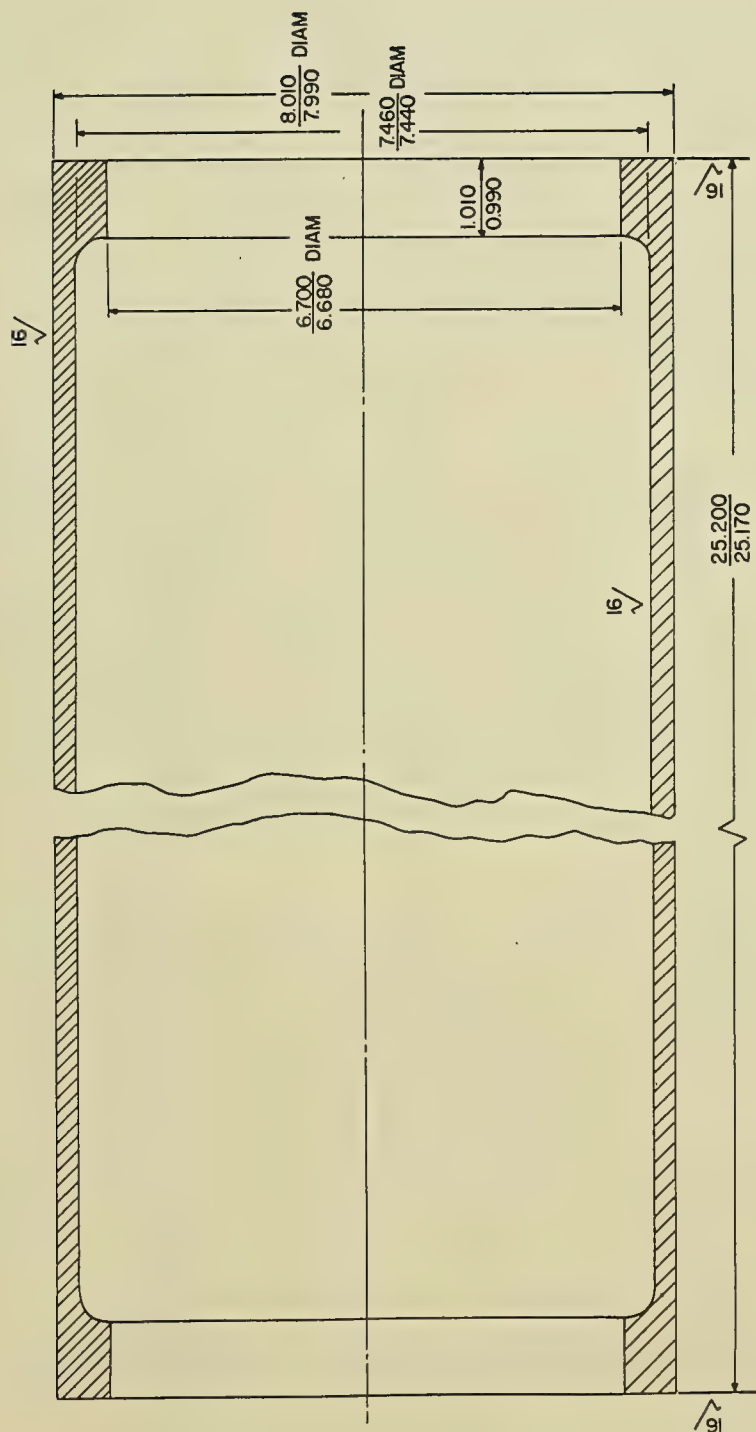


FIGURE 2 NINETY-NINE-PERCENT ALUMINA CERAMIC SHELL,  
IMPLODED AT 13,500 psi



stiffener in the middle, as well as the end stiffeners (Figure 3), while another had a series of stiffeners in addition to those at the ends (Figure 4). All the shells were tested with flat 7075-T6 aluminum alloy end closures that permitted the ends of the shells to slide upon them. Besides being subjected to slowly increasing hydrostatic pressure, some of the shells were pressure cycled, some were subjected to dynamic pressure loadings, while some were notched prior to hydrostatic pressure tests.

The results of the tests conducted with the exploratory cylindrical shell series in 1963 at the Southwest Research Institute, San Antonio, Texas, were very encouraging. It was found that the elastic stability and stress distribution formulas available for rib-stiffened metallic cylinders apply in identical manner to ceramic cylinders, except that in the ceramic cylinders all of the deformations take place in the elastic stress region of the material. When stress raisers, such as deep scratches or sharp fillets, are located in an area of the shell where only compressive stresses occur, no degradation of the ceramic rib-stiffened cylinder's collapse strength occurred. No creep has been observed at biaxial stresses below 200,000 psi generated in the ceramic cylinders by hydrostatic pressure for one day. The implosion resistance of ceramic rib-stiffened cylinders to underwater shock waves has been found to increase with depth, while that of metallic cylinders of identical dimensions decreased. When the #9606 Pyroceram rib-stiffened cylinder (Figure 4) was subjected to 3000 pressure cycles which generated compressive stresses of 200,000 psi magnitude in the cylinder, no failure of the cylinder occurred although some flaking of the material was observed in areas where the highest compressive stresses occurred (Figures 5-7). No failure or flaking of any kind occurred at the joints where the ceramic cylinders rested on the smooth 7075-T6 aluminum closures.

The ceramic cylinders tested were not of large diameter; however, their buoyancy was of sufficient magnitude that, if several of these cylindrical shell sections were joined together into a long hull, it would support a useful oceanographic instrumentation payload. Using an L/D ratio of 6-8 which insures minimum hydrodynamic drag, a 60-inch-long cylindrical hull made up of the already proven 8-inch-OD ceramic shell sections could carry a 30-pound payload to a depth of 20,000 feet and yet retain 5-10 pounds of buoyancy for the return trip to the surface. But this could be feasible only if a mechanical joint were developed that not only would withstand the stresses generated by hydrostatic loading, but also would insure the hull's integrity during launch and retrieval operations.

#### Experimental Joints for Ceramic Shells

Several approaches were tried to the design of a reliable cylindrical shell section joint (Figure 8) that, in addition to withstanding

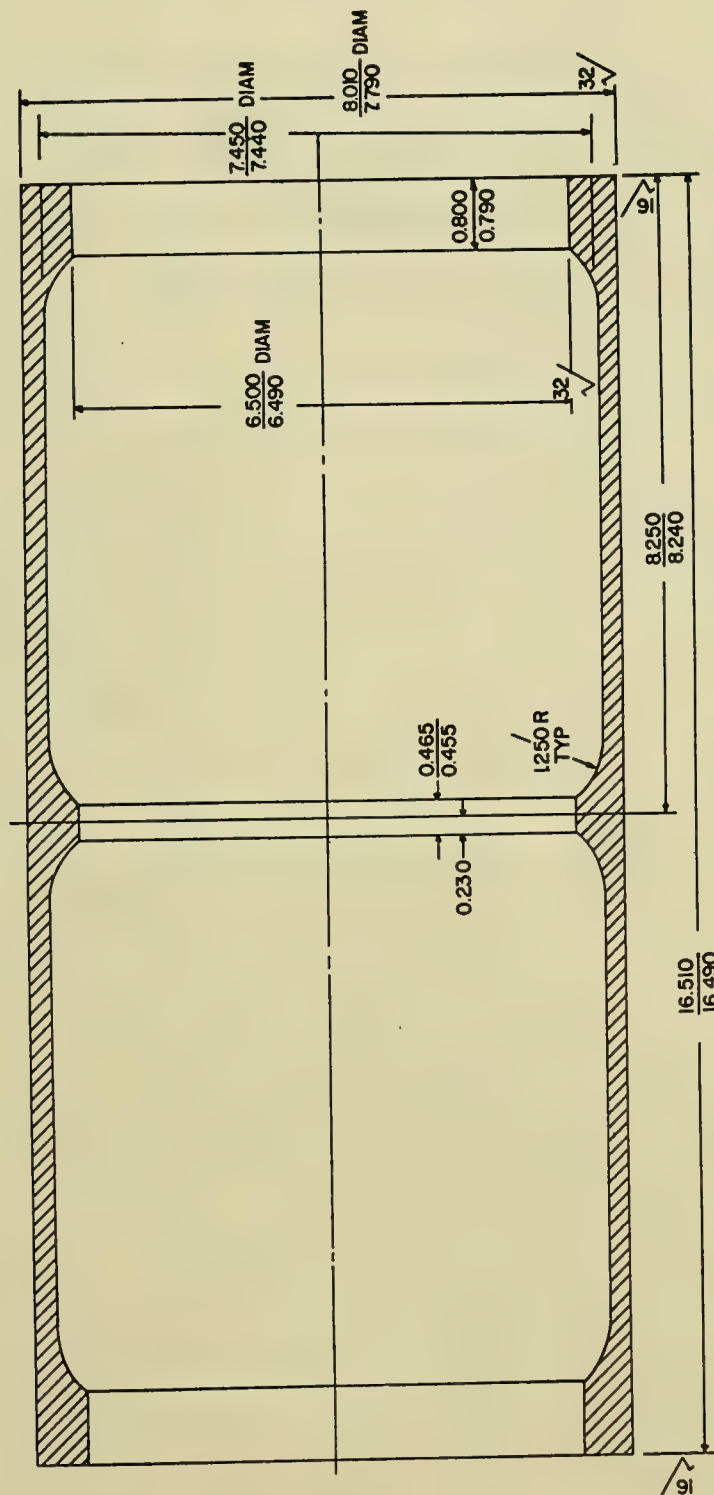


FIGURE 3 PYROCERAM #9606 SHELL, WITHSTOOD 10,000 psi



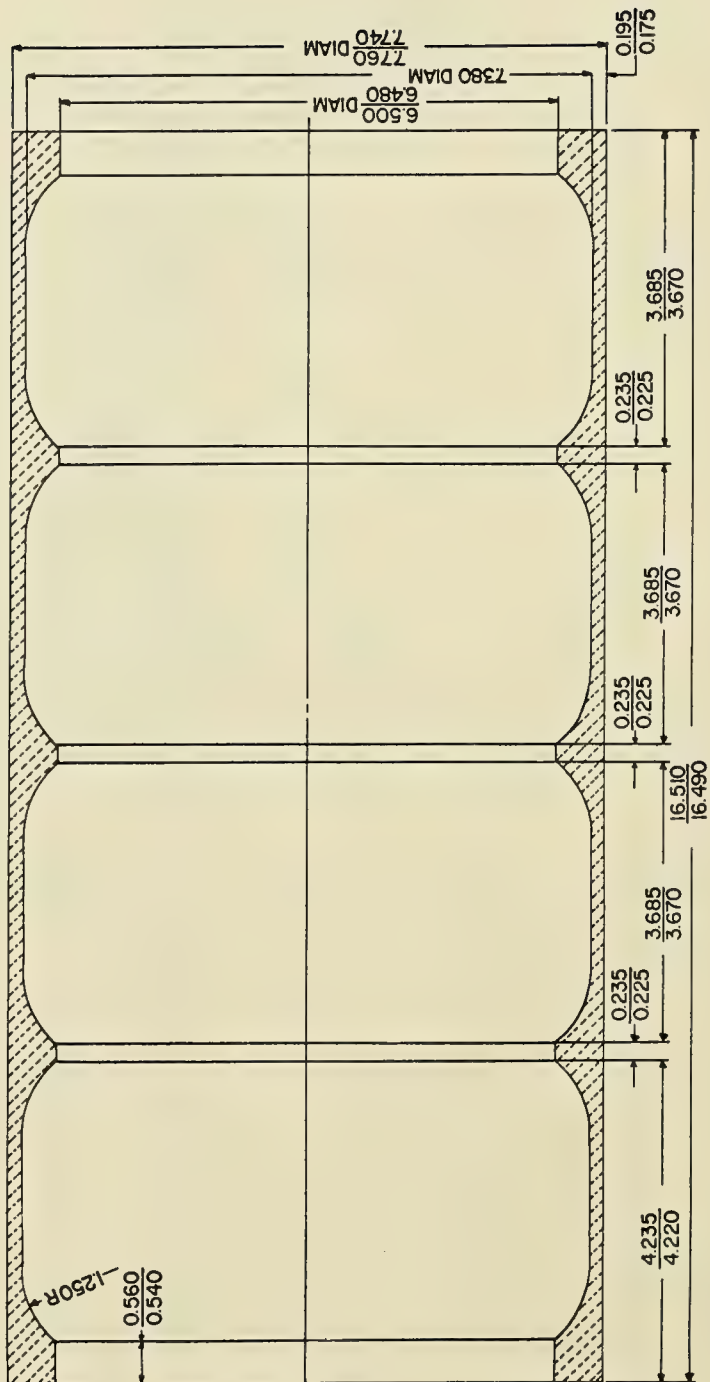


FIGURE 4 PYROCERAM #9606 SHELL, IMPLoded AT 11,000 psi

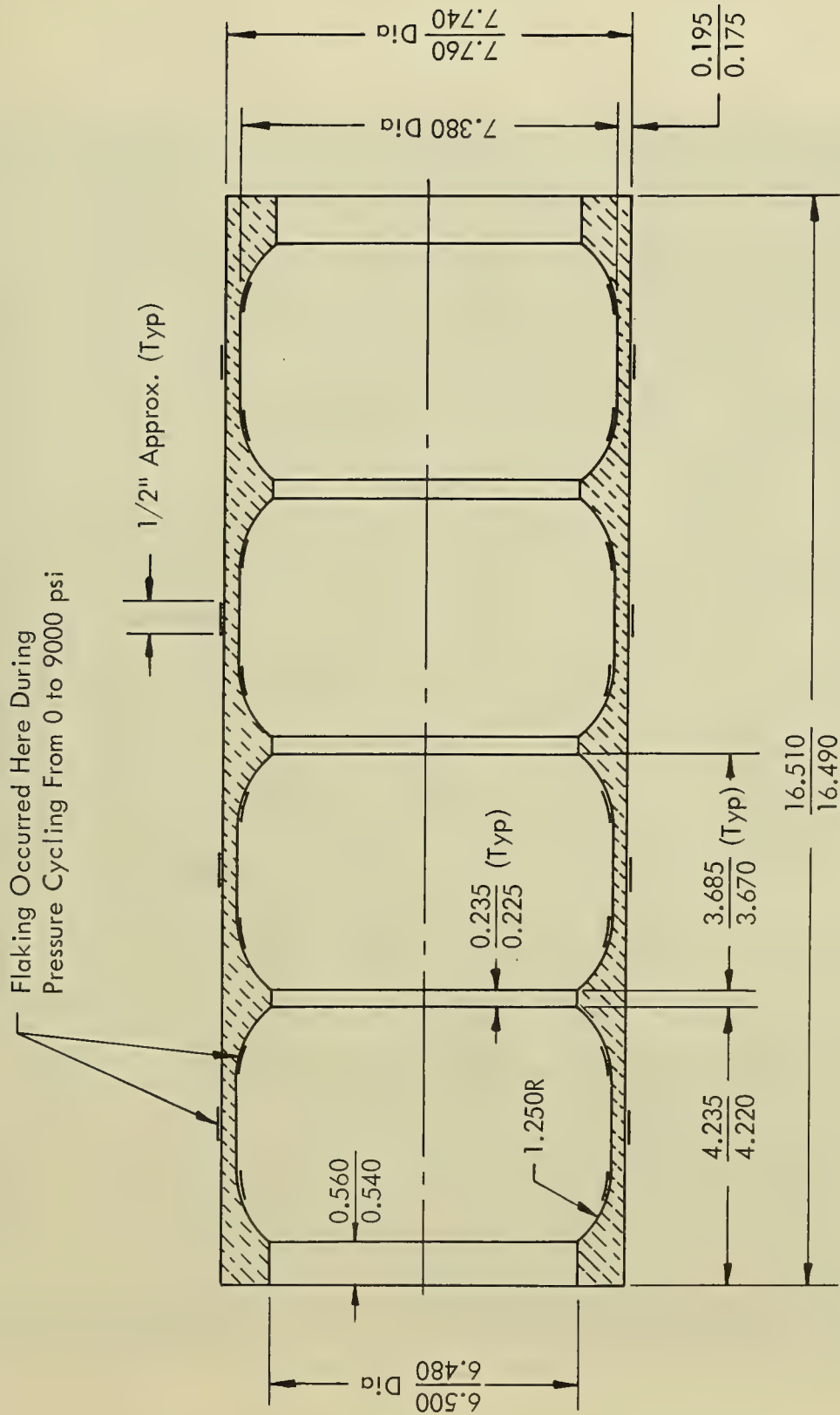


FIGURE 5 LOCATION OF AREAS ON RIB-STIFFENED PYROCERAM #9606 SHELL WHERE FLAKING OF SURFACE OCCURRED DURING CYCLING

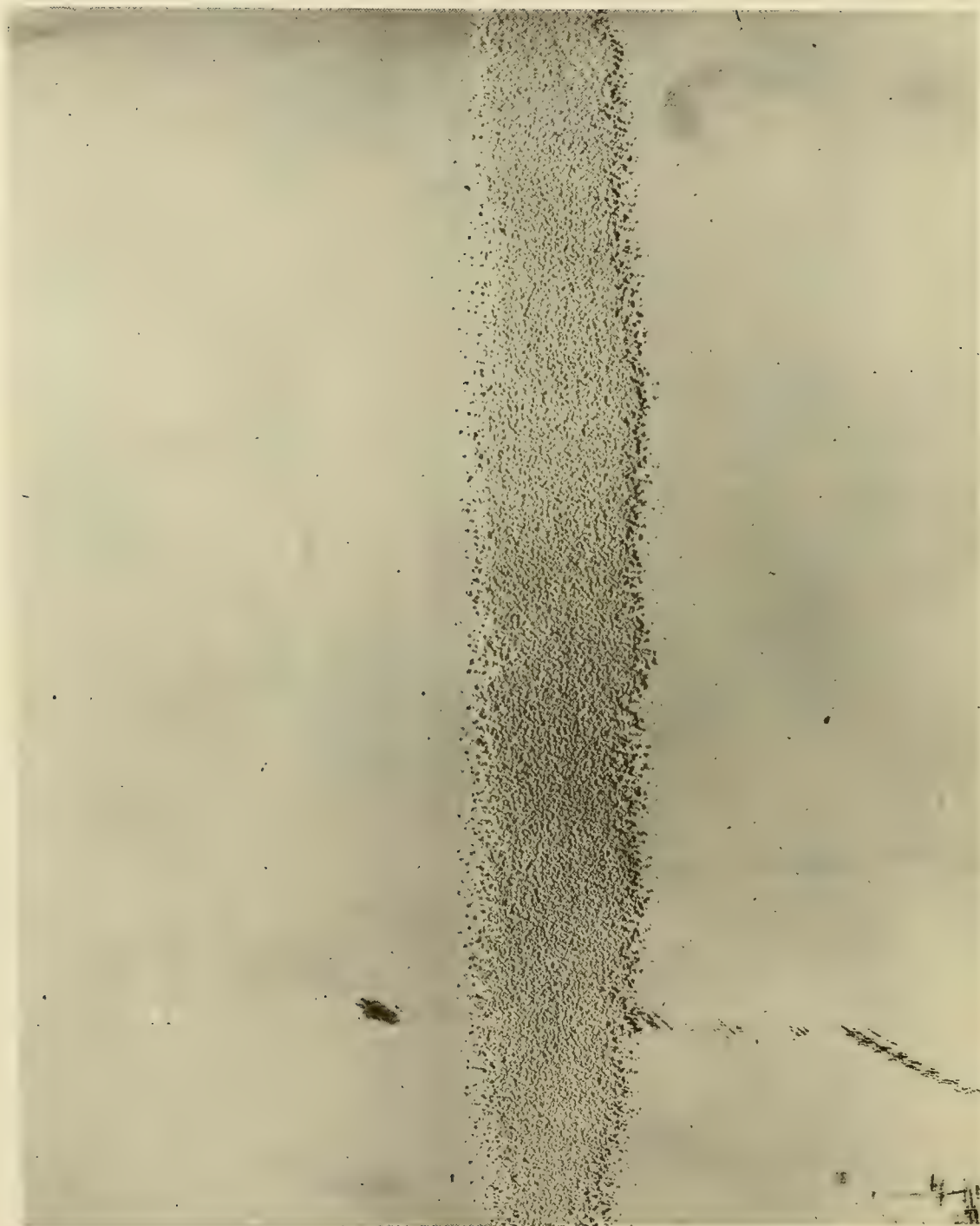


FIGURE 6 DETAIL OF FLAKED EXTERNAL SURFACE OF PYROCERAM #9606 SHELL (FIGURE 4)  
AFTER 3,000 PRESSURE CYCLES FROM 0 TO 9,000 psi

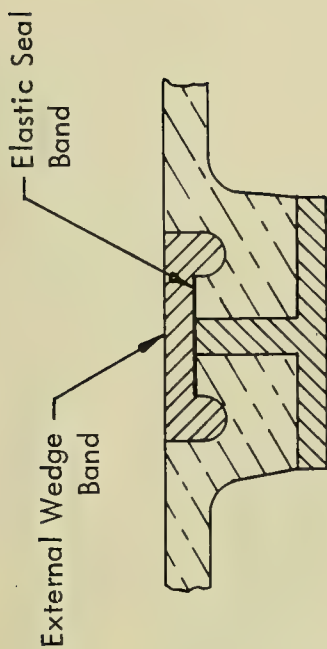


FIGURE 7 DETAIL OF FLAKED INTERIOR SURFACE OF PYROCERAM #9606 SHELL (FIGURE 4)  
AFTER 3,000 PRESSURE CYCLES FROM 0 TO 9,000 psi

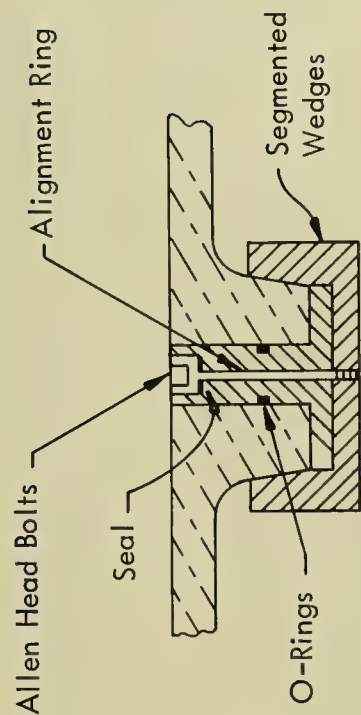


an operational hydrostatic pressure of 10,000 psi, would also withstand the bending moments generated inside the hull by launching from a shipboard-mounted air-operated launcher. One other requirement complicated the design further, the requirement being that the joint be flush with the external hull surface so as not to generate additional hydrodynamic drag for the hull. Of the three designs considered, only one has been found to satisfy all the above-mentioned operational requirements. One of the designs (Figure 8a), an internal expanding wedge joint, was rejected because it imposed tensile stresses on the ceramic flanges when two shell sections were locked together with this joint. In this particular case, the tensile stresses were caused by the upward thrust of the joint wedges used to draw the two adjoining cylinders' flanges together. The other design, an external wedge band joint (Figures 8b and 9), was rejected because the deep grooves cut in the external surface of the cylinder would cause shear stresses to be generated in the ceramic under column loading imposed on the hull by hydrostatic pressure. To determine accurately at what depth the shear failure of the ceramic cylinders would occur if joined by such a joint, two hemisphere capped ceramic cylinders were joined by the external wedge band joint and were tested hydrostatically to destruction. The shear failure, which occurred at 1480 psi, proved that this joint, although simple and fast in its lock operation, causes the cylinder to fail in shear. The only externally flush joint design that was found to meet the design depth requirement and at the same time did not introduce any additional stresses into the cylinder under hydrostatic loading was the breech-lock joint (Figure 10). When two ceramic cylinders of identical dimensions as those that were equipped with external wedge band joints were fitted with the breech-lock joint, they successfully withstood 16,000 psi of hydrostatic pressure without implosion. Thus a workable design was born for hydrodynamically streamlined joining of ceramic shells of cylindrical shape for deep submergence applications. Regardless of diameter, cylindrical sections could be joined now into hulls of any length to carry the desired payload to the ocean's greatest depths. Needless to say, a continuous screw thread could be substituted for the interrupted screw thread if extremely high bending moments were to be carried by the joint and the additional time and effort required to lock a continuous screw joint were of no particular consequence. If the requirement that the external joint surface be flush with the ceramic surface is waived for applications where extremely smooth hydrodynamic surfaces are not of importance, then another joint design can be added to the already described series of joints. This joint, a modified wedge band design (Figures 8d and 11), incorporates all that is best in a wedge band concept without having any of the drawbacks that can be associated with this joint concept. It does not require O-rings for sealing or any threads on the metallic joint surfaces. During locking of ceramic sections, only compressive stresses are generated in them, and bending moments applied to the

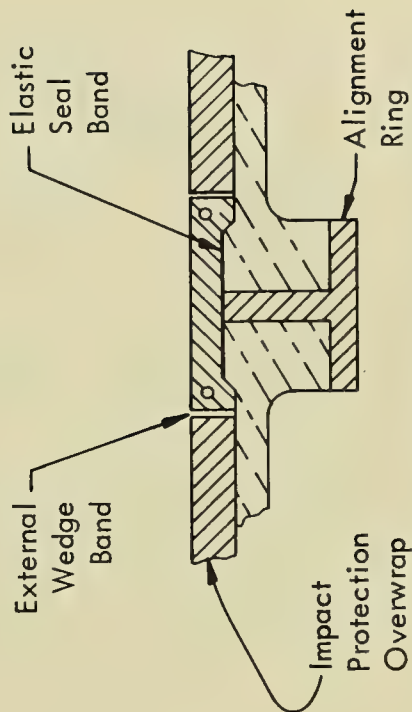




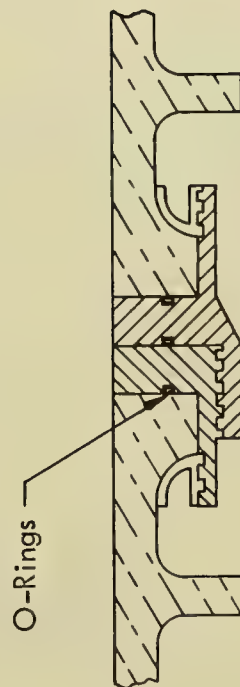
B. Externally Flush Wedge Band Joint



A. Externally Flush, Internally Expanding Segmented Wedge Joint



D. Externally Projecting Wedge Band Joint



C. Externally Flush Breech-Lock Joint

FIGURE 8 JOINTS FOR GLASS AND CERAMIC RIB-STIFFENED CYLINDERS

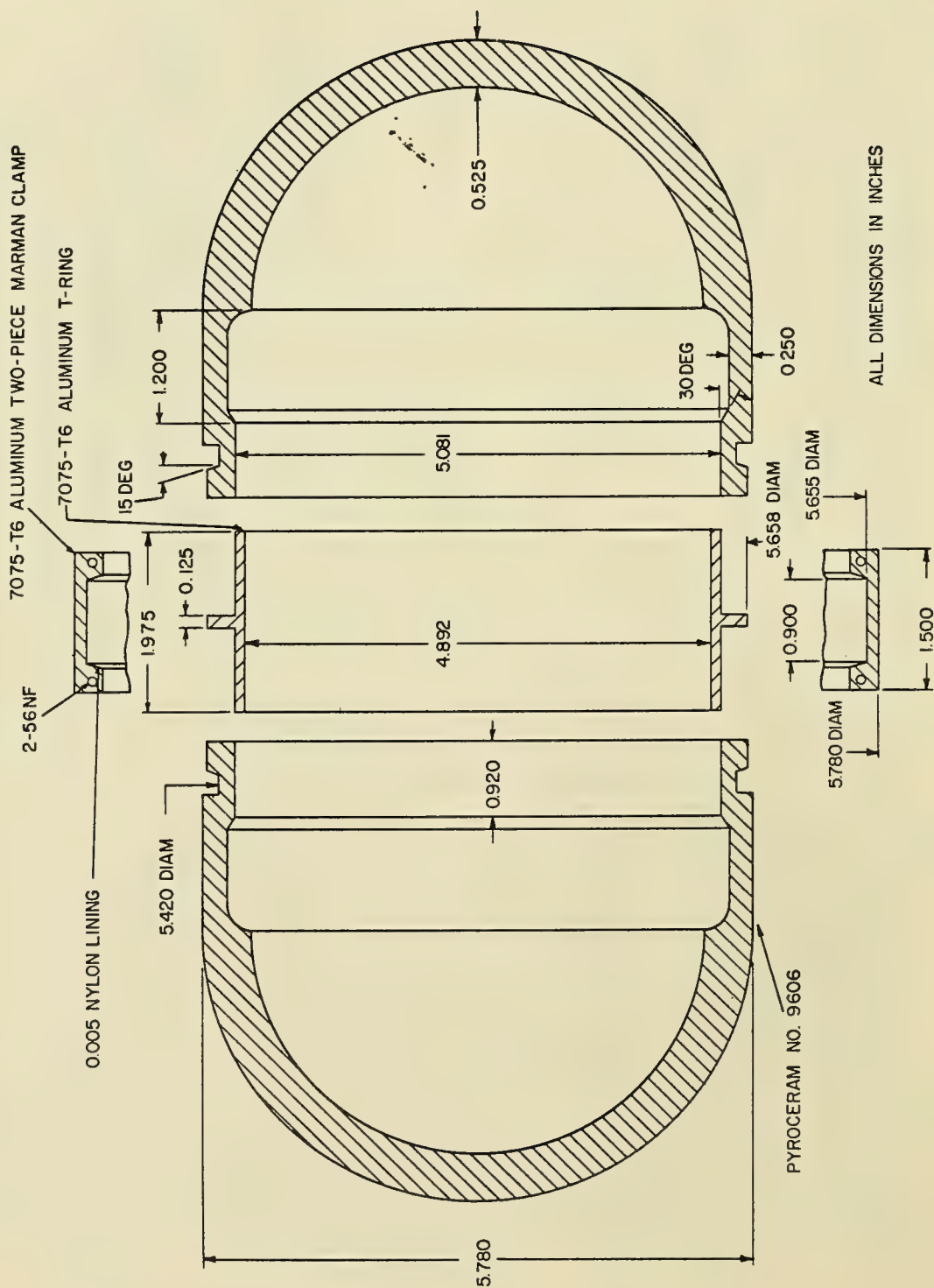


FIGURE 9 EXTERNALLY FLUSH WEDGE-BANK JOINT, IMPOLODED AT 14,800 psi

MATERIAL : SHELLS - PYROCERAM NO. 9606  
 JOINT RINGS - 7075-T6 ALUMINUM  
 (all dimensions in inches)

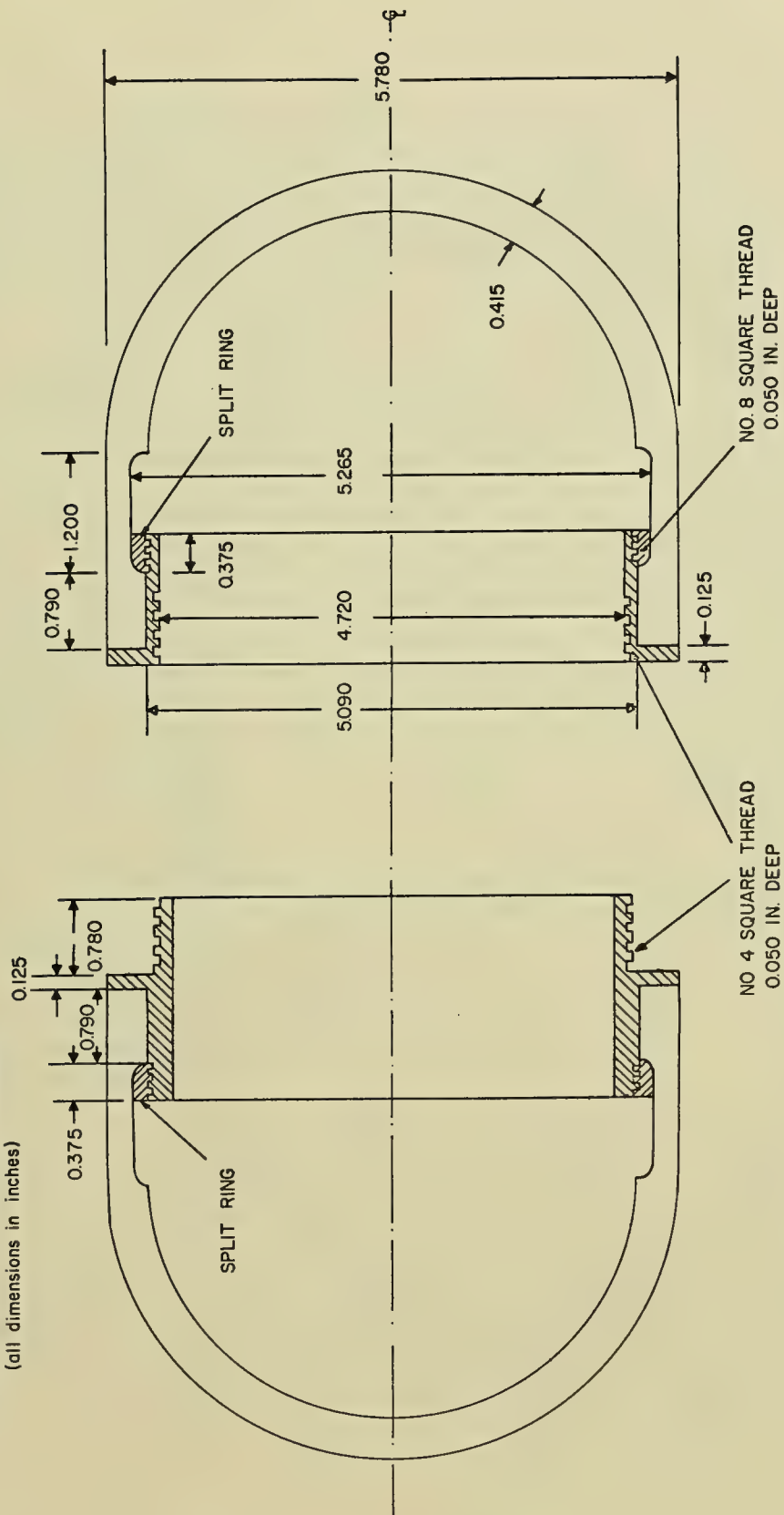
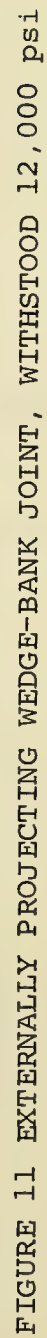


FIGURE 10 EXTERNALLY FLUSH BREECH-LOCK JOINT, WITHSTOOD 16,000 psi



joint during launching of the cylindrical buoy generate only modest shear stresses in the ceramic lock flanges as the flanges can be kept extremely short. Wrapping of the cylinders with protective overwraps can restore to the hull its streamlined shape, as then the protruding wedge bands are flush with the overwrap at shallow depths and protrude only moderately at abyssal depths where the overwrap is flattened somewhat by the hydrostatic pressure.

Although experimental data generated by the author<sup>8</sup> and others<sup>9</sup> show that highest bearing stresses are carried only by a ceramic to ceramic joint interface, its application is limited as it requires beveled perfectly polished hand-lapped surfaces for its successful operation. If ceramic hulls for ASW weapons or oceanographic instrumentation capsules are ever to be mass produced and assembled on an interchangeable basis, then hand-lapped and hand-fitted ceramic to ceramic joints cannot be considered a desirable type of joint although its bearing stress-carrying ability may be the best among joints. The mechanical shell section joints found workable for deep submergence cylindrical ceramic hulls incorporate the bearing surfaces into a structural ring member of the joint, so that the whole ring material can be considered as a gasket. Since the bearing stresses encountered at the ends of monocoque ceramic cylinders amount at the most to only one half of hoop stresses in the cylinder, the largest bearing stresses that can be expected will be less than 170,000 psi. In the rib-stiffened cylinders tested,<sup>8</sup> the bearing stresses are further reduced below 170,000 psi by the presence of end flanges, whose bearing area is generally at least two times as large as that of the shell wall between stiffeners. Thus, the maximum bearing stresses that generally have to be contended with at the end flanges of rib-stiffened cylinders are in the vicinity of 60,000 psi. Such a bearing stress is low enough where a variety of metallic joint materials can withstand it. There is, however, one further requirement that must be considered when selecting the material for the structural members of the ceramic shell section joint. The additional requirement is the compliance of the joint under hydrostatic loading.

If the metallic joint behaves as an integral part of the ceramic shell during hydrostatic loading, then it is a good joint and will not cause any additional stresses in the ceramic portions of the shell joint. On the other hand, a severe mismatch between the moduli of elasticity of the metallic and ceramic parts of the joint will invariably cause additional stresses to be generated in the joint which may cause its premature failure. For this reason, the choice of joint materials is very much limited to high-strength aluminum, titanium, and steel alloys. Ideally, the moduli of the metallic parts and the ceramic shell should be matched, but since this is rarely possible or feasible, the ideal match between the moduli remains but a goal. In reality, a decision always must be made whether



the metal or the ceramic is to have higher modulus of elasticity. Since the compressive strength of the metal in the joint is invariably less than that of the ceramic shell, it is imperative that the modulus of elasticity of the metal never surpass that of ceramic. In this manner, the stresses in the metallic joint held rigidly between the ceramic shells and undergoing the same strains as the flanges at the ends of the shell will be equal or less than those in the ceramic flanges. Since the hoop stresses in the ceramic shell flanges are generally more than 100,000 psi but less than 200,000 psi, the metallic joint with matching modulus of elasticity must be made of metallic alloy with at least 150,000 psi yield strength.

The ceramics used in the construction of the experimental shell series were Pyroceram #9606 and 99-percent alumina with  $17.5 \times 10^6$  and  $50 \times 10^6$  moduli of elasticity, respectively. In ideal terms, the use of titanium would be the logical choice for joints in Pyroceram #9606 shells and beryllium for joints in the 99-percent alumina shells. If the high cost, or low strength of the ideally matching modulus joint materials is a deterrent to their application, then high strength aluminum alloys like 7075-T6, 7178-T6, or 7001-T6 can be substituted for the ideal joint material in Pyroceram shells, while high strength steel alloys can be used in conjunction with 99-percent alumina. As a matter of fact, 7075-T6 aluminum alloy was the material from which the experimental joints were machined for the Pyroceram #9606 material. Although different metals should be used in the joints for different glasses and ceramics as explained above, titanium will, in all probability, emerge as the sole joint material for ceramic shells. It not only matches with its modulus of elasticity all of the Corning's glass Pyroceram ceramic series, but also is quite compatible with the alumina ceramics whose moduli are higher than that of titanium. When one adds to this the other mechanical and physical properties of titanium, like its high compressive and tensile strength and its excellent resistance to corrosion, then its selection for joint application becomes much more desirable. The only cylindrical shells that would perform better with high-strength aluminum joints are glasses whose moduli of elasticity generally match that of aluminum. Needless to say, other factors, like absolute minimum of weight, and need for economical fabrication of joints, may dictate the use of high-strength aluminum. But, regardless of what considerations are employed in the selection of materials for the mechanical joint, the field from which the alloy is chosen is limited because of the magnitude of compressive stresses and moduli of elasticity involved. Some tests have been performed with nylon and teflon gaskets of 1/16 to 1/8 inch thickness on bearing surfaces and so far have been generally found less desirable than bare metallic bearing surfaces because of their tendency to extrude. The cold flow of these plastics under even very moderate compressive stresses makes them definitely undesirable for applications when the hydrostatic pressure on the

shells is maintained for longer periods of time. When nylon or teflon gaskets are employed that are only .010 to .030 thick, then their tendency to extrude is less pronounced, but benefits accruing from their use are still questionable.

#### PRACTICAL DEEP SUBMERGENCE CERAMIC AND GLASS OCEANOGRAPHIC INSTRUMENTATION CAPSULES

Once the design and fabrication of cylindrical rib-stiffened shells and their mechanical joints were proven feasible by the experimental deep submergence ceramic shell series described beforehand, no further impediments remained in the path for the design and fabrication of glass and ceramic capsules that would be capable of carrying commercially available oceanographic instrumentation to abyssal depths. Decision, however, had to be made on the type of glass or ceramic to use and how to fabricate it.

Besides the choice of several different ceramic materials available at the time and experimented with previously, there are many other ceramics and glasses that could be utilized for the construction of glass or ceramic oceanographic capsules. The choice, to say the least, was not easy, particularly when only limited funding was available. Since the requirements at that time were for two distinct capsule operational requirements, it was decided to approach the design and fabrication of these capsules from two different viewpoints. The operational requirements for the two-capsule systems differed considerably. One capsule system, to be composed of several individual capsules diving simultaneously, was to collect data on the relationship between depth, water temperature and sound propagation parameters. Since low dive and rise velocities are more desirable for this system than fast ones, and no restrictions were placed on the overall weight and size of the individual capsules, no effort was made to optimize the structural or fabrication parameters of these capsules. The other capsule system, in which the capsules were to be used individually, was to perform measurements of hydrodynamic parameters as the capsule's ballast was varied to achieve different rise velocities. As the hydrodynamic performance of the capsule was its main operational requirement, low weight, larger displacement and optimum hydrodynamic shape were of utmost importance. Since these two approaches used in the design and fabrication of the glass or ceramic capsules are quite different, they bear further discussion.

In the design for external pressure shells, there are basically two approaches to the utilization of a given structural material. One approach, generally applied to vehicles where strength to weight ratio of the hull, regardless of cost, is the overriding requirement, relies on exhaustive quality control of the material, and painstaking adherence to very tight dimensional tolerances. Being assured of the quality of the material and

tolerances, in regard to roundness and uniformity of wall thickness, the designer can set the operational depth of the structure as close to its theoretical collapse pressure as he desires, in which case, the difference between the operational depth and the collapse depth is a true safety factor.

The second approach is a compromise between fabrication cost and the desirable strength to weight ratio of the structure. In such a case, quality control and dimensional tolerances are relaxed sufficiently to bring the cost of fabrication down, and yet the tolerances are not so relaxed as to make the structure lose the attractive strength to weight ratio imparted to it by the good mechanical properties of the material.

Both approaches to the design of external pressure vessels have their place in engineering practice, and in this particular example, both have been applied to the design and fabrication of the first practical glass and ceramic oceanographic instrumentation capsules, which has resulted in a cost ratio of approximately five to one. Since the cost difference is considerable, it bears examining as to what the additional cost has purchased for one capsule system in comparison to the other capsule system.

#### DIVEAR Capsule System

The hull of the DIVEAR capsule<sup>12</sup> [Diving Instrumentation Vehicle for Environmental and Acoustic Research] (Figure 12) has been designed for a low stress level so that considerable deviation from nominal dimensions could be tolerated without failure of the hull at its operational depth. The hull of DIVEAR is a Pyrex cylinder (Figure 13) which has an OD of 16 inches, is 58 inches long with integral ribs, and has a wall thickness of 13/16 inch. The glass hull was fabricated by fusing several tubular glass sections (Figure 14) that had been hand blown separately within an external cylindrical mold. Since each of the tubular glass sections was actually a flat-bottom jar whose bottom had been only partially removed, the remaining bottom rim served, after extensive flame working on a lathe, as a rib for stiffening the hull. After all of the glass sections were fused together, the ends of the hull were ground and the whole structure annealed. Since the primary concern during the fabrication of the glass hull was the evaluation of standard hand blowing and flame working techniques for their applicability to the construction of underwater vehicle structures, no special emphasis was placed on the elimination of air bubbles or external ridges in the glass welds. Thus the finished glass structure (Figures 15-16) has pronounced ridges and some trapped air bubbles in the areas of the fusion welds. No attention was paid, also, to the optical properties of the finished glass structure. Nevertheless,



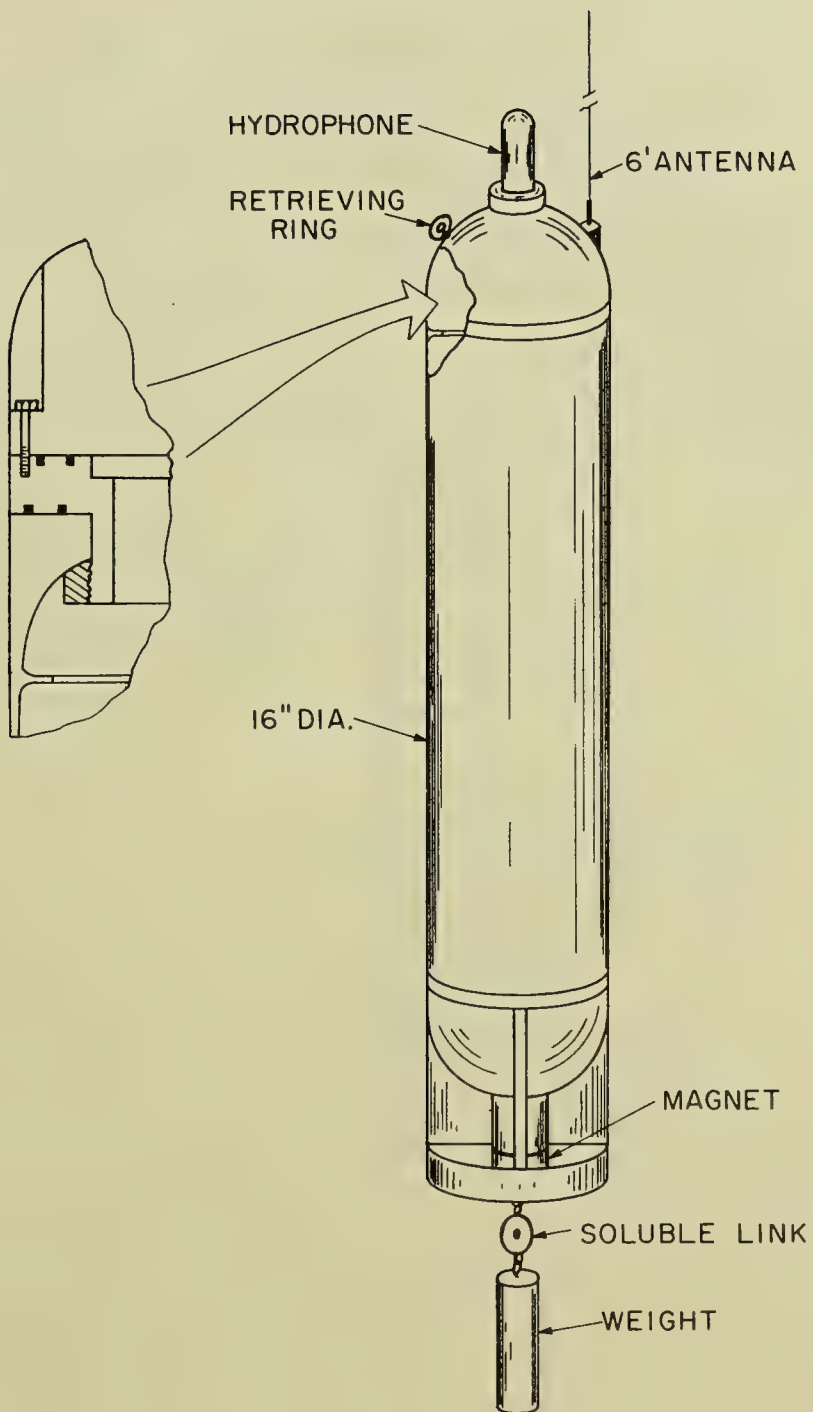


FIGURE 12 DIVEAR CAPSULE ASSEMBLY

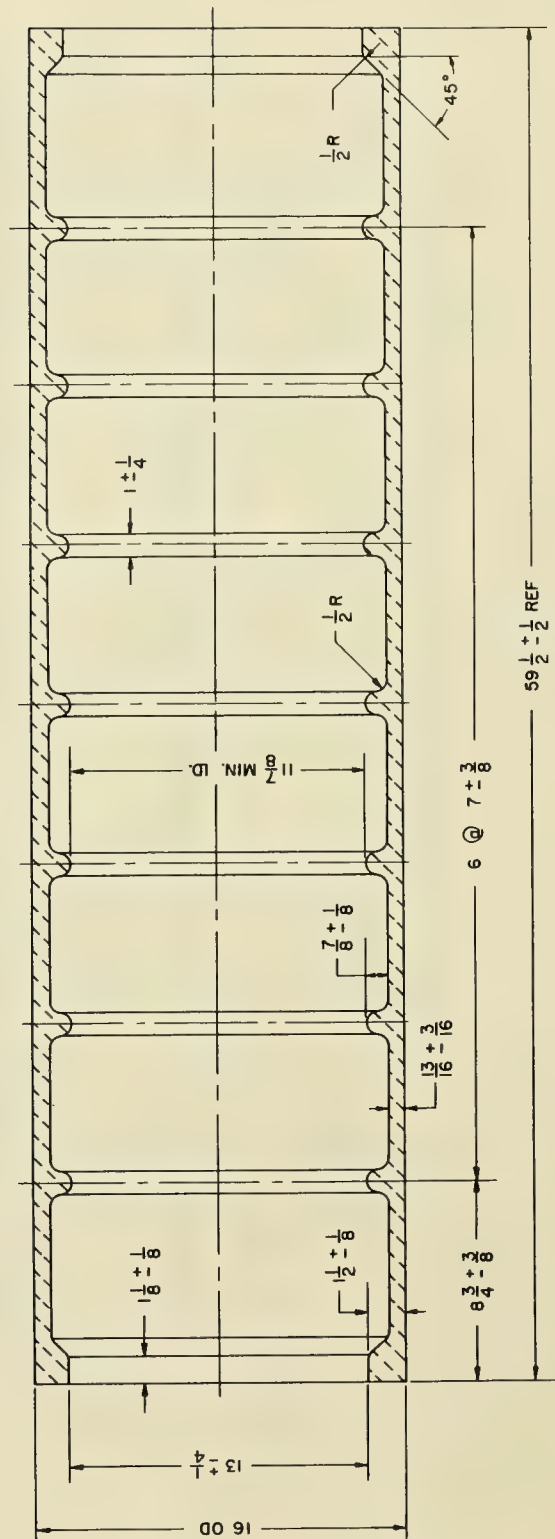


FIGURE 13 PYREX SHELL FOR DIVEAR CAPSULE, DESIGNED FOR 20,000-FOOT OPERATIONAL DEPTH





FIGURE 14 ASSEMBLY OF DIVEAR SHELL FROM TUBULAR SECTIONS BY FUSION BONDING



FIGURE 15 FUSION BONDED MONOLITHIC DIVER SHELL, INTERIOR VIEW



FIGURE 16 FUSION BONDED MONOLITHIC DIVER SHELL, SIDE VIEW



the finished product represents a fairly homogeneous glass mass of surprisingly good quality when one considers the 215-pound monolithic mass of glass involved in the structure.

The ends of the hull were capped with 7075-T6 aluminum hemispheres machined to accept internal and external attachments plus several feed-throughs (Figure 17). The bearing area between the end caps and the glass cylinder is a generous one and relies on the flatness of the aluminum and glass flanges for elimination of point loadings. Sealing is accomplished with an O-ring located in an O-ring groove in the aluminum flange under axial compression.

In general, the DIVEAR structure has the minimum of structural refinements necessary to withstand the operational depth of 20,000 feet. Furthermore, to keep the cost down to an absolute minimum, extremely generous dimensional tolerances are permitted which vary from  $\pm 1/8$  to  $\pm 3/8$ , depending on the dimension described. Thus, to insure the integrity of the glass cylinder at the operational depth, even with stress concentrations produced by the eccentricity and variation in thickness of the cylinder and stiffeners, maximum design stress for the nominal dimensions of the cylinder is only 87,000 psi, definitely a low stress level for glass but still considerably higher than the stress experienced by current models<sup>11</sup> of spherical submarine hulls tested to 20,000 feet. Still, this design stress surpasses the operational stress level that could be safely specified for any commercial high-strength aluminum, glass fiber epoxy laminate, or HY80 steel. Only the more expensive high-strength titanium alloys or steels could carry such design stress safely, and then only if the dimensional tolerances were appreciably tighter than those specified for DIVEAR. The cost of the DIVEAR structure then, if fabricated from any other material that would give it the same weight (aluminum end closures included) to displacement ratio of .65 at 20,000 feet, would be higher than incurred in fabrication of Pyrex DIVEAR. The cost of this 280-pound aluminum-capped Pyrex hull is approximately \$35 per pound of payload-carrying buoyancy. Thus, although in this particular design the design stresses have been set low to capitalize on the cost savings afforded by the loose dimensional tolerances of the glass hand-blowing process, the structure is still competitive in cost with similar structures fabricated from the commercially available maraging steel and titanium alloys which give the structure the same weight to displacement ratio and 20,000-foot depth capability. If Pyrex DIVEAR hull performs in hydrostatic proof tests as predicted, then this approach to fabrication of inexpensive glass instrumentation capsules is justified. It is worthwhile to note here, however, that by discounting the mechanical strength of glass to meet the loose tolerances of the more economical fabrication method, the DIVEAR glass hull has been placed in a weight to displacement ratio category where the major justification for the use of glass as the structural



FIGURE 17 STRUCTURAL COMPONENTS OF THE DIVEAR CAPSULE ASSEMBLY



material over that of some other material is based on cost per pound of buoyance. For oceanographic instrumentation systems that do not need the payload-carrying performance afforded only by the lowest obtainable weight to displacement ratios, the above-mentioned approach to fabrication of glass hulls is reasonable, and if proven successful in testing of actual hardware, acceptable.

### Benthos System

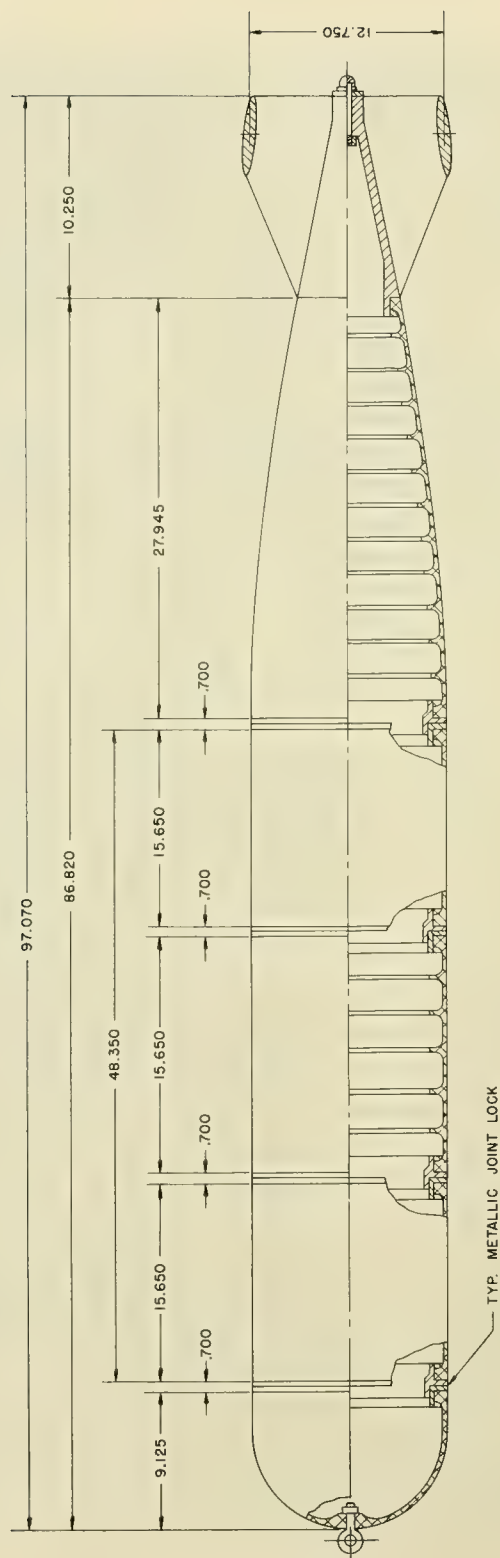
The approach to the design and fabrication of ceramic hulls for Benthos<sup>4</sup> (Figure 18) has been just the opposite used in the design and fabrication of DIVEAR glass hull. The different approach used to design and fabricate Benthos followed from a completely different set of systems' operational requirements. The requirements were, in this case, for a hydrodynamically streamlined vehicle with smallest weight to displacement ratio, capable of carrying out oceanographic or ASW missions to depths of 35,000 feet. To accomplish these requirements the hull proportions and finishes had to present minimum hydrodynamic drag, while the design stresses had to be of maximum allowable magnitude in order to give the vehicle the utmost in payload-carrying capability for its displacement.

To meet the low hydrodynamic drag requirements, a cylindrical shape was chosen which was capped at the front with a hemispherical nose and at the rear with a gradually tapered afterbody (Figure 19) terminating in shrouded cruciform fins. Both the ceramic and metallic sections of the hull were fabricated to 32 RMS finish requirements to insure low hydrodynamic drag. To make the interior of the vehicle accessible and the fabrication costs more economical, the hull was conceived as an assembly of five ceramic and one metallic shell sections joined together by metallic breech-lock joints. As much of the hull was made of ceramic as possible to capitalize on the material's high-strength (Figures 20-22), and only the shrouded fins mounted on a short conical plug were made from metal (Figure 23).

The structure itself had to be designed to operate under very high working stresses. Only by stressing the materials to the maximum possible stress level could the hull provide Benthos with the utmost in payload-carrying capability. The fact that Benthos was to provide the utmost in buoyancy for a given displacement at 35,000 feet dictated that only materials with maximum compressive strength-weight ratios and reliable fabrication methods with predictable dimensional control could be employed in the construction of this vehicle. Although all glasses and ceramics are described as being capable of withstanding extremely high compressive stresses, only those could be considered for the construction of Benthos whose compressive strength had been experimentally proven by hydrostatic



FIGURE 18 MODEL OF BENTHOS





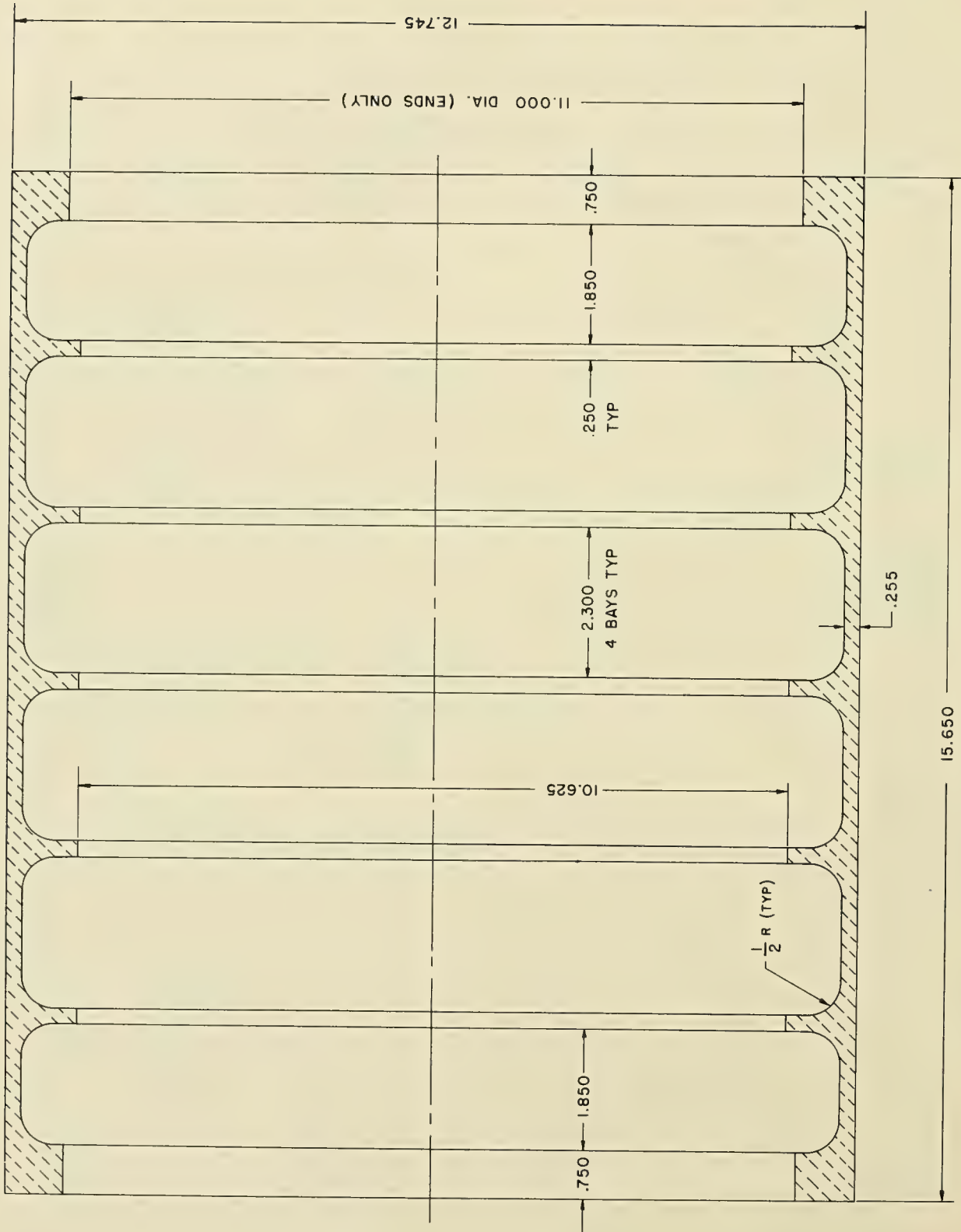


FIGURE 21 PYROCERAM #9606 CYLINDRICAL SECTION OF BENTHOS







testing of spherical or cylindrical shells of these materials. When the scanty experimental data was reviewed, only Pyroceram #9606 and 99-percent alumina shells were found capable of withstanding, consistently, compressive stresses above 200,000 psi level. Since both materials are about equally strong in compression, the choice had to be made on some other basis. Ninety-nine-percent alumina ceramic has qualities which make it quite an attractive choice. It possesses modulus of elasticity of  $50 \times 10^6$  psi; the raw material is inexpensive and can be easily produced in many different shapes with very little investment in molds. The high modulus of elasticity makes it an extremely desirable choice as it permits the design and construction of rib-stiffened shells with shallow ribs and wide rib spacing. Still, it suffers one very important disadvantage for use in deep-diving vehicles when compared to Pyroceram #9606. Its specific gravity is 3.85, while that of Pyroceram #9606 is 2.61. Since this amounts to more than 20 percent in weight penalty, it hardly could be ignored in the selection considerations for a vehicle that is to represent a cylindrical structure with the lowest weight to displacement ratio that today's underwater hull technology is capable of producing.

Although the shell section joints can be made in different designs and materials, only the already proven breech-lock joints and aluminum and titanium alloys were considered. The only departure from the already proven joint design was the incorporation of O-ring seals and a decrease in the size of the ceramic flanges (Figures 24-27). Both modifications are thought to be improvements over the original design (Figure 10) as the axially compressed static O-ring seals afford good sealing at both launch and retrieval, while smaller ceramic flanges on the shell ends permit the metallic joint to be further recessed into the shell wall, and thus make the shell capable of receiving payloads with larger outside diameter.

The first choice for the joint material was high-strength aluminum which had proven itself before during the experimentation with different joint designs. Furthermore, aluminum joints would contribute less weight to the structure than titanium joints. The aluminum alloy selected for the joints was 7001-T6, which, after being forged into rings, was machined to the desired dimensions. The compressive strength of this alloy in excess of 90,000 psi is thought to be sufficient for most of the stresses imposed upon the joint by the ceramic shell sections under hydrostatic or launch loadings. The only apparent drawback of aluminum joints is their corrodibility under repeated exposure to sea water environment. For this reason, a second set of joints has been prepared for Benthos fabricated from Ti-6Al-6V-2Sn titanium alloy. For repeated dives or long-term ocean bottom submergence where the additional weight of titanium joints is compensated for by their resistance to corrosion, they will find their employment.



FIGURE 24 TYPICAL BREECH-LOCK JOINT FOR BENTHOS

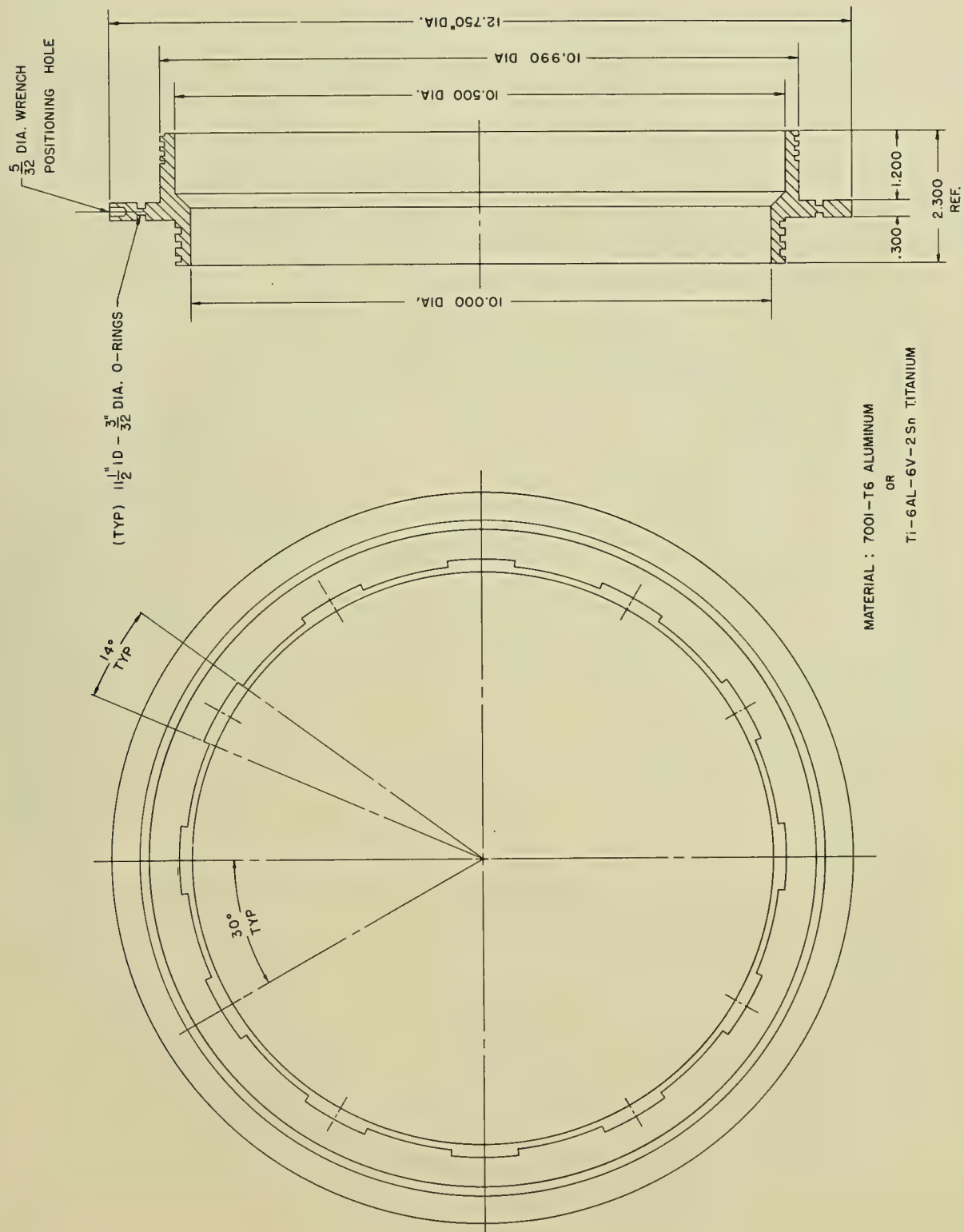


FIGURE 25 TYPICAL MALE JOINT RING FOR BENTHOS



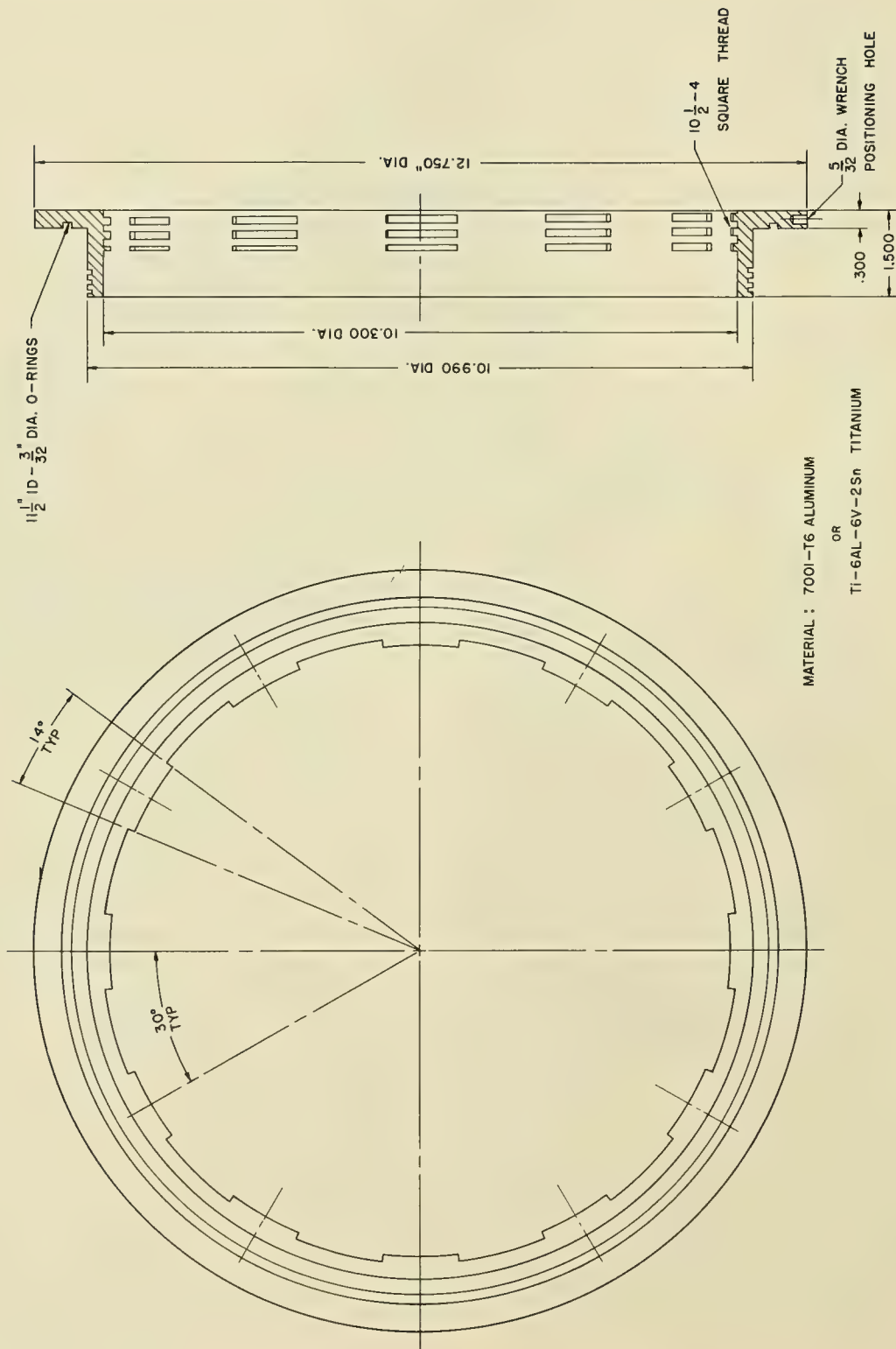


FIGURE 26 TYPICAL FEMALE JOINT RING FOR BENTHOS

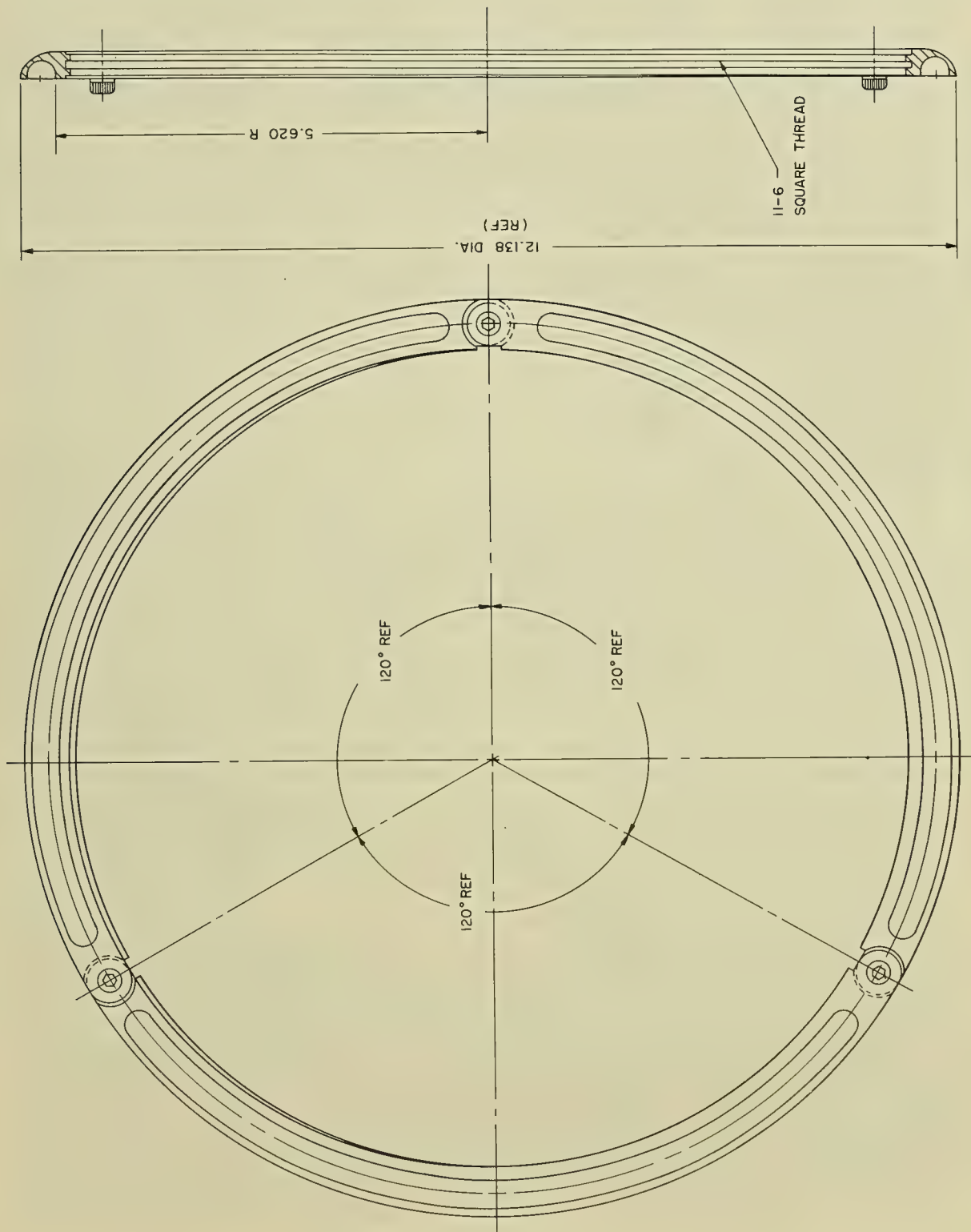


FIGURE 27 TYPICAL COLLAPSIBLE RETAINER UNIT FOR BENTHOS BREECH-LOCK JOINTS

One of the requirements which the joint must satisfy is an ability to withstand large bending moments to which Benthos will be subjected when launched on ASW missions from deck-mounted air-operated tube launchers. For this reason, a prototype model of the joint was built and tested to destruction under bending moments. Since alloys used in the production version of the joint were not available at that time, the prototype joint was built from 7075-T6 aluminum alloy. For the flexure tests, the joint was mounted to steel cylinders with end flanges identical to those in the ceramic Benthos shells. Under a two-point flexure test (Figure 28), the joint failed at 170,000 pound inches of bending moment by shearing of threads in the breech-lock at the point of highest tensile stress. When the test data obtained from testing the 7075-T6 aluminum joint is extrapolated to 7001-T6 aluminum and Ti-6Al-6V-2Sn titanium alloy joints, their fracture strengths are predicted to be 220,000 and 340,000 pound inches, respectively. Since these bending moments are in all probability larger than moments required to fracture the ceramic shell sections, the strength of the metallic joints to withstand bending moments is considered more than adequate.

During the fabrication of the shell sections, the highest possible quality control was exercised. Unlike any other ceramic material, Pyroceram ceramics are transparent in the initial stages of fabrication, and visual inspection methods are used to examine them for internal defects (Figure 30). Optical glass-melting techniques are used to assure uniform composition, constant density, freedom from bubbles and striations, and uniform electrical properties. Subsequent controlled heat-treating cycles activate special nucleating agents in the body to produce a fine-grained, uniform crystal growth. No problems have been encountered in the ceraming of the thick-walled cylindrical, hemispherical, and conical blanks from which subsequently excess material is removed by grinding. Using a tracer lathe and proper guide templates, the excess material is removed until a rib-stiffened structure with integral ribs results (Figure 29). The grinding operation lends itself to very close dimensional tolerance control; the final product of the fabrication is within  $\pm .010$  inch of specified nominal dimensions.

Summarizing, it can be stated that Benthos is an antithesis to DIVEAR. Whereas the latter downrates design stresses in glass for the sake of economy in fabrication, the former demands and obtains reliable design stresses in the ceramic hull unattainable by the employment of any other commercially available material, except possibly 99-percent alumina ceramic. In Benthos, ceramics do not have to justify their application on a basis of cost in competition with other materials, but on the basis of being the peer without rivals among high-strength structural materials. No other material can provide Benthos with its unmatched deep submergence design

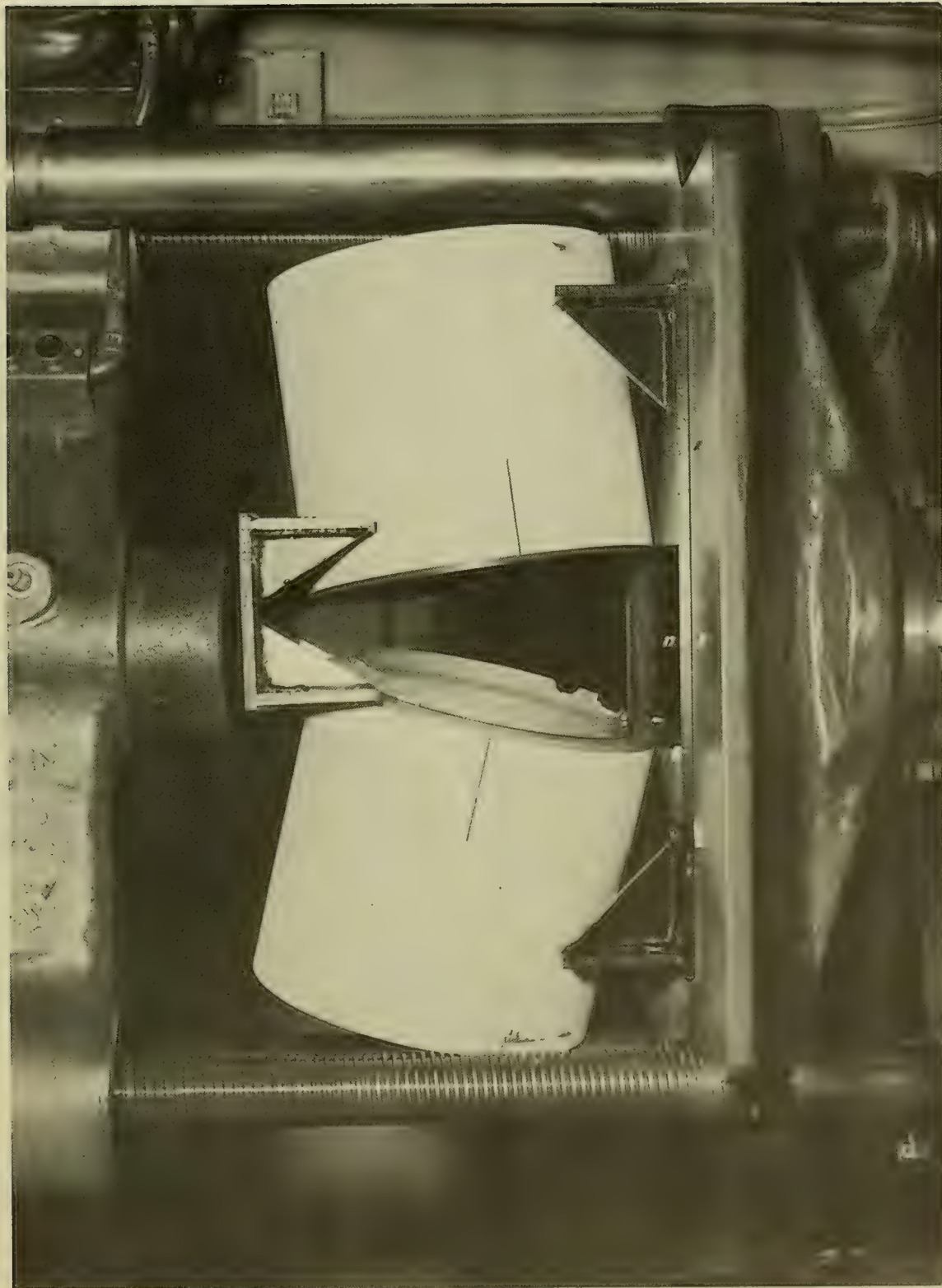


FIGURE 28 BENTHOS BREECH-LOCK JOINT OF 7075-T6 ALUMINUM AFTER DESTRUCTIVE TESTING AT 170,000 POUND INCHES OF BENDING MOMENT



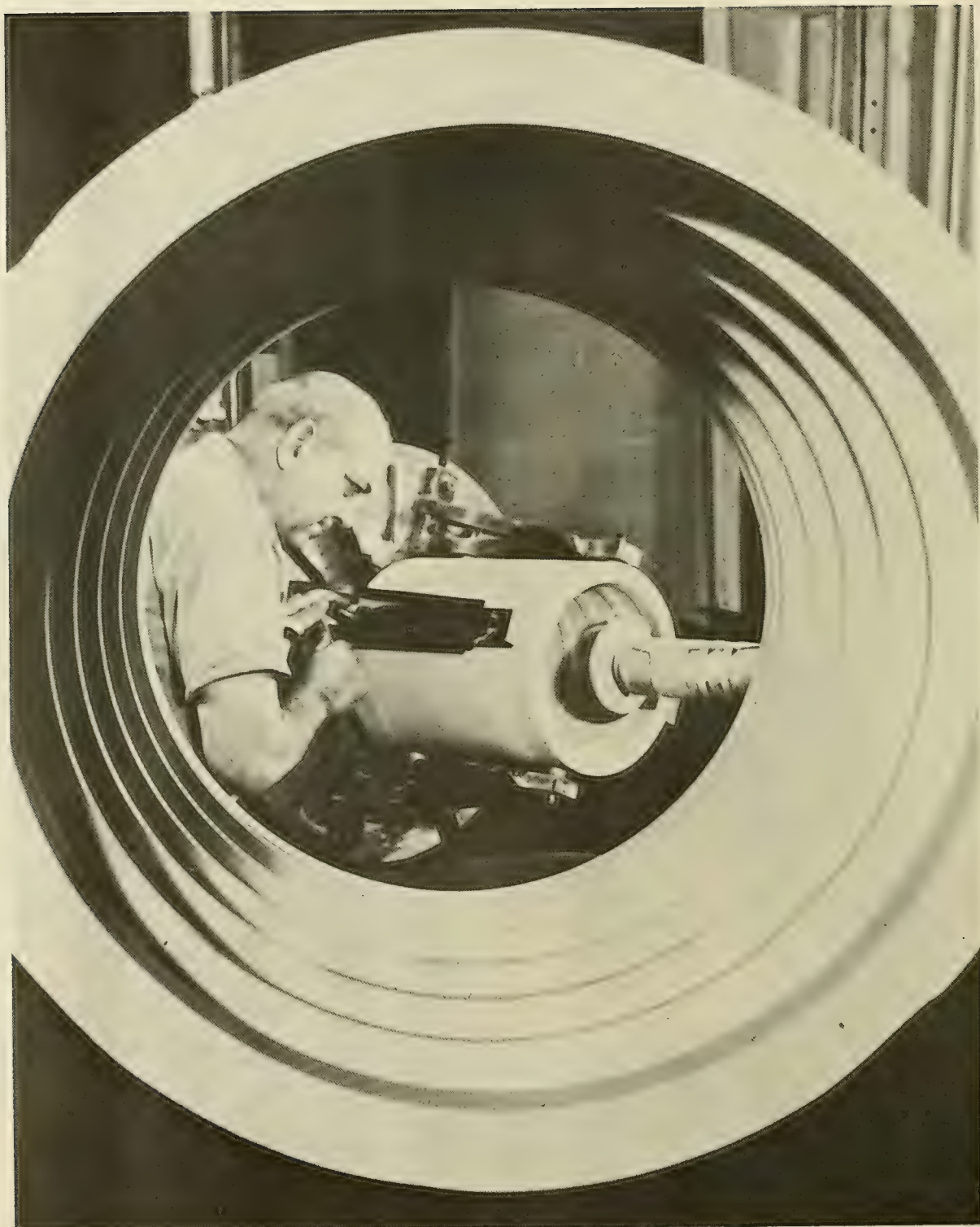


FIGURE 29 GRINDING OF BENTHOS CYLINDRICAL SECTION





FIGURE 30 STRIKING COMPARISON BETWEEN BENTHOS AFTERBODY AND NOSE SECTIONS PRIOR TO CERAMING AND GRINDING. CYLINDRICAL SECTION HAS BEEN ALREADY CERAMED AND GROUND

capability of 35,000 feet at .51 weight to displacement ratio. The smooth hydrodynamic shape of the hull will make the ascent of the 370-pound vehicle carrying a 150-pound payload with an integral buoyancy of 30 pounds after release of ballast at the bottom of the ocean a fast operation. For oceanographic missions, Benthos will be launched and retrieved, like DIVEAR, by sliding on an inclined ramp at the stern of the boat. For ASW missions, it will be launched from shipboard or submarine torpedo tubes. Although free-diving capsule Benthos relies solely upon its buoyancy for return to the ocean's surface, the addition of an electric or closed cycle thermal power plant will convert the free-diving capsule into an oceanographic or ASW vehicle with unsurpassable operational depth capabilities. If Benthos, when proof tested this summer, withstands the hydrostatic pressure at its design depth, the repeated pressure cycling, and the tube launchings, then the approach used in the design and fabrication of its deep submergence hull can be considered a success, and the five to one increase in cost over DIVEAR justifiable, when one considers the exceptional performance parameters achieved.

#### GUIDEPOSTS FOR FUTURE DEVELOPMENTS

The glass and ceramic construction materials, although already proven applicable to small and intermediate size and oceanographic free-diving capsules, must also be found useful for the construction of large oceanographic buoys and vehicles in order to maintain their position as desirable materials for deep submergence hulls. At the present time, the capability of the glass and ceramic industry to produce large glass or ceramic monolithic external pressure shells of spherical or cylindrical shape is severely limited. Monolithic spheres, of approximately 4 feet diameter, and monolithic cylinders of monocoque or rib-stiffened design of 2 feet diameter and 5 feet length are considered today the practical limits of monolithic glass or ceramic hull construction. Large investment in glass or ceramic furnaces, holding tanks, molds and grinding equipment would probably raise the capability of the industry to produce monolithic spheres or cylinders of twice the size that they are capable of today. Assuming that the money (\$5 to \$10 million) can be invested immediately, the ability to produce monolithic shapes of twice the size possible today will in turn become a new size limitation on glass or ceramic hulls that will be exceedingly difficult and expensive (\$10 to \$50 million) to overcome. It is obvious then that steps have to be taken today to develop construction techniques which will permit the design and fabrication of spheres and cylinders larger than the future size limit imposed by the fabrication capability limitation on monolithic construction.

Such steps should and are actually taken in conjunction with the program of raising the present fabrication maximum size limits. That very elementary steps have already been taken is evidenced by the successful assembly of glass and ceramic spheres from hemispheres and of long cylindrical hulls from short cylindrical shell sections. While the 5-foot-long hull of glass DIVEAR symbolizes the present approach to monolithic construction technique, the 9-foot-long Benthos exemplifies the only proven polyolithic construction technique available today for cylindrical hulls. The assembly of spheres from hemispheres, and cylinders from cylindrical sections or rings is only the beginning of the polyolithic construction design philosophy; more advanced concepts for this design philosophy and construction technique are already in the offing which promise to permit the design and fabrication of ceramic and glass hulls from smaller and smaller modular units.

In the design and construction of cylindrical hulls, additional methods, besides those of making the hull from cylindrical sections or rings, are being sought for breaking down the basic structural module to a smaller size (Figure 31). The additional methods, circumscribed by the geometry of the cylinder, limit themselves to breaking down further the basic component of the cylinder, the cylindrical shell section. The ultimate solution to this problem is the decomposition of the cylindrical section into small modules, the curved bricks. The intermediate solution, on the other hand, is the assembly of cylindrical sections from  $180^\circ$  or less trough-like cylindrical segments. Both the fundamental and the intermediate polyolithic construction techniques for cylinders have been already tried and found successful.

The assembly of monocoque and rib-stiffened cylinders from two or more segments, or of spheres from several spherical polygons,<sup>13</sup> has been experimented with so far only with acrylic resin models and found successful (Figures 32-33). Not only has it been proven that the elastic stability and the compressive strength of the polyolithic structures is the same as of monolithic structures, but that the fabrication costs are much less than if the structures were made simply of hemispheres or long cylindrical sections. If such structures were to be produced in glass or ceramic in larger quantities, the savings would be quite substantial, as pressing of individual structural modules would be substituted for the present laborious grinding of glass or ceramic castings. Only edges of the modules would require grinding for better fit in the joints.

Attempts<sup>14</sup> also have been made to by-pass the intermediate size module stage for cylinders and to go directly to the ultimate modular size. The structures experimented with were monocoque cylinders (Figures 34-35) made up of 99-percent alumina ceramic segments whose length was approximately



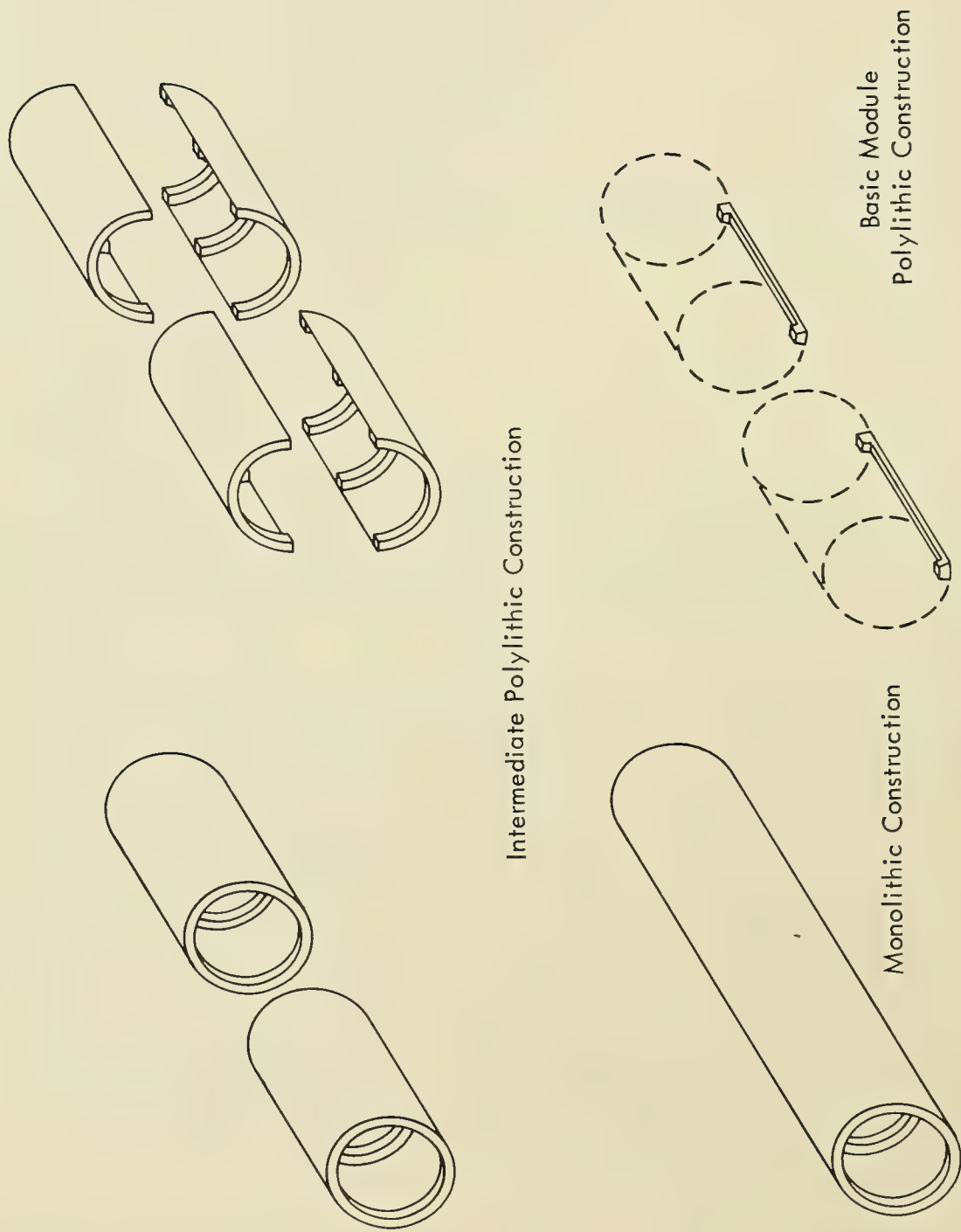


FIGURE 31 EXAMPLES OF MONOLITHIC AND POLYLITHIC TYPES OF CONSTRUCTION

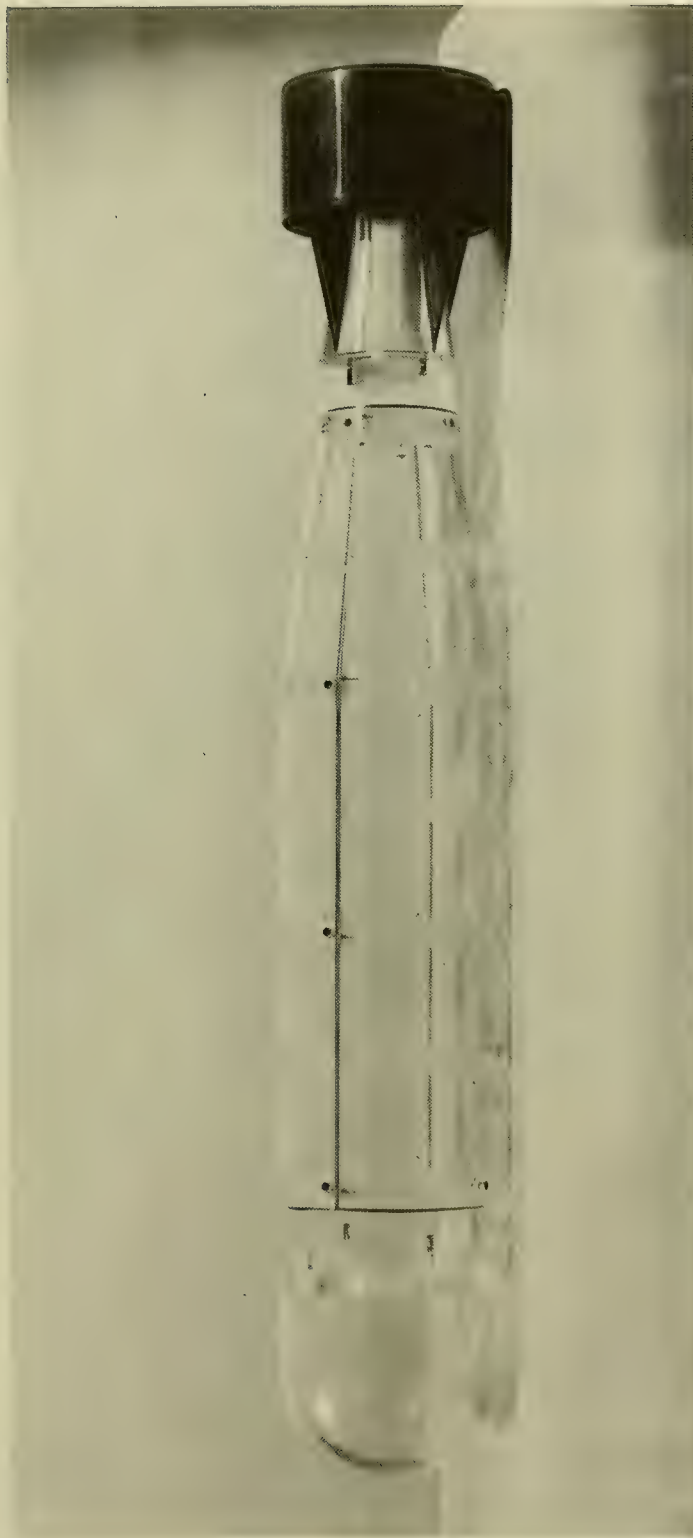


FIGURE 32 ACRYLIC RESIN MODEL OF A CYLINDRICAL INSTRUMENTATION  
CAPSULE WITH LONGITUDINAL JOINTS





FIGURE 33 ACRYLIC RESIN MODEL OF NEMO (NAVAL EDREOBENTHIC MANNED OBSERVATORY OF  
PACIFIC MISSILE RANGE) HULL ASSEMBLED FROM SPHERICAL POLYGONS

From: "Design Concepts Study For Deep Submersibles," Aerojet General Report TR-328: 64-207, July 1964

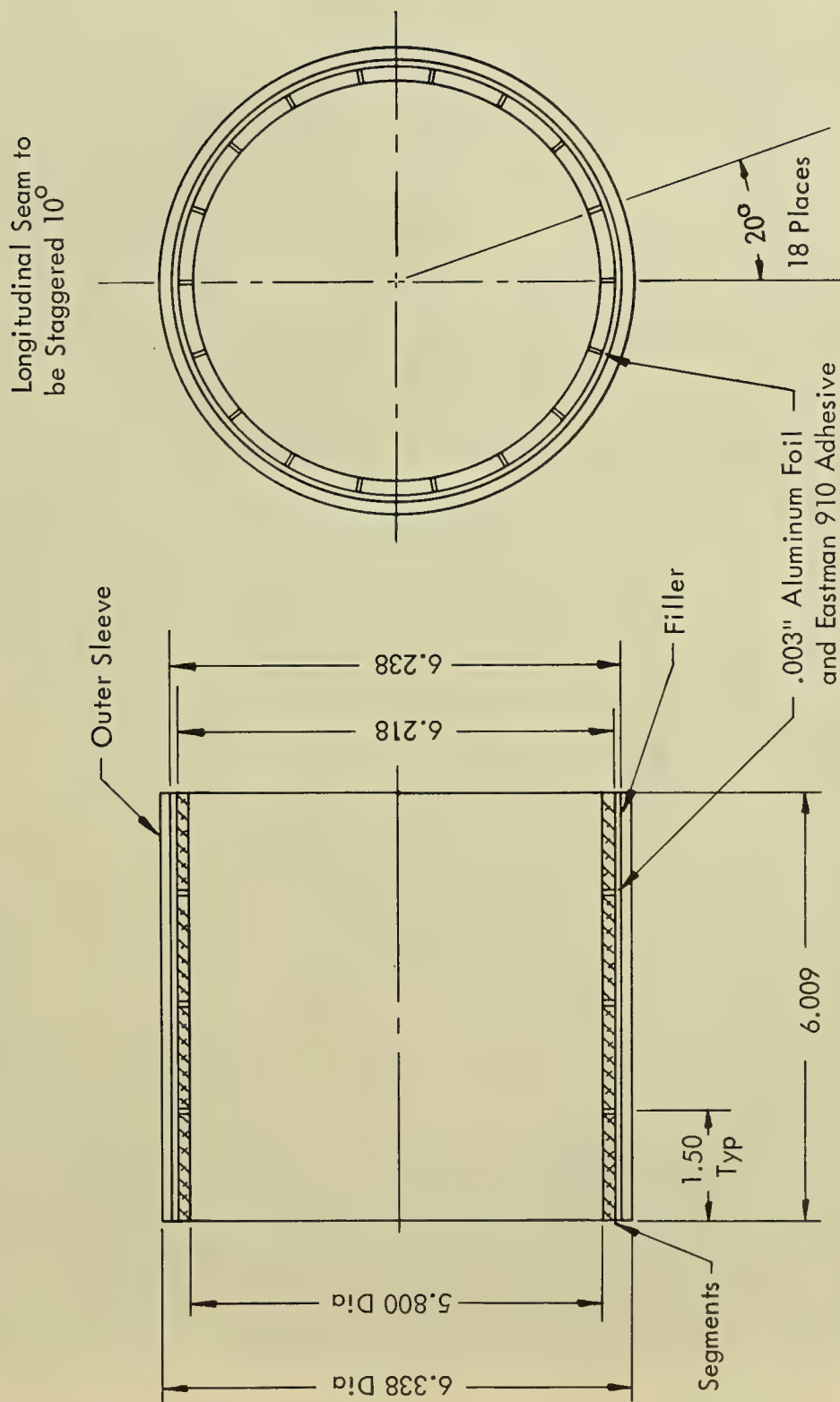


FIGURE 34 NINETY-NINE AND FIVE TENTHS PERCENT ALUMINUM CERAMIC POLYLITHIC SHELL, COLLAPSED AT 11,700 psi

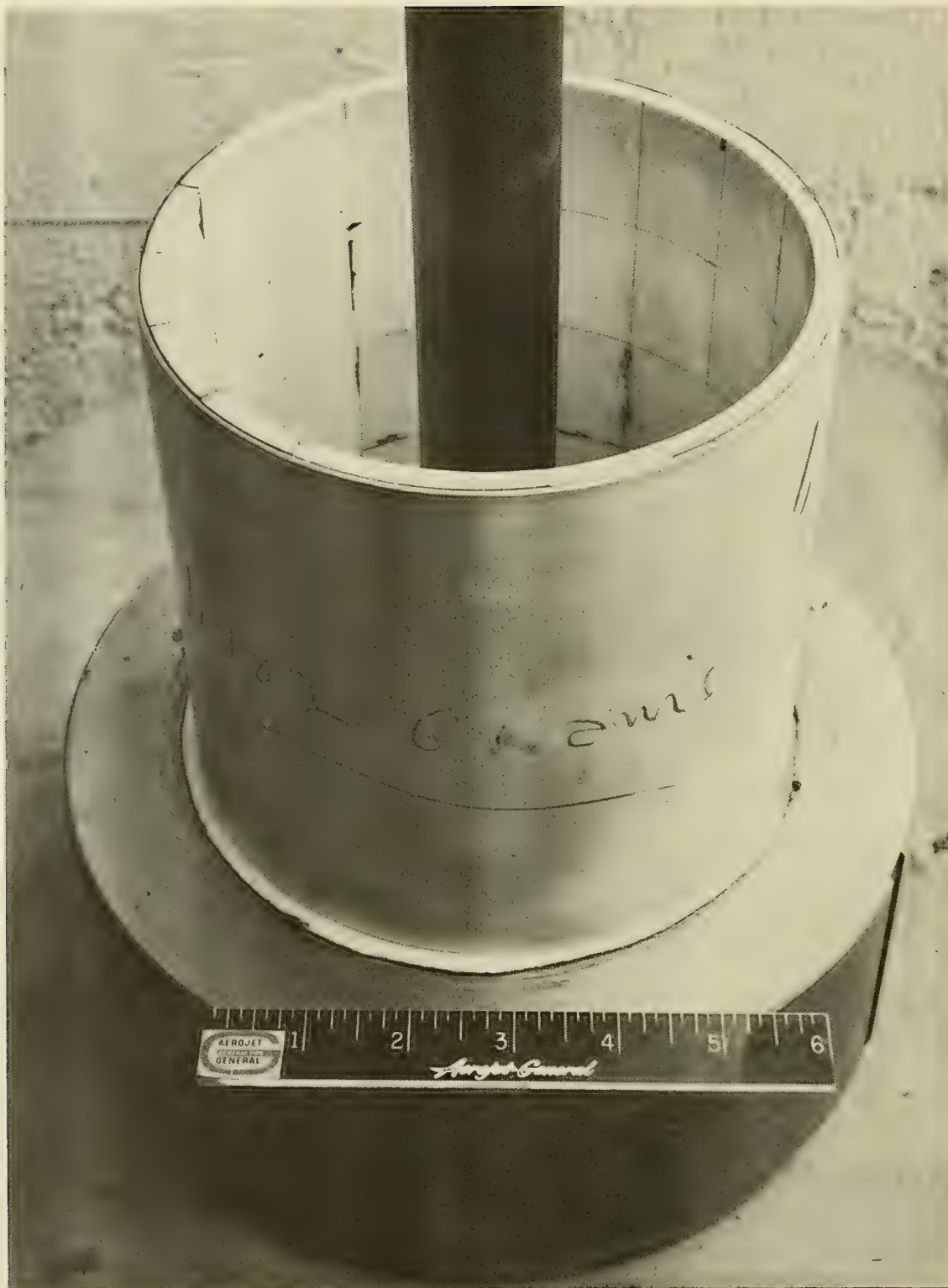


FIGURE 35 ASSEMBLY OF A TYPICAL POLYLITHIC SHELL

equal to their width. Since sufficient polyolithic cylinders were not tested to establish optimum gasket materials and their thickness, compressive stresses of only 200,000 psi were carried by these polyolithic cylinders before failure. The need for an external envelope to make such ceramic structure waterproof makes it heavier than if it was a monolithic cylinder. Depending on the material and thickness of such an envelope, the weight penalty to be sustained by the glass or ceramic cylindrical would vary anywhere from 10 to 20 percent of the monolithic hull's weight. Some penalty must also be paid for the presence of the many joint surfaces which necessitate the lowering of the compressive design stress in the structure so that surface imperfections in the joints will not cause the structure to fail.

Since it appears that the proliferation of joints in a glass or ceramic structure for the reduction of size of the modular structure components carries with it a penalty in reduced design stresses, the polyolithic hull construction should be resorted to only when absolutely necessary. It is for this reason that the glass and ceramic industry's present size fabrication capability should be doubled before major emphasis is placed on basic modular polyolithic construction techniques for deep submergence hulls. The intermediate polyolithic construction techniques — cylindrical hulls assembled either from several monolithic or several segmented cylindrical shell sections and spheres assembled from two hemispheres or several spherical polygons — promise to be a happy medium between the high reliability and high cost of one-piece monolithic hull construction, and the low cost and low reliability of basic module polyolithic construction. When to the already developing intermediate polyolithic construction capability will be added soon the increased size fabrication capability of the United States glass and ceramic industry, there will be available by 1970 a design and fabrication technology that will permit the construction of deep submergence oceanographic capsules of 5 to 10 tons displacement.

#### POST SCRIPT

Glass and ceramics are at the present time exotic and expensive materials<sup>15</sup> resorted to by oceanographers only in cases where extremely great depths (Figures 36-38) are to be penetrated by their buoyant research probes. As the usage of these materials increases in the oceanographic capsule field, they will lose some of their exotic lustre and instead gain the sheen of reliable noncorrodible and inexpensive every-day hull construction materials.



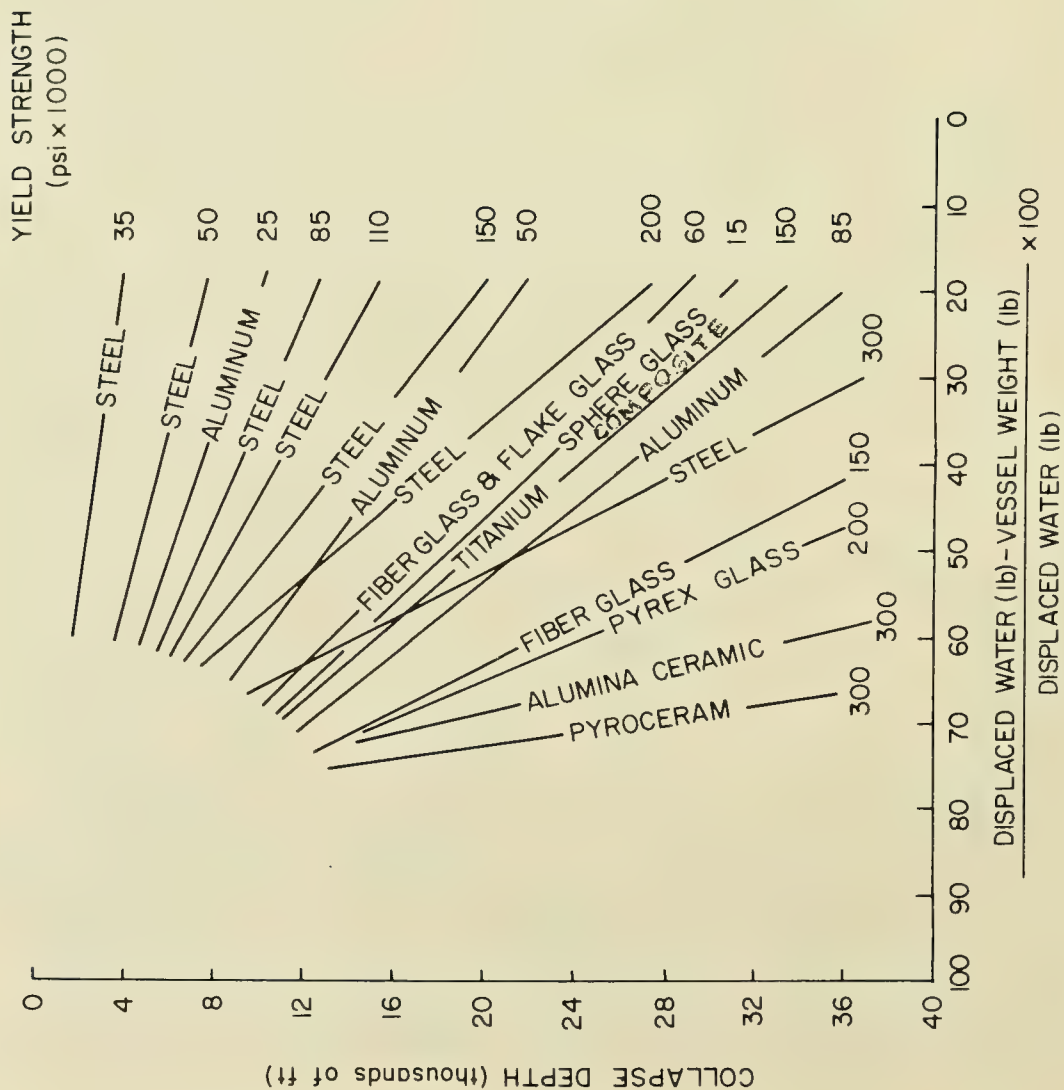


FIGURE 36 STRENGTH OF RIB-STIFFENED CYLINDERS MADE OF VARIOUS MATERIALS



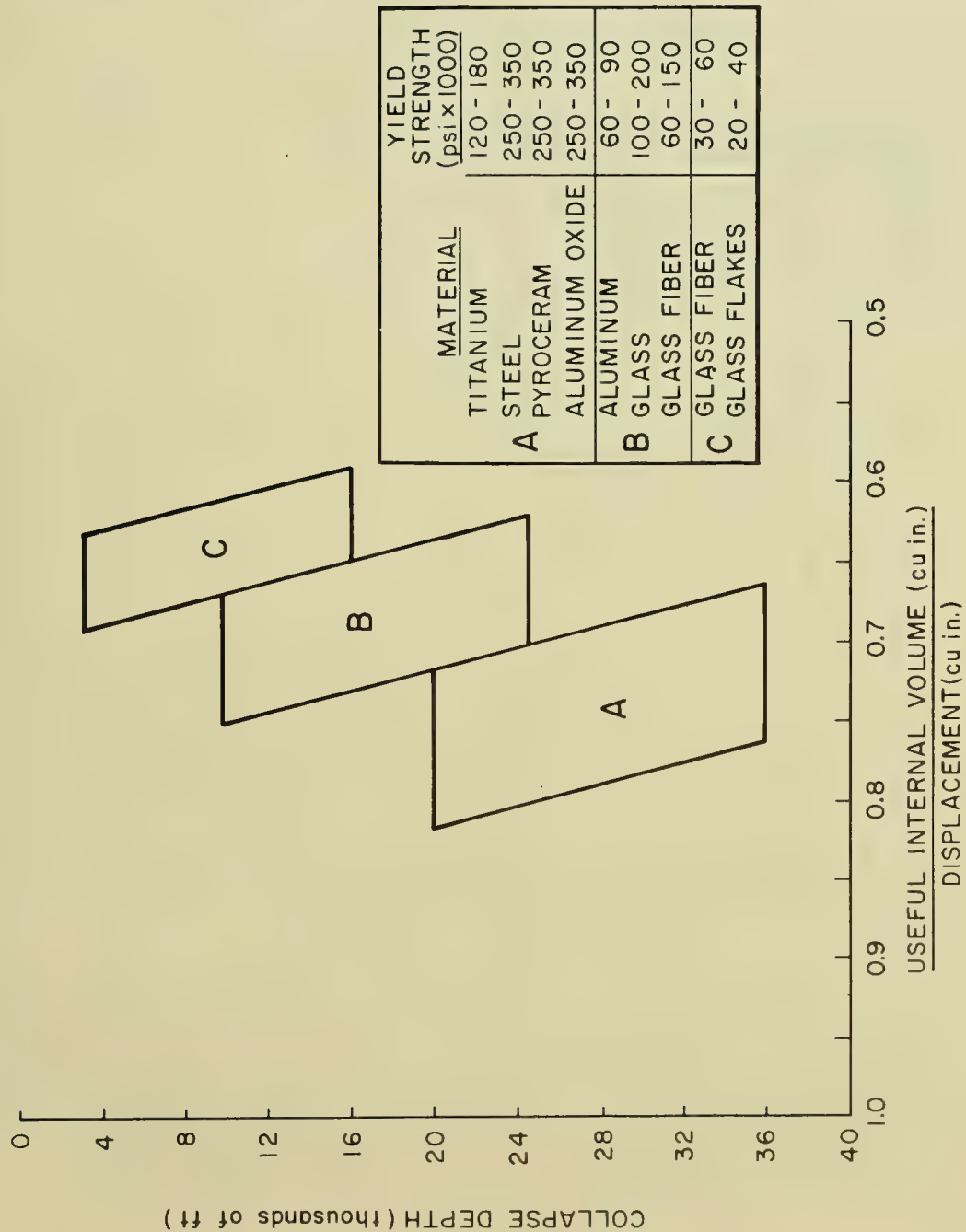
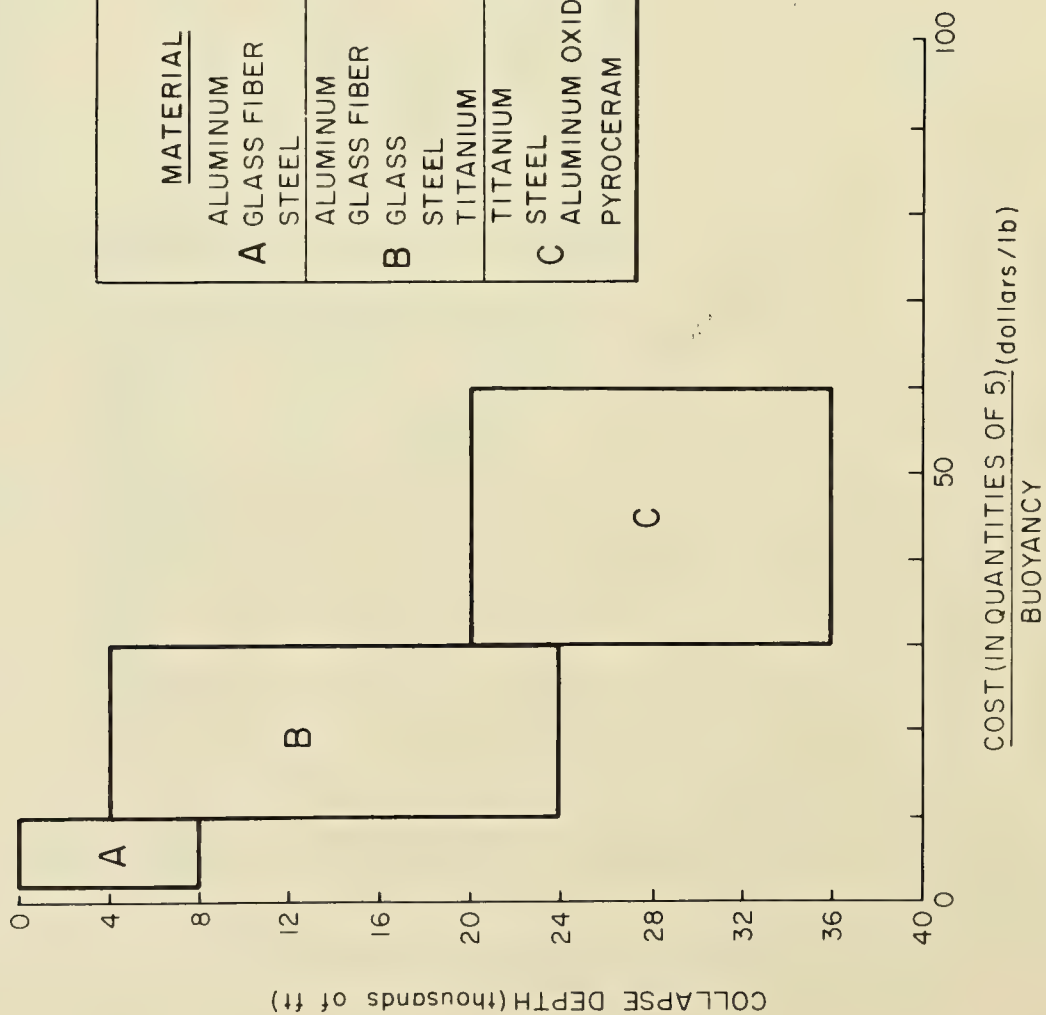


FIGURE 37 USEFUL INTERNAL VOLUME OF RIB-STIFFENED CYLINDERS MADE OF VARIOUS MATERIALS



YIELD STRENGTH (psi x 1000)	
MATERIAL	
A	ALUMINUM
	GLASS FIBER
	STEEL
B	ALUMINUM
	GLASS FIBER
	GLASS
	STEEL
C	TITANIUM
	TITANIUM
	STEEL
	ALUMINUM OXIDE
	PYROCERAM

FIGURE 38 COST OF RIB-STIFFENED CYLINDERS MADE OF VARIOUS MATERIALS

## REFERENCES

1. Perry, H. A., "Feasibility of Transparent Hulls for Deep Submergence," Paper No. 63-WA-219, American Society of Mechanical Engineers, Winter Meeting, Philadelphia, Pennsylvania, November 1963.
2. Stachiw, J. D., "Glass and Ceramics for Underwater Vehicle Structures," Undersea Technology, January 1964.
3. Stachiw, J. D., "Glass and Ceramics for Underwater Structures," Ceramic Age, July 1964.
4. Stachiw, J. D., "A Practical Glass Deep Sea Vehicle," Undersea Technology, July 1964.
5. David Taylor Model Basin. Report No. 1759: The Elastic Buckling Strength of Spherical Glass Shells, by M. A. Krenzke and R. J. Charles. September 1963.
6. David Taylor Model Basin. Report No. 1641: Exploratory Tests of Long Glass Cylinders Under External Hydrostatic Pressure, by M. A. Krenzke. 1963.
7. Pennsylvania State University, Ordnance Research Laboratory. External Report NOrd 16597-89: Shells for Underwater Vehicles, by J. D. Stachiw. 1962.
8. Pennsylvania State University, Ordnance Research Laboratory. External Report NOW 63-0209-C-2: Solid Glass and Ceramic External-Pressure Vessels, by J. D. Stachiw. 1964.
9. David Taylor Model Basin. Taylor Model Basin Progress Report on Solid Glass Structures Program, by Thomas J. Kiernan. March 1965.
10. Isaacs, J. D., and H. E. Maxwell, "The Ball Breaker, A Deep-Water Signalling Device," The Journal of Marine Research (1952) XI, Vol. 1, p. 63.
11. Perry, H. A., "The Argument for Glass Submersibles," Undersea Technology, September 1964.
12. Stachiw, J. D., and R. F. Snyder, "The Design and Fabrication of Glass and Ceramic Deep Submergence Free-Diving Instrumentation Capsules," National Underwater Technology Conference, New London, Connecticut, May 5-7, 1965.

13. Pennsylvania State University, Ordnance Research Laboratory.  
TN-26.3111-03: The Elastic Stability of Segmented Cylinders and  
Spheres Under External Hydrostatic Pressure, by J. D. Stachiw.  
February 5, 1963.
14. AeroJet-General Corporation, Van Korman Center. Report No.  
TR-328:64-207: Design Concepts Study for Deep Submersibles  
(Ceramic), by R. D. Saunders. July 1964.
15. Stachiw, J. D., "Design Parameters for Glass and Ceramic Underwater  
Structures," Ceramic Age, Vol. 81, No. 5, 1965.
16. Ernsberger, F. M., "Submarines of Glass", Machine Design, Vol. 37,  
No. 10, 1965.

SYNTACTIC FOAM BUOYANCY MATERIALS  
FOR SUBMERGED RESEARCH VEHICLE

by

Israel Resnick

U. S. Naval Applied Science Laboratory





# SYNTACTIC FOAM BUOYANCY MATERIALS FOR SUBMERGED RESEARCH VEHICLE

by

Israel Resnick  
U. S. Naval Applied Science Laboratory

## INTRODUCTION

Buoyancy materials are needed for deep submergence vehicles to permit them to carry an adequate payload and still remain buoyant. Buoyancy materials are also needed to support ocean platforms and acoustic arrays. This paper describes the development of syntactic foam buoyancy material by the U. S. Naval Applied Science Laboratory, for deep research vehicles and other applications.

At the inception of the development program on buoyancy materials, the Applied Science Laboratory studied and investigated a large number of low-density materials, both liquids and solids, and considered their potentials and limitations.

## LOW DENSITY LIQUIDS AND SOLIDS

### Low Density Liquids

A comparison of low density liquids is shown in Table 1. Low density liquids have limited usefulness since all these materials require a thin walled shell to contain them (e.g. Trieste) and damage to the shell can be catastrophic. This becomes increasingly significant during handling of the vessel and during operation at great depths.

### Low Density Solids

A comparison of the properties of low density solids is given in Table 2. The low density solids which may be considered for deep submergence buoyancy include low density metals such as lithium, woods, organic polymers such as polyethylene, or polypropylene, expanded plastics, inorganic (metal or ceramic) foams, and syntactic foams. The potential for lithium or wood as a buoyancy material for deep submergence is limited. As described in Table 2, lithium is very reactive and needs a container; woods have low strength and high water absorption. The foamed plastics

TABLE 1. COMPARISON OF LOW DENSITY LIQUIDS

Property	Gasoline & Naphtha	Ammonia Solutions	Silicone Oil
Cost	Low	Low	High
Compressibility	High. Loses buoyancy at great depth.	Low, nearly the same as sea water.	High
Bulk Modulus x 10 <sup>5</sup> psi	1.4	4	1.5
Fire Hazard	High, both aboard the vehicle and the mother ship.	None	None
Thermal contraction	High, causing a loss in buoyancy.	—	—
Relative buoyancy, pcf. (at 20°C) in 20°C water	17	17.5	3.7
Effect on aluminum and copper base alloys	None	Highly corrosive	None

TABLE 1 COMPARISON OF LOW DENSITY LIQUIDS

Material	Density	Bulk Modulus x 10 <sup>5</sup> psi	Comments and Limitation
Lithium metal	0.53	22	Reacts with water. Requires noncorrosive container which reduces buoyancy.
Wood	0.4-1.3	—	Low compressive strength, absorbs water rapidly at pressures greater than 500 psi.
Solid Polyethylene, Polypropylene	0.9-0.95	2.6	Marginal compressive strength. Low buoyancy.
Expanded plastics	wide range	—	Low strength. Permeable to water, must be packaged.
Inorganic foams	wide range	—	Low strength or open celled structure.
Syntactic foam	0.65-0.75	5.5	Offer exceptional promise for use at 10,000 psi.

TABLE 2 COMPARISON OF LOW DENSITY SOLIDS

and inorganic foams have the serious limitations of permeability and low strength. The low density plastics have limited buoyancy as a class, but they might be used as thick walled spheres or sections at moderate pressures. However, in this form they are air filled structures rather than buoyancy materials which are the subject of this paper. The syntactic foams however, offer exceptional promise for use at deep submergence pressures.

### Syntactic Foam

Syntactic foam is defined as a material consisting of a resin matrix containing a low density hollow sphere filler. This definition describes a family of materials whose density and other properties depend on the type of resin system, filler, percentages of each component, and fabrication techniques. The specific system developed at the U. S. Naval Applied Science Laboratory to provide buoyancy for the Submersible Research Vehicle (SRV) planned by the Bureau of Ships consisted of hollow glass spheres, with an outside diameter of 20 to 90 microns, in a rigid epoxy resin matrix. Figure 1, shows an exploded view of a cross-section of the NASL ML-B3 syntactic foam magnified 250 times. The hollow glass spheres in a range of sizes are visible. The formulation consists of approximately 40 per cent hollow spheres and 60 per cent resin by weight. The principal properties of the foam are also listed in the figure. The specimen shown in Figure 1, and the specimens used for test had cut or milled faces. The effect of a molded "skin" or a coating on specimen properties will be discussed later.

### Physical Properties

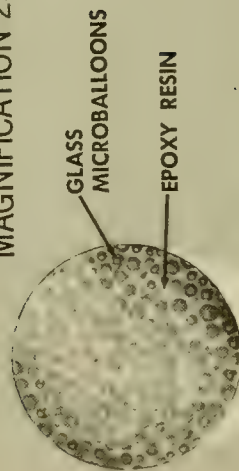
The syntactic foams when used in an equalized pressure design, eliminate the disadvantages of liquid buoyancy materials used at present and offer reliability and reasonable economy. Studies of syntactic foam show that several of them are suitable for underwater use if the hydrostatic pressure does not exceed 10,000 psi. NASL formulation ML-B3 and the best commercially available formulations meet this requirement and may be expected to have represented physical properties such as listed in Tables 3A and 3B.

### Bulk Modulus

Bulk modulus characterizes the incompressibility of a material; it is the ratio of the stress to the change in volume. Figure 2 shows the bulk modulus of water and that of the low density liquid and solid buoyancy materials listed in Tables 1 and 2; the values are representative for the respective classes of materials. Bulk modulus for expanded plastics and woods have not been included since at 10,000 psi these materials



MAGNIFICATION 250X



ML-B3

FORMULATION % BY WT.

Glass Microballoons \_\_\_\_\_ 40

Anhydride cured

Epoxy Resin System \_\_\_\_\_ 60

MAJOR PROPERTIES

Buoyancy 20 pcf

Uniaxial Compressive Strength 18,000 psi

Uniaxial Compressive Modulus 550,000 psi

Water Absorption < 1.0 %

Bulk Modulus Similar to Water

Cost/lb. of Buoyancy \$8.60

FIGURE 1 EXPLODED VIEW OF NASL DEVELOPED ML-B3

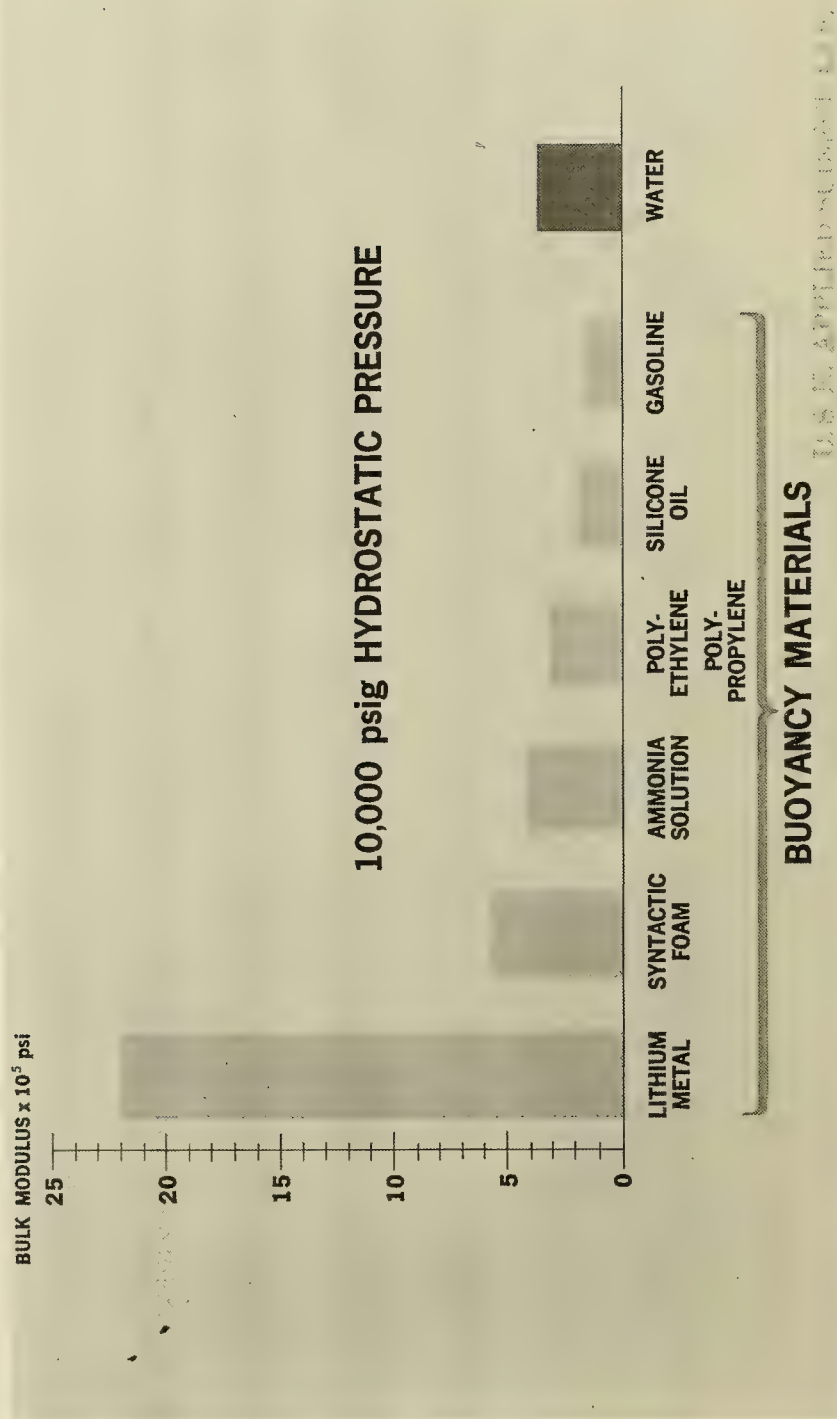


FIGURE 2 BULK MODULUS OF BUOYANCY MATERIALS

## PRINCIPAL PROPERTIES

Nominal density, pcf	44
Net buoyancy, pcf	20
Initial compressive strength	
.2% offset yield, psi	15,000
Ultimate, psi	18,000
Compressive modulus, psi	550,000
Compressive strength after hydrostatic immersion	
.2% offset yield, psi	14,000
Ultimate, psi	17,000
Compressive modulus, psi	520,000
Water absorption %	1.5

NAVAPLSCIENLAB REPORT 1950-104

TABLE 3A NAVAPLSCIENLAB AND COMMERCIALLY DEVELOPED  
SYNTACTIC FOAMS PRINCIPAL PROPERTIES

## ADDITIONAL PROPERTIES

Shear strength, psi	6,000
Tensile strength, psi	5,000
Tensile modulus, psi	600,000
Bulk modulus, psi	550,000
Impact strength, ft./lbs./in.	0.25
Fatigue (No. of cycles- atmos. to 10,000 psi)	More than 10,000
Creep, none to	12,000 psi

TABLE 3B NAVAPLSCIENLAB AND COMMERCIALY DEVELOPED  
SYNTACTIC FOAMS, ADDITIONAL PROPERTIES

would be permanently deformed. Only lithium and syntactic foam have a bulk modulus greater than that of water.

## HYDROSTATIC TESTS AND HYDROSTATIC TEST FACILITIES

In order to determine the effect of simulated service conditions on the syntactic foams, some specimens were subjected to hydrostatic pressures of 10,000 psi for 1000 hours. Other specimens were subjected to 1000 cycles of hydrostatic pressure between atmospheric and 10,000 psi. Figure 3 shows a view of the NASL hydrospace test facility. This consists of four pressure vessels, which are modified 16 inch Naval projectiles, with auxiliary piping and instrumentation. Two of the pressure vessels are used at test pressures to 10,000 psi, these are not shielded. The other two vessels, with the shielding, are used at pressures up to 25,000 psi. Figure 4 shows a cross section of one pressure vessel and its auxiliary piping. The vessels may be held at a designated pressure or may be cycled between two pressures for selected time intervals.

### Water Absorption

#### Static Exposure

Figure 5 shows a graph of the water absorption of several types of syntactic foam after exposure to hydrostatic pressure of 10,000 psi for periods of immersion up to 1000 hours. In addition to ML-B3, two earlier formulations, ML-B2 and ML-B1, and a commercially available syntactic foam are shown. Each week the pressure was released, the specimens were removed, blotted, weighed and measured. The specimens were then replaced in the pressure vessel and the test was continued. The epoxy-resin hardener system was identical in each of the Applied Science Laboratory foams. The hollow glass sphere filler however differed. It should be noted that the specimen size for each group was 2 x 2 x 1 and that each specimen had cut or milled faces. The effect of specimen size, and the effect of a residual molded "skin" on water absorption will be discussed later.

#### Cyclic Exposure

Figure 6 shows water absorption of several syntactic foams; after exposure to 1000 cycles of pressure between atmospheric and 10,000 psi. Each cycle lasted 20 minutes. The pressure was raised from atmospheric to 10,000 psi during a four minute period and was held at this pressure for 12 minutes, then released in several seconds. The pressure was then held at atmospheric for four minutes and the cycle was repeated. Specimens exposed to this cyclic exposure showed a slightly higher water absorption than those subjected to continuous static exposure at 10,000 psi for 1000 hours. The increased water absorption and slightly lower



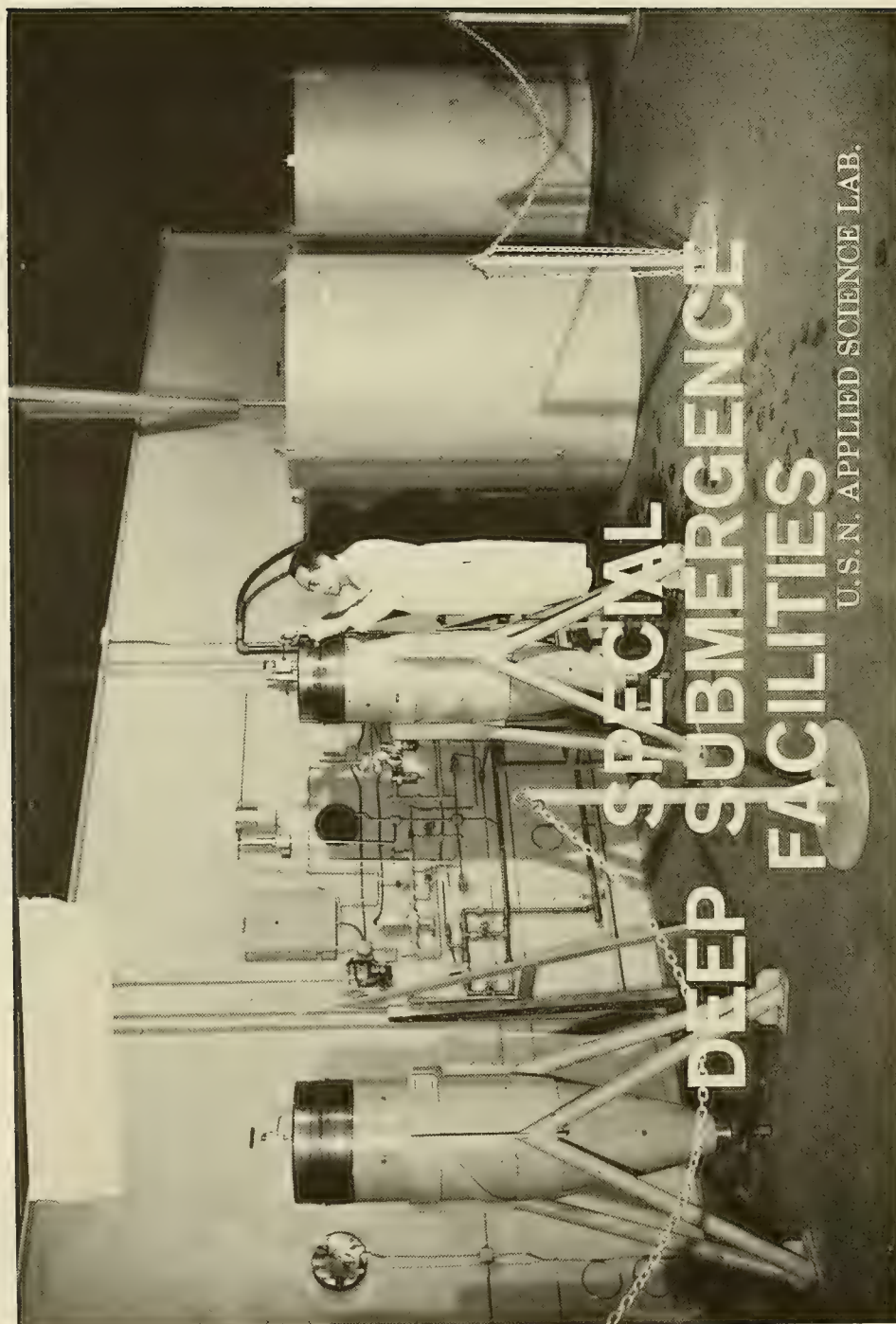
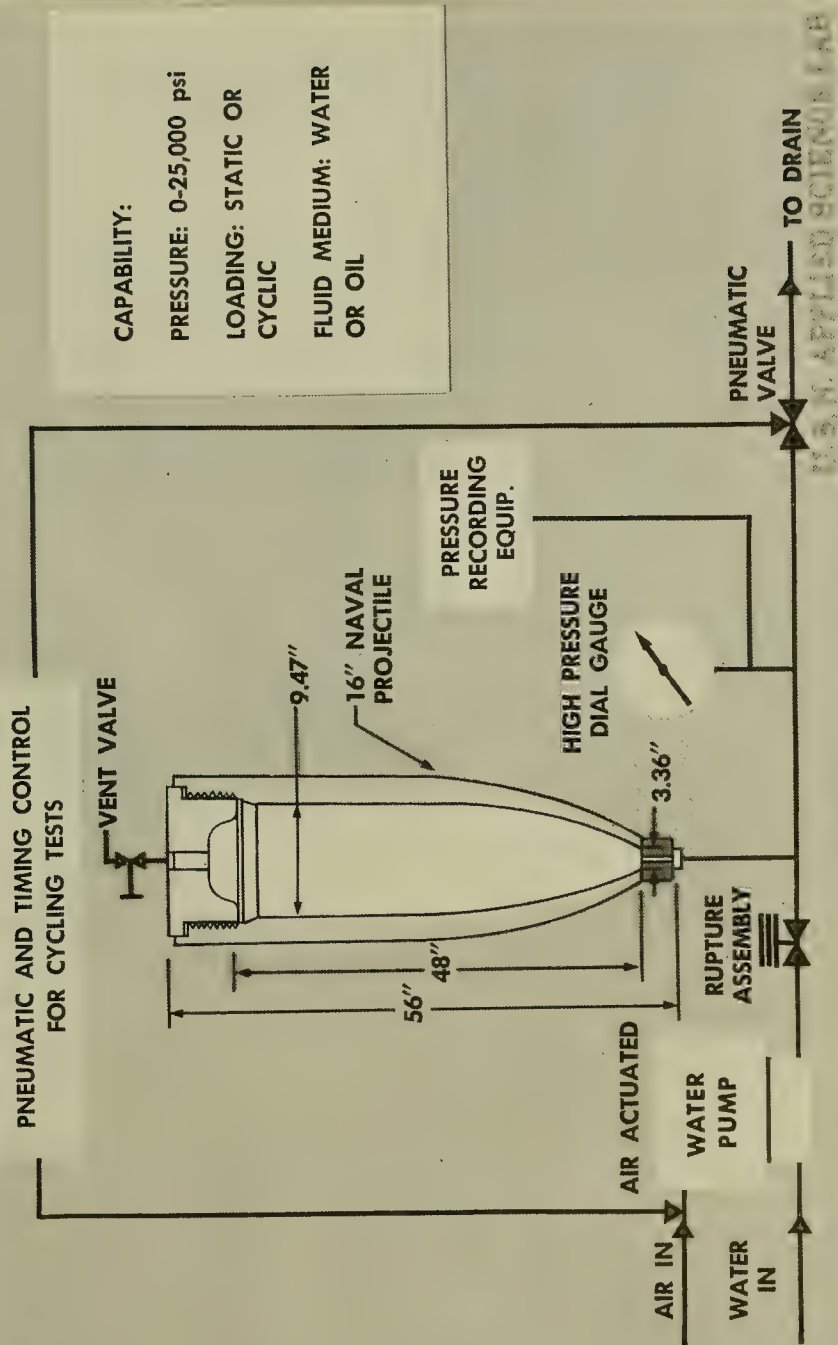


FIGURE 3 NASL SPECIAL DEEP SUBMERGENCE FACILITIES



**CAPABILITY:**

**PRESSURE: 0-25,000 psi**

**LOADING: STATIC OR CYCLIC**

**FLUID MEDIUM: WATER OR OIL**

FIGURE 4 NASL 25,000 psi HYDROSPACE CHAMBER

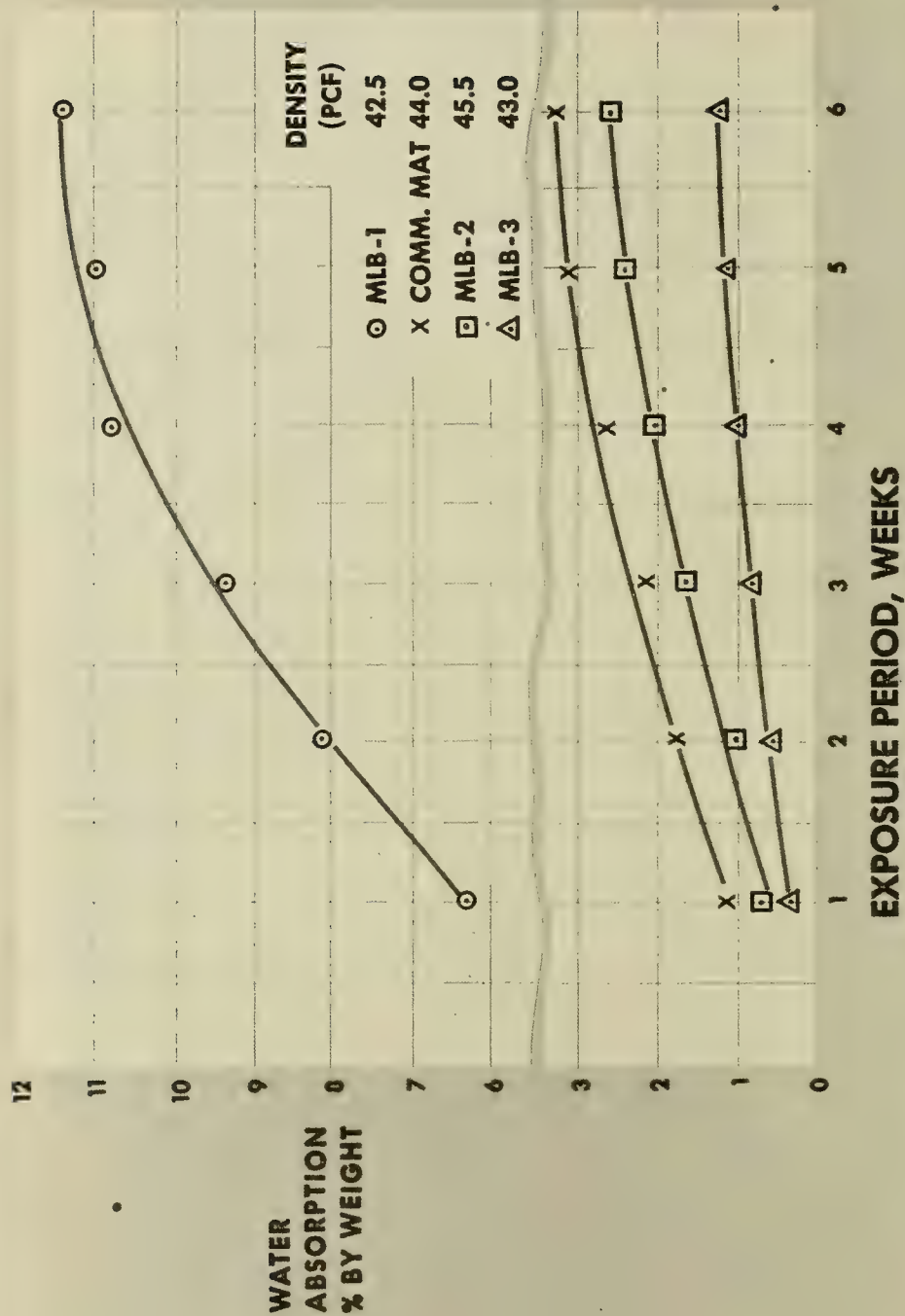


FIGURE 5 WATER ABSORPTION AT 10,000 psi HYDROSTATIC PRESSURE

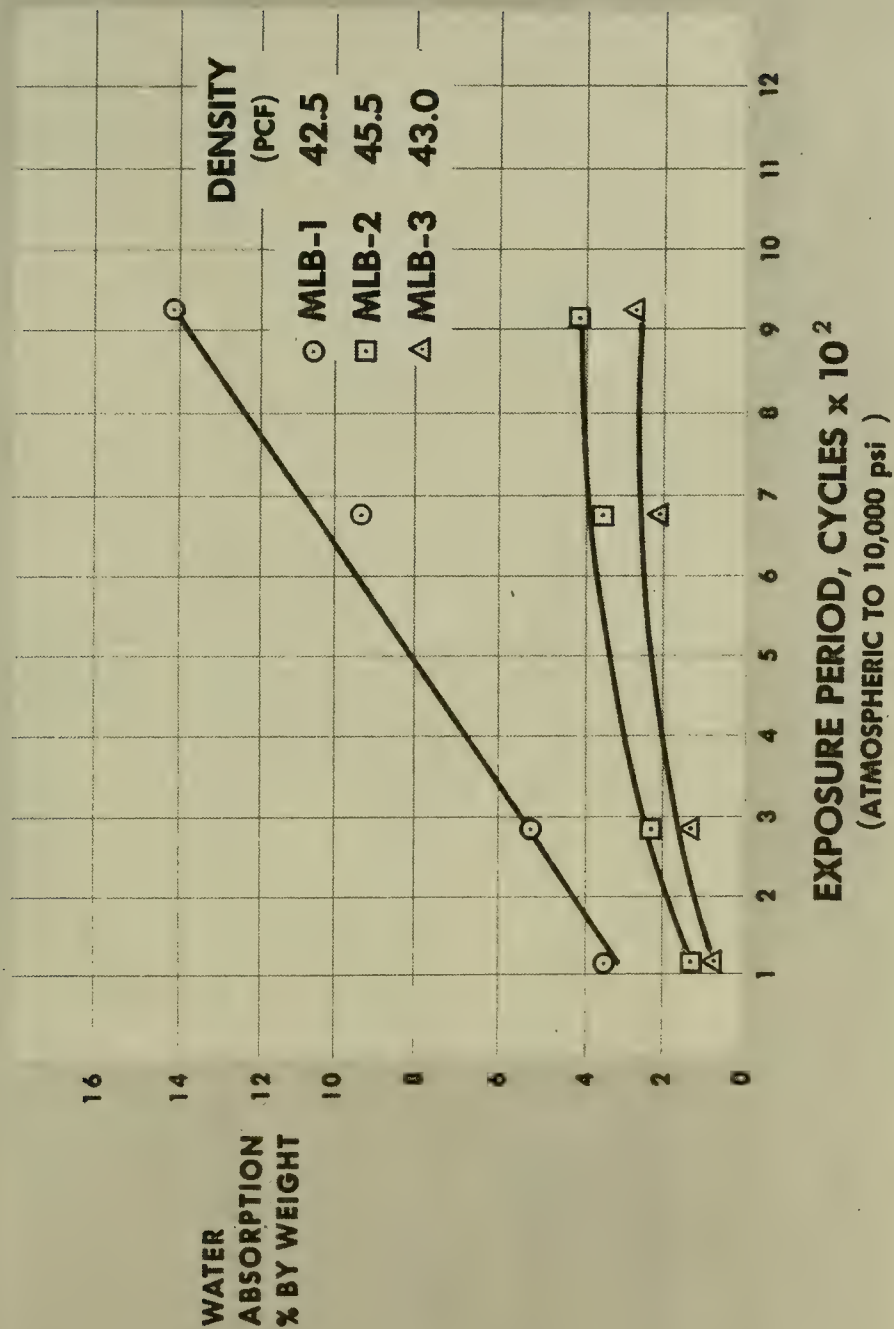


FIGURE 6 EFFECT OF CYCLING ON WATER ABSORPTION



retention of compressive strength are attributed to the sudden release of pressure from 10,000 psi which may have caused tensile failure of surface hollow spheres. Tests using a longer, eight hour, cycle of exposure with a slower rate of increase and decrease of pressure are now underway.

### Effect of Specimen Size

Table 4 shows the relationship between specimen size and water absorption. As the specimen size increases and therefore the surface area to volume ratio decreases, the percentage of water absorbed decreases. The syntactic foam modules that will be used for service applications are expected to have a volume of several cubic feet. Under similar conditions of pressure, the percentage of water absorbed for these specimens which have a much smaller surface area/volume ratio, should be substantially lower than that absorbed by the small specimens.

### Effect of Coatings

A molded block of foam when removed from its mold has a "skin" or outer resin-rich surface on most or all of its faces. As reported previously, all of the above data on water absorption was obtained from specimens prepared with cut or milled faces. In order to obtain information on the effect of the normal "skin", a slightly lower strength sample of ML-B3 was selected. The original skin remained on some surfaces and a thin coat of the ML-B3 resin was painted on the cut surface. In addition, to obtain information on the effect of a coating, a commercial sample of syntactic foam with a proprietary coating (not the normal molded "skin") was selected for test. The 1 x 1 x 1 inch specimens were exposed to 1000 cycles of hydrostatic pressure between atmospheric and 10,000 psi. In the NASL ML-B3 sample with the molded "skin" surface, the water adsorption was reduced 66%. In the commercial specimens, the coating reduced the water absorption 92%.

### Exposure of Syntactic Foam to Mineral Oil

Preliminary plans for the submerged research vehicle called for mineral oil to be used as the fluid surrounding the syntactic foam. To determine the stability of the syntactic foam in mineral oil (Humble Oil Company Zerice 37 Brand) specimens were immersed at 10,000 psi for 1000 hours. Table 5A shows that 0.54 per cent was absorbed after the 1000 hours of immersion. By comparison 2.6% water was absorbed when similar specimens were immersed in water for 1000 hours at 10,000 psi. The specimens immersed in oil showed 0.5 per cent absorption when weighed after a week of immersion, then oil absorption remained constant during the next five weeks. This indicates that oil absorption is primarily a surface phenomenon. Table 5B shows the effect of coupling agents on the



SIZE IN INCHES	1 x 1/2 x 1 1/2	1 x 1 x 1	2 x 2 x 1	2 x 2 x 2	4 x 4 x 4	6 x 6 x 6
AREA/VOLUME	10	6	4	3	1.5	1
ML-B3						
1st BATCH	2.67	1.47	1.43	1.01	—	—
2nd BATCH	—	4.4	—	—	1.00	0.70
2nd BATCH (WITH SKIN)	—	1.5	—	—	—	—
COMMERCIAL MAT.						
1st BATCH	5.65	3.39	3.02	—	—	—
2nd BATCH	—	3.2	—	—	1.00	0.40
2nd BATCH (COATED)	—	0.24	—	—	—	—

NOTE: NO MEASURABLE DIMENSIONAL CHANGES IN ANY SPECIMENS

TABLE 4 WATER ABSORPTION, BY WEIGHT AFTER 1000 CYCLES  
(0 - 10,000 psi HYDROSTATIC PRESSURE)



SYNTACTIC FOAM ML-B3	OIL ABSORPTION % BY WEIGHT	WATER ABSORPTION % BY WEIGHT
STANDARD FORMULATION	0.54	2.64
TREATED SPHERES	0.45	—
TREATED RESIN SYSTEM	0.46	—
TREATED RESIN & SPHERES	0.45	—

NOTE: 1 x 1 x 1 IN. CUBES USED FOR EXPOSURE

TABLE 5A OIL ABSORPTION, % BY WEIGHT AFTER EXPOSURE FOR  
1000 HOURS AT 10,000 psi HYDROSTATIC PRESSURE

SYNTACTIC FOAM ML-B3	ULTIMATE COMPRESSIVE STRENGTH (psi)		
	EXPOSURE		% CHANGE
	BEFORE	AFTER	
STANDARD FORMULATION	15,600	14,700	-5.7
TREATED SPHERES	16,700	16,500	-1.2
TREATED RESIN SYSTEM	16,600	16,600	0
TREATED RESIN & SPHERES	16,000	16,000	0

NOTE: 1 x 1 x 1 IN. CUBES USED FOR COMPRESSION

TABLE 5B COMPRESSIVE STRENGTH AFTER OIL EXPOSURE FOR 1000 HOURS  
AT 10,000 psi ISOSTATIC PRESSURE

glass-resin interface. The purpose of a coupling agent is to produce a better bond between the glass and the resin. In formulation ML-B3A the spheres were treated with a solution containing gamma Aminopropyltriethoxysilane coupling agent. In formulation ML-B3B, 0.5 per cent of this silane coupling agent was added to the resin. In formulation ML-B3C both the hollow glass spheres, as in A, and the resin system, as in B, were treated with the coupling agent. The ML-B3 without coupling agent, shows a 5.7 per cent loss in compressive strength after 1000 hours in oil immersion. After treatment with coupling agent, there was negligible deterioration in compressive strength after oil immersion.

#### Lower Density Syntactic Foam

Hollow spheres of lower density are now becoming available. These should permit the development of lower density foams. These spheres have lower specific gravities than the Type 45 high-strength spheres used in ML-B3 foam, and will thus permit the development of lower density foams. Table 6 shows four foam formulations made with the same resin system but with different types of hollow sphere filler. As the specific gravity of the spheres decreases, as may be expected the density of the foam decreases and the compressive strength is reduced. Formulation NASL-B13 was made with the same spheres as formulation NASL-B12 except that the spheres were pressure screened by subjecting them to 2000 psi hydrostatic pressure. The unbroken "floaters", which were the stronger spheres, were used in formulation NASL-B13. The resulting foam shows a slight increase in density over the NASL-B12 foam but a compressive strength comparable to the NASL-B11 foam made with the higher density spheres having a nominal specific gravity of 0.4.

#### FORECAST OF FUTURE (1970) PROPERTIES

##### Compressive Strength

The strength properties of syntactic foams are dependent on the strength of the resin and filler components and on fabrication procedures. Values for existing foam in Tables 3A and 3B are based on formulations containing a resin system having an ultimate compressive strength of 22,000 psi and hollow glass spheres which are reported to show approximately 50 per cent breakage at 10,000 psi. Formulations for normal 44 pcf density foam are based on optimum resin to glass ratios. The resin has greater compressive strength than the filler; therefore, as the percentage of lightweight filler is increased, the compressive strength of the foam as well as its density will decrease. Development of higher strength resin systems and higher strength glass spheres would be expected to improve the compressive strength of the nominal 44 pcf density foam as shown in Figure 7.



FOAM DESIGNATION	sp. gr. OF SPHERES	FOAM DENSITY	COMPRESSIVE STRENGTH (psi)		WATER ABSORPTION % BY WEIGHT
			BEFORE	AFTER	
ML-B3	0.45	44.2	17.5	16.8	1.1
NASL-B11	0.40	42.0	14.5	12.7	1.4
NASL-B12	0.35	38.5	12.4	10.5	3.0
NASL-B13 *(SCREENED SPHERES)	0.35	39.4	14.2	12.5	1.3

U.S. N. A. PPLIED SCIENCE LAB.

TABLE 6 EFFECT OF SPHERE TYPES



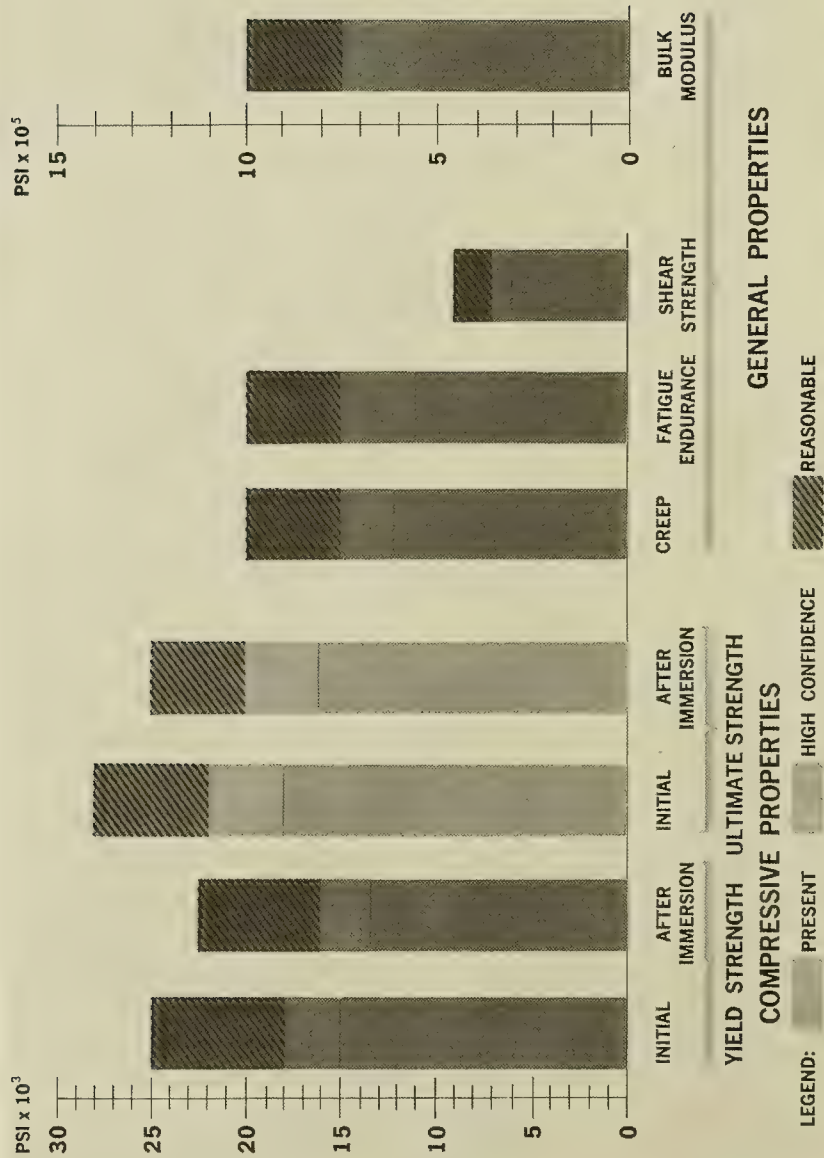


FIGURE 7 FORECAST OF PROPERTIES

Projections for increases in compressive strength properties as well as other properties are based on the following considerations:

A 50 per cent improvement in resin compressive strength by 1970. Polyester and epoxy resin systems having 30,000 psi compressive yield strength representing an increase of 50 per cent over the present strength are now under laboratory investigation.

A 50 per cent improvement in the strength of newly available glass and ceramic materials which may be used as hollow sphere filler, and the development of better coupling agents and fabrication technology.

#### Other Strength Properties

An increase in the strength of the resin, and hollow spheres and an improvement in fabrication procedures can be expected to improve other properties such as tensile, shear and fatigue strengths.

#### Density

Development of resin systems having either higher strength or lower density or both, and of stronger and more uniform low density fillers will result in lower density buoyancy materials than those cited in Table 3. Figure 8 projects improvements in buoyancy for 3 types of materials. The use of larger size hollow glass spheres, up to several inches outside diameter, in a syntactic foam matrix offers opportunities for density reduction. To produce an optimum material, one with highest buoyancy, the problem of relative sphere size, sphere thickness and spacing of spheres in the matrix is being studied both mathematically and experimentally. The Naval Applied Science Laboratory is now investigating the use of large, coated glass and ceramic spheres distributed in a syntactic foam matrix with a target of developing a buoyancy system with a density of 25 pcf and capable of withstanding a pressure of 13,500 psi.

#### Costs

The present 44 pcf syntactic foam suitable for use at 10,000 psi hydrostatic pressure ranges in price from \$4.00 to \$9.00 per pound depending on quantity used; the price per pound of net buoyancy is between \$8.00 and \$18.00. These values are based on resin system costs of approximately \$0.90 per pound, glass spheres at \$5.00 to \$12.00 per pound plus fabrication costs. Lower strength spheres which may be suitable for use up to 5000 psi are available at a price of \$0.65 per pound. Figure 8 shows projected costs for 3 types of buoyancy materials. The most promising area for decrease in the price of the higher strength syntactic foam is the reduction in manufacturing costs of the highest priced ingredient, the glass sphere filler. This may be expected, if and when, there is a substantial increase in demand for the material.

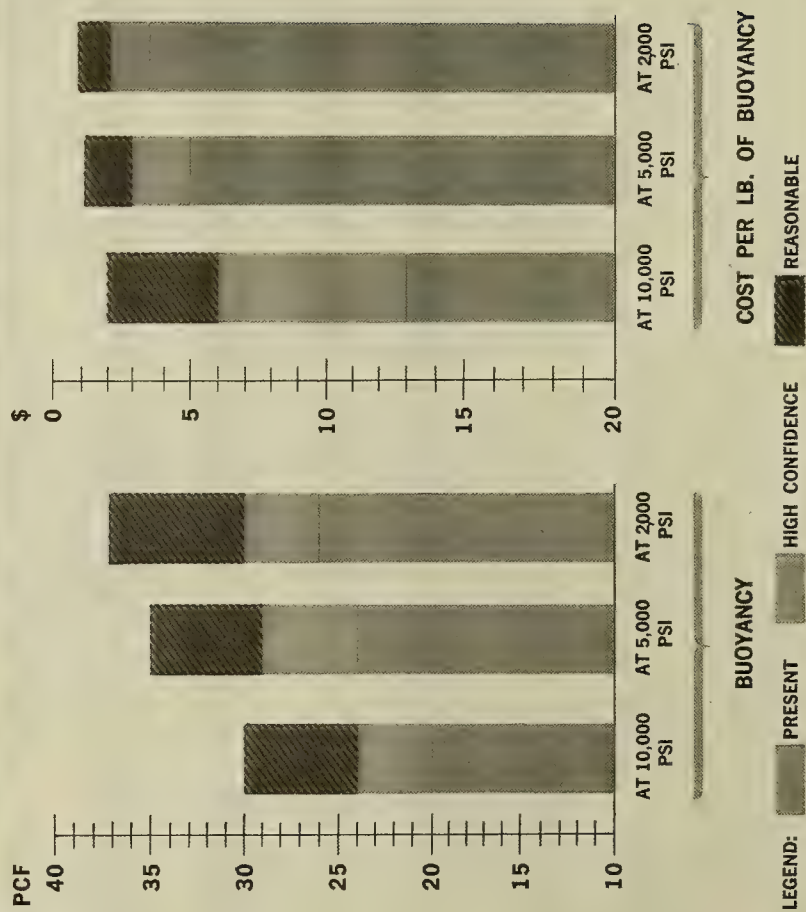


FIGURE 8 BUOYANCY PROPERTIES AND COST

## SUMMARY

This paper discussed the potentials and limitations of liquid and solid buoyancy materials studied or evaluated by the U. S. Naval Applied Science Laboratory. The development and properties of NASL ML-B3 and other syntactic foams were given. The NASL Deep Submergence Facilities were illustrated and the procedures used to evaluate the properties of the syntactic foam were described. All the information developed at the Laboratory indicates that the NASL ML-B3 type of syntactic foam is suitable buoyancy material for underwater use if the hydrostatic pressure does not exceed 10,000 psi. Significant material developments forecast for the next few years were also described.

## REFERENCES

- (1) Bukzin, E. A. and Resnick, I., Buoyancy Materials from NRL Report 6167. Status and Projections of Developments in Hull Structural Materials for Deep Ocean Vehicles and Fixed Bottom Installations. Edited by W. S. Pillini. U. S. Naval Research Laboratory - Nov 4, 1964
- (2) Report on the Development of Buoyancy Materials for Deep Submergence. NAVAPLSCIENLAB Project 6411-1, Technical Memorandum #1 of 17 Oct 1963
- (3) Resnick, I. and Macander, A. Report on the Development of Buoyancy Materials for Deep Submergence. NAVAPLSCIENLAB Project 6411-1, Technical Memorandum #2 of 13 Jul 1964
- (4) Resnick, I. and Macander, A. Report on the Development of Buoyancy Materials for Deep Submergence. NAVAPLSCIENLAB Project 6411-1, Technical Memorandum #3 (in preparation)





THERMAL AND SOUND VELOCITY MICROSTRUCTURE DATA  
TAKEN WITH AN UNMANNED RESEARCH VEHICLE

by

S. R. Murphy and G. E. Lord

Applied Physics Laboratory, University of Washington



THERMAL AND SOUND VELOCITY MICROSTRUCTURE DATA  
TAKEN WITH AN UNMANNED RESEARCH VEHICLE

by

S. R. Murphy and G. E. Lord  
Applied Physics Laboratory, University of Washington

ABSTRACT

For the past several years the Applied Physics Laboratory, University of Washington, has operated torpedo-like research vehicles in a series of investigations of thermal microstructure. Readings have been taken with thermistor probes and a sound velocimeter for isobaric trajectories of 6 to 20 nautical miles in length. The depth of the measurements range from 50 m down to 2500 m. Cruises have been to areas several hundred miles west of San Diego and near Oahu, Hawaii.

These data have been subjected to several statistical treatments. The root-mean-square deviation from the mean, autocorrelation and cross-correlation functions for temperature and sound velocity, and power spectra have all been computed. Digital filtering has been employed to enhance portions of the spectra. It has been essential for the interpretation of the results of these analyses to determine carefully the control characteristics of the vehicle and the limitations of the data system in order to determine the "noise" level of the measurements. Preliminary results show temperature deviations of the order of  $0.3^{\circ}\text{C}$  at 50 m falling to  $0.02^{\circ}\text{C}$  at 1500 m with correlation lengths of several thousand feet. Likewise, horizontal gradients are of the order of  $0.1^{\circ}\text{C/nautical mile}$  near the surface and  $0.001^{\circ}\text{C/nautical mile}$  at 2000 m.

## INTRODUCTION

This paper presents a summary of some of the oceanographic data taken with a torpedo-like instrument carrier. The details of the complete system will be presented elsewhere. However, generally, the device is launched from a surface vessel (Fig 1) and dives to one of several preset pressure levels. It runs for 4 to 6 hours at 6 knots and is capable of operation down to 14,000 feet. An acoustic system gives position with respect to the surface ship and accepts commands to change depth and heading during the run.

Figure 2 gives a list of the variables recorded on the operations reported here. Thermistor number 1, located on the nose, is recorded 12 times per second. Thermistor number 2, located on the tail, is recorded three times per second. These sensors have a time constant of 40 ms. The Gulton Thermometer is a quartz oscillator having a time constant of several seconds and is located on the nose. Sound velocity, as noted here, is recorded 12 times per second. This instrument is seldom operated below 1000 m depth since the resolution of recording, 0.1 m/sec is insufficient to detect the variations normally observed. The data are recorded digitally on magnetic tape and can be played directly into an IBM computer or converted back to an analog voltage for direct recording. The last column of Figure 2 lists the resolution per bit of the digital recordings.

## DATA DESCRIPTION

The data reported here were taken on three cruises. The first in March 1964 was about 230 miles west of San Diego in 2000-fathom water. The second cruise was near Oahu in the Hawaiian Islands as shown in Figure 3. This was one week in September 1964. The third cruise in March of this year was in the Southern California area and near the island of Guadaloupe. Figure 4 shows some of these run trajectories. As can be seen, some of these runs have 90° turns which allow the determination of two components of the horizontal gradient.

The next few figures are presented in order to give a general impression of the results obtained in operations of this type. Figure 5 is a photograph of the analog playback of a run at 30 m depth. Eighteen nautical miles of record are represented along the horizontal scale. The upper temperature trace was off scale and limited during portions of the large excursions at the beginning and end of the record. With this exception, temperature and sound velocity "track" very closely. As can be seen, the depth excursions are less than one meter. A vertical profile taken one

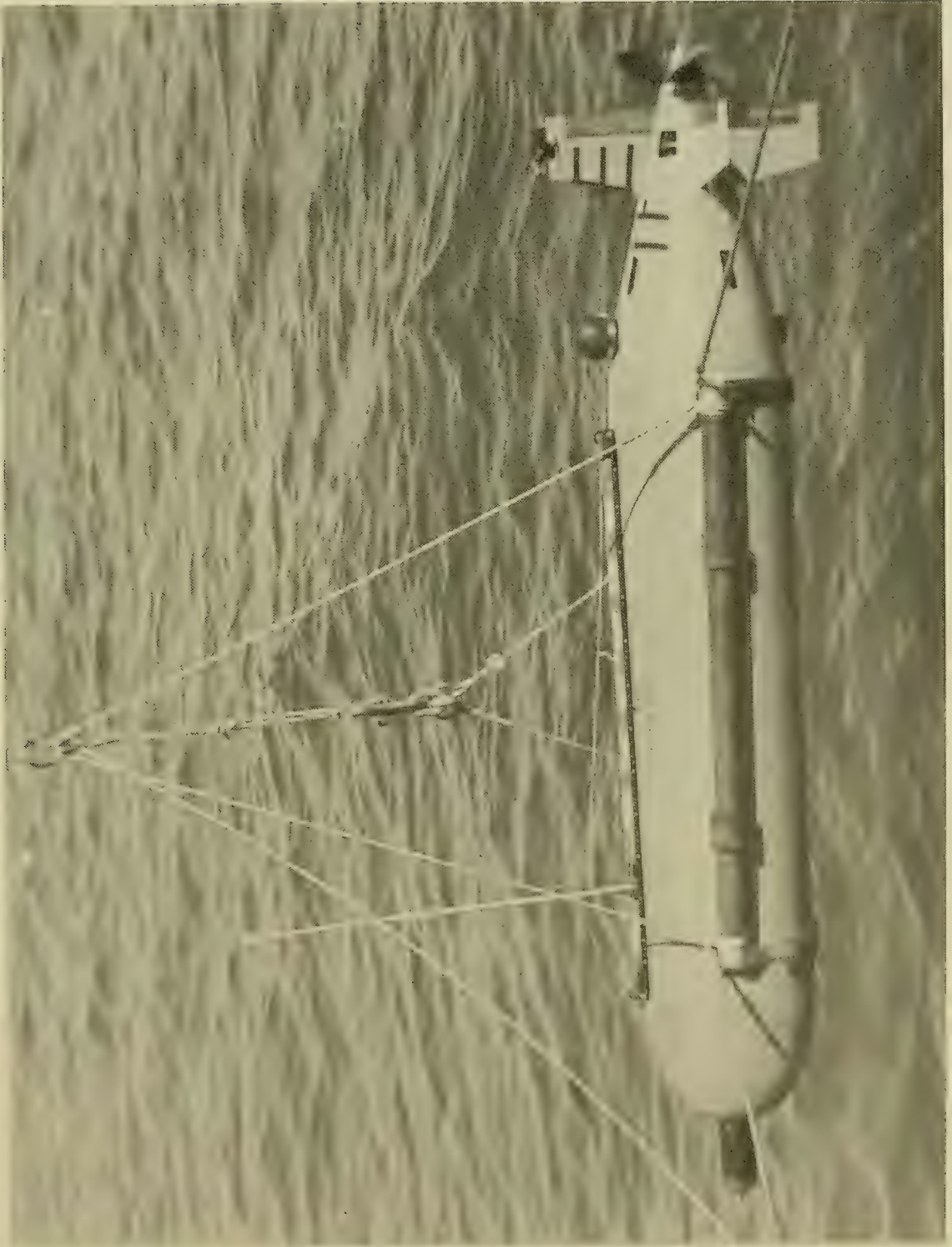


FIGURE 1 THE VEHICLE READY FOR LAUNCH



<u>Function</u>	<u>Type of Conversion</u>	<u>Frequency of Recording readings /second</u>	<u>Resolution</u>
Thermistor no. 1	* A - D	12	0.001 °C
" no. 2	A - D	3	0.001 °C
Gulton Thermometer	** F - D	1	0.0005 °C
Sound Velocity	F - D	12	0.1 m/s
Pressure	A - D	12	0.1% of full scale
Pitch	A - D	3	0.1°
Roll	A - D	1	0.1°
Propulsion Voltage	A - D	1	50 mv
Data Supply "	A - D	1	32 mv
Tape "Write"	A - D	1	5 mv
Elevator Position	go-no go	12	
Rudder Position	go-no go	12	
Transponder Returns	go-no go	12	
Minute Marker	go-no go	12	
* Analog to Digital		** Frequency to Digital	

FIGURE 2 A SUMMARY OF DATA RECORDED IN THE VEHICLE



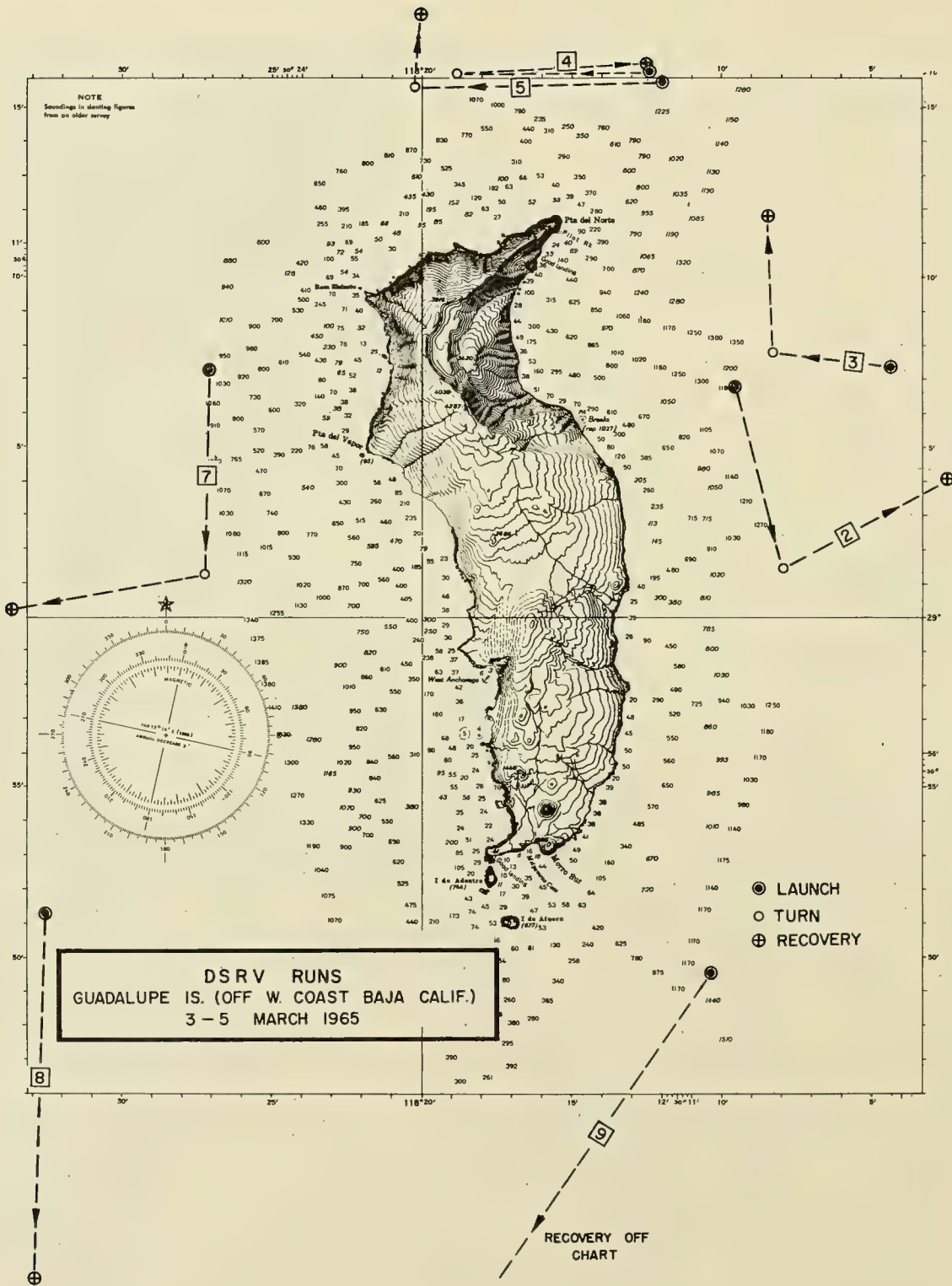
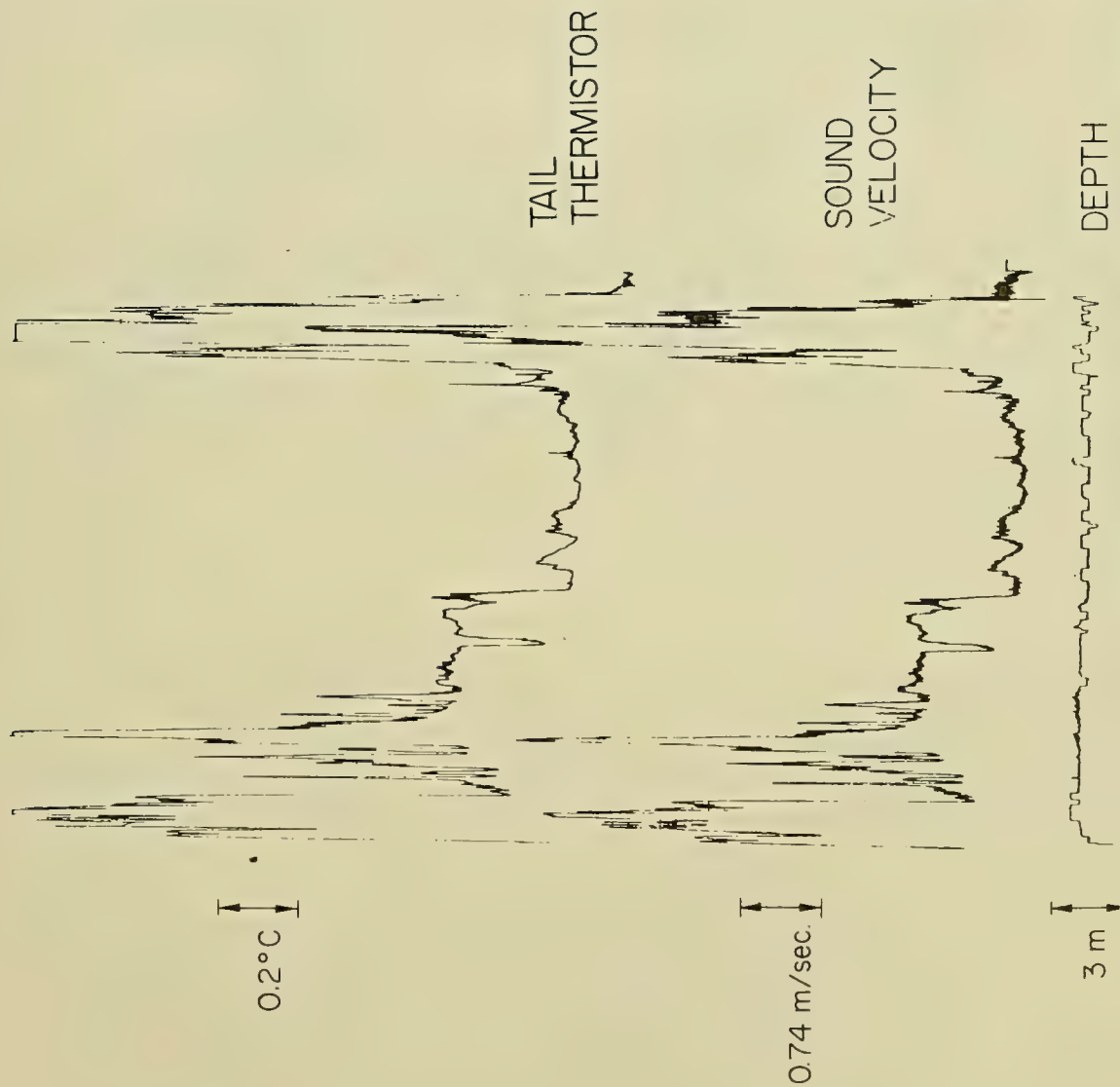


FIGURE 4 EXAMPLE OF RUN TRAJECTORIES FOR CRUISE OF MARCH 1965



RUN 65C19  
 March 11, 1965  
 30 m Depth  
 18 naut. mi. long

FIGURE 5 TEMPERATURE, SOUND VELOCITY, AND DEPTH FOR  
 AN 18 NAUTICAL MILE RUN AT 30 m DEPTH



hour before the run showed a layer depth of 70 m with no discernible vertical gradients.

Figure 5 shows the results of a deeper run at 800 m. The temperature scale is twice as sensitive as in the previous figure. One of the interesting features here is the departure of the tail thermistor reading from the other two instruments. Subsequent investigation showed a high resistance salt water short on that thermistor. This illustrates one of the problems that can arise with non-redundant instrumentation.

Figure 6 is a run at 1300 m. Once again, the three instruments track very well and the smoothing caused by the longer time constant of the Gulton Thermometer can be seen.

One of the useful features of the vehicle is the ease of maneuverability at depth. Figure 7 shows the result of a 180° course change half-way through a two hour run. The two paths are displaced about 200 feet horizontally with respect to each other. The top trace is the total sound velocity record as recorded. The bottom trace is the upper trace expanded twice in length and folded at the turn. Data near the right hand portion of these curves are only a few minutes apart in time while at the left they are two hours apart. The large slowly varying excursions (internal waves?) are reproduced very well but the small high frequency variations are not. This is not unexpected in view of the horizontal displacement in the two paths and the passage of time.

## DATA ANALYSIS

In analyzing these data, care must be taken to assure that changes in run depth resulting from control system perturbations are noted. In the following summaries only the data in which this source of error is negligible are included. The criterion used is that the temperature or sound velocity variations observed must be at least 10 times the product of the depth variation and the local vertical gradient.

The primary interest in taking these data has been for acoustical applications. One of the primary acoustical questions has been horizontal gradients and their magnitudes. The results from these measurements are shown in Figure 8. Here the data from the March 1965 cruise are summarized. The horizontal temperature gradient has been plotted as a function of depth over a run length of 6 - 12 nautical miles. The solid points are the total gradient on runs in which 90° turns were made. The crosses are single gradient components derived from straight runs. In





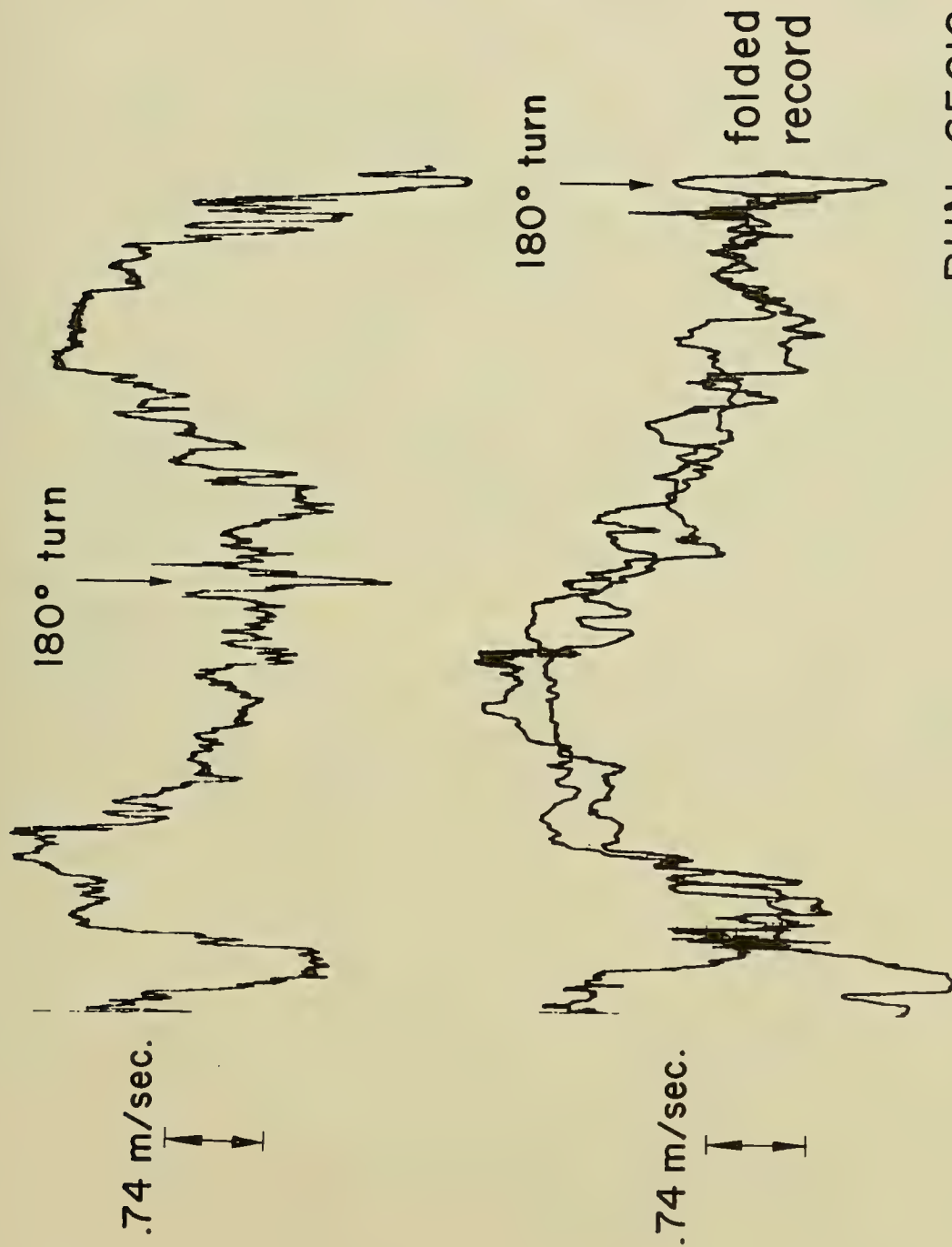
RUN 65C8  
 MARCH 3, 1965  
 800 M DEPTH  
 12 NAUT. MI. LONG

FIGURE 6 THREE TEMPERATURE RECORDS FOR A 12 NAUTICAL MILE RUN AT 800 m DEPTH



RUN 65C10  
 March 7, 1965  
 1300 m depth  
 12 naut. mi. long

FIGURE 7 THREE TEMPERATURE RECORDS FOR A 12 NAUTICAL MILE RUN AT 1300 m DEPTH



RUN 65C16  
 200 m DEPTH  
 March 10, 1965  
 12 Nautical Miles Long

FIGURE 8 AN EXAMPLE OF THE SOUND VELOCITY OBSERVED IN A 180° TURN

this presentation, no geographical distinction has been made although results are included from runs a few miles from shore as well as 250 miles at sea. In spite of the heterogeneous collection a general trend of horizontal gradients is clearly indicated.

Most of the statistical calculations have been limited so far to the early California and Hawaii data. However, Figure 9 shows the variance in degrees centigrade for runs of about 12 nautical miles long. These data indicate a possible difference between data taken in Hawaii and California. A comparison with Figure 8 shows that the horizontal gradient in  $^{\circ}\text{C}/\text{nm}$  covers two decades down to 2000 m whereas the variance is contained within one decade. In order to estimate the effects of these sound velocity variations on the fluctuation of acoustical signals, we need the auto-correlation function as well as the variance. Only preliminary results are available as yet. Figure 10 is typical for the early California data and the Hawaii data. The first zero crossing is several thousand feet. This has complicated the analysis since long records must be processed. In order to emphasize the higher frequency, short correlation variations, two shallow (50 m depth) Hawaii runs were filtered digitally to remove space wave lengths longer than 20 feet. Figure 11 shows a typical result. The correlation function is not significant since, as noted on the figure, the variance is less than  $0.002^{\circ}\text{C}$ .

Analysis of these data is continuing with the expectation that acoustical applications will be forthcoming. A large amount of data is required before generalizations are reasonable and adequate summaries can be presented. In addition, we must appreciate that the sea is incomparably larger than the minute areas covered in the three cruises reported here.

MARCH 1965 DATA  
CALIFORNIA COAST  
6-12 NAUT. MI.

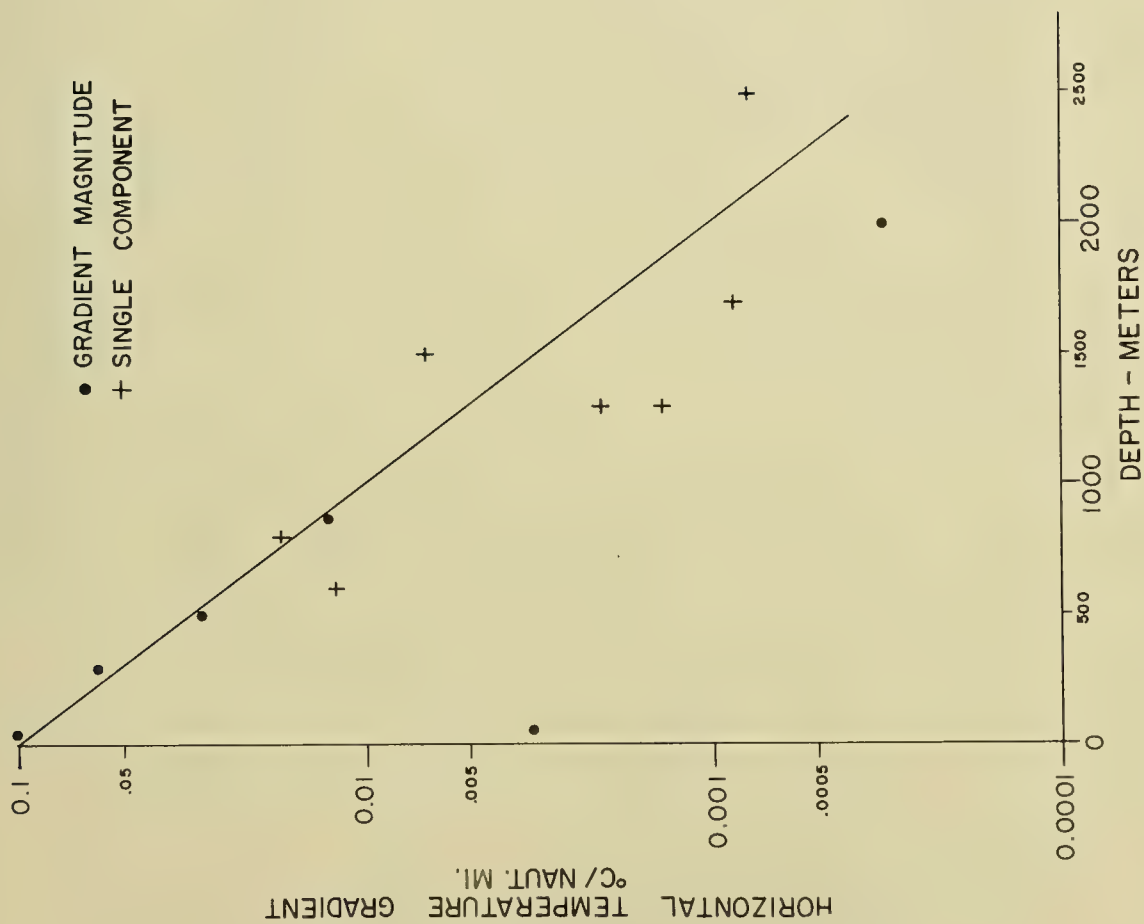
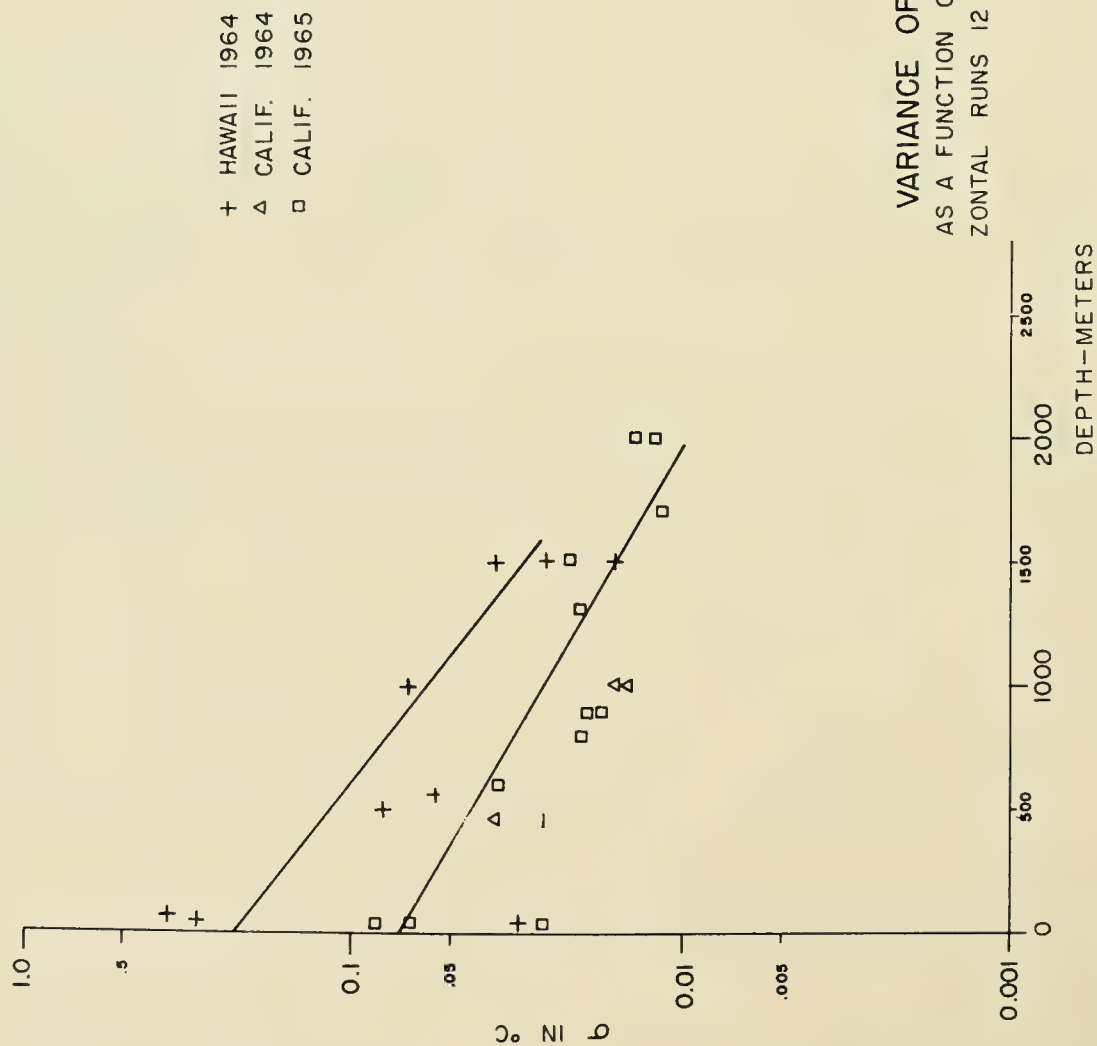


FIGURE 9 HORIZONTAL TEMPERATURE GRADIENT IN ° C/NAUTICAL MILE AS A FUNCTION OF DEPTH





VARIANCE OF TEMPERATURE  
AS A FUNCTION OF DEPTH FOR HORIZONTAL  
RUNS 12 NAUT. MI. LONG

FIGURE 10 VARIANCE IN  $^{\circ}\text{C}$  AS A FUNCTION OF DEPTH  
FOR RUNS 12 NAUTICAL MILES LONG

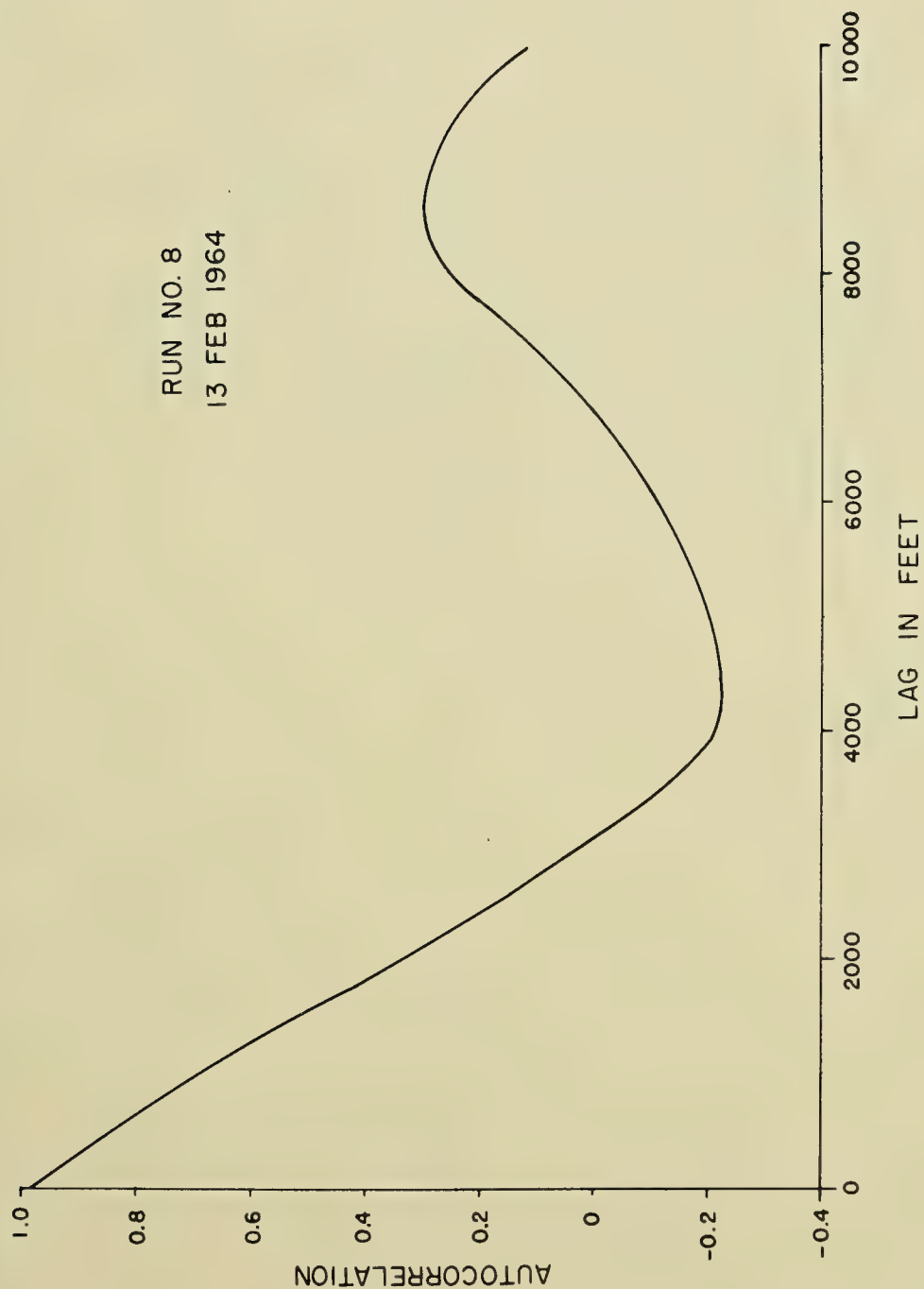


FIGURE 11 A TYPICAL AUTOCORRELATION FUNCTION OF THE TEMPERATURE  
DATA FROM THE HAWAIIAN CRUISE

RUN H-13

$\sigma = 0.0016$  °C

5000 FT. SAMPLE

FILTERED SAMPLE WITH  
WAVE LENGTHS 2 FEET  
TO 20 FEET

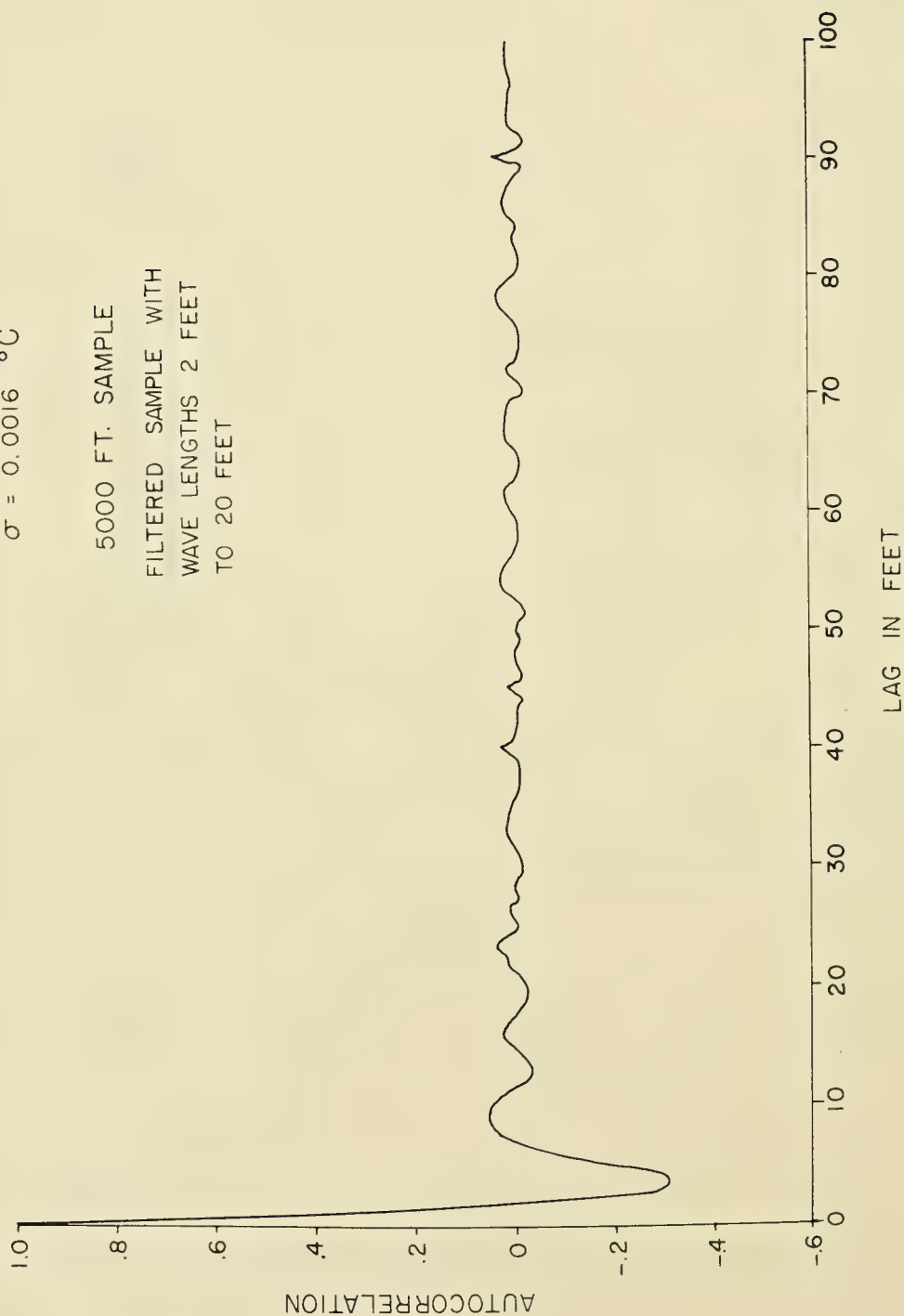


FIGURE 12 THE RESULTS OF DIGITAL FILTERING OF A 5000 FT SAMPLE AT 50 M DEPTH

ECONOMIC CONSTRAINTS ON THE DESIGN OF AN  
EXPENDABLE INSTRUMENT SYSTEM

by

W. V. A. Clark, Jr.

Francis Associates, Inc., Marion, Massachusetts





## ECONOMIC CONSTRAINTS ON THE DESIGN OF AN EXPENDABLE INSTRUMENT SYSTEM

by

W. V. A. Clark, Jr.

Francis Associates, Inc., Marion, Massachusetts

The purpose of this paper is to explain a few of the economic constraints which have influenced the development of an expendable oceanographic instrument. Economics control almost any engineering development; an expendable device causes the cost per unit to be multiplied by large numbers and therefore is an interesting problem.

The particular instrument involved in this development is an expendable electronic BT developed by Francis Associates, Inc. The device in its final form consists of a weighted thermistor probe which falls freely through the water paying out wire from a spool contained in a tear-drop shaped after-body. Wire is also paid out from a shipboard spool so that no strains are placed on the wire link between the probe and the ship. The device weighs about 2 pounds, is useful up to 1,500 feet, may be deployed at ship speeds up to 30 knots, and in its present form has an accuracy plus or minus  $.2^{\circ}\text{C}$ . and a depth accuracy of plus or minus 2% or 15 feet, whichever is greater.

The first exercise in this development was that of determining the nature of the demand curve, that is, the amounts likely to be used at varying prices. Indeed it was an early assumption that expendable BT's might be procured in large volume which led Francis Associates to initiate the development. The exploration of a demand curve is an old and, I must confess, a disorderly process. Depending upon the industry we are in, it is called economic analysis, merchandising, market research, or perhaps just hustling. In its best form it consists of analyzing a market before entering it, so that various levels of pricing can be traced through to their ultimate effects. Perhaps the application of orderly demand curve exploration which touches our lives most closely is that of large merchandising establishments such as Sears Roebuck. In the olden days manufacturers would present products to buyers; buyers, from these available products,

would select and price those items which they hoped to sell. The converse of this practice is now normal. A firm such as Sears will examine a market; examine the price levels and all the features of competitive products; will examine and predict the movement of technology in the field; will examine the growth and dynamic development of the market itself; and finally from this, prepare specifications for a line and range of products aimed at fitting different segments of the market. Sears Roebuck has "good, better, and best" based upon a three-level pricing strategy. General Motors has its range of automobiles aimed at reaching into many different strata of the predicted demand.

The exploration of the demand curve for expendable BT was an interesting journey. BT's are used for a number of purposes and in a number of tactical settings, and in many cases the cost of making a BT drop is obscured by the fact that most of the costs surrounding this drop are fixed. It is known to all of us that all costs are variable in the long run, yet it is hard to demonstrate the value of an expensive expendable device when the destroyer and sailor will be there on the payroll anyway. However, a long-run demand curve did materialize and it showed a highly elastic demand. The total market for an expendable BT appeared to be perhaps hundreds of units per year at the \$100 plus price level. At the \$50 to \$60 price level the market was clearly one of thousands. At a \$25 to \$30 price level the long-run market per year was in the tens of thousands. Another 50% reduction in price, or something approaching \$12 to \$15, produced a potential market in hundreds of thousands of units per year. A demand curve of this nature is what is known as a highly elastic demand. In other words for successive 50% reductions, it showed ten-fold increases in items called for; a 5X slope. Given this type of demand-curve evidence the ground rules for engineering efforts were fairly clear. It is known from learning curves and from production experience in many industries that a 50% reduction in cost from initial high volume manufacture is often feasible, especially if one has not backed oneself into a corner where the basic prices of raw materials make an asymptote. It was therefore concluded that to aim for a price of \$30 and an initial per year usage in the thousands. High volume manufacture from this point would permit over the long run major reductions in price as long as the materials' price "floor" was carefully observed.

Granting the above market study, we were then in a position to place some dollar constraints on the basic design of our device. If we granted an original price of \$30 and assumed that we were going to look for a profit somewhat commensurate with the risk (as well as some amortization of

our engineering outlays) we would end up with an acceptable cost of around \$20 to \$25. Within this cost there would have to be what we know as "G & A" and some sales costs. Although we squirm at their presence and their amounts, these costs seldom run below 20 to 25%, which would point to a manufacturing cost of \$15 to \$20. Examination of the costs of any instrument system shows that labor costs including manufacturing overhead run in the neighborhood of 50% with a range of 40 to 60%. Since our expendable BT is going to have to be a simple device we shoot for 40% labor and 60% material which tells us that our material will cost around \$9 to \$12 and our labor \$6 to \$8. Proceeding backwards through the jungle of costing, we know that labor will involve overhead. In this case, it probably will be high because we know that this device will demand extensive Quality Control. This would finally say that our labor cost must be in the order of \$3 to \$4 or somewhere in the line of one manhour all the way from raw materials to accepted, packed, and shipped finished products.

We know now more and more about our design. We know that it must be small, it must be brutally simple, and that we are not going to dance unless our raw materials are in total around \$10 with downward revision possible. Since we know we are dealing with a ballast weight to sink the device and a group of molded parts and electrical connections, we begin to see that our budget for temperature sensor and our transmission link to the ship are in total something like \$6. We also know that our electrical design should concentrate the electronics in the shipboard gear, keeping the expendable sensor simple.

We are now ready to examine the constraints which accuracy places upon our economics and here we find a favorable effect. When we say the word accuracy, it is important that we know what we are saying; and in the case of expendable BT, our meaning is clearly the classic QC meaning: lack of unintentional deviation between different units. (Under this definition a Chevrolet is a higher quality automobile than a Rolls Royce.) If our BT is to be as cheap as we want it to be, it will not permit skilled hand operations; it will demand highly automated machined processes. Automated machined processes tend to produce identical units; dispersions are typically narrow. These are the logical results of die casting, injection molding and automatic screw machine, and mechanized chemical processes especially continuous ones.

A further constraint which emerged early in the design was one which said that the manufacturing technologies should be processes which lent themselves to thorough process control and easy acceptance testing. It is



expensive to test any expendable device by using it. In the case of an expendable BT, which requires a 1,500 foot instrumented test tank for even the simplest test, acceptance tests are terribly costly. It is mandatory that our technology provide for very low consumers' risk sampling plans of the materials, coupled with final assembly processes which do not degrade the quality of the parts. This feature of the planning also supports the inevitable need for multiple sources of the same instrument; final tests will not possibly control this product. The pieces chosen on the final parts list reflected in each case a selection based upon easy and reliable sampling inspections.

In summary we commenced our design efforts only after concluding four simple economic studies. First, a price-volume analysis; secondly, a cost-size and complexity analysis; third, an accuracy-cost analysis; and finally, a manufacturing quality control analysis. We recommend this as typical of the type of contribution which economic thinking can provide as a guide line for the application of the engineering and development efforts.

A SHIPBOARD NAVIGATIONAL AND GEOPHYSICAL PROCESSING SYSTEM

by

Carl O. Bowin

Woods Hole Oceanographic Institution  
Woods Hole, Massachusetts





# A SHIPBOARD NAVIGATIONAL AND GEOPHYSICAL PROCESSING SYSTEM

by

Carl O. Bowin  
Woods Hole Oceanographic Institution  
Woods Hole, Massachusetts  
02543

## INTRODUCTION

Technological developments in the last five years have made it practical to collect large amounts of bathymetric, gravity, and magnetic information during a single cruise. The reduction of these data involve the processing of a similar amount of navigational information. It is difficult for analysis to keep pace with the collection at present, and without the utilization of modern data processing techniques it will become increasingly so. Since June 1962, the Geophysics Department of the Woods Hole Oceanographic Institution has used a digital computer (IBM 1710) aboard the Research Vessel CHAIN for the real-time collection and processing of navigational and geophysical data. This system was developed by the Woods Hole Oceanographic Institution. The engineering design and computer programming was accomplished by the International Business Machines Corporation under subcontract to Woods Hole. This project was supported at the Woods Hole Oceanographic Institution under Contracts Nonr-1367(00) and Nonr-4029(00) with the Office of Naval Research, Department of the Navy. Our goal is to accomplish at sea as much data analysis and interpretation as possible while the investigation is being conducted.

## DATA PROCESSING SYSTEM

The first shipboard system consisted simply of an analog-to-digital converter, a digital computer, a console typewriter, and a paper-tape reader and punch (Bernstein and Bowin, 1963; Bowin, 1963). The system automatically sampled the ship's heading and speed, two inputs from a shipboard gravity meter, and switches manually set the depth of the water. Ship's position information was inserted via manual entry switches that are standard equipment on the IBM Analog to Digital Converter (1711). Only the water-depth switches were remote from the computer system

and they were placed adjacent to the echo sounder in another laboratory on the ship.

Improvements were continually made to the system as experience was gained with it. The system was considerably expanded in November 1963. See Figure 1 for a diagram of the present system. These changes included the addition of an output typewriter (buffered), capability for the computer to control switches and stepping motors, a digital plotter, remote digital displays, remote latitude-longitude displays, remote navigation input units, remote alarm units, and three remote input-output typewriters. Further, the paper-tape reader and punch was replaced by a card reader and punch, and three magnetic disk drive units were installed. The three random access magnetic disk storage units, with removable magnetic disk packs, offer very rapid input and output of data and the ability to merge real-time, on-line computations with background off-line computations. The three remote, input-output typewriters are being used in experiments to improve the collection, dissemination, and availability of the scientific and navigational information logged in the various laboratories and bridge of the ship during the course of the cruise.

The computer program changes required to utilize the added features and equipment were of course extensive. Figure 2 summarizes the growth of the computer program that has attended the development of this ship-board data-processing system. It is especially illuminating in relation to the statements of the programmers who first looked at our requirements in 1961 and questioned whether our problem really needed a computer at all. The memory storage required by the real-time program has shown a ten-fold increase in less than three years - from twenty-thousand to two hundred and thirty thousand character locations - and there are still many programs yet to be implemented.

## NAVIGATION

Our main interests in navigation concern our need to know the ship's position and ground speed. The reduction of the gravity measurements appears to place the most stringent requirements upon this knowledge where positional accuracy to 0.1 minute of latitude and longitude, and ground speed accuracy to 0.1 knot are desired. Unfortunately, it is only possible to achieve these accuracies in very limited portions of the world's oceans. The basic navigational capability aboard the R/V CHAIN include radar and visual bearings, celestial navigation, Loran-A, and Loran-C. At times, a gyro-erected optical navigation system (GEON) under development by Dr. W. S. von Arx of the Woods Hole Oceanographic Institution has been utilized. In addition, we have been experimenting in the utilization of very low frequency transmissions for navigation, and we hope to

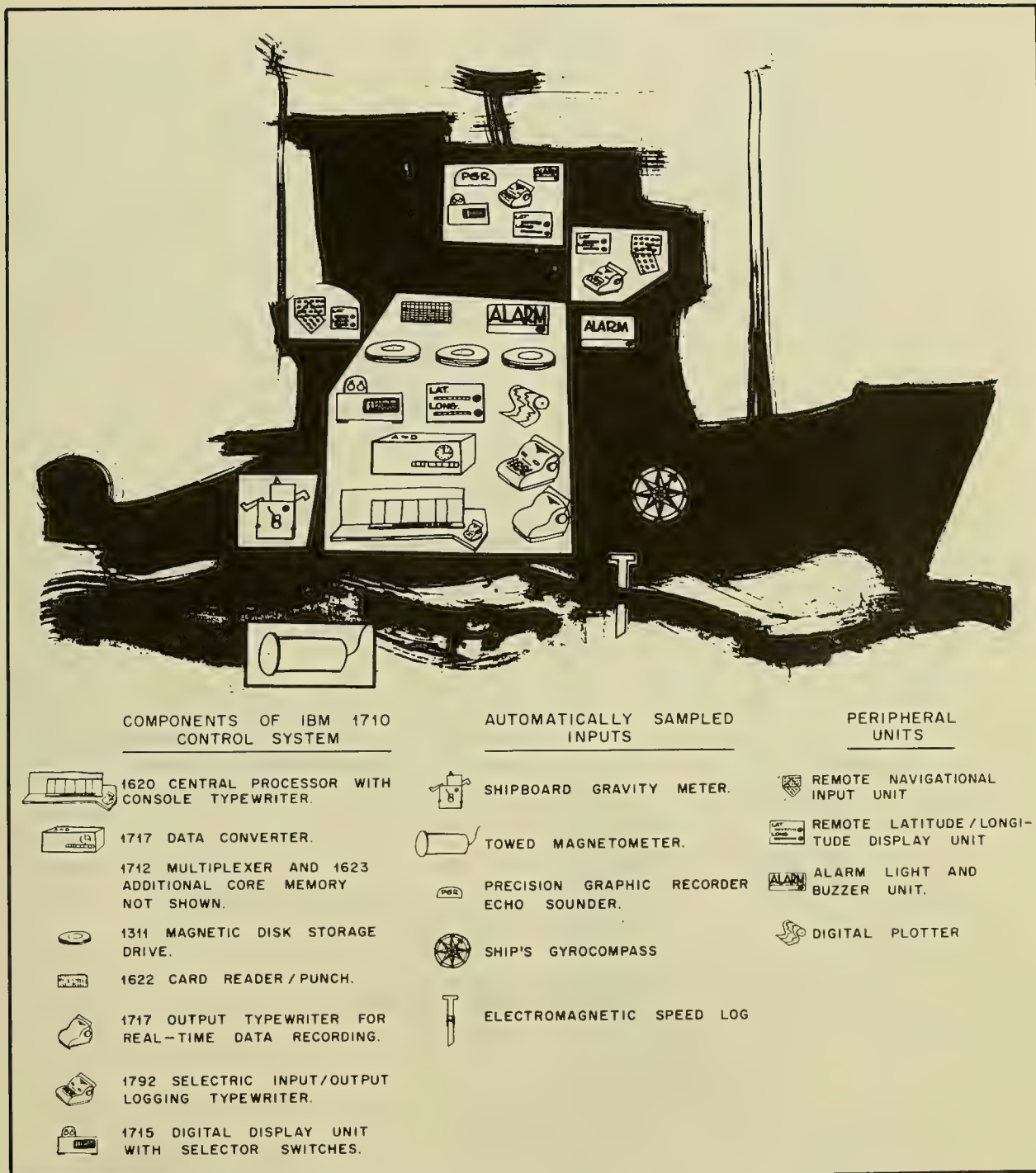


FIGURE 1 DIAGRAMMATIC REPRESENTATION OF THE GEOPHYSICAL AND NAVIGATIONAL DATA PROCESSING SYSTEM ABOARD R V CHAIN



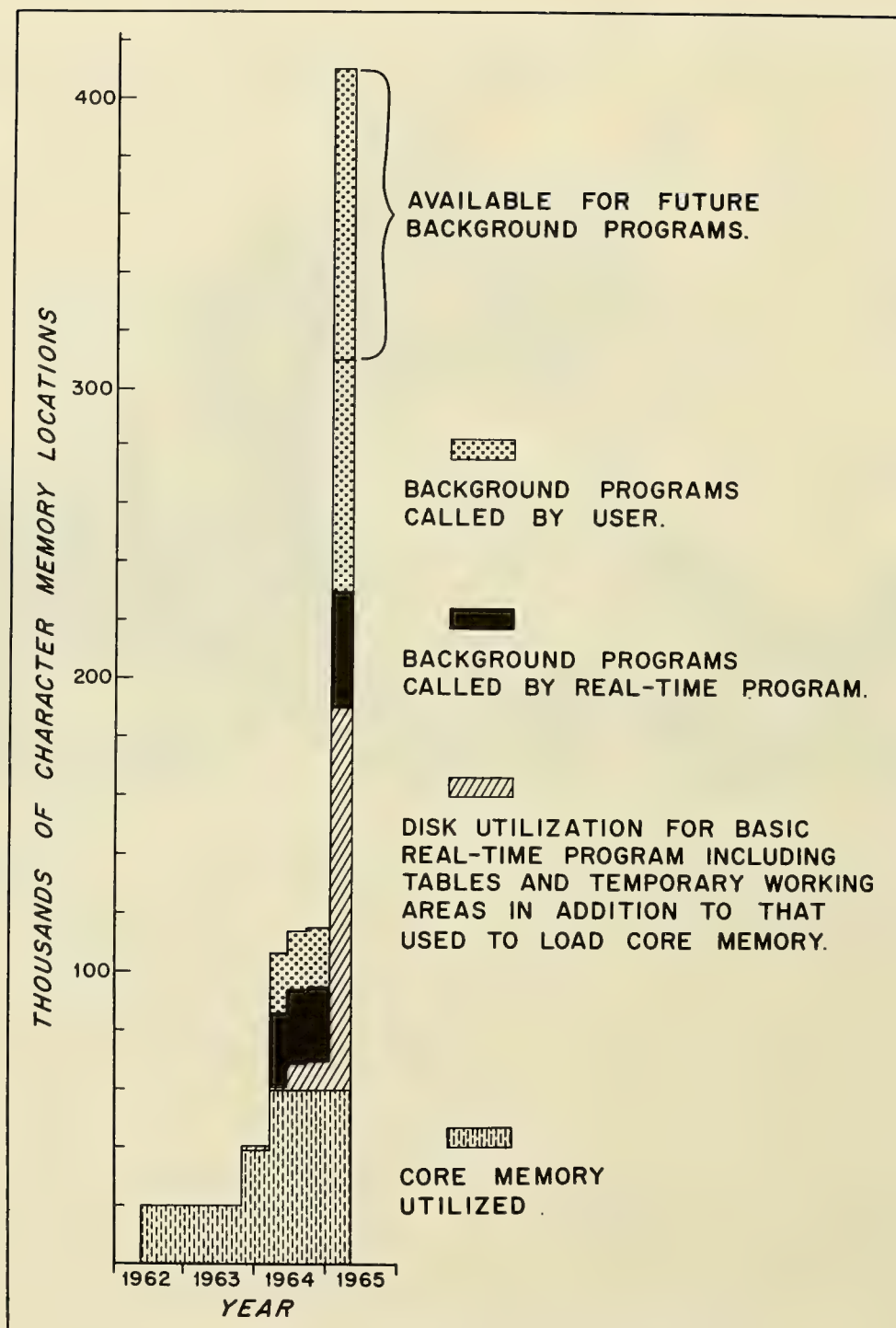


FIGURE 2 GROWTH OF COMPUTER PROGRAM ATTENDANT WITH THE DEVELOPMENT OF THE SHIPBOARD SYSTEM



obtain a satellite navigation receiver in the near future. Position information can be entered into the computer either via the manual entry switches at the computer site itself or from either of two remote input units. Upon entry of the fix information the computer calculates the differences between this fix and the dead reckoning position at the time of the fix, and records this information on the main lab output typewriter and on the three remote input-output typewriters on the bridge and in the science laboratories. These differences are used in judging the quality of the fix in relation to previous fixes, and in helping the operator to decide whether or not to use the present fix for up-dating of the dead reckoning navigation carried on by the computer program. Latitude and longitude, regardless of how it is obtained, can be accepted by the computer. Computer programs have been generated for the on-line processing of Loran-C and VLF micro-second delays, and the latitude and longitude determined by these computer programs are similarly recorded on the several typewriters. This process is considerably faster and more accurate than the manual plotting and reading of Loran positions. Similar programming for Loran-A micro-second delays are in progress. The ship's position information processed by the computer is also stored on a magnetic disk, and these data disks may be later reprocessed using off-line programs to up date the dead reckoning navigation to agree with selected navigational fixes. Although this procedure improves the continuity of position information along the ship's track, it does not appear to significantly improve knowledge of instantaneous ground speed. The ship's electromagnetic speed log is our best available source of ground speed information. It will, of course, be in error by any ocean currents that may be present, sets due to wind, or water turbulence along the hull of the ship. Surface ocean currents are generally greater than 0.1 knot and therefore our desired accuracy is not obtained. However, there have been rare occasions when the computer dead reckoning did not differ from navigation fixes by more than 3 nautical miles for periods up to twenty hours. The determination of ground speed indirectly from two navigational fixes may yield accurate values of average ground speed if the time between the two fixes is sufficiently long. Even if good fixes with an uncertainty of 0.1 nautical mile are available, at least two hours between such fixes are required in order that the error in determining ground speed be within 0.1 knot; and a two-hour average is hardly an instantaneous value. Continuous 0.1 knot accuracy in ground speed does not appear to be generally possible at present. Even inertial systems do not appear to be adequate for this accuracy, especially in areas of rough bottom topography producing local deflections of the vertical which cause erroneous accelerometer readings. We are presently trying to improve on the existing situation by developing, in collaboration

with Westinghouse Electric Corporation, a deep-towed speed log which should yield a better estimate of ground speed than speed logs operating in the near-surface waters.

## CONCLUSIONS

The need for a shipboard computer with the capacity of a 7090-type machine is not far off. It is presently possible to define the basic requirements of future shipboard computer systems. It is not possible, however, to anticipate all the things one would like to do a year hence, thus versatility and flexibility of design are extremely important if the ability to follow up on experience is desired. Multiprogramming capability is essential, including the ability to time-share real-time and off-line programs. The program should be written with a modular construction and preferably in a Fortran-like language with sampling and control instructions. This would allow the user greater ability to modify and expand the program as desired. Core memory should be made as large as practical; the tendency is for best estimates to be too small. Equipment and programs should exist that will prevent failures in peripheral units or external input units from halting or destroying the operation of the other activities of the computer system. It also appears that the use of several similar output devices for the visual recording of the various types of scientific data processed is preferable to one large unit recording everything in a necessarily less flexible format. And last, but not least, reliability should be maximized to the extent that urgency demands, and design and money permit.

## REFERENCES

- Bernstein, R. and C. O. Bowin, 1963, Real-Time Digital Computer Acquisition and Computation of Gravity Data at Sea: IEEE Transactions on Geoscience Electronics, Vol. GE-1, No. 1, 1-10.
- Bowin, Carl O. , 1963, WHOI Reference No. 63-40, Supplementary Report on the Automatic Gravity System Used Aboard R/V CHAIN July 1962 - September 1963, 88 pp.

INVESTIGATIONS OF SEDIMENT PROPERTIES IN SONAR  
BOTTOM REFLECTIVITY STUDIES

by

James J. Gallagher

U. S. Navy Underwater Sound Laboratory, New London, Conn.

and

Vito A. Nacci

Civil Engineering Department, University of Rhode Island  
Kingston, R. I.



# INVESTIGATIONS OF SEDIMENT PROPERTIES IN SONAR BOTTOM REFLECTIVITY STUDIES

by

James J. Gallagher

U. S. Navy Underwater Sound Laboratory, New London, Conn.

and

Vito A. Nacci

Civil Engineering Department, University of Rhode Island, Kingston, R. I.

## INTRODUCTION

The objective of the investigation of sediment properties in acoustic bottom loss studies is to develop a capability to predict acoustic energy loss in various types of ocean depositional areas. This capability is being developed primarily by laboratory experiments on sediment samples and by model studies, utilizing the laboratory-derived sediment properties values.

This problem has been under study in this country for about ten years. The general approach has been to establish the relationships between the structural and acoustical properties of the sediments. Various mathematical expressions have been derived relating principally density, median grain size, and porosity to sound velocity. However, these expressions appear to be restricted to localized physiographic provinces, and perhaps to geographic sectors or soil types. The problem of the acoustic energy absorbing properties of the sediments is more severe, and the solution is less developed. Many investigators of acoustic energy loss utilize core samples, selected at relatively large distance intervals, as being representative of the bottom. However, variability in acoustic energy loss occurs over rather small distances along the bottom, well within the limits of a physiographic province.

Rather than seek relationships of wide-spread application, the Acoustics Research Division of the Underwater Sound Laboratory is formulating a program to explain this variability over specified areas of the ocean bottom. We have chosen our test sites as those with little bottom slope and almost no bottom roughness features. Sedimentation and soil mechanics relationships will also be studied. The properties of those sediments that would most likely be found in a flat-bottom depositional area are being intensively examined for energy absorbing qualities, for their effect on a passing acoustic wave, and for the effect of a passing acoustic wave on the properties of the sediment aggregate. In adopting the approach it is felt that the effects of



bottom roughness on energy loss are omitted and, therefore, the accuracy of results is improved. Usually these depositional areas contain dramatic stratigraphy, and some contain many sub-bottom acoustic reflectors.

## SURVEY DISCUSSION

Two sites have been surveyed thus far, one rather insufficiently because of equipment failure.

In an area about 30 miles south of Bermuda, two core samples of about 5-foot length were obtained about 1/2 mile apart. The sub-bottom layering is quite fine, and it is felt that at least two more cores would be required before a cross-sectional diagram of the sub-bottom structure could be constructed with some reliability. Recent Naval Research Laboratory photographs taken by J. Gennari have shown this bottom section to be extremely flat. A study of the area will be continued when the other cores are obtained.

Five cores were obtained from the Tongue of the Ocean, off Middle Bight (Fig. 1). They were taken from an area less than two miles in diameter and ranged in length from 10 to 16 feet. While stereo-photographic attempts were made, no photographs were obtained. However, the echo sounding trace revealed a flat, though slightly inclined, bottom.

The in-situ determination of the thin impedance layers in the upper 100 feet of sediments has been a difficult task. In deep water they are not readily identifiable by echo sounding or sub-bottom reflection techniques. The standard 12-kcps hull-mounted or towed UQN source produces very little penetration in deep water. The approach to increased proficiency in acoustic surveying of the ocean bottom has thus far been narrowly limited to two basic interests: (1) detailed study of the water-sediment interface using high-frequency sources, and (2) vertical delineation of the major structural provinces from the bottom interface to the earth's core, using seismic techniques. In the first case very little penetration is sought or achieved. In the second thicknesses of the fine layers are considerably smaller than the wavelengths of the signals employed and therefore go undetected.

The 100-kilojoule EG and G sparker source was used about the AGOR-4 with a band pass filter range of 500-2000 cps. The penetration was excellent and apparently the detection of the finer structure was good, since a number of layers were indicated. However, the bubble pulse returns overlapped the fine layer and other bubble pulse returns to the extent that the records could not be interpreted.

During a recent 3.5-kcps normal incidence test a magnetostrictive scroll source was towed about 1000 feet above the bottom and the signals were recorded on a PGR. The existence of the individual layers was evident, although the definition was somewhat



poor. The technique looks promising. A means and variance program was developed and promises to reveal sub-bottom impedance layers from the acoustic data. However, the results of this particular test indicated that the shallowest major reflector was approximately 100 feet down, or considerably greater than the core samples obtained. Further tests will be made using varying pulse lengths for a given frequency, and the presentation of the structures will be compared. This technique is in the formative stage and is undergoing modification.

A similar approach will be made on the next bottom study cruise. A 12-kcps capacitance discharge device will be towed near the bottom. When a 0.5-msec pulse length is used, the layer thickness resolution should be about one foot, with penetration of from 50 to 100 feet. This device is similar to the pinger unit used in most underwater camera systems; but it will not be battery powered, it will serve as a receiver as well as transmitter, and the repetition rate will be varied and controlled from the surface ship, as deemed necessary. Later, if the evaluation of this technique proves satisfactory, this device will be modified to operate in the 1 to 4 kcps frequency range. Whether acoustic impedance layers several inches thick or less are significant contributors to the overall energy loss is a subject currently under study. It appears that the controlling feature is not the thickness of the layer but the magnitude of the rate of change in impedance.

As more is known about the geologic-acoustic relationships and about the behavioral reactions of each property in the soil mass, we shall embark upon a program to measure the absolute values of a number of the parameters in situ. This will include the use of: (1) gamma radiation devices which are available to determine bulk density in a sediment mass; (2) vane shear devices, fall cone penetrometers, etc., which are available for in-situ measurement of shear strength; and (3) the acoustic probe technique which has been utilized at NEL and will be attempted this year at USL using lower frequencies and greater depth penetration. Hopefully, coring pipes or other elongated tubes will be instrumented for in-situ measurements of sound velocity.

This instrumented probe technique is well developed in the petroleum and well-logging industries. With the advances in marine drilling, this realization may be more immediate than we are at present prepared for.

## LABORATORY DISCUSSION

The laboratory analyses of the core samples have been performed at the University of Rhode Island's Soil Mechanics Laboratory, in the Department of Civil Engineering. The following engineering properties were determined at one-foot intervals along the core, and at smaller intervals where required: specific gravity, water content (based upon 100% saturation), atterberg limits, void ratio, bulk wet density, organic content, carbonate content, median grain size, sorting coefficient, gross determination of grain shape, and sound velocity.



The sound velocity values thus far determined were direct measurements using an Underwater Systems, Inc., sediment velocimeter, model no. US1-101, on loan from NAVOCEANO. These values will soon be compared with those determined by four sources discussed below.

a. Direct measurements are being made at the URI laboratory by using a longitudinal wave vibration apparatus (Fig. 2). This device utilizes an air chamber to provide confining pressure, ceramic transducers placed at both ends of the sample, an oscillator, a pulse generator, an amplifier, and an oscilloscope. The wave forms are displayed on the oscilloscope and can thus be measured in time units. The velocity is computed from the time value and the known length of the sample. This apparatus will soon be modified to provide water as the confining medium.

b. A table of estimated sound velocities was constructed to relate porosity, density, and median grain size to sound velocity. This table is a compilation of published reports in which the values of all these properties are given, Hamilton, et al. (1956), Laughton (1957), Sutton (1957), and Shumway (1960), and was tabulated irrespective of physiographic province or soil type.

c. Using most of this same data, M. McDonald (1965) categorized the source areas into shelf, slope, shelf-slope, deep, and slope-deep provinces. He then ran a regression analysis on the data to determine the significant variables affecting the sound velocity value for a given province.

d. Sound velocity was computed from laboratory elastic moduli determinations. This technique will be discussed in the following section.

All these sound velocities will then be used in the mathematical model to note their effect on the impedance layering and consequently on the value of reflection coefficients.

In order to understand the acoustic properties of the sediment aggregate, the elastic qualities of the mass must also be examined. Therefore, a more intensive treatment of analysis was given to core no. 2 of the TOTO cores as a pilot study, to include the determination of several elastic moduli by various techniques. This experiment will be performed on the remaining core samples and on ensuing samples.

### Elastic Moduli Experiments

The behavior of soil under seismic forces, vibrations, or dynamic loadings is dependent upon some soil properties and loading conditions. An experimental study on dry Ottawa sand and saturated calcium carbonate clay (core no. 2 of the TOTO cores) revealed some relationship and some validity to the elastic theory. From this study there is reason to believe that a field soil modulus type of test can be used to determine field sound velocities.

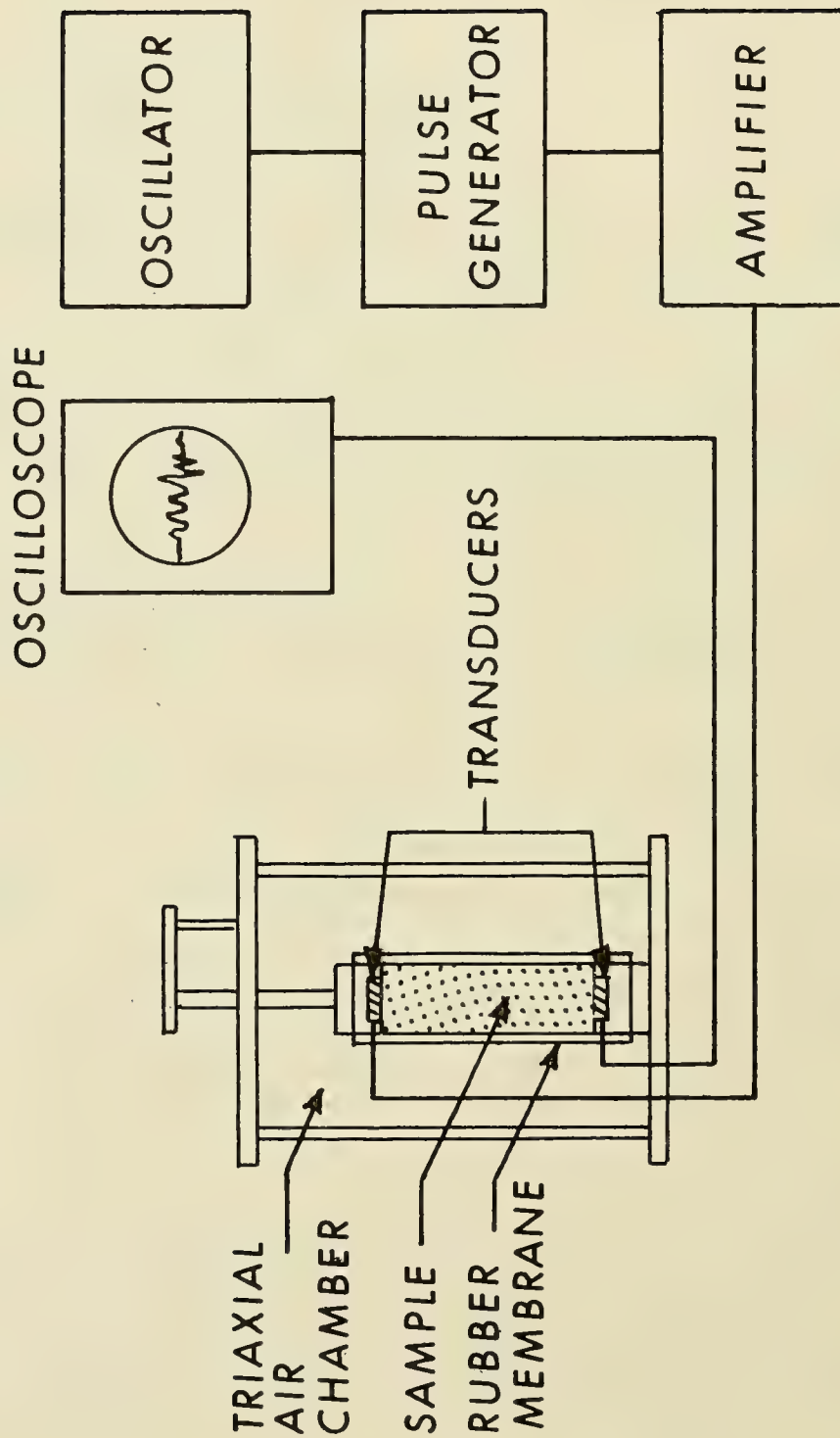


FIGURE 2 LONGITUDINAL WAVE VIBRATION APPARATUS



## Wave Velocity by Dynamic Loading

The stress conditions of a loaded elastic medium build up according to its stiffness and mass:

$$c = \left( \frac{E}{\gamma} \right)^{1/2}, \quad (1)$$

where

$c$  = wave velocity  
 $E$  = young modulus  
 $\gamma$  = mass density.

For usual soil types, the mass densities are relatively stable. Therefore, the variations of the soil properties affecting the soil modulus  $E$  would be expected to influence wave velocities. It should be noted that the applicability of an elastic theory to soil may be seriously questioned; yet, any system of particles may be considered elastic within the following limitations: (1) the volume of the specimen must be large in comparison to individual particle dimensions; (2) the stresses and strains considered average and small in value; and (3) the sample must be essentially isotropic. The wave velocity noted in Eq. (1) may be longitudinal or transverse. The longitudinal may be either a dilatation wave caused by a fully constrained sample or a rod wave for which deformation is allowed laterally. The transverse waves are shear waves and are slower. A second theoretical equation relates the resonant frequency of a mass to wave velocity and soil modulus:

$$c = 4 L f_n = \sqrt{\frac{E}{\gamma}}, \quad (2)$$

where

$f_n$  = resonant frequency  
 $L$  = length of sample

And finally we arrive at the correlation of the various moduli:

$$G = \frac{1}{2(1 + \nu)} E \quad (3)$$

$$M = \frac{(1 - \nu)}{(1 + \nu)(1 - 2\nu)} E \quad (4)$$

where

$G$  = modulus of elasticity in shear

$\nu$  = Poisson's ratio (0.5 for fully saturated soils under dynamic loading)

$M$  = constrained modulus of elasticity.

### Equipment

The longitudinal wave vibration apparatus is used to determine the soil modulus by utilizing a resonant frequency technique. The wave forms are displayed on the oscilloscope.

For the torsional wave vibration apparatus, Fig. 3, a loudspeaker is mechanically attached to rotate a pedestal in torsion. The sample is placed on the pedestal and phonograph cartridge pickups are placed in contact with the top and bottom of the sample and connected to the oscilloscope. The resonant frequency in shear is obtained by varying the frequency to obtain the maximum torsional displacement output in comparison to the input.

### Results and Discussion

#### a. Dry Ottawa Sand

From a test series on dry Ottawa sand, the variation of longitudinal wave velocity with confining pressure, void ratio, length-diameter ratio and lateral constraint was determined.

In each test, the Ottawa sand was confined in a thin rubber membrane, and sound velocities were determined as shown in Fig. 4. This series of tests also revealed the reduction in velocity due to increased side friction of the longer samples. (A separate short study of sound velocities in samples confined in steel tubes with varying degrees of skin roughness also confirmed the fact that wave propagation is reduced by side friction.)

Curve "C" represents an Ottawa sand sample confined in a rather stiff rubber tube within the air chamber. This might be considered anisotropic consolidation with resultant reduction in velocity.

Some of the specimens were tested first at high pressure and later at low pressures with little correlation to the virgin pressure-velocity line. This undoubtedly reflects the over-consolidation effects found in consolidation and shear tests.

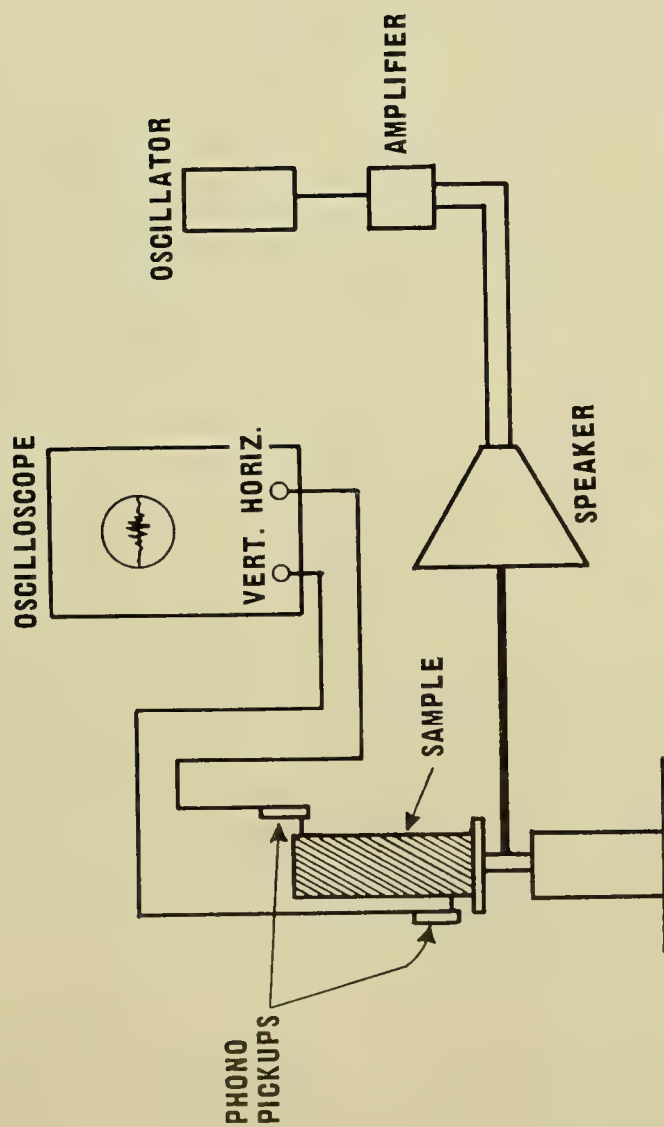


FIGURE 3 TORSIONAL WAVE VIBRATION APPARATUS

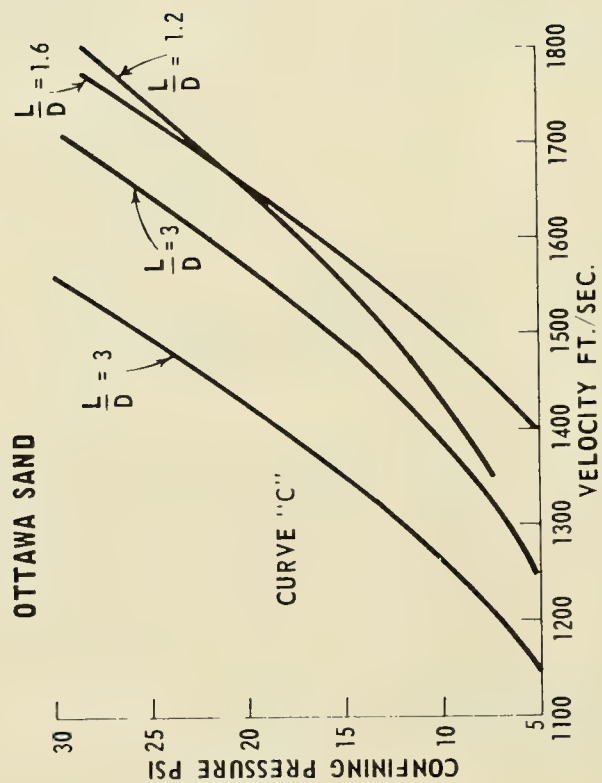


FIGURE 4 SOUND VELOCITY AS A FUNCTION OF LENGTH-TO-DIAMETER RATIO AND CONFINING PRESSURE-OTTAWA SAND

Some further work on a finer Ottawa sand were in fair agreement although of somewhat faster velocity. This is probably due to a lower porosity rather than smaller grain size.

Summarizing the work on dry Ottawa sand, we find that the void ratio or porosity exerts the principal effect on sound velocity, which for normally consolidated samples is a manifestation of the confining pressures.

#### b. Saturated Calcium Carbonate Clay Size Samples

A series of tests on core no. 2 of the TOTO cores, including static confined compression (consolidation), static triaxial shear tests, torsional vibration tests, and sound velocity tests, were performed on a saturated calcium carbonate clay in order to reveal any correlation of the various soil moduli, Fig. 5. Table 1 presents the numerical data associated with Fig. 5. It is known that soils stressed rapidly can exhibit properties quite unlike those observed under static conditions. Further, in this series, because of the limitations of the equipment, some of the moduli were entirely constrained, some unconfined, and some isotropically confined. Nevertheless, the results are quite informative and interesting.

#### c. Static Confined Moduli

The compression moduli determined from a drained consolidation test were quite low since strains are relatively large. These values, as shown in Fig. 5, are many orders of magnitude away from the seismic moduli and, except for the lateral confinement, bear little resemblance to the behavior under seismic pulses.

#### d. Triaxial Shear Test

The modulus of an isotropically confined triaxial sample is determined by applying an axial stress undrained. The separation of the elastic strain from the secondary strain or creep is desirable. The method used was a repetitive axial loading and unloading until a constant relation of stress to strain was obtained (Fig. 6). This can be considered the static modulus of elasticity. The clay triaxial samples were consolidated in steps from 1.5 to 2 psi before the axial pressures were applied; the resulting moduli vary almost linearly with confining pressure.

#### e. Torsional Vibration

This device, similar to that used by the investigators Wilson and Dietrich (1960) was used to obtain the resonant torsional frequency. The samples used were entirely unconfined and saturated and had been previously consolidated to some confining pressure. The dynamic torsional modulus,



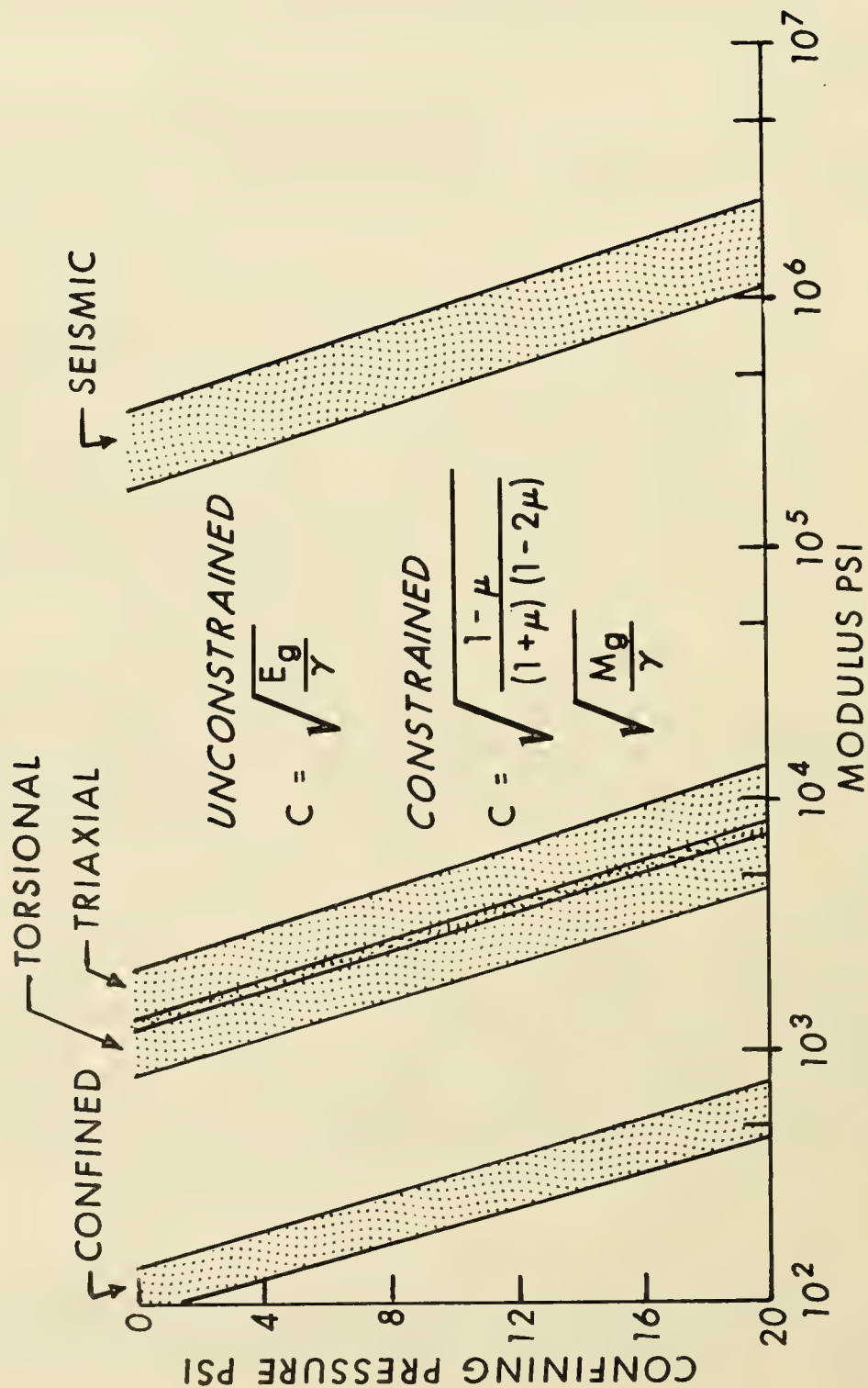


FIGURE 5 ELASTIC MODULI DETERMINATIONS FROM VARIOUS TESTS—  
CALCIUM CARBONATE CLAY

Table 1

NUMERICAL VALUES USED IN CONSTRUCTING  
ELASTIC MODULI CURVES OF FIG. 5

Consolidation Pressure psi	Water Content	$M_s$	Modulus of elasticity psi				$M_d (10^3)$	$C$ ft/sec.
			$E_s$	$G_d$	$E_d$			
1.5	56.2	--	---	338	---		---	---
1.75	56.0	--	1610	---	1600		200	3400
2.0	54.2	--	720	---	---		---	---
2.5	53.0	--	2300	---	---		---	---
4.0	51.3	183	---	---	2400		300	4600
7.1	50.0	--	3220	1150	---		---	---
7.1	49.8	--	3940	---	---		---	---
8.0	49.8	262	---	---	4000		500	4860
14.2	48.4	--	6390	2362	5200		650	5480
14.2	46.2	--	---	4700	8050		1000	6800
16.0	47.0	345	---	---	---		---	---
21.0	46.5	--	8380	---	---		---	---

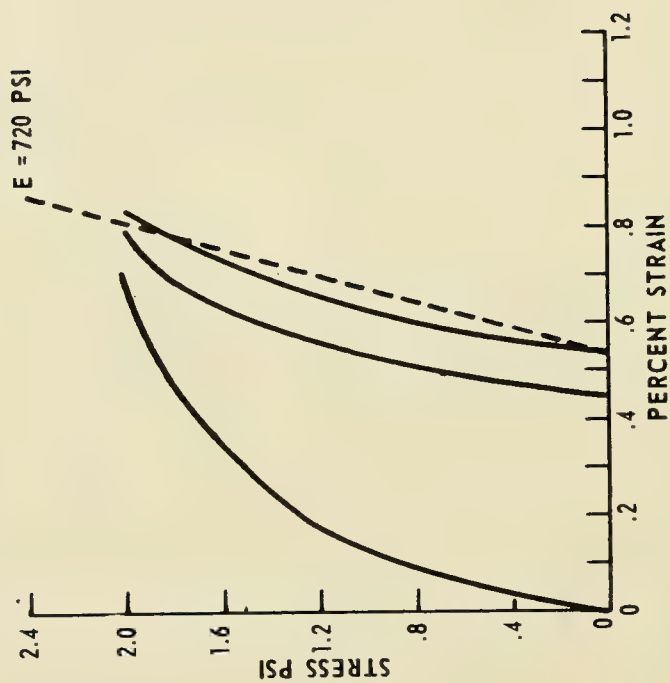


FIGURE 6 STATIC ELASTIC MODULUS FROM TRIAXIAL SHEAR TEST—CALCIUM CARBONATE CLAY

$$G_d = \frac{16 f_s^2 L^2 \gamma}{g}$$

is obtained from the resonant frequency, and the dynamic elastic modulus,

$$E_d = \frac{2 (1 + \nu)}{G_d} ,$$

is computed from the measured  $G_d$  and Poisson's ratio, which was assumed to be 0.5 for undrained saturated clays. The plots of dynamic elastic modulus  $E_d$  obtained in this manner compare fairly well with the static elastic modulus  $E$  of the triaxial test. Future tests planned for the torsional apparatus will utilize samples confined in thin rubber membranes, with an internal vacuum providing a more positive confining pressure. At the low confining pressure the curves for the dynamic and static moduli are almost superimposed. Perhaps this is the reason for the favorable comparison. This question will be explored further.

#### f. Seismic Wave Velocity

The observed seismic velocity determined from the sweep speed of the trace across the oscilloscope is used to compute the modulus either from

$$c = \sqrt{\frac{E g}{\gamma}}$$

or

$$c = \sqrt{\frac{1 - \nu}{(1 + \nu) (1 - 2\nu)}} \sqrt{\frac{E g}{\gamma}} = \sqrt{\frac{M g}{\gamma}}$$

Because of the dynamic effects, the relationship between wave velocity and modulus lies somewhere between unconstrained and fully constrained, probably closer to fully constrained. Completely saturated materials have a high constrained modulus because water is not able to drain and its bulk modulus is  $3 \times 10^5$  psi. Other investigators have reported saturated constrained moduli ranging from  $1 \times 10^5$  to  $1 \times 10^6$  psi.

#### g. Relation Between Unconstrained and Constrained Moduli

Theoretically a constrained modulus may be obtained from an unconstrained modulus.

$$M = (E) \frac{1 - \nu}{(1 + \nu) (1 - 2\nu)}$$

For fully saturated or nearly saturated samples this relationship is too sensitive to slight variations of Poisson's ratio to be useful. For instance the proper relationship between  $M$  and  $E$  in these tests result in  $\nu = 0.495$ . A true test to the relation between the various moduli would have to come from dry or partially saturated samples of known Poisson's ratio. Sediment samples are rarely completely homogeneous, and therefore a range of moduli results.

### Conclusions Drawn from Moduli Tests on the Clay Samples

The following conclusions can be drawn from this study:

- a. The stress-strain relationship for static and dynamic loading for confined or unconfined soil samples is considerably influenced by the void ratio or confining pressures.
- b. Young's modulus for soil may be determined by static triaxial tests or dynamic vibration test.
- c. The theoretical relationship between constrained modulus and unconstrained modulus  $E$  may be quite valid, but requires further investigation.
- d. In the determination of field sound velocity within a homogeneous strata, the propagation of the acoustic wave should be primarily the function of void ratio or confining pressure, and a short term field load or penetration test should be a valid indicator of the velocity.

### Structural Properties

Vertical profiles of several engineering properties, sound velocity, and impedance for TOTO cores 5 and 6 are shown in Figs. 7 through 9. The numerical data are presented in Tables 2 and 3. The lithologic structure of the cores, based upon Shepard's triangular diagram are shown in Fig. 1. A plot of these structural features indicates that there is a predominant advancing of coarse material from the northwest and later regression.

Note the trend toward increasing sound velocity with depth, which is similar to that of the moduli with increasing pressure. The velocity profiles then indicate that factors other than the void ratio, or confining pressure, are affecting the sound velocity. Note also that core no. 6 does not reveal an apparent reason for the large increase in velocity in the 3- to 4-foot layer. Similarly, these properties are affecting the elastic moduli. Therefore, the object of immediate concern is to determine the relationships between the engineering properties and the elastic moduli of the saturated marine sediments.



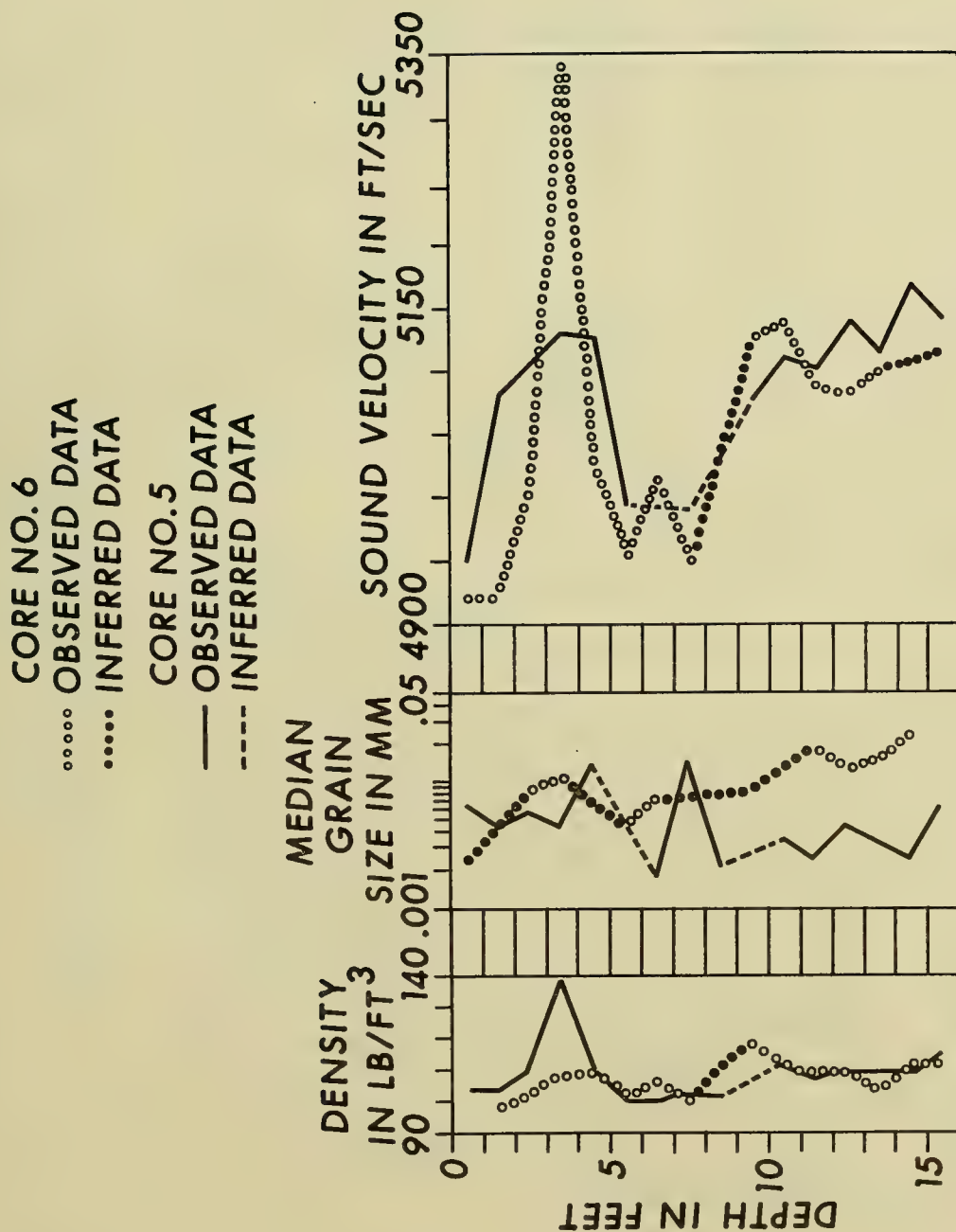


FIGURE 7 VERTICAL VARIATIONS IN DENSITY, MEDIAN GRAIN SIZE AND SOUND VELOCITY WITH DEPTH

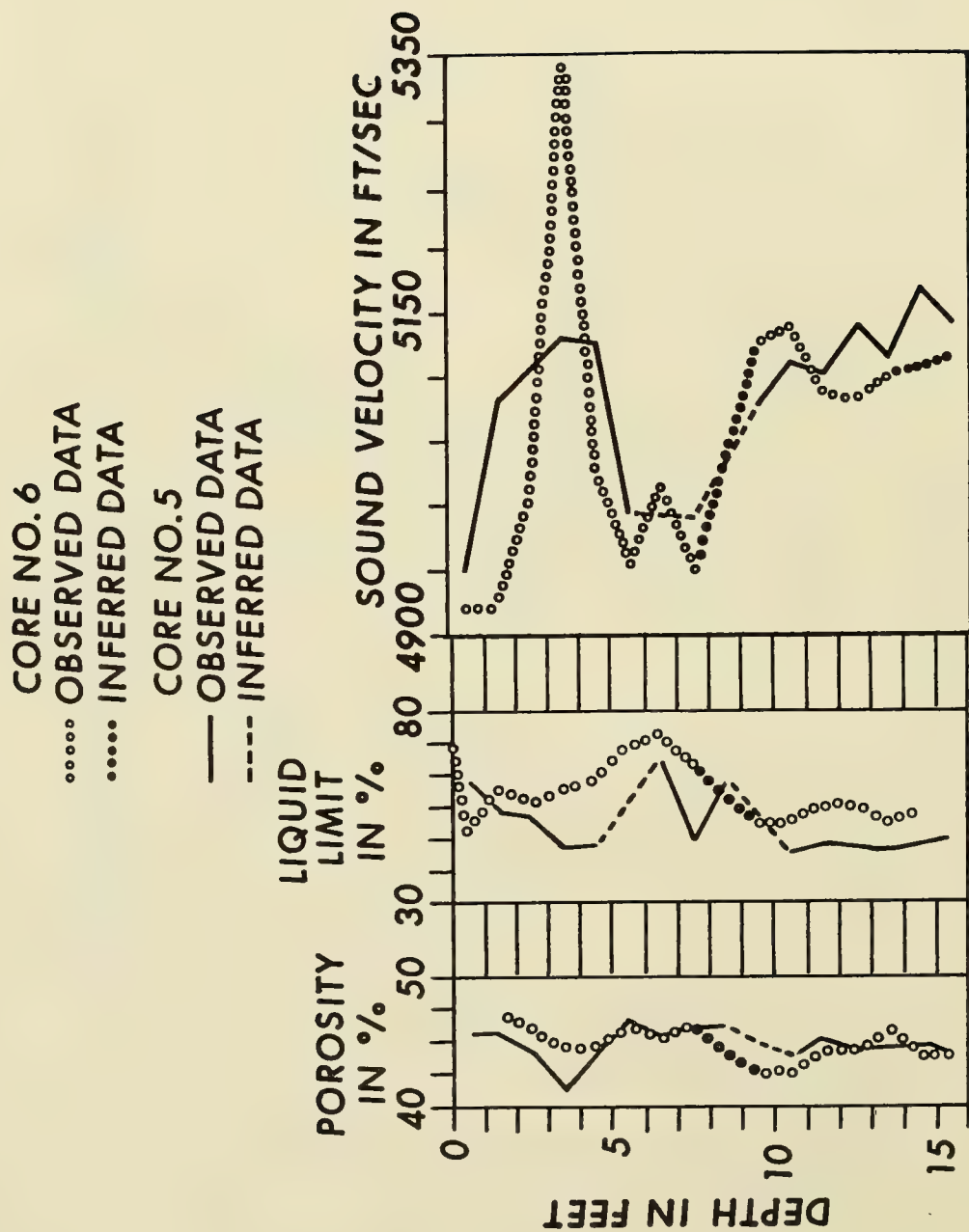


FIGURE 8 VERTICAL VARIATIONS IN POROSITY, LIQUID LIMIT AND SOUND VELOCITY WITH DEPTH

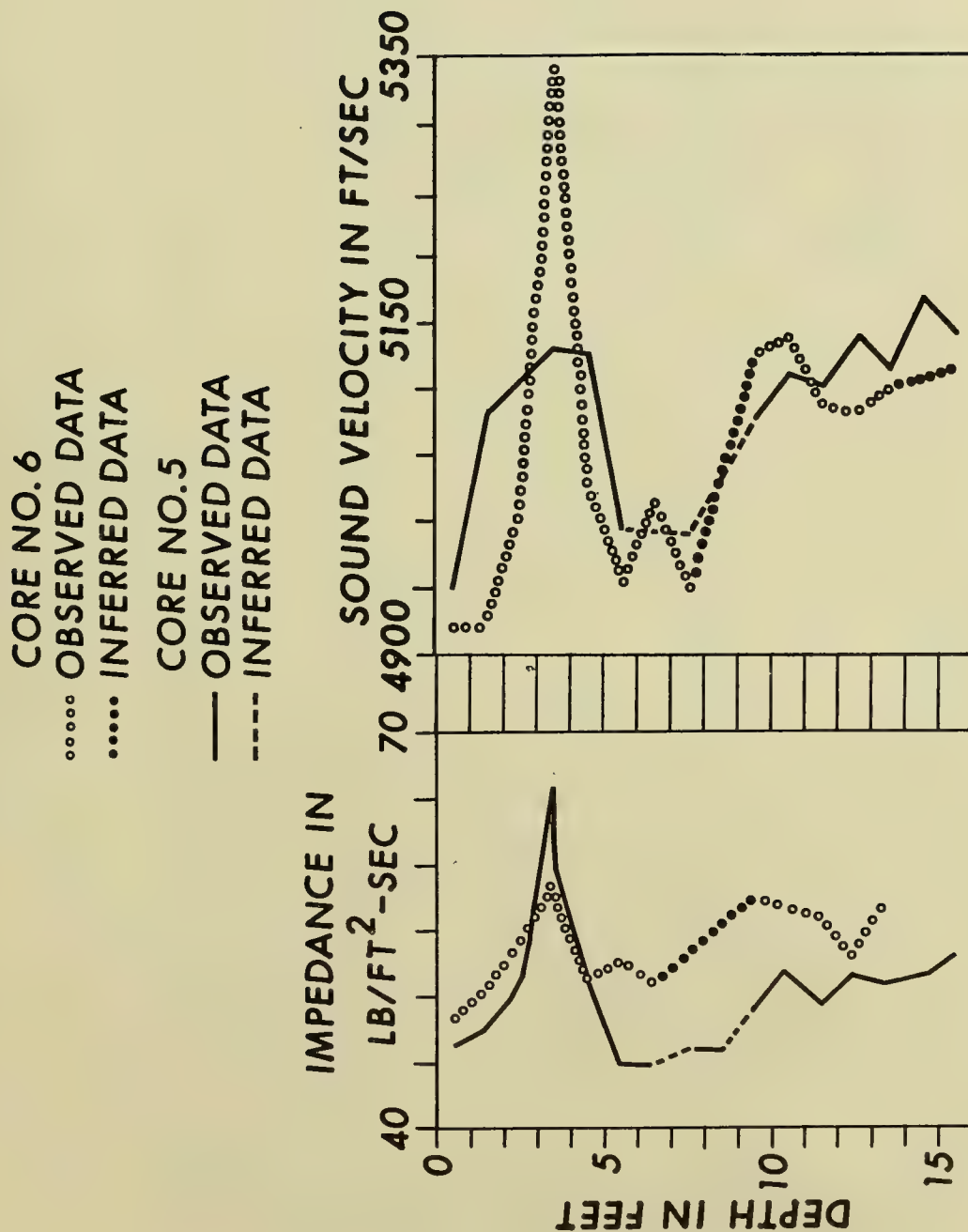


FIGURE 9 VERTICAL VARIATIONS IN SOUND VELOCITY AND IMPEDANCE WITH DEPTH

Table No. 2 - PHYSICAL PROPERTIES DATA - Core No. 5

Latitude	24° 21' N																	
Longitude	77° 31.3' W																	
Topo Feature	Flat narrow basin																	
Water Depth	810 fathoms																	
Sample Method	2300 lb. Ewing Corer, Piston Type																	
Sample Thickness	16 feet																	
Pos. of Layer	0-1	1-2	2-3	3-4	4-5	5-6	6-7	7-8	8-9	9-10	10-11	11-12	12-13	13-14	14-15	15-16		
Sand %	13	18	16	15	21		13	21	17		11	14	17	11	14	15		
Silt %	48	44	45	47	49		36	48	34		45	40	47	44	40	50		
Clay %	39	38	39	38	30		51	31	49		44	46	36	45	46	35		
Organic %	0	→																
Sort. Coef.	6.73	5.71	1.77	5.90	5.9		6.156	5.89	8.54		7.07	5.345	5.85	4.071	5.35	5.35		
Med Grain Diam (mm)	.0065	.0046	.0056	.0045	.0135		.0017	.014	.0022		.0034	.0025	.0042	.0033	.0025	.0065		
Grain Density																		
Wet Density #/ft <sup>3</sup>	104	104	110	138	110	100	100	102	102		111	107	110	110	110	113		
Spec. Gravity	2.8	→																
CO <sub>2</sub> Cont. %	100	→																
Water Cont. %	60.1	58.9	47.8	29.8	47.07	70.3	70.9	64.9	64.7		44.7	54.6	47.6	48.7	48.1	43		
Saturation %	100	→																
Porosity %	63	62	57	45.5	57	66	61	64.7	64.4		55.5	60.5	57	57.5	57.5	54.2		
Liquid Limit %	59.2	49.8	46.75	37.80	38.20		65.60	38.20	59.20		35.30	38.90	36.90	35.60	39.00	40.40		
Plastic Limit %	33.15	37.54	48.71	Gran	29.30		42.00	36.16	41.05		28.45	32.87	30.28	31.04	30.58	31.99		
Void Ratio	1.68	1.65	1.34	.84	1.32	1.97	1.98	1.82	1.81		1.25	1.53	1.33	1.36	1.35	1.2		
Soil Type	Clay Silt	Clay Silt	Clay Silt	Clay Silt	Clay Silt		Silty Clay	Clay Silt	Silty Clay		Clay Silt	Clay Silt	Clay Silt	Clay Silt	Clay Silt	Clay Silt		
Snd Vel, Long ft/sec	4950.7	5077.8	5102.9	5130.5	5126.5	4997.4		4991.0		5079.9	5110.2	5103.8	5140.7	5116.1	5168.8	5142.2		
Impedance	51.49	52.81	56.13	70.80	56.39	49.97		50.91		54.35	56.72	54.61	56.55	56.28	56.86	58.11		

Note: The figures in the impedance line should be multiplied by 10<sup>4</sup> lb/ft<sup>2</sup>.sec.

Table No. 3 - PHYSICAL PROPERTIES DATA - Core No. 6

Latitude 24° 21' N  
 Longitude 77° 30.9' W  
 Topo Feature Flat narrow basin  
 Water Depth 810 fathoms  
 Sample Method 2300 lb. Ewing Corer, Piston Type  
 Sample Thickness 15 feet

Pos. of Layer	0-1	1-2	2-3	3-4	4-5	5-6	6-7	7-8	8-9	9-10	10-11	11-12	12-13	13-14	14-15
Sand %	21		32	32		28	30			31		34	32	33	30
Silt %	51		61	63		53	56			63		66	66	67	70
Clay %	28		7	5		19	14			6		--	2	--	--
Organic %	0	→													
Sort. Coef.															
Med Grain Diam (mm)	.0022		.0086	.01		.0044	.0070			.0086		.018	.013	.015	.024
Grain Density															
Wet Density #/ft <sup>3</sup>	98.2	102.8	108.6	109.0	102.3	106.4	101.5		118	112.2	110.5	110.3	104.0	112.2	113.0
Spec. Gravity	2.8	→													
CO <sub>2</sub> Cont. %	100	→													
Water Cont. %	76.2	64.1	48.9	50.2	64.3	56.2	67.1		35.9	45.4	47.4	48	60.2	45.2	43.5
Saturation %	100	→													
Porosity %	68	64.2	58	58.4	64.3	61	65		50	50	57	57.2	62.7	56	55
Liquid Limit %	32.21	46.31	42.50	44.62	48.76	57.46	62.85	52.51	62.44	34.68	35.01	39.49	39.61	35.59	37.96
Plastic Limit %	38.92	34.14	31.24	32.07	32.27	40.33	39.70	37.79	37.79	29.48	31.19	31.85	30.89	31.36	29.02
Void Ratio	2.13	1.79	1.37	1.4	1.8	1.57	1.88		1.01	1.27	1.33	1.34	1.69	1.26	1.22
Soil Type	Sand Clay		Sandy Silt	Sandy Silt		Sandy Silt	Sandy Silt			Sandy Silt (shells)		Sandy Silt	Sandy Silt	Sandy Silt	Sandy Silt
SndVel, Long ft/sec	4922.6	4924.6	5006.4	5344.3	5029.0	4954.0	5015.6	4949.9		5123.4	5138.6	5085.2	5082.2	5097.4	5114.1
Impedance	48.34	50.62	54.37	58.25	51.45	52.71	50.91			57.48	56.78	56.09	52.85	57.19	

Note: The figures in the impedance line should be multiplied by 10<sup>4</sup> lb/ft<sup>2</sup>-sec.



Towards this end it is intended to artificially sediment core samples with known grain sizes, grain shapes, and mineral characteristics in the cohesionless and cohesive soil types. If these properties are held constant, the normality and temperature of the receiving water will be varied to obtain differences in settling characteristics and, therefore, structure. Also, the degree of sorting will be varied to obtain varying degrees of stiffness. These samples will then be subjected to the various tests for determinations of the moduli. An interesting experiment in this regard will be to determine the moduli while holding the void ratio constant and varying the confining pressure.

Essentially, the measure of compressibility reveals the relative ability of the soil to resist shear. Measurements of shear strength then should be linked with those of elastic moduli. Looking at the associated data required for effective shear strength measurements, such as void ratio, friction coefficient, over-consolidation ratio, temperature, strain and rate of strain, and cohesion, it can be seen that these properties are very similar to those required for interpreting moduli measurements. Therefore, it can be inferred, at this time, that a shear strength determination would be the most effective single indicator of the elastic moduli and, thus, longitudinal sound velocity. The shear strength also can be related to shear velocity.

This study may lead to a more intensive investigation of the cohesive or physio-chemical characteristic of the fine grained sediments and its relationship to acoustic behavior.

## CONSIDERATION OF BEHAVIORAL CHARACTERISTICS

It was noted in several of the Bermuda cores that the median grain size determinations revealed a predominantly silt layer, whereas the atterberg tests indicated that the sediment aggregate behaved like a clay. The degree of deflocculation of the fine silt and clay particles can not always be accurately determined. This usually results in larger particle diameter size than that which actually exists. Also, inaccuracies are inherent in the application of Stokes' Law to this measurement, since the particle shape is assumed to be spheroidal. Perhaps we should focus our attention on the behavioral characteristics of the sediment mass. Should we explore the action and reaction between the acoustic wave stress and the soil particle as a contributing factor in energy absorption? It is the opinion of the authors that this well may be the most fundamental approach to the problem, and therefore we shall attempt to devote some study to the cohesive characteristics of the sediments. Since little absorption occurs in the cohesionless sediments, perhaps this approach is justified.

When the subject of pore water in the clay aggregate is discussed, is the double layer water, which may occupy a large portion of the volume of the aggregate, considered? It is quite likely to assume that this water will not subscribe to the alteration of temperature and pressure when the sample is raised to the surface, as

per Wilson's tables, in predicting in-situ sound velocity in the pore water. The double layer water phenomenon may be more influential in acoustic energy absorption than we have imagined.

## MATHEMATICAL MODEL DISCUSSION

The data obtained from the laboratory and in-situ measurements are being submitted to the multi-layered mathematical model for determination of reflection coefficients. These results will then be compared with the field acoustic measurements over the same bottom.

The primary data inputs to the model are density, velocity, and layer thickness, where the layer thickness refers to that of the acoustic impedance layer. It should be noted here that the lithologic strata in the sediment column do not necessarily correspond to the acoustic impedance strata. In order to determine the impedance values we must know the values of sound velocity. This has not been a readily measurable quantity and, for the most part, has been inferred from the engineering properties of the sediment. The value of the absorption coefficient is required and has been estimated using Shumway's data (1960) as a guide. Use of the first-power frequency dependence, as recommended by B. F. Cole (1964), has compared favorably with the field acoustic data. By utilizing these data we then compute the reflection coefficients.

In the Bermuda area study the sound velocity values were obtained from the table of estimated values and were used to compute the impedances. The model derived amplitude reflection coefficients were then compared with those from the corresponding field acoustic test. At the large incident angles, where the depth of acoustic penetration is approximately comparable to the core lengths, the curve fit was fairly close, Menotti, et al., (1965). However, it is felt that there is insufficient geological data to effectively describe the insonified area of the bottom.

## SUMMARY

The motivating factor in undertaking this investigation is to obtain significant behavioral relationships between geological and acoustical properties of the soil mass which will lead to development of a predictive capability of acoustic energy loss in bottom bounce sonar operations, based upon ocean bottom environmental data. To this end our approach is to thoroughly examine small, smooth areas of the bottom, thereby eliminating extensive horizontal variations in lithology and reverberation effects caused by a rough surface. The data gathered will be used as inputs to the multi-layered mathematical model which assumes a smooth bottom interface.

It appears that the state of the art of soil science in the marine sediments prevents proclamation of precision analysis and, thus, prediction of acoustic energy

loss over an extended area. Initially, we only hope to narrow the contributions to this loss by eliminating some secondary effects. Such a great deal of fundamental investigation into the physiochemical and behavior characteristics of the sediment aggregate within small areas of the bottom is required that one is not permitted the license to sample at widely scattered stations over a broad area and interpolate accurately the conditions existing between stations.

To increase the density of stations sampled per unit time and to eliminate the problems of pressure change caused by elevating bottom samples to the surface, disturbances during sampling, transportation, storage, etc., as now exists in many coring operations, consideration is being given to the use of in-situ density and water content measuring devices, a field shear strength apparatus, and in-situ acoustic probes. These measurements must be accompanied by core sampling (and laboratory analysis) for comparative purposes for some, as yet, undetermined period. The coring operation will be discontinued when the in-situ measurements are believed to be independently reliable.

Laboratory analyses and experimentation techniques will continue to provide the basic information concerning geologic-acoustic relationships. Shear strength measurements in the triaxial chamber will be made on all forthcoming core samples. The shear strength parameter may prove to be the most significant single measurement required in determining the geologic-acoustic relationships. Since deep ocean sediments possess some rigidity, we can expect some shear wave propagation to take place. Because of the relatively large amplitudes of the shear wave, absorption of this waveform may be a significant parameter to consider in studies of acoustic energy loss.

In the development of the laboratory analysis program we are working toward the inclusion of an intensive investigation of the dynamic properties of the saturated unconsolidated sediments. The results of a pilot study indicate that the stress-strain relationship for static and dynamic loading of confined or unconfined homogeneous soil samples is considerably influenced by the void ratio or confining pressures. This results in a general trend of increasing modulus with depth. However, variations occur in the vertical sound velocity profile in the non-homogeneous core samples, indicating that other parameters are influencing the sound velocity structure. Therefore, the object of primary concern is to determine the relationships between the geological properties and the elastic moduli. On the basis of the results of the pilot study, it is assumed that at the low confining pressures (overburden pressures) a Young's modulus can be determined by either a static triaxial or dynamic vibration test. If this assumption is indeed valid, then a transition zone exists in which we hope to develop valid experiments and techniques for dynamic testing of these saturated sediments.



## REFERENCES

- Hamilton, E. L. , Shumway, G. , Menard, H. W. , and Shipek, C. J. , 1956, Acoustic and other physical properties of shallow water sediments off San Diego. *Journal of the Acoustical Society of America*, v. 28, p. 1-15.
- Laughton, A. S. , 1957, Sound propagation in compacted ocean sediments. *Geophysics*, v. 22, p. 233-260.
- Sutton, G. , Berckhemer, H. , Nafe, J. E. , 1957, Physical analysis of deep sea sediments. *Geophysics*, v. 22, p. 779-812.
- Shumway, G. , 1960, Sound speed and absorption studies of marine sediments by a resonance method, *Geophysics*, v. 25, Part I, p. 451-467, Part II p. 659-682.
- McDonald, M. , 1965, (personal communication) General Dynamics, Electric Boat Division.
- Wilson, S. D. , Dietrich, R. J. , 1960, Effect of consolidation pressure on elastic and shear strength properties of clay, *Research Conference on Shear Strength of Cohesive Soils*, ASCE, p. 419-435.
- Cole, B. F. , 1964, Marine sediment attenuation and ocean-bottom reflected sound, *Journal of the Acoustical Society of America*, v. 36, no. 10, Oct. 1964. Abstract of paper presented at 68th meeting of the Acoustical Society of America.
- Menotti, F. R. , Santaniello, S. R. , and Schumacher, W. R. , 1965, Studies of observed and predicted values of bottom reflectivity as a function of incident angle, *USL Report No. 657*, 28 April 1965.





TEMPERATURE STRUCTURE IN THE TRANSITION REGION  
OF THE NORTH PACIFIC

by

Margaret K. Robinson

University of California, Scripps Institution of Oceanography  
La Jolla, California

and

John Northrop

University of California, Marine Physical Laboratory  
San Diego, California



# TEMPERATURE STRUCTURE IN THE TRANSITION REGION OF THE NORTH PACIFIC

by

Margaret K. Robinson  
University of California  
Scripps Institution of Oceanography  
La Jolla, California - 92038

and

John Northrop  
University of California  
Marine Physical Laboratory  
San Diego, California - 92152

## INTRODUCTION

The floating instrument platform, FLIP, was towed by the R.V. HORIZON to  $39^{\circ} 30'N$ ,  $148^{\circ}W$ , where she remained on station for 27 days, September 2 to 29, 1963.

This location (Fig 1), midway between the Hawaiian Islands, California, and Yakutat, Alaska, in the boundary region between the Subarctic and the Subtropics (Sverdrup, et al., 1946), was selected by Professor Walter Munk, Scientist-Director of the expedition. His primary purpose was to monitor surface waves in midocean in an attempt to track, from Australia to Alaska, ocean swell generated by storms in the South Pacific. Snodgrass, et al. (1965) have reported the results of this phase of the operation.

FLIP (Fig 2) is an ideal platform for monitoring the variability of the physical properties of the ocean, including internal and surface waves, (Fisher and Spiess, 1963). Her vertical motion is minimal. Rudnick (1964) has described in detail FLIP's response to wave motion. He reports behavior in accord with theory; hence, FLIP can be considered to follow the vertical motion of the sea surface very closely at all frequencies well below the resonant frequency (133 cycles per hour--27-second period). At higher frequencies, the total rms vertical displacement was of the order of 10 cms., even though she encountered storm winds of 20 m/sec and waves of 15 m, under whose battering the R.V. HORIZON rolled  $45^{\circ}$ .

The amplitude of the tides at this open ocean location are unknown. Tidal amplitudes in the Hawaiian Islands range between 1.6 to 2.5 feet. It is assumed that the tidal amplitude at FLIP's location is less than or equal to those in the Hawaiian area.

The program of oceanographic observations was planned to take advantage of the fact that FLIP would remain in approximately the same location for almost an entire month. She actually drifted a rhumb line distance of 47 nautical miles (87 kms) to the southwest ( $225^{\circ}$ ) at an average rate of 1.7 nm per day, though her true course was erratic and the total scaled track was 86 nautical miles (159 kms).

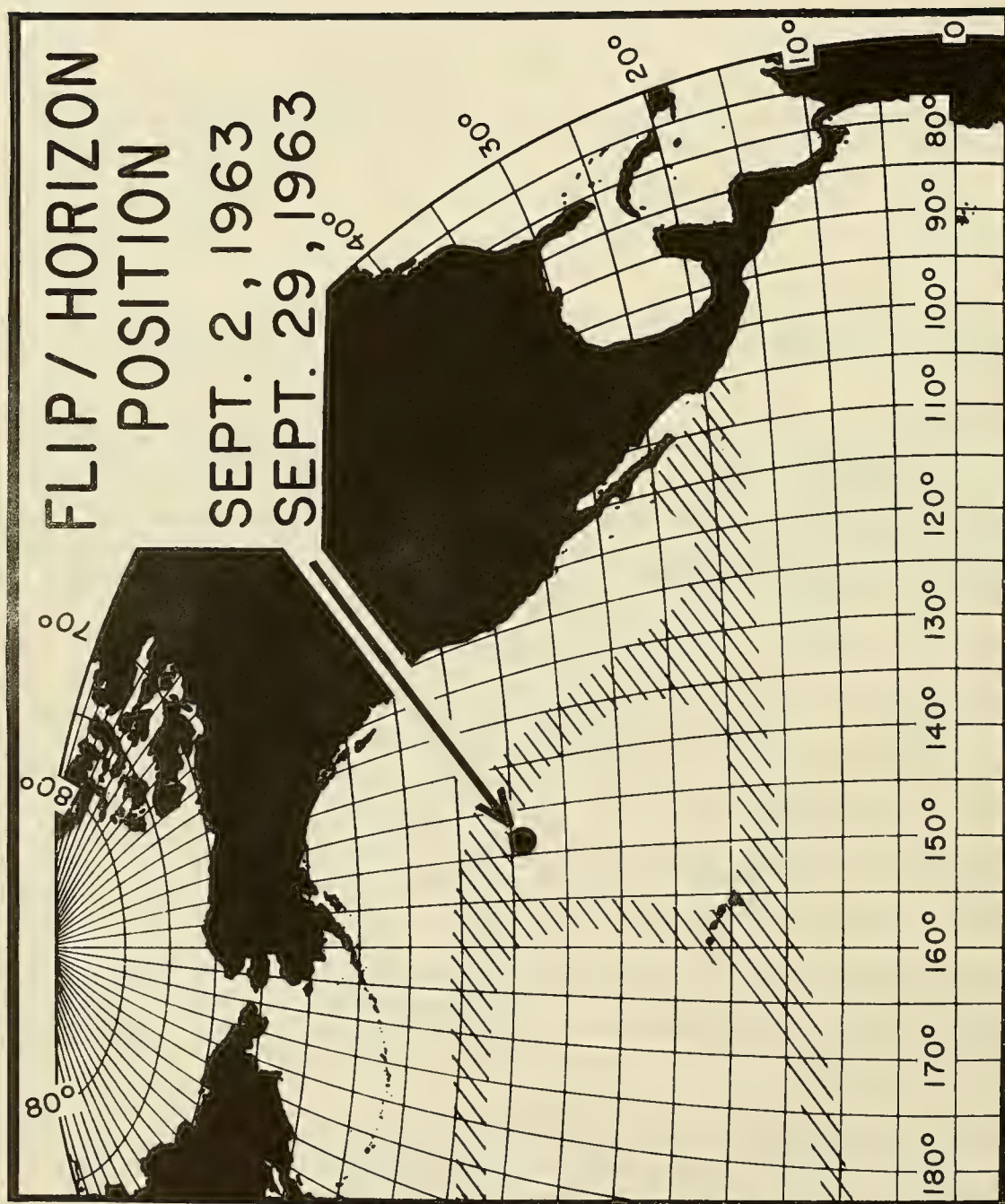


FIGURE 1 LOCATION CHART (WATER MASS BOUNDARIES AFTER SVERDRUP, ET AL., 1942)

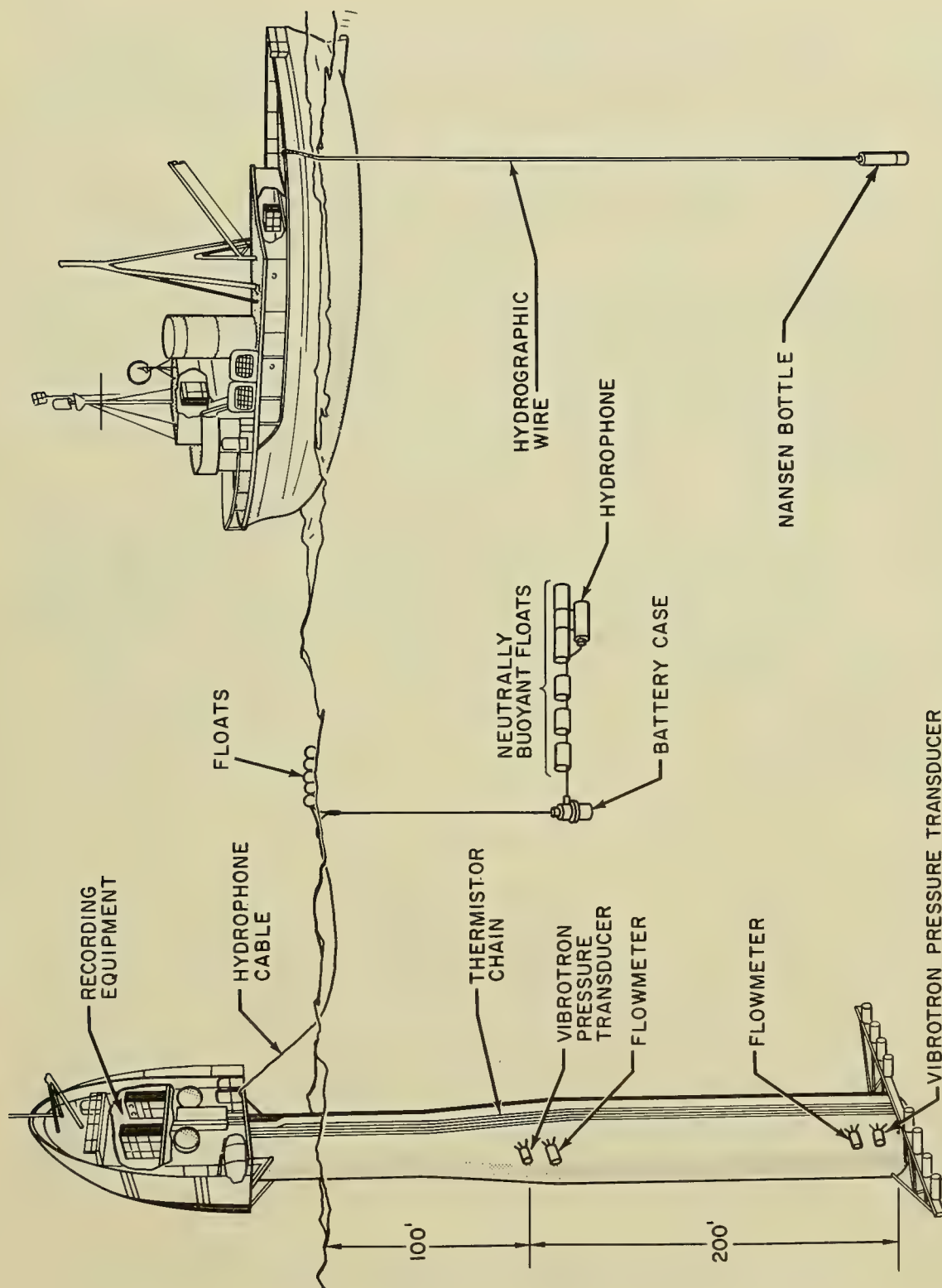


FIGURE 2 SCHEMATIC DIAGRAM OF FLIP IN VERTICAL POSITION, AND TOWING SHIP R.V. HORIZON



A thermistor chain was attached to FLIP with 30 thermistors located at 10-foot intervals between depths of 10 and 300 feet (3.3 and 91m). The thermistors were scanned at 6-minute intervals for periods of 18 hours a day, and at 50-second intervals for two 3-hour periods a day and for two 27-hour periods. Unfortunately, several breaks occurred in both the 6-minute and 50-second series.

From the R.V. HORIZON, 23 hydrographic casts were made--one each day except on September 5th and 10th when seas were too rough. The first two and the last casts were made to 1,200 meters; the others, to 600 meters. Salinity determinations were made aboard the R.V. HORIZON by use of the conductive-type salinometer developed at the University of Washington. Oxygen determinations were made by the Winkler method. Just prior to each cast, a bathythermograph (BT) temperature observation was taken so that the Nansen bottles might be arranged to sample more closely the layers where and when temperature inversions were present. A total of 1,004 BT observations were taken. These included an almost continuous hourly series from September 4th to 26th, and two 24-hour series taken at 10-minute intervals.

Only those aspects of the oceanographic program related to the variability of the temperature-depth structure and, indirectly, to the sound velocity-depth structure will be discussed here. They will include: (1) variability of the temperature-depth structure related to internal waves and to season; (2) results of the time-series analysis of the 6-minute thermistor-chain temperature record, including power spectra, auto-correlation functions, and time lag statistics of the oscillations of selected isotherms; (3) T-S curves and envelope of observed T and S values showing changes in T-S depth structure which produce a secondary sound channel at approximately 100 meters depth; and (4) implications of these observations for prediction of oceanographic parameters and for Navy operational and observational programs.

## DISCUSSION

The time variation in the temperature-depth (T-D) structure is illustrated by the selection of BT traces shown in Figure 3<sup>1</sup>. The three single traces in the top row indicate the three principal variants in the T-D structure encountered at FLIP's location: (1) no separation between seasonal and permanent thermoclines; (2) seasonal and permanent thermoclines separated by a 50-meter layer of almost isothermal water; and (3) a temperature inversion at the bottom of the seasonal thermocline.

In the last figure on the top row, traces 1 and 3 have been superimposed, indicating differences observed in a 4-hour period. The additional figures indicate, in time intervals of 20 minutes to 26 days, differences in depth

---

<sup>1</sup> Figures 3, 4 and 5 have been included in the text to take the place of the time-lapse movie of the hourly and 10-minute BT series presented at the Symposium.

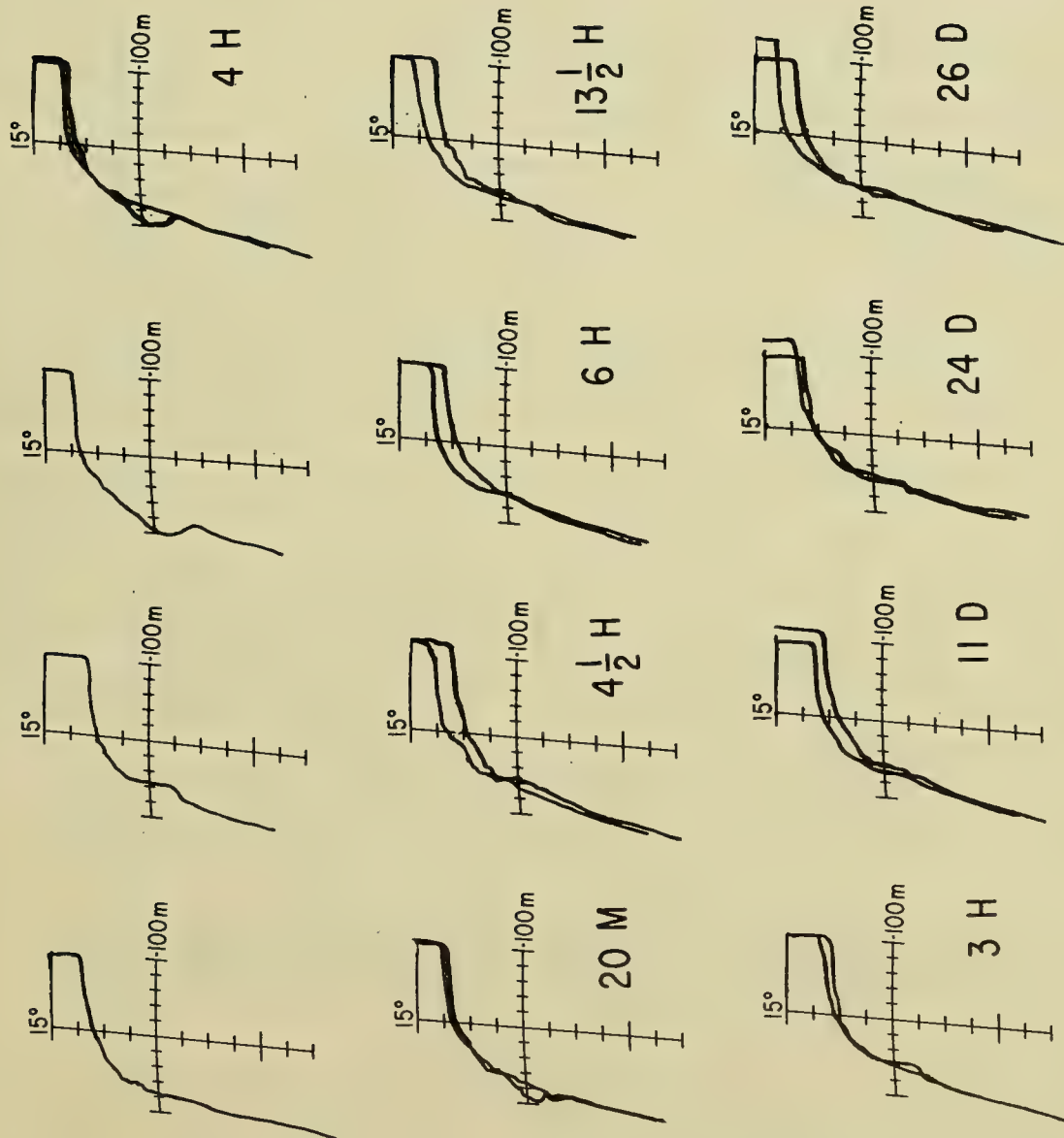


FIGURE 3 SELECTED BT TRACES SHOWING CHANGES IN TEMPERATURE-DEPTH STRUCTURE IN PERIODS OF 20 MINUTES TO 26 DAYS

of thermocline; changes of temperature between 75 and 125 meters due to the intrusion of cold or warm water; and minimum temperature differences below 125 meters. The last figure indicates differences in structure between the first and last BT observations, a time interval of 26 days, 3 hours, and a space interval of 47 nautical miles (84 km). The temperature in the isothermal layer decreased from  $21.0^{\circ}\text{C}$  to  $19.8^{\circ}\text{C}$  during the period of observation. Although the amplitude of the thermocline depth oscillations was almost the same on the first day as on the last, the mean depth of the thermocline increased from 84 to 102 feet between September 2nd and 28th.

The decrease of temperature in the isothermal layer, and the increase in mean depth of the thermocline are in agreement with the expected seasonal changes at this location during the month of September.

In order to convert the T-D variations into a continuous spectrum, the depths of occurrence of individual isotherms were read from the analog thermistor chain record. Figures 4 and 5 are plots of the selected isotherms for two periods of 30 hours, based on the 6-minute thermistor chain data record. The relation of the selected isotherms to the T-D structure is illustrated in Figure 6.

In these figures, no attempt has been made to indicate the existence of the temperature inversions shown in Figure 3, primarily because their full extent was not visible on the 300 foot (91 m) thermistor chain records. The appearance and disappearance of the temperature inversions, however, does appear, from the deeper BT observations, to be related to the low frequency internal waves which are clearly seen in Figures 4 and 5 at shallower depths.

These two sections of the total record were selected to illustrate that there were appreciable differences in the height of the low frequency internal waves at these two phases of the moon. The maximum height of the low frequency internal wave at the top of the thermocline, as shown by the oscillations of the  $20^{\circ}$ ,  $17^{\circ}$  and  $15.5^{\circ}$  isotherms, occurred at the time of the full moon (Fig 5). The height of the wave at the bottom of the thermocline was at near maximum at the three-quarter moon phase (Fig 4 and Table 1). The maximum height of the wave at the bottom of the thermocline, 110 ft., however, occurred on September 16th, one day prior to the time of the full moon. The height of the wave at the top of the thermocline at this period was only 48 feet.

The mean depth of the  $17^{\circ}$  isotherm was the same during the two periods but the standard deviation was larger during the full moon. The mean depth of the  $12.5^{\circ}$  isotherm was 35 feet deeper at full moon but the standard deviation was smaller at this time (Table 1).

Table 2 summarizes statistics of the depth variability of the 5 selected isotherms for the entire series. The standard deviation is least for the  $17^{\circ}$  isotherm--15.45 ft., and largest for the  $12.5^{\circ}$  isotherm--18.38 ft. The range of observed depths increases from 66 ft. for the  $20^{\circ}$  isotherm to 148 ft. for the  $12.5^{\circ}$  isotherm. Tables 1 and 2 indicate that variability of the

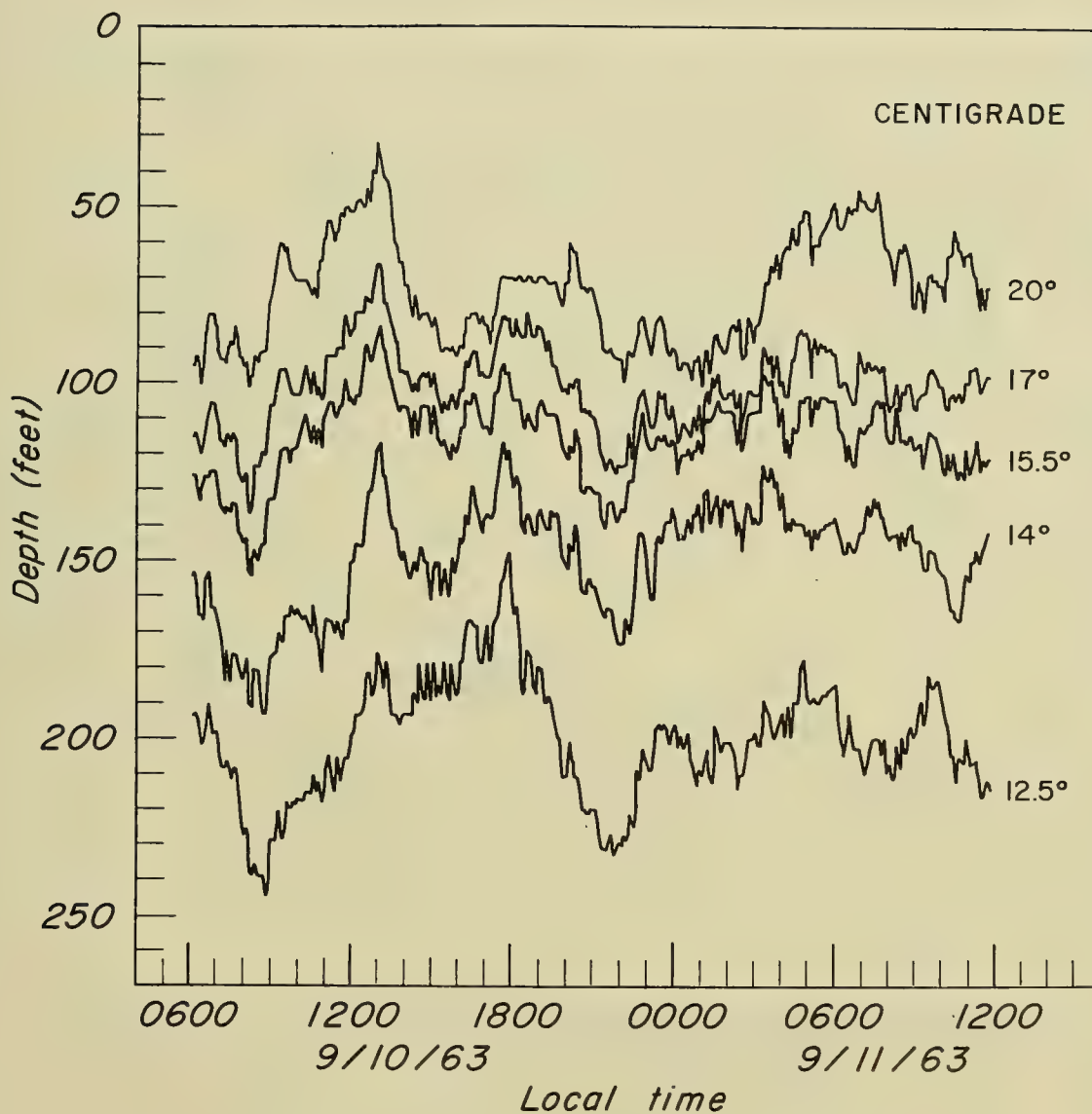


FIGURE 4 VARIATION IN DEPTH OF SELECTED ISOTHERMS,  
SEPTEMBER 10-11, 1963, BASED ON 6-MINUTE  
THERMISTOR CHAIN SERIES



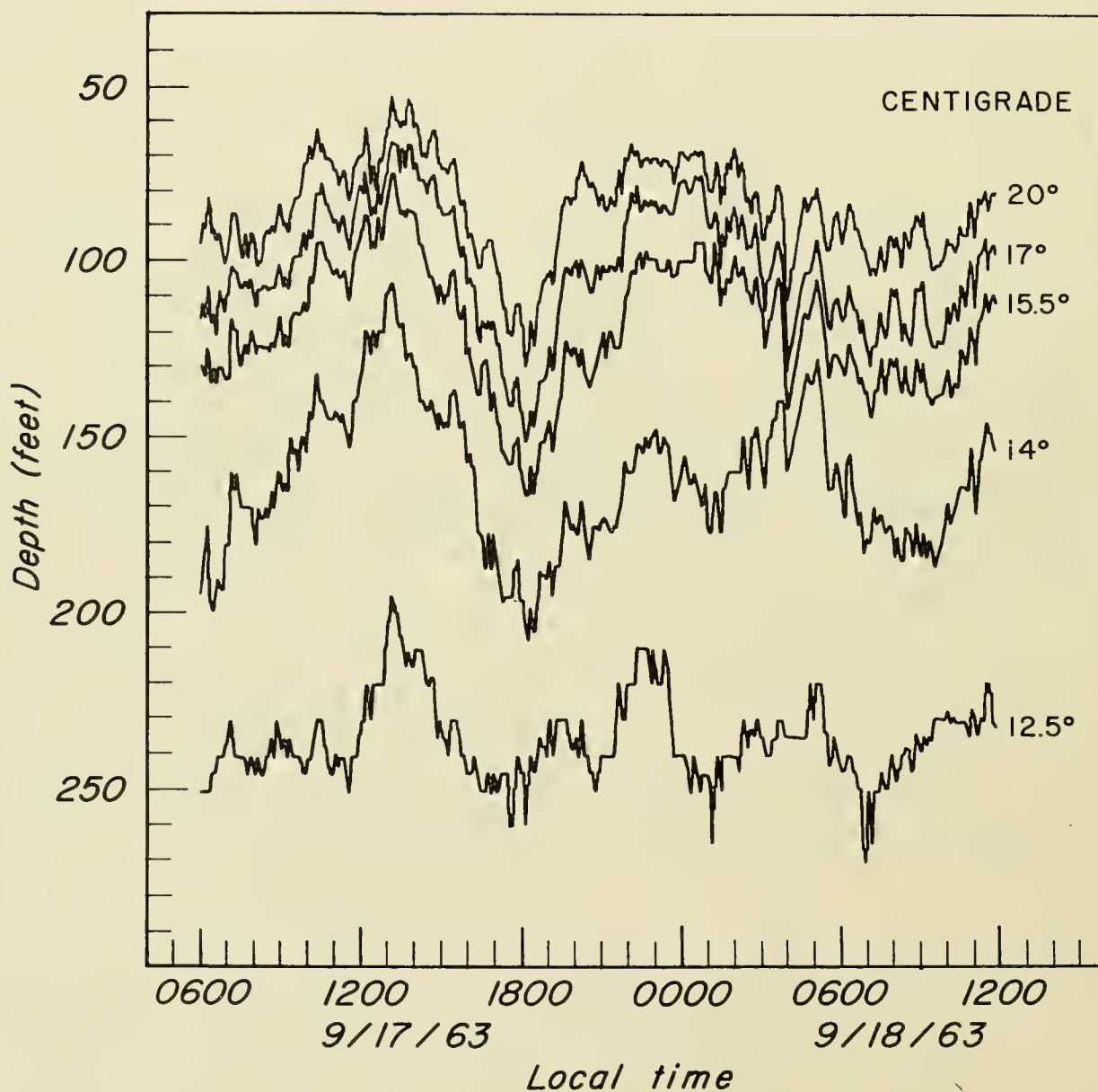


FIGURE 5 VARIATION IN DEPTH OF SELECTED ISOTHERMS,  
SEPTEMBER 17-18, 1963, BASED ON 6-MINUTE  
THERMISTOR CHAIN SERIES



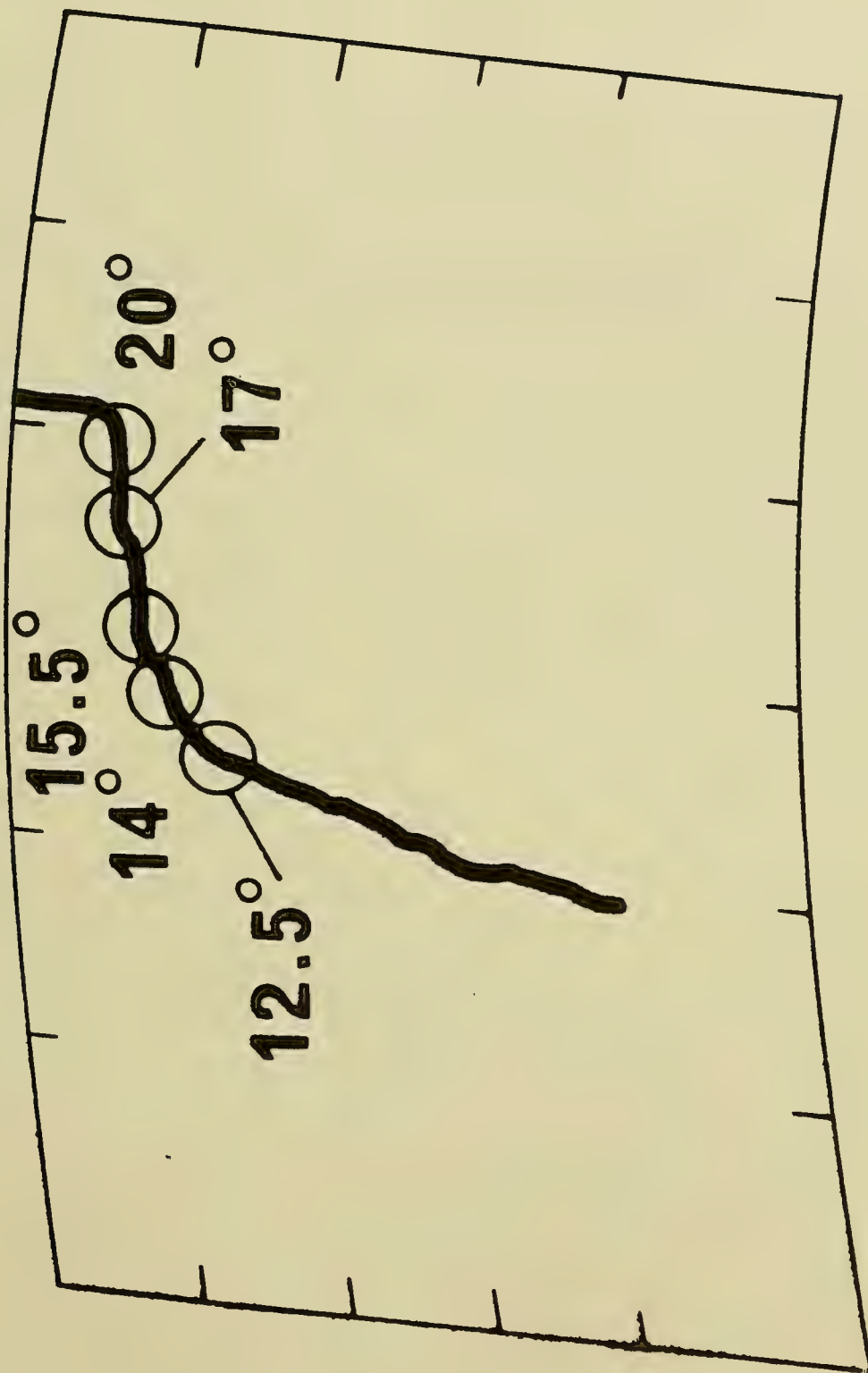


FIGURE 6 RELATION OF SELECTED ISOTHERMS TO TEMPERATURE-DEPTH STRUCTURE

TABLE 1

COMPARISON OF MEAN DEPTHS, STANDARD DEVIATIONS AND MAXIMUM  
INTERNAL WAVE HEIGHTS FOR THE  $17^{\circ}$  AND  $12.5^{\circ}$  ISOTHERMS

	<u>Sept. 10-11</u>	<u>Sept. 17-18</u>
	<u>Ft.</u>	<u>Ft.</u>
Mean depth $17^{\circ}$	101	102
Mean depth $12.5^{\circ}$	200	235
Standard deviation of depth of $17^{\circ}$	11.2	17.4
Standard deviation of depth of $12.5^{\circ}$	17.8	12.2
Maximum height of internal wave, $17^{\circ}$	65	85
Maximum height of internal wave, $12.5^{\circ}$	96	70
N	274	267

TABLE 2

STATISTICS OF VARIABILITY OF DEPTHS OF SELECTED  
ISOTHERMS, FROM 6-MINUTE SERIES

	$\frac{20.0^{\circ}}{\text{Ft.}}$	$\frac{17.0^{\circ}}{\text{Ft.}}$	$\frac{15.5^{\circ}}{\text{Ft.}}$	$\frac{14.0^{\circ}}{\text{Ft.}}$	$\frac{12.5^{\circ}}{\text{Ft.}}$
Mean	87.8	105.7	121.2	154.4	223.5
Standard deviation	16.15	15.45	15.54	16.48	18.38
Minimum	66	67	76	106	148
Maximum	141	157	172	207	300
Range	75	90	96	101	152
N	4762	4762	4762	4762	4749

depth of the selected isotherms in the two 30-hour samples were sometimes as great as the variability of the entire sample.

Although we do not fully understand the causes, by means of statistical time-series analysis, we are able to describe certain features of the temperature variability associated with internal waves.

The relatively complete 6-minute thermistor chain series of 5,332 observations extended from 0918 September 6, 1963 to 1624 September 28, 1963, a period of 22 days, 7 hours. These data have been analyzed to determine quantitatively the characteristics of both the low and high frequency internal waves which can be seen in Figures 4 and 5. Time-series computer analysis programs, developed at Scripps Institution of Oceanography by Bullard, Oglebay, Munk and Miller (1964), were used.

In Figure 7 are presented power spectra for the  $20^{\circ}$ ,  $14^{\circ}$  and  $12.5^{\circ}$  isotherms whose T-D relation is shown in Figure 6. The spectra for the  $17^{\circ}$  and  $15.5^{\circ}$  isotherms are essentially the same as that of the  $20^{\circ}$  isotherm and are omitted from Figure 7. High frequencies have been filtered from these spectra, the cutoff frequency being .5 CPH. The significant low frequency peaks occur at .08 CPH (the semi-diurnal tidal period) and at .055 CPH (the 18.6 hour inertial period at this latitude). For 90% confidence limits, the ratio of computed to true values for these spectra fall between 0.49 and 1.85

The ratio of the power in the semi-diurnal and inertial peaks to the total power in these spectra (Fig 7) and the amplitude of these peaks are given in Table 3. Amplitudes and ratios were summed over the peak and the two adjacent frequencies.

In the case of the  $14^{\circ}$  isotherm, the peak inertial frequency has shifted to the right to .06 CPH. There is no peak at any of the inertial frequencies on the  $12.5^{\circ}$  spectrum. There is, however, a small "blip" at .07 CPH on the shoulder of the semi-diurnal peak. When the three spectra of Figure 7 are considered together, there appears to be a shift in the inertial peak toward the high frequencies in the semi-diurnal peak. This shift may be an artifact caused by a diminution in the height of the inertial wave component as shown in Table 3 by the amplitude summed over the inertial frequencies for the  $12.5^{\circ}$  isotherm.

Defant (1940) reported a change in phase but no diminution of strength of inertial components of currents with depth in his discussion of the ALTAIR anchor station data in the Gulf Stream area north of the Azores ( $44.6^{\circ}\text{N}$ ,  $34.0^{\circ}\text{W}$ , 16-20 June 1938). His interpretation of the ALTAIR data was that the change in phase with depth indicated that the inertial oscillations were coupled with semi-diurnal internal waves. The FLIP data, on the other hand, show a diminution of amplitude of the inertial component but no systematic phase shift in the internal waves within FLIP's depth range, although, occasionally, both low and high frequency internal waves in the  $14^{\circ}$  and  $12.5^{\circ}$  series (located near the bottom of the thermocline) are out of

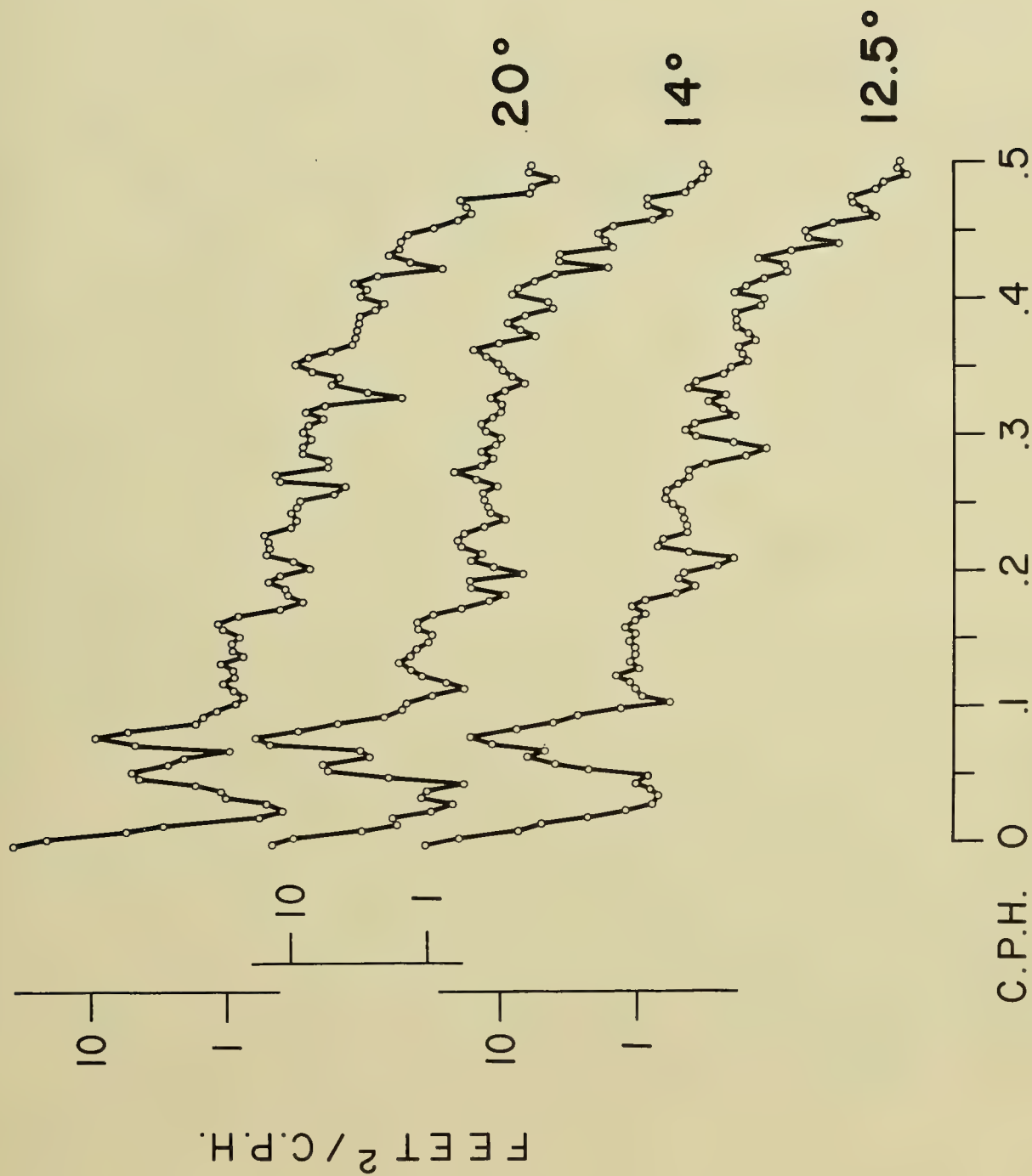


FIGURE 7 POWER SPECTRA OF DEPTH CHANGE OF SELECTED ISOTHERMS



TABLE 3

RATIO OF THE POWER IN THE SEMI-DIURNAL AND INERTIAL PEAKS TO THE  
TOTAL POWER AND PEAK AMPLITUDES. (POWER AND AMPLITUDES  
SUMMED OVER THE PEAK AND ADJACENT FREQUENCIES.)

	Semi-diurnal Freqs. (.075, .080, .085)		Inertial Freqs. (.050, .055, .060)	
	<u>Ratio</u>	<u>Amplitude</u>	<u>Ratio</u>	<u>Amplitude</u>
		Ft.		Ft.
20°	.14	8.8	.08	5.4
17°	.22	10.5	.06	5.8
15.5°	.29	12.0	.06	5.5
14°	.35	12.2	.10	7.1
12.5°	.20	10.6	(.04)	(4.6)*

\* No peaks, see text.

phase with the oscillations of the  $20^{\circ}$ ,  $17^{\circ}$  and  $15.5^{\circ}$  isotherms located in the main part of the thermocline.

A systematic phase shift of the inertial wave with depth would not alter the power spectra, nor cause the apparent frequency shift seen in Figure 7. Further analysis of the series will be carried out in an attempt to determine if the apparent frequency shift is real or artifact.

A power spectrum of the  $20^{\circ}$  isotherm was also computed for frequencies between 0 and 5 CPH without lowpass filtering. The area under the curve, in the low frequencies, .014 to .11 CPH (72 to 9-hr. periods) accounted for .65 of the total power. In the higher frequencies, between .11 and .4 CPH (9 to 2.5-hr. periods), there was .24 of the total power and between .4 and 5 CPH (2.5 hr to 12 min. periods), .11. There were several small but statistically non-significant peaks in the high frequencies between .42 and .12 CPH (2.4 and 8-hr. periods).

If the assumption is made that the semi-diurnal period internal waves revealed by the power spectra are progressive waves, a calculation based on the observed density distribution and on Fjeldstad's (1933) theory of internal waves would give a wave velocity of 92 cm/sec., and a wave length of 22 nm.

The auto-correlation functions for selected isotherms for lags between 6 minutes and 20 hours are shown in Figure 8. The three curves show sharp drops to minimum correlations at 6 hours, then increase to peaks between 12 and 13 hours. The values of the auto-correlation function in this peak range from 0.46 to 0.54. Not shown in the figure are the curves for the  $17^{\circ}$  isotherm, which is very close to that of the  $12.5^{\circ}$  isotherm, and the curve for the  $15.5^{\circ}$  isotherm which falls mid-way between the curves of the  $12.5^{\circ}$  and  $14^{\circ}$  isotherms. The dominance of the semi-diurnal period at all depths is clearly shown by these auto-correlation curves. It is also noteworthy that within two hours the correlation has decreased to values near 0.5, or approximately to those of the functions in the 12 to 13-hr. peak.

The variability of the depth of the thermocline is further demonstrated in Figure 9 by curves showing the percentage of occurrence of depth differences of the  $20^{\circ}$  isotherm computed for lags of 50 seconds to 1 hour. For a 50-second lag, 50% of the time there was no change in depth between observations. For a lag of 1 hour, 5% of the time there was no change, and 5% of the time the difference was greater than 25 feet.

From similar curves for the other selected isotherms, the percentages of time that the depth changes exceeded 25 feet for lags of 1 hour were as follows:  $17^{\circ}$ - 4%;  $15.5^{\circ}$ - 5%;  $14.0^{\circ}$ - 9%; and  $12.5^{\circ}$ - 7%. Statistical summaries of the lag differences for the selected isotherms are given in Tables 4, 5, 6, 7 and 8. Note that the standard deviations for lags of 1 hour are approximately one-half as large as the standard deviations computed for the entire series, listed in Table 2.

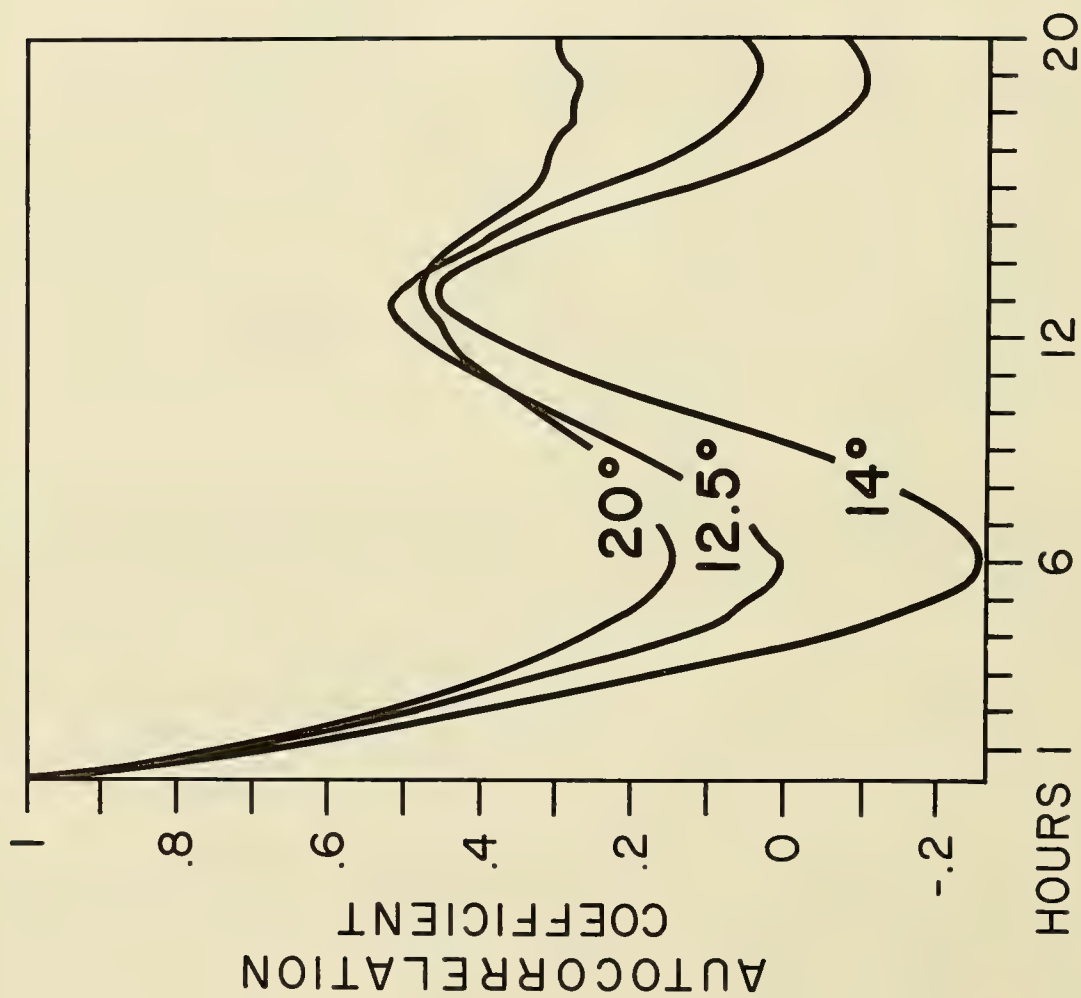


FIGURE 8 AUTO-CORRELATION FUNCTIONS OF DEPTH CHANGE OF SELECTED ISOTHERMS FOR LAGS OF 6 MINUTES TO 20 HOURS

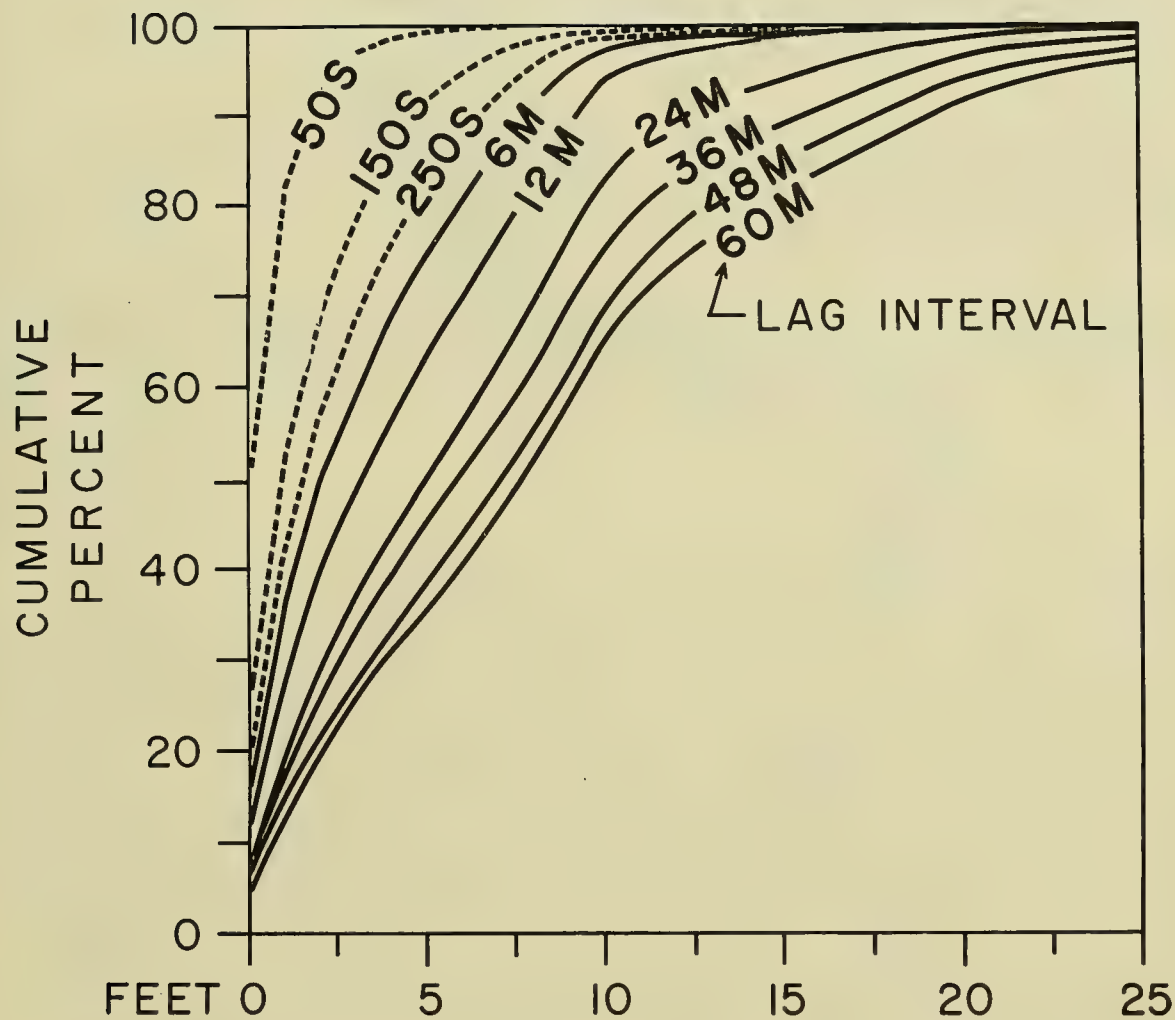


FIGURE 9 DISTRIBUTION OF ABSOLUTE DEPTH DIFFERENCES OF  $20^{\circ}$  ISOTHERM FOR LAGS OF 50 SECONDS TO 1 HOUR

To relate the temperature variability to the associated salinity-depth structure, the T-S curves of hydrographic stations 13 and 14 are shown in Figure 10, enclosed by the T-S envelope of the data for the 23 stations taken during the expedition (See statistical summary, Table 9).

The sound velocity-depth curves based on station 13, 0800 September 17, and station 14, 1522 September 28, are given in Figure 11. The sound velocity inversion which can be seen on the station 13 curve results from the temperature inversion in the halocline shown in Figure 10.

The sound velocity inversion is sufficient to produce a secondary sound channel at this level (Fig 12). The sound channel is approximately 40 m in thickness.

Computations based on the sound velocity structure when no inversion existed (Station 14) were as follows: With a source depth of 100 m, the maximum range of the limiting ray at 100 m was 1 nm. The axis of the permanent sound channel was at 600 m and the convergence zone was at 25.6 nm.

The intermittent existence of the secondary sound channel in this boundary region appears to be associated with changes in the vertical structure due to internal waves. Use can be made of such a secondary sound channel because its existence can be inferred from synoptic BT observations.

## SUMMARY

The analysis of the oceanographic data collected by FLIP and the R.V. HORIZON during September 1963 indicates: (1) that the variability in the temperature-depth structure beneath the isothermal layer is primarily dependent upon internal waves; (2) the variation in depth of the top of the thermocline was as great during a 12-hour period at the time of the full moon as over the period of 26 days, and was almost as large in any given 12-hour period; (3) the temperature in the isothermal layer decreased from  $21^{\circ}$  to  $19.8^{\circ}$  during the observational period. Although the range of the depth oscillations in the thermocline was almost the same on the first day as the last, the mean depth of the thermocline increased from 65 to 110 feet (20-34 m) during the same period. The decrease of temperature in the isothermal layer and the increase in mean depth of the thermocline are in agreement with the expected seasonal changes; and (4) the basic sound velocity-depth structure remained essentially the same throughout the period, excepting, of course, the intermittent inversion near 300 ft. (91 m).

## CONCLUSION

These results have important implications for Navy operations. The variability in the temperature-depth structure associated with internal waves will always be the limiting factor in prediction. It is the environmental condition which must be lived with. However, if the envelope of



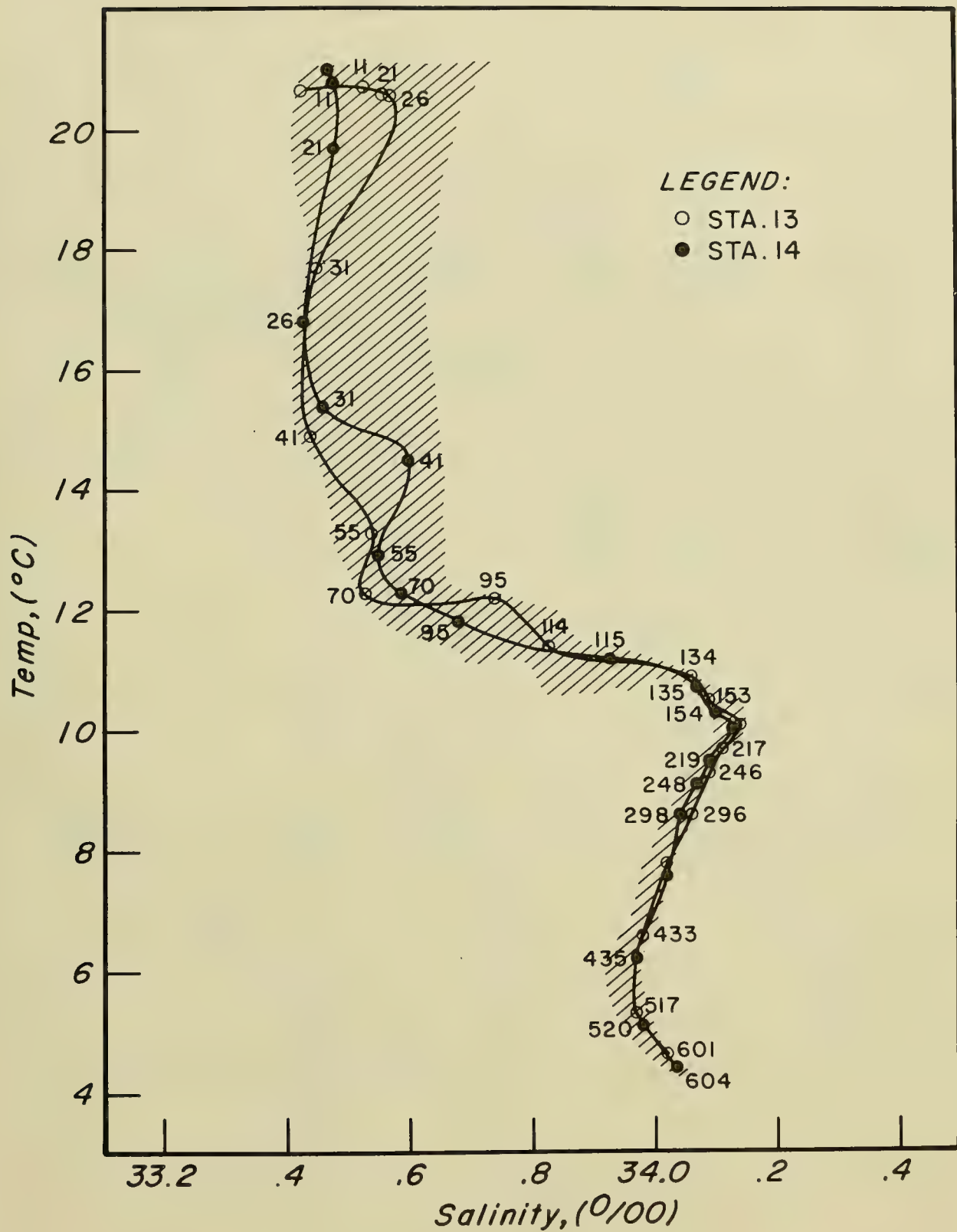


FIGURE 10 T-S CURVES FOR HYDROGRAPHIC STATIONS 13 AND 14

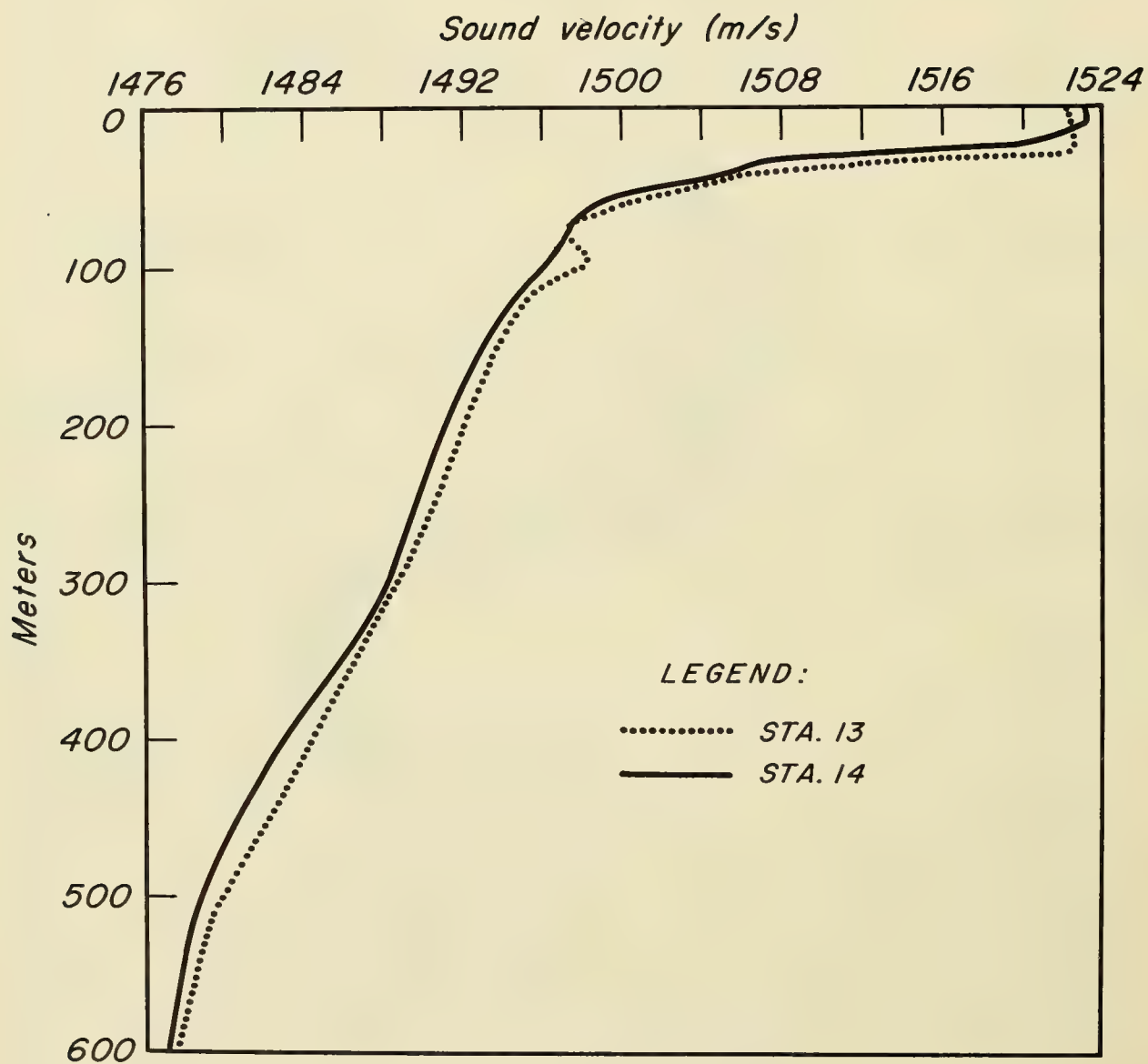


FIGURE 11 SOUND VELOCITY-DEPTH CURVES, STATIONS 13 AND 14

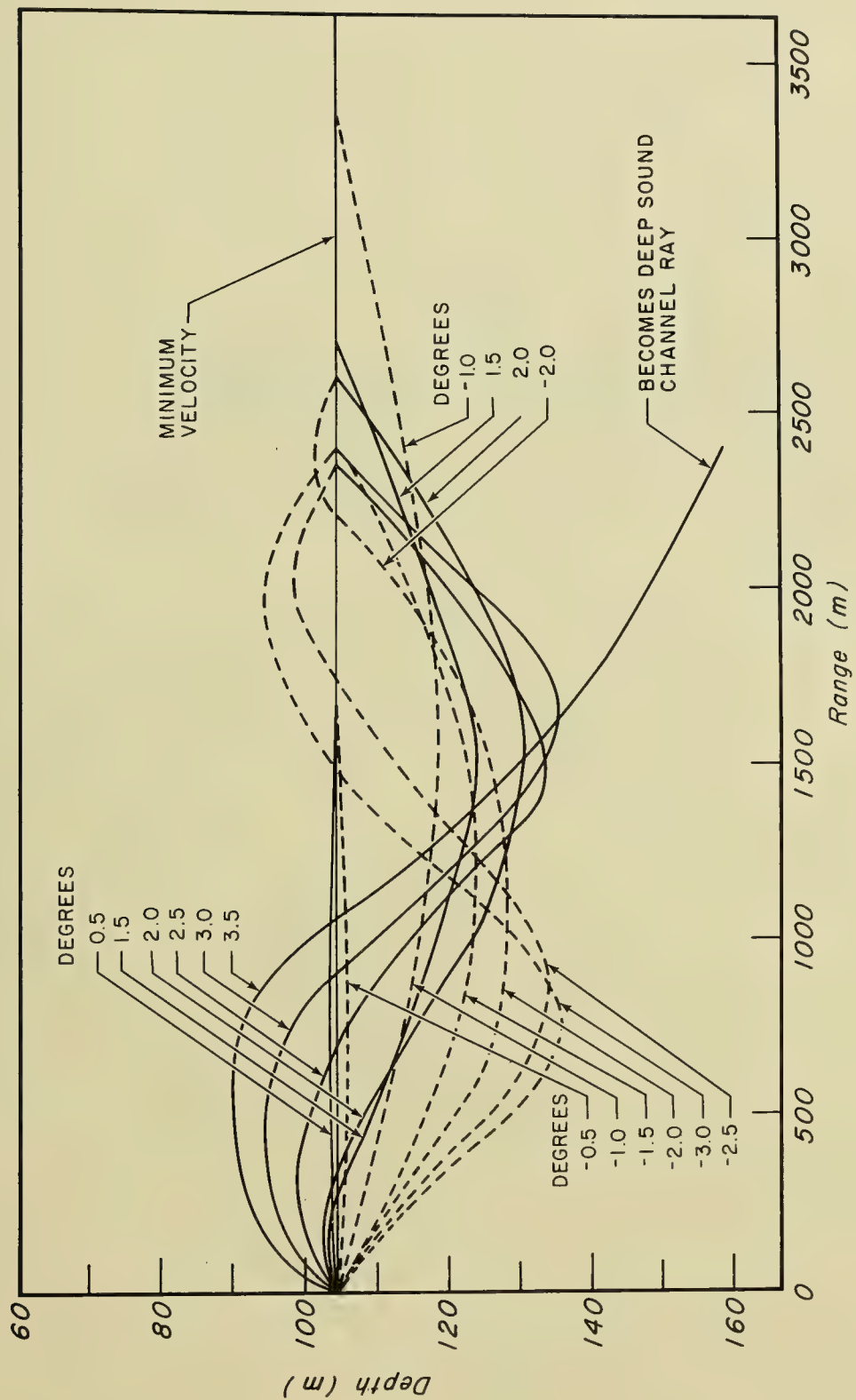


FIGURE 12 RAY DIAGRAM OF SECONDARY SOUND CHANNEL

TABLE 4  
STATISTICS OF DIFFERENCES IN DEPTH (IN FEET) OF  
20° ISOTHERMS FOR LAGS OF DIFFERENT INTERVALS

<u>Lags</u>	<u>N</u>	<u>Mean</u>	<u>Standard Deviations</u>	<u>Extreme Differences</u>
50-second series:				
50"	9075	0.82	1.16	22
100"	9031	1.50	1.73	35
150"	8991	2.07	2.14	21
200"	8954	2.52	2.48	19
250"	8920	2.89	2.75	21
300"	8887	3.17	2.94	22
350"	8854	3.40	3.09	24
6-minute series:				
6'	4718	3.48	3.22	26
12'	4689	3.53	3.88	33
18'	4662	5.44	4.59	35
24'	4642	6.26	5.11	41
30'	4620	6.88	5.64	43
36'	4603	7.42	6.09	40
42'	4589	7.95	6.43	38
48'	4576	8.47	6.78	45
54'	4563	8.84	7.12	46
60'	4554	9.30	7.40	53

TABLE 5

STATISTICS OF DIFFERENCES IN DEPTH (IN FEET) OF  
17° ISOTHERMS FOR LAGS OF DIFFERENT INTERVALS

<u>Lags</u>	<u>N</u>	<u>Mean</u>	<u>Standard Deviations</u>	<u>Extreme Differences</u>
50-second series:				
50"	9076	0.79	1.01	20
100"	9033	1.48	1.59	30
150"	8994	2.07	2.03	26
200"	8958	2.57	2.38	18
250"	8925	2.98	2.67	27
300"	8893	3.30	2.90	27
350"	8861	3.55	3.07	28
6-minute series:				
6'	4718	3.72	3.31	28
12'	4689	4.70	3.96	35
18'	4662	5.66	4.70	37
24'	4642	6.47	5.27	34
30'	4620	7.13	5.71	39
36'	4603	7.70	6.15	38
42'	4589	8.19	6.49	38
48'	4576	8.70	6.83	42
54'	4563	9.04	7.15	42
60'	4554	9.44	7.42	44



TABLE 6

STATISTICS OF DIFFERENCES IN DEPTH (IN FEET) OF  
15.5° ISOTHERMS FOR LAGS OF DIFFERENT INTERVALS

<u>Lags</u>	<u>N</u>	<u>Mean</u>	<u>Standard Deviations</u>	<u>Extreme Differences</u>
50-second series:				
50"	9078	0.81	1.13	20
100"	9035	1.52	1.74	30
150"	8996	2.13	2.21	28
200"	8960	2.65	2.57	19
250"	8927	3.09	2.89	28
300"	8895	3.45	3.12	29
350"	8863	3.74	3.30	31
6-minute series:				
6'	4718	3.93	3.48	31
12'	4689	5.03	4.22	38
18'	4662	6.12	5.03	40
24'	4642	6.94	5.65	42
30'	4620	7.64	6.17	49
36'	4603	8.22	6.62	43
42'	4589	8.76	6.99	45
48'	4576	9.32	7.32	46
54'	4563	9.76	7.64	48
60'	4554	10.15	7.93	49

TABLE 7

STATISTICS OF DIFFERENCES IN DEPTH (IN FEET) OF  
14° ISOTHERMS FOR LAGS OF DIFFERENT INTERVALS

<u>Lags</u>	<u>N</u>	<u>Mean</u>	<u>Standard Deviations</u>	<u>Extreme Differences</u>
50-second series:				
50"	9076	0.93	1.30	22
100"	9033	1.73	1.97	23
150"	8994	2.44	2.48	25
200"	8958	3.03	2.88	23
250"	8925	3.53	3.22	22
300"	8861	4.26	3.73	28
6-minute series:				
6'	4718	4.45	4.04	39
12'	4689	5.65	4.91	43
18'	4662	6.89	5.73	43
24'	4642	7.82	6.49	45
30'	4620	8.69	7.07	52
36'	4603	9.40	7.72	58
42'	4589	10.03	8.19	54
48'	4576	10.68	8.68	56
54'	4563	11.27	9.05	55
60'	4554	11.81	9.33	54

TABLE 8

STATISTICS OF DIFFERENCES IN DEPTH (IN FEET) OF  
12.5° ISOTHERMS FOR LAGS OF DIFFERENT INTERVALS

<u>Lags</u>	<u>N</u>	<u>Mean</u>	<u>Standard Deviations</u>	<u>Extreme Differences</u>
50-second series:				
50"	9061	0.97	2.54	104
100"	9018	1.73	3.14	105
150"	8977	2.39	3.58	104
200"	8940	2.95	3.92	103
250"	8906	3.46	4.23	102
300"	8873	3.88	4.46	101
350"	8840	4.23	4.65	103
6-minute series:				
6'	4701	4.32	5.29	110
12'	4672	5.47	5.83	110
18'	4645	6.51	6.51	112
24'	4624	7.46	7.08	103
30'	4601	8.18	7.57	102
36'	4583	8.94	7.90	107
42'	4568	9.52	8.17	101
48'	4554	10.15	8.56	102
54'	4541	10.58	8.68	106
60'	4532	11.14	9.15	109

TABLE 9

STATISTICS OF VARIABILITY AT STANDARD DEPTHS  
BASED ON HYDROGRAPHIC STATION DATA

Depth	N	Temperature °C.		Salinity ‰		Oxygen ml/L		Sound Velocity m/s	
		Mean	Std.Dev.	Mean	Std.Dev.	Mean	Std.Dev.	Mean	Std.Dev.
0	22	20.50	.32	33.55	.08	5.48	.06	1521.79	.81
10	22	20.48	.31	33.56	.08	5.49	.06	1521.89	.84
20	22	20.36	.30	33.57	.07	5.51	.08	1521.74	.73
30	22	18.61	1.67	33.54	.06	6.01	.46	1516.87	4.48
50	22	13.84	.54	33.53	.06	6.76	.11	1502.61	1.70
75	22	12.20	.19	33.58	.05	6.40	.09	1497.59	.65
100	22	11.74	.24	33.72	.06	5.92	.09	1496.55	.73
125	22	11.04	.13	33.96	.06	5.54	.09	1494.80	.52
200	22	9.78	.08	34.11	.01	5.40	.03	1491.68	.24
250	22	9.12	.08	34.06	.01	5.37	.06	1489.96	.26
300	22	8.52	.07	34.04	.01	5.04	.10	1488.46	.29
400	22	6.94	.09	33.99	.01	4.03	.09	1483.93	.34
500	22	5.45	.09	33.97	.01	3.13	.08	1479.54	.42
600	22	4.54	.06	34.02	.01	2.24	.10	1477.50	.21

variability can be measured for a 12-hr. period, we may expect these conditions to prevail over periods up to one month. The duration will probably be longer in tropical regions, shorter in current regions. In boundary or confluence regions, the usefulness of the envelope will be limited by the time-scale of the changes in location of the boundary.

#### ACKNOWLEDGEMENTS

This paper represents results of research sponsored by the Office of Naval Research under Contract NONR 2216 (01), (05).

#### REFERENCES

- Bullard, E. C., F. E. Oglebay, W. H. Munk, G. R. Miller 1964 A user's guide to Bomm. University of California, Inst. Geophy. and Plan. Phys., La Jolla, California. 111. 1964.
- Defant, Albert 1940 Die ozeanogr. Verhältnisse während der Ankerstation des ALTAIR am Nordrand des Hauptstromstriches des Golfstromes nordlich der Azoren. Aus den Wiss. Erg. der Intern. Golfstrom-Unternahmen 1938. Ann. Hydr. Mar. Met. Beih. November 1940.
- Fisher, F. H. and F. N. Spiess 1963 FLIP, floating instrument platform J. Acoust. Soc. Am., 35, 1633-44. 1963.
- Fjeldstad, J. E. 1933 Interne Wellen, Geofysiske Publikasjoner, 10, 53, Oslo 1933.
- Rudnick, Philip 1964 FLIP: An oceanographic buoy. Science, 146, No. 3649, pp. 1268-1273. December 1964.
- Snodgrass, F., G. Groves, K. Hausselman, G. Miller, W. H. Munk and R. Powers. Propagation of Ocean Swell across the Pacific. Phil. Trans. Royal Society of London, in press.
- Sverdrup, H. U., M. W. Johnson and R. H. Fleming 1946 The Oceans. Prentice Hall, Inc., New York, 1060. 1946.



SOUND VELOCITY STRUCTURE OF THE OCEAN BETWEEN  
BERMUDA AND THE ANTILLES

by

R. E. Payne and J. C. Beckerle

Woods Hole Oceanographic Institution  
Woods Hole, Massachusetts



# SOUND VELOCITY STRUCTURE OF THE OCEAN BETWEEN BERMUDA AND THE ANTILLES

by

R. E. Payne and J. C. Beckerle

Woods Hole Oceanographic Institution, Woods Hole, Mass. 02543

## INTRODUCTION

The Geophysics Department of the Woods Hole Oceanographic Institution is conducting a continuing study to determine the variations of the sound velocity structure of the broad ocean area between Bermuda and the Antilles as a function of time and of the geographical coordinates. The first survey in this study was made in July and August of 1962 by J. Reitzel. During the same months of 1964 we made a large number of sound velocity profiles on Cruise 11 of the R/V ATLANTIS II. Figure 1 shows the positions of the profiles made in the two studies. The large dots are positions of profiles in 1962; the small dots and the large dots with numbers are positions of profiles in 1964. We chose the positions of our profiles so as to give a broad coverage of the area and also to give some detailed information about areas which appeared to be interesting in 1962. The numbers at the positions give the profile numbers. Sound velocities were measured with a commercial model of the National Bureau of Standards "sing - around" velocimeter. Depths were measured with an Inverted Echo Sounder, (Dow, 1963) using the measured sound velocities to correct the depths. Sound velocities were calculated at 1 to 2 meter depth intervals with the assistance of a GE 225 computer.

## SHORT TERM VARIATIONS

We were interested in learning the magnitude of fluctuations of sound velocity at any given depth that may take place within the duration of a cruise. This information is necessary to determine within what limits we can compare profiles made at different times in a cruise. To this end we made three pairs of lowerings, the two members of a pair being made at locations as close as was practical, 7 miles apart in the worst instance and 1 mile in the best. Figure 2 shows Profiles 21 and 22 which were made in the Puerto Rican Trench about 6 hours apart. Although the

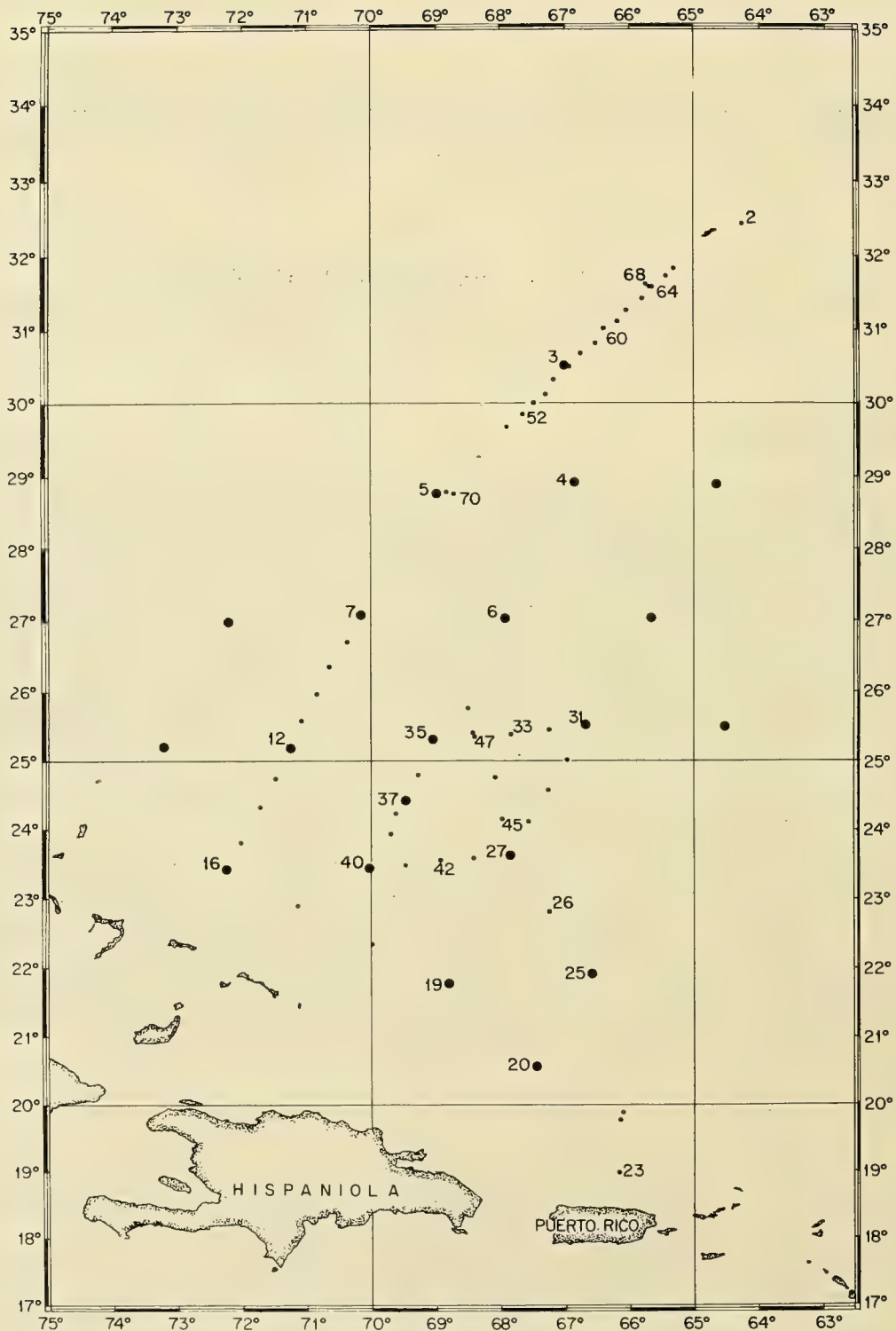


FIGURE 1 PROFILE POSITIONS IN 1962 AND 1964

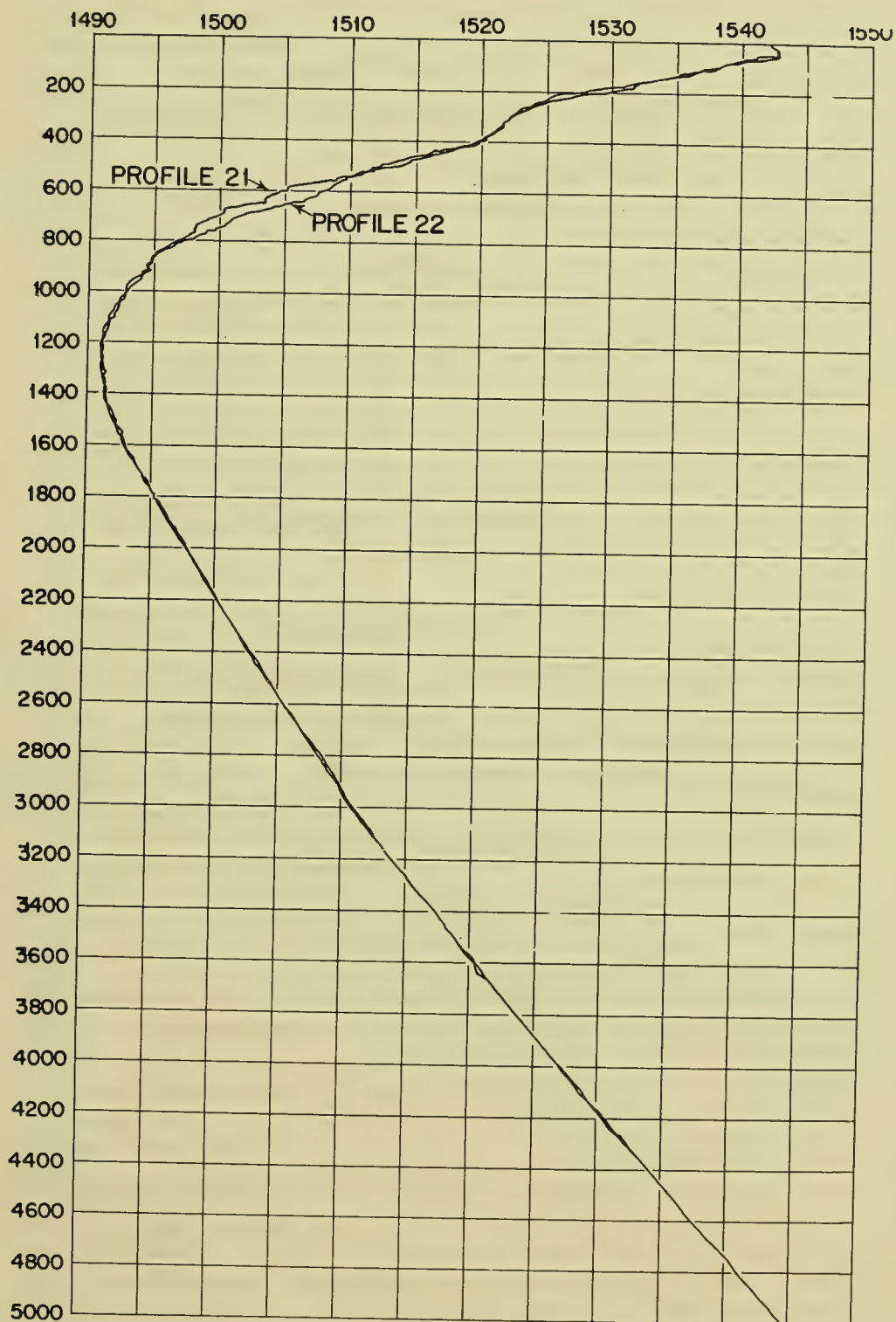


FIGURE 2 PROFILES 21 AND 22



shapes are similar the magnitude of the sound velocity shows differences up to 2 m/sec at various depths in the thermocline. Differences of this order of magnitude are not surprising. A. Piip (personal communication) of the Bermuda Sofar Station has found a semidiurnal variation in the sound velocity at a depth of 1150 m. of a little over 1 m/sec in this area. Figure 3 shows Profiles 34 and 47 which were made 4 days apart about half way between Bermuda and Puerto Rico. The differences between them in the magnitude of the sound velocity are small. However, one significant difference occurs at 300 m. In Profile 34 the sound velocity gradient becomes positive for a short distance below 300 m. causing a secondary sound channel while in Profile 47 the gradient is negative throughout the thermocline and there is no secondary sound channel. We shall return to this point later. Figure 4 shows profiles 5 and 49 made 34 days apart. Differences in magnitude of the sound velocity of up to 4 to 5 m/sec are found in the main thermocline with somewhat larger fluctuations near the surface. Again the general shape has not changed and both profiles have a decidedly positive sound gradient near 300 m.

## LONG TERM VARIATIONS

Comparison of the data taken in 1962 with that acquired in 1964 gives us an idea of some changes which have taken place during this two year period. The 1962 data were spread over a greater area but the 1964 profiles were closer together. From his data Reitzel drew isovelocity contour curves from 200, 300, 400, 500, 600, 800, and 1000 m. Contours of course, are an interpretation of results, but the 1962 data have been contoured independently by three people all skeptical of the others' interpretations. The contours of all three are essentially the same. The 1964 profiles do not cover a broad enough area to be contoured but we can determine whether they agree even generally with the 1962 data. Figure 5 shows the 1962 contours and the 1964 sound velocities at a depth of 800 m. Contour plots at all depths between 300 m. and 1000 m. are qualitatively similar to that at 800 m. except as noted below. Sound velocities have been rounded off to the nearest meter per second and are close to 1500 m/sec. 1400 or 1500 must be added as appropriate to give the true sound velocity. The minimum and maximum sound velocities at a given depth may differ slightly from the two years but the range is strikingly similar at all depths. The next most general feature is a regional decrease in sound velocity from NW. to SE. near the surface which gradually rotates around to N. to S. as one progresses down to 1000 m. If we chose to call this the zero order mode of change then the first order change manifests itself as a maximum of the sound velocity in the SW. and a minimum in the NE. in the 1962 contours. The numbers from 1964 show a reversal

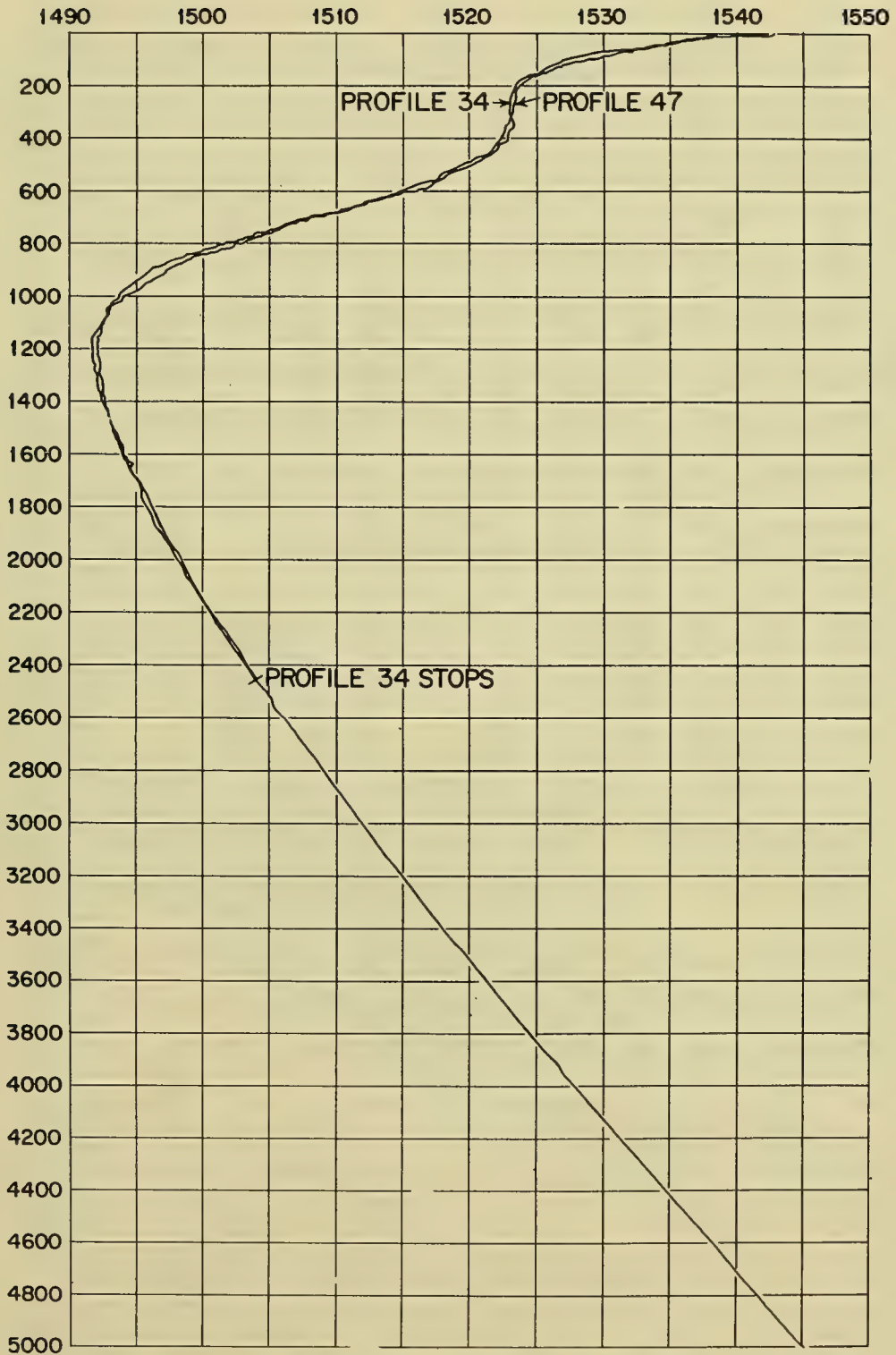


FIGURE 3 PROFILES 34 AND 47

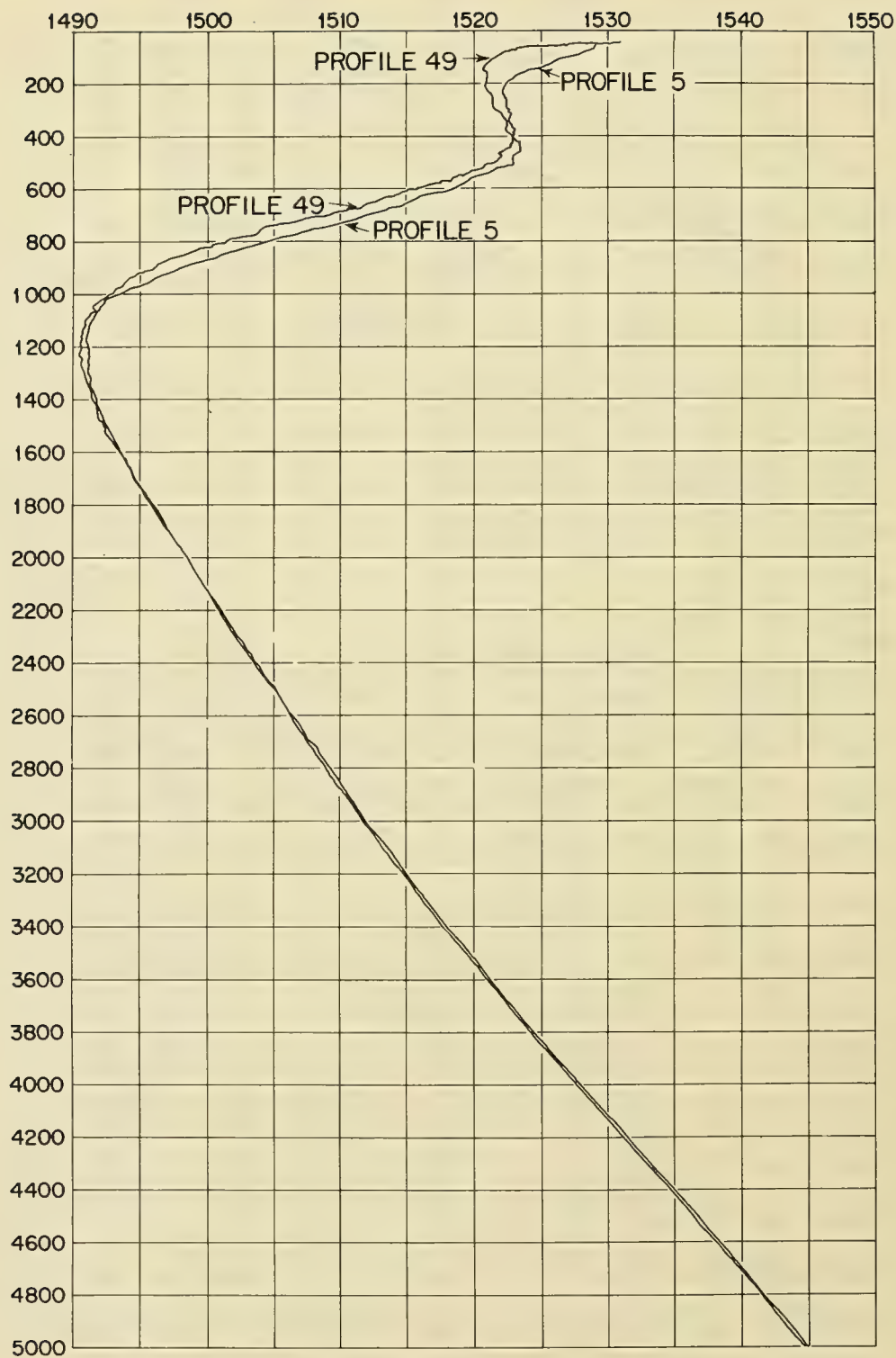


FIGURE 4 PROFILES 5 AND 49

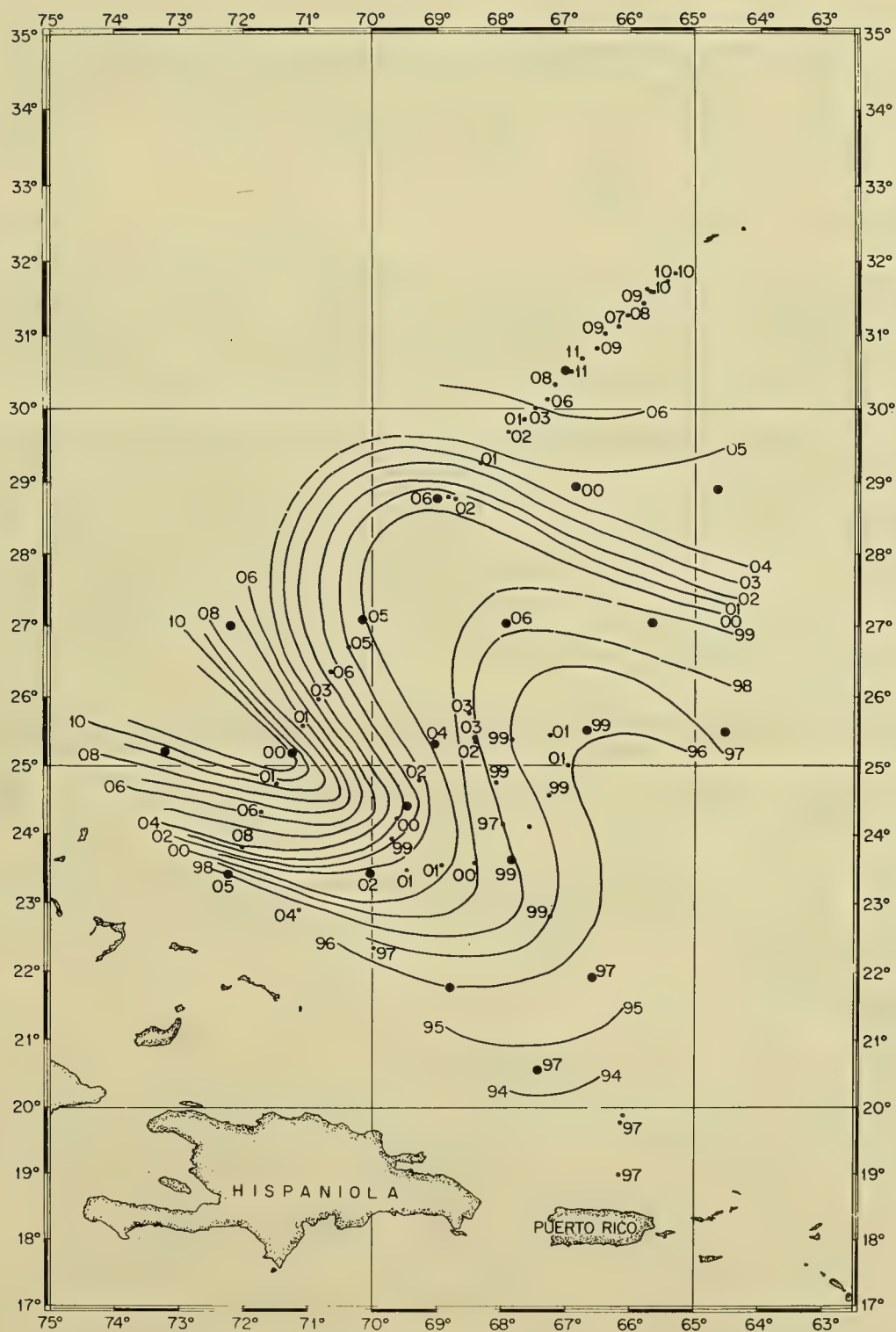


FIGURE 5 CONTOURS AT 800 m



of this with a minimum in the SW. and a maximum in the NE. In 1962 the gradients characteristic of the sound velocity high in the southwest were much higher than any found in 1964. Differences over the period of one month as mentioned above cannot obliterate those features and so we feel justified in these comparisons of regional features.

## GEOGRAPHICAL VARIATIONS

The area can be divided into three regions depending upon the shape of the sound velocity profiles above 500 m. Figure 6 illustrates typical profile shapes in those three regions. In Profile 45 an 18°C isothermal region between 200 m. and 500 m. causes the sound velocity gradient to be positive in this interval. The central profiles have gradients close to zero in this depth interval but the southern profile has a negative gradient from the surface to the SOFAR axis. Thus Profile 45 has a definite secondary sound channel in addition to the SOFAR channel. The others do not. Figure 7 shows the boundaries of the three regions considering all the profiles. These boundaries occur between two adjacent profiles of the 1964 data. Near Profile 47 and 48 the boundary apparently moved north of Profile 48, a distance of at least 30 miles, during the four days which elapsed between Profile 34 and Profiles 47 and 48.

The 1962 data show that the northernmost profile, whose position is the same as Profile 3 in 1964, has a shape similar to the profiles in the central section. It might be inferred from this that in 1962 the 18°C water lay north of 30°N.

Below the SOFAR velocity minimum there is little variation in sound velocity over the area at any given depth; e. g. , at 5000 m. the variation is less 1 1/2 m/sec.

## DISCUSSION

These are only two studies made in the same season two years apart and we cannot determine from them the periods of the large scale changes described. We can, however, put a lower limit of two months on them since it seems reasonable from the results that the regional structure did not change radically over the time required to collect the data. The similarities and changes between the two years and the remarkably consistent geographic pattern in one year suggest either an oscillatory phenomenon such as internal waves or some very long period transient in the circulation of the North Atlantic. Time series observations over several years will probably be required to determine the true scales of the



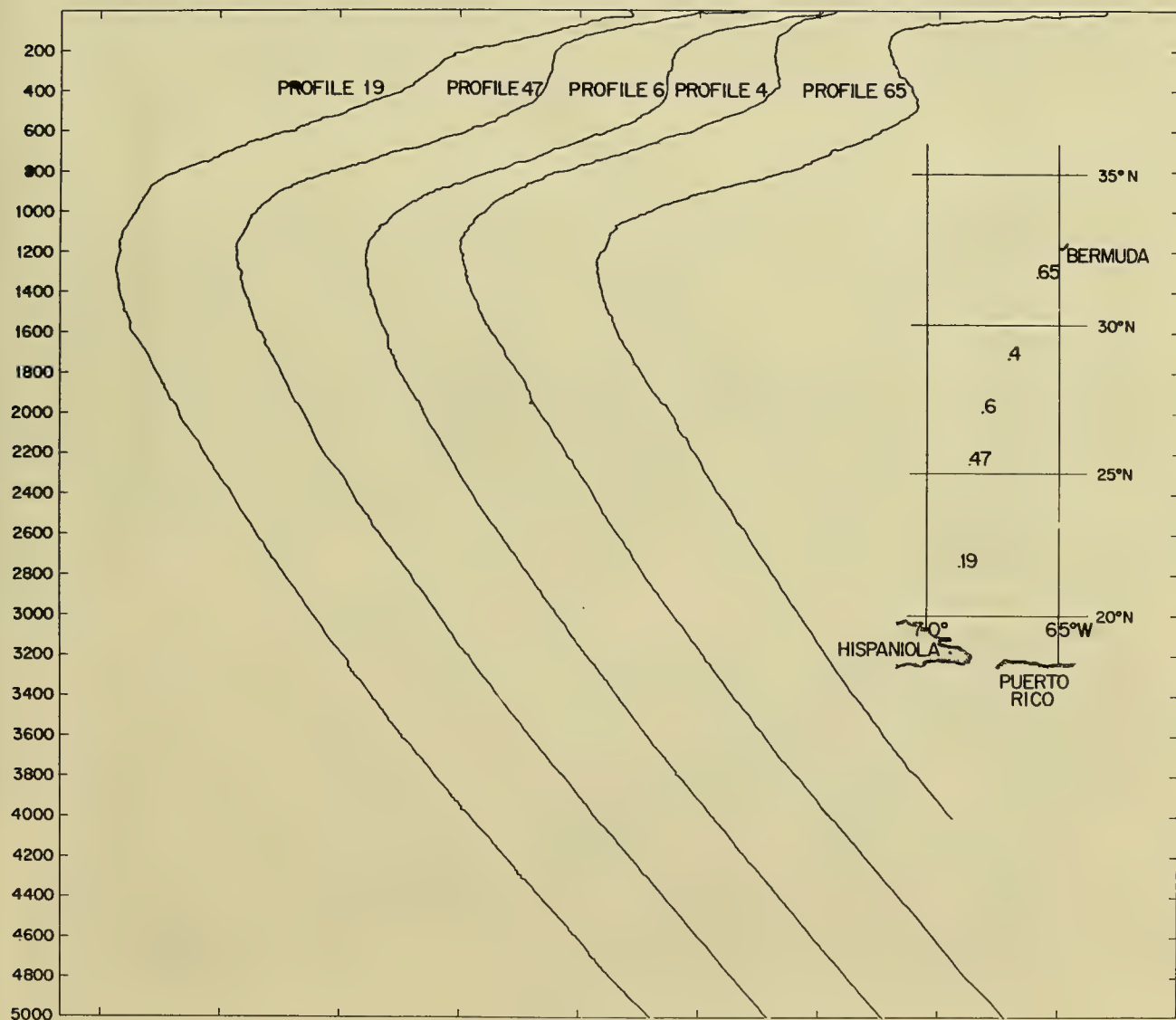


FIGURE 6

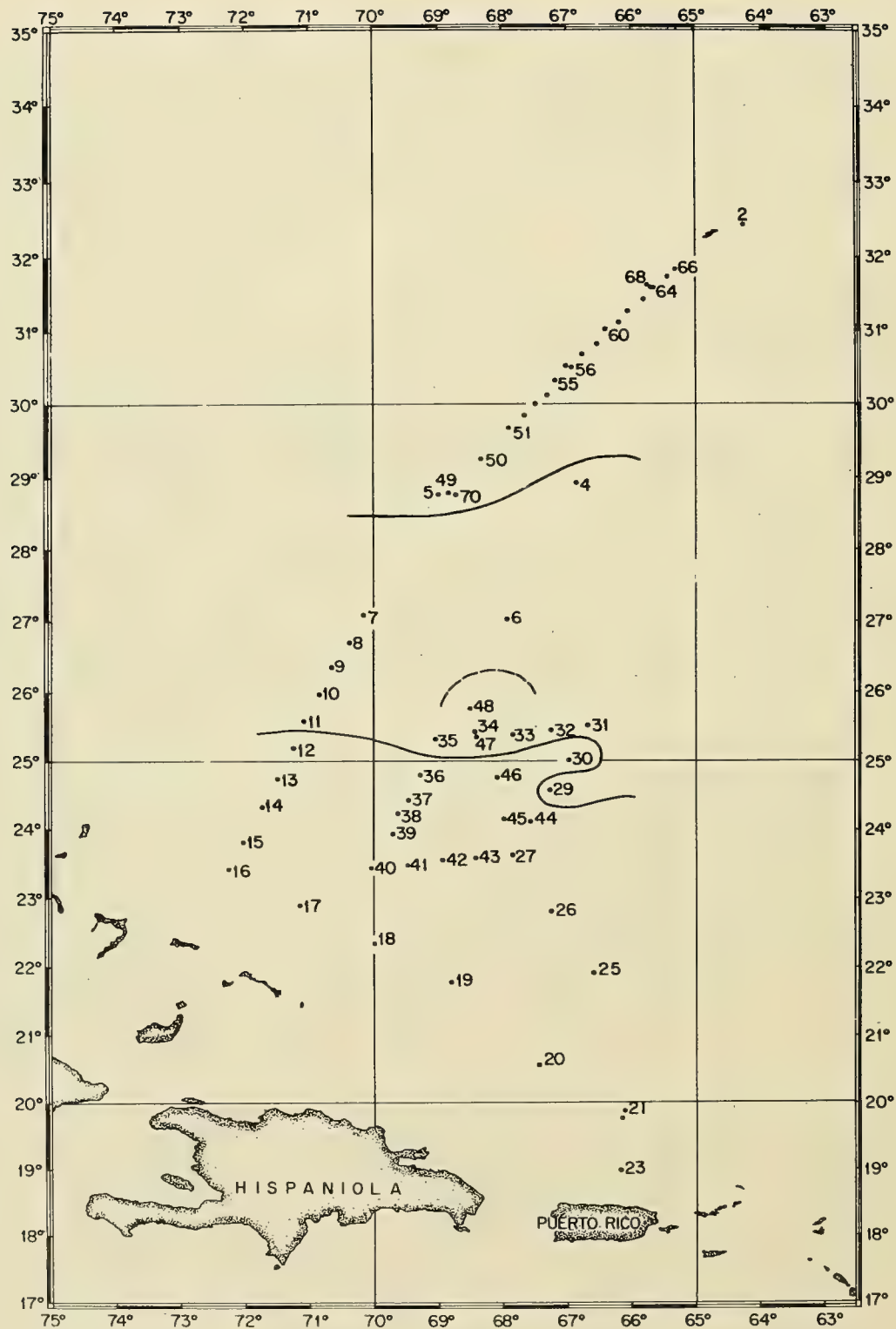


FIGURE 7 ZONES FOR UPPER 500 m

change and their driving mechanisms. Valuable understanding can be achieved by continuing to work from ships with lowered instruments, but it seems that anchored buoys and towed instruments could be especially advantageous for this work.

The occurrence of the depressed shallow sound channel has long been known, and sound transmission studies have been made along it. Nevertheless it seems worthwhile to remind ourselves that this is a good sound channel, near the surface, and near home, where existing variable depth sonar can be used to considerable advantage. Sonars which can be towed at 600 feet will find great advantage there throughout the year. But it does have rather distinct limits about which we know little. These limits almost certainly change, but we now have little idea how fast and only a vague idea how far. It would be worthwhile to find out.

### Conclusion

Sound velocity data from two cruises to the area between Bermuda and the Antilles in 1962 and 1964 have closely the same range of velocities at any depth, differing at most by only a few meters per second. This difference is the same as the change which took place between two measurements at the same location during a single cruise. A general decrease in sound velocity from north to south was found at all depths from 300 m. to 1000 m. in both studies. A maximum of sound velocity in the western half of the area with an accompanying minimum in the east found in the 1962 results have become reversed in 1964. Evidence is inadequate to distinguish between recurrent internal waves and circulation transients as the explanation for these large scale characteristics of the water.

The whole area is divisible into three regions depending on the sound velocity structure above 500 meters. Near Bermuda this part of the water column is partially a sound channel. Farther south and west the same depth has nearly constant sound velocity as a function of depth. Still further south the sound velocity gradient is continuously negative. The secondary sound channel which appears between the surface and 500 m. in the northern profiles in 1964 was absent in 1962, the corresponding structure being isovelocity. This and other evidence of change in the position of the boundaries between these water masses indicate changes in sound transmission. The time scale and magnitude of these changes is not known.



## Acknowledgement

We should like to thank Dr. J. B. Hersey for his advice and assistance in the preparation of this paper.

## REFERENCES

Dow, W. and S. L. Stillman, (1962) Inverted Echo Sounder. Marine Sciences Instrumentation, Vol. 1, 263-272 (Plenum Press Inc. , New York).





